

Lecture Notes on Nonlinear Dynamics (A Work in Progress)

Daniel Arovas
Department of Physics
University of California, San Diego

May 5, 2023

Contents

Contents	i
List of Figures	vii
0.1 Preface	xv
0 Reference Materials	1
0.1 Dynamical Systems	1
0.2 Hamiltonian Mechanics	2
0.3 Differential Equations	2
0.4 Synchronization	3
0.5 Nonlinear Wave Equations	3
0.6 Hydrodynamics	3
0.7 Pattern Formation	4
0.8 Biological Applications	4
1 Introduction to Dynamics	5
1.1 Introduction	5
1.1.1 Phase space and phase curves	5
1.1.2 Vector fields	6
1.1.3 Existence / uniqueness / extension theorems	7
1.1.4 Linear differential equations	8
1.1.5 Lyapunov functions	8

1.2	<i>N = 1</i> Systems	9
1.2.1	Classification of fixed points ($N = 1$)	10
1.2.2	Logistic equation	10
1.2.3	Singular $f(u)$	11
1.2.4	Recommended exercises	13
1.2.5	Non-autonomous ODEs	13
1.3	Flows on the Circle	14
1.3.1	Nonuniform oscillator	14
1.4	Appendix I : Evolution of Phase Space Volumes	16
1.5	Appendix II : Lyapunov Characteristic Exponents	17
1.6	Appendix III : Normal Matrices, Non-Normal Matrices, and Jordan Blocks	19
2	Bifurcations	25
2.1	Types of Bifurcations	25
2.1.1	Saddle-node bifurcation	25
2.1.2	Transcritical bifurcation	26
2.1.3	Pitchfork bifurcation	28
2.1.4	Imperfect bifurcation	29
2.2	Examples	31
2.2.1	Population dynamics	31
2.3	Appendix I : The Bletch	34
2.4	Appendix II : Landau Theory of Phase Transitions	36
2.4.1	Landau coefficients from mean field theory	38
2.4.2	Magnetization dynamics	39
2.4.3	Cubic terms in Landau theory : first order transitions	42
2.4.4	Magnetization dynamics	44
2.4.5	Sixth order Landau theory : tricritical point	47
2.4.6	Hysteresis for the sextic potential	48

3 Two-Dimensional Phase Flows	51
3.1 Harmonic Oscillator and Pendulum	51
3.1.1 Simple harmonic oscillator	51
3.1.2 Pendulum	53
3.2 General $N = 2$ Systems	53
3.2.1 The damped driven pendulum	54
3.2.2 Classification of $N = 2$ fixed points	56
3.2.3 The fixed point zoo	58
3.2.4 Fixed points for $N = 3$ systems	61
3.3 Andronov-Hopf Bifurcation	62
3.4 Population Biology : Lotka-Volterra Models	63
3.4.1 Rabbits and foxes	64
3.4.2 Rabbits and sheep	65
3.5 Poincaré-Bendixson Theorem	67
3.6 Index Theory	68
3.6.1 Gauss-Bonnet Theorem	72
3.6.2 Singularities and topology	73
3.7 Appendix : Example Problem	75
4 Nonlinear Oscillators	79
4.1 Weakly Perturbed Linear Oscillators	79
4.1.1 Naïve Perturbation theory and its failure	79
4.1.2 Poincaré-Lindstedt method	81
4.2 Multiple Time Scale Method	83
4.2.1 Duffing oscillator	85
4.2.2 Van der Pol oscillator	86
4.3 Forced Nonlinear Oscillations	87
4.3.1 Forced Duffing oscillator	89
4.3.2 Forced van der Pol oscillator	91

4.4	Synchronization	95
4.5	Relaxation Oscillations	99
4.5.1	Example problem	102
4.5.2	Multiple limit cycles	104
4.5.3	Example problem	105
4.6	Appendix I : Multiple Time Scale Analysis to $\mathcal{O}(\epsilon^2)$	106
4.7	Appendix II : MSA and Poincaré-Lindstedt Methods	108
4.7.1	Problem using multiple time scale analysis	108
4.7.2	Solution using Poincaré-Lindstedt method	112
4.8	Appendix III : Modified van der Pol Oscillator	114
5	Maps, Strange Attractors, and Chaos	121
5.1	Motion on Resonant Tori	121
5.1.1	The twist map	121
5.1.2	The perturbed twist map	122
5.2	Maps from Time-Dependent Hamiltonian Systems	123
5.2.1	Parametric Oscillator	123
5.2.2	Kicked dynamics	126
5.3	Local Stability and Lyapunov Exponents	129
5.3.1	The fate of nearly separated initial conditions under iteration	129
5.3.2	Kolmogorov-Sinai entropy	130
5.4	The Poincaré-Birkhoff Theorem	132
5.5	One-dimensional Maps	134
5.5.1	Lyapunov Exponents	136
5.5.2	Chaos in the logistic map	136
5.5.3	Intermittency	138
5.6	Attractors	139
5.7	The Lorenz Model	139
5.7.1	Fixed point analysis	141

5.7.2	Poincaré section	143
5.7.3	Rössler System	144
6	Front Propagation	147
6.1	Reaction-Diffusion Systems	147
6.1.1	Single component systems	147
6.1.2	Propagating front solutions	148
6.1.3	Stability and zero mode	151
6.1.4	Fisher's equation	153
6.1.5	Velocity selection and stability	154
6.2	Multi-Species Reaction-Diffusion Systems	156
6.2.1	Propagating front solutions	158
6.3	Excitable Media	161
6.3.1	Front propagation in excitable media	163
7	Pattern Formation	169
7.1	Reaction-Diffusion Dynamics Revisited	169
7.2	Turing and Hopf Instabilities	171
7.3	The Brusselator	172
7.3.1	The amplitude equation	174
7.4	Rayleigh-Bénard Instability	177
7.5	Center Manifold Reduction	179
7.6	Selection and Stability of Spatial Patterns	180
7.6.1	$d = 1$	181
7.6.2	Remarks on the amplitude equations for $d > 1$	181
7.6.3	$d = 2$	182
7.6.4	$d = 3$	189
7.7	Anisotropy	189
7.8	Phase Diffusion : Eckhaus and Zigzag Instabilities	190

8 Solitons	195
8.1 The Korteweg-deVries Equation	196
8.1.1 KdV solitons	197
8.1.2 Periodic solutions : soliton trains	198
8.1.3 Interlude: primer on elliptic functions	199
8.1.4 The soliton lattice	200
8.1.5 N -soliton solutions to KdV	201
8.1.6 Bäcklund transformations	205
8.2 Sine-Gordon Model	207
8.2.1 Tachyon solutions	210
8.2.2 Hamiltonian formulation	210
8.2.3 Phonons	211
8.2.4 Mechanical realization	211
8.2.5 Kinks and antikinks	212
8.2.6 Bäcklund transformation for the sine-Gordon system	213
8.3 Nonlinear Schrödinger Equation	215
8.3.1 Amplitude-phase representation	216
8.3.2 Phonons	217
8.3.3 Soliton solutions for NLS(+)	217
8.3.4 Dark solitons for NLS(−)	219
9 Shock Waves	221
9.1 Nonlinear Chiral Wave Equation	221
9.1.1 The method of characteristics	222
9.1.2 Breaking waves: when characteristics intersect	224
9.2 Shocks	227
9.3 Internal Shock Structure	228
9.3.1 Quadratic $J(\rho)$	229
9.4 Shock Fitting	230

9.4.1	An important caveat	230
9.4.2	Recipe for shock fitting when $J'''(\rho) = 0$	231
9.4.3	Example : shock fitting an inverted parabola	232
9.5	Long-time Behavior of Shocks	234
9.5.1	Fate of a hump	234
9.5.2	N-wave and P-wave	235
9.6	Shock Merging	237
9.7	Shock Fitting for General $J(\rho)$	238
9.8	Sources	239
9.8.1	Examples	239
9.8.2	Moving sources	240
9.9	Burgers' Equation	241
9.9.1	The limit $\nu \rightarrow 0$	242
9.9.2	Examples	243
9.9.3	Confluence of shocks	246
9.10	Appendix I : The Method of Characteristics	247
9.10.1	Example	248
9.11	Appendix II : Worked Problem in Shock Fitting	249
9.12	Appendix III : The Traffic Light	252
9.13	Appendix IV : Characteristics for a Periodic Signal	254
9.14	Appendix V : Car-Following Models	261

List of Figures

1.1	An example of a phase curve	6
1.2	Phase flow for an $N = 1$ system	10
1.3	Flow diagram for the logistic equation	11
1.4	$f(u) = A u - u^* ^\alpha$, for $\alpha > 1$ and $\alpha < 1$	12
1.5	Solutions to $\dot{e} = \mp A e^\alpha$	13
1.6	Flow for the nonuniform oscillator $\dot{\theta} = \omega - \sin \theta$	15
2.1	Evolution of $F(x, \alpha)$ as a function of the control parameter α	26
2.2	Flow diagrams for $\dot{u} = r + u^2$ and $\dot{u} = ru - u^2$	27
2.3	Extended phase space flow for the saddle-node and transcritical bifurcations	27
2.4	Supercritical and subcritical pitchfork bifurcations	28
2.5	Extended phase space flow for supercritical and subcritical pitchfork bifurcations	29
2.6	Scaled free energy and phase diagram	30
2.7	Imperfect pitchfork bifurcation	31
2.8	Phase flow for the constantly harvested population	32
2.9	Plot of $h(n) = n/(n^2 + 1)$	33
2.10	Phase diagram for the equation $\dot{n} = \gamma(1 - n/c) n - n^2/(n^2 + 1)$	34
2.11	Phase flow for the scaled bletch population, $\dot{n} = n^2 - n^3$	35
2.12	Phase flow for the harvested bletch population, $\dot{n} = -\nu n + n^2 - n^3$	36
2.13	Scaled bletch harvest r versus scaled harvesting rate ν	37
2.14	Phase diagram for the quartic mean field theory $f = f_0 + \frac{1}{2}am^2 + \frac{1}{4}bm^4 - hm$	39

2.15 Mean field free energy $f(m)$ at $h = 0.1$	40
2.16 Dissipative magnetization dynamics $\dot{m} = -f'(m)$	41
2.17 Hysteretic dynamics	42
2.18 Behavior of the quartic free energy $f(m) = \frac{1}{2}am^2 - \frac{1}{3}ym^3 + \frac{1}{4}bm^4$	44
2.19 Fixed points for $\varphi(u) = \frac{1}{2}\bar{r}u^2 - \frac{1}{3}u^3 + \frac{1}{4}u^4$	45
2.20 Behavior of the sextic free energy $f(m) = \frac{1}{2}am^2 + \frac{1}{4}bm^4 + \frac{1}{6}cm^6$	46
2.21 Free energy $\varphi(u) = \frac{1}{2}\bar{r}u^2 - \frac{1}{4}u^4 + \frac{1}{6}u^6$	48
2.22 Fixed points $\varphi'(u^*) = 0$ for the sextic potential	49
3.1 Phase curves for the harmonic oscillator	52
3.2 Phase curves for the simple pendulum	54
3.3 The resistively and capacitively shunted Josephson junction	55
3.4 Phase flows for the equation $\ddot{\phi} + \gamma^{-1}\dot{\phi} + \sin \phi = j$	57
3.5 Complete classification of fixed points for the $N = 2$ system	58
3.6 Fixed point zoo for $N = 2$ systems	59
3.7 Phase portrait for an $N = 2$ flow	60
3.8 Stable, unstable, and half-stable limit cycles	60
3.9 Limit cycle of the Van der Pol oscillator for $\mu \gg 1$	61
3.10 Hopf bifurcation	63
3.11 Phase flow for the rabbits vs. foxes Lotka-Volterra model	65
3.12 Two possible phase flows for the rabbits vs. sheep model	67
3.13 Two singularities with index +1	67
3.14 Two singularities with index -1	69
3.15 Left panel: a singularity with index +2	70
3.16 A vector field with index -2	71
3.17 Two smooth vector fields on the sphere \mathbb{S}^2	72
3.18 Smooth vector fields on the torus and on a 2-manifold of genus $g = 2$	73
3.19 Composition of two circles	74
3.20 Sketch of phase flow for $\dot{x} = \frac{1}{2}x + xy - 2x^3$, $\dot{y} = \frac{5}{2}y + xy - y^2$	76

4.1	Phase diagram for the forced Duffing oscillator	89
4.2	Amplitude A versus detuning ν for the forced Duffing oscillator (I)	90
4.3	Amplitude versus detuning ν for the forced Duffing oscillator (II)	90
4.4	Amplitude versus detuning for the forced van der Pol oscillator	92
4.5	Phase diagram for the weakly forced van der Pol oscillator in the (ν^2, f_0^2) plane	93
4.6	Forced van der Pol system with $\epsilon = 0.1$, $\nu = 0.4$ for three values of f_0	94
4.7	Isochrones of the complex amplitude equation $\dot{A} = (1 + i\alpha)A - (1 + i\beta) A ^2 A$	97
4.8	Analysis of the equation $\dot{\psi} = -\nu + \varepsilon G(\psi)$	98
4.9	Relaxation oscillations in the Liénard plane (x, y)	100
4.10	Limit cycle for the relaxation oscillation	101
4.11	Limit cycle for large μ relaxation oscillations	102
4.12	Relaxation oscillations for $\ddot{x} + \mu(x - 1)\dot{x} + x = 0$	103
4.13	Liénard plots for systems with one and two relaxation oscillations	104
4.14	Three instances of $\Phi(x)$	105
4.15	Phase flows in the Liénard plane for the three examples in fig. 4.14	106
4.16	Phase flow and nullclines for the oscillator $\ddot{x} + \epsilon(x^4 - 1)\dot{x} + x = 0$	115
4.17	Vector field and phase curves for the oscillator $\ddot{x} + \epsilon(x^4 - 1)\dot{x} + x = 0$	117
4.18	Solution to the oscillator equation $\ddot{x} + \epsilon(x^4 - 1)\dot{x} + x = 0$	117
4.19	Vector field and phase curves for the oscillator $\ddot{x} + \epsilon(x^4 - 1)\dot{x} + x = 0$	119
4.20	Solution to the oscillator equation $\ddot{x} + \epsilon(x^4 - 1)\dot{x} + x = 0$	119
5.1	Motion of an $n = 2$ system on an invariant torus	122
5.2	Phase diagram for the parametric oscillator in the (θ, ϵ) plane	125
5.3	The standard map	127
5.4	The kicked Harper map	128
5.5	The baker's transformation	131
5.6	The iterated twist map	132
5.7	Self-similar structures in the iterated twist map	133
5.8	Homoclinic tangle for the map $x_{n+1} = y_n$ and $y_{n+1} = (a + by_n^2)y_n - x_n$	134

5.9 Cobweb diagram showing iterations of the logistic map $f(x) = rx(1 - x)$	135
5.10 Iterates of the logistic map $f(x) = rx(1 - x)$	137
5.11 Lyapunov exponent (in red) for the logistic map	138
5.12 Iterates of the sine map $f(x) = r \sin(\pi x)$	139
5.13 Intermittency in the logistic map in the vicinity of the 3-cycle	140
5.14 Evolution of the Lorenz equations for $\sigma = 10$, $b = \frac{8}{3}$ and both $r = 15$ and $r = 28$	141
5.15 Evolution of the Lorenz equations showing the strange attractor	142
5.16 $X(t)$ for the Lorenz equations with $\sigma = 10$, $b = \frac{8}{3}$, and $r = 28$	143
5.17 Lorenz attractor and relations between successive maxima Z_N	144
5.18 Period doubling bifurcations of the Rössler attractor for $a = b = \frac{1}{10}$	145
5.19 Period doubling bifurcations of the Rössler attractor for $a = b = \frac{1}{5}$	145
6.1 Reaction functions $R(u) = ru(a - u)$ and stable fixed points for local reaction kinetics	149
6.2 Evolution of a blip in the Fisher equation	154
6.3 Analysis of the characteristic polynomial for the Jacobian of the linearized map	159
6.4 Sketch of the type-II front	160
6.5 Sketch of the nullclines for the dynamical system described in the text	161
6.6 Sketch of the fizzle	162
6.7 Sketch of $u(t)$ and $v(t)$ for the fizzle and burst	162
6.8 With three nullcline crossings, there are two stable fixed points and two types of burst	163
6.9 Excitation cycle for the FitzHugh-Nagumo model	164
6.10 Sketch of the excitation pulse of the FitzHugh-Nagumo model	165
6.11 Mechanical analog for the front solution, showing force $F(x)$ and potential $U(x)$	166
7.1 Instabilities in linear systems $\dot{\eta} = L\eta$ are determined by the real parts of their eigenvalues	170
7.2 Instability lines for the Brusselator	173
7.3 Bénard convection cells in a fluid heated from below	178
7.4 Sketch showing separation of frequency scales owing to gap Δ	179
7.5 Flow diagrams for one-dimensional bifurcations	182
7.6 Phase diagram for the $M = 2$ system	183

7.7	Points of high symmetry in the honeycomb lattice	187
7.8	Two-dimensional stationary Turing patterns	188
7.9	Dimensionless amplitude S versus dimensionless coupling η	189
7.10	Zigzag, Eckhaus, and Benjamin-Feir instabilities	191
7.11	Boundary curves for Eckhaus and zigzag instabilities	192
8.1	Soliton solutions to the KdV equation	198
8.2	he Jacobi elliptic functions $\text{sn}(\zeta, k)$ (solid) and $\text{cn}(\zeta, k)$ (dot-dash)	199
8.3	The cubic function $P(u)$ and the soliton lattice (I)	200
8.4	The cubic function $P(u)$ and the soliton lattice (II)	201
8.5	Early and late time configuration of the two soliton solution to the KdV equation	203
8.6	Spacetime diagram (x versus t) for the collision of two KdV solitons	205
8.7	"Wrestling's living legend" Bob Backlund, in a 1983 match	206
8.8	A superconducting transmission	208
8.9	The inverted potential $-U(\phi) = \cos \phi - 1$ for the sine-Gordon problem	210
8.10	Kink and antikink solutions to the sine-Gordon equation	212
9.1	Forward and backward breaking waves for the nonlinear chiral wave equation	223
9.2	Crossing of characteristics of the nonlinear chiral wave equation $\rho_t + c(\rho) \rho_x = 0$ (I)	225
9.3	Crossing of characteristics of the nonlinear chiral wave equation $\rho_t + c(\rho) \rho_x = 0$ (II)	226
9.4	Current conservation in the shock frame yields the shock velocity, $v_s = \Delta j / \Delta \rho$	227
9.5	A resulting shock wave arising from $c_- = \frac{5}{4}$ and $c_+ = \frac{3}{4}$	228
9.6	Shock fitting for quadratic $J(\rho)$	231
9.7	Evolution of the inverted parabola profile	233
9.8	Initial and late time configurations for a hump profile	235
9.9	N-wave and P-wave	236
9.10	Merging of two shocks	237
9.11	Evolution of profiles for Burgers' equation	245
9.12	Merging of two shocks for piecewise constant initial data	246
9.13	Crossing characteristics without and with shock fitting	250

9.14 Evolution of $c(x, t)$ for a series of time values	251
9.15 Characteristics for the green light problem	253
9.16 Density <i>versus</i> position for the green light problem at three successive times	254
9.17 Evolution of traffic density before, during, and after a red light	255
9.18 Phase diagram for the shock merge analysis	258
9.19 Characteristics for the light cycle problem	260

0.1 Preface

This is a proto-preface. A fuller preface will be included when these lecture notes are completed.

Chapter 0

Reference Materials

No one book contains all the relevant material. Here I list several resources, arranged by topic. My personal favorites are marked with a diamond (\diamond).

0.1 Dynamical Systems

- \diamond S. Strogatz, *Nonlinear Dynamics and Chaos* (Addison-Wesley, 1994)
- \diamond S. Neil Rasband, *Chaotic Dynamics of Nonlinear Systems* (Wiley, 1990)
- \diamond J. Guckenheimer and P. Holmes, *Nonlinear Oscillations, Dynamical Systems, and Bifurcations of Vector Fields* (Springer, 1983)
- E. A. Jackson, *Perspectives of Nonlinear Dynamics*, 2 vols. (Cambridge, 1991)
- A. J. Lichtenberg and M. A. Lieberman, *Regular and Stochastic Motion* (Springer, 1983)
- M. Lakshmanan and S. Rajasekar, *Nonlinear Dynamics : Integrability, Chaos, and Patterns* (Springer, 2003)
- H. G. Schuster and W. Just, *Deterministic Chaos*, 4th ed. (Wiley-VCH, 2005)
- M. Tabor, *Chaos and Integrability in Nonlinear Dynamics* (Wiley, 1989)
- E. Ott, *Chaos in Dynamical Systems*, 2nd ed. (Cambridge, 2002)

0.2 Hamiltonian Mechanics

- R. Z. Sagdeev, D. A. Usikov, and G. M. Zaslavsky, *Nonlinear Physics from the Pendulum to Turbulence and Chaos* (Harwood Academic, 1988)
- ◊ G. M. Zaslavsky, *Hamiltonian Chaos and Fractional Dynamics* (Oxford, 2005)
- ◊ J. V. José and E. J. Saletan, *Classical Dynamics : A Contemporary Approach* (Cambridge, 1998)
- V. I. Arnold, V. V. Kozlov, and A. I. Neishtadt, *Mathematical Aspects of Classical and Celestial Mechanics* (Springer, 2006)
- A. L. Fetter and J. D. Walecka, *Nonlinear Mechanics* (Dover, 2006)
- I. Percival and D. Richards, *Introduction to Dynamics* (Cambridge, 1982)
- W. Dittrich and M. Reuter, *Classical and Quantum Dynamics* (Springer, 2001)

0.3 Differential Equations

- ◊ D. Zwillinger, *Handbook of Differential Equations*, 3rd ed. (Academic Press, 1998)
- ◊ A. H. Nayfeh, *Introduction to Perturbation Techniques* (Wiley, 1981)
- ◊ C. M. Bender and S. A. Orszag, *Advanced Mathematical Methods for Scientists and Engineers* (Springer, 1999)
- ◊ V. I. Arnold, *Ordinary Differential Equations* (MIT Press, 1973)
- V. I. Arnold, *Geometrical Methods in the Theory of Ordinary Differential Equations* (Springer, 1988)
- L. Perko, *Differential Equations and Dynamical Systems*, 3rd ed. (Springer, 2001)

- J. A. Sanders and F. Verhulst, *Averaging Methods in Nonlinear Dynamical Systems* (Springer, 1985).

0.4 Synchronization

- ◊ Y. Kuramoto, *Chemical Oscillations, Waves, and Turbulence* (Dover, 2003)
- A. Pikovsky, M. Rosenblum, and J. Kurths, *Synchronization : A Universal Concept in Nonlinear Sciences* (Cambridge, 2001)

0.5 Nonlinear Wave Equations

- ◊ G. B. Whitham, *Linear and Nonlinear Waves* (Wiley, 1999)
- ◊ A. Scott, *Nonlinear Science*, 2nd ed. (Oxford, 2003)
- E. Infeld and G. Rowlands, *Nonlinear Waves, Solitons, and Chaos* (Cambridge, 2000)
- R. Rajaraman, *Solitons and Instantons* (North-Holland, 1987)
- H.-K. Rhee, R. Aris, and N. R. Amundson, *First-Order Partial Differential Equations* (2 vols.) (Dover, 1986)
- L. I. Pismen, *Vortices in Nonlinear Fields* (Oxford, 1999)

0.6 Hydrodynamics

- ◊ C. Godreche and P. Manneville (eds.), *Hydrodynamics and Nonlinear Instabilities* (Cambridge, 1998)
- P. G. Saffman, *Vortex dynamics* (Cambridge, 1992)

0.7 Pattern Formation

- ◊ M. Cross and H. Greenside, *Pattern Formation and Dynamics in Nonequilibrium Systems* (Cambridge, 2009)
- ◊ P. Manneville, *Instabilities, Chaos, and Turbulence* (Imperial College Press, 2004)
- ◊ D. Walgraef, *Spatio-Temporal Pattern Formation* (Springer, 1996)
- J. García-Ojalvo and J. M. Sancho, *Noise in Spatially Extended Systems* (Springer, 1999)
- P. Manneville, *Dissipative Structures and Weak Turbulence* (Academic Press, 1990)
- L. M. Pismen, *Patterns and Interfaces in Dissipative Dynamics* (Springer, 2006)
- M. I. Rabinovich, A. B. Ezersky, and P. D. Weidman, *The Dynamics of Patterns* (World Scientific, 2000)
- R. Hoyle, *Pattern Formation : An Introduction to Methods* (Cambridge, 2006)

0.8 Biological Applications

- ◊ J. D. Murray, *Mathematical Biology*, (3rd ed., 2 vols.) (Springer, 2002)
- E. M. Izhikevich, *Dynamical Systems in Neuroscience* (MIT Press, 2007)
- L. Edelstein-Keshet, *Mathematical Models in Biology* (SIAM, 2005)
- J. Hofbauer and K. Sigmund, *Evolutionary Games and Population Dynamics* (Cambridge, 1998)
- M. A. Nowak, *Evolutionary Dynamics* (Harvard, 2006)

Chapter 1

Introduction to Dynamics

1.1 Introduction

1.1.1 Phase space and phase curves

Dynamics is the study of motion through phase space. The phase space of a given dynamical system is described as an N -dimensional manifold, \mathcal{M} . A (differentiable) manifold \mathcal{M} is a topological space that is locally diffeomorphic to \mathbb{R}^N .¹ Typically in this course \mathcal{M} will \mathbb{R}^N itself, but other common examples include the circle \mathbb{S}^1 , the torus \mathbb{T}^2 , the sphere \mathbb{S}^2 , etc.

Let $g_\tau: \mathcal{M} \rightarrow \mathcal{M}$ be a one-parameter family of transformations from \mathcal{M} to itself, with $g_{\tau=0} = 1$, the identity, and $\tau \in \mathbb{R}$. We call g_τ the τ -advance mapping. It satisfies the composition rule

$$g_\tau g_\sigma = g_{\tau+\sigma} . \quad (1.1)$$

Let us choose an arbitrary point $\varphi_0 = \varphi(t_0) \in \mathcal{M}$ to be the phase space coordinate at an initial time t_0 . We then write $\varphi(t_0 + \tau) \equiv g_\tau \varphi(t_0)$, which also is in \mathcal{M} . The set

$$\{g_\tau \varphi_0 \mid \tau \in \mathbb{R}, \varphi_0 \in \mathcal{M}\} \quad (1.2)$$

is called a *phase curve*. A graph of the motion $\varphi(t)$ in the product space $\mathcal{M} \times \mathbb{R}$ is called an *integral curve*. In a more general setting, we could define the two-parameter dynamical map $G_{t_0}^{t_0+\tau}$, which evolves the phase space coordinate from $\varphi(t_0)$ to $\varphi(t_0 + \tau)$ to depend on t_0 as well. Thus

$$G_{t_0}^{t_0+\tau} \varphi(t_0) = \varphi(t_0 + \tau) . \quad (1.3)$$

But then $G_t^t = 1$ must be the identity for all t , and $G_t^{t'}$ must satisfy a composition rule,

$$G_{t_0}^{t_2} = G_{t_1}^{t_2} G_{t_0}^{t_1} \quad (1.4)$$

¹A *diffeomorphism* $F: \mathcal{M} \rightarrow \mathcal{N}$ is a differentiable map with a differentiable inverse. This is a special type of *homeomorphism*, which is a continuous map with a continuous inverse.

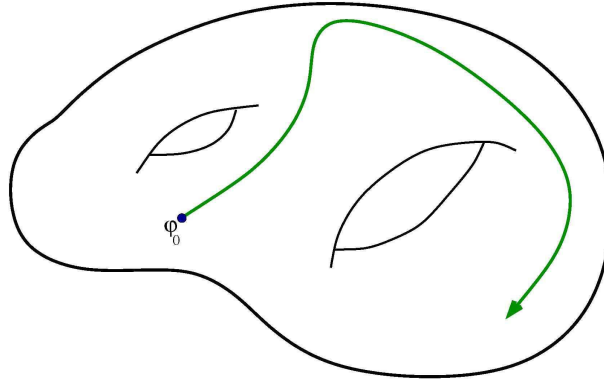


Figure 1.1: An example of a phase curve.

for any time t_1 . This says that to evolve the phase space coordinate φ between times t_0 and t_2 , we can first evolve from t_0 to t_1 and then from t_1 to t_2 , for any t_1 . By extending the phase space \mathcal{M} to $\mathcal{M}' \equiv \mathcal{M} \times \mathbb{R}$, where $\dim(\mathcal{M}') = N + 1$, then defining the $(N + 1)$ -dimensional phase space vector $\psi^T = (\varphi_1, \dots, \varphi_N, t)$, we define the one-parameter map on \mathcal{M}' , \tilde{g}_τ , by

$$\tilde{g}_\tau \begin{pmatrix} \varphi \\ t \end{pmatrix} = \begin{pmatrix} G_t^{t+\tau} \varphi \\ t + \tau \end{pmatrix} . \quad (1.5)$$

Unless otherwise stated, and without loss of generality, we will always consider our dynamical systems to be governed by a one-parameter τ -advance map g_τ .

1.1.2 Vector fields

The *velocity* vector $\mathbf{V}(\varphi)$ is given by the derivative

$$\mathbf{V}(\varphi) = \frac{d}{dt} \Big|_{t=0} g_t \varphi . \quad (1.6)$$

The velocity $\mathbf{V}(\varphi)$ is an element of the *tangent space* to \mathcal{M} at φ , abbreviated $T\mathcal{M}_\varphi$. If \mathcal{M} is N -dimensional, then so is each $T\mathcal{M}_\varphi$ (for all φ). However, \mathcal{M} and $T\mathcal{M}_\varphi$ may differ topologically. For example, if $\mathcal{M} = \mathbb{S}^1$, the circle, the tangent space at any point is isomorphic to \mathbb{R} .

For our purposes, we will take $\varphi = (\varphi_1, \dots, \varphi_N)$ to be an N -tuple, *i.e.* a point in \mathbb{R}^N . The equation of motion is then

$$\frac{d}{dt} \varphi(t) = \mathbf{V}(\varphi(t)) . \quad (1.7)$$

Note that any N^{th} order ODE, of the general form

$$\frac{d^N x}{dt^N} = F \left(x, \frac{dx}{dt}, \dots, \frac{d^{N-1}x}{dt^{N-1}} \right) , \quad (1.8)$$

may be represented by the first order system $\dot{\varphi} = \mathbf{V}(\varphi)$. To see this, define $\varphi_k = d^{k-1}x/dt^{k-1}$, with $k = 1, \dots, N$. Thus, for $j < N$ we have $\dot{\varphi}_j = \varphi_{j+1}$, and $\dot{\varphi}_N = f$. In other words,

$$\underbrace{\frac{d}{dt} \begin{pmatrix} \varphi_1 \\ \vdots \\ \varphi_{N-1} \\ \varphi_N \end{pmatrix}}_{\dot{\varphi}} = \underbrace{\begin{pmatrix} \mathbf{V}(\varphi) \\ \varphi_2 \\ \vdots \\ \varphi_N \\ F(\varphi_1, \dots, \varphi_N) \end{pmatrix}}_{\mathbf{V}(\varphi)} . \quad (1.9)$$

1.1.3 Existence / uniqueness / extension theorems

Theorem : Given $\dot{\varphi} = \mathbf{V}(\varphi)$ and $\varphi(0)$, if each $\mathbf{V}(\varphi)$ is a smooth vector field over some open set $\mathcal{D} \in \mathcal{M}$, then for $\varphi(0) \in \mathcal{D}$ the initial value problem has a solution on some finite time interval $(-\tau, +\tau)$ and the solution is unique. Furthermore, the solution has a unique extension forward or backward in time, either indefinitely or until $\varphi(t)$ reaches the boundary of \mathcal{D} .

Corollary : Different trajectories never intersect!

More generally, we might ask the following: *under what conditions does the dynamical system $\dot{\varphi} = \mathbf{V}(\varphi, t)$ with initial conditions $\varphi(0) = \varphi_0$ have a unique solution?*. This is specified by the *Picard-Lindelöf theorem*², which says that if $D \subseteq \mathbb{R}^N \times \mathbb{R}$, is a closed rectangle and $\mathbf{V}: D \rightarrow \mathbb{R}^N$ is a function which is continuous in t and *Lipschitz continuous* in φ , then there exists some $\varepsilon > 0$ such that the initial value problem $\dot{\varphi}(t) = \mathbf{V}(\varphi(t), t)$ with $(\varphi_0, t_0) \in D$, has a unique solution $\varphi(t)$ on the interval $t \in [t_0 - \varepsilon, t_0 + \varepsilon]$. In this case the solution is

$$\varphi(t) = \varphi(t_0) + \int_{t_0}^t ds \mathbf{V}(\varphi(s), s) . \quad (1.10)$$

In general, Lipschitz continuity³ is a condition on a function $f: \mathcal{X} \rightarrow \mathcal{Y}$ between two metric spaces $(\mathcal{X}, d_{\mathcal{X}})$ and $(\mathcal{Y}, d_{\mathcal{Y}})$, where $d_{\mathcal{X}}(X_1, X_2)$ and $d_{\mathcal{Y}}(Y_1, Y_2)$ are distance functions on \mathcal{X} and \mathcal{Y} , respectively, with $X_{1,2} \in \mathcal{X}$ and $Y_{1,2} \in \mathcal{Y}$. The function f is then Lipschitz continuous if there exists a real constant $K \geq 0$ such that

$$d_{\mathcal{Y}}(f(X_1), f(X_2)) \leq K d_{\mathcal{X}}(X_1, X_2) . \quad (1.11)$$

For our application, this means $\exists K \geq 0$ such that

$$|\mathbf{V}(\varphi_1, t) - \mathbf{V}(\varphi_2, t)| \leq K |\varphi_1 - \varphi_2| \quad (1.12)$$

for all $t \in [t_0 - \varepsilon, t_0 + \varepsilon]$, where

$$|\varphi' - \varphi| = \sqrt{\sum_{n=1}^N (\varphi'_n - \varphi_n)^2} \quad (1.13)$$

is the Euclidean distance in phase space. An example where this fails is given in §1.2.3 below.

²See Wikipedia: https://en.wikipedia.org/wiki/Picard-Lindelöf_theorem.

³See https://en.wikipedia.org/wiki/Lipschitz_continuity.

1.1.4 Linear differential equations

A homogeneous linear N^{th} order ODE,

$$\frac{d^N x}{dt^N} + c_{N-1} \frac{d^{N-1} x}{dt^{N-1}} + \dots + c_1 \frac{dx}{dt} + c_0 x = 0 \quad (1.14)$$

may be written in matrix form, as

$$\frac{d}{dt} \begin{pmatrix} \varphi_1 \\ \varphi_2 \\ \vdots \\ \varphi_N \end{pmatrix} = \underbrace{\begin{pmatrix} 0 & 1 & 0 & \cdots & 0 \\ 0 & 0 & 1 & \cdots & 0 \\ \vdots & \vdots & \vdots & & \vdots \\ -c_0 & -c_1 & -c_2 & \cdots & -c_{N-1} \end{pmatrix}}_M \begin{pmatrix} \varphi_1 \\ \varphi_2 \\ \vdots \\ \varphi_N \end{pmatrix}. \quad (1.15)$$

Thus,

$$\dot{\varphi} = M\varphi, \quad (1.16)$$

and if the coefficients c_k are time-independent, *i.e.* the ODE is *autonomous*, the solution is obtained by exponentiating the constant matrix Q :

$$\varphi(t) = \exp(Mt) \varphi(0); \quad (1.17)$$

the exponential of a matrix may be given meaning by its Taylor series expansion. If the ODE is not autonomous, then $M = M(t)$ is time-dependent, and the solution is given by the path-ordered exponential,

$$\varphi(t) = \mathcal{P} \exp \left\{ \int_0^t dt' M(t') \right\} \varphi(0), \quad (1.18)$$

As defined, the equation $\dot{\varphi} = V(\varphi)$ is autonomous, since g_t depends only on t and on no other time variable. However, by extending the phase space from \mathcal{M} to $\mathbb{R} \times \mathcal{M}$, which is of dimension $(N+1)$, one can describe arbitrary time-dependent ODEs.

1.1.5 Lyapunov functions

For a general dynamical system $\dot{\varphi} = V(\varphi)$, a *Lyapunov function* $L(\varphi)$ is a function which satisfies

$$\nabla L(\varphi) \cdot V(\varphi) \leq 0. \quad (1.19)$$

There is no simple way to determine whether a Lyapunov function exists for a given dynamical system, or, if it does exist, what the Lyapunov function is. However, if a Lyapunov function can be found, then this severely limits the possible behavior of the system. This is because $L(\varphi(t))$ must be a monotonic function of time:

$$\frac{d}{dt} L(\varphi(t)) = \nabla L \cdot \frac{d\varphi}{dt} = \nabla L \cdot V(\varphi) \leq 0. \quad (1.20)$$

Thus, the system evolves toward a local minimum of the Lyapunov function. In general this means that oscillations are impossible in systems for which a Lyapunov function exists. For example, the relaxational dynamics of the magnetization M of a system are sometimes modeled by the equation

$$\frac{dM}{dt} = -\Gamma \frac{\partial F}{\partial M} , \quad (1.21)$$

where $F(M, T)$ is the *free energy* of the system. In this model, assuming constant temperature T , $\dot{F} = F'(M) \dot{M} = -\Gamma [F'(M)]^2 \leq 0$. So the free energy $F(M)$ itself is a Lyapunov function, and it monotonically decreases during the evolution of the system. We shall meet up with this example again in the next chapter when we discuss imperfect bifurcations.

1.2 $N = 1$ Systems

We now study phase flows in a one-dimensional phase space, governed by the equation

$$\frac{du}{dt} = f(u) . \quad (1.22)$$

Again, the equation $\dot{u} = h(u, t)$ is first order, but not autonomous, and it corresponds to the $N = 2$ system,

$$\frac{d}{dt} \begin{pmatrix} u \\ t \end{pmatrix} = \begin{pmatrix} h(u, t) \\ 1 \end{pmatrix} . \quad (1.23)$$

The equation 1.22 is easily integrated:

$$\frac{du}{f(u)} = dt \implies t - t_0 = \int_{u_0}^u \frac{du'}{f(u')} . \quad (1.24)$$

This gives $t(u)$; we must then invert this relationship to obtain $u(t)$.

Example : Suppose $f(u) = a - bu$, with a and b constant. Then

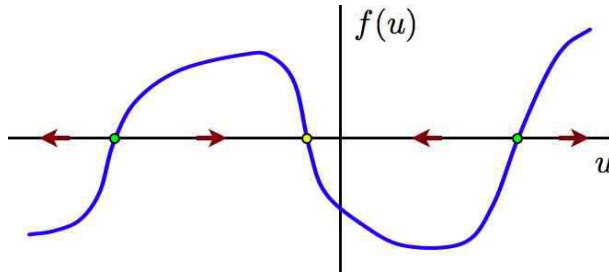
$$dt = \frac{du}{a - bu} = -b^{-1} d \ln(a - bu) \quad (1.25)$$

whence

$$t = \frac{1}{b} \ln \left(\frac{a - bu(0)}{a - bu(t)} \right) \implies u(t) = \frac{a}{b} + \left(u(0) - \frac{a}{b} \right) \exp(-bt) . \quad (1.26)$$

Even if one cannot analytically obtain $u(t)$, the behavior is very simple, and easily obtained by graphical analysis. Sketch the function $f(u)$. Then note that

$$\dot{u} = f(u) \implies \begin{cases} f(u) > 0 & \dot{u} > 0 \Rightarrow \text{move to right} \\ f(u) < 0 & \dot{u} < 0 \Rightarrow \text{move to left} \\ f(u) = 0 & \dot{u} = 0 \Rightarrow \text{fixed point} \end{cases} \quad (1.27)$$

Figure 1.2: Phase flow for an $N = 1$ system.

The behavior of $N = 1$ systems is particularly simple: $u(t)$ flows to the first stable fixed point encountered, where it then (after a logarithmically infinite time) stops. The motion is monotonic – the velocity \dot{u} never changes sign. Thus, *oscillations never occur for $N = 1$ phase flows*.⁴

1.2.1 Classification of fixed points ($N = 1$)

A *fixed point* u^* satisfies $f(u^*) = 0$. Generically, $f'(u^*) \neq 0$ at a fixed point.⁵ Suppose $f'(u^*) < 0$. Then to the left of the fixed point, the function $f(u < u^*)$ is positive, and the flow is to the right, *i.e.* toward u^* . To the right of the fixed point, the function $f(u > u^*)$ is negative, and the flow is to the left, *i.e.* again toward u^* . Thus, when $f'(u^*) < 0$ the fixed point is said to be *stable*, since the flow in the vicinity of u^* is to u^* . Conversely, when $f'(u^*) > 0$, the flow is always away from u^* , and the fixed point is then said to be *unstable*. Indeed, if we linearize about the fixed point, and let $\epsilon \equiv u - u^*$, then

$$\dot{\epsilon} = f'(u^*) \epsilon + \frac{1}{2} f''(u^*) \epsilon^2 + \mathcal{O}(\epsilon^3) , \quad (1.28)$$

and dropping all terms past the first on the RHS gives

$$\epsilon(t) = \exp \left[f'(u^*) t \right] \epsilon(0) . \quad (1.29)$$

The deviation decreases exponentially for $f'(u^*) < 0$ and increases exponentially for $f'(u^*) > 0$. Note that

$$t(\epsilon) = \frac{1}{f'(u^*)} \ln \left(\frac{\epsilon}{\epsilon(0)} \right) , \quad (1.30)$$

so the approach to a stable fixed point takes a logarithmically infinite time. For the unstable case, the deviation grows exponentially, until eventually the linearization itself fails.

1.2.2 Logistic equation

This model for population growth was first proposed by Verhulst in 1838. Let N denote the population in question. The dynamics are modeled by the first order ODE,

$$\frac{dN}{dt} = rN \left(1 - \frac{N}{K} \right) , \quad (1.31)$$

⁴When I say ‘never’ I mean ‘sometimes’ – see the section 1.3.

⁵The system $f(u^*) = 0$ and $f'(u^*) = 0$ is overdetermined, with two equations for the single variable u^* .

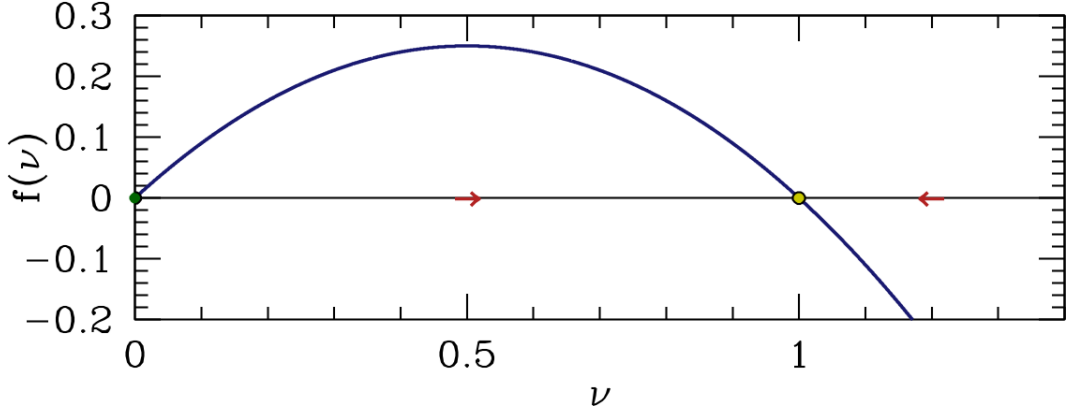


Figure 1.3: Flow diagram for the logistic equation.

where N , r , and K are all positive. For $N \ll K$ the growth rate is r , but as N increases a quadratic nonlinearity kicks in and the rate vanishes for $N = K$ and is negative for $N > K$. The nonlinearity models the effects of competition between the organisms for food, shelter, or other resources. Or maybe they crap all over each other and get sick. Whatever.

There are two fixed points, one at $N^* = 0$, which is unstable ($f'(0) = r > 0$). The other, at $N^* = K$, is stable ($f'(K) = -r$). The equation is adimensionalized by defining $\nu = N/K$ and $s = rt$, whence

$$\dot{\nu} = \nu(1 - \nu) . \quad (1.32)$$

Integrating,

$$\frac{d\nu}{\nu(1 - \nu)} = d\ln\left(\frac{\nu}{1 - \nu}\right) = ds \implies \nu(s) = \frac{\nu_0}{\nu_0 + (1 - \nu_0)\exp(-s)} . \quad (1.33)$$

As $s \rightarrow \infty$, $\nu(s) = 1 - (\nu_0^{-1} - 1)e^{-s} + \mathcal{O}(e^{-2s})$, and the relaxation to equilibrium ($\nu^* = 1$) is exponential, as usual.

Another application of this model is to a simple autocatalytic reaction, such as



i.e. X catalyses the reaction $A \rightarrow X$. Assuming a fixed concentration of A , we have

$$\dot{x} = \kappa_+ a x - \kappa_- x^2 , \quad (1.35)$$

where x is the concentration of X , and κ_{\pm} are the forward and backward reaction rates.

1.2.3 Singular $f(u)$

Suppose that in the vicinity of a fixed point we have $f(u) = A|u - u^*|^\alpha$, with $A, \alpha > 0$. We now analyze both sides of the fixed point.

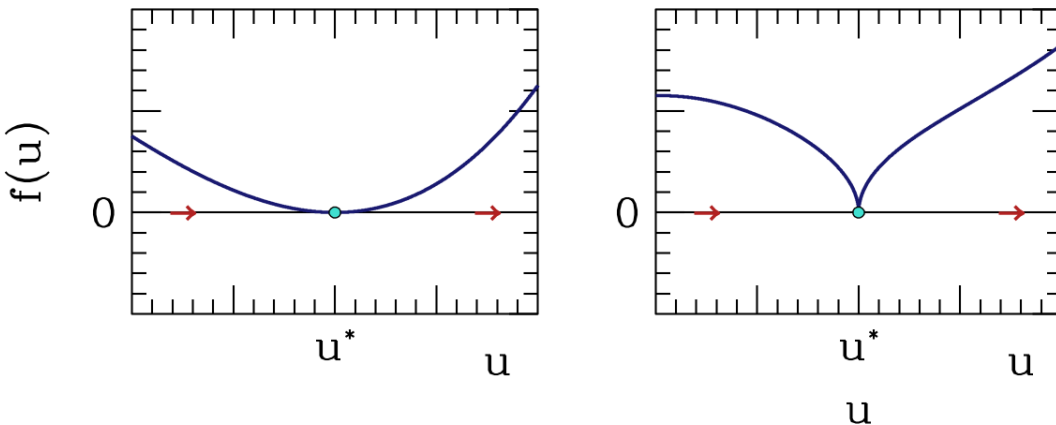


Figure 1.4: $f(u) = A |u - u^*|^\alpha$ for $\alpha > 1$ (left) and $0 < \alpha < 1$ (right).

$u < u^*$: Let $\epsilon = u^* - u$. Then

$$\dot{\epsilon} = -A \epsilon^\alpha \implies \frac{\epsilon^{1-\alpha}}{1-\alpha} = \frac{\epsilon_0^{1-\alpha}}{1-\alpha} - At \quad , \quad (1.36)$$

hence

$$\epsilon(t) = \left[\epsilon_0^{1-\alpha} + (\alpha-1)At \right]^{1/(1-\alpha)} \quad . \quad (1.37)$$

This, for $\alpha < 1$ the fixed point $\epsilon = 0$ is reached in a finite time: $\epsilon(t_c) = 0$, with

$$t_c = \frac{\epsilon_0^{1-\alpha}}{(1-\alpha)A} \quad . \quad (1.38)$$

For $\alpha > 1$, we have $\lim_{t \rightarrow \infty} \epsilon(t) = 0$, but $\epsilon(t) > 0$ for all finite t .

The fixed point $u = u^*$ is now *half-stable* – the flow from the left is toward u^* but from the right is away from u^* . Let's now analyze the flow on either side of u^* .

$u > u^*$: Let $\epsilon = u - u^*$. Then $\dot{\epsilon} = A \epsilon^\alpha$, and

$$\epsilon(t) = \left[\epsilon_0^{1-\alpha} + (1-\alpha)At \right]^{1/(1-\alpha)} \quad . \quad (1.39)$$

For $\alpha < 1$, $\epsilon(t)$ escapes to $\epsilon = \infty$ only after an infinite time. For $\alpha > 1$, the escape to infinity takes a finite time: $\epsilon(t_c) = \infty$, with

$$t_c = \frac{\epsilon_0^{1-\alpha}}{(\alpha-1)A} \quad . \quad (1.40)$$

In both cases, higher order terms in the (nonanalytic) expansion of $f(u)$ about $u = u^*$ will eventually come into play.

The case $\alpha < 1$ provides a nice illustration of the Picard-Lindelöf theorem in §1.1.3, for consider the equation $dx/ds = -A|x|^\alpha$ with $\alpha \in (0, 1)$ and initial condition $x(s=0) = x_0 > 0$. The solution is

$$x(s) = \left[x_0^{1-\alpha} - (1-\alpha)As \right]^{1/(1-\alpha)} \Theta(t_c - s) \quad , \quad (1.41)$$

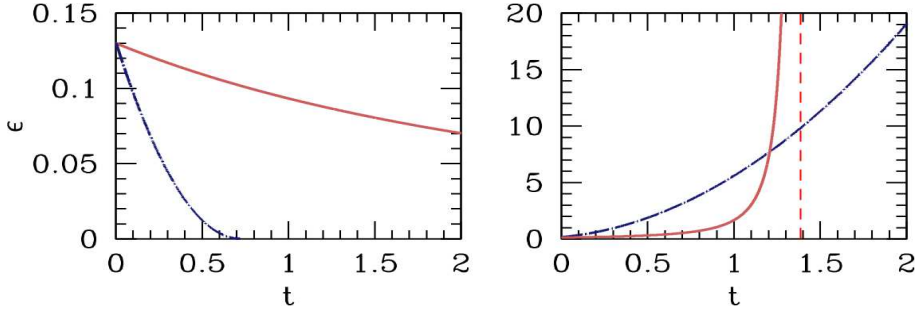


Figure 1.5: Solutions to $\dot{\epsilon} = \mp A \epsilon^\alpha$. Left panel: $\epsilon = u^* - u$, with $\alpha = 1.5$ (solid red) and $\alpha = 0.5$ (dot-dashed blue); $A = 1$ in both cases. Right panel: $\epsilon = u - u^*$, $\alpha = 1.5$ (solid red) and $\alpha = 0.5$ (dot-dashed blue); $A = 4$ in both cases.

where t_c is given above. Now let's run time backwards and define $t \equiv -s + t_c + \tau$ with $\tau > 0$. The dynamical system is then $dx/dt = A |x|^\alpha$ and the solution is

$$x(t) = \left[x_0^{1-\alpha} - (1-\alpha)A(t_c + \tau - t) \right]^{1/(1-\alpha)} \Theta(t - \tau) , \quad (1.42)$$

where $x(t_c + \tau) = x_0$. This is a valid solution for *any* $\tau \geq 0$. Thus for any positive τ , we have a solution to the equation $\dot{x} = A |x|^\alpha$ with initial condition $x(t = 0) = 0$, and therefore *the solution to the initial value problem is not unique!* The difficulty can be traced to the fact that the vector field $V(x) = A|x|^\alpha$ is not Lipschitz continuous at $x = 0$, since for any $K > 0$ we may find an x such that

$$|V(x) - V(0)| = A|x|^\alpha > K|x| , \quad (1.43)$$

which is the case for all $|x| < (A/K)^{1/(1-\alpha)}$.

1.2.4 Recommended exercises

It is constructive to sketch the phase flows for the following examples:

$$\begin{array}{ll} \dot{v} = -g & \dot{u} = A \sin(u) \\ m\dot{v} = -mg - \gamma v & \dot{u} = A(u-a)(u-b)(u-c) \\ m\dot{v} = -mg - cv^2 \operatorname{sgn}(v) & \dot{u} = au^2 - bu^3 . \end{array}$$

In each case, identify all the fixed points and assess their stability. Assume all constants A, a, b, c, γ , etc. are positive.

1.2.5 Non-autonomous ODEs

Non-autonomous ODEs of the form $\dot{u} = h(u, t)$ are in general impossible to solve by quadratures. One can always go to the computer, but it is worth noting that in the *separable* case, $h(u, t) = f(u)g(t)$, one

can obtain the solution

$$\frac{du}{f(u)} = g(t) dt \implies \int_{u_0}^u \frac{du'}{f(u')} = \int_0^t dt' g(t') , \quad (1.44)$$

which implicitly gives $u(t)$. Note that \dot{u} may now change sign, and $u(t)$ may even oscillate. For an explicit example, consider the equation

$$\dot{u} = A(u + 1) \sin(\beta t) , \quad (1.45)$$

the solution of which is

$$u(t) = -1 + (u_0 + 1) \exp \left\{ \frac{A}{\beta} [1 - \cos(\beta t)] \right\} . \quad (1.46)$$

In general, the non-autonomous case defies analytic solution. Many have been studied, such as the Riccati equation,

$$\frac{du}{dt} = P(t)u^2 + Q(t)u + R(t) . \quad (1.47)$$

Riccati equations have the special and remarkable property that one can generate *all* solutions (*i.e.* with arbitrary boundary condition $u(0) = u_0$) from *any* given solution (*i.e.* with any boundary condition).

1.3 Flows on the Circle

We had remarked that oscillations are impossible for the equation $\dot{u} = f(u)$ because the flow is to the first stable fixed point encountered. If there are no stable fixed points, the flow is unbounded. However, suppose phase space itself is bounded, *e.g.* a circle \mathbb{S}^1 rather than the real line \mathbb{R} . Thus,

$$\dot{\theta} = f(\theta) , \quad (1.48)$$

with $f(\theta + 2\pi) = f(\theta)$. Now if there are no fixed points, $\theta(t)$ endlessly winds around the circle, and in this sense we can have oscillations.

1.3.1 Nonuniform oscillator

A particularly common example is that of the nonuniform oscillator,

$$\dot{\theta} = \omega - \sin \theta , \quad (1.49)$$

which has applications to electronics, biology, classical mechanics, and condensed matter physics. Note that the general equation $\dot{\theta} = \omega - A \sin \theta$ may be rescaled to the above form. A simple application is to the dynamics of a driven, overdamped pendulum. The equation of motion is

$$I\ddot{\theta} + b\dot{\theta} + I\omega_0^2 \sin \theta = N , \quad (1.50)$$

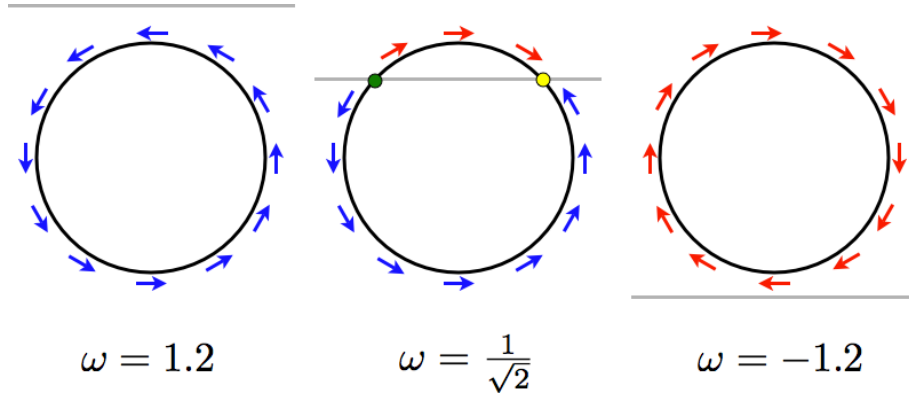


Figure 1.6: Flow for the nonuniform oscillator $\dot{\theta} = \omega - \sin \theta$ for three characteristic values of ω .

where I is the moment of inertia, b is the damping parameter, N is the external torque (presumed constant), and ω_0 is the frequency of small oscillations when $b = N = 0$. When b is large, the inertial term $I\ddot{\theta}$ may be neglected, and after rescaling we arrive at eqn. 1.49.

The book by Strogatz provides a biological example of the nonuniform oscillator: fireflies. An individual firefly will on its own flash at some frequency f . This can be modeled by the equation $\dot{\phi} = \beta$, where $\beta = 2\pi f$ is the angular frequency. A flash occurs when $\phi = 2\pi n$ for $n \in \mathbb{Z}$. When subjected to a periodic stimulus, fireflies will attempt to synchronize their flash to the flash of the stimulus. Suppose the stimulus is periodic with angular frequency Ω . The firefly synchronization is then modeled by the equation

$$\dot{\phi} = \beta - A \sin(\phi - \Omega t) \quad . \quad (1.51)$$

Here, A is a measure of the firefly's ability to modify its natural frequency in response to the stimulus. Note that when $0 < \phi - \Omega t < \pi$, i.e. when the firefly is leading the stimulus, the dynamics tell the firefly to slow down. Conversely, when $-\pi < \phi - \Omega t < 0$, the firefly is lagging the stimulus, the dynamics tell it to speed up. Now focus on the difference $\theta \equiv \phi - \Omega t$. We have

$$\dot{\theta} = \beta - \Omega - A \sin \theta \quad , \quad (1.52)$$

which is the nonuniform oscillator. We can adimensionalize by defining

$$s \equiv At \quad , \quad \omega \equiv \frac{\beta - \Omega}{A} \quad , \quad (1.53)$$

yielding $\frac{d\theta}{ds} = f(\theta) = \omega - \sin \theta$.

Fixed points θ^* occur only for $|\omega| < 1$, at $\sin \theta^* = \omega$, in which case $f'(\theta^*) = -\cos \theta^*$. As we have seen above, stability requires $f'(\theta^*) < 0$, which means $\theta^* \in (-\frac{\pi}{2}, \frac{\pi}{2})$, i.e. θ^* must lie on the right half of the circle. For $|\omega| > 1$, the angular velocity never vanishes anywhere along the circle, and there are no fixed points. In this case the motion is eternally clockwise ($\omega < -1$) or counterclockwise ($\omega > +1$). The situation is depicted in Fig. 1.6.

To integrate, set $z = \exp(i\theta)$, in which case

$$\frac{dz}{ds} = -\frac{1}{2}(z^2 - 2i\omega z - 1) = -\frac{1}{2}(z - \xi_-)(z - \xi_+) \quad , \quad (1.54)$$

where $\xi_{\pm} = i\omega \pm \sqrt{1 - \omega^2} \equiv i\omega \pm \nu$ with $\nu \equiv \sqrt{1 - \omega^2}$. This yields

$$d \log \left(\frac{z - \xi_+}{z - \xi_-} \right) = \frac{1}{2} (\xi_- - \xi_+) ds = -\nu ds \quad (1.55)$$

which integrates to

$$z(s) = \frac{(\xi_+ - e^{-\nu s} \xi_-) z(0) + (e^{-\nu s} - 1) \xi_+ \xi_-}{(1 - e^{-\nu s}) z(0) + (\xi_+ e^{-\nu s} - \xi_-)} \quad . \quad (1.56)$$

When $\omega^2 > 1$, ν is pure imaginary and $\exp(-\nu s)$ continually winds about the unit circle. When $\omega^2 < 1$, ν is real and positive. We then have that $z(s \rightarrow \infty) = \xi_+$ while $z(s \rightarrow -\infty) = \xi_-$. Note that ξ_{\pm} lie on the appropriate halves of the circle as depicted in fig. 1.6.

For $|\omega| > 1$, the motion is periodic, with period

$$T = \int_0^{2\pi} \frac{d\theta}{|\omega| - \sin \theta} = \frac{2\pi}{\sqrt{\omega^2 - 1}} \quad . \quad (1.57)$$

1.4 Appendix I : Evolution of Phase Space Volumes

Recall the general form of a dynamical system, $\dot{\varphi} = \mathbf{V}(\varphi)$. Usually we are interested in finding integral curves $\varphi(t)$. However, consider for the moment a collection of points in phase space comprising a region \mathcal{R} . As the dynamical system evolves, this region will also evolve, so that $\mathcal{R} = \mathcal{R}(t)$. We now ask: how does the volume of $\mathcal{R}(t)$,

$$\text{vol}[\mathcal{R}(t)] = \int_{\mathcal{R}(t)} d\mu \quad , \quad (1.58)$$

where $d\mu = d\varphi_1 d\varphi_2 \cdots d\varphi_N$ is the phase space measure, change with time. We have, explicitly,

$$\begin{aligned} \text{vol}[\mathcal{R}(t + dt)] &= \int_{\mathcal{R}(t+dt)} d\mu = \int_{\mathcal{R}(t)} d\mu \left\| \frac{\partial \varphi_i(t + dt)}{\partial \varphi_j(t)} \right\| \\ &= \int_{\mathcal{R}(t)} d\mu \left\{ 1 + \nabla \cdot \mathbf{V} dt + \mathcal{O}((dt)^2) \right\} \quad , \end{aligned} \quad (1.59)$$

since

$$\frac{\partial \varphi_i(t + dt)}{\partial \varphi_j(t)} = \delta_{ij} + \frac{\partial V_i}{\partial \varphi_j} \Big|_{\varphi(t)} dt + \mathcal{O}((dt)^2) \quad , \quad (1.60)$$

and, using $\ln \det M = \text{Tr} \ln M$,

$$\det(1 + \epsilon A) = 1 + \epsilon \text{Tr} A + \mathcal{O}(\epsilon^2) \quad . \quad (1.61)$$

Thus,

$$\frac{d}{dt} \text{vol}[\mathcal{R}(t)] = \int_{\mathcal{R}(t)} d\mu \nabla \cdot \mathbf{V} = \int_{\partial \mathcal{R}(t)} d\Sigma \hat{\mathbf{n}} \cdot \mathbf{V} \quad , \quad (1.62)$$

where in the last line we have used Stokes' theorem to convert the volume integral over \mathcal{R} to a surface integral over its boundary $\partial \mathcal{R}$.

1.5 Appendix II : Lyapunov Characteristic Exponents

Suppose $\varphi(t)$ is an integral curve – *i.e.* a solution of $\dot{\varphi} = \mathbf{V}(\varphi)$. We now ask: how do nearby trajectories behave? Do they always remain close to $\varphi(t)$ for all t ? To answer this, we write $\tilde{\varphi}(t) \equiv \varphi(t) + \eta(t)$, in which case

$$\frac{d}{dt} \eta_i(t) = M_{ij}(t) \eta_j(t) + \mathcal{O}(\eta^2) , \quad (1.63)$$

where

$$M_{ij}(t) = \left. \frac{\partial V_i}{\partial \varphi_j} \right|_{\varphi(t)} . \quad (1.64)$$

The solution, valid to first order in $\delta\varphi$, is

$$\eta_i(t) = Q_{ij}(t, t_0) \eta_j(t_0) , \quad (1.65)$$

where the matrix $Q(t, t_0)$ is given by the *path ordered exponential*,

$$\begin{aligned} Q(t, t_0) &= \mathcal{P} \exp \left\{ \int_{t_0}^t dt' M(t') \right\} \\ &\equiv \lim_{N \rightarrow \infty} \left(1 + \frac{\Delta t}{N} M(t_{N-1}) \right) \cdots \left(1 + \frac{\Delta t}{N} M(t_1) \right) \left(1 + \frac{\Delta t}{N} M(t_0) \right) , \end{aligned} \quad (1.66)$$

with $\Delta t = t - t_0$ and $t_j = t_0 + (j/N)\Delta t$. \mathcal{P} is the *path ordering operator*, which places earlier times to the right:

$$\mathcal{P} A(t) B(t') = \begin{cases} A(t) B(t') & \text{if } t > t' \\ B(t') A(t) & \text{if } t < t' \end{cases} . \quad (1.67)$$

The distinction is important if $[A(t), B(t')] \neq 0$. Note that Q satisfies the composition property,

$$Q(t, t_0) = Q(t, t_1) Q(t_1, t_0) \quad (1.68)$$

for any $t_1 \in [t_0, t]$. When M is time-independent, as in the case of a *fixed point* where $\mathbf{V}(\varphi^*) = 0$, the path ordered exponential reduces to the ordinary exponential, and $Q(t, t_0) = \exp(M(t - t_0))$.

Generally it is impossible to analytically compute path-ordered exponentials. However, the following example may be instructive. Suppose

$$M(t) = \begin{cases} M_1 & \text{if } t/T \in [2j, 2j+1] \\ M_2 & \text{if } t/T \in [2j+1, 2j+2] \end{cases} , \quad (1.69)$$

for all integer j . $M(t)$ is a ‘matrix-valued square wave’, with period $2T$. Then, integrating over one period, from $t = 0$ to $t = 2T$, we have

$$\begin{aligned} A &\equiv \exp \left\{ \int_0^{2T} dt M(t) \right\} = e^{(M_1 + M_2)T} \\ A_{\mathcal{P}} &\equiv \mathcal{P} \exp \left\{ \int_0^{2T} dt M(t) \right\} = e^{M_2 T} e^{M_1 T} . \end{aligned} \quad (1.70)$$

In general, $A \neq A_{\mathcal{P}}$, so the path ordering has a nontrivial effect⁶.

The Lyapunov exponents are defined in the following manner. Let \hat{e} be an N -dimensional unit vector. Define

$$\Lambda(\varphi_0, \hat{e}) \equiv \lim_{t \rightarrow \infty} \lim_{b \rightarrow 0} \frac{1}{t - t_0} \ln \left(\frac{\|\boldsymbol{\eta}(t)\|}{\|\boldsymbol{\eta}(t_0)\|} \right)_{\boldsymbol{\eta}(t_0)=b\hat{e}} , \quad (1.71)$$

where $\|\cdot\|$ denotes the Euclidean norm of a vector, and where $\varphi_0 = \varphi(t_0)$. A theorem due to Oseledec guarantees that there are N such values $\Lambda_i(\varphi_0)$, depending on the choice of \hat{e} , for a given φ_0 . Specifically, the theorem guarantees that the matrix

$$W \equiv (Q^T Q)^{1/(t-t_0)} \quad (1.72)$$

converges in the limit $t \rightarrow \infty$ for almost all φ_0 . The eigenvalues Λ_i correspond to the different eigenspaces of W . Oseledec's theorem (also called the 'multiplicative ergodic theorem') guarantees that the eigenspaces of W either grow ($\Lambda_i > 1$) or shrink ($\Lambda_i < 1$) exponentially fast. That is, the norm any vector lying in the i^{th} eigenspace of W will behave as $\Lambda_i^t = \exp(t \ln \Lambda_i)$ as $t \rightarrow \infty$.

Note that while $W = W^T$ is symmetric by construction, Q is simply a general real-valued $N \times N$ matrix. The left and right eigenvectors of a matrix $M \in \text{GL}(N, \mathbb{R})$ will in general be different. The set of eigenvalues λ_α is, however, common to both sets of eigenvectors. Let $\{\psi_\alpha\}$ be the right eigenvectors and $\{\chi_\alpha^*\}$ the left eigenvectors, such that

$$\begin{aligned} M_{ij} \psi_{\alpha,j} &= \lambda_\alpha \psi_{\alpha,i} \\ \chi_{\alpha,i}^* M_{ij} &= \lambda_\alpha \chi_{\alpha,j}^* . \end{aligned} \quad (1.73)$$

We can always choose the left and right eigenvectors to be orthonormal, *viz.*

$$\langle \chi_\alpha | \psi_\beta \rangle = \chi_{\alpha,i}^* \psi_{\beta,i} = \delta_{\alpha\beta} . \quad (1.74)$$

Indeed, we can define the matrix $S_{i\alpha} = \psi_{\alpha,i}$, in which case $S_{\alpha j}^{-1} = \chi_{\alpha,j}^*$, and

$$S^{-1} M S = \text{diag}(\lambda_1, \dots, \lambda_N) . \quad (1.75)$$

The matrix M can always be decomposed into its eigenvectors, as

$$M_{ij} = \sum_\alpha \lambda_\alpha \psi_{\alpha,i} \chi_{\alpha,j}^* . \quad (1.76)$$

If we expand u in terms of the right eigenvectors,

$$\boldsymbol{\eta}(t) = \sum_\beta C_\beta(t) \psi_\beta(t) , \quad (1.77)$$

then upon taking the inner product with χ_α , we find that C_α obeys

$$\dot{C}_\alpha + \langle \chi_\alpha | \dot{\psi}_\beta \rangle C_\beta = \lambda_\alpha C_\alpha . \quad (1.78)$$

⁶If $[M_1, M_2] = 0$ then $A = A_{\mathcal{P}}$.

If $\dot{\psi}_\beta = 0$, e.g. if M is time-independent, then $C_\alpha(t) = C_\alpha(0) e^{\lambda_\alpha t}$, and

$$\eta_i(t) = \sum_{\alpha} \overbrace{\sum_j \eta_j(0) \chi_{\alpha,j}^*}^{C_\alpha(0)} e^{\lambda_\alpha t} \psi_{\alpha,i} . \quad (1.79)$$

Thus, the component of $\eta(t)$ along ψ_α increases exponentially with time if $\text{Re}(\lambda_\alpha) > 0$, and decreases exponentially if $\text{Re}(\lambda_\alpha) < 0$.

Nota bene: If $M \in \text{GL}(N, \mathbb{R})$ is not symmetric – more generally if it does not commute with its transpose M^\top – then it may be that the right eigenvectors of M do not span \mathbb{R}^N . In this case, the canonical decomposition of M contains one or more *Jordan blocks*. See §1.6 below.

1.6 Appendix III: Normal Matrices, Non-Normal Matrices, and Jordan Blocks

Normal matrices and eigenspectra : Quantum mechanical Hamiltonians can be represented as Hermitian matrices. In elementary school linear algebra class, we all learned that any Hermitian matrix H is diagonalizable by a unitary transformation, its eigenvalues are real, and eigenvectors corresponding to different eigenvalues are necessarily orthogonal. In the case of degenerate eigenvalues, their associated eigenvectors may be chosen to be mutually orthogonal via the Gram-Schmidt process. In the following discussion, we will assume our matrices are in general complex, but we can of course restrict to the real case, as is appropriate for real linear dynamical systems.

Any complex square matrix A which satisfies $A^\dagger A = AA^\dagger$ is called *normal*. Hermitian matrices are normal, but so are antihermitian and unitary matrices⁷. Real symmetric, antisymmetric, and orthogonal matrices satisfy $A^\top A = AA^\top$. The *Schur decomposition theorem* guarantees that any $n \times n$ matrix A may be decomposed as $A = VTV^\dagger$, where $V \in \text{U}(n)$ and T is upper triangular. Now if A is normal, $[A, A^\dagger] = V [T, T^\dagger] V^\dagger = 0$, hence T is normal. However, it is easy to show that any normal upper triangular matrix must be diagonal⁸, so $A = VDV^\dagger$, which means $D = V^\dagger AV$ is the diagonal matrix of eigenvalues of A . Conversely, if $A = VDV^\dagger$ is unitarily equivalent to a diagonal matrix, it is trivial to show that A is normal. Thus *any $n \times n$ matrix A is diagonalizable by a unitary transformation if and only if A is normal*.

There is a real version of Schur decomposition whereby a real matrix B satisfying $B^\top B = BB^\top$ may be decomposed as $B = RSR^\top$, where R is a real orthogonal matrix, and S is *block upper triangular*. The diagonal blocks of S are either 1×1 , corresponding to real eigenvalues, or 2×2 , corresponding to complex eigenvalues. One eventually concludes that real symmetric matrices have real eigenvalues, real antisymmetric matrices have pure imaginary (or zero) eigenvalues, and real orthogonal matrices have unimodular complex eigenvalues.

⁷There are many examples of normal matrices which are neither Hermitian, antihermitian, nor unitary. For example, any diagonal matrix with arbitrary complex diagonal entries is normal.

⁸ $T^\dagger T = TT^\dagger$ says that $\sum_j |T_{ij}|^2 = \sum_j |T_{ji}|^2$, i.e. the sum of the square moduli of the elements in the i^{th} row is the same as that for the i^{th} column. Starting with $i = 1$, the only possible nonzero entry in the first column is $T_{1,1}$, hence all the remaining entries in the first row must vanish. Filling in all these zeros, proceed to $i = 2$. Since we just showed $T_{1,2} = 0$, we conclude that the only possible nonzero entry in the second column is $T_{2,2}$, hence all remaining entries in the second row must vanish. Continuing in this manner, we conclude that T is diagonal if it is both normal and upper triangular.

Now let's set $A = VDV^\dagger$ and consider different classes of matrix A . If A is Hermitian, $A = A^\dagger$ immediately yields $D = D^\dagger$, which says that all the eigenvalues of A must be real. If $A^\dagger = -A$, then $D^\dagger = -D$ and all the eigenvalues are purely imaginary. And if $A^\dagger = A^{-1}$, then $D^\dagger = D^{-1}$ and we conclude that all the eigenvalues are unimodular, *i.e.* of the form $e^{i\omega_j}$. This analysis also tells us that any unitary matrix U can be written in the form $U = \exp(iH)$ for some Hermitian matrix H .

Jordan blocks: What happens when an $n \times n$ matrix A is not normal? In this case A is not diagonalizable by a unitary transformation, and while the sum of the dimensions of its eigenspaces is generically equal to the matrix dimension $\dim(A) = n$, this is not guaranteed; it may be less than n . For example, consider the matrix

$$A = \begin{pmatrix} a & 1 \\ 0 & a \end{pmatrix}. \quad (1.80)$$

The eigenvalues are solutions to $\det(\lambda I - A) = 0$, hence $\lambda = a$, but there is only one eigenvector, $\psi = \begin{pmatrix} 1 \\ 0 \end{pmatrix}$. What is always true for any complex matrix A is that it can be brought to *Jordan canonical form* by a similarity transformation $J = P^{-1}AP$, where P is invertible, and

$$J = \begin{pmatrix} J^{(1)} & & \\ & \ddots & \\ & & J^{(b)} \end{pmatrix}, \quad (1.81)$$

where b is the number of *Jordan blocks* and where each block $J^{(r)}$ is an $n_r \times n_r$ matrix of the form

$$J^{(r)} = \begin{pmatrix} \lambda_r & 1 & & \\ & \lambda_r & \ddots & \\ & & \ddots & 1 \\ & & & \lambda_r \end{pmatrix}. \quad (1.82)$$

Thus each $J^{(r)}$ is tridiagonal, with diagonal elements all given by λ_r and each element directly above the diagonal equal to one. Clearly $J^{(r)}$ has only one eigenvalue, λ_r , and writing the corresponding *right* eigenvector as $\vec{R}^{(r)}$, the condition $J^{(r)} \vec{R}^{(r)} = \lambda^{(r)} \vec{R}^{(r)}$ yields the equations

$$\lambda_r R_1^{(r)} + R_2^{(r)} = \lambda_r R_1^{(r)}, \quad \lambda_r R_2^{(r)} + \psi_3 = \lambda_r R_2^{(r)}, \quad \dots \quad \lambda_r R_{n_r-1}^{(r)} + R_{n_r}^{(r)} = \lambda_r R_{n_r-1}^{(r)}, \quad (1.83)$$

where $n_r = \dim(J^{(r)})$. These equations entail $R_2^{(r)} = R_3^{(r)} = \dots = R_{n_r}^{(r)} = 0$, which says that there is only one such eigenvector, whose components are $R_j^{(r)} = \delta_{j,1}$. Note that the corresponding *left* eigenvector $\vec{L}^{(r)}$ then has components $L_j^{(r)} = \delta_{j,n_r}$. If $n_r > 1$ we then have $\langle L^{(r)} | R^{(r)} \rangle \equiv \vec{L}^{(r)} \cdot \vec{R}^{(r)} = 0$, which means that the left and right eigenvectors of A which correspond to the Jordan blocks with $n_r > 1$ are orthogonal. *Nota bene*: It may be the case that there are degeneracies among the eigenvalues $\{\lambda_r\}$.

To summarize⁹, for every general complex $n \times n$ matrix A ,

⁹See https://en.wikipedia.org/wiki/Jordan_normal_form.

- A may be brought to Jordan canonical form by a similarity transformation $J = P^{-1}AP$, where $J = \text{bdiag}(J^{(1)}, \dots, J^{(b)})$ is block diagonal, with each $(J^{(r)})_{ij} = \lambda_r \delta_{i,j} + \delta_{i,j-1}$ with $\dim(J^{(r)}) = n_r$, for $r \in \{1, \dots, b\}$.
- There are $b \leq n$ eigenvalues $\{\lambda_1, \dots, \lambda_b\}$ (again, not necessarily all distinct) and b corresponding eigenvectors $\{\vec{R}^{(1)}, \dots, \vec{R}^{(b)}\}$. If $b = n$ then the matrix is diagonalizable.
- The dimension n of the matrix A satisfies $n = n_1 + \dots + n_b$, i.e. it is the sum of the dimensions of all its Jordan blocks.
- Let $\lambda \in \{\lambda_1, \dots, \lambda_b\}$ be an eigenvalue, and define

$$t_k(\lambda) = \dim \ker(\lambda \mathbb{I}_{n \times n} - A)^k , \quad (1.84)$$

which is the *dimension of the null space* of the matrix $\lambda \mathbb{I}_{n \times n} - A$. Then

- ◊ $t_k(\lambda)$ is the number of Jordan blocks corresponding to the eigenvalue λ .
- ◊ The number of Jordan blocks of size greater than k is $t_{k+1}(\lambda) - t_k(\lambda)$. Thus the number of Jordan blocks of size k for the eigenvalue λ is

$$N_k(\lambda) = 2t_k(\lambda) - t_{k+1}(\lambda) - t_{k-1}(\lambda) . \quad (1.85)$$

Singular value decomposition : Note the difference between the decomposition into Jordan canonical form and singular value decomposition (SVD), in which we write an $m \times n$ matrix A as $A = USV^\dagger$, where U is $m \times k$, V is $n \times k$ (hence V^\dagger is $k \times n$), $U^\dagger U = V^\dagger V = \mathbb{I}_{k \times k}$, and $S = \text{diag}(s_1, \dots, s_k)$ is a $k \times k$ real matrix with $k \leq \min(m, n)$ and each $s_j > 0$. The elements s_j are the singular values and the rows of U and V are the singular vectors. Note that $A^\dagger A = VS^2 V^\dagger$ is $n \times n$ and $AA^\dagger = US^2 U^\dagger$ is $m \times m$. If we define

$$F(\lambda) = \prod_{j=1}^k (\lambda - s_j^2) , \quad (1.86)$$

Then

$$P(\lambda) \equiv \det(\lambda - A^\dagger A) = \lambda^{n-k} F(\lambda) , \quad Q(\lambda) \equiv \det(\lambda - AA^\dagger) = \lambda^{m-k} F(\lambda) . \quad (1.87)$$

Some comments:

- When $A \in \mathbb{R}$ is real, then both U and V may be chosen to be real, and we may write $A = USV^\top$.
- We may also adopt a convention where U is $m \times m$, V is $n \times n$, and S to be $m \times n$, where only the first k diagonal elements S_{ii} are the (nonzero and real) singular values. In this case, $U^\dagger U = \mathbb{I}_{m \times m}$ and $V^\dagger V = \mathbb{I}_{n \times n}$.
- For any square $n \times n$ complex matrix A we therefore have two decompositions, via JCF and SVD, *viz.*

$$A = P^{-1}JP = USV^\dagger , \quad (1.88)$$

where J is the Jordan canonical form of A . When A is normal, $k = n$ and $P = U^\dagger = V^\dagger$, in which case the two decompositions are equivalent.

Example: As an example highlighting the difference between eigenvalues and singular values, consider

$$A = \begin{pmatrix} 1 & 0 & 1 \\ 0 & 1 & 1 \\ 0 & 0 & 0 \end{pmatrix} = RDL^T = USV^T , \quad (1.89)$$

where

$$L^T = \begin{pmatrix} 1 & -1 & 0 \\ 0 & 1 & 1 \\ 0 & 0 & 1 \end{pmatrix} , \quad D = \begin{pmatrix} 1 & 0 & 0 \\ 0 & 1 & 0 \\ 0 & 0 & 0 \end{pmatrix} , \quad R = \begin{pmatrix} 1 & 1 & -1 \\ 0 & 1 & -1 \\ 0 & 0 & 1 \end{pmatrix} \quad (1.90)$$

and

$$U = \frac{1}{\sqrt{2}} \begin{pmatrix} 1 & -1 \\ 1 & 1 \\ 0 & 0 \end{pmatrix} , \quad S = \begin{pmatrix} \sqrt{3} & 0 \\ 0 & 1 \end{pmatrix} , \quad V^T = \frac{1}{\sqrt{6}} \begin{pmatrix} 1 & 1 & 2 \\ -\sqrt{3} & \sqrt{3} & 0 \end{pmatrix} . \quad (1.91)$$

Note that U and V^T are both chosen to be real, which is a consequence of the fact that A itself is real. One can check that R is the matrix of right column eigenvectors, L^T is the matrix of left row eigenvectors, and Λ is the matrix of eigenvalues. Thus, the three eigenvalues are $\{\lambda_1, \lambda_2, \lambda_3\} = \{1, 1, 0\}$. One also has $L^T R = \mathbb{I}$, i.e. $L^T = R^{-1}$, which says that $L_i^{(a)} R_i^{(b)} = \delta^{ab}$ – the row and column eigenvectors satisfy orthonormality. Thus $R^{-1} A R = D$ and A is diagonalizable by R , which is a consequence of there being no Jordan blocks. Note that there are only two singular values, $\{s_1, s_2\} = \{\sqrt{3}, 1\}$, and that U has dimensions 3×2 while V^T has dimensions 2×3 . One can further check that $U^T U = V^T V = \mathbb{I}_{2 \times 2}$.

Had we adopted the convention where both U and V are square, we would have

$$U = \frac{1}{\sqrt{2}} \begin{pmatrix} 1 & -1 & 0 \\ 1 & 1 & 0 \\ 0 & 0 & \sqrt{2} \end{pmatrix} , \quad S = \begin{pmatrix} \sqrt{3} & 0 & 0 \\ 0 & 1 & 0 \\ 0 & 0 & 0 \end{pmatrix} , \quad V^T = \frac{1}{\sqrt{6}} \begin{pmatrix} 1 & 1 & 2 \\ -\sqrt{3} & \sqrt{3} & 0 \\ -\sqrt{2} & -\sqrt{2} & \sqrt{2} \end{pmatrix} , \quad (1.92)$$

for which $U^T U = V^T V = \mathbb{I}_{3 \times 3}$. The extra zeroes in the matrix S are padding, and there are only two singular values, $\sqrt{3}$ and 1.

For this example, both the set of eigenvalues and the set of singular values are distinct. Furthermore,

$$A^\dagger A = \begin{pmatrix} 1 & 0 & 1 \\ 0 & 1 & 1 \\ 1 & 1 & 2 \end{pmatrix} = V S^2 V^T , \quad AA^\dagger = \begin{pmatrix} 2 & 1 & 0 \\ 1 & 2 & 0 \\ 0 & 0 & 0 \end{pmatrix} = U S^2 U^\dagger . \quad (1.93)$$

The singular values of A are thus the positive square roots of the eigenvalues of the nonnegative definite Hermitian matrix $A^\dagger A$ (or, equivalently, of AA^\dagger). In general, the eigenvalues λ_j of a non-normal matrix A may not be real, even if $A \in \mathrm{GL}(n, \mathbb{R})$ is itself real. (In this case the eigenvalues are either real or come in complex conjugate pairs.) The singular values, however, are always real and positive.

As a second example, consider the matrix

$$B = \begin{pmatrix} 1 & 1 \\ -3 & 3 \end{pmatrix} = RDL^T = USV^T , \quad (1.94)$$

where

$$L^\top = \frac{i}{2\sqrt{2}} \begin{pmatrix} +\sqrt{3}e^{-i\phi} & -1 \\ -\sqrt{3}e^{+i\phi} & 1 \end{pmatrix}, \quad D = \begin{pmatrix} 2+i\sqrt{2} & 0 \\ 0 & 2-i\sqrt{2} \end{pmatrix}, \quad R = \begin{pmatrix} 1 & 1 \\ \sqrt{3}e^{+i\phi} & \sqrt{3}e^{-i\phi} \end{pmatrix} \quad (1.95)$$

with $e^{i\phi} = \frac{1}{\sqrt{3}}(1 + i\sqrt{2})$ and

$$U = \begin{pmatrix} 1 & 0 \\ 0 & 1 \end{pmatrix}, \quad S = \begin{pmatrix} 3\sqrt{2} & 0 \\ 0 & \sqrt{2} \end{pmatrix}, \quad V^\top = \frac{1}{\sqrt{2}} \begin{pmatrix} 1 & 1 \\ -1 & 1 \end{pmatrix}. \quad (1.96)$$

Note that the two right eigenvectors form a complex conjugate pair, as do the two left eigenvectors. This situation pertains for every complex eigenvalue, since if $\lambda_r \in \mathbb{C}$ is an eigenvalue then so is λ_r^* . Again, since $B \in \mathrm{GL}(2, \mathbb{R})$, the U and V matrices may be chosen real. There are two singular values $\{s_1, s_2\} = \{3\sqrt{2}, \sqrt{2}\}$. But unlike the matrix A in the previous example, B has complex eigenvalues $\lambda_{\pm} = 2 \pm i\sqrt{2}$, and the matrices L^\top and R of the left (row) and right (column) eigenvectors are complex. As in the previous case, $L^\top = R^{-1}$, hence $R^{-1}BR = D$, i.e. B is diagonalized by the matrix R , which is possible because there are no nontrivial Jordan blocks when it is brought to canonical form.

Chapter 2

Bifurcations

2.1 Types of Bifurcations

2.1.1 Saddle-node bifurcation

We remarked above how $f'(u)$ is in general nonzero when $f(u)$ itself vanishes, since two equations in a single unknown is an overdetermined set. However, consider the function $F(x, \alpha)$, where α is a control parameter. If we demand $F(x, \alpha) = 0$ and $\partial_x F(x, \alpha) = 0$, we have two equations in two unknowns, and in general there will be a zero-dimensional solution set consisting of points (x_c, α_c) . The situation is depicted in Fig. 2.1.

Let's expand $F(x, \alpha)$ in the vicinity of such a point (x_c, α_c) :

$$\begin{aligned} F(x, \alpha) &= F(x_c, \alpha_c) + \frac{\partial F}{\partial x} \Big|_{(x_c, \alpha_c)} (x - x_c) + \frac{\partial F}{\partial \alpha} \Big|_{(x_c, \alpha_c)} (\alpha - \alpha_c) + \frac{1}{2} \frac{\partial^2 F}{\partial x^2} \Big|_{(x_c, \alpha_c)} (x - x_c)^2 \\ &\quad + \frac{\partial^2 F}{\partial x \partial \alpha} \Big|_{(x_c, \alpha_c)} (x - x_c)(\alpha - \alpha_c) + \frac{1}{2} \frac{\partial^2 F}{\partial \alpha^2} \Big|_{(x_c, \alpha_c)} (\alpha - \alpha_c)^2 + \dots \end{aligned} \quad (2.1)$$
$$= A(\alpha - \alpha_c) + B(x - x_c)^2 + \dots ,$$

where we keep terms of lowest order in the deviations δx and $\delta \alpha$. Note that we can separately change the signs of A and B by redefining $\alpha \rightarrow -\alpha$ and/or $x \rightarrow -x$, so without loss of generality we may assume both A and B are positive. If we now rescale $u \equiv \sqrt{B/A}(x - x_c)$, $r \equiv \alpha - \alpha_c$, and $\tau = \sqrt{AB}t$, we have, neglecting the higher order terms, we obtain the ‘normal form’ of the saddle-node bifurcation,

$$\frac{du}{d\tau} = r + u^2 . \quad (2.2)$$

The evolution of the flow is depicted in Fig. 2.2. For $r < 0$ there are two fixed points – one stable ($u^* = -\sqrt{-r}$) and one unstable ($u = +\sqrt{-r}$). At $r = 0$ these two nodes coalesce and annihilate each other. (The point $u^* = 0$ is half-stable precisely at $r = 0$.) For $r > 0$ there are no longer any fixed points

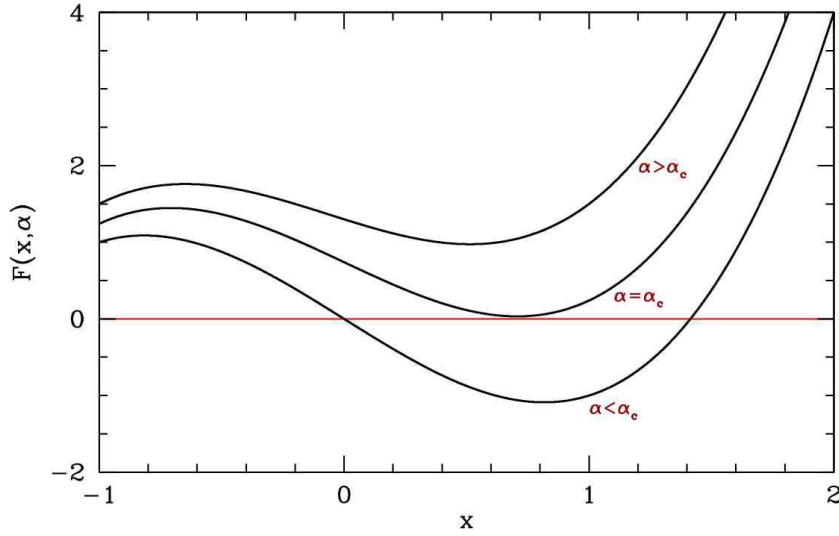


Figure 2.1: Evolution of $F(x, \alpha)$ as a function of the control parameter α .

in the vicinity of $u = 0$. In the left panel of Fig. 2.3 we show the flow in the extended (r, u) plane. The unstable and stable nodes annihilate at $r = 0$.

2.1.2 Transcritical bifurcation

Another situation which arises frequently is the *transcritical bifurcation*. Consider the equation $\dot{x} = f(x)$ in the vicinity of a fixed point x^* .

$$\frac{dx}{dt} = f'(x^*)(x - x^*) + \frac{1}{2}f''(x^*)(x - x^*)^2 + \dots . \quad (2.3)$$

We rescale $u \equiv \beta(x - x^*)$ with $\beta = -\frac{1}{2}f''(x^*)$ and define $r \equiv f'(x^*)$ as the control parameter, to obtain, to order u^2 ,

$$\frac{du}{dt} = ru - u^2 . \quad (2.4)$$

Note that the sign of the u^2 term can be reversed relative to the others by sending $u \rightarrow -u$.

Consider a crude model of a laser threshold. Let n be the number of photons in the laser cavity, and N the number of excited atoms in the cavity. The dynamics of the laser are approximated by the equations

$$\begin{aligned} \dot{n} &= GNn - kn \\ N &= N_0 - \alpha n . \end{aligned} \quad (2.5)$$

Here G is the gain coefficient and k the photon decay rate. N_0 is the pump strength, and α is a numerical factor. The first equation tells us that the number of photons in the cavity grows with a rate $GN - k$; gain is proportional to the number of excited atoms, and the loss rate is a constant cavity-dependent quantity (typically through the ends, which are semi-transparent). The second equation says that the number of

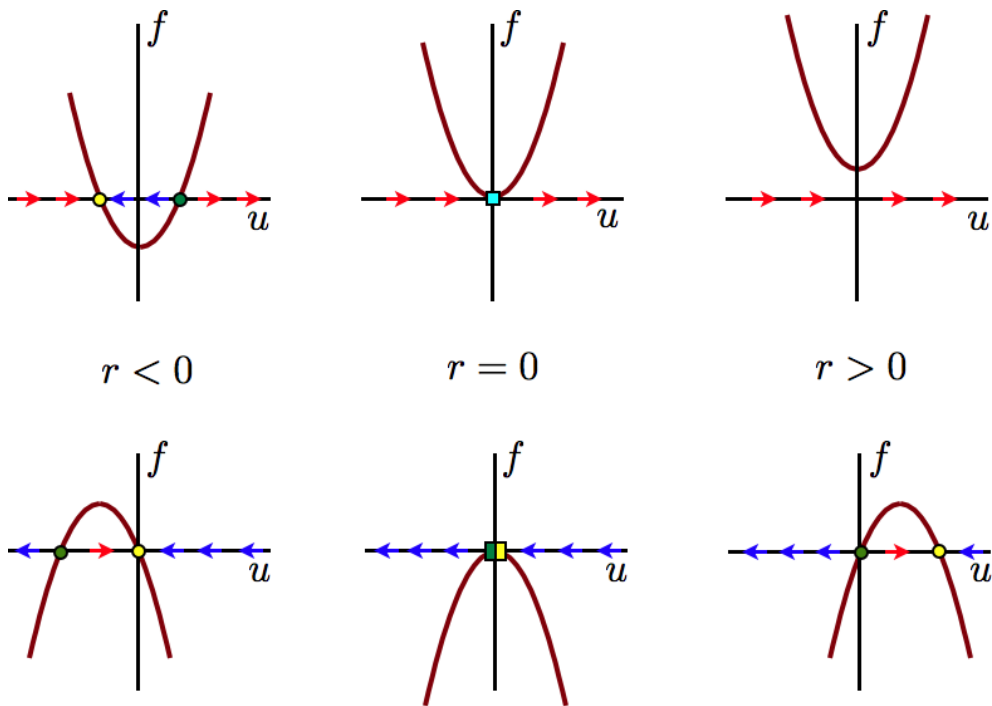


Figure 2.2: Flow diagrams for the saddle-node bifurcation $\dot{u} = r + u^2$ (top) and the transcritical bifurcation $\dot{u} = ru - u^2$ (bottom).

excited atoms is equal to the pump strength minus a term proportional to the number of photons (since the presence of a photon means an excited atom has decayed). Putting them together,

$$\dot{n} = (GN_0 - k)n - \alpha Gn^2 , \quad (2.6)$$

which exhibits a transcritical bifurcation at pump strength $N_0 = k/G$. For $N_0 < k/G$ the system acts as a lamp; for $N_0 > k/G$ the system acts as a laser.

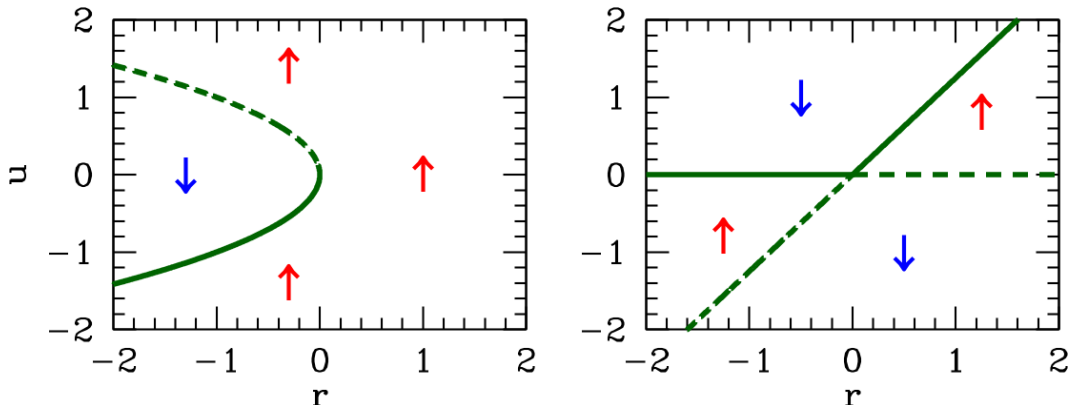


Figure 2.3: Extended phase space (r, u) flow diagrams for the saddle-node bifurcation $\dot{u} = r + u^2$ (left) and the transcritical bifurcation $\dot{u} = ru - u^2$ (right).

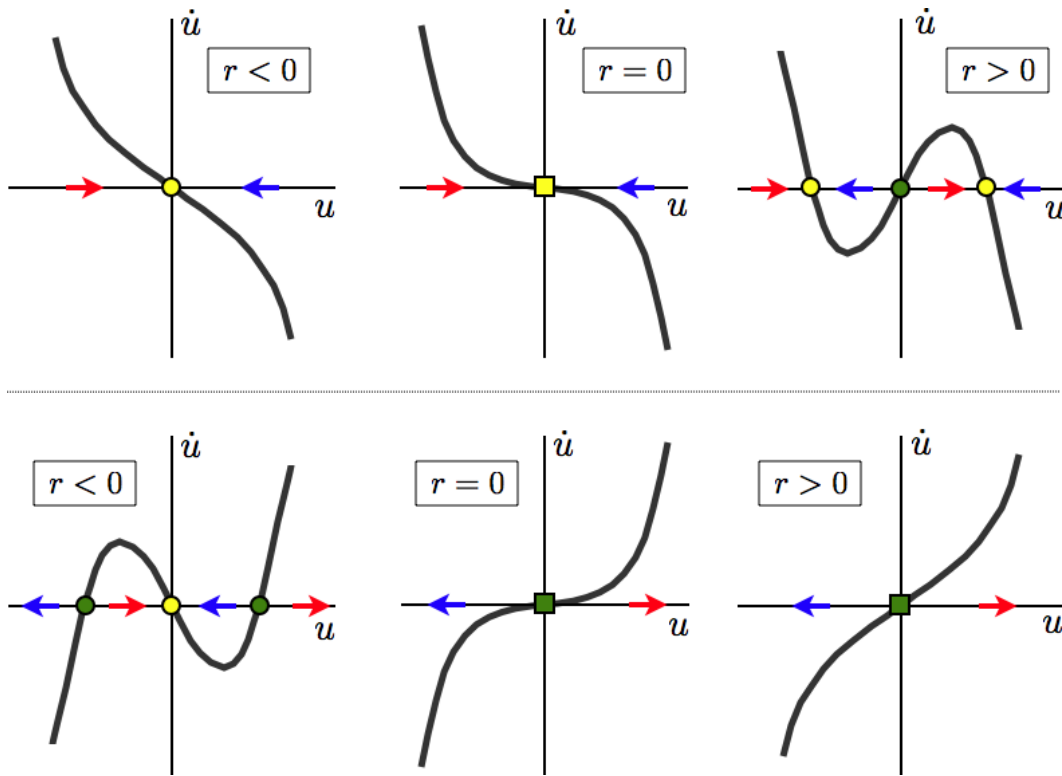


Figure 2.4: Top: supercritical pitchfork bifurcation $\dot{u} = ru - u^3$. Bottom: subcritical pitchfork bifurcation $\dot{u} = ru + u^3$.

What happens in the transcritical bifurcation is an exchange of stability of the fixed points at $u^* = 0$ and $u^* = r$ as r passes through zero. This is depicted graphically in the bottom panel of Fig. 2.2.

2.1.3 Pitchfork bifurcation

The pitchfork bifurcation is commonly encountered in systems in which there is an overall parity symmetry ($u \rightarrow -u$). There are two classes of pitchfork: supercritical and subcritical. The normal form of the supercritical bifurcation is

$$\dot{u} = ru - u^3 \quad , \quad (2.7)$$

which has fixed points at $u^* = 0$ and $u^* = \pm\sqrt{r}$. Thus, the situation is as depicted in fig. 2.4 (top panel). For $r < 0$ there is a single stable fixed point at $u^* = 0$. For $r > 0$, $u^* = 0$ is unstable, and flanked by two stable fixed points at $u^* = \pm\sqrt{r}$.

If we send $u \rightarrow -u$, $r \rightarrow -r$, and $t \rightarrow -t$, we obtain the *subcritical pitchfork*, depicted in the bottom panel of fig. 2.4. The normal form of the subcritical pitchfork bifurcation is

$$\dot{u} = ru + u^3 \quad . \quad (2.8)$$

The fixed point structure in both supercritical and subcritical cases is shown in Fig. 2.5.

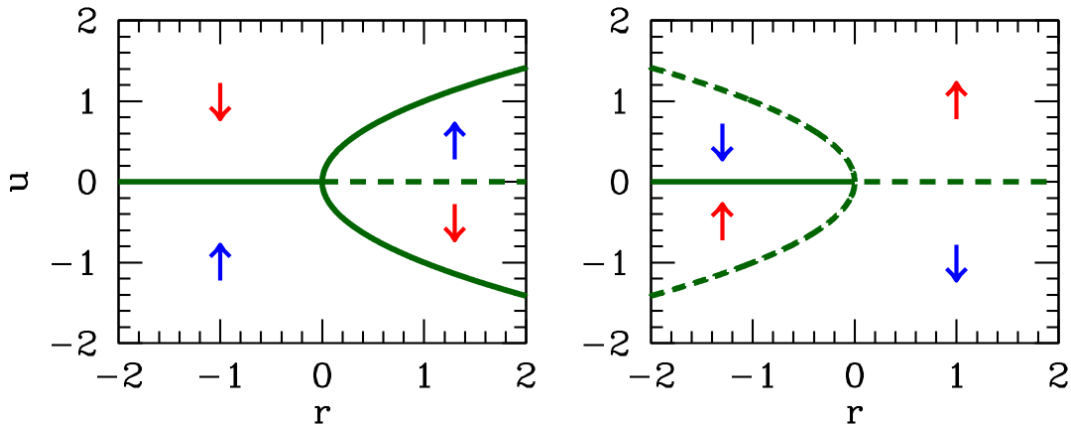


Figure 2.5: Extended phase space (r, u) flow diagrams for the supercritical pitchfork bifurcation $\dot{u} = ru - u^3$ (left), and subcritical pitchfork bifurcation $\dot{u} = ru + u^3$ (right).

2.1.4 Imperfect bifurcation

The imperfect bifurcation occurs when a symmetry-breaking term is added to the pitchfork. The normal form contains two control parameters:

$$\dot{u} = h + ru - u^3 \quad . \quad (2.9)$$

Here, the constant h breaks the parity symmetry if $u \rightarrow -u$.

This equation arises from a crude model of magnetization dynamics. Let M be the magnetization of a sample, and $F(M)$ the free energy. Assuming M is small, we can expand $F(M)$ as

$$F(M) = -HM + \frac{1}{2}aM^2 + \frac{1}{4}bM^4 + \dots \quad , \quad (2.10)$$

where H is the external magnetic field, and a and b are temperature-dependent constants. This is called the *Landau expansion* of the free energy. We assume $b > 0$ in order that the minimum of $F(M)$ not lie at infinity. The dynamics of $M(t)$ are modeled by

$$\frac{dM}{dt} = -\Gamma \frac{\partial F}{\partial M} \quad , \quad (2.11)$$

with $\Gamma > 0$. Thus, the magnetization evolves toward a local minimum in the free energy. Note that the free energy is a decreasing function of time:

$$\frac{dF}{dt} = \frac{\partial F}{\partial M} \frac{dM}{dt} = -\Gamma \left(\frac{\partial F}{\partial M} \right)^2 \quad . \quad (2.12)$$

By rescaling $M \equiv uM_0$ with $M_0 = (b\Gamma)^{-1/2}$ and defining $r \equiv -a\Gamma$ and $h \equiv (\Gamma^3 b)^{1/2} H$, we obtain the normal form

$$\begin{aligned} \dot{u} &= h + ru - u^3 = -\frac{\partial f}{\partial u} \\ f(u) &= -\frac{1}{2}ru^2 + \frac{1}{4}u^4 - hu \quad . \end{aligned} \quad (2.13)$$

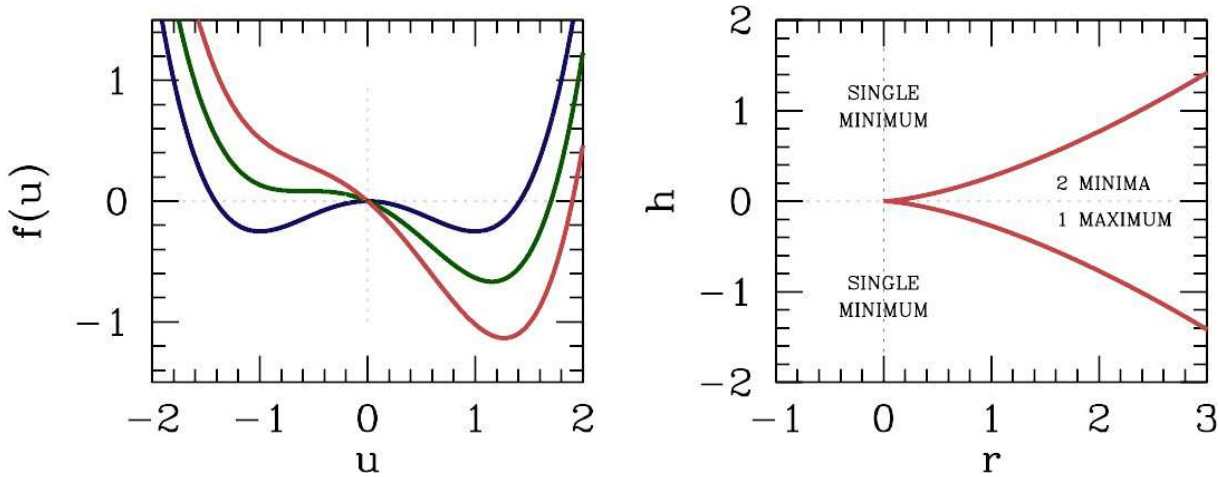


Figure 2.6: Left: scaled free energy $f(u) = -\frac{1}{2}ru^2 + \frac{1}{4}u^4 - hu$, with $h = 0$ (blue), $h = h_c$ (green), and $h = 2h_c$ (red), where $h_c = \frac{2}{3\sqrt{3}}r^{3/2}$. Right: phase diagram for the imperfect bifurcation $\dot{u} = -f'(u) = h + ru - u^3$ in the (r, h) plane.

Here, $f(u)$ is a scaled version of the free energy.

Fixed points satisfy the equation

$$u^3 - ru - h = 0 \quad , \quad (2.14)$$

and correspond to extrema in $f(u)$. By the fundamental theorem of algebra, this cubic polynomial may be uniquely factorized over the complex plane. Since the coefficients are real, the complex conjugate \bar{u} satisfies the same equation as u , hence there are two possibilities for the roots: either (i) all three roots are real, or (ii) one root is real and the other two are a complex conjugate pair. Clearly for $r < 0$ we are in situation (ii) since $u^3 - ru$ is then monotonically increasing for $u \in \mathbb{R}$, and therefore takes the value h precisely once for u real. For $r > 0$, there is a region $h \in [-h_c(r), h_c(r)]$ over which there are three real roots. To find $h_c(r)$, we demand $f''(u) = 0$ as well as $f'(u) = 0$, which says that two roots have merged in a saddle-node bifurcation, forming an inflection point. Thus $f''(u) = 3u^2 - r = 0$ yields $u = \pm(r/3)^{1/2}$, which requires $r > 0$, and using this to eliminate u from the equation $f(u) = 0$ yields the critical value of h as a function of r , viz. $h_c(r) = \frac{2}{3\sqrt{3}}r^{3/2}\Theta(r)$.

Examples of the function $f(u)$ for $r > 0$ are shown in the left panel of Fig. 2.6 for three different values of h . For $|h| < h_c(r)$ there are three extrema satisfying $f'(u^*) = 0$: $u_1^* < u_2^* < 0 < u_3^*$, assuming (without loss of generality) that $h > 0$. Clearly u_1^* is a local minimum, u_2^* a local maximum, and u_3^* the global minimum of the function $f(u)$. The ‘phase diagram’ for this system, plotted in the (r, h) control parameter space, is shown in the right panel of Fig. 2.6.

In Fig. 2.7 we plot the fixed points $u^*(r)$ for fixed h . A saddle-node bifurcation occurs at $r = r_c(h) = \frac{3}{2^{2/3}}|h|^{2/3}$. For $h = 0$ this reduces to the supercritical pitchfork; for finite h the pitchfork is deformed and even changed topologically. Finally, in Fig. 2.7 we show the behavior of $u^*(h)$ for fixed r . When $r < 0$ the curve retraces itself as h is ramped up and down, but for $r > 0$ the system exhibits the phenomenon of *hysteresis*, i.e. there is an irreversible aspect to the behavior. Fig. 2.7 shows a *hysteresis loop* when $r > 0$.

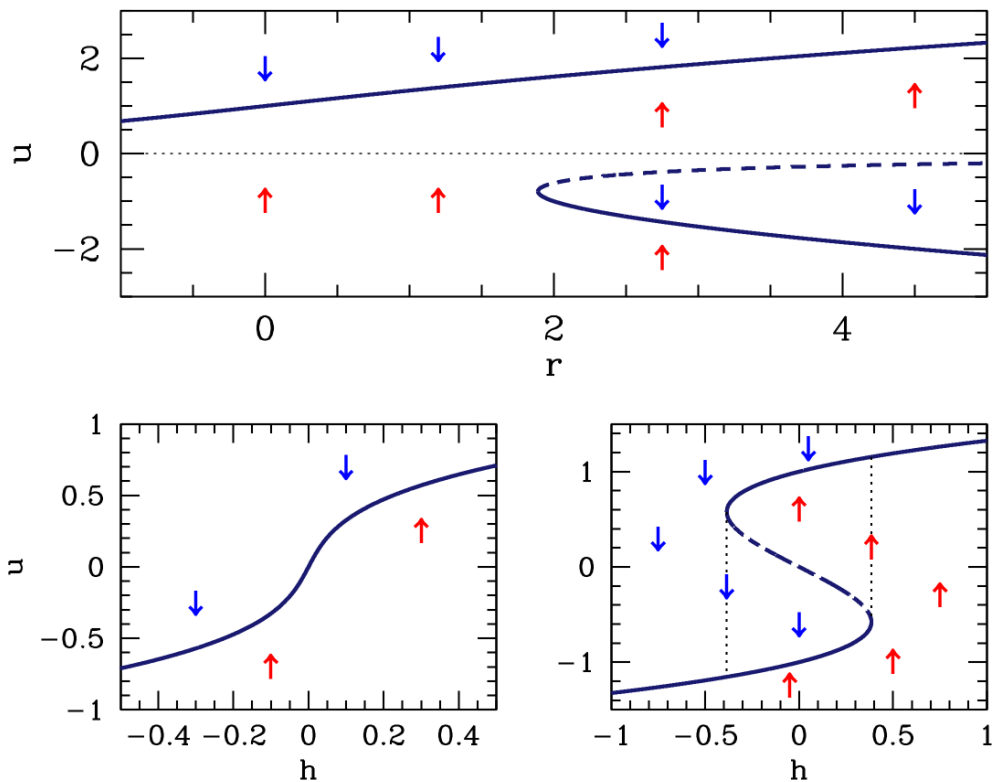


Figure 2.7: Top: extended phase space \$(r, u)\$ flow diagram for \$\dot{u} = h + ru - u^3\$, the imperfect pitchfork bifurcation, at \$h = 1\$. This is in a sense a deformed supercritical pitchfork. The saddle-node bifurcation occurs at \$r_c = (3/2^{2/3})|h|^{2/3} = 1.8899\$. Bottom: extended phase space \$(h, u)\$ flow diagram for the imperfect pitchfork bifurcation \$r = -0.2\$ (left panel) and \$r = 1\$ (right panel). For \$r < 0\$ the behavior is completely reversible. For \$r > 0\$, a regime of irreversibility sets in between \$-h_c\$ and \$+h_c\$, where \$h_c = 2(r/3)^{3/2}\$. The system then exhibits the phenomenon of hysteresis. The dotted vertical lines show the boundaries of the hysteresis loop.

2.2 Examples

2.2.1 Population dynamics

Consider the dynamics of a harvested population,

$$\dot{N} = rN\left(1 - \frac{N}{K}\right) - H(N) \quad , \quad (2.15)$$

where \$r, K > 0\$, and where \$H(N)\$ is the *harvesting rate*.

(a) Suppose \$H(N) = H_0\$ is a constant. Sketch the phase flow, and identify and classify all fixed points.

Solution : We examining \$\dot{N} = f(N)\$ with

$$f(N) = rN - \frac{r}{K}N^2 - H_0 \quad . \quad (2.16)$$

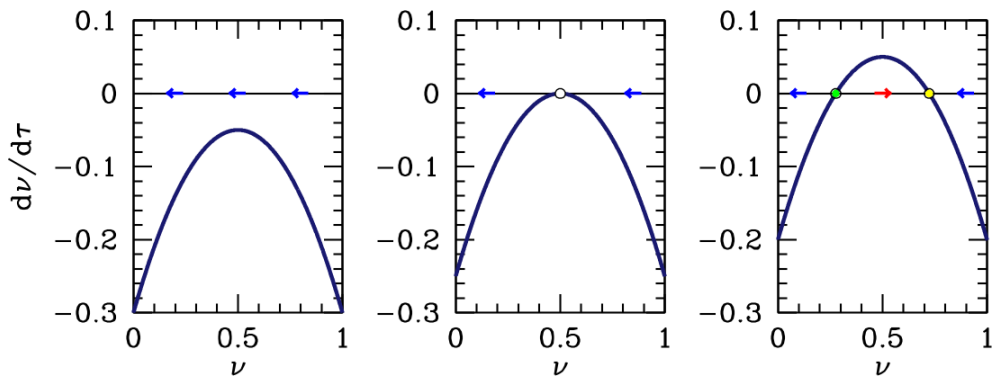


Figure 2.8: Phase flow for the constantly harvested population, $\dot{\nu} = \nu(1 - \nu) - h$, for $h = 0.30$ (left), $h = 0.25$ (center), and $h = 0.20$ (right). The critical harvesting rate is $h_c = \frac{1}{4}$.

Setting $f'(N) = 0$ yields $N = \frac{1}{2}K$. $f(N)$ is a downward-opening parabola whose maximum value is $f(\frac{1}{2}K) = \frac{1}{4}rK - H_0$. Thus, if $H_0 > \frac{1}{4}rK$, the harvesting rate is too large and the population always shrinks. A saddle-node bifurcation occurs at this value of H_0 , and for larger harvesting rates, there are fixed points at

$$N_{\pm} = \frac{1}{2}K \pm \frac{1}{2}K \sqrt{1 - \frac{4H_0}{rK}} \quad , \quad (2.17)$$

with N_- unstable and N_+ stable. By rescaling the population $\nu = N/K$, time $\tau = rt$ and harvesting rate $h = H_0/rK$, we arrive at the equation

$$\dot{\nu} = \nu(1 - \nu) - h \quad . \quad (2.18)$$

The critical harvesting rate is then $h_c = \frac{1}{4}$. See fig. 2.8.

(b) One defect of the constant harvesting rate model is that $N = 0$ is not a fixed point. To remedy this, consider the following model for $H(N)$ ¹:

$$H(N) = \frac{BN^2}{N^2 + A^2} \quad , \quad (2.19)$$

where A and B are (positive) constants. Show that one can rescale (N, t) to (n, τ) , such that

$$\frac{dn}{d\tau} = \gamma n \left(1 - \frac{n}{c}\right) - \frac{n^2}{n^2 + 1} \quad , \quad (2.20)$$

where γ and c are positive constants. Provide expressions for n , τ , γ , and c .

Solution : Examining the denominator of $H(N)$, we must take $N = An$. Dividing both sides of $\dot{N} = f(N)$ by B , we obtain

$$\frac{A}{B} \frac{dN}{dt} = \frac{rA}{B} n \left(1 - \frac{A}{K} n\right) - \frac{n^2}{n^2 + 1} \quad , \quad (2.21)$$

¹This is a model for the dynamics of the spruce budworm population, taken from ch. 1 of J. D. Murray, *Mathematical Biology* (2nd edition, Springer, 1993).

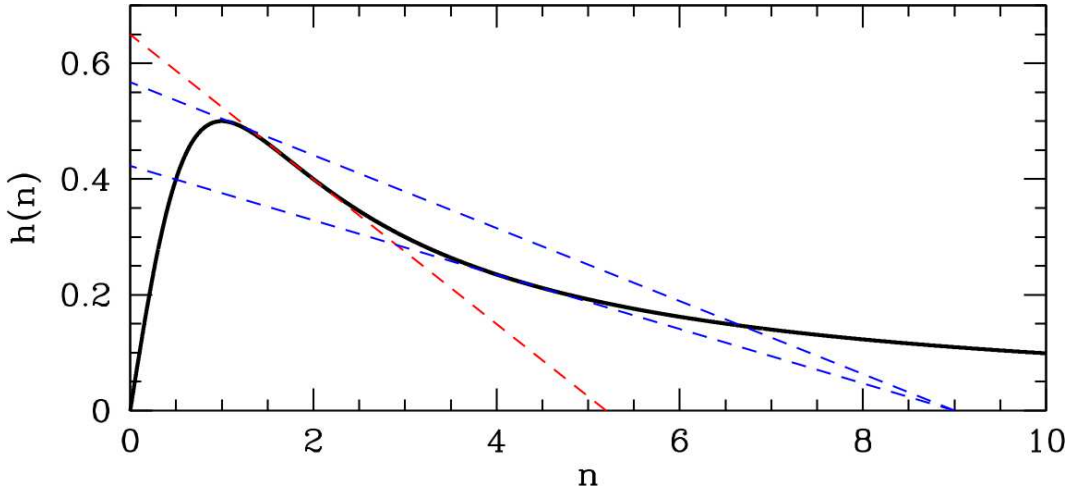


Figure 2.9: Plot of $h(n) = n/(n^2+1)$ (thick black curve). Straight lines show the function $y(n) = \gamma(1 - \frac{n}{c})$ for different values of c and γ . The red line is tangent to the inflection point of $h(n)$ and determines the minimum value $c^* = 3\sqrt{3}$ for a bifurcation. The blue lines show the construction for determining the location of the two bifurcations for $c > c^*$ (in this case, $c = 9$). See the analysis in the text.

from which we glean $\tau = Bt/A$, $\gamma = rA/B$, and $c = K/A$.

(c) Show that for c sufficiently small that there is a unique asymptotic ($\tau \rightarrow \infty$) value for the (scaled) population n , for any given value of γ . Thus, there are no bifurcations as a function of the control parameter γ for c fixed and $c < c^*$.

(d) Show that for $c > c^*$, there are two bifurcations as a function of γ , and that for $\gamma_1^* < \gamma < \gamma_2^*$ the asymptotic solution is bistable, *i.e.* there are two stable values for $n(\tau \rightarrow \infty)$. Sketch the solution set ‘phase diagram’ in the (c, γ) plane. Hint: Sketch the functions $\gamma(1 - n/c)$ and $n/(n^2 + 1)$. The $n \neq 0$ fixed points are given by the intersections of these two curves. Determine the boundary of the bistable region in the (c, γ) plane parametrically in terms of n . Find c^* and $\gamma_1^*(c) = \gamma_2^*(c)$.

Solution (c) and (d) : We examine

$$\frac{dn}{d\tau} = g(n) = \left\{ \gamma \left(1 - \frac{n}{c} \right) - \frac{n}{n^2 + 1} \right\} n . \quad (2.22)$$

There is an unstable fixed point at $n = 0$, where $g'(0) = \gamma > 0$. The other fixed points occur when the term in the curly brackets vanishes. In fig. 2.9 we plot the function $h(n) \equiv n/(n^2 + 1)$ versus n . We seek the intersection of this function with a two-parameter family of straight lines, given by $y(n) = \gamma(1 - n/c)$. The n -intercept is c and the y -intercept is γ . Provided $c > c^*$ is large enough, there are two bifurcations as a function of γ , which we call $\gamma_{\pm}(c)$. These are shown as the dashed blue lines in figure 2.9 for $c = 9$.

Both bifurcations are of the saddle-node type. We determine the curves $\gamma_{\pm}(c)$ by requiring that $h(n)$ is

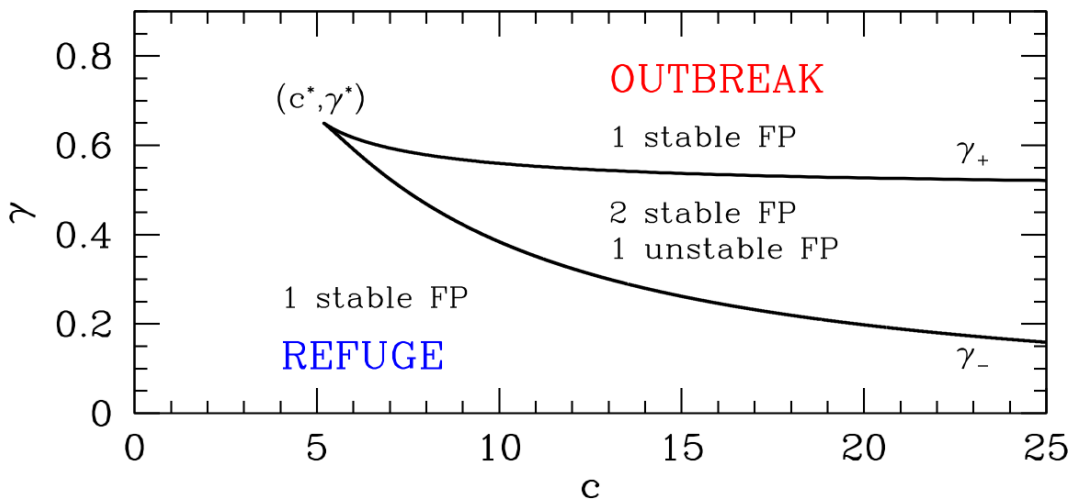


Figure 2.10: Phase diagram for the equation $\dot{n} = \gamma(1 - n/c)n - n^2/(n^2 + 1)$, labeling $n \neq 0$ fixed points. (The point $n = 0$ is always unstable.)

tangent to $y(n)$, which gives two equations:

$$\begin{aligned} h(n) &= \frac{n}{n^2 + 1} = \gamma\left(1 - \frac{n}{c}\right) = y(n) \\ h'(n) &= \frac{1 - n^2}{(n^2 + 1)^2} = -\frac{\gamma}{c} = y'(n) . \end{aligned} \quad (2.23)$$

Together, these give $\gamma(c)$ parametrically, i.e. as $\gamma(n)$ and $c(n)$:

$$\gamma(n) = \frac{2n^3}{(n^2 + 1)^2} , \quad c(n) = \frac{2n^3}{(n^2 - 1)} . \quad (2.24)$$

Since $h(n)$ is maximized for $n = 1$, where $h(1) = \frac{1}{2}$, there is no bifurcation occurring at values $n < 1$. If we plot $\gamma(n)$ versus $c(n)$ over the allowed range of n , we obtain the phase diagram in fig. 2.10. The cusp occurs at (c^*, γ^*) , and is determined by the requirement that the two bifurcations coincide. This supplies a third condition, namely that $h'(n) = 0$, where

$$h''(n) = \frac{2n(n^2 - 3)}{(n^2 + 1)^3} . \quad (2.25)$$

Hence $n = \sqrt{3}$, which gives $c^* = 3\sqrt{3}$ and $\gamma^* = \frac{3\sqrt{3}}{8}$. For $c < c^*$, there are no bifurcations at any value of γ .

2.3 Appendix I : The Bletch

Problem: The bletch is a disgusting animal native to the Forest of Jkroo on the planet Barney. The bletch population obeys the equation

$$\frac{dN}{dt} = aN^2 - bN^3 , \quad (2.26)$$



Figure 2.11: Phase flow for the scaled bletch population, $\dot{n} = n^2 - n^3$.

where N is the number of blettes, and a and b are constants. (Blettes reproduce asexually, but only when another blette is watching. However, when there are three blettes around, they beat the @! !*\$&* out of each other.)

- (a) Sketch the phase flow for N . (Strange as the blette is, you can still rule out $N < 0$.) Identify and classify all fixed points.
- (b) The blette population is now *harvested* (they make nice shoes). To model this, we add an extra term to the dynamics:

$$\frac{dN}{dt} = -hN + aN^2 - bN^3 \quad , \quad (2.27)$$

where h is the harvesting rate. Show that the phase flow now depends crucially on h , in that there are two qualitatively different flows, depending on whether $h < h_c(a, b)$ or $h > h_c(a, b)$. Find the critical harvesting rate $h_c(a, b)$ and sketch the phase flows for the two different regimes.

- (c) In equilibrium, the rate at which blettes are harvested is $R = hN^*$, where N^* is the equilibrium blette population. Suppose we start with $h = 0$, in which case N^* is given by the value of N at the stable fixed point you found in part (a). Now let h be increased very slowly from zero. As h is increased, the equilibrium population changes. Sketch R versus h . What value of h achieves the biggest blette harvest? What is the corresponding value of R_{\max} ?

Solution:

- (a) Setting the RHS of eqn. 2.26 to zero suggests the rescaling

$$N = \frac{a}{b} n \quad , \quad t = \frac{b}{a^2} \tau \quad . \quad (2.28)$$

This results in

$$\frac{dn}{d\tau} = n^2 - n^3 \quad . \quad (2.29)$$

The point $n = 0$ is a (nonlinearly) repulsive fixed point, and $n = 1$, corresponding to $N = a/b$, is attractive. The flow is shown in fig. 2.11.

By the way, the dynamics can be integrated, using the method of partial fractions, to yield

$$\frac{1}{n_0} - \frac{1}{n} + \ln \left(\frac{n}{n_0} \cdot \frac{1-n_0}{1-n} \right) = \tau \quad . \quad (2.30)$$

(b) Upon rescaling, the harvested bletch dynamics obeys the equation

$$\frac{dn}{d\tau} = -\nu n + n^2 - n^3 \quad , \quad (2.31)$$

where $\nu = bh/a^2$ is the dimensionless harvesting rate. Setting the RHS to zero yields $n(n^2 - n + \nu) = 0$, with solutions $n^* = 0$ and

$$n_{\pm}^* = \frac{1}{2} \pm \sqrt{\frac{1}{4} - \nu} \quad . \quad (2.32)$$

At $\nu = \frac{1}{4}$ there is a saddle-node bifurcation, and for $\nu > \frac{1}{4}$ the only fixed point (for real n) is at $n^* = 0$ (stable) – the bletch population is then *overharvested*. For $\nu > \frac{1}{4}$, there are three solutions: a stable fixed point at $n^* = 0$, an unstable fixed point at $n^* = \frac{1}{2} - \sqrt{\frac{1}{4} - \nu}$, and a stable fixed point at $n^* = \frac{1}{2} + \sqrt{\frac{1}{4} - \nu}$. The critical harvesting rate is $\nu_c = \frac{1}{4}$, which means $h_c = a^2/4b$.

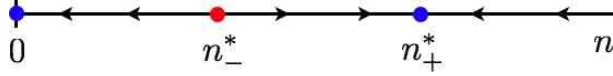


Figure 2.12: Phase flow for the harvested bletch population, $\dot{n} = -\nu n + n^2 - n^3$.

(c) The scaled bletch harvest is given by $r = \nu n_+^*(\nu)$. Note $R = h N_+^* = \frac{a^3}{b^2} r$. The optimal harvest occurs when νn^* is a maximum, which means we set

$$\frac{d}{d\nu} \left\{ \frac{1}{2}\nu + \nu \sqrt{\frac{1}{4} - \nu} \right\} = 0 \quad \Rightarrow \quad \nu_{\text{opt}} = \frac{2}{9} \quad . \quad (2.33)$$

Thus, $n_+^*(\nu_{\text{opt}}) = \frac{2}{3}$ and $r_{\text{opt}} = \frac{4}{27}$, meaning $R = 4a^3/27b^2$. Note that at $\nu = \nu_c = \frac{1}{4}$ that $n_+^*(\nu_c) = \frac{1}{2}$, hence $r(\nu_c) = \frac{1}{8}$, which is smaller than $(\nu_{\text{opt}}) = \frac{2}{9}$. The harvest $r(\nu)$ discontinuously drops to zero at $\nu = \nu_c$, since for $\nu > \nu_c$ the flow is to the only stable fixed point at $n^* = 0$.

2.4 Appendix II : Landau Theory of Phase Transitions

Landau's theory of phase transitions is based on an expansion of the free energy of a thermodynamic system in terms of an *order parameter*, which is nonzero in an ordered phase and zero in a disordered phase. For example, the magnetization M of a ferromagnet in zero external field but at finite temperature typically vanishes for temperatures $T > T_c$, where T_c is the *critical temperature*, also called the *Curie temperature* in a ferromagnet. A low order expansion in powers of the order parameter is appropriate sufficiently close to T_c , i.e. at temperatures such that the order parameter, if nonzero, is still small.

The simplest example is the quartic free energy,

$$f(m) = f_0 + \frac{1}{2}am^2 + \frac{1}{4}bm^4 \quad , \quad (2.34)$$

where m is a dimensionless measure of the magnetization density, and where f_0 , a , and b are all functions of the dimensionless temperature θ , which in a ferromagnet is the ratio $\theta = k_B T / \mathcal{J}$, where $\mathcal{J} = \sum_j J_{ij}$

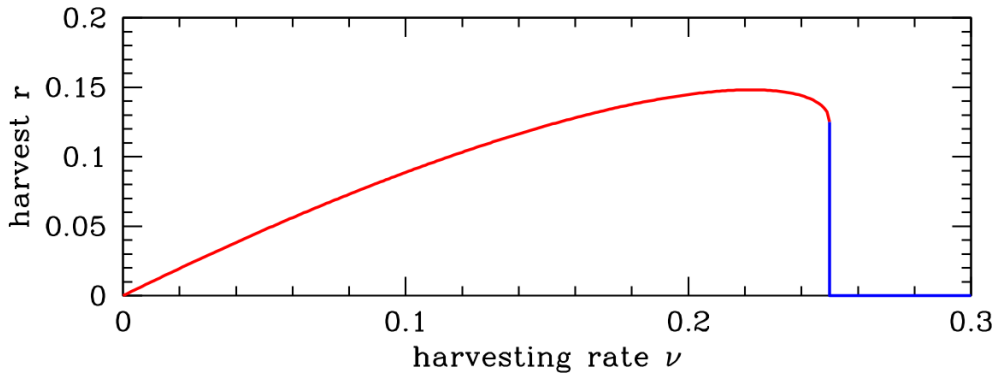


Figure 2.13: Scaled bletch harvest r versus scaled harvesting rate ν . Optimal harvesting occurs for $\nu_{\text{opt}} = \frac{2}{9}$. The critical harvesting rate is $\nu_c = \frac{1}{4}$, at which point the harvest discontinuously drops to zero.

is a sum over the couplings. Let us assume $b > 0$, which is necessary if the free energy is to be bounded from below². The equation of state ,

$$\frac{\partial f}{\partial m} = 0 = am + bm^3 \quad , \quad (2.35)$$

has three solutions in the complex m plane: (i) $m = 0$, (ii) $m = \sqrt{-a/b}$, and (iii) $m = -\sqrt{-a/b}$. The latter two solutions lie along the (physical) real axis if $a < 0$. We assume that $a(\theta)$ is monotonically increasing, and that there exists a unique temperature θ_c where $a(\theta_c) = 0$. Minimizing f , we find

$$\begin{aligned} \theta < \theta_c &: f = f_0 - \frac{a^2}{4b} \\ \theta > \theta_c &: f = f_0 \quad . \end{aligned} \quad (2.36)$$

The free energy is continuous at θ_c since $a(\theta_c) = 0$. The specific heat, however, is discontinuous across the transition, with

$$c(\theta_c^+) - c(\theta_c^-) = -\theta_c \left. \frac{\partial^2 f}{\partial \theta^2} \right|_{\theta=\theta_c} \left(\frac{a^2}{4b} \right) = -\frac{\theta_c [a'(\theta_c)]^2}{2b(\theta_c)} \quad . \quad (2.37)$$

The presence of a magnetic field h breaks the \mathbb{Z}_2 symmetry of $m \rightarrow -m$. The free energy becomes

$$f(m) = f_0 + \frac{1}{2}am^2 + \frac{1}{4}bm^4 - hm \quad , \quad (2.38)$$

and the mean field equation is

$$bm^3 + am - h = 0 \quad . \quad (2.39)$$

This is a cubic equation for m with real coefficients, and as such it can either have three real solutions or one real solution and two complex solutions related by complex conjugation. Clearly we must have $a < 0$ in order to have three real roots, since $bm^3 + am$ is monotonically increasing otherwise. The

²It is always the case that f is bounded from below, on physical grounds. Were b negative, we'd have to consider higher order terms in the Landau expansion.

boundary between these two classes of solution sets occurs when two roots coincide, which means $f''(m) = 0$ as well as $f'(m) = 0$. Simultaneously solving these two equations, we find

$$h^*(a) = \pm \frac{2}{3^{3/2}} \frac{(-a)^{3/2}}{b^{1/2}} , \quad (2.40)$$

or, equivalently,

$$a^*(h) = -\frac{3}{2^{2/3}} b^{1/3} |h|^{2/3}. \quad (2.41)$$

If, for fixed h , we have $a < a^*(h)$, then there will be three real solutions to the mean field equation $f'(m) = 0$, one of which is a global minimum (the one for which $m \cdot h > 0$). For $a > a^*(h)$ there is only a single global minimum, at which m also has the same sign as h . If we solve the mean field equation perturbatively in h/a , we find

$$\begin{aligned} m(a, h) &= \frac{h}{a} - \frac{b h^3}{a^4} + \mathcal{O}(h^5) & (a > 0) \\ &= \frac{h}{2|a|} - \frac{3 b^{1/2} h^2}{8|a|^{5/2}} + \mathcal{O}(h^3) & (a < 0) \end{aligned} . \quad (2.42)$$

2.4.1 Landau coefficients from mean field theory

A simple variational density matrix for the Ising ferromagnet yields the dimensionless free energy density

$$f(m, h, \theta) = -\frac{1}{2} m^2 - hm + \theta \left\{ \left(\frac{1+m}{2}\right) \ln \left(\frac{1+m}{2}\right) + \left(\frac{1-m}{2}\right) \ln \left(\frac{1-m}{2}\right) \right\} . \quad (2.43)$$

When m is small, it is appropriate to expand $f(m, h, \theta)$, obtaining

$$f(m, h, \theta) = -\theta \ln 2 - hm + \frac{1}{2}(\theta - 1)m^2 + \frac{\theta}{12}m^4 + \frac{\theta}{30}m^6 + \frac{\theta}{56}m^8 + \dots . \quad (2.44)$$

Thus, we identify

$$a(\theta) = \theta - 1 , \quad b(\theta) = \frac{1}{3}\theta . \quad (2.45)$$

We see that $a(\theta) = 0$ at a critical temperature $\theta_c = 1$.

The free energy of eqn. 2.43 behaves qualitatively just like it does for the simple Landau expansion, where one stops at order m^4 . Consider without loss of generality the case $h > 0$. The minimum of the free energy $f(m, h, \theta)$ then lies at $m > 0$ for any θ . At low temperatures, the double well structure we found in the $h = 0$ case is tilted so that the right well lies lower in energy than the left well. This is depicted in fig. 2.15. As the temperature is raised, the local minimum at $m < 0$ vanishes, annihilating with the local maximum in a saddle-node bifurcation. To find where this happens, one sets $\frac{\partial f}{\partial m} = 0$ and $\frac{\partial^2 f}{\partial m^2} = 0$ simultaneously, resulting in

$$h^*(\theta) = \sqrt{1-\theta} - \frac{\theta}{2} \ln \left(\frac{1+\sqrt{1-\theta}}{1-\sqrt{1-\theta}} \right) . \quad (2.46)$$

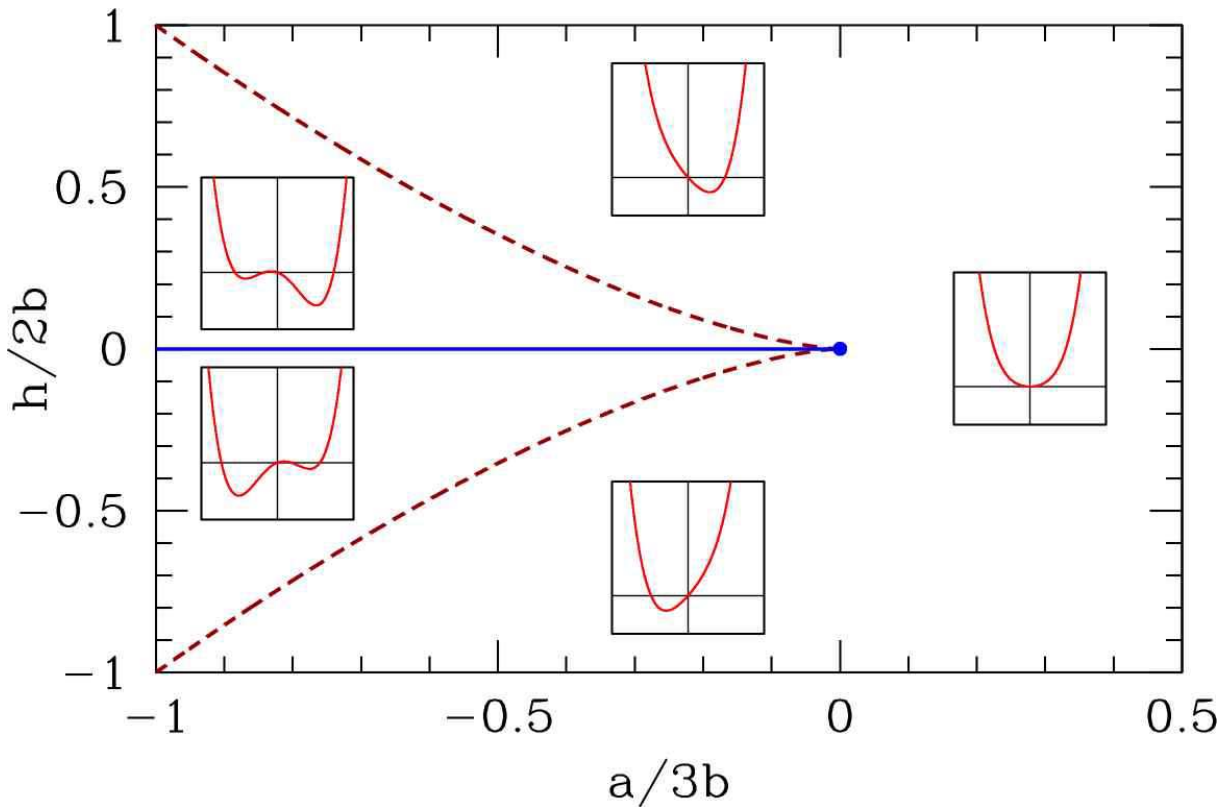


Figure 2.14: Phase diagram for the quartic mean field theory $f = f_0 + \frac{1}{2}am^2 + \frac{1}{4}bm^4 - hm$, with $b > 0$. There is a first order line at $h = 0$ extending from $a = -\infty$ and terminating in a critical point at $a = 0$. For $|h| < h^*(a)$ (dashed red line) there are three solutions to the mean field equation, corresponding to one global minimum, one local minimum, and one local maximum. Insets show behavior of the free energy $f(m)$.

The solutions lie at $h = \pm h^*(\theta)$. For $\theta < \theta_c = 1$ and $h \in [-h^*(\theta), +h^*(\theta)]$, there are three solutions to the mean field equation. Equivalently we could in principle invert the above expression to obtain $\theta^*(h)$. For $\theta > \theta^*(h)$, there is only a single global minimum in the free energy $f(m)$ and there is no local minimum. Note $\theta^*(h=0) = 1$.

2.4.2 Magnetization dynamics

Dissipative processes drive physical systems to minimum energy states. We can crudely model the dissipative dynamics of a magnet by writing the phenomenological equation

$$\frac{dm}{dt} = -\Gamma \frac{\partial f}{\partial m} . \quad (2.47)$$

This drives the free energy f to smaller and smaller values:

$$\frac{df}{dt} = \frac{\partial f}{\partial m} \frac{dm}{dt} = -\Gamma \left(\frac{\partial f}{\partial m} \right)^2 \leq 0 . \quad (2.48)$$

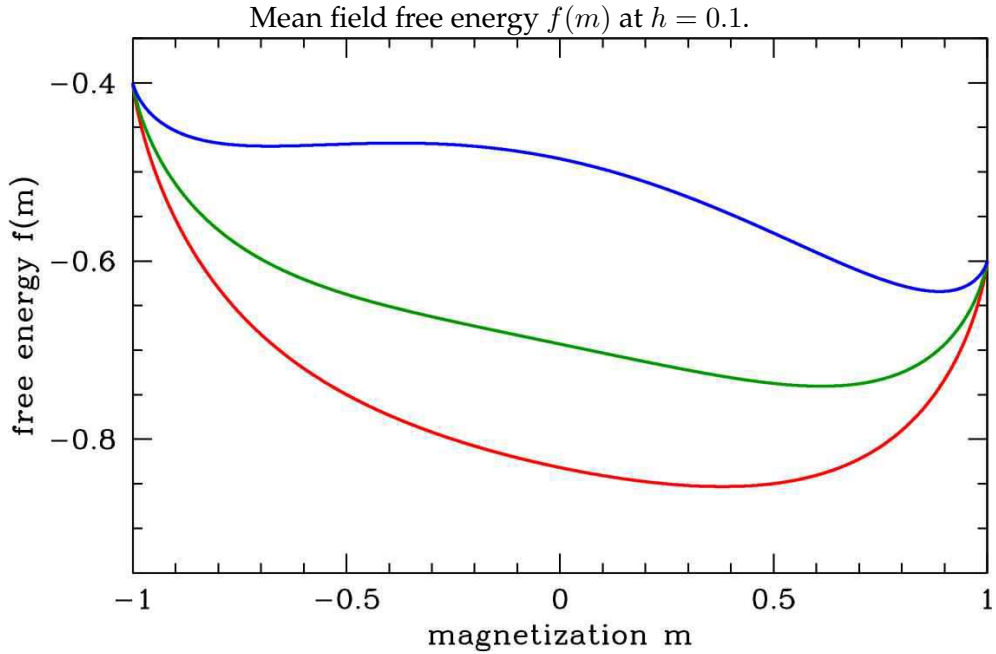


Figure 2.15: Mean field free energy $f(m)$ at $h = 0.1$. Temperatures shown: $\theta = 1.2$ (red), $\theta = 1.0$ (dark green), and $\theta = 0.7$ (blue).

Clearly the *fixed point* of these dynamics, where $\dot{m} = 0$, is a solution to the mean field equation $\frac{\partial f}{\partial m} = 0$. At the solution to the mean field equation, one has

$$\frac{\partial f}{\partial m} = 0 \quad \Rightarrow \quad m = \tanh\left(\frac{m + h}{\theta}\right) . \quad (2.49)$$

The phase flow for the equation $\dot{m} = -\Gamma f'(m)$ is shown in fig. 2.16. As we have seen, for any value of h there is a temperature θ^* below which the free energy $f(m)$ has two local minima and one local maximum. When $h = 0$ the minima are degenerate, but at finite h one of the minima is a global minimum. Thus, for $\theta < \theta^*(h)$ there are three solutions to the mean field equations. In the language of dynamical systems, under the dynamics of eqn. 2.47, minima of $f(m)$ correspond to attractive fixed points and maxima to repulsive fixed points. If $h > 0$, the rightmost of these fixed points corresponds to the global minimum of the free energy. As θ is increased, this fixed point evolves smoothly. At $\theta = \theta^*$, the (metastable) local minimum and the local maximum coalesce and annihilate in a saddle-node bifurcation. However at $h = 0$ all three fixed points coalesce at $\theta = \theta_c$ and the bifurcation is a supercritical pitchfork. As a function of t at finite h , the dynamics are said to exhibit an *imperfect bifurcation*, which is a deformed supercritical pitchfork.

The solution set for the mean field equation is simply expressed by inverting the tanh function to obtain $h(\theta, m)$. One readily finds

$$h(\theta, m) = \frac{\theta}{2} \ln\left(\frac{1+m}{1-m}\right) - m . \quad (2.50)$$

As we see in the bottom panel of fig. 2.17, $m(h)$ becomes multivalued for field values $h \in [-h^*(\theta), +h^*(\theta)]$, where $h^*(\theta)$ is given in eqn. 2.46. Now imagine that $\theta < \theta_c$ and we slowly ramp the field h from a large

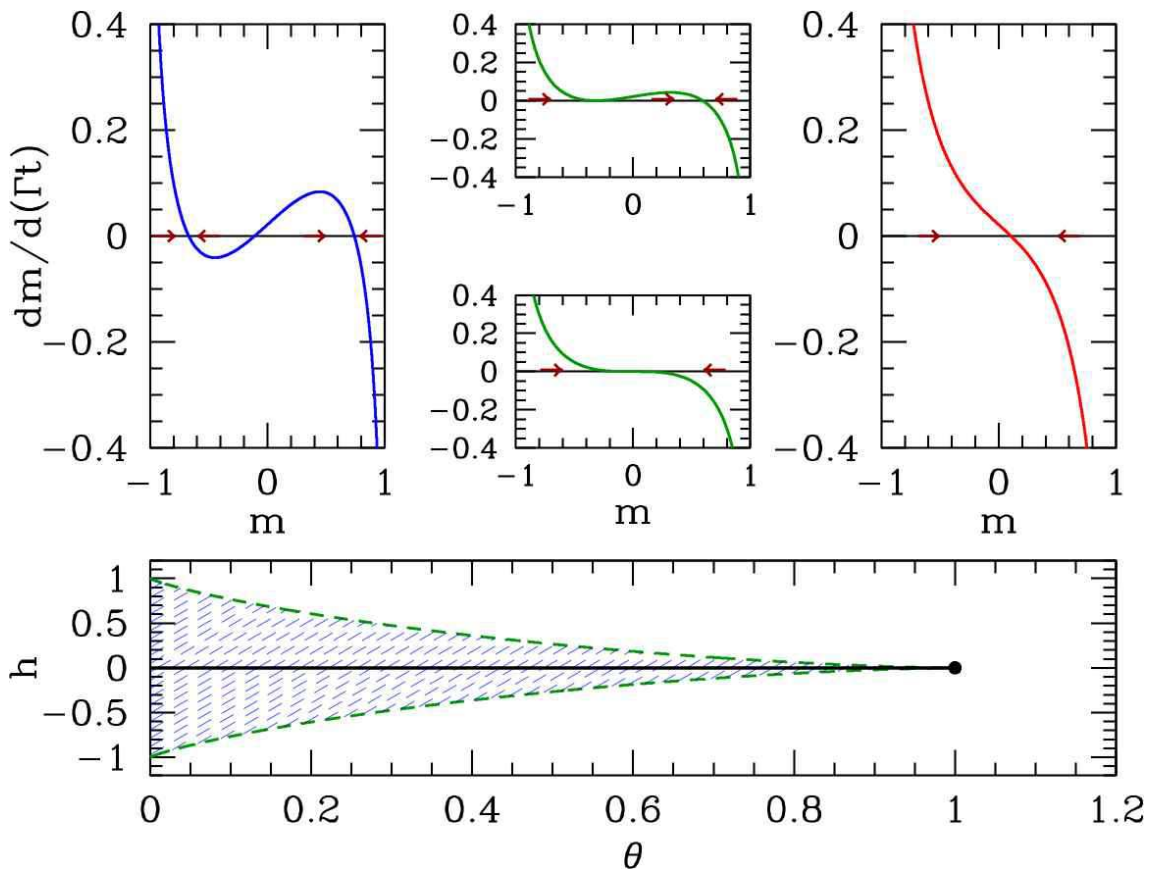


Figure 2.16: Dissipative magnetization dynamics $\dot{m} = -f'(m)$. Bottom panel shows $h^*(\theta)$ from eqn. 2.46. For (θ, h) within the blue shaded region, the free energy $f(m)$ has a global minimum plus a local minimum and a local maximum. Otherwise $f(m)$ has only a single global maximum. Top panels show an imperfect bifurcation in the magnetization dynamics at $h = 0.0215$, for which $\theta^* = 0.90$. Temperatures shown: $\theta = 0.80$ (blue), $\theta = \theta^*(h) = 0.90$ (green), and $\theta = 1.2$. The rightmost stable fixed point corresponds to the global minimum of the free energy. The bottom of the middle two upper panels shows $h = 0$, where both of the attractive fixed points and the repulsive fixed point coalesce into a single attractive fixed point (supercritical pitchfork bifurcation).

negative value to a large positive value, and then slowly back down to its original value. On the time scale of the magnetization dynamics, we can regard $h(t)$ as a constant. Thus, $m(t)$ will flow to the nearest stable fixed point. Initially the system starts with $m = -1$ and h large and negative, and there is only one fixed point, at $m^* \approx -1$. As h slowly increases, the fixed point value m^* also slowly increases. As h exceeds $-h^*(\theta)$, a saddle-node bifurcation occurs, and two new fixed points are created at positive m , one stable and one unstable. The global minimum of the free energy still lies at the fixed point with $m^* < 0$. However, when h crosses $h = 0$, the global minimum of the free energy lies at the most positive fixed point m^* . The dynamics, however, keep the system stuck in what is a metastable phase. This persists until $h = +h^*(\theta)$, at which point another saddle-node bifurcation occurs, and the attractive fixed point at $m^* < 0$ annihilates with the repulsive fixed point. The dynamics then act quickly to drive m to the only remaining fixed point. This process is depicted in the top panel of fig. 2.17. As one can

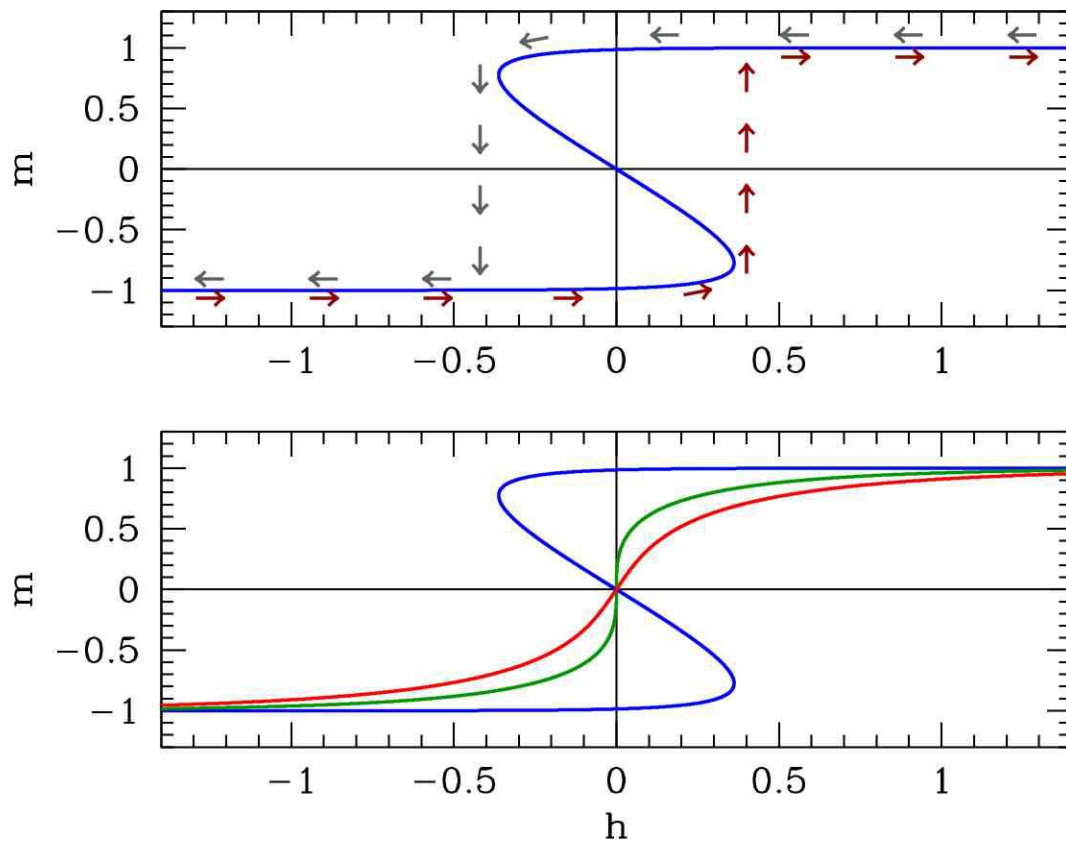


Figure 2.17: Top panel : hysteresis as a function of ramping the dimensionless magnetic field h at $\theta = 0.40$. Dark red arrows below the curve follow evolution of the magnetization on slow increase of h . Dark grey arrows above the curve follow evolution of the magnetization on slow decrease of h . Bottom panel : solution set for $m(\theta, h)$ as a function of h at temperatures $\theta = 0.40$ (blue), $\theta = \theta_c = 1.0$ (dark green), and $t = 1.25$ (red).

see from the figure, the system follows a stable fixed point until the fixed point disappears, even though that fixed point may not always correspond to a global minimum of the free energy. The resulting $m(h)$ curve is then not reversible as a function of time, and it possesses a characteristic shape known as a *hysteresis loop*. Etymologically, the word *hysteresis* derives from the Greek *υστερησις*, which means ‘lagging behind’. Systems which are hysteretic exhibit a *history-dependence* to their status, which is not uniquely determined by external conditions. Hysteresis may be exhibited with respect to changes in applied magnetic field, changes in temperature, or changes in other externally determined parameters.

2.4.3 Cubic terms in Landau theory : first order transitions

Next, consider a free energy with a cubic term,

$$f = f_0 + \frac{1}{2}am^2 - \frac{1}{3}ym^3 + \frac{1}{4}bm^4 , \quad (2.51)$$

with $b > 0$ for stability. Without loss of generality, we may assume $y > 0$ (else send $m \rightarrow -m$). Note that we no longer have $m \rightarrow -m$ (*i.e.* \mathbb{Z}_2) symmetry. The cubic term favors positive m . What is the phase diagram in the (a, y) plane?

Extremizing the free energy with respect to m , we obtain

$$\frac{\partial f}{\partial m} = 0 = am - ym^2 + bm^3 \quad . \quad (2.52)$$

This cubic equation factorizes into a linear and quadratic piece, and hence may be solved simply. The three solutions are $m = 0$ and

$$m = m_{\pm} \equiv \frac{y}{2b} \pm \sqrt{\left(\frac{y}{2b}\right)^2 - \frac{a}{b}} \quad . \quad (2.53)$$

We now see that for $y^2 < 4ab$ there is only one real solution, at $m = 0$, while for $y^2 > 4ab$ there are three real solutions. Which solution has lowest free energy? To find out, we compare the energy $f(0)$ with $f(m_+)$ ³. Thus, we set

$$f(m) = f(0) \implies \frac{1}{2}am^2 - \frac{1}{3}ym^3 + \frac{1}{4}bm^4 = 0 \quad , \quad (2.54)$$

and we now have two quadratic equations to solve simultaneously:

$$\begin{aligned} 0 &= a - ym + bm^2 \\ 0 &= \frac{1}{2}a - \frac{1}{3}ym + \frac{1}{4}bm^2 = 0 \quad . \end{aligned} \quad (2.55)$$

Eliminating the quadratic term gives $m = 3a/y$. Finally, substituting $m = m_+$ gives us a relation between a , b , and y :

$$y^2 = \frac{9}{2}ab \quad . \quad (2.56)$$

Thus, we have the following:

$$\begin{aligned} a > \frac{y^2}{4b} &: 1 \text{ real root } m = 0 \\ \frac{y^2}{4b} > a > \frac{2y^2}{9b} &: 3 \text{ real roots; minimum at } m = 0 \\ \frac{2y^2}{9b} > a &: 3 \text{ real roots; minimum at } m = \frac{y}{2b} + \sqrt{\left(\frac{y}{2b}\right)^2 - \frac{a}{b}} \end{aligned} \quad (2.57)$$

The solution $m = 0$ lies at a local minimum of the free energy for $a > 0$ and at a local maximum for $a < 0$. Over the range $\frac{y^2}{4b} > a > \frac{2y^2}{9b}$, then, there is a global minimum at $m = 0$, a local minimum at $m = m_+$, and a local maximum at $m = m_-$, with $m_+ > m_- > 0$. For $\frac{2y^2}{9b} > a > 0$, there is a local minimum at $a = 0$, a global minimum at $m = m_+$, and a local maximum at $m = m_-$, again with $m_+ > m_- > 0$. For $a < 0$, there is a local maximum at $m = 0$, a local minimum at $m = m_-$, and a global minimum at $m = m_+$, with $m_+ > 0 > m_-$. See fig. 2.18.

³We needn't waste our time considering the $m = m_-$ solution, since the cubic term prefers positive m .

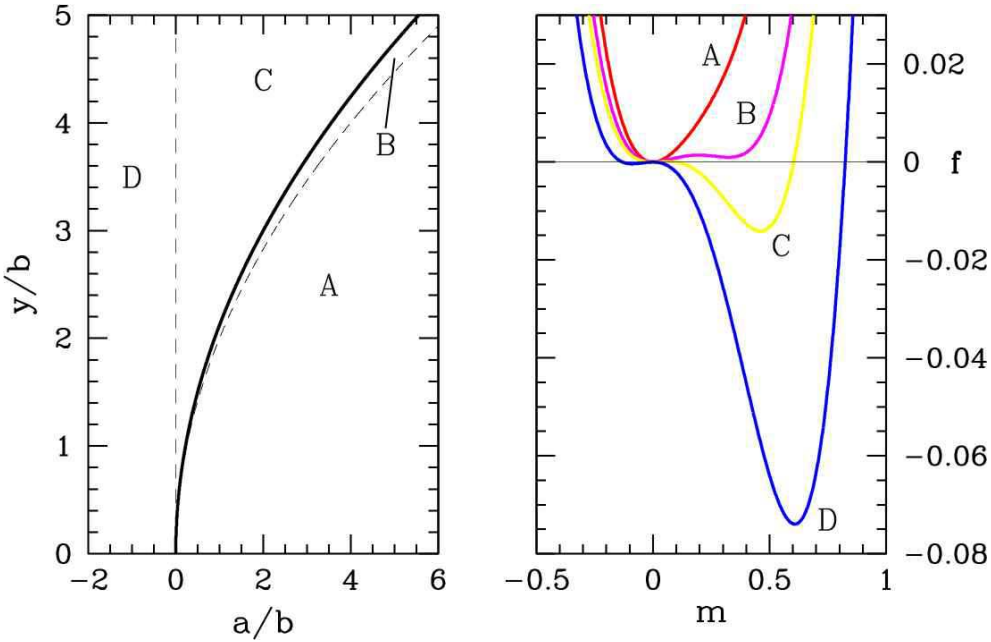


Figure 2.18: Behavior of the quartic free energy $f(m) = \frac{1}{2}am^2 - \frac{1}{3}ym^3 + \frac{1}{4}bm^4$. A: $y^2 < 4ab$; B: $4ab < y^2 < \frac{9}{2}ab$; C and D: $y^2 > \frac{9}{2}ab$. The thick black line denotes a line of first order transitions, where the order parameter is discontinuous across the transition.

2.4.4 Magnetization dynamics

Suppose we now impose some dynamics on the system, of the simple relaxational type

$$\frac{dm}{dt} = -\Gamma \frac{\partial f}{\partial m} , \quad (2.58)$$

where Γ is a phenomenological kinetic coefficient. Assuming $y > 0$ and $b > 0$, it is convenient to adimensionalize by writing

$$m \equiv \frac{y}{b} \cdot u \quad , \quad a \equiv \frac{y^2}{b} \cdot \bar{r} \quad , \quad t \equiv \frac{b}{\Gamma y^2} \cdot s \quad . \quad (2.59)$$

Then we obtain

$$\frac{\partial u}{\partial s} = -\frac{\partial \varphi}{\partial u} \quad , \quad (2.60)$$

where the dimensionless free energy function is

$$\varphi(u) = \frac{1}{2}\bar{r}u^2 - \frac{1}{3}u^3 + \frac{1}{4}u^4 \quad . \quad (2.61)$$

We see that there is a single control parameter, \bar{r} . The fixed points of the dynamics are then the stationary points of $\varphi(u)$, where $\varphi'(u) = 0$, with

$$\varphi'(u) = u(\bar{r} - u + u^2) \quad . \quad (2.62)$$

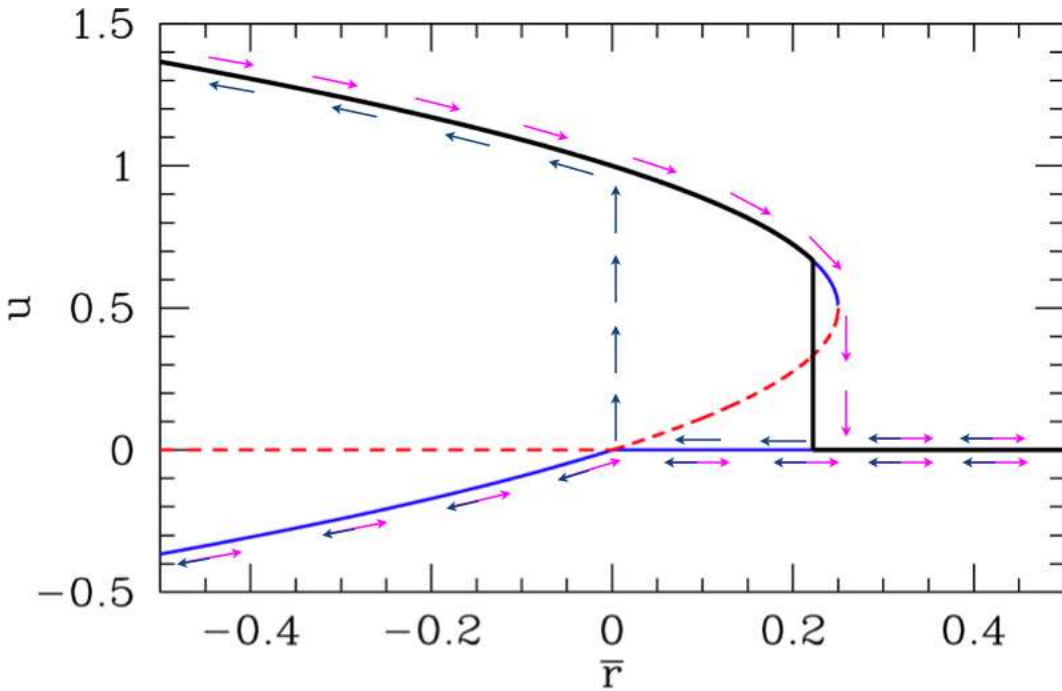


Figure 2.19: Fixed points for $\varphi(u) = \frac{1}{2}\bar{r}u^2 - \frac{1}{3}u^3 + \frac{1}{4}u^4$ and flow under the dynamics $\dot{u} = -\varphi'(u)$. Solid curves represent stable fixed points and dashed curves unstable fixed points. Magenta arrows show behavior under slowly increasing control parameter \bar{r} and dark blue arrows show behavior under slowly decreasing \bar{r} . For $u > 0$ there is a hysteresis loop. The thick black curve shows the equilibrium thermodynamic value of $u(\bar{r})$, i.e. that value which minimizes the free energy $\varphi(u)$. There is a first order phase transition at $\bar{r} = \frac{2}{9}$, where the thermodynamic value of u jumps from $u = 0$ to $u = \frac{2}{3}$.

The solutions to $\varphi'(u) = 0$ are then given by

$$u^* = 0 \quad , \quad u^* = \frac{1}{2} \pm \sqrt{\frac{1}{4} - \bar{r}} \quad . \quad (2.63)$$

For $r > \frac{1}{4}$ there is one fixed point at $u = 0$, which is attractive under the dynamics $\dot{u} = -\varphi'(u)$ since $\varphi''(0) = \bar{r}$. At $\bar{r} = \frac{1}{4}$ there occurs a saddle-node bifurcation and a pair of fixed points is generated, one stable and one unstable. As we see from fig. 2.14, the interior fixed point is always unstable and the two exterior fixed points are always stable. At $r = 0$ there is a transcritical bifurcation where two fixed points of opposite stability collide and bounce off one another (metaphorically speaking).

At the saddle-node bifurcation, $\bar{r} = \frac{1}{4}$ and $u = \frac{1}{2}$, and we find $\varphi(u = \frac{1}{2}; \bar{r} = \frac{1}{4}) = \frac{1}{192}$, which is positive. Thus, the thermodynamic state of the system remains at $u = 0$ until the value of $\varphi(u_+)$ crosses zero. This occurs when $\varphi(u) = 0$ and $\varphi'(u) = 0$, the simultaneous solution of which yields $\bar{r} = \frac{2}{9}$ and $u = \frac{2}{3}$.

Suppose we slowly ramp the control parameter \bar{r} up and down as a function of the dimensionless time s . Under the dynamics of eqn. 2.60, $u(s)$ flows to the first stable fixed point encountered – this is always the case for a dynamical system with a one-dimensional phase space. Then as \bar{r} is further varied, u follows the position of whatever locally stable fixed point it initially encountered. Thus, $u(\bar{r}(s))$ evolves smoothly until a bifurcation is encountered. The situation is depicted by the arrows in fig. 2.19. The

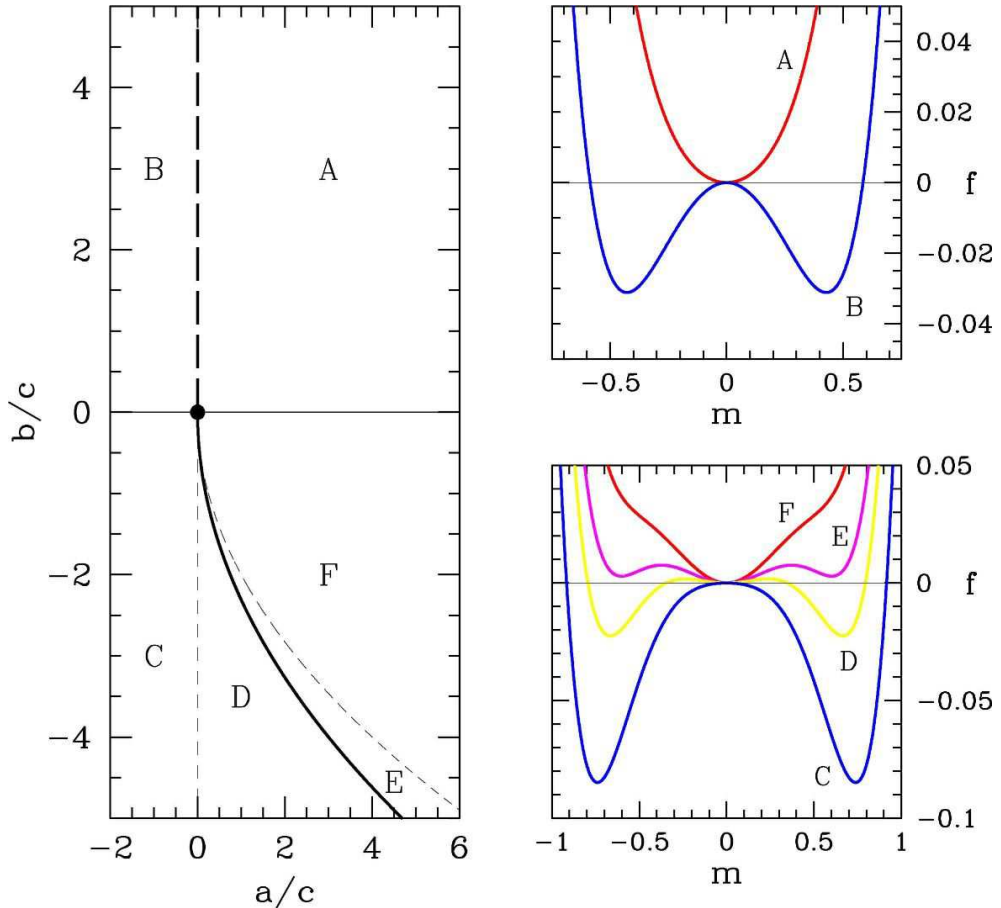


Figure 2.20: Behavior of the sextic free energy $f(m) = \frac{1}{2}am^2 + \frac{1}{4}bm^4 + \frac{1}{6}cm^6$. A: $a > 0$ and $b > 0$; B: $a < 0$ and $b > 0$; C: $a < 0$ and $b < 0$; D: $a > 0$ and $b < -\frac{4}{\sqrt{3}}\sqrt{ac}$; E: $a > 0$ and $-\frac{4}{\sqrt{3}}\sqrt{ac} < b < -2\sqrt{ac}$; F: $a > 0$ and $-2\sqrt{ac} < b < 0$. The thick dashed line is a line of second order transitions, which meets the thick solid line of first order transitions at the tricritical point, $(a, b) = (0, 0)$.

equilibrium thermodynamic value for $u(\bar{r})$ is discontinuous; there is a first order phase transition at $\bar{r} = \frac{2}{9}$, as we've already seen. As r is increased, $u(\bar{r})$ follows a trajectory indicated by the magenta arrows. For an negative initial value of u , the evolution as a function of \bar{r} will be *reversible*. However, if $u(0)$ is initially positive, then the system exhibits *hysteresis*, as shown. Starting with a large positive value of \bar{r} , $u(s)$ quickly evolves to $u = 0^+$, which means a positive infinitesimal value. Then as r is decreased, the system remains at $u = 0^+$ even through the first order transition, because $u = 0$ is an attractive fixed point. However, once r begins to go negative, the $u = 0$ fixed point becomes repulsive, and $u(s)$ quickly flows to the stable fixed point $u_+ = \frac{1}{2} + \sqrt{\frac{1}{4} - \bar{r}}$. Further decreasing r , the system remains on this branch. If \bar{r} is later increased, then $u(s)$ remains on the upper branch past $r = 0$, until the u_+ fixed point annihilates with the unstable fixed point at $u_- = \frac{1}{2} - \sqrt{\frac{1}{4} - \bar{r}}$, at which time $u(s)$ quickly flows down to $u = 0^+$ again.

2.4.5 Sixth order Landau theory : tricritical point

Finally, consider a model with \mathbb{Z}_2 symmetry, with the Landau free energy

$$f = f_0 + \frac{1}{2}am^2 + \frac{1}{4}bm^4 + \frac{1}{6}cm^6 , \quad (2.64)$$

with $c > 0$ for stability. We seek the phase diagram in the (a, b) plane. Extremizing f with respect to m , we obtain

$$\frac{\partial f}{\partial m} = 0 = m(a + bm^2 + cm^4) , \quad (2.65)$$

which is a quintic with five solutions over the complex m plane. One solution is obviously $m = 0$. The other four are

$$m = \pm \sqrt{-\frac{b}{2c} \pm \sqrt{\left(\frac{b}{2c}\right)^2 - \frac{a}{c}}} . \quad (2.66)$$

For each \pm symbol in the above equation, there are two options, hence four roots in all.

If $a > 0$ and $b > 0$, then four of the roots are imaginary and there is a unique minimum at $m = 0$.

For $a < 0$, there are only three solutions to $f'(m) = 0$ for real m , since the $-$ choice for the \pm sign under the radical leads to imaginary roots. One of the solutions is $m = 0$. The other two are

$$m = \pm \sqrt{-\frac{b}{2c} + \sqrt{\left(\frac{b}{2c}\right)^2 - \frac{a}{c}}} . \quad (2.67)$$

The most interesting situation is $a > 0$ and $b < 0$. If $a > 0$ and $b < -2\sqrt{ac}$, all five roots are real. There must be three minima, separated by two local maxima. Clearly if m^* is a solution, then so is $-m^*$. Thus, the only question is whether the outer minima are of lower energy than the minimum at $m = 0$. We assess this by demanding $f(m^*) = f(0)$, where m^* is the position of the largest root (*i.e.* the rightmost minimum). This gives a second quadratic equation,

$$0 = \frac{1}{2}a + \frac{1}{4}bm^2 + \frac{1}{6}cm^4 , \quad (2.68)$$

which together with equation 2.65 gives

$$b = -\frac{4}{\sqrt{3}}\sqrt{ac} . \quad (2.69)$$

Thus, we have the following, for fixed $a > 0$:

$$\begin{aligned} b > -2\sqrt{ac} &: 1 \text{ real root } m = 0 \\ -2\sqrt{ac} > b > -\frac{4}{\sqrt{3}}\sqrt{ac} &: 5 \text{ real roots; minimum at } m = 0 \\ -\frac{4}{\sqrt{3}}\sqrt{ac} > b &: 5 \text{ real roots; minima at } m = \pm \sqrt{-\frac{b}{2c} + \sqrt{\left(\frac{b}{2c}\right)^2 - \frac{a}{c}}} \end{aligned} \quad (2.70)$$

The point $(a, b) = (0, 0)$, which lies at the confluence of a first order line and a second order line, is known as a *tricritical point*.

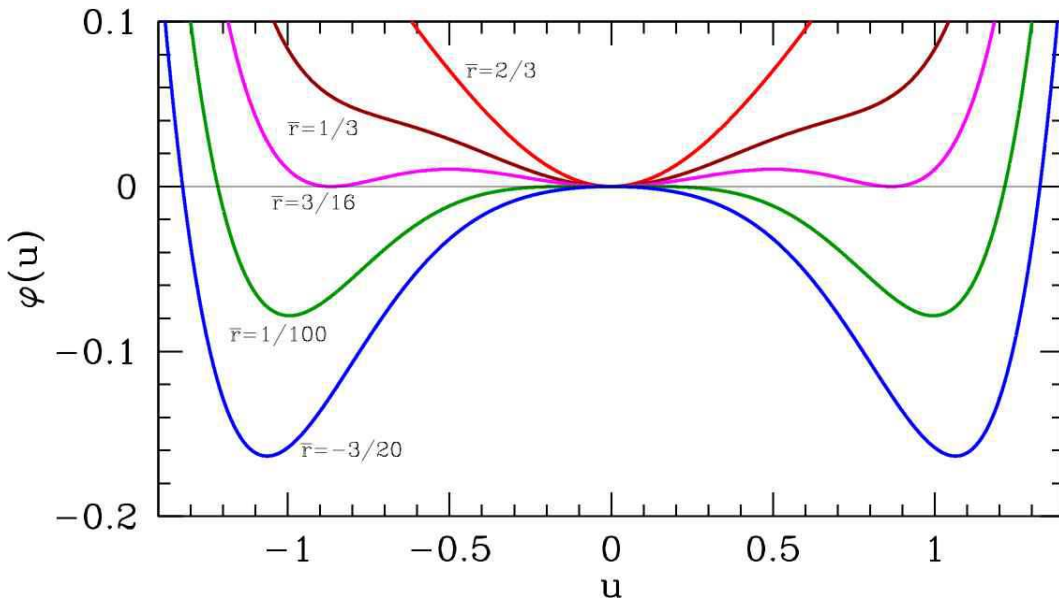


Figure 2.21: Free energy $\varphi(u) = \frac{1}{2}\bar{r}u^2 - \frac{1}{4}u^4 + \frac{1}{6}u^6$ for several different values of the control parameter \bar{r} .

2.4.6 Hysteresis for the sextic potential

Once again, we consider the dissipative dynamics $\dot{m} = -\Gamma f'(m)$. We adimensionalize by writing

$$m \equiv \sqrt{\frac{|b|}{c}} \cdot u \quad , \quad a \equiv \frac{b^2}{c} \cdot \bar{r} \quad , \quad t \equiv \frac{c}{\Gamma b^2} \cdot s \quad . \quad (2.71)$$

Then we obtain once again the dimensionless equation

$$\frac{\partial u}{\partial s} = -\frac{\partial \varphi}{\partial u} \quad , \quad (2.72)$$

where

$$\varphi(u) = \frac{1}{2}\bar{r}u^2 \pm \frac{1}{4}u^4 + \frac{1}{6}u^6 \quad . \quad (2.73)$$

In the above equation, the coefficient of the quartic term is positive if $b > 0$ and negative if $b < 0$. That is, the coefficient is $\text{sgn}(b)$. When $b > 0$ we can ignore the sextic term for sufficiently small u , and we recover the quartic free energy studied earlier. There is then a second order transition at $r = 0$.

New and interesting behavior occurs for $b > 0$. The fixed points of the dynamics are obtained by setting $\varphi'(u) = 0$. We have

$$\begin{aligned} \varphi(u) &= \frac{1}{2}\bar{r}u^2 - \frac{1}{4}u^4 + \frac{1}{6}u^6 \\ \varphi'(u) &= u(\bar{r} - u^2 + u^4) \quad . \end{aligned} \quad (2.74)$$

Thus, the equation $\varphi'(u) = 0$ factorizes into a linear factor u and a quartic factor $u^4 - u^2 + \bar{r}$ which is

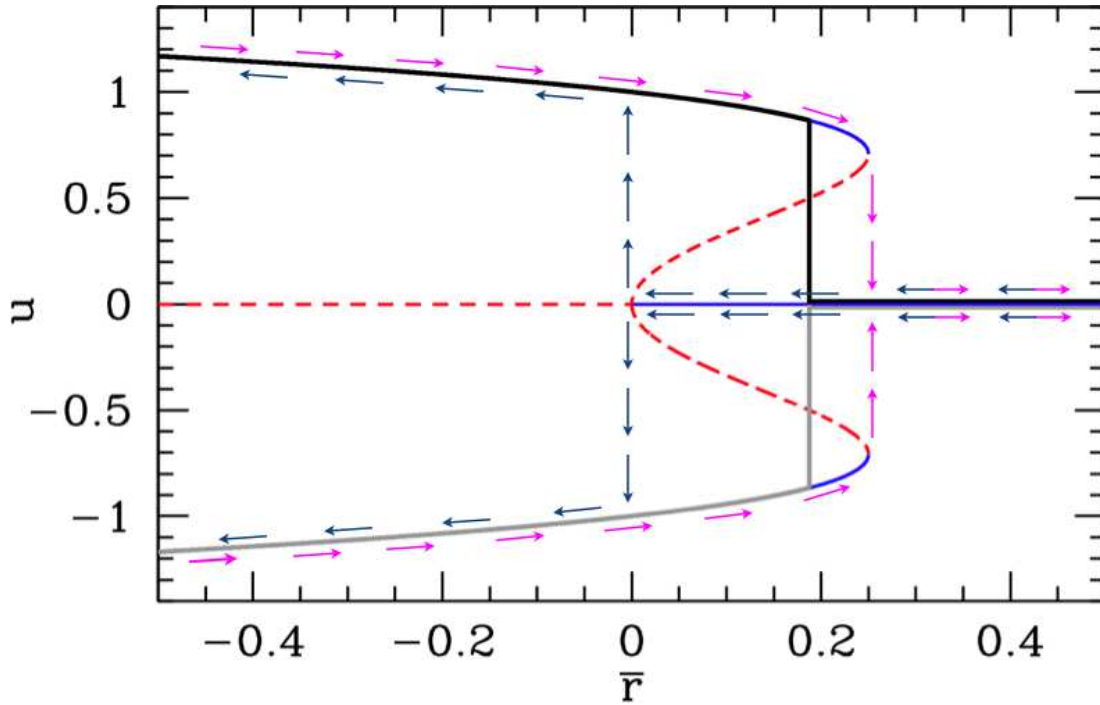


Figure 2.22: Fixed points $\varphi'(u^*) = 0$ for the sextic potential $\varphi(u) = \frac{1}{2}\bar{r}u^2 - \frac{1}{4}u^4 + \frac{1}{6}u^6$, and corresponding dynamical flow (arrows) under $\dot{u} = -\varphi'(u)$. Solid curves show stable fixed points and dashed curves show unstable fixed points. The thick solid black and solid grey curves indicate the equilibrium thermodynamic values for u ; note the overall $u \rightarrow -u$ symmetry. Within the region $\bar{r} \in [0, \frac{1}{4}]$ the dynamics are irreversible and the system exhibits the phenomenon of hysteresis. There is a first order phase transition at $\bar{r} = \frac{3}{16}$.

quadratic in u^2 . Thus, we can easily obtain the roots:

$$\begin{aligned} \bar{r} < 0 &: u^* = 0, u^* = \pm \sqrt{\frac{1}{2} + \sqrt{\frac{1}{4} - \bar{r}}} \\ 0 < \bar{r} < \frac{1}{4} &: u^* = 0, u^* = \pm \sqrt{\frac{1}{2} + \sqrt{\frac{1}{4} - \bar{r}}}, u^* = \pm \sqrt{\frac{1}{2} - \sqrt{\frac{1}{4} - \bar{r}}} \\ \bar{r} > \frac{1}{4} &: u^* = 0. \end{aligned} \quad (2.75)$$

In fig. 2.22, we plot the fixed points and the hysteresis loops for this system. At $\bar{r} = \frac{1}{4}$, there are two symmetrically located saddle-node bifurcations at $u = \pm \frac{1}{\sqrt{2}}$. We find $\varphi(u = \pm \frac{1}{\sqrt{2}}, \bar{r} = \frac{1}{4}) = \frac{1}{48}$, which is positive, indicating that the stable fixed point $u^* = 0$ remains the thermodynamic minimum for the free energy $\varphi(u)$ as \bar{r} is decreased through $\frac{1}{4}$. Setting $\varphi(u) = 0$ and $\varphi'(u) = 0$ simultaneously, we obtain $\bar{r} = \frac{3}{16}$ and $u = \pm \frac{\sqrt{3}}{2}$. The thermodynamic value for u therefore jumps discontinuously from $u = 0$ to $u = \pm \frac{\sqrt{3}}{2}$ (either branch) at $\bar{r} = \frac{3}{16}$; this is a first order transition.

Under the dissipative dynamics considered here, the system exhibits hysteresis, as indicated in the figure, where the arrows show the evolution of $u(s)$ for very slowly varying $\bar{r}(s)$. When the control param-

eter \bar{r} is large and positive, the flow is toward the sole fixed point at $u^* = 0$. At $\bar{r} = \frac{1}{4}$, two simultaneous saddle-node bifurcations take place at $u^* = \pm\frac{1}{\sqrt{2}}$; the outer branch is stable and the inner branch unstable in both cases. At $r = 0$ there is a subcritical pitchfork bifurcation, and the fixed point at $u^* = 0$ becomes unstable.

Suppose one starts off with $\bar{r} \gg \frac{1}{4}$ with some value $u > 0$. The flow $\dot{u} = -\varphi'(u)$ then rapidly results in $u \rightarrow 0^+$. This is the ‘high temperature phase’ in which there is no magnetization. Now let r increase slowly, using s as the dimensionless time variable. The scaled magnetization $u(s) = u^*(\bar{r}(s))$ will remain pinned at the fixed point $u^* = 0^+$. As \bar{r} passes through $\bar{r} = \frac{1}{4}$, two new stable values of u^* appear, but our system remains at $u = 0^+$, since $u^* = 0$ is a stable fixed point. But after the subcritical pitchfork, $u^* = 0$ becomes unstable. The magnetization $u(s)$ then flows rapidly to the stable fixed point at $u^* = \frac{1}{\sqrt{2}}$, and follows the curve $u^*(\bar{r}) = \left(\frac{1}{2} + (\frac{1}{4} - \bar{r})^{1/2}\right)^{1/2}$ for all $r < 0$.

Now suppose we start increasing r (*i.e.* increasing temperature). The magnetization follows the stable fixed point $u^*(\bar{r}) = \left(\frac{1}{2} + (\frac{1}{4} - \bar{r})^{1/2}\right)^{1/2}$ past $\bar{r} = 0$, beyond the first order phase transition point at $\bar{r} = \frac{3}{16}$, and all the way up to $\bar{r} = \frac{1}{4}$, at which point this fixed point is annihilated at a saddle-node bifurcation. The flow then rapidly takes $u \rightarrow u^* = 0^+$, where it remains as r continues to be increased further.

Within the region $\bar{r} \in [0, \frac{1}{4}]$ of control parameter space, the dynamics are said to be *irreversible* and the behavior of $u(s)$ is said to be *hysteretic*.

Chapter 3

Two-Dimensional Phase Flows

We've seen how, for one-dimensional dynamical systems $\dot{u} = f(u)$, the possibilities in terms of the behavior of the system are in fact quite limited. Starting from an arbitrary initial condition $u(0)$, the phase flow is monotonically toward the first stable fixed point encountered. (That point may lie at infinity.) No oscillations are possible¹. For $N = 2$ phase flows, a richer set of possibilities arises, as we shall now see.

3.1 Harmonic Oscillator and Pendulum

3.1.1 Simple harmonic oscillator

A one-dimensional harmonic oscillator obeys the equation of motion,

$$m \frac{d^2x}{dt^2} = -kx \quad , \tag{3.1}$$

where m is the mass and k the force constant (of a spring). If we define $v = \dot{x}$, this may be written as the $N = 2$ system,

$$\frac{d}{dt} \begin{pmatrix} x \\ v \end{pmatrix} = \begin{pmatrix} 0 & 1 \\ -\Omega^2 & 0 \end{pmatrix} \begin{pmatrix} x \\ v \end{pmatrix} = \begin{pmatrix} v \\ -\Omega^2 x \end{pmatrix} \quad , \tag{3.2}$$

where $\Omega = \sqrt{k/m}$ has the dimensions of frequency (inverse time). The solution is well known:

$$\begin{aligned} x(t) &= x_0 \cos(\Omega t) + \frac{v_0}{\Omega} \sin(\Omega t) \\ v(t) &= v_0 \cos(\Omega t) - \Omega x_0 \sin(\Omega t) \quad . \end{aligned} \tag{3.3}$$

The phase curves are ellipses:

$$\Omega x^2(t) + \Omega^{-1} v^2(t) = C \quad , \tag{3.4}$$

¹If phase space itself is multiply connected, e.g. a circle, then the system can oscillate by moving around the circle.

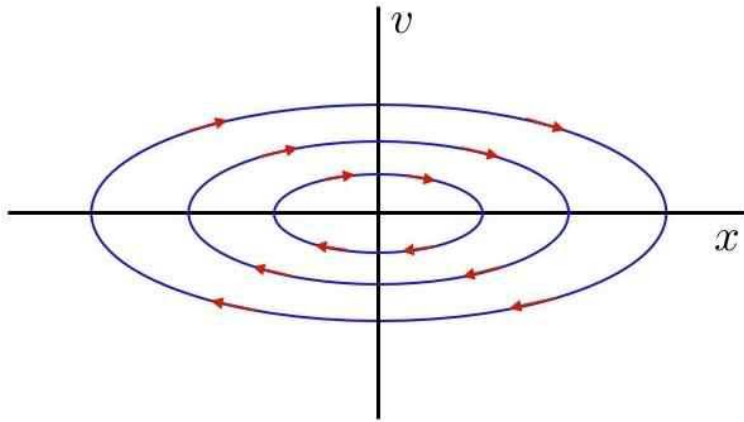


Figure 3.1: Phase curves for the harmonic oscillator.

where the constant $C = \Omega x_0^2 + \Omega^{-1} v_0^2$. A sketch of the phase curves and of the phase flow is shown in Fig. 3.1. Note that the x and v axes have different dimensions. Note also that the origin is a fixed point, however, unlike the $N = 1$ systems studied in the first lecture, here the phase flow can avoid the fixed points, and oscillations can occur.

Incidentally, eqn. 3.2 is linear, and may be solved by the following method. Write the equation as $\dot{\varphi} = M\varphi$, with

$$\varphi = \begin{pmatrix} x \\ \dot{x} \end{pmatrix} \quad \text{and} \quad M = \begin{pmatrix} 0 & 1 \\ -\Omega^2 & 0 \end{pmatrix} \quad (3.5)$$

The formal solution to $\dot{\varphi} = M\varphi$ is

$$\varphi(t) = e^{Mt} \varphi(0) \quad . \quad (3.6)$$

What do we mean by the exponential of a matrix? We mean its Taylor series expansion:

$$e^{Mt} = \mathbb{I} + Mt + \frac{1}{2!} M^2 t^2 + \frac{1}{3!} M^3 t^3 + \dots \quad . \quad (3.7)$$

Note that

$$\begin{aligned} M^2 &= \begin{pmatrix} 0 & 1 \\ -\Omega^2 & 0 \end{pmatrix} \begin{pmatrix} 0 & 1 \\ -\Omega^2 & 0 \end{pmatrix} \\ &= \begin{pmatrix} -\Omega^2 & 0 \\ 0 & -\Omega^2 \end{pmatrix} = -\Omega^2 \mathbb{I} \quad , \end{aligned} \quad (3.8)$$

hence

$$M^{2k} = (-\Omega^2)^k \mathbb{I} \quad , \quad M^{2k+1} = (-\Omega^2)^k M \quad . \quad (3.9)$$

Thus,

$$\begin{aligned}
 e^{Mt} &= \sum_{k=0}^{\infty} \frac{1}{(2k)!} (-\Omega^2 t^2)^k \cdot \mathbb{I} + \sum_{k=0}^{\infty} \frac{1}{(2k+1)!} (-\Omega^2 t^2)^k \cdot Mt \\
 &= \cos(\Omega t) \cdot \mathbb{I} + \Omega^{-1} \sin(\Omega t) \cdot M \\
 &= \begin{pmatrix} \cos(\Omega t) & \Omega^{-1} \sin(\Omega t) \\ -\Omega \sin(\Omega t) & \cos(\Omega t) \end{pmatrix} .
 \end{aligned} \tag{3.10}$$

Plugging this into eqn. 3.6, we obtain the desired solution.

For the damped harmonic oscillator, we have

$$\ddot{x} + 2\beta\dot{x} + \Omega^2 x = 0 \quad \Rightarrow \quad M = \begin{pmatrix} 0 & 1 \\ -\Omega^2 & -2\beta \end{pmatrix} . \tag{3.11}$$

The phase curves then spiral inward to the fixed point at $(0, 0)$.

3.1.2 Pendulum

Next, consider the simple pendulum, composed of a mass point m affixed to a massless rigid rod of length ℓ .

$$m\ell^2 \ddot{\theta} = -mg\ell \sin \theta . \tag{3.12}$$

This is equivalent to

$$\frac{d}{dt} \begin{pmatrix} \theta \\ \omega \end{pmatrix} = \begin{pmatrix} \omega \\ -\Omega^2 \sin \theta \end{pmatrix} , \tag{3.13}$$

where $\omega = \dot{\theta}$ is the angular velocity, and where $\Omega = \sqrt{g/\ell}$ is the natural frequency of small oscillations.

The phase curves for the pendulum are shown in Fig. 3.2. The small oscillations of the pendulum are essentially the same as those of a harmonic oscillator. Indeed, within the small angle approximation, $\sin \theta \approx \theta$, and the pendulum equations of motion are exactly those of the harmonic oscillator. These oscillations are called *librations*. They involve a back-and-forth motion in real space, and the phase space motion is contractable to a point, in the topological sense. However, if the initial angular velocity is large enough, a qualitatively different kind of motion is observed, whose phase curves are *rotations*. In this case, the pendulum bob keeps swinging around in the same direction, because, as we'll see in a later lecture, the total energy is sufficiently large. The phase curve which separates these two topologically distinct motions is called a *separatrix*.

3.2 General $N = 2$ Systems

The general form to be studied is

$$\frac{d}{dt} \begin{pmatrix} x \\ y \end{pmatrix} = \begin{pmatrix} V_x(x, y) \\ V_y(x, y) \end{pmatrix} . \tag{3.14}$$

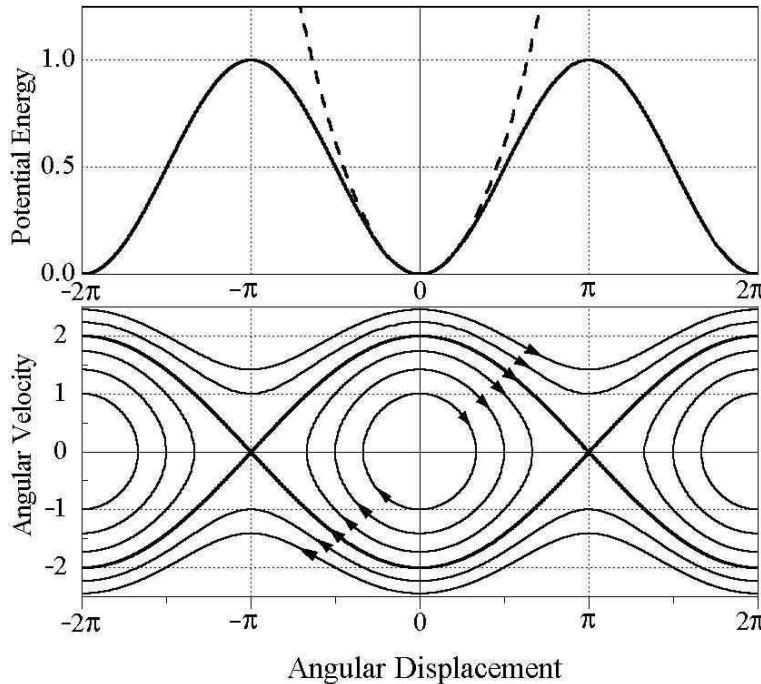


Figure 3.2: Phase curves for the simple pendulum. The *separatrix* divides phase space into regions of vibration and libration.

Special cases include autonomous second order ODEs, *viz.*

$$\ddot{x} = f(x, \dot{x}) \quad \Rightarrow \quad \frac{d}{dt} \begin{pmatrix} x \\ v \end{pmatrix} = \begin{pmatrix} v \\ f(x, v) \end{pmatrix} \quad , \quad (3.15)$$

of the type which occur in one-dimensional mechanics.

3.2.1 The damped driven pendulum

Another example is that of the damped and driven harmonic oscillator,

$$\frac{d^2\phi}{ds^2} + \gamma \frac{d\phi}{ds} + \sin \phi = j \quad . \quad (3.16)$$

This is equivalent to a model of a resistively and capacitively shunted Josephson junction, depicted in fig. 3.3. If ϕ is the superconducting phase difference across the junction, the current through the junction is given by $I_J = I_c \sin \phi$, where I_c is the *critical current*. The current carried by the resistor is $I_R = V/R$ from Ohm's law, and the current from the capacitor is $I_C = \dot{\phi}$. Finally, the *Josephson relation* relates the voltage V across the junction to the superconducting phase difference ϕ : $V = (\hbar/2e) \dot{\phi}$. Summing up the parallel currents, we have that the total current I is given by

$$I = \frac{\hbar C}{2e} \ddot{\phi} + \frac{\hbar}{2eR} \dot{\phi} + I_c \sin \phi \quad , \quad (3.17)$$

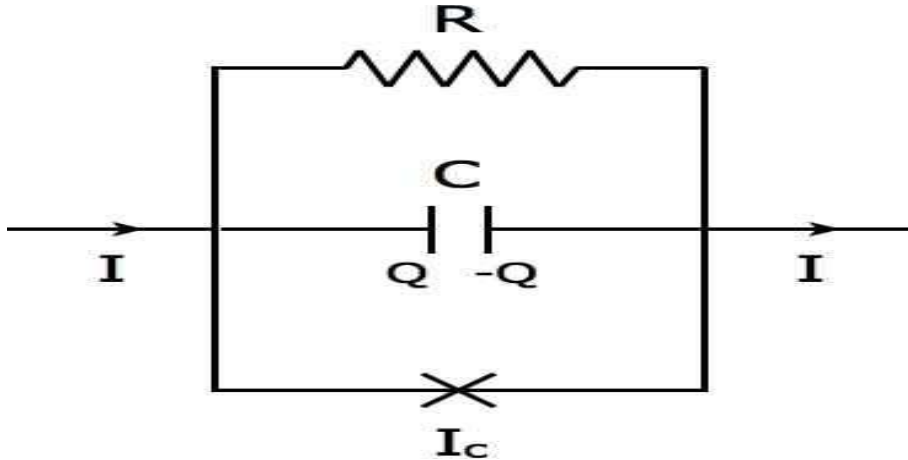


Figure 3.3: . The resistively and capacitively shunted Josephson junction. The Josephson junction is the X element at the bottom of the figure.

which, again, is equivalent to a damped, driven pendulum.

This system also has a mechanical analog. Define the ‘potential’

$$U(\phi) = -I_c \cos \phi - I\phi \quad . \quad (3.18)$$

The equation of motion is then

$$\frac{\hbar C}{2e} \ddot{\phi} + \frac{\hbar}{2eR} \dot{\phi} = -\frac{\partial U}{\partial \phi} \quad . \quad (3.19)$$

Thus, the combination $\hbar C / 2e$ plays the role of the inertial term (mass, or moment of inertia), while the combination $\hbar / 2eR$ plays the role of a damping coefficient. The potential $U(\phi)$ is known as the *tilted washboard potential*, for obvious reasons. (Though many of you have perhaps never seen a washboard.)

The model is adimensionalized by defining the Josephson plasma frequency ω_p and the RC time constant τ :

$$\omega_p \equiv \sqrt{\frac{2eI_c}{\hbar C}} \quad , \quad \tau \equiv RC \quad . \quad (3.20)$$

The dimensionless combination $\omega_p \tau$ then enters the adimensionalized equation as the sole control parameter:

$$\frac{I}{I_c} = \frac{d^2\phi}{ds^2} + \frac{1}{\omega_p \tau} \frac{d\phi}{ds} + \sin \phi \quad , \quad (3.21)$$

where $s = \omega_p t$. In the Josephson junction literature, the quantity $\beta \equiv 2eI_c R^2 C / \hbar = (\omega_p \tau)^2$, known as the *McCumber-Stewart* parameter, is a dimensionless measure of the damping (large β means small damping). In terms of eqn. 3.16, we have $\gamma = (\omega_p \tau)^{-1}$ and $j = I/I_c$.

We can write the second order ODE of eqn. 3.16 as two coupled first order ODEs:

$$\frac{d}{dt} \begin{pmatrix} \phi \\ \omega \end{pmatrix} = \begin{pmatrix} \omega \\ j - \sin \phi - \gamma \omega \end{pmatrix} \quad , \quad (3.22)$$

where $\omega = \dot{\phi}$. Phase space is a cylinder, $\mathbb{S}^1 \times \mathbb{R}^1$.

The quantity $\omega_p\tau$ typically ranges from 10^{-3} to 10^3 in Josephson junction applications. If $\omega_p\tau$ is small, then the system is heavily damped, and the inertial term $d^2\phi/ds^2$ can be neglected. One then obtains the $N = 1$ system

$$\gamma \frac{d\phi}{ds} = j - \sin \phi \quad . \quad (3.23)$$

If $|j| < 1$, then $\phi(s)$ evolves to the first stable fixed point encountered, where $\phi^* = \sin^{-1}(j)$ and $\cos \phi^* = \sqrt{1 - j^2}$. Since $\phi(s) \rightarrow \phi^*$ is asymptotically a constant, the voltage drop V must then vanish, as a consequence of the Josephson relation $V = (\hbar/2e)\dot{\phi}$. This, there is current flowing with no voltage drop!

If $|j| > 1$, the RHS never vanishes, in which case $\phi(s)$ is monotonic. We then can integrate the differential equation

$$dt = \frac{\hbar}{2eR} \cdot \frac{d\phi}{I - I_c \sin \phi} \quad . \quad (3.24)$$

Asymptotically the motion is periodic, with the period T obtained by integrating over the interval $\phi \in [0, 2\pi]$. One finds

$$T = \frac{\hbar}{2eR} \cdot \frac{2\pi}{\sqrt{I^2 - I_c^2}} \quad . \quad (3.25)$$

The time-averaged voltage drop is then

$$\langle V \rangle = \frac{\hbar}{2e} \langle \dot{\phi} \rangle = \frac{\hbar}{2e} \cdot \frac{2\pi}{T} = R\sqrt{I^2 - I_c^2} \quad . \quad (3.26)$$

This is the physics of the *current-biased resistively and capacitively shunted Josephson junction* in the strong damping limit. It is ‘current-biased’ because we are specifying the current I . Note that Ohm’s law is recovered at large values of I .

For general $\omega_p\tau$, we can still say quite a bit. At a fixed point, both components of the vector field $\mathbf{V}(\phi, \omega)$ must vanish. This requires $\omega = 0$ and $j = \sin \phi$. Therefore, there are two fixed points for $|j| < 1$, one a saddle point and the other a stable spiral. For $|j| > 1$ there are no fixed points, and asymptotically the function $\phi(t)$ tends to a periodic *limit cycle* $\phi_{LC}(t)$. The flow is sketched for two representative values of j in Fig. 3.4.

3.2.2 Classification of $N = 2$ fixed points

Suppose we have solved the fixed point equations $V_x(x^*, y^*) = 0$ and $V_y(x^*, y^*) = 0$. Let us now expand about the fixed point, writing

$$\begin{aligned} \dot{x} &= \left. \frac{\partial V_x}{\partial x} \right|_{(x^*, y^*)} (x - x^*) + \left. \frac{\partial V_x}{\partial y} \right|_{(x^*, y^*)} (y - y^*) + \dots \\ \dot{y} &= \left. \frac{\partial V_y}{\partial x} \right|_{(x^*, y^*)} (x - x^*) + \left. \frac{\partial V_y}{\partial y} \right|_{(x^*, y^*)} (y - y^*) + \dots \end{aligned} \quad . \quad (3.27)$$

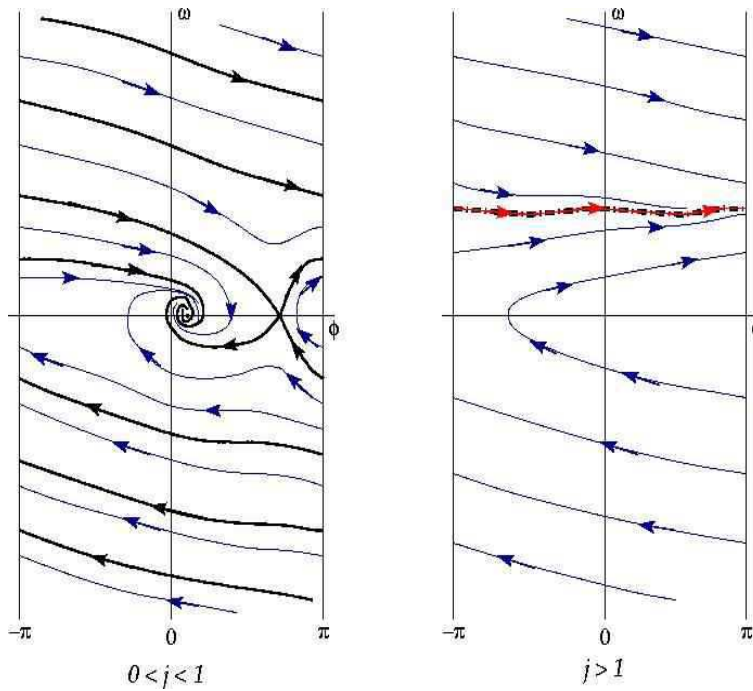


Figure 3.4: Phase flows for the equation $\ddot{\phi} + \gamma^{-1}\dot{\phi} + \sin \phi = j$. Left panel: $0 < j < 1$; note the separatrix (in black), which flows into the stable and unstable fixed points. Right panel: $j > 1$. The red curve overlying the thick black dot-dash curve is a *limit cycle*.

We define

$$u_1 = x - x^* \quad , \quad u_2 = y - y^* \quad , \quad (3.28)$$

which, to linear order, satisfy

$$\frac{d}{dt} \begin{pmatrix} u_1 \\ u_2 \end{pmatrix} = \underbrace{\begin{pmatrix} a & b \\ c & d \end{pmatrix}}_M \begin{pmatrix} u_1 \\ u_2 \end{pmatrix} + \mathcal{O}(u^2) \quad . \quad (3.29)$$

The formal solution to $\dot{\mathbf{u}} = M\mathbf{u}$ is

$$\mathbf{u}(t) = \exp(Mt) \mathbf{u}(0) \quad , \quad (3.30)$$

where $\exp(Mt) = \sum_{n=0}^{\infty} \frac{1}{n!} (Mt)^n$ is the exponential of the matrix Mt .

The behavior of the system is determined by the eigenvalues of M , which are roots of the characteristic equation $P(\lambda) = 0$, where

$$\begin{aligned} P(\lambda) &= \det(\lambda\mathbb{I} - M) \\ &= \lambda^2 - T\lambda + D \quad , \end{aligned} \quad (3.31)$$

with $T = a + d = \text{Tr}(M)$ and $D = ad - bc = \det(M)$. The two eigenvalues are therefore

$$\lambda_{\pm} = \frac{1}{2} \left(T \pm \sqrt{T^2 - 4D} \right) \quad . \quad (3.32)$$

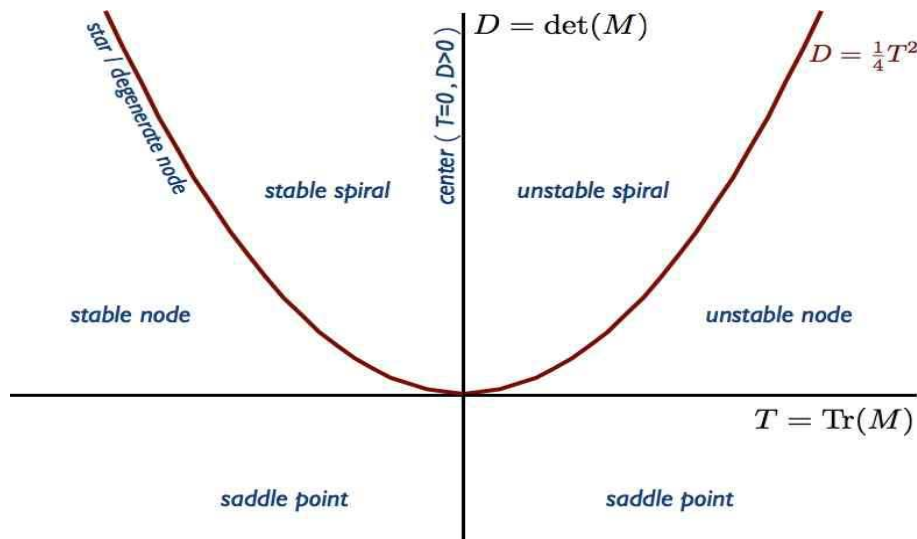


Figure 3.5: Complete classification of fixed points for the $N = 2$ system.

To see why the eigenvalues control the behavior, let us expand $\mathbf{u}(0)$ in terms of the eigenvectors of M . Since M is not necessarily symmetric, we should emphasize that we expand $\mathbf{u}(0)$ in terms of the *right* eigenvectors of M , which satisfy

$$M\psi_a = \lambda_a \psi_a \quad , \quad (3.33)$$

where the label a runs over the symbols $+$ and $-$, as in (3.32). We write

$$\mathbf{u}(t) = \sum_a C_a(t) \psi_a \quad . \quad (3.34)$$

Since (we assume) the eigenvectors are *linearly independent*, the equation $\dot{\mathbf{u}} = M\mathbf{u}$ becomes

$$\dot{C}_a = \lambda_a C_a \quad , \quad (3.35)$$

with solution

$$C_a(t) = e^{\lambda_a t} C_a(0) \quad . \quad (3.36)$$

Thus, the coefficients of the eigenvectors ψ_a will grow in magnitude if $|\lambda_a| > 1$, and will shrink if $|\lambda_a| < 1$.

3.2.3 The fixed point zoo

- **Saddles** : When $D < 0$, both eigenvalues are real; one is positive and one is negative, i.e. $\lambda_+ > 0$ and $\lambda_- < 0$. The right eigenvector ψ_- is thus the *stable direction* while ψ_+ is the *unstable direction*.
- **Nodes** : When $0 < D < \frac{1}{4}T^2$, both eigenvalues are real and of the same sign. Thus, both right eigenvectors correspond to stable or to unstable directions, depending on whether $T < 0$ (stable; $\lambda_- < \lambda_+ < 0$) or $T > 0$ (unstable; $\lambda_+ > \lambda_- > 0$). If λ_\pm are distinct, one can distinguish *fast* and *slow* eigendirections, based on the magnitude of the eigenvalues.

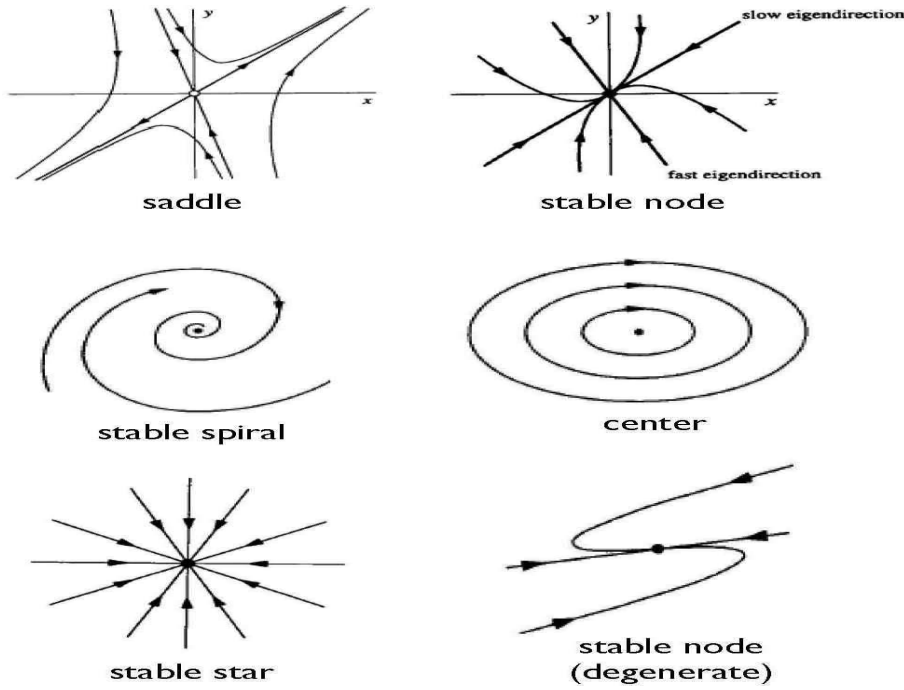


Figure 3.6: Fixed point zoo for $N = 2$ systems. Not shown: unstable versions of node, spiral, and star (reverse direction of arrows to turn stable into unstable).

- **Spirals :** When $D > \frac{1}{4}T^2$, the discriminant $T^2 - 4D$ is negative, and the eigenvalues come in a complex conjugate pair: $\lambda_- = \lambda_+^*$. The real parts are given by $\text{Re}(\lambda_{\pm}) = \frac{1}{2}T$, so the motion is stable (*i.e.* collapsing to the fixed point) if $T < 0$ and unstable (*i.e.* diverging from the fixed point) if $T > 0$. The motion is easily shown to correspond to a spiral. One can check that the spiral rotates counterclockwise for $a > d$ and clockwise for $a < d$.

- **Degenerate Cases :** When $T = 0$ we have $\lambda_{\pm} = \pm\sqrt{-D}$. For $D < 0$ we have a saddle, but for $D > 0$ both eigenvalues are imaginary: $\lambda_{\pm} = \pm i\sqrt{D}$. The orbits do not collapse to a point, nor do they diverge to infinity, in the $t \rightarrow \infty$ limit, as they do in the case of the stable and unstable spiral. The fixed point is called a *center*, and it is surrounded by closed trajectories.

When $D = \frac{1}{4}T^2$, the discriminant vanishes and the eigenvalues are degenerate. If the rank of M is two, the fixed point is a stable ($T < 0$) or unstable ($T > 0$) *star*. If M is degenerate and of rank one, the fixed point is a *degenerate node*.

When $D = 0$, one of the eigenvalues vanishes. This indicates a *fixed line* in phase space, since any point on that line will not move. The fixed line can be stable or unstable, depending on whether the remaining eigenvalue is negative (stable, $T < 0$), or positive (unstable, $T > 0$).

Putting it all together, an example of a phase portrait is shown in Fig. 3.7. Note the presence of an *isolated, closed trajectory*, which is called a *limit cycle*. Many self-sustained physical oscillations, *i.e.* oscillations with no external forcing, exhibit limit cycle behavior. Limit cycles, like fixed points, can be stable or unstable, or partially stable. Limit cycles are inherently nonlinear. While the linear equation $\dot{\varphi} = M\varphi$

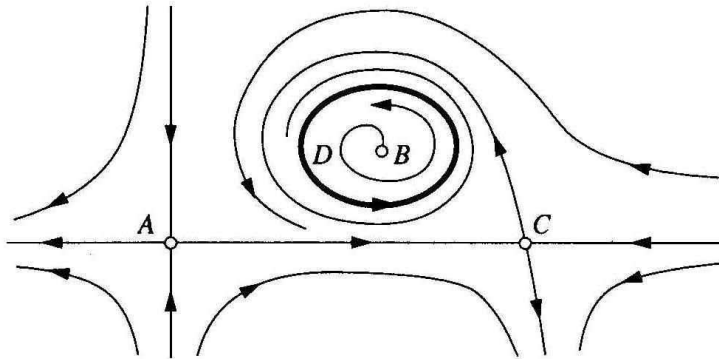


Figure 3.7: Phase portrait for an $N = 2$ flow including saddles (A,C), unstable spiral (B), and limit cycle (D).

can have periodic solutions if M has purely imaginary eigenvalues, these periodic trajectories are not *isolated*, because $\lambda \varphi(t)$ is also a solution. The amplitude of these linear oscillations is fixed by the initial conditions, whereas for limit cycles, the amplitude is inherent from the dynamics itself, and the initial conditions are irrelevant (for a stable limit cycle).

In fig. 3.8 we show simple examples of stable, unstable, and half-stable limit cycles. As we shall see when we study nonlinear oscillations, the Van der Pol oscillator,

$$\ddot{x} + \mu(x^2 - 1)\dot{x} + x = 0 \quad , \quad (3.37)$$

with $\mu > 0$ has a stable limit cycle. The physics is easy to apprehend. The coefficient of the \dot{x} term in the equation of motion is positive for $|x| > 1$ and negative for $|x| < 1$. Interpreting this as a coefficient of friction, we see that the friction is positive, *i.e.* dissipating energy, when $|x| > 1$ but *negative*, *i.e.* accumulating energy, for $|x| < 1$. Thus, any small motion with $|x| < 1$ is *amplified* due to the negative friction, and would increase without bound were it not for the fact that the friction term reverses its sign and becomes dissipative for $|x| > 1$. The limit cycle for $\mu \gg 1$ is shown in fig. 3.9.

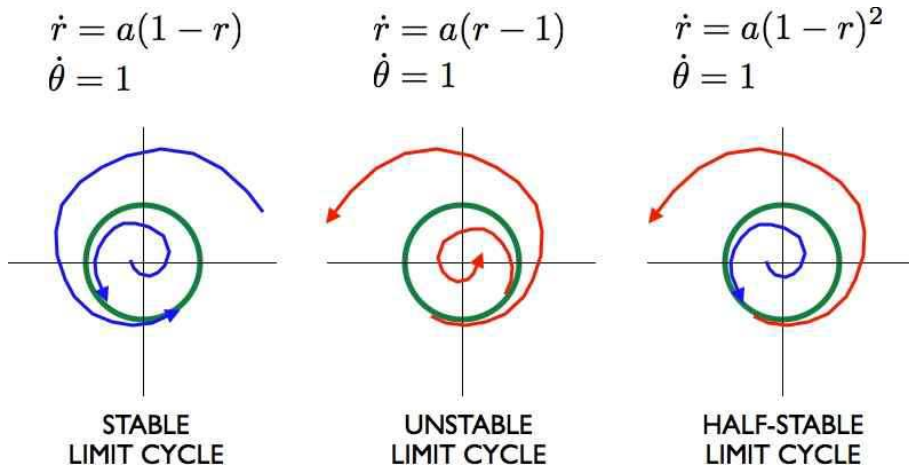


Figure 3.8: Stable, unstable, and half-stable limit cycles.

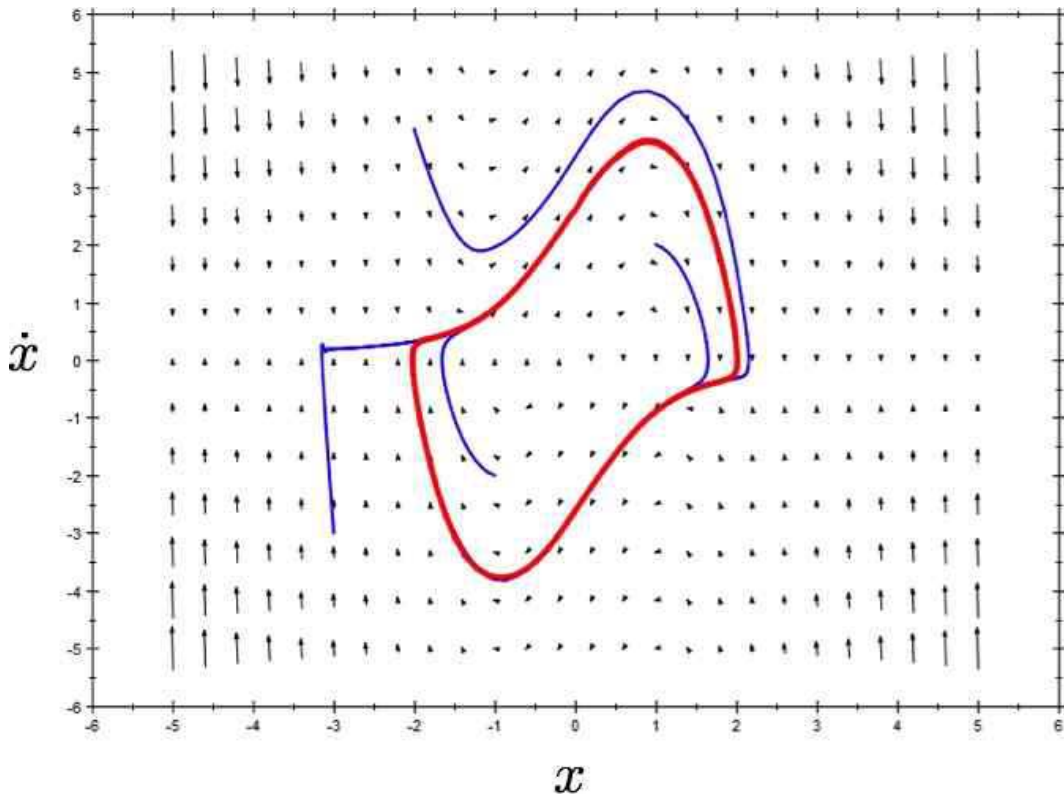


Figure 3.9: Limit cycle of the Van der Pol oscillator for $\mu \gg 1$. (Source: Wikipedia)

3.2.4 Fixed points for $N = 3$ systems

For an $N = 2$ system, there are five generic types of fixed points. They are classified according to the eigenvalues of the linearized dynamics at the fixed point. For a real 2×2 matrix, the eigenvalues must be real or else must be a complex conjugate pair. The five types of fixed points are then

$$\begin{aligned}
 \lambda_1 > 0, \lambda_2 > 0 &: (1) \text{unstable node} \\
 \lambda_1 > 0, \lambda_2 < 0 &: (2) \text{saddle point} \\
 \lambda_1 < 0, \lambda_2 < 0 &: (3) \text{stable node} \\
 \operatorname{Re} \lambda_1 > 0, \lambda_2 = \lambda_1^* &: (4) \text{unstable spiral} \\
 \operatorname{Re} \lambda_1 < 0, \lambda_2 = \lambda_1^* &: (5) \text{stable spiral}
 \end{aligned} \tag{3.38}$$

How many possible generic fixed points are there for an $N = 3$ system?

For a general real 3×3 matrix M , the characteristic polynomial $P(\lambda) = \det(\lambda - M)$ satisfies $P(\lambda^*) = P(\lambda)$. Thus, if λ is a root then so is λ^* . This means that the eigenvalues are either real or else come in complex

conjugate pairs. There are then ten generic possibilities for the three eigenvalues:

- | | | |
|------|-----------------------|--|
| (1) | unstable node | : $\lambda_1 > \lambda_2 > \lambda_3 > 0$ |
| (2) | (+ + -) saddle | : $\lambda_1 > \lambda_2 > 0 > \lambda_3$ |
| (3) | (+ - -) saddle | : $\lambda_1 > 0 > \lambda_2 > \lambda_3$ |
| (4) | stable node | : $0 > \lambda_1 > \lambda_2 > \lambda_3$ |
| (5) | unstable spiral-node | : $\lambda_1 > \operatorname{Re} \lambda_{2,3} > 0 ; \operatorname{Im} \lambda_2 = -\operatorname{Im} \lambda_3$ |
| (6) | unstable spiral-node | : $\operatorname{Re} \lambda_{1,2} > \lambda_3 > 0 ; \operatorname{Im} \lambda_1 = -\operatorname{Im} \lambda_2$ |
| (7) | stable spiral-node | : $0 > \lambda_1 > \operatorname{Re} \lambda_{2,3} ; \operatorname{Im} \lambda_2 = -\operatorname{Im} \lambda_3$ |
| (8) | stable spiral-node | : $0 > \operatorname{Re} \lambda_{1,2} > \lambda_3 ; \operatorname{Im} \lambda_1 = -\operatorname{Im} \lambda_2$ |
| (9) | (+ - -) spiral-saddle | : $\lambda_1 > 0 > \operatorname{Re} \lambda_{2,3} ; \operatorname{Im} \lambda_2 = -\operatorname{Im} \lambda_3$ |
| (10) | (+ + -) spiral-saddle | : $\operatorname{Re} \lambda_{1,2} > 0 > \lambda_3 ; \operatorname{Im} \lambda_1 = -\operatorname{Im} \lambda_2 .$ |

3.3 Andronov-Hopf Bifurcation

A bifurcation between a spiral and a limit cycle is known as an *Andronov-Hopf bifurcation*. As a simple example, consider the $N = 2$ system,

$$\begin{aligned}\dot{x} &= ax - by - C(x^2 + y^2)x \\ \dot{y} &= bx + ay - C(x^2 + y^2)y ,\end{aligned}\tag{3.39}$$

where a , b , and C are real. Clearly the origin is a fixed point, at which one finds the eigenvalues $\lambda = a \pm ib$. Thus, the fixed point is a stable spiral if $a < 0$ and an unstable spiral if $a > 0$.

Written in terms of the complex variable $z = x + iy$, these two equations collapse to the single equation

$$\dot{z} = (a + ib)z - C|z|^2z .\tag{3.40}$$

The dynamics are also simple in polar coordinates $r = |z|$, $\theta = \arg(z)$:

$$\begin{aligned}\dot{r} &= ar - Cr^3 \\ \dot{\theta} &= b .\end{aligned}\tag{3.41}$$

The phase diagram, for fixed $b > 0$, is depicted in Fig. 3.10. For positive a/C , there is a limit cycle at $r = \sqrt{a/C}$. In both cases, the limit cycle disappears as a crosses the value $a^* = 0$ and is replaced by a stable ($a < 0, C > 0$) or unstable ($a > 0, C < 0$) spiral.

This example also underscores the following interesting point. Adding a small nonlinear term C has no fundamental effect on the fixed point behavior so long as $a \neq 0$, when the fixed point is a stable or unstable spiral. In general, fixed points which are attractors (stable spirals or nodes), repellers (unstable spirals or nodes), or saddles are *robust* with respect to the addition of a small nonlinearity. But the fixed point behavior in the marginal cases – centers, stars, degenerate nodes, and fixed lines – is strongly affected by the presence of even a small nonlinearity. In this example, the FP is a center when $a = 0$. But as the (r, θ) dynamics shows, a small nonlinearity will destroy the center and turn the FP into an attractor ($C > 0$) or a repeller ($C < 0$).

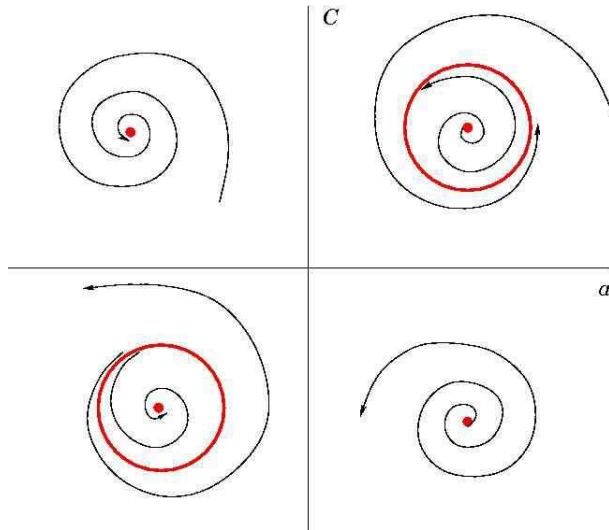


Figure 3.10: Hopf bifurcation: for $C > 0$ the bifurcation is supercritical, between stable spiral and stable limit cycle. For $C < 0$ the bifurcation is subcritical, between unstable spiral and unstable limit cycle. The bifurcation occurs at $a = 0$ in both cases.

3.4 Population Biology : Lotka-Volterra Models

Consider two species with populations N_1 and N_2 , respectively². We model the evolution of these populations by the coupled ODEs

$$\begin{aligned} \frac{dN_1}{dt} &= aN_1 + bN_1N_2 + cN_1^2 \\ \frac{dN_2}{dt} &= dN_2 + eN_1N_2 + fN_2^2 \end{aligned} \quad , \quad (3.42)$$

where $\{a, b, c, d, e, f\}$ are constants. We can eliminate some constants by rescaling $N_{1,2}$. This results in the following:

$$\begin{aligned} \dot{x} &= x(r - \mu x - ky) \\ \dot{y} &= y(r' - \mu'y - k'x) \end{aligned} \quad , \quad (3.43)$$

where μ , and μ' can each take on one of three possible values $\{0, \pm 1\}$. By rescaling time, we can eliminate the scale of either of r or r' as well. Typically, intra-species competition guarantees $\mu = \mu' = +1$. The remaining coefficients (r, k, k') are real may also be of either sign. The values and especially the signs of the various coefficients have a physical (or biological) significance. For example, if $k < 0$ it means that x grows due to the presence of y . The effect of y on x may be of the same sign ($kk' > 0$) or of opposite sign ($kk' < 0$).

²This discussion is adapted from S. Strogatz, *Nonlinear Dynamics and Chaos*.

3.4.1 Rabbits and foxes

As an example, consider the model

$$\begin{aligned}\dot{x} &= x - xy \\ \dot{y} &= -\beta y + xy\end{aligned}. \quad (3.44)$$

The quantity x might represent the (scaled) population of rabbits and y the population of foxes in an ecosystem. There are two fixed points: at $(0, 0)$ and at $(\beta, 1)$. Linearizing the dynamics about these fixed points, one finds that $(0, 0)$ is a saddle while $(\beta, 1)$ is a center. Let's do this explicitly.

The first step is to find the fixed points (x^*, y^*) . To do this, we set $\dot{x} = 0$ and $\dot{y} = 0$. From $\dot{x} = x(1-y) = 0$ we have that $x = 0$ or $y = 1$. Suppose $x = 0$. The second equation, $\dot{y} = (x - \beta)y$ then requires $y = 0$. So $P_1 = (0, 0)$ is a fixed point. The other possibility is that $y = 1$, which then requires $x = \beta$. So $P_2 = (\beta, 1)$ is the second fixed point. Those are the only possibilities.

We now compute the linearized dynamics at these fixed points. The linearized dynamics are given by $\dot{\varphi} = M\varphi$, with

$$M = \begin{pmatrix} \partial\dot{x}/\partial x & \partial\dot{x}/\partial y \\ \partial\dot{y}/\partial x & \partial\dot{y}/\partial y \end{pmatrix} = \begin{pmatrix} 1-y & -x \\ y & x-\beta \end{pmatrix} . \quad (3.45)$$

Evaluating M at P_1 and P_2 , we find

$$M_1 = \begin{pmatrix} 1 & 0 \\ 0 & -\beta \end{pmatrix} , \quad M_2 = \begin{pmatrix} 0 & -\beta \\ 1 & 0 \end{pmatrix} . \quad (3.46)$$

The eigenvalues are easily found:

$$\begin{aligned}P_1 : \lambda_+ &= 1 & \lambda_- &= -\beta \\ P_2 : \lambda_+ &= i\sqrt{\beta} & \lambda_- &= -i\sqrt{\beta}\end{aligned} . \quad (3.47)$$

Thus P_1 is a saddle point and P_2 is a center.

As we saw earlier, generally speaking we expect nonlinear terms to transform centers to stable or unstable spirals, possibly with a limit cycle. However for the Lotka-Volterra system there is a conserved quantity. Consider the general predator-prey system

$$\begin{aligned}\dot{x} &= (a - b y) x \\ \dot{y} &= -(c - d x) y\end{aligned}, \quad (3.48)$$

where a, b, c , and d are all positive constants. Now consider the function

$$H \equiv dx + b y - c \ln x - a \ln y . \quad (3.49)$$

Then

$$\frac{\partial H}{\partial x} = d - \frac{c}{x} , \quad \frac{\partial H}{\partial y} = b - \frac{a}{y} . \quad (3.50)$$

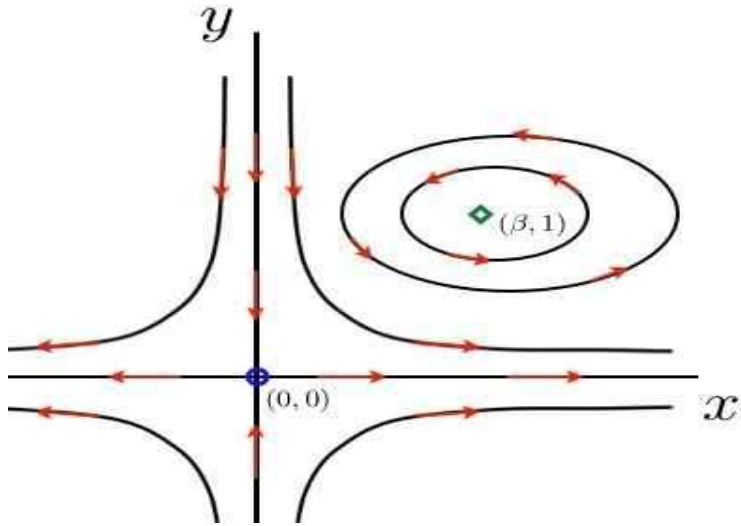


Figure 3.11: Phase flow for the rabbits *vs.* foxes Lotka-Volterra model of eqs. 3.44.

Thus, we have $\dot{x} = -xy \frac{\partial H}{\partial y}$ and $\dot{y} = xy \frac{\partial H}{\partial x}$. If we define $p \equiv \ln x$ and $q \equiv \ln y$, then we have

$$\dot{q} = \frac{\partial H}{\partial p} \quad , \quad \dot{p} = -\frac{\partial H}{\partial q} \quad (3.51)$$

with

$$H(q, p) = d e^p + b e^q - c p - a q . \quad (3.52)$$

So the system is a Hamiltonian system in disguise, and we know that for Hamiltonian systems the only possible fixed points are saddles and centers. The phase curves are level sets of the function H .

3.4.2 Rabbits and sheep

In the rabbits and foxes model of eqs. 3.44, the rabbits are the food for the foxes. This means $k = 1$ but $k' = -1$, *i.e.* the fox population is enhanced by the presence of rabbits, but the rabbit population is diminished by the presence of foxes. Consider now a model in which the two species (rabbits and sheep, say) compete for food:

$$\begin{aligned} \dot{x} &= x(r - x - ky) \\ \dot{y} &= y(1 - y - k'x) \end{aligned} , \quad (3.53)$$

with r , k , and k' all positive. Note that when either population x or y vanishes, the remaining population is governed by the logistic equation, *i.e.* it will flow to a nonzero fixed point.

The matrix of derivatives, which is to be evaluated at each fixed point in order to assess its stability, is

$$M = \begin{pmatrix} \partial \dot{x} / \partial x & \partial \dot{x} / \partial y \\ \partial \dot{y} / \partial x & \partial \dot{y} / \partial y \end{pmatrix} = \begin{pmatrix} r - 2x - ky & -kx \\ -k'y & 1 - 2y - k'x \end{pmatrix} . \quad (3.54)$$

At each fixed point, we must evaluate $D = \det(M)$ and $T = \text{Tr}(M)$ and apply the classification scheme of Fig. 3.5.

- $\mathbf{P}_1 = (0, 0)$: This is the trivial state with no rabbits ($x = 0$) and no sheep ($y = 0$). The linearized dynamics gives $M_1 = \begin{pmatrix} r & 0 \\ 0 & 1 \end{pmatrix}$, which corresponds to an unstable node.
- $\mathbf{P}_2 = (r, 0)$: Here we have rabbits but no sheep. The linearized dynamics gives $M_2 = \begin{pmatrix} -r & -rk \\ 0 & 1 - rk' \end{pmatrix}$. For $rk' > 1$ this is a stable node; for $rk' < 1$ it is a saddle point.
- $\mathbf{P}_3 = (0, 1)$: Here we have sheep but no rabbits. The linearized dynamics gives $M_3 = \begin{pmatrix} r - k & 0 \\ -k' & -1 \end{pmatrix}$. For $k > r$ this is a stable node; for $k < r$ it is a saddle.
- There is one remaining fixed point – a nontrivial one where both x and y are nonzero. To find it, we set $\dot{x} = \dot{y} = 0$, and divide out by x and y respectively, to get

$$\begin{aligned} x + ky &= r \\ kx' + y &= 1 \quad . \end{aligned} \tag{3.55}$$

This is a simple rank 2 inhomogeneous linear system. If the fixed point \mathbf{P}_4 is to lie in the physical quadrant ($x > 0, y > 0$), then either (i) $k > r$ and $k' > r^{-1}$ or (ii) $k < r$ and $k' < r^{-1}$. The solution is

$$\mathbf{P}_4 = \begin{pmatrix} 1 & k \\ k' & 1 \end{pmatrix}^{-1} \begin{pmatrix} r \\ 1 \end{pmatrix} = \frac{1}{1 - kk'} \begin{pmatrix} r - k \\ 1 - rk' \end{pmatrix} \quad . \tag{3.56}$$

The linearized dynamics then gives

$$M_4 = \frac{1}{1 - kk'} \begin{pmatrix} k - r & k(k - r) \\ k'(rk' - 1) & rk' - 1 \end{pmatrix} \quad , \tag{3.57}$$

yielding

$$\begin{aligned} T &= \frac{rk' - 1 + k - r}{1 - kk'} \\ D &= \frac{(k - r)(rk' - 1)}{1 - kk'} \quad . \end{aligned} \tag{3.58}$$

The classification of this fixed point can vary with parameters. Consider the case $r = 1$. If $k = k' = 2$ then both \mathbf{P}_2 and \mathbf{P}_3 are stable nodes. At \mathbf{P}_4 , one finds $T = -\frac{2}{3}$ and $D = -\frac{1}{3}$, corresponding to a saddle point. In this case it is the fate of one population to die out at the expense of the other, and which one survives depends on initial conditions. If instead we took $k = k' = \frac{1}{2}$, then $T = -\frac{4}{3}$ and $D = \frac{1}{3}$, corresponding to a stable node (node $D < \frac{1}{4}T^2$ in this case). The situation is depicted in Fig. 3.12.

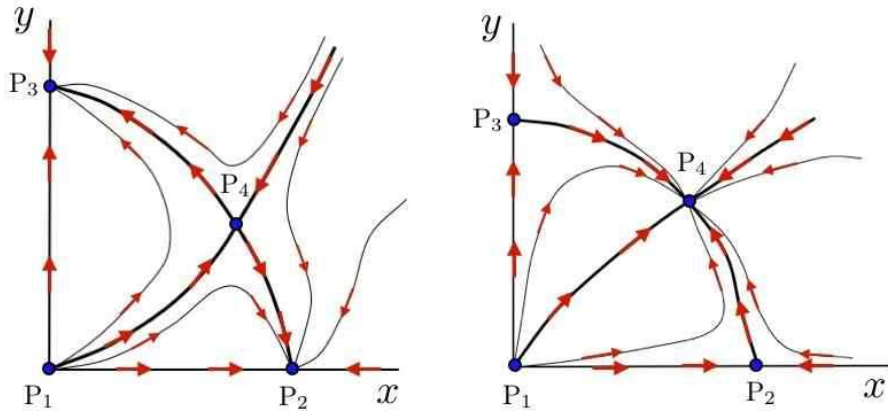


Figure 3.12: Two possible phase flows for the rabbits vs. sheep model of eqs. 3.53. Left panel: $k > r > k'^{-1}$. Right panel: $k < r < k'^{-1}$.

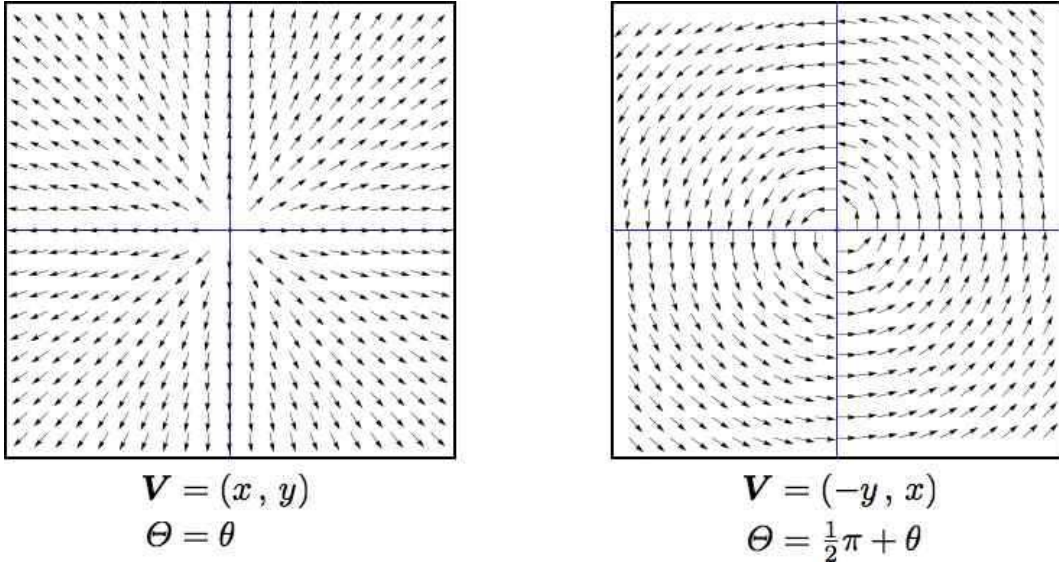


Figure 3.13: Two singularities with index +1. The direction field $\hat{\mathbf{V}} = \mathbf{V}/|\mathbf{V}|$ is shown in both cases.

3.5 Poincaré-Bendixson Theorem

Although $N = 2$ systems are much richer than $N = 1$ systems, they are still ultimately rather impoverished in terms of their long-time behavior. If an orbit does not flow off to infinity or asymptotically approach a stable fixed point (node or spiral or nongeneric example), the only remaining possibility is limit cycle behavior. This is the content of the *Poincaré-Bendixson theorem*, which states:

- IF Ω is a compact (*i.e.* closed and bounded) subset of phase space,
- AND $\dot{\varphi} = \mathbf{V}(\varphi)$ is continuously differentiable on Ω ,
- AND Ω contains no fixed points (*i.e.* $\mathbf{V}(\varphi)$ never vanishes in Ω),

- AND a phase curve $\varphi(t)$ is always confined to Ω ,
- ◊ THEN $\varphi(t)$ is either closed or approaches a closed trajectory in the limit $t \rightarrow \infty$.

Thus, under the conditions of the theorem, Ω must contain a closed orbit.

One way to prove that $\varphi(t)$ is confined to Ω is to establish that $\mathbf{V} \cdot \hat{\mathbf{n}} \leq 0$ everywhere on the boundary $\partial\Omega$, which means that the phase flow is always directed inward (or tangent) along the boundary. Let's analyze an example from the book by Strogatz. Consider the system

$$\begin{aligned}\dot{r} &= r(1 - r^2) + \lambda r \cos \theta \\ \dot{\theta} &= 1\end{aligned}, \quad (3.59)$$

with $0 < \lambda < 1$. Then define

$$a \equiv \sqrt{1 - \lambda} \quad , \quad b \equiv \sqrt{1 + \lambda} \quad (3.60)$$

and

$$\Omega \equiv \left\{ (r, \theta) \mid a < r < b \right\} \quad . \quad (3.61)$$

On the boundaries of Ω , we have

$$\begin{aligned}r = a &\Rightarrow \dot{r} = \lambda a (1 + \cos \theta) \\ r = b &\Rightarrow \dot{r} = -\lambda b (1 - \cos \theta)\end{aligned}. \quad (3.62)$$

We see that the radial component of the flow is inward along both $r = a$ and $r = b$. Thus, any trajectory which starts inside Ω can never escape. The Poincaré-Bendixson theorem tells us that the trajectory will approach a stable limit cycle in the limit $t \rightarrow \infty$.

It is only with $N \geq 3$ systems that the interesting possibility of chaotic behavior emerges.

3.6 Index Theory

Consider a smooth two-dimensional vector field $\mathbf{V}(\varphi)$. The angle that the vector \mathbf{V} makes with respect to the $\hat{\varphi}_1$ and $\hat{\varphi}_2$ axes is a scalar field,

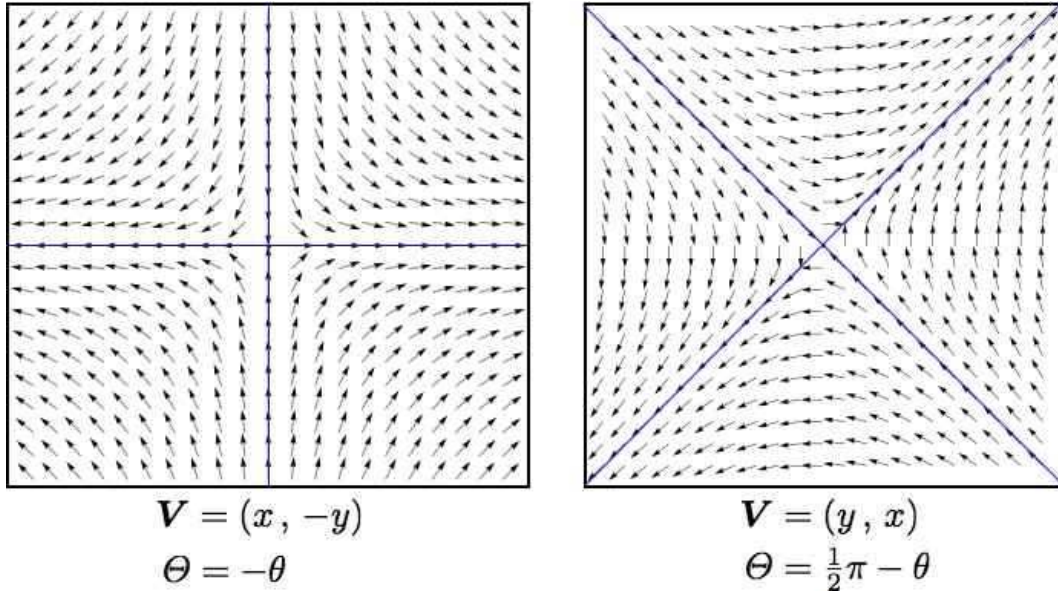
$$\Theta(\varphi) = \tan^{-1} \left(\frac{V_2(\varphi)}{V_1(\varphi)} \right) \quad . \quad (3.63)$$

So long as \mathbf{V} has finite length, the angle Θ is well-defined. In particular, we expect that we can integrate $\nabla\Theta$ over a closed curve \mathcal{C} in phase space to get

$$\oint_{\mathcal{C}} d\varphi \cdot \nabla\Theta = 0 \quad . \quad (3.64)$$

However, this can fail if $\mathbf{V}(\varphi)$ vanishes (or diverges) at one or more points in the interior of \mathcal{C} . In general, if we define

$$W_{\mathcal{C}}(\mathbf{V}) = \frac{1}{2\pi} \oint_{\mathcal{C}} d\varphi \cdot \nabla\Theta \quad , \quad (3.65)$$

Figure 3.14: Two singularities with index -1 .

then $W_{\mathcal{C}}(\mathbf{V}) \in \mathbb{Z}$ is an integer valued function of \mathcal{C} , which is the change in Θ around the curve \mathcal{C} . This must be an integer, because Θ is well-defined only up to multiples of 2π . Note that *differential changes* of Θ are in general well-defined.

Thus, if $\mathbf{V}(\varphi)$ is finite, meaning neither infinite nor infinitesimal, *i.e.* \mathbf{V} neither diverges nor vanishes anywhere in $\text{int}(\mathcal{C})$, then $W_{\mathcal{C}}(\mathbf{V}) = 0$. Assuming that \mathbf{V} never diverges, any singularities in Θ must arise from points where $\mathbf{V} = 0$, which in general occurs at isolated points, since it entails two equations in the two variables (φ_1, φ_2) .

The index of a two-dimensional vector field $\mathbf{V}(\varphi)$ at a *point* φ is the integer-valued winding of \mathbf{V} about that point:

$$\begin{aligned} \text{ind } (\mathbf{V}) &= \lim_{a \rightarrow 0} \frac{1}{2\pi} \oint_{\mathcal{C}_a(\varphi_0)} d\varphi \cdot \nabla \Theta \\ &= \lim_{a \rightarrow 0} \frac{1}{2\pi} \oint_{\mathcal{C}_a(\varphi_0)} d\varphi \cdot \frac{V_1 \nabla V_2 - V_2 \nabla V_1}{V_1^2 + V_2^2} , \end{aligned} \quad (3.66)$$

where $\mathcal{C}_a(\varphi_0)$ is a circle of radius a surrounding the point φ_0 . The index of a closed curve \mathcal{C} is given by the sum of the indices at all the singularities enclosed by the curve:³

$$W_{\mathcal{C}}(\mathbf{V}) = \sum_{\varphi_i \in \text{int}(\mathcal{C})} \text{ind } (\mathbf{V}) . \quad (3.67)$$

³Technically, we should weight the index at each enclosed singularity by the signed number of times the curve \mathcal{C} encloses that singularity. For simplicity and clarity, we assume that the curve \mathcal{C} is homeomorphic to the circle \mathbb{S}^1 .

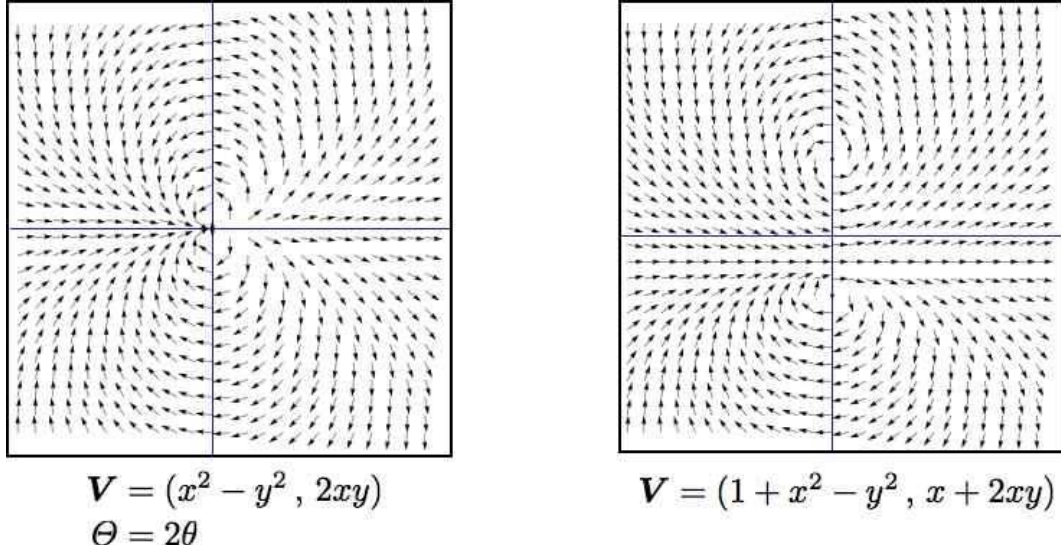


Figure 3.15: Left panel: a singularity with index +2. Right panel: two singularities each with index +1. Note that the long distance behavior of \mathbf{V} is the same in both cases.

As an example, consider the vector fields plotted in fig. 3.13. We have:

$$\begin{aligned}\mathbf{V} &= (x, y) \quad \Rightarrow \quad \Theta = \theta \\ \mathbf{V} &= (-y, x) \quad \Rightarrow \quad \Theta = \theta + \frac{1}{2}\pi\end{aligned}. \quad (3.68)$$

The index is the same, +1, in both cases, even though the first corresponds to an unstable node and the second to a center. Any $N = 2$ fixed point with $\det M > 0$ has index +1.

Fig. 3.14 shows two vector fields, each with index -1:

$$\begin{aligned}\mathbf{V} &= (x, -y) \quad \Rightarrow \quad \Theta = -\theta \\ \mathbf{V} &= (y, x) \quad \Rightarrow \quad \Theta = -\theta + \frac{1}{2}\pi\end{aligned}. \quad (3.69)$$

In both cases, the fixed point is a saddle.

As an example of the content of eqn. 3.67, consider the vector fields in eqn. 3.15. The left panel shows the vector field $\mathbf{V} = (x^2 - y^2, 2xy)$, which has a single fixed point, at the origin $(0, 0)$, of index +2. The right panel shows the vector field $\mathbf{V} = (1 + x^2 - y^2, x + 2xy)$, which has fixed points (x^*, y^*) at $(0, 1)$ and $(0, -1)$. The linearized dynamics is given by the matrix

$$M = \begin{pmatrix} \frac{\partial \dot{x}}{\partial x} & \frac{\partial \dot{x}}{\partial y} \\ \frac{\partial \dot{y}}{\partial x} & \frac{\partial \dot{y}}{\partial y} \end{pmatrix} = \begin{pmatrix} 2x & -2y \\ 1 + 2y & 2x \end{pmatrix}. \quad (3.70)$$

Thus,

$$M_{(0,1)} = \begin{pmatrix} 0 & -2 \\ 2 & 0 \end{pmatrix}, \quad M_{(0,-1)} = \begin{pmatrix} 0 & 2 \\ -2 & 0 \end{pmatrix}. \quad (3.71)$$

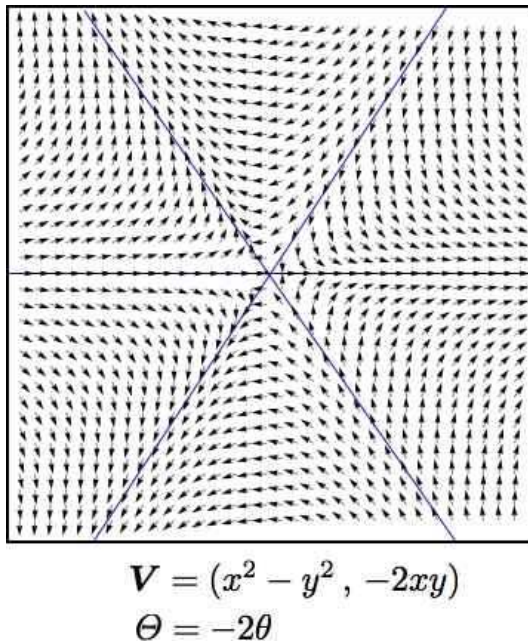


Figure 3.16: A vector field with index -2 .

At each of these fixed points, we have $T = 0$ and $D = 4$, corresponding to a center, with index $+1$. If we consider a square-ish curve \mathcal{C} around the periphery of each figure, the vector field is almost the same along such a curve for both the left and right panels, and the winding number is $W_{\mathcal{C}}(\mathbf{V}) = +2$.

Finally, consider the vector field shown in fig. 3.16, with $\mathbf{V} = (x^2 - y^2, -2xy)$. Clearly $\Theta = -2\theta$, and the index of the singularity at $(0, 0)$ is -2 .

To recapitulate some properties of the index / winding number:

- The index $\text{ind}_{\varphi_0}(\mathbf{V})$ of an $N = 2$ vector field \mathbf{V} at a point φ_0 is the winding number of \mathbf{V} about that point.
- The winding number $W_{\mathcal{C}}(\mathbf{V})$ of a curve \mathcal{C} is the sum of the indices of the singularities enclosed by that curve.
- Smooth deformations of \mathcal{C} do not change its winding number. One must instead “stretch” \mathcal{C} over a fixed point singularity in order to change $W_{\mathcal{C}}(\mathbf{V})$.
- Uniformly rotating each vector in the vector field by an angle β has the effect of sending $\Theta \rightarrow \Theta + \beta$; this leaves all indices and winding numbers invariant.
- Nodes and spirals, whether stable or unstable, have index $+1$ (ss do the special cases of centers, stars, and degenerate nodes). Saddle points have index -1 .
- Clearly any closed orbit must lie on a curve \mathcal{C} of index $+1$.

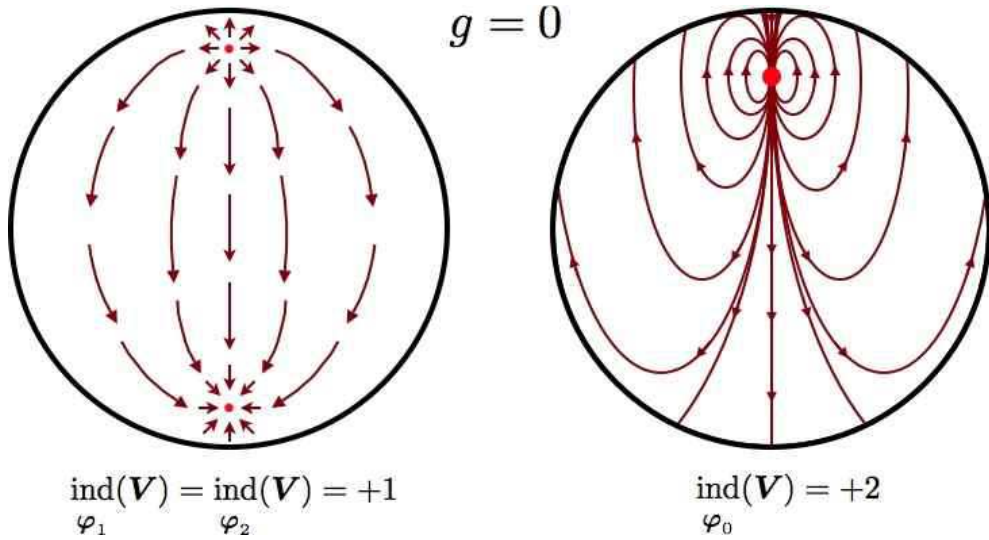


Figure 3.17: Two smooth vector fields on the sphere S^2 , which has genus $g = 0$. Left panel: two index +1 singularities. Right panel: one index +2 singularity.

3.6.1 Gauss-Bonnet Theorem

There is a deep result in mathematics, the Gauss-Bonnet theorem, which connects the local *geometry* of a two-dimensional manifold to its global *topological structure*. The content of the theorem is as follows:

$$\int_{\mathcal{M}} dA K = 2\pi \chi(\mathcal{M}) = 2\pi \sum_i \text{ind}(\mathbf{V}) \quad , \quad (3.72)$$

where \mathcal{M} is a 2-manifold (a topological space locally homeomorphic to \mathbb{R}^2), K is the local *Gaussian curvature* of \mathcal{M} , which is given by $K = (R_1 R_2)^{-1}$, where $R_{1,2}$ are the principal radii of curvature at a given point, and dA is the differential area element. The quantity $\chi(\mathcal{M})$ is called the *Euler characteristic* of \mathcal{M} and is given by $\chi(\mathcal{M}) = 2 - 2g$, where g is the *genus* of \mathcal{M} , which is the number of holes (or handles) of \mathcal{M} . Furthermore, $\mathbf{V}(\varphi)$ is *any* smooth vector field on \mathcal{M} , and φ_i are the singularity points of that vector field, which are fixed points of the dynamics $\dot{\varphi} = \mathbf{V}(\varphi)$.

To apprehend the content of the Gauss-Bonnet theorem, it is helpful to consider an example. Let $\mathcal{M} = S^2$ be the unit 2-sphere, as depicted in fig. 3.17. At any point on the unit 2-sphere, the radii of curvature are degenerate and both equal to $R = 1$, hence $K = 1$. If we integrate the Gaussian curvature over the sphere, we thus get $4\pi = 2\pi \chi(S^2)$, which says $\chi(S^2) = 2 - 2g = 2$, which agrees with $g = 0$ for the sphere. Furthermore, the Gauss-Bonnet theorem says that *any* smooth vector field on S^2 must have a singularity or singularities, with the total index summed over the singularities equal to +2. The vector field sketched in the left panel of fig. 3.17 has two index +1 singularities, which could be taken at the north and south poles, but which could be anywhere. Another possibility, depicted in the right panel of fig. 3.17, is that there is a one singularity with index +2.

In fig. 3.18 we show examples of manifolds with genii $g = 1$ and $g = 2$. The case $g = 1$ is the familiar 2-torus, which is topologically equivalent to a product of circles: $\mathbb{T}^2 \simeq S^1 \times S^1$, and is thus coordinatized

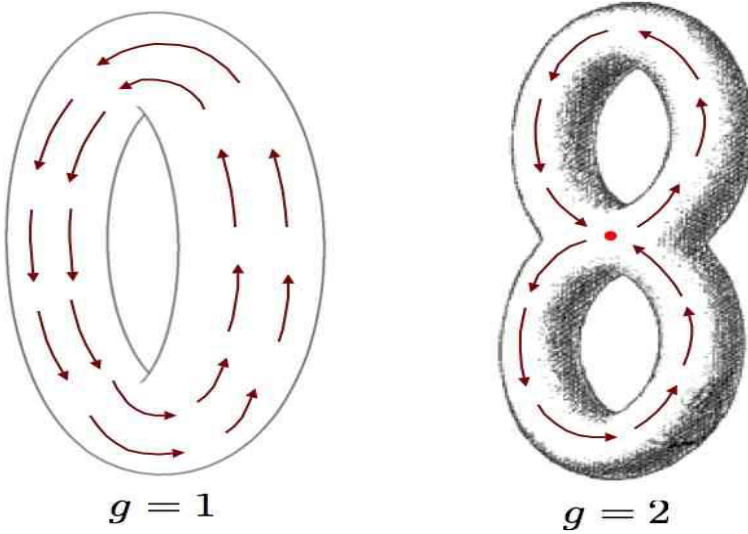


Figure 3.18: Smooth vector fields on the torus \mathbb{T}^2 ($g = 1$), and on a 2-manifold \mathcal{M} of genus $g = 2$.

by two angles θ_1 and θ_2 . A smooth vector field pointing in the direction of increasing θ_1 never vanishes, and thus has no singularities, consistent with $g = 1$ and $\chi(\mathbb{T}^2) = 0$. Topologically, one can define a torus as the quotient space $\mathbb{R}^2/\mathbb{Z}^2$, or as a square with opposite sides identified. This is what mathematicians call a ‘flat torus’ – one with curvature $K = 0$ everywhere. Of course, such a torus cannot be embedded in three-dimensional Euclidean space; a two-dimensional figure embedded in a three-dimensional Euclidean space inherits a metric due to the embedding, and for a physical torus, like the surface of a bagel, the Gaussian curvature is only zero *on average*.

The $g = 2$ surface \mathcal{M} shown in the right panel of fig. 3.18 has Euler characteristic $\chi(\mathcal{M}) = -2$, which means that any smooth vector field on \mathcal{M} must have singularities with indices totalling -2 . One possibility, depicted in the figure, is to have two saddle points with index -1 ; one of these singularities is shown in the figure (the other would be on the opposite side).

3.6.2 Singularities and topology

For any $N = 1$ system $\dot{x} = f(x)$, we can identify a ‘charge’ Q with any generic fixed point x^* by setting

$$Q = \text{sgn}[f'(x^*)] \quad , \quad (3.73)$$

where $f(x^*) = 0$. The total charge contained in a region $[x_1, x_2]$ is then

$$Q_{12} = \frac{1}{2} \text{sgn}[f(x_2)] - \frac{1}{2} \text{sgn}[f(x_1)] \quad . \quad (3.74)$$

It is easy to see that Q_{12} is the sum of the charges of all the fixed points lying within the interval $[x_1, x_2]$. In higher dimensions, we have the following general construction. Consider an N -dimensional dynam-

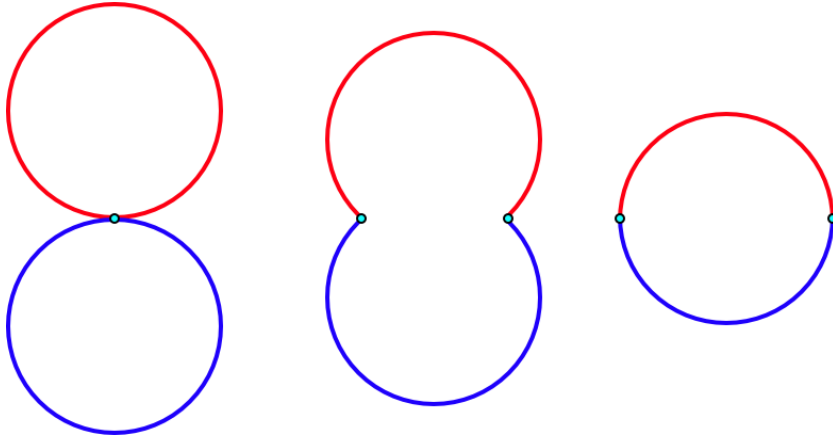


Figure 3.19: Composition of two circles. The same general construction applies to the merging of n -spheres \mathbb{S}^n , called the *wedge sum*.

ical system $\dot{x} = \mathbf{V}(x)$, and let $\hat{n}(x)$ be the unit vector field defined by

$$\hat{n}(x) = \frac{\mathbf{V}(x)}{|\mathbf{V}(x)|} . \quad (3.75)$$

Consider now a unit sphere in \hat{n} space, which is of dimension $(N - 1)$. If we integrate over this surface, we obtain

$$\Omega_N = \oint d\sigma_a n^a = \frac{2\pi^{(N-1)/2}}{\Gamma(\frac{N-1}{2})} , \quad (3.76)$$

which is the surface area of the unit sphere \mathbb{S}^{N-1} . Thus, $\Omega_2 = 2\pi$, $\Omega_3 = 4\pi$, $\Omega_4 = 2\pi^2$, etc.

Now consider a change of variables over the surface of the sphere, to the set $(\xi_1, \dots, \xi_{N-1})$. We then have

$$\Omega_N = \oint_{\mathbb{S}^{N-1}} d\sigma_a n^a = \oint d^{N-1}\xi \epsilon_{a_1 \dots a_N} n^{a_1} \frac{\partial n^{a_2}}{\partial \xi_1} \dots \frac{\partial n^{a_N}}{\partial \xi_{N-1}} \quad (3.77)$$

The topological charge is then

$$Q = \frac{1}{\Omega_N} \oint d^{N-1}\xi \epsilon_{a_1 \dots a_N} n^{a_1} \frac{\partial n^{a_2}}{\partial \xi_1} \dots \frac{\partial n^{a_N}}{\partial \xi_{N-1}} \quad (3.78)$$

The quantity Q is an *integer topological invariant* which characterizes the map from the surface $(\xi_1, \dots, \xi_{N-1})$ to the unit sphere $|\hat{n}| = 1$. In mathematical parlance, Q is known as the *Pontrjagin index* of this map.

This analytical development recapitulates some basic topology. Let \mathcal{M} be a topological space and consider a map from the circle \mathbb{S}^1 to \mathcal{M} . We can compose two such maps by merging the two circles, as shown in fig. 3.19. Two maps are said to be *homotopic* if they can be smoothly deformed into each other. Any two homotopic maps are said to belong to the same *equivalence class* or *homotopy class*. For general \mathcal{M} , the homotopy classes may be multiplied using the composition law, resulting in a group structure. The group is called the *fundamental group* of the manifold \mathcal{M} , and is abbreviated $\pi_1(\mathcal{M})$. If $\mathcal{M} = \mathbb{S}^2$, then

any such map can be smoothly contracted to a point on the 2-sphere, which is to say a trivial map. We then have $\pi_1(\mathcal{M}) = 0$. If $\mathcal{M} = \mathbb{S}^1$, the maps can wind nontrivially, and the homotopy classes are labeled by a single integer winding number: $\pi_1(\mathbb{S}^1) = \mathbb{Z}$. The winding number of the composition of two such maps is the sum of their individual winding numbers. If $\mathcal{M} = \mathbb{T}^2$, the maps can wind nontrivially around either of the two cycles of the 2-torus. We then have $\pi_1(\mathbb{T}^2) = \mathbb{Z}^2$, and in general $\pi_1(\mathbb{T}^n) = \mathbb{Z}^n$. This makes good sense, since an n -torus is topologically equivalent to a product of n circles. In some cases, $\pi_1(\mathcal{M})$ can be nonabelian, as is the case when \mathcal{M} is the genus $g = 2$ structure shown in the right hand panel of fig. 3.18.

In general we define the n^{th} homotopy group $\pi_n(\mathcal{M})$ as the group under composition of maps from \mathbb{S}^n to \mathcal{M} . For $n \geq 2$, $\pi_n(\mathcal{M})$ is abelian. If $\dim(\mathcal{M}) < n$, then $\pi_n(\mathcal{M}) = 0$. In general, $\pi_n(\mathbb{S}^n) = \mathbb{Z}$. These n^{th} homotopy classes of the n -sphere are labeled by their Pontrjagin index Q .

Finally, we ask what is Q in terms of the eigenvalues and eigenvectors of the linearized map

$$M_{ij} = \left. \frac{\partial V_i}{\partial x_j} \right|_{x^*} . \quad (3.79)$$

For simple cases where all the λ_i are nonzero, we have

$$Q = \text{sgn} \left(\prod_{i=1}^N \lambda_i \right) . \quad (3.80)$$

3.7 Appendix : Example Problem

Consider the two-dimensional phase flow,

$$\begin{aligned} \dot{x} &= \frac{1}{2}x + xy - 2x^3 \\ \dot{y} &= \frac{5}{2}y + xy - y^2 . \end{aligned} \quad (3.81)$$

(a) Find and classify all fixed points.

Solution : We have

$$\begin{aligned} \dot{x} &= x \left(\frac{1}{2} + y - 2x^2 \right) \\ \dot{y} &= y \left(\frac{5}{2} + x - y \right) . \end{aligned} \quad (3.82)$$

The matrix of first derivatives is

$$M = \begin{pmatrix} \frac{\partial \dot{x}}{\partial x} & \frac{\partial \dot{x}}{\partial y} \\ \frac{\partial \dot{y}}{\partial x} & \frac{\partial \dot{y}}{\partial y} \end{pmatrix} = \begin{pmatrix} \frac{1}{2} + y - 6x^2 & x \\ y & \frac{5}{2} + x - 2y \end{pmatrix} . \quad (3.83)$$

There are six fixed points.

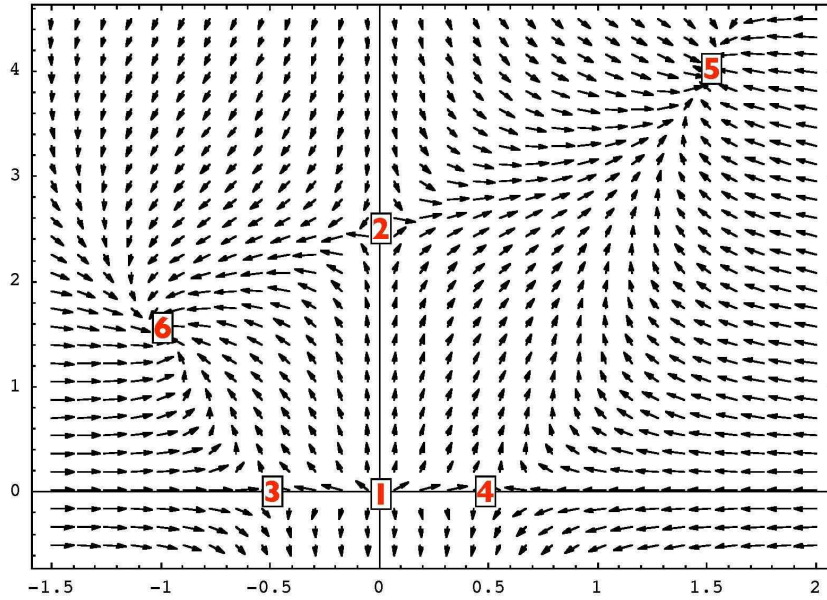


Figure 3.20: Sketch of phase flow for $\dot{x} = \frac{1}{2}x + xy - 2x^3$, $\dot{y} = \frac{5}{2}y + xy - y^2$. Fixed point classifications are in the text.

$(x, y) = (0, 0)$: The derivative matrix is

$$M = \begin{pmatrix} \frac{1}{2} & 0 \\ 0 & \frac{5}{2} \end{pmatrix} . \quad (3.84)$$

The determinant is $D = \frac{5}{4}$ and the trace is $T = 3$. Since $D < \frac{1}{4}T^2$ and $T > 0$, this is an unstable node. (Duh! One can read off both eigenvalues are real and positive.) Eigenvalues: $\lambda_1 = \frac{1}{2}$, $\lambda_2 = \frac{5}{2}$.

$(x, y) = (0, \frac{5}{2})$: The derivative matrix is

$$M = \begin{pmatrix} 3 & 0 \\ \frac{5}{2} & -\frac{5}{2} \end{pmatrix} , \quad (3.85)$$

for which $D = -\frac{15}{2}$ and $T = \frac{1}{2}$. The determinant is negative, so this is a saddle. Eigenvalues: $\lambda_1 = -\frac{5}{2}$, $\lambda_2 = 3$.

$(x, y) = (-\frac{1}{2}, 0)$: The derivative matrix is

$$M = \begin{pmatrix} -1 & -\frac{1}{2} \\ 0 & 2 \end{pmatrix} , \quad (3.86)$$

for which $D = -2$ and $T = +1$. The determinant is negative, so this is a saddle. Eigenvalues: $\lambda_1 = -1$, $\lambda_2 = 2$.

$(x, y) = (\frac{1}{2}, 0)$: The derivative matrix is

$$M = \begin{pmatrix} -1 & \frac{1}{2} \\ 0 & 3 \end{pmatrix} , \quad (3.87)$$

for which $D = -3$ and $T = +2$. The determinant is negative, so this is a saddle. Eigenvalues: $\lambda_1 = -1$, $\lambda_2 = 3$.

$(x, y) = (\frac{3}{2}, 4)$: This is one root obtained by setting $y = x + \frac{5}{2}$ and the solving $\frac{1}{2} + y - 2x^2 = 3 + x - 2x^2 = 0$, giving $x = -1$ and $x = +\frac{3}{2}$. The derivative matrix is

$$M = \begin{pmatrix} -9 & \frac{3}{2} \\ 4 & -4 \end{pmatrix} \quad , \quad (3.88)$$

for which $D = 30$ and $T = -13$. Since $D < \frac{1}{4}T^2$ and $T < 0$, this corresponds to a stable node. Eigenvalues: $\lambda_1 = -10$, $\lambda_2 = -3$.

$(x, y) = (-1, \frac{3}{2})$: This is the second root obtained by setting $y = x + \frac{5}{2}$ and the solving $\frac{1}{2} + y - 2x^2 = 3 + x - 2x^2 = 0$, giving $x = -1$ and $x = +\frac{3}{2}$. The derivative matrix is

$$M = \begin{pmatrix} -4 & -1 \\ \frac{3}{2} & -\frac{3}{2} \end{pmatrix} \quad , \quad (3.89)$$

for which $D = \frac{15}{2}$ and $T = -\frac{11}{2}$. Since $D < \frac{1}{4}T^2$ and $T < 0$, this corresponds to a stable node. Eigenvalues: $\lambda_1 = -3$, $\lambda_2 = -\frac{5}{2}$.

(b) Sketch the phase flow.

Solution : The flow is sketched in fig. 3.20. Thanks to Evan Bierman for providing the Mathematica code.

Chapter 4

Nonlinear Oscillators

4.1 Weakly Perturbed Linear Oscillators

Consider a nonlinear oscillator described by the equation of motion

$$\ddot{x} + \Omega_0^2 x = \epsilon h(x) . \quad (4.1)$$

Here, ϵ is a dimensionless parameter, assumed to be small, and $h(x)$ is a nonlinear function of x . In general, we might consider equations of the form

$$\ddot{x} + \Omega_0^2 x = \epsilon h(x, \dot{x}) , \quad (4.2)$$

such as the van der Pol oscillator,

$$\ddot{x} + \mu(x^2 - 1)\dot{x} + \Omega_0^2 x = 0 . \quad (4.3)$$

First, we will focus on nondissipative systems, *i.e.* where we may write $m\ddot{x} = -\partial_x V$, with $V(x)$ some potential.

As an example, consider the simple pendulum, which obeys

$$\ddot{\theta} + \Omega_0^2 \sin \theta = 0 , \quad (4.4)$$

where $\Omega_0^2 = g/\ell$, with ℓ the length of the pendulum. We may rewrite his equation as

$$\begin{aligned} \ddot{\theta} + \Omega_0^2 \theta &= \Omega_0^2 (\theta - \sin \theta) \\ &= \frac{1}{6} \Omega_0^2 \theta^3 - \frac{1}{120} \Omega_0^2 \theta^5 + \dots \end{aligned} \quad (4.5)$$

The RHS above is a nonlinear function of θ . We can define this to be $h(\theta)$, and take $\epsilon = 1$.

4.1.1 Naïve Perturbation theory and its failure

Let's assume though that ϵ is small, and write a formal power series expansion of the solution $x(t)$ to equation 4.1 as

$$x = x_0 + \epsilon x_1 + \epsilon^2 x_2 + \dots . \quad (4.6)$$

We now plug this into 4.1. We need to use Taylor's theorem,

$$h(x_0 + \eta) = h(x_0) + h'(x_0) \eta + \frac{1}{2} h''(x_0) \eta^2 + \dots \quad (4.7)$$

with

$$\eta = \epsilon x_1 + \epsilon^2 x_2 + \dots \quad . \quad (4.8)$$

Working out the resulting expansion in powers of ϵ is tedious. One finds

$$h(x) = h(x_0) + \epsilon h'(x_0) x_1 + \epsilon^2 \left\{ h'(x_0) x_2 + \frac{1}{2} h''(x_0) x_1^2 \right\} + \dots \quad . \quad (4.9)$$

Equating terms of the same order in ϵ , we obtain a hierarchical set of equations,

$$\begin{aligned} \ddot{x}_0 + \Omega_0^2 x_0 &= 0 \\ \ddot{x}_1 + \Omega_0^2 x_1 &= h(x_0) \\ \ddot{x}_2 + \Omega_0^2 x_2 &= h'(x_0) x_1 \\ \ddot{x}_3 + \Omega_0^2 x_3 &= h'(x_0) x_2 + \frac{1}{2} h''(x_0) x_1^2 \end{aligned} \quad (4.10)$$

et cetera, where prime denotes differentiation with respect to argument. The first of these is easily solved: $x_0(t) = A \cos(\Omega_0 t + \varphi)$, where A and φ are constants. This solution then is plugged in at the next order, to obtain an inhomogeneous equation for $x_1(t)$. Solve for $x_1(t)$ and insert into the following equation for $x_2(t)$, etc. It looks straightforward enough.

The problem is that resonant forcing terms generally appear in the RHS of each equation of the hierarchy past the first. Define $\theta \equiv \Omega_0 t + \varphi$. Then $x_0(\theta)$ is an even periodic function of θ with period 2π , hence so is $h(x_0)$. We may then expand $h(x_0(\theta))$ in a Fourier series:

$$h(A \cos \theta) = \sum_{n=0}^{\infty} h_n(A) \cos(n\theta) \quad . \quad (4.11)$$

The $n = 1$ term leads to resonant forcing. Thus, the solution for $x_1(t)$ is

$$x_1(t) = \frac{1}{\Omega_0^2} \sum_{\substack{n=0 \\ (n \neq 1)}}^{\infty} \frac{h_n(A)}{1 - n^2} \cos(n\Omega_0 t + n\varphi) + \frac{h_1(A)}{2\Omega_0} t \sin(\Omega_0 t + \varphi) \quad , \quad (4.12)$$

which increases linearly with time. As an example, consider a cubic nonlinearity with $h(x) = r x^3$, where r is a constant. Then using

$$\cos^3 \theta = \frac{3}{4} \cos \theta + \frac{1}{4} \cos(3\theta) \quad , \quad (4.13)$$

we have $h_1 = \frac{3}{4} r A^3$ and $h_3 = \frac{1}{4} r A^3$.

4.1.2 Poincaré-Lindstedt method

The problem here is that the nonlinear oscillator has a different frequency than its linear counterpart. Indeed, if we assume the frequency Ω is a function of ϵ , with

$$\Omega(\epsilon) = \Omega_0 + \epsilon \Omega_1 + \epsilon^2 \Omega_2 + \dots , \quad (4.14)$$

then subtracting the unperturbed solution from the perturbed one and expanding in ϵ yields

$$\begin{aligned} \cos(\Omega t) - \cos(\Omega_0 t) &= -\sin(\Omega_0 t) (\Omega - \Omega_0) t - \frac{1}{2} \cos(\Omega_0 t) (\Omega - \Omega_0)^2 t^2 + \dots \\ &= -\epsilon \sin(\Omega_0 t) \Omega_1 t - \epsilon^2 \left\{ \sin(\Omega_0 t) \Omega_2 t + \frac{1}{2} \cos(\Omega_0 t) \Omega_1^2 t^2 \right\} + \mathcal{O}(\epsilon^3) . \end{aligned} \quad (4.15)$$

What perturbation theory can do for us is to provide a good solution *up to a given time*, provided that ϵ is *sufficiently small*. It *will not* give us a solution that is close to the true answer for *all* time. We see above that in order to do that, and to recover the shifted frequency $\Omega(\epsilon)$, we would have to resum perturbation theory to all orders, which is a daunting task.

The Poincaré-Lindstedt method obviates this difficulty by assuming $\Omega = \Omega(\epsilon)$ from the outset. Define a dimensionless time $s \equiv \Omega t$ and write 4.1 as

$$\Omega^2 \frac{d^2x}{ds^2} + \Omega_0^2 x = \epsilon h(x) , \quad (4.16)$$

where

$$\begin{aligned} x &= x_0 + \epsilon x_1 + \epsilon^2 x_2 + \dots \\ \Omega^2 &= a_0 + \epsilon a_1 + \epsilon^2 a_2 + \dots . \end{aligned} \quad (4.17)$$

We now plug the above expansions into 4.16:

$$\begin{aligned} (a_0 + \epsilon a_1 + \epsilon^2 a_2 + \dots) \left(\frac{d^2x_0}{ds^2} + \epsilon \frac{d^2x_1}{ds^2} + \epsilon^2 \frac{d^2x_2}{ds^2} + \dots \right) + \Omega_0^2 (x_0 + \epsilon x_1 + \epsilon^2 x_2 + \dots) \\ \epsilon h(x_0) + \epsilon^2 h'(x_0) x_1 + \epsilon^3 \left\{ h'(x_0) x_2 + \frac{1}{2} h''(x_0) x_1^2 \right\} + \dots \end{aligned} \quad (4.18)$$

Now let's write down equalities at each order in ϵ :

$$\begin{aligned} a_0 \frac{d^2x_0}{ds^2} + \Omega_0^2 x_0 &= 0 \\ a_0 \frac{d^2x_1}{ds^2} + \Omega_0^2 x_1 &= h(x_0) - a_1 \frac{d^2x_0}{ds^2} \\ a_0 \frac{d^2x_2}{ds^2} + \Omega_0^2 x_2 &= h'(x_0) x_1 - a_2 \frac{d^2x_0}{ds^2} - a_1 \frac{d^2x_1}{ds^2} , \end{aligned} \quad (4.19)$$

et cetera.

The first equation of the hierarchy is immediately solved by

$$a_0 = \Omega_0^2 \quad , \quad x_0(s) = A \cos(s + \varphi) \quad . \quad (4.20)$$

At $\mathcal{O}(\epsilon)$, then, we have

$$\frac{d^2x_1}{ds^2} + x_1 = \Omega_0^{-2} h(A \cos(s + \varphi)) + \Omega_0^{-2} a_1 A \cos(s + \varphi) \quad . \quad (4.21)$$

The LHS of the above equation has a natural frequency of unity (in terms of the dimensionless time s). We expect $h(x_0)$ to contain resonant forcing terms, per 4.11. However, we now have the freedom to adjust the undetermined coefficient a_1 to *cancel* any such resonant term. Clearly we must choose

$$a_1 = -\frac{h_1(A)}{A} \quad . \quad (4.22)$$

The solution for $x_1(s)$ is then

$$x_1(s) = \frac{1}{\Omega_0^2} \sum_{\substack{n=0 \\ (n \neq 1)}}^{\infty} \frac{h_n(A)}{1-n^2} \cos(ns + n\varphi) \quad , \quad (4.23)$$

which is periodic and hence does not increase in magnitude without bound, as does 4.12. The perturbed frequency is then obtained from

$$\Omega^2 = \Omega_0^2 - \frac{h_1(A)}{A} \epsilon + \mathcal{O}(\epsilon^2) \implies \Omega(\epsilon) = \Omega_0 - \frac{h_1(A)}{2A\Omega_0} \epsilon + \mathcal{O}(\epsilon^2) \quad . \quad (4.24)$$

Note that Ω depends on the amplitude of the oscillations.

As an example, consider an oscillator with a quartic nonlinearity in the potential, *i.e.* $h(x) = r x^3$. Then

$$h(A \cos \theta) = \frac{3}{4} r A^3 \cos \theta + \frac{1}{4} r A^3 \cos(3\theta) \quad . \quad (4.25)$$

We then obtain, setting $\epsilon = 1$ at the end of the calculation,

$$\Omega = \Omega_0 - \frac{3rA^2}{8\Omega_0} + \dots \quad (4.26)$$

where the remainder is higher order in the amplitude A . In the case of the pendulum,

$$\ddot{\theta} + \Omega_0^2 \theta = \frac{1}{6} \Omega_0^2 \theta^3 + \mathcal{O}(\theta^5) \quad , \quad (4.27)$$

and with $r = \frac{1}{6} \Omega_0^2$ and $\theta_0(t) = \theta_0 \sin(\Omega t)$, we find

$$T(\theta_0) = \frac{2\pi}{\Omega} = \frac{2\pi}{\Omega_0} \cdot \left\{ 1 + \frac{1}{16} \theta_0^2 + \dots \right\} \quad . \quad (4.28)$$

One can check that this is correct to lowest nontrivial order in the amplitude, using the exact result for the period,

$$T(\theta_0) = \frac{4}{\Omega_0} \mathbb{K}\left(\sin^2 \frac{1}{2}\theta_0\right) \quad , \quad (4.29)$$

where $\mathbb{K}(x)$ is the complete elliptic integral.

The procedure can be continued to the next order, where the free parameter a_2 is used to eliminate resonant forcing terms on the RHS.

A good exercise to test one's command of the method is to work out the lowest order nontrivial corrections to the frequency of an oscillator with a quadratic nonlinearity, such as $h(x) = rx^2$. One finds that there are no resonant forcing terms at first order in ϵ , hence one must proceed to second order to find the first nontrivial corrections to the frequency.

4.2 Multiple Time Scale Method

Another method of eliminating secular terms (*i.e.* driving terms which oscillate at the resonant frequency of the unperturbed oscillator), and one which has applicability beyond periodic motion alone, is that of multiple time scale analysis. Consider the equation

$$\ddot{x} + x = \epsilon h(x, \dot{x}) \quad , \quad (4.30)$$

where ϵ is presumed small, and $h(x, \dot{x})$ is a nonlinear function of position and/or velocity. We define a hierarchy of time scales: $T_n \equiv \epsilon^n t$. There is a normal time scale $T_0 = t$, slow time scale $T_1 = \epsilon t$, a 'superslow' time scale $T_2 = \epsilon^2 t$, etc. Thus,

$$\begin{aligned} \frac{d}{dt} &= \frac{\partial}{\partial T_0} + \epsilon \frac{\partial}{\partial T_1} + \epsilon^2 \frac{\partial}{\partial T_2} + \dots \\ &= \sum_{n=0}^{\infty} \epsilon^n \frac{\partial}{\partial T_n} \quad . \end{aligned} \quad (4.31)$$

Next, we expand

$$x(t) = \sum_{n=0}^{\infty} \epsilon^n x_n(T_0, T_1, \dots) \quad . \quad (4.32)$$

Thus, we have

$$\left(\sum_{n=0}^{\infty} \epsilon^n \frac{\partial}{\partial T_n} \right)^2 \left(\sum_{k=0}^{\infty} \epsilon^k x_k \right) + \sum_{k=0}^{\infty} \epsilon^k x_k = \epsilon h \left(\sum_{k=0}^{\infty} \epsilon^k x_k \quad , \quad \sum_{n=0}^{\infty} \epsilon^n \frac{\partial}{\partial T_n} \left(\sum_{k=0}^{\infty} \epsilon^k x_k \right) \right) \quad .$$

We now evaluate this order by order in ϵ :

$$\begin{aligned} \mathcal{O}(\epsilon^0) : \quad &\left(\frac{\partial^2}{\partial T_0^2} + 1 \right) x_0 = 0 \\ \mathcal{O}(\epsilon^1) : \quad &\left(\frac{\partial^2}{\partial T_0^2} + 1 \right) x_1 = -2 \frac{\partial^2 x_0}{\partial T_0 \partial T_1} + h \left(x_0, \frac{\partial x_0}{\partial T_0} \right) \\ \mathcal{O}(\epsilon^2) : \quad &\left(\frac{\partial^2}{\partial T_0^2} + 1 \right) x_2 = -2 \frac{\partial^2 x_1}{\partial T_0 \partial T_1} - 2 \frac{\partial^2 x_0}{\partial T_0 \partial T_2} - \frac{\partial^2 x_0}{\partial T_1^2} + \frac{\partial h}{\partial x} \Big|_{\{x_0, \dot{x}_0\}} x_1 + \frac{\partial h}{\partial \dot{x}} \Big|_{\{x_0, \dot{x}_0\}} \left(\frac{\partial x_1}{\partial T_0} + \frac{\partial x_0}{\partial T_1} \right) \quad , \end{aligned} \quad (4.33)$$

et cetera. The expansion gets more and more tedious with increasing order in ϵ .

Let's carry this procedure out to first order in ϵ . To order ϵ^0 ,

$$x_0 = A \cos(T_0 + \phi) , \quad (4.34)$$

where A and ϕ are arbitrary (at this point) functions of $\{T_1, T_2, \dots\}$. Now we solve the next equation in the hierarchy, for x_1 . Let $\theta \equiv T_0 + \phi$. Then $\frac{\partial}{\partial T_0} = \frac{\partial}{\partial \theta}$ and we have

$$\left(\frac{\partial^2}{\partial \theta^2} + 1 \right) x_1 = 2 \frac{\partial A}{\partial T_1} \sin \theta + 2A \frac{\partial \phi}{\partial T_1} \cos \theta + h(A \cos \theta, -A \sin \theta) . \quad (4.35)$$

Since the arguments of h are periodic under $\theta \rightarrow \theta + 2\pi$, we may expand h in a Fourier series:

$$h(\theta) \equiv h(A \cos \theta, -A \sin \theta) = \sum_{k=1}^{\infty} \alpha_k(A) \sin(k\theta) + \sum_{k=0}^{\infty} \beta_k(A) \cos(k\theta) . \quad (4.36)$$

The inverse of this relation is

$$\begin{aligned} \alpha_k(A) &= \int_0^{2\pi} \frac{d\theta}{\pi} h(\theta) \sin(k\theta) , \quad k > 0 \\ \beta_0(A) &= \int_0^{2\pi} \frac{d\theta}{2\pi} h(\theta) \\ \beta_k(A) &= \int_0^{2\pi} \frac{d\theta}{\pi} h(\theta) \cos(k\theta) , \quad k > 0 . \end{aligned} \quad (4.37)$$

We now demand that the secular terms on the RHS – those terms proportional to $\cos \theta$ and $\sin \theta$ – must vanish. This means

$$\begin{aligned} 2 \frac{\partial A}{\partial T_1} + \alpha_1(A) &= 0 \\ 2A \frac{\partial \phi}{\partial T_1} + \beta_1(A) &= 0 . \end{aligned} \quad (4.38)$$

These two first order equations require two initial conditions, which is sensible since our initial equation $\ddot{x} + x = \epsilon h(x, \dot{x})$ is second order in time.

With the secular terms eliminated, we may solve for x_1 :

$$x_1 = \sum_{k \neq 1}^{\infty} \left\{ \frac{\alpha_k(A)}{1 - k^2} \sin(k\theta) + \frac{\beta_k(A)}{1 - k^2} \cos(k\theta) \right\} + C_0 \cos \theta + D_0 \sin \theta . \quad (4.39)$$

Note: (i) the $k = 1$ terms are excluded from the sum, and (ii) an arbitrary solution to the homogeneous equation, *i.e.* eqn. 4.35 with the right hand side set to zero, is included. The constants C_0 and D_0 are arbitrary functions of $T_1, T_2, \text{etc.}$.

The equations for A and ϕ are both first order in T_1 . They will therefore involve two constants of integration – call them A_0 and ϕ_0 . At second order, these constants are taken as dependent upon the superslow time scale T_2 . *The method itself may break down at this order.* (See if you can find out why.)

Let's apply this to the nonlinear oscillator $\ddot{x} + \sin x = 0$, also known as the simple pendulum. We'll expand the sine function to include only the lowest order nonlinear term, and consider

$$\ddot{x} + x = \frac{1}{6}\epsilon x^3 . \quad (4.40)$$

We'll assume ϵ is small and take $\epsilon = 1$ at the end of the calculation. This will work provided the amplitude of the oscillation is itself small. To zeroth order, we have $x_0 = A \cos(t + \phi)$, as always. At first order, we must solve

$$\begin{aligned} \left(\frac{\partial^2}{\partial \theta^2} + 1 \right) x_1 &= 2 \frac{\partial A}{\partial T_1} \sin \theta + 2A \frac{\partial \phi}{\partial T_1} \cos \theta + \frac{1}{6} A^3 \cos^3 \theta \\ &= 2 \frac{\partial A}{\partial T_1} \sin \theta + 2A \frac{\partial \phi}{\partial T_1} \cos \theta + \frac{1}{24} A^3 \cos(3\theta) + \frac{1}{8} A^3 \cos \theta . \end{aligned} \quad (4.41)$$

We eliminate the secular terms by demanding

$$\frac{\partial A}{\partial T_1} = 0 , \quad \frac{\partial \phi}{\partial T_1} = -\frac{1}{16} A^2 , \quad (4.42)$$

hence $A = A_0$ and $\phi = -\frac{1}{16} A_0^2 T_1 + \phi_0$, and

$$x(t) = A_0 \cos \left(t - \frac{1}{16} \epsilon A_0^2 t + \phi_0 \right) - \frac{1}{192} \epsilon A_0^3 \cos \left(3t - \frac{3}{16} \epsilon A_0^2 t + 3\phi_0 \right) + \dots , \quad (4.43)$$

which reproduces the result obtained from the Poincaré-Lindstedt method.

4.2.1 Duffing oscillator

Consider the equation

$$\ddot{x} + 2\epsilon\mu\dot{x} + x + \epsilon x^3 = 0 . \quad (4.44)$$

This describes a damped nonlinear oscillator. Here we assume both the damping coefficient $\tilde{\mu} \equiv \epsilon\mu$ as well as the nonlinearity both depend linearly on the small parameter ϵ . We may write this equation in our standard form $\ddot{x} + x = \epsilon h(x, \dot{x})$, with $h(x, \dot{x}) = -2\mu\dot{x} - x^3$.

For $\epsilon > 0$, which we henceforth assume, it is easy to see that the only fixed point is $(x, \dot{x}) = (0, 0)$. The linearized flow in the vicinity of the fixed point is given by

$$\frac{d}{dt} \begin{pmatrix} x \\ \dot{x} \end{pmatrix} = \begin{pmatrix} 0 & 1 \\ -1 & -2\epsilon\mu \end{pmatrix} \begin{pmatrix} x \\ \dot{x} \end{pmatrix} + \mathcal{O}(x^3) . \quad (4.45)$$

The determinant is $D = 1$ and the trace is $T = -2\epsilon\mu$. Thus, provided $\epsilon\mu < 1$, the fixed point is a stable spiral; for $\epsilon\mu > 1$ the fixed point becomes a stable node.

We employ the multiple time scale method to order ϵ . We have $x_0 = A \cos(T_0 + \phi)$ to zeroth order, as usual. The nonlinearity is expanded in a Fourier series in $\theta = T_0 + \phi$:

$$\begin{aligned} h\left(x_0, \frac{\partial x_0}{\partial T_0}\right) &= 2\mu A \sin \theta - A^3 \cos^3 \theta \\ &= 2\mu A \sin \theta - \frac{3}{4}A^3 \cos \theta - \frac{1}{4}A^3 \cos 3\theta . \end{aligned} \quad (4.46)$$

Thus, $\alpha_1(A) = 2\mu A$ and $\beta_1(A) = -\frac{3}{4}A^3$. We now solve the first order equations,

$$\frac{\partial A}{\partial T_1} = -\frac{1}{2} \alpha_1(A) = -\mu A \quad \implies \quad A(T) = A_0 e^{-\mu T_1} \quad (4.47)$$

as well as

$$\frac{\partial \phi}{\partial T_1} = -\frac{\beta_1(A)}{2A} = \frac{3}{8}A_0^2 e^{-2\mu T_1} \quad \implies \quad \phi(T_1) = \phi_0 + \frac{3A_0^2}{16\mu} (1 - e^{-2\mu T_1}) . \quad (4.48)$$

After elimination of the secular terms, we may read off

$$x_1(T_0, T_1) = \frac{1}{32}A^3(T_1) \cos(3T_0 + 3\phi(T_1)) . \quad (4.49)$$

Finally, we have

$$\begin{aligned} x(t) &= A_0 e^{-\epsilon \mu t} \cos\left(t + \frac{3A_0^2}{16\mu} (1 - e^{-2\epsilon \mu t}) + \phi_0\right) \\ &\quad + \frac{1}{32}\epsilon A_0^3 e^{-3\epsilon \mu t} \cos\left(3t + \frac{9A_0^2}{16\mu} (1 - e^{-2\epsilon \mu t}) + 3\phi_0\right) . \end{aligned} \quad (4.50)$$

4.2.2 Van der Pol oscillator

Let's apply this method to another problem, that of the van der Pol oscillator,

$$\ddot{x} + \epsilon(x^2 - 1)\dot{x} + x = 0 , \quad (4.51)$$

with $\epsilon > 0$. The nonlinear term acts as a frictional drag for $x > 1$, and as a 'negative friction' (*i.e.* increasing the amplitude) for $x < 1$. Note that the linearized equation at the fixed point ($x = 0, \dot{x} = 0$) corresponds to an unstable spiral for $\epsilon < 2$.

For the van der Pol oscillator, we have $h(x, \dot{x}) = (1 - x^2)\dot{x}$, and plugging in the zeroth order solution $x_0 = A \cos(t + \phi)$ gives

$$\begin{aligned} h\left(x_0, \frac{\partial x_0}{\partial T_0}\right) &= (1 - A^2 \cos^2 \theta) (-A \sin \theta) \\ &= (-A + \frac{1}{4}A^3) \sin \theta + \frac{1}{4}A^3 \sin(3\theta) , \end{aligned} \quad (4.52)$$

with $\theta \equiv t + \phi$. Thus, $\alpha_1 = -A + \frac{1}{4}A^3$ and $\beta_1 = 0$, which gives $\phi = \phi_0$ and

$$2 \frac{\partial A}{\partial T_1} = A - \frac{1}{4}A^3 . \quad (4.53)$$

The equation for A is easily integrated:

$$\begin{aligned} dT_1 = -\frac{8dA}{A(A^2-4)} &= \left(\frac{2}{A} - \frac{1}{A-2} - \frac{1}{A+2} \right) dA = d \ln \left(\frac{A}{A^2-4} \right) \\ \implies A(T_1) &= \frac{2}{\sqrt{1 - \left(1 - \frac{4}{A_0^2}\right) \exp(-T_1)}} . \end{aligned} \quad (4.54)$$

Thus,

$$x_0(t) = \frac{2 \cos(t + \phi_0)}{\sqrt{1 - \left(1 - \frac{4}{A_0^2}\right) \exp(-\epsilon t)}} . \quad (4.55)$$

This behavior describes the approach to the limit cycle $2 \cos(t + \phi_0)$. With the elimination of the secular terms, we have

$$x_1(t) = -\frac{1}{32} A^3 \sin(3\theta) = -\frac{\frac{1}{4} \sin(3t + 3\phi_0)}{\left[1 - \left(1 - \frac{4}{A_0^2}\right) \exp(-\epsilon t)\right]^{3/2}} . \quad (4.56)$$

4.3 Forced Nonlinear Oscillations

The forced, damped linear oscillator,

$$\ddot{x} + 2\mu\dot{x} + x = f_0 \cos \Omega t \quad (4.57)$$

has the solution

$$x(t) = x_h(t) + C(\Omega) \cos(\Omega t + \delta(\Omega)) , \quad (4.58)$$

where

$$x_h(t) = A_+ e^{\lambda_+ t} + A_- e^{\lambda_- t} , \quad (4.59)$$

where $\lambda_{\pm} = -\mu \pm \sqrt{\mu^2 - 1}$ are the roots of $\lambda^2 + 2\mu\lambda + 1 = 0$. The ‘susceptibility’ C and phase shift δ are given by

$$C(\Omega) = \frac{1}{\sqrt{(\Omega^2 - 1)^2 + 4\mu^2\Omega^2}} , \quad \delta(\Omega) = \tan^{-1} \left(\frac{2\mu\Omega}{1 - \Omega^2} \right) . \quad (4.60)$$

The homogeneous solution, $x_h(t)$, is a transient and decays exponentially with time, since $\text{Re}(\lambda_{\pm}) < 0$. The asymptotic behavior is a phase-shifted oscillation at the driving frequency Ω .

Now let’s add a nonlinearity. We study the equation

$$\ddot{x} + x = \epsilon h(x, \dot{x}) + \epsilon f_0 \cos(t + \epsilon\nu t) . \quad (4.61)$$

Note that amplitude of the driving term, $\epsilon f_0 \cos(\Omega t)$, is assumed to be small, *i.e.* proportional to ϵ , and the driving frequency $\Omega = 1 + \epsilon\nu$ is assumed to be close to resonance. (The resonance frequency of the unperturbed oscillator is $\omega_{\text{res}} = 1$.) Were the driving frequency far from resonance, it could be dealt

with in the same manner as the non-secular terms encountered thus far. The situation when Ω is close to resonance deserves our special attention.

At order ϵ^0 , we still have $x_0 = A \cos(T_0 + \phi)$. We write

$$\Omega t = t + \epsilon\nu t = T_0 + \nu T_1 \equiv \theta - \psi \quad , \quad (4.62)$$

where $\theta = T_0 + \phi(T_1)$ as before, and $\psi(T_1) \equiv \phi(T_1) - \nu T_1$. At order ϵ^1 , we must then solve

$$\begin{aligned} \left(\frac{\partial^2}{\partial \theta^2} + 1 \right) x_1 &= 2A' \sin \theta + 2A\phi' \cos \theta + h(A \cos \theta, -A \sin \theta) + f_0 \cos(\theta - \psi) \\ &= \sum_{k \neq 1} \left(\alpha_k \sin(k\theta) + \beta_k \cos(k\theta) \right) + \left(2A' + \alpha_1 + f_0 \sin \psi \right) \sin \theta \\ &\quad + \left(2A\psi' + 2A\nu + \beta_1 + f_0 \cos \psi \right) \cos \theta \quad , \end{aligned} \quad (4.63)$$

where the prime denotes differentiation with respect to T_1 . We thus have the $N = 2$ dynamical system

$$\begin{aligned} \frac{dA}{dT_1} &= -\frac{1}{2}\alpha_1(A) - \frac{1}{2}f_0 \sin \psi \\ \frac{d\psi}{dT_1} &= -\nu - \frac{\beta_1(A)}{2A} - \frac{f_0}{2A} \cos \psi \quad . \end{aligned} \quad (4.64)$$

If we assume that $\{A, \psi\}$ approaches a fixed point of these dynamics, then at the fixed point these equations provide a relation between the amplitude A , the ‘detuning’ parameter ν , and the drive f_0 :

$$\left[\alpha_1(A) \right]^2 + \left[2\nu A + \beta_1(A) \right]^2 = f_0^2 \quad . \quad (4.65)$$

In general this is a nonlinear equation for $A(f_0, \nu)$. The linearized (A, ψ) dynamics in the vicinity of a fixed point is governed by the matrix

$$M = \begin{pmatrix} \partial \dot{A} / \partial A & \partial \dot{A} / \partial \psi \\ \partial \dot{\psi} / \partial A & \partial \dot{\psi} / \partial \psi \end{pmatrix} = \begin{pmatrix} -\frac{1}{2}\alpha'_1(A) & \nu A + \frac{1}{2}\beta_1(A) \\ -\frac{\beta'_1(A)}{2A} - \frac{\nu}{A} & -\frac{\alpha_1(A)}{2A} \end{pmatrix} \quad . \quad (4.66)$$

If the (A, ψ) dynamics exhibits a stable fixed point (A^*, ψ^*) , then one has

$$x_0(t) = A^* \cos(T_0 + \nu T_1 + \psi^*) = A^* \cos(\Omega t + \psi^*) \quad . \quad (4.67)$$

The oscillator’s frequency is then the forcing frequency $\Omega = 1 + \epsilon\nu$, in which case the oscillator is said to be *entrained*, or *synchronized*, with the forcing. Note that

$$\det M = \frac{F'(A^*)}{8A^*} \quad .$$

4.3.1 Forced Duffing oscillator

Thus far our approach has been completely general. We now restrict our attention to the Duffing equation, for which

$$\alpha_1(A) = 2\mu A \quad , \quad \beta_1(A) = -\frac{3}{4}A^3 \quad , \quad (4.68)$$

which yields the cubic equation

$$A^6 - \frac{16}{3}\nu A^4 + \frac{64}{9}(\mu^2 + \nu^2)A^2 - \frac{16}{9}f_0^2 = 0 \quad . \quad (4.69)$$

Analyzing the cubic is a good exercise. Setting $y = A^2$, we define

$$G(y) \equiv y^3 - \frac{16}{3}\nu y^2 + \frac{64}{9}(\mu^2 + \nu^2) y \quad , \quad (4.70)$$

and we seek a solution to $G(y) = \frac{16}{9}f_0^2$. Setting $G'(y) = 0$, we find roots at

$$y_{\pm} = \frac{16}{9}\nu \pm \frac{8}{9}\sqrt{\nu^2 - 3\mu^2} \quad . \quad (4.71)$$

If $\nu^2 < 3\mu^2$ the roots are imaginary, which tells us that $G(y)$ is monotonically increasing for real y . There is then a unique solution to $G(y) = \frac{16}{9}f_0^2$.

If $\nu^2 > 3\mu^2$, then the cubic $G(y)$ has a local maximum at $y = y_-$ and a local minimum at $y = y_+$. For $\nu < -\sqrt{3}\mu$, we have $y_- < y_+ < 0$, and since $y = A^2$ must be positive, this means that once more there is a unique solution to $G(y) = \frac{16}{9}f_0^2$.

For $\nu > \sqrt{3}\mu$, we have $y_+ > y_- > 0$. There are then three solutions for $y(\nu)$ for $f_0 \in [f_0^-, f_0^+]$, where $f_0^{\pm} = \frac{3}{4}\sqrt{G(y_{\mp})}$. If we define $\kappa \equiv \nu/\mu$, then

$$f_0^{\pm} = \frac{8}{9}\mu^{3/2}\sqrt{\kappa^3 + 9\kappa \pm \sqrt{\kappa^2 - 3}} \quad . \quad (4.72)$$

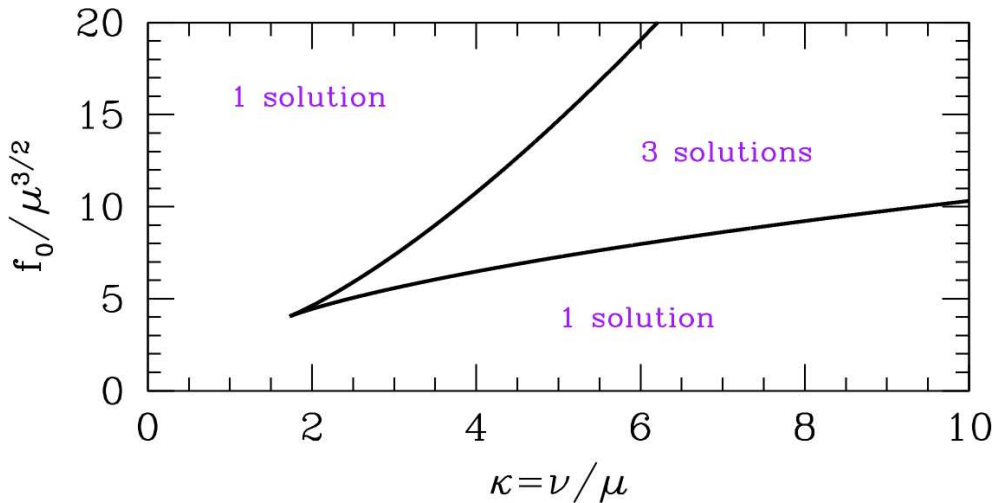


Figure 4.1: Phase diagram for the forced Duffing oscillator.

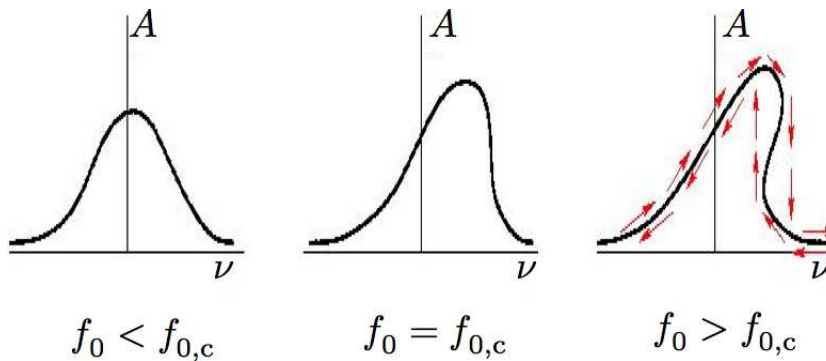


Figure 4.2: Amplitude A versus detuning ν for the forced Duffing oscillator for three values of the drive f_0 . The critical drive is $f_{0,c} = \frac{16}{3^{5/4}} \mu^{3/2}$. For $f_0 > f_{0,c}$, there is hysteresis as a function of the detuning.

The phase diagram is shown in Fig. 4.1. The minimum value for f_0 is $f_{0,c} = \frac{16}{3^{5/4}} \mu^{3/2}$, which occurs at $\kappa = \sqrt{3}$.

Thus far we have assumed that the (A, ψ) dynamics evolves to a fixed point. We should check to make sure that this fixed point is in fact stable. To do so, we evaluate the linearized dynamics at the fixed point. Writing $A = A^* + \delta A$ and $\psi = \psi^* + \delta\psi$, we have

$$\frac{d}{dT_1} \begin{pmatrix} \delta A \\ \delta\psi \end{pmatrix} = M \begin{pmatrix} \delta A \\ \delta\psi \end{pmatrix} , \quad (4.73)$$

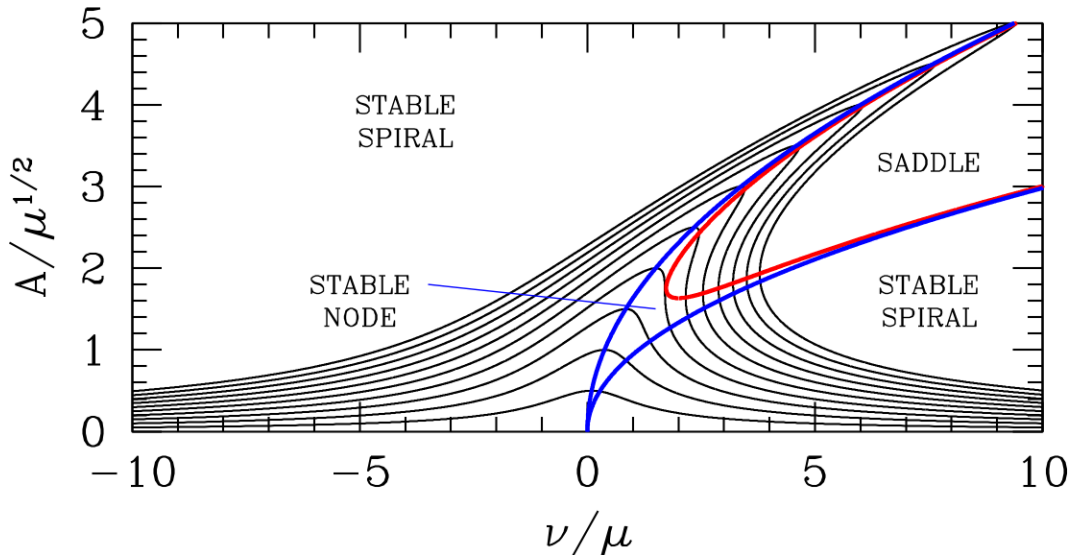


Figure 4.3: Amplitude versus detuning ν for the forced Duffing oscillator for ten equally spaced values of f_0 between $\mu^{3/2}$ and $10\mu^{3/2}$. The critical value is $f_{0,c} = 4.0525 \mu^{3/2}$. The red and blue curves are boundaries for the fixed point classification.

with

$$M = \begin{pmatrix} \frac{\partial \dot{A}}{\partial A} & \frac{\partial \dot{A}}{\partial \psi} \\ \frac{\partial \dot{\psi}}{\partial A} & \frac{\partial \dot{\psi}}{\partial \psi} \end{pmatrix} = \begin{pmatrix} -\mu & -\frac{1}{2}f_0 \cos \psi \\ \frac{3}{4}A + \frac{f_0}{2A^2} \cos \psi & \frac{f_0}{2A} \sin \psi \end{pmatrix} = \begin{pmatrix} -\mu & \nu A - \frac{3}{8}A^3 \\ \frac{9}{8}A - \frac{\nu}{A} & -\mu \end{pmatrix} . \quad (4.74)$$

One then has $T = -2\mu$ and

$$D = \mu^2 + (\nu - \frac{3}{8}A^2)(\nu - \frac{9}{8}A^2) . \quad (4.75)$$

Setting $D = \frac{1}{4}T^2 = \mu^2$ sets the boundary between stable spiral and stable node. Setting $D = 0$ sets the boundary between stable node and saddle. The fixed point structure is as shown in Fig. 4.3. Though the amplitude exhibits hysteresis, the oscillator frequency is always synchronized with the forcing as one varies the detuning.

4.3.2 Forced van der Pol oscillator

Consider now a weakly dissipative, weakly forced van der Pol oscillator, governed by the equation

$$\ddot{x} + \epsilon(x^2 - 1)\dot{x} + x = \epsilon f_0 \cos(t + \epsilon\nu t) , \quad (4.76)$$

where the forcing frequency is $\Omega = 1 + \epsilon\nu$, which is close to the natural frequency $\omega_0 = 1$. We apply the multiple time scale method, with $h(x, \dot{x}) = (1 - x^2)\dot{x}$. As usual, the lowest order solution is $x_0 = A(T_1) \cos(T_0 + \phi(T_1))$, where $T_0 = t$ and $T_1 = \epsilon t$. Again, we define $\theta \equiv T_0 + \phi(T_1)$ and $\psi(T_1) \equiv \phi(T_1) - \nu T_1$. From

$$h(A \cos \theta, -A \sin \theta) = \left(\frac{1}{4}A^3 - A\right) \sin \theta + \frac{1}{4}A^3 \sin(3\theta) , \quad (4.77)$$

we arrive at

$$\begin{aligned} \left(\frac{\partial^2}{\partial \theta^2} + 1\right)x_1 &= -2\frac{\partial^2 x_0}{\partial T_0 \partial T_1} + h\left(x_0, \frac{\partial x_0}{\partial T_0}\right) \\ &= \left(\frac{1}{4}A^3 - A + 2A' + f_0 \sin \psi\right) \sin \theta \\ &\quad + (2A\psi' + 2\nu A + f_0 \cos \psi) \cos \theta + \frac{1}{4}A^3 \sin(3\theta) . \end{aligned} \quad (4.78)$$

We eliminate the secular terms, proportional to $\sin \theta$ and $\cos \theta$, by demanding

$$\begin{aligned} \frac{dA}{dT_1} &= \frac{1}{2}A - \frac{1}{8}A^3 - \frac{1}{2}f_0 \sin \psi \\ \frac{d\psi}{dT_1} &= -\nu - \frac{f_0}{2A} \cos \psi . \end{aligned} \quad (4.79)$$

Stationary solutions have $A' = \psi' = 0$, hence $\cos \psi = -2\nu A / f_0$, and hence

$$\begin{aligned} f_0^2 &= 4\nu^2 A^2 + \left(1 - \frac{1}{4}A^2\right)^2 A^2 \\ &= \frac{1}{16}A^6 - \frac{1}{2}A^4 + (1 + 4\nu^2)A^2 . \end{aligned} \quad (4.80)$$

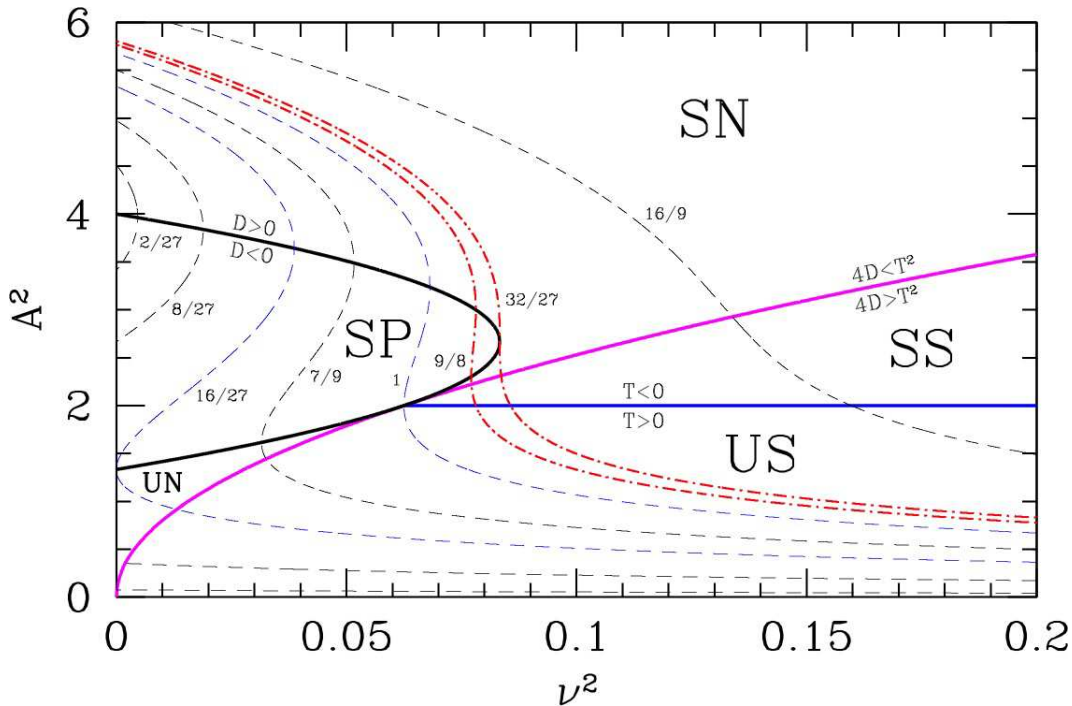


Figure 4.4: Amplitude *versus* detuning for the forced van der Pol oscillator. Fixed point classifications are abbreviated SN (stable node), SS (stable spiral), UN (unstable node), US (unstable spiral), and SP (saddle point). The dot-dashed red curves mark the boundaries of the region in which hysteresis occurs.

For this solution, we have

$$x_0 = A^* \cos(T_0 + \nu T_1 + \psi^*) \quad , \quad (4.81)$$

and the oscillator's frequency is the forcing frequency $\Omega = 1 + \varepsilon\nu$.

To proceed further, let $y = A^2$, and consider the cubic equation

$$G(y) = \frac{1}{16}y^3 - \frac{1}{2}y^2 + (1 + 4\nu^2)y = f_0^2 \quad . \quad (4.82)$$

Setting $G'(y) = 0$, we find the roots of $G'(y)$ lie at $y_{\pm} = \frac{4}{3}(2 \pm u)$, where $u = (1 - 12\nu^2)^{1/2}$. Thus, the roots are complex for $\nu^2 > \frac{1}{12}$, in which case $G(y)$ is monotonically increasing, and there is a unique solution to $G(y) = f_0^2$. Since $G(0) = 0 < f_0^2$, that solution satisfies $y > 0$. For $\nu^2 < \frac{1}{12}$, there are two local extrema at $y = y_{\pm}$. When $G_{\min} = G(y_+) < f_0^2 < G(y_-) = G_{\max}$, the cubic equation $G(y) = f_0^2$ has three real, positive roots. This is equivalent to the condition

$$-\frac{8}{27}u^3 + \frac{8}{9}u^2 < \frac{32}{27} - f_0^2 < \frac{8}{27}u^3 + \frac{8}{9}u^2 \quad . \quad (4.83)$$

We can say even more by exploring the behavior of eqs. (4.80) in the vicinity of the fixed points. Writing $A = A^* + \delta A$ and $\psi = \psi^* + \delta\psi$, we have

$$\frac{d}{dT_1} \begin{pmatrix} \delta A \\ \delta\psi \end{pmatrix} = \begin{pmatrix} \frac{1}{2}(1 - \frac{3}{4}A^{*2}) & \nu A^* \\ -\nu/A^* & \frac{1}{2}(1 - \frac{1}{4}A^{*2}) \end{pmatrix} \begin{pmatrix} \delta A \\ \delta\psi \end{pmatrix} \quad . \quad (4.84)$$

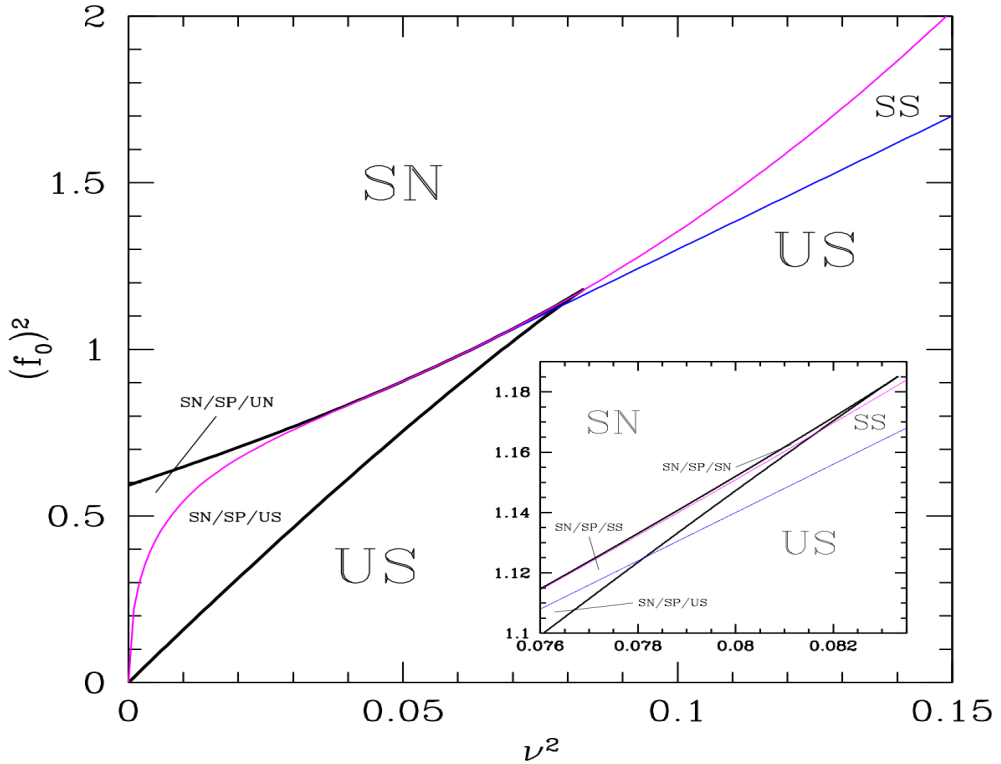


Figure 4.5: Phase diagram for the weakly forced van der Pol oscillator in the (ν^2, f_0^2) plane. Inset shows detail. Abbreviations for fixed point classifications are as in Fig. 4.4.

The eigenvalues of the linearized dynamics at the fixed point are given by $\lambda_{\pm} = \frac{1}{2}(T \pm \sqrt{T^2 - 4D})$, where T and D are the trace and determinant of the linearized equation. Recall now the classification scheme for fixed points of two-dimensional phase flows. When $D < 0$, we have $\lambda_- < 0 < \lambda_+$ and the fixed point is a saddle. For $0 < 4D < T^2$, both eigenvalues have the same sign, so the fixed point is a node. For $4D > T^2$, the eigenvalues form a complex conjugate pair, and the fixed point is a spiral. A node/spiral fixed point is stable if $T < 0$ and unstable if $T > 0$. For our forced van der Pol oscillator, we have

$$\begin{aligned} T &= 1 - \frac{1}{2}A^{*2} \\ D &= \frac{1}{4}(1 - A^{*2} + \frac{3}{16}A^{*4}) + \nu^2 \end{aligned} \quad . \quad (4.85)$$

From these results we can obtain the plot of Fig. 4.4, where amplitude is shown *versus* detuning. We now ask: for what values of f_0^2 is there hysteretic behavior over a range $\nu \in [\nu_-, \nu_+]$? Suppose, following the curves of constant f_0^2 in Fig. 4.4, we start somewhere in the upper left corner of the diagram, in the region $D > 0$ and $f_0^2 < \frac{32}{27}$. Now ramp up ν^2 while keeping f_0^2 constant until we arrive on the upper branch of the $D = 0$ curve. An infinitesimal further increase in ν^2 will cause a discontinuous drop in $y = A^2$ to a value below the saddle point region. Clearly if $f_0^2 = 1$, we will wind up on a branch of this curve for which $A^2 < 2$, which is unstable, and so in order to end up on a stable branch, we must start with $f_0^2 > 1$. To find the minimum such value of f_0^2 for which this is possible, we first demand $G(y) = 0$ as well as $D = 0$. The second of these conditions is equivalent to $G'(y) = 0$. Eliminating y , we obtain the

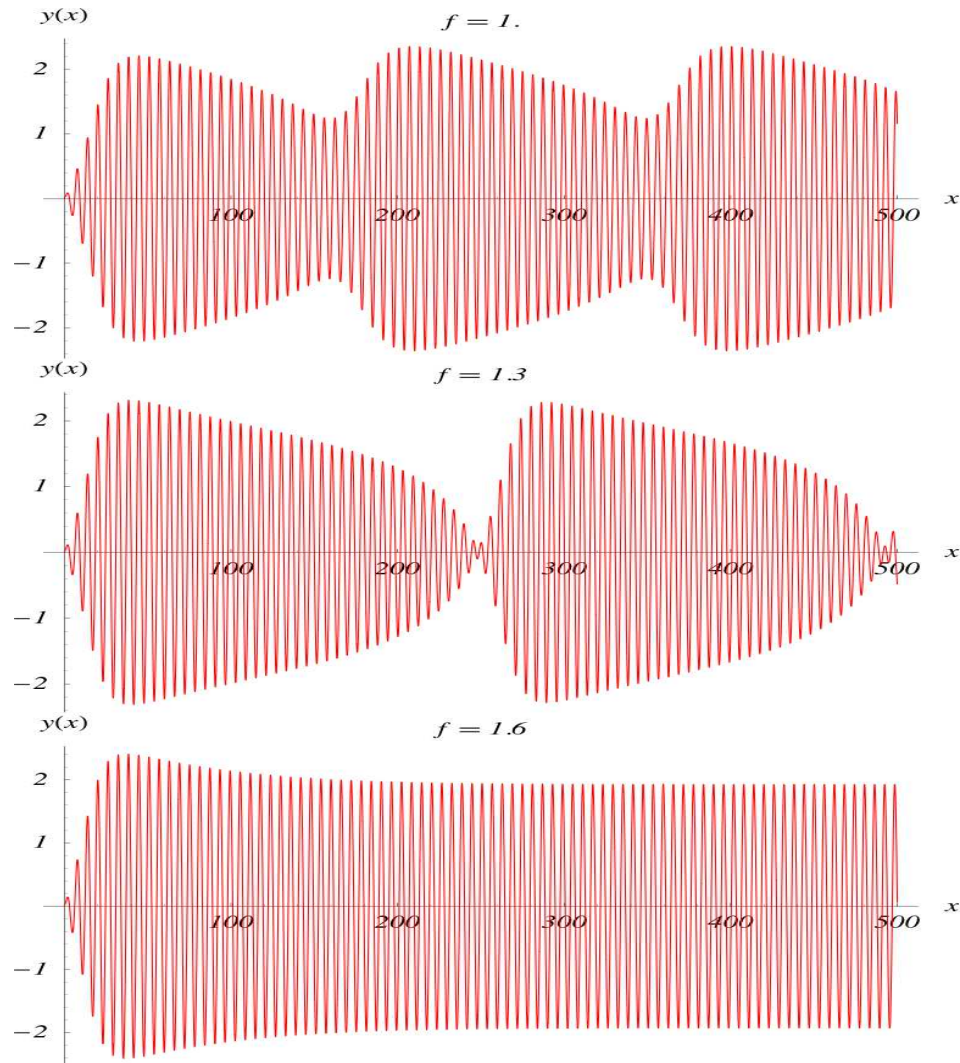


Figure 4.6: Forced van der Pol system with $\epsilon = 0.1$, $\nu = 0.4$ for three values of f_0 . The limit entrained solution becomes unstable at $f_0 = 1.334$.

equation $\frac{8}{27}(2+u)^2(1-u) = f_0^2$, where $u = \sqrt{1-12\nu^2}$ as above. Next, we demand that $G(y) = 0$ at $y = 2$ (*i.e.* the blue line in Fig. 4.4) for the *same values* of f_0^2 and ν^2 . Thus says $f_0^2 = \frac{1}{6}(7-4u^2)$. Eliminating f_0^2 , we obtain the equation

$$\frac{8}{27}(2+u)^2(1-u) = \frac{1}{6}(7-4u^2) , \quad (4.86)$$

which is equivalent to the factorized cubic $(4u-1)(2u+1)^2 = 0$. The root we seek is $u = \frac{1}{4}$, corresponding to $\nu^2 = \frac{15}{192}$ and $f_0^2 = \frac{9}{8}$. Thus, hysteretic behavior is possible only in the narrow regime $f_0^2 \in [\frac{9}{8}, \frac{32}{27}]$. The phase diagram in the (ν^2, f_0^2) plane is shown in Fig. 4.5. Hysteresis requires two among the three fixed points be stable, so the system can jump from one stable branch to another as ν is varied. These regions are so small they are only discernible in the inset.

Finally, we can make the following statement about the *global* dynamics (*i.e.* not simply in the vicinity of

a fixed point). For large A , we have

$$\frac{dA}{dT_1} = -\frac{1}{8}A^3 + \dots \quad , \quad \frac{d\psi}{dT_1} = -\nu + \dots \quad . \quad (4.87)$$

This flow is inward, hence if the flow is not to a stable fixed point, it must be attracted to a limit cycle. The limit cycle necessarily involves several frequencies. This result – the generation of new frequencies by nonlinearities – is called *heterodyning*.

We can see heterodyning in action in the van der Pol system. In Fig. 4.5, the blue line which separates stable and unstable spiral solutions is given by $f_0^2 = 8\nu^2 + \frac{1}{2}$. For example, if we take $\nu = 0.40$ then the boundary lies at $f_0 = 1.334$. For $f_0 < 1.334$, we expect heterodyning, as the entrained solution is unstable. For $f_0 > 1.334$ the solution is entrained and oscillates at a fixed frequency. This behavior is exhibited in Fig. 4.6.

4.4 Synchronization

Thus far we have assumed both the nonlinearity as well as the perturbation are weak. In many systems, we are confronted with a strong nonlinearity which we can perturb weakly. How does an attractive limit cycle in a strongly nonlinear system respond to weak periodic forcing? Here we shall follow the nice discussion in the book of Pikovsky *et al.*

Consider a forced dynamical system,

$$\dot{\varphi} = \mathbf{V}(\varphi) + \varepsilon \mathbf{f}(\varphi, t) \quad . \quad (4.88)$$

When $\varepsilon = 0$, we assume that the system has at least one attractive limit cycle $\gamma(t) = \gamma(t + T_0)$. All points on the limit cycle are fixed under the T_0 -advance map g_{T_0} , where $g_\tau \varphi(t) = \varphi(t + \tau)$. The idea is now to parameterize the points along the limit cycle by a phase angle ϕ which runs from 0 to 2π such that $\phi(t)$ increases by 2π with each orbit of the limit cycle, with ϕ increasing uniformly with time, so that $\dot{\phi} = \omega_0 = 2\pi/T_0$. Now consider the action of the T_0 -advance map g_{T_0} on points in the vicinity of the limit cycle. Since each point $\gamma(\phi)$ on the limit cycle is a fixed point, and since the limit cycle is presumed to be attractive, we can define the ϕ -isochrone as the set of points $\{\varphi\}$ in phase space which flow to the fixed point $\gamma(\phi)$ under repeated application of g_{T_0} . The isochrones are $(N - 1)$ -dimensional hypersurfaces.

Equivalently, consider a point $\varphi_0 \in \Omega_\gamma$ lying within the basin of attraction Ω_γ of the limit cycle $\gamma(t)$. We say that φ_0 lies along the ϕ -isochrone if

$$\lim_{t \rightarrow \infty} \left| \varphi(t) - \gamma\left(t + \frac{\phi}{2\pi} T_0\right) \right| = 0 \quad , \quad (4.89)$$

where $\varphi(0) = \varphi_0$. For each $\varphi_0 \in \Omega_\gamma$, there exists a unique corresponding value of $\phi(\varphi_0) \in [0, 2\pi]$. This is called the *asymptotic* (or *latent*) *phase* of φ_0 .

To illustrate this, we analyze the example in Pikovsky *et al.* of the complex amplitude equation (CAE),

$$\frac{dA}{dt} = (1 + i\alpha) A - (1 + i\beta) |A|^2 A \quad , \quad (4.90)$$

where $A \in \mathbb{C}$ is a complex number. It is convenient to work in polar coordinates, writing $A = R e^{i\Theta}$, in which case the real and complex parts of the CAE become

$$\begin{aligned}\dot{R} &= (1 - R^2) R \\ \dot{\Theta} &= \alpha - \beta R^2 \quad .\end{aligned}\tag{4.91}$$

These equations can be integrated to yield the solution

$$\begin{aligned}R(t) &= \frac{R_0}{\sqrt{R_0^2 + (1 - R_0^2) e^{-2t}}} \\ \Theta(t) &= \Theta_0 + (\alpha - \beta)t - \frac{1}{2}\beta \ln[R_0^2 + (1 - R_0^2) e^{-2t}] \\ &= \Theta_0 + (\alpha - \beta)t + \beta \ln(R/R_0) \quad .\end{aligned}\tag{4.92}$$

As $t \rightarrow \infty$, we have $R(t) \rightarrow 1$ and $\dot{\Theta}(t) \rightarrow \omega_0$. Thus the limit cycle is the circle $R = 1$, and its frequency is $\omega_0 = \alpha - \beta$.

Since all points on each isochrone share the same phase, we can evaluate $\dot{\phi}$ along the limit cycle, and thus we have $\dot{\phi} = \omega_0$. The functional form of the isochrones is dictated by the rotational symmetry of the vector field, which requires $\phi(R, \Theta) = \Theta - f(R)$, where $f(R)$ is an as-yet undetermined function. Taking the derivative, we immediately find $f(R) = \beta \ln R$, i.e.

$$\phi(R, \Theta) = \Theta - \beta \ln R + c \quad ,\tag{4.93}$$

where c is a constant. We can now check that

$$\dot{\phi} = \dot{\Theta} - \beta \frac{\dot{R}}{R} = \alpha - \beta = \omega_0 \quad .\tag{4.94}$$

Without loss of generality we may take $c = 0$. Thus the ϕ -isochrone is given by the curve $\Theta(R) = \phi + \beta \ln R$, which is a logarithmic spiral. These isochrones are depicted in fig. 4.7.

At this point we have defined a phase function $\phi(\varphi)$ as the phase of the fixed point along the limit cycle to which φ flows under repeated application of the T_0 -advance map g_{T_0} . Now let us examine the dynamics of ϕ for the weakly perturbed system of eqn. 4.88. We have

$$\begin{aligned}\frac{d\phi}{dt} &= \sum_{j=1}^N \frac{\partial \phi}{\partial \varphi_j} \frac{d\varphi_j}{dt} \\ &= \omega_0 + \varepsilon \sum_{j=1}^N \frac{\partial \phi}{\partial \varphi_j} f_j(\varphi, t) \quad .\end{aligned}\tag{4.95}$$

We will assume that φ is close to the limit cycle, so that $\varphi - \gamma(\phi)$ is small. As an example, consider once more the complex amplitude equation (4.90), but now adding in a periodic forcing term.

$$\frac{dA}{dt} = (1 + i\alpha) A - (1 + i\beta) |A|^2 A + \varepsilon \cos \omega t \quad .\tag{4.96}$$

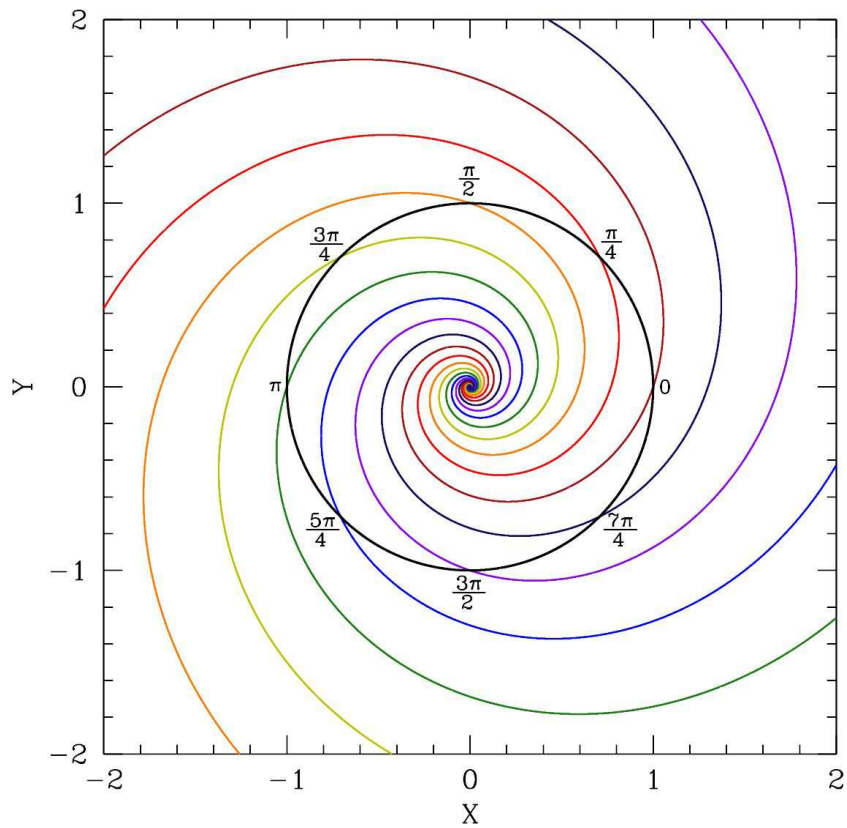


Figure 4.7: Isochrones of the complex amplitude equation $\dot{A} = (1 + i\alpha)A - (1 + i\beta)|A|^2A$, where $A = X + iY$.

Writing $A = X + iY$, we have

$$\begin{aligned}\dot{X} &= X - \alpha Y - (X - \beta Y)(X^2 + Y^2) + \varepsilon \cos \omega t \\ \dot{Y} &= Y + \alpha X - (\beta X + Y)(X^2 + Y^2) .\end{aligned}\tag{4.97}$$

In Cartesian coordinates, the isochrones for the $\varepsilon = 0$ system are

$$\phi = \tan^{-1}(Y/X) - \frac{1}{2}\beta \ln(X^2 + Y^2) ,\tag{4.98}$$

hence

$$\begin{aligned}\frac{d\phi}{dt} &= \omega_0 + \varepsilon \frac{\partial \phi}{\partial X} \cos \omega t \\ &= \alpha - \beta - \varepsilon \left(\frac{\beta X + Y}{X^2 + Y^2} \right) \cos \omega t \\ &\approx \omega_0 - \varepsilon (\beta \cos \phi + \sin \phi) \cos \omega t \\ &= \omega_0 - \varepsilon \sqrt{1 + \beta^2} \cos(\phi - \phi_\beta) \cos \omega t .\end{aligned}\tag{4.99}$$

where $\phi_\beta = \operatorname{ctn}^{-1} \beta$. Note that in the third line above we have invoked $R \approx 1$, i.e. we assume that we are close to the limit cycle.

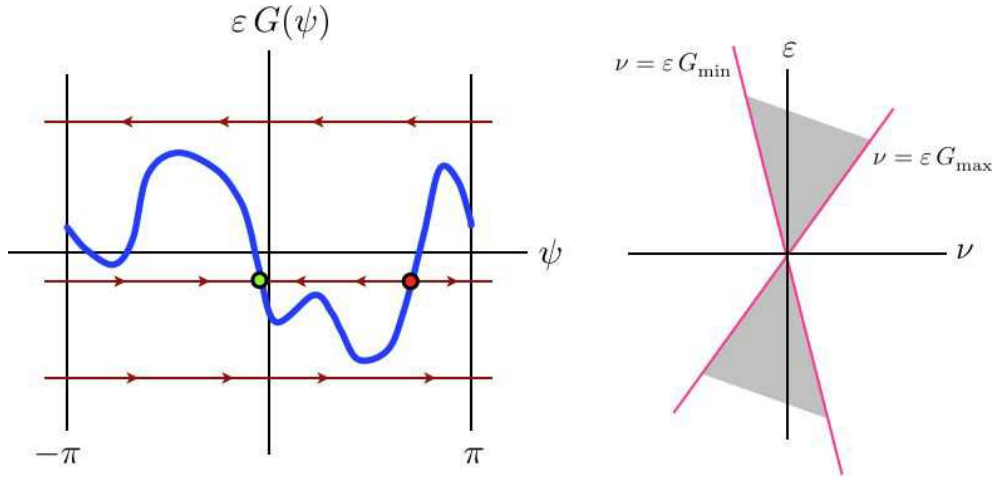


Figure 4.8: Left panel: graphical analysis of the equation $\dot{\psi} = -\nu + \varepsilon G(\psi)$. Right panel: Synchronization region (gray) as a function of detuning ν .

We now define the function

$$F(\phi, t) \equiv \sum_{j=1}^N \frac{\partial \phi}{\partial \varphi_j} \Big|_{\gamma(\phi)} f_j(\gamma(\phi), t) \quad . \quad (4.100)$$

The phase dynamics for ϕ are now written as

$$\dot{\phi} = \omega_0 + \varepsilon F(\phi, t) \quad . \quad (4.101)$$

Now $F(\phi, t)$ is periodic in both its arguments, so we may write

$$F(\phi, t) = \sum_{k,l} F_{kl} e^{i(k\phi + l\omega t)} \quad . \quad (4.102)$$

For the unperturbed problem, we have $\dot{\phi} = \omega_0$, hence resonant terms in the above sum are those for which $k\omega_0 + l\omega \approx 0$. This occurs when $\omega \approx \frac{p}{q}\omega_0$, where p and q are relatively prime integers. In this case the resonance condition is satisfied for $k = jp$ and $l = -jq$ for all $j \in \mathbb{Z}$. We now separate the resonant from the nonresonant terms in the (k, l) sum, writing

$$\dot{\phi} = \omega_0 + \varepsilon \sum_j F_{jp, -jq} e^{ij(p\phi - q\omega t)} + \text{NRT} \quad , \quad (4.103)$$

where NRT denotes nonresonant terms, *i.e.* those for which $(k, l) \neq (jp, -jq)$ for some integer j . We now average over short time scales to eliminate the nonresonant terms, and focus on the dynamics of this averaged phase $\langle \phi \rangle$.

We define the angle $\psi \equiv p\langle \phi \rangle - q\omega t$, which obeys

$$\begin{aligned} \dot{\psi} &= p\langle \dot{\phi} \rangle - q\omega \\ &= (p\omega_0 - q\omega) + \varepsilon p \sum_j F_{jp, -jq} e^{ij\psi} = -\nu + \varepsilon G(\psi) \quad , \end{aligned} \quad (4.104)$$

where $\nu \equiv q\omega - p\omega_0$ is the detuning and $G(\psi) = p \sum_j F_{jp,-jq} e^{ij\psi}$ is the sum over resonant terms. Note that the nonresonant terms have been eliminated by the aforementioned averaging procedure. This last equation is a simple $N = 1$ dynamical system on the circle – a system we have already studied. The dynamics are depicted in fig. 4.8. If the detuning ν falls within the range $[\varepsilon G_{\min}, \varepsilon G_{\max}]$, then ψ flows to a fixed point, and the nonlinear oscillator is synchronized with the periodic external force, with $\langle \dot{\phi} \rangle \rightarrow \frac{q}{p}\omega$. If the detuning is too large and lies outside this region, then there is no synchronization. Rather, $\psi(t)$ increases on average linearly with time. In this case we have $\langle \phi(t) \rangle = \phi_0 + \frac{q}{p}\omega t + \frac{1}{p}\psi(t)$, where

$$dt = \frac{d\psi}{\varepsilon G(\psi) - \nu} \quad \Rightarrow \quad T_\psi = \int_{-\pi}^{\pi} \frac{d\psi}{\varepsilon G(\psi) - \nu} \quad . \quad (4.105)$$

Thus, $\psi(t) = \Omega_\psi t + \Psi(t)$, where $\Psi(t) = \Psi(t + T)$ is periodic with period $T_\psi = 2\pi/\Omega_\psi$. This leads to heterodyning with a beat frequency $\Omega_\psi(\nu, \varepsilon)$.

Why do we here find the general resonance condition $\omega = \frac{p}{q}\omega_0$, whereas for weakly forced, weakly nonlinear oscillators resonance could only occur for $\omega = \omega_0$? There are two reasons. The main reason is that in the latter case, the limit cycle is harmonic to zeroth order, with $x_0(t) = A \cos(t + \phi)$. There are only two frequencies, then, in the Fourier decomposition of the limit cycle: $\omega_0 = \pm 1$. In the strongly nonlinear case, the limit cycle is decomposed into what is in general a countably infinite set of frequencies which are all multiples of a fundamental ω_0 . In addition, if the forcing $f(\varphi, t)$ is periodic in t , its Fourier decomposition in t will involve all integer multiples of some fundamental ω . Thus, the most general resonance condition is $k\omega_0 + l\omega = 0$.

Our analysis has been limited to the lowest order in ε , and we have averaged out the nonresonant terms. When one systematically accounts for both these features, there are two main effects. One is that the boundaries of the synchronous region are no longer straight lines as depicted in the right panel of fig. 4.8. The boundaries themselves can be curved. Moreover, even if there are no resonant terms in the (k, l) sum to lowest order, they can be generated by going to higher order in ε . In such a case, the width of the synchronization region $\Delta\nu$ will be proportional to a higher power of ε : $\Delta\nu \propto \varepsilon^n$, where n is the order of ε where resonant forcing terms first appear in the analysis.

4.5 Relaxation Oscillations

We saw how to use multiple time scale analysis to identify the limit cycle of the van der Pol oscillator when ϵ is small. Consider now the opposite limit, where the coefficient of the damping term is very large. We generalize the van der Pol equation to

$$\ddot{x} + \mu \Phi(x) \dot{x} + x = 0 \quad , \quad (4.106)$$

and suppose $\mu \gg 1$. Define now the variable

$$y \equiv \frac{\dot{x}}{\mu} + \int_0^x dx' \Phi(x') \equiv \frac{\dot{x}}{\mu} + F(x) \quad , \quad (4.107)$$

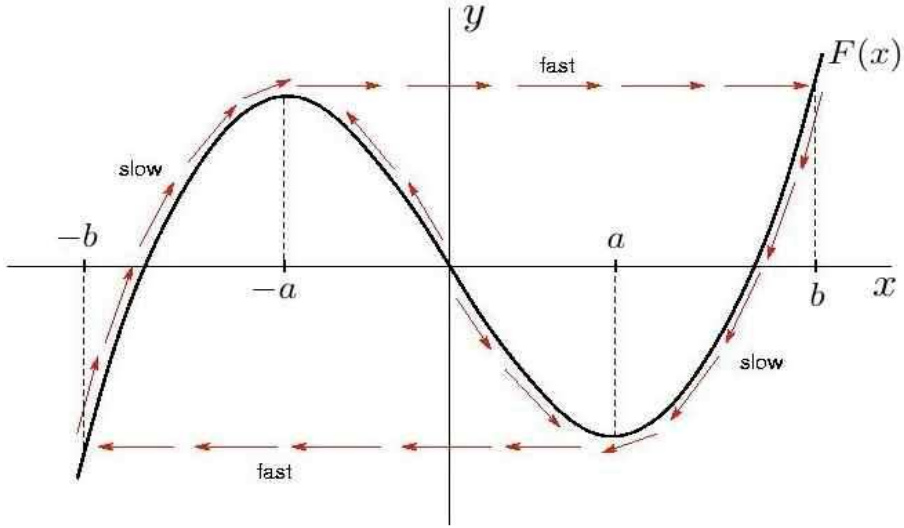


Figure 4.9: Relaxation oscillations in the Liénard plane (x, y). The system rapidly flows to a point on the curve $y = F(x)$, and then crawls slowly along this curve. The slow motion takes x from $-b$ to $-a$, after which the system executes a rapid jump to $x = +b$, then a slow retreat to $x = +a$, followed by a rapid drop to $x = -b$.

where $F'(x) = \Phi(x)$. (y is sometimes called the *Liénard variable*, and (x, y) the *Liénard plane*.) Then the original second order equation may be written as two coupled first order equations:

$$\begin{aligned}\dot{x} &= \mu(y - F(x)) \\ \dot{y} &= -\frac{x}{\mu}.\end{aligned}\tag{4.108}$$

Since $\mu \gg 1$, the first of these equations is *fast* and the second one *slow*. The dynamics rapidly achieves $y \approx F(x)$, and then slowly evolves along the curve $y = F(x)$, until it is forced to make a large, fast excursion.

A concrete example is useful. Consider $F(x)$ of the form sketched in Fig. 4.9. This is what one finds for the van der Pol oscillator, where $\Phi(x) = x^2 - 1$ and $F(x) = \frac{1}{3}x^3 - x$. The limit cycle behavior $x_{LC}(t)$ is sketched in Fig. 4.10. We assume $\Phi(x) = \Phi(-x)$ for simplicity.

Assuming $\Phi(x) = \Phi(-x)$ is symmetric, $F(x)$ is antisymmetric. For the van der Pol oscillator and other similar cases, $F(x)$ resembles the sketch in fig. 4.9. There are two local extrema: a local maximum at $x = -a$ and a local minimum at $x = +a$. We define b such that $F(b) = F(-a)$, as shown in the figure; antisymmetry then entails $F(-b) = F(+a)$. Starting from an arbitrary initial condition, the y dynamics are slow, since $\dot{y} = -\mu^{-1}x$ (we assume $\mu \gg x(0)$). So y can be regarded as essentially constant for the fast dynamics in the second of eqn. 4.108, according to which $x(t)$ flows rapidly to the right if $y > F(x)$ and rapidly to the left if $y < F(x)$. This fast motion stops when $x(t)$ reaches a point where $y = F(x)$. At this point, the slow dynamics takes over. Assuming $y \approx F(x)$, we have

$$y \approx F(x) \quad \Rightarrow \quad \dot{y} = -\frac{x}{\mu} \approx F'(x) \dot{x},\tag{4.109}$$

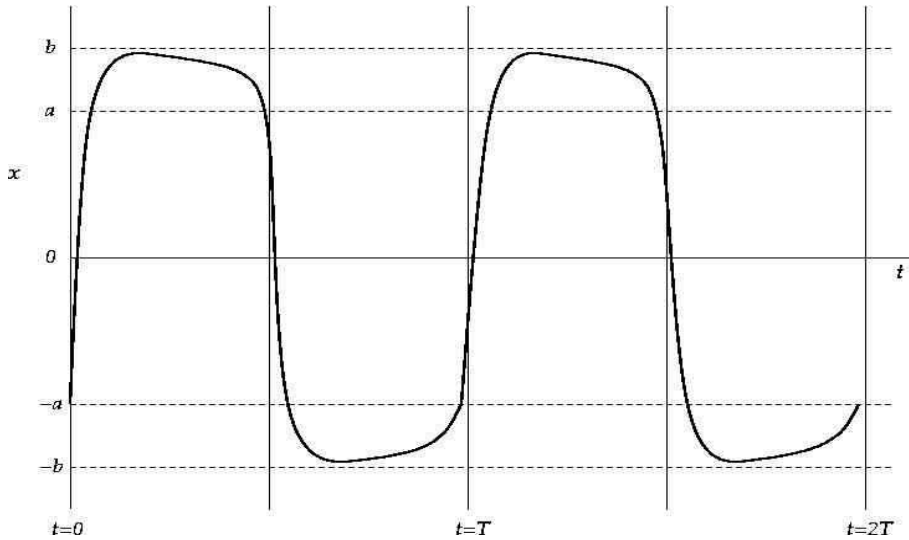


Figure 4.10: A sketch of the limit cycle for the relaxation oscillation studied in this section.

which says that

$$\dot{x} \approx -\frac{x}{\mu F'(x)} \quad \text{if } y \approx F(x) \quad (4.110)$$

over the slow segments of the motion, which are the regions $x \in [-b, -a]$ and $x \in [a, b]$. The relaxation oscillation is then as follows. Starting at $x = -b$, $x(t)$ increases slowly according to eqn. 4.110. At $x = -a$, the motion can no longer follow the curve $y = F(x)$, since $\dot{y} = -\mu^{-1}x$ is still positive. The motion thus proceeds quickly to $x = +b$, with

$$\dot{x} \approx \mu(F(b) - F(x)) \quad x \in [-a, +b] \quad . \quad (4.111)$$

After reaching $x = +b$, the motion once again is slow, and again follows eqn. 4.110, according to which $x(t)$ now decreases slowly until it reaches $x = +a$, at which point the motion is again fast, with

$$\dot{x} \approx \mu(F(a) - F(x)) \quad x \in [-b, +a] \quad . \quad (4.112)$$

The cycle then repeats.

Thus, the limit cycle is given by the following segments:

$$x \in [-b, -a] \quad (\dot{x} > 0) : \quad \dot{x} \approx -\frac{x}{\mu F'(x)} \quad (4.113)$$

$$x \in [-a, b] \quad (\dot{x} > 0) : \quad \dot{x} \approx \mu[F(b) - F(x)] \quad (4.114)$$

$$x \in [a, b] \quad (\dot{x} < 0) : \quad \dot{x} \approx -\frac{x}{\mu F'(x)} \quad (4.115)$$

$$x \in [-b, a] \quad (\dot{x} < 0) : \quad \dot{x} \approx \mu[F(a) - F(x)] \quad . \quad (4.116)$$

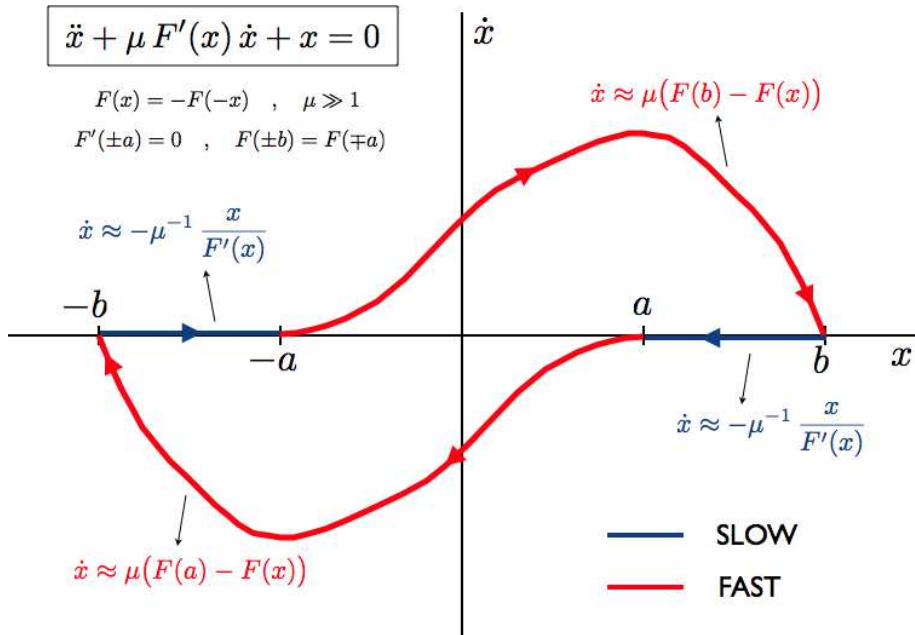


Figure 4.11: Limit cycle for large μ relaxation oscillations, shown in the phase plane (x, \dot{x}) .

A sketch of the limit cycle is given in fig. 4.11, showing the slow and fast portions.

When $\mu \gg 1$ we can determine approximately the period of the limit cycle. Clearly the period is twice the time for either of the slow portions, hence

$$T \approx 2\mu \int_a^b dx \frac{\Phi(x)}{x} , \quad (4.117)$$

where $F'(\pm a) = \Phi(\pm a) = 0$ and $F(\pm b) = F(\mp a)$. For the van der Pol oscillator, with $\Phi(x) = x^2 - 1$, we have $a = 1$, $b = 2$, and $T \simeq (3 - 2 \ln 2) \mu$.

4.5.1 Example problem

Consider the equation

$$\ddot{x} + \mu(|x| - 1)\dot{x} + x = 0 . \quad (4.118)$$

Sketch the trajectory in the Liénard plane, and find the approximate period of the limit cycle for $\mu \gg 1$.

Solution : We define

$$F'(x) = |x| - 1 \Rightarrow F(x) = \begin{cases} +\frac{1}{2}x^2 - x & \text{if } x > 0 \\ -\frac{1}{2}x^2 - x & \text{if } x < 0 \end{cases} . \quad (4.119)$$

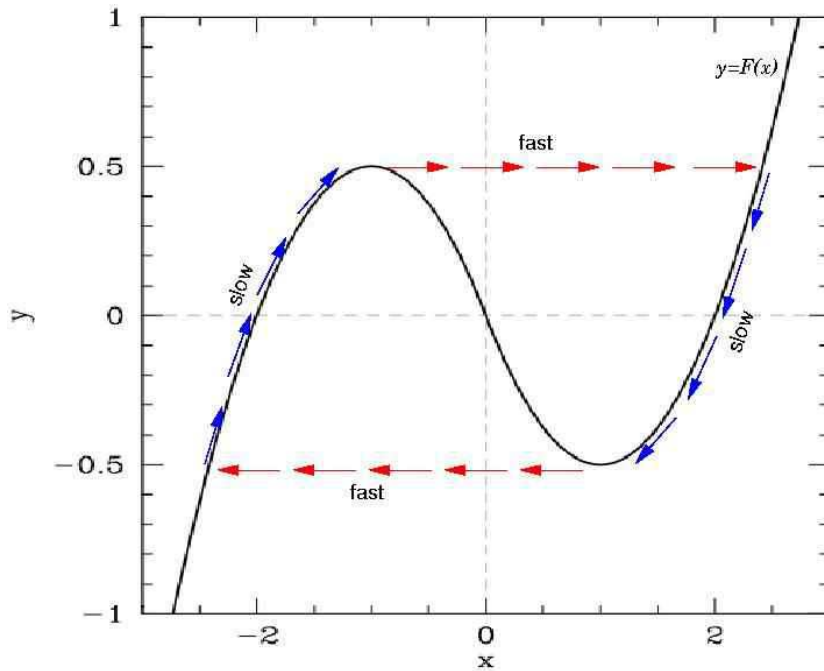


Figure 4.12: Relaxation oscillations for $\ddot{x} + \mu(|x| - 1)\dot{x} + x = 0$ plotted in the Liénard plane. The solid black curve is $y = F(x) = \frac{1}{2}x^2 \operatorname{sgn}(x) - x$. The variable y is defined to be $y = \mu^{-1}\dot{x} + F(x)$. Along slow portions of the limit cycle, $y \simeq F(x)$.

We therefore have

$$\dot{x} = \mu\{y - F(x)\} \quad , \quad \dot{y} = -\frac{x}{\mu} \quad , \quad (4.120)$$

with $y \equiv \mu^{-1}\dot{x} + F(x)$.

Setting $F'(x) = 0$ we find $x = \pm a$, where $a = 1$ and $F(\pm a) = \mp \frac{1}{2}$. We also find $F(\pm b) = F(\mp a)$, where $b = 1 + \sqrt{2}$. Thus, the limit cycle is as follows: (i) fast motion from $x = -a$ to $x = +b$, (ii) slow relaxation from $x = +b$ to $x = +a$, (iii) fast motion from $x = +a$ to $x = -b$, and (iv) slow relaxation from $x = -b$ to $x = -a$. The period is approximately the time it takes for the slow portions of the cycle. Along these portions, we have $y \simeq F(x)$, and hence $\dot{y} \simeq F'(x)\dot{x}$. But $\dot{y} = -x/\mu$, so

$$F'(x)\dot{x} \simeq -\frac{x}{\mu} \quad \Rightarrow \quad dt = -\mu \frac{F'(x)}{x} dx \quad , \quad (4.121)$$

which we integrate to obtain

$$\begin{aligned} T &\simeq -2\mu \int_b^a dx \frac{F'(x)}{x} = 2\mu \int_1^{1+\sqrt{2}} dx \left(1 - \frac{1}{x}\right) \\ &= 2\mu \left[\sqrt{2} - \ln(1 + \sqrt{2}) \right] \simeq 1.066 \mu \quad . \end{aligned} \quad (4.122)$$

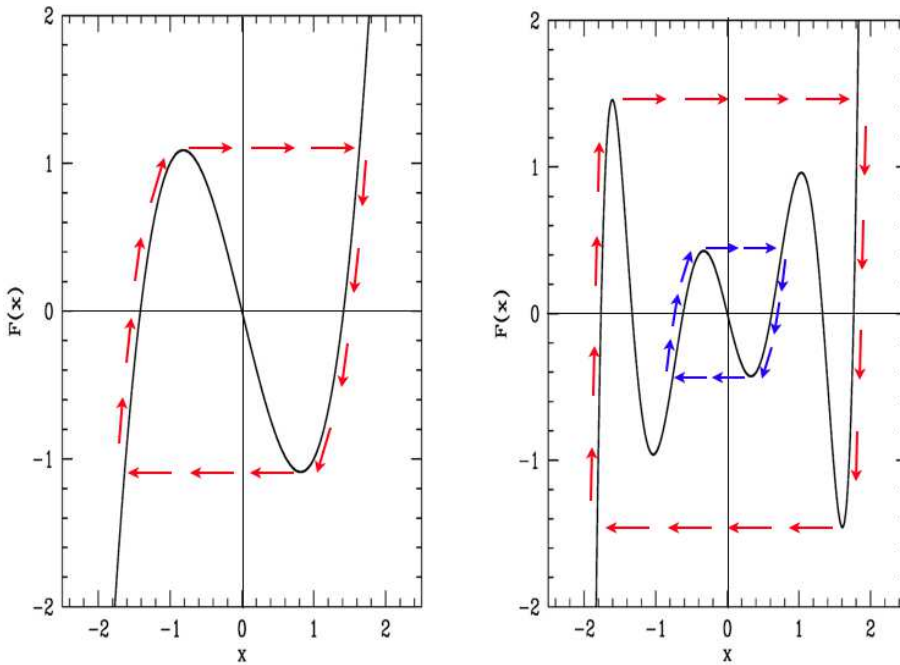


Figure 4.13: Liénard plots for systems with one (left) and two (right) relaxation oscillations.

4.5.2 Multiple limit cycles

For the equation

$$\ddot{x} + \mu F'(x) \dot{x} + x = 0 \quad , \quad (4.123)$$

it is illustrative to consider what sort of $F(x)$ would yield more than one limit cycle. Such an example is shown in fig. 4.13.

In polar coordinates, it is very easy to construct such examples. Consider, for example, the system

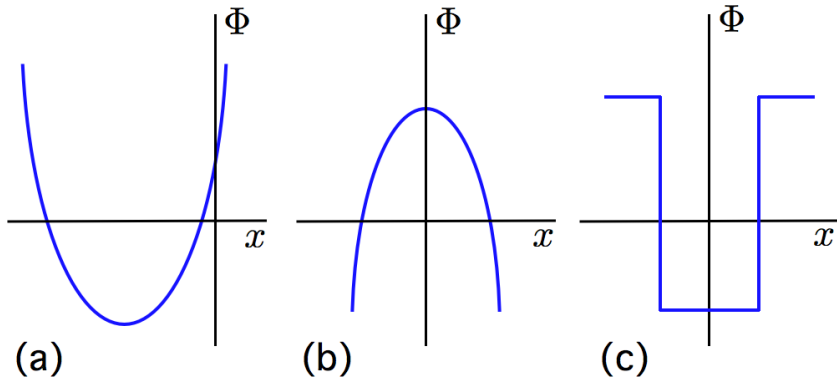
$$\begin{aligned} \dot{r} &= \sin(\pi r) + \epsilon \cos \theta \\ \dot{\theta} &= b r \end{aligned} \quad , \quad (4.124)$$

with $|\epsilon| < 1$. First consider the case $\epsilon = 0$. Clearly the radial flow is outward for $\sin(\pi r) > 0$ and inward for $\sin(\pi r) < 0$. Thus, we have stable limit cycles at $r = 2n + 1$ and unstable limit cycles at $r = 2n$, for all $n \in \mathbb{Z}$. With $0 < |\epsilon| < 1$, we have

$$\begin{aligned} r \in \left[2n + \frac{1}{\pi} \sin^{-1} \epsilon, 2n + 1 - \frac{1}{\pi} \sin^{-1} \epsilon \right] &\Rightarrow \dot{r} > 0 \\ r \in \left[2n + 1 + \frac{1}{\pi} \sin^{-1} \epsilon, 2n + 2 - \frac{1}{\pi} \sin^{-1} \epsilon \right] &\Rightarrow \dot{r} < 0 \end{aligned} \quad (4.125)$$

The Poincaré-Bendixson theorem then guarantees the existence of stable and unstable limit cycles. We can put bounds on the radial extent of these limit cycles.

$$\begin{aligned} r \in \left[2n + 1 - \frac{1}{\pi} \sin^{-1} \epsilon, 2n + 1 + \frac{1}{\pi} \sin^{-1} \epsilon \right] &\Rightarrow \text{stable limit cycle} \\ t \in \left[2n - \frac{1}{\pi} \sin^{-1} \epsilon, 2n + \frac{1}{\pi} \sin^{-1} \epsilon \right] &\Rightarrow \text{unstable limit cycle} \end{aligned} \quad (4.126)$$

Figure 4.14: Three instances of $\Phi(x)$.

Note that an unstable limit cycle is a repeller, which is to say that it is stable (an attractor) if we run the dynamics backwards, sending $t \rightarrow -t$.

4.5.3 Example problem

Consider the nonlinear oscillator,

$$\ddot{x} + \mu \Phi(x) \dot{x} + x = 0 \quad , \quad (4.127)$$

with $\mu \gg 1$. For each case in fig. 4.14, sketch the flow in the Liénard plane, starting with a few different initial conditions. For which case(s) do relaxation oscillations occur?

Solution : Recall the general theory of relaxation oscillations. We define

$$y \equiv \frac{\dot{x}}{\mu} + \int_0^x dx' \Phi(x') = \frac{\dot{x}}{\mu} + F(x) \quad , \quad (4.128)$$

in which case the second order ODE for the oscillator may be written as two coupled first order ODEs:

$$\dot{y} = -\frac{x}{\mu} \quad , \quad \dot{x} = \mu(y - F(x)) \quad . \quad (4.129)$$

Since $\mu \gg 1$, the first of these equations is *slow* and the second one *fast*. The dynamics rapidly achieves $y \approx F(x)$, and then slowly evolves along the curve $y = F(x)$, until it is forced to make a large, fast excursion.

To explore the dynamics in the Liénard plane, we plot $F(x)$ versus x , which means we must integrate $\Phi(x)$. This is done for each of the three cases in fig. 4.14.

Note that a fixed point corresponds to $x = 0$ and $\dot{x} = 0$. In the Liénard plane, this means $x = 0$ and $y = F(0)$. Linearizing by setting $x = \delta x$ and $y = F(0) + \delta y$, we have¹

$$\frac{d}{dt} \begin{pmatrix} \delta x \\ \delta y \end{pmatrix} = \begin{pmatrix} \mu \delta y - \mu F'(0) \delta x \\ -\mu^{-1} \delta x \end{pmatrix} = \begin{pmatrix} -\mu F'(0) & \mu \\ -\mu^{-1} & 0 \end{pmatrix} \begin{pmatrix} \delta x \\ \delta y \end{pmatrix} \quad . \quad (4.130)$$

¹We could, of course, linearize about the fixed point in (x, \dot{x}) space and obtain the same results.

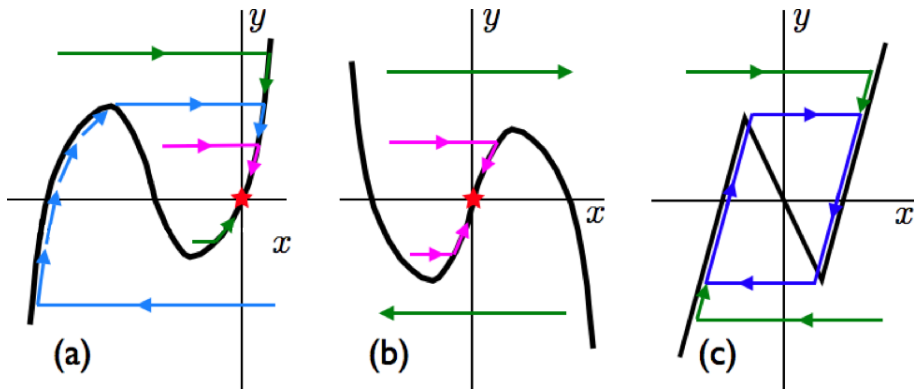


Figure 4.15: Phase flows in the Liénard plane for the three examples in fig. 4.14.

The linearized map has trace $T = -\mu F'(0)$ and determinant $D = 1$. Since $\mu \gg 1$ we have $0 < D < \frac{1}{4}T^2$, which means the fixed point is either a stable node, for $F'(0) > 0$, or an unstable node, for $F'(0) < 0$. In cases (a) and (b) the fixed point is a stable node, while in case (c) it is unstable. The flow in case (a) always collapses to the stable node. In case (b) the flow either is unbounded or else it collapses to the stable node. In case (c), all initial conditions eventually flow to a unique limit cycle exhibiting relaxation oscillations.

4.6 Appendix I : Multiple Time Scale Analysis to $\mathcal{O}(\epsilon^2)$

Problem : A particle of mass m moves in one dimension subject to the potential

$$U(x) = \frac{1}{2}m\omega_0^2 x^2 + \frac{1}{3}\epsilon m\omega_0^2 \frac{x^3}{a} , \quad (4.131)$$

where ϵ is a dimensionless parameter.

(a) Find the equation of motion for x . Show that by rescaling x and t you can write this equation in dimensionless form as

$$\frac{d^2u}{ds^2} + u = -\epsilon u^2 . \quad (4.132)$$

Solution : The equation of motion is

$$m\ddot{x} = -U'(x) = -m\omega_0^2 x - \epsilon m\omega_0^2 \frac{x^2}{a} . \quad (4.133)$$

We now define $s \equiv \omega_0 t$ and $u \equiv x/a$, yielding

$$\frac{d^2u}{ds^2} + u = -\epsilon u^2 . \quad (4.134)$$

(b) You are now asked to perform an $\mathcal{O}(\epsilon^2)$ multiple time scale analysis of this problem, writing

$$T_0 = s , \quad T_1 = \epsilon s , \quad T_2 = \epsilon^2 s , \quad (4.135)$$

and

$$u = u_0 + \epsilon u_1 + \epsilon^2 u_2 + \dots . \quad (4.136)$$

This results in a hierarchy of coupled equations for the functions $\{u_n\}$. Derive the first three equations in the hierarchy.

Solution : We have

$$\frac{d}{ds} = \frac{\partial}{\partial T_0} + \epsilon \frac{\partial}{\partial T_1} + \epsilon^2 \frac{\partial}{\partial T_2} + \dots . \quad (4.137)$$

Therefore

$$\begin{aligned} \left(\frac{\partial}{\partial T_0} + \epsilon \frac{\partial}{\partial T_1} + \epsilon^2 \frac{\partial}{\partial T_2} + \dots \right)^2 (u_0 + \epsilon u_1 + \epsilon^2 u_2 + \dots) &+ (u_0 + \epsilon u_1 + \epsilon^2 u_2 + \dots) \\ &= -\epsilon (u_0 + \epsilon u_1 + \epsilon^2 u_2 + \dots)^2 . \end{aligned} \quad (4.138)$$

Expanding and then collecting terms order by order in ϵ , we derive the hierarchy. The first three levels are

$$\begin{aligned} \frac{\partial^2 u_0}{\partial T_0^2} + u_0 &= 0 \\ \frac{\partial^2 u_1}{\partial T_0^2} + u_1 &= -2 \frac{\partial^2 u_0}{\partial T_0 \partial T_1} - u_0^2 \\ \frac{\partial^2 u_2}{\partial T_0^2} + u_2 &= -2 \frac{\partial^2 u_0}{\partial T_0 \partial T_2} - \frac{\partial^2 u_0}{\partial T_1^2} - 2 \frac{\partial^2 u_1}{\partial T_0 \partial T_1} - 2 u_0 u_1 . \end{aligned} \quad (4.139)$$

(c) Show that there is no frequency shift to first order in ϵ .

Solution : At the lowest (first) level of the hierarchy, the solution is

$$u_0 = A(T_1, T_2) \cos(T_0 + \phi(T_1, T_2)) . \quad (4.140)$$

At the second level, then,

$$\frac{\partial^2 u_1}{\partial T_0^2} + u_1 = 2 \frac{\partial A}{\partial T_1} \sin(T_0 + \phi) + 2A \frac{\partial \phi}{\partial T_1} \cos(T_0 + \phi) - A^2 \cos^2(T_0 + \phi) . \quad (4.141)$$

We eliminate the resonant forcing terms on the RHS by demanding

$$\frac{\partial A}{\partial T_1} = 0 \quad \text{and} \quad \frac{\partial \phi}{\partial T_1} = 0 . \quad (4.142)$$

Thus, we must have $A = A(T_2)$ and $\phi = \phi(T_2)$. To $\mathcal{O}(\epsilon)$, then, ϕ is a constant, which means there is no frequency shift at this level of the hierarchy.

(d) Find $u_0(s)$ and $u_1(s)$.

Solution : The equation for u_1 is that of a non-resonantly forced harmonic oscillator. The solution is easily found to be

$$u_1 = -\frac{1}{2}A^2 + \frac{1}{6}A^2 \cos(2T_0 + 2\phi) . \quad (4.143)$$

We now insert this into the RHS of the third equation in the hierarchy:

$$\begin{aligned} \frac{\partial^2 u_2}{\partial T_0^2} + u_2 &= -2 \frac{\partial^2 u_0}{\partial T_0 \partial T_2} - 2 u_0 u_1 \\ &= 2 \frac{\partial A}{\partial T_2} \sin(T_0 + \phi) + 2A \frac{\partial \phi}{\partial T_2} \cos(T_0 + \phi) - 2A \cos(T_0 + \phi) \left\{ -\frac{1}{2}A^2 + \frac{1}{6}A^2 \cos(2T_0 + 2\phi) \right\} \\ &= 2 \frac{\partial A}{\partial T_2} \sin(T_0 + \phi) + \left(2A \frac{\partial \phi}{\partial T_2} + \frac{5}{6}A^3 \right) \cos(T_0 + \phi) - \frac{1}{6}A^3 \cos(3T_0 + 3\phi) . \end{aligned} \quad (4.144)$$

Setting the coefficients of the resonant terms on the RHS to zero yields

$$\begin{aligned} \frac{\partial A}{\partial T_2} &= 0 \quad \Rightarrow \quad A = A_0 \\ 2A \frac{\partial \phi}{\partial T_2} + \frac{5}{6}A^3 &= 0 \quad \Rightarrow \quad \phi = -\frac{5}{12}A_0^2 T_2 . \end{aligned} \quad (4.145)$$

Therefore,

$$u(s) = \overbrace{A_0 \cos \left(s - \frac{5}{12}\epsilon^2 A_0^2 s \right)}^{u_0(s)} + \overbrace{\frac{1}{6}\epsilon A_0^2 \cos \left(2s - \frac{5}{6}\epsilon^2 A_0^2 s \right) - \frac{1}{2}\epsilon A_0^2}^{\epsilon u_1(s)} + \mathcal{O}(\epsilon^2) \quad (4.146)$$

4.7 Appendix II : MSA and Poincaré-Lindstedt Methods

4.7.1 Problem using multiple time scale analysis

Consider the central force law $F(r) = -k r^{\beta^2-3}$.

(a) Show that a stable circular orbit exists at radius $r_0 = (\ell^2/\mu k)^{1/\beta^2}$.

Solution : For a circular orbit, the effective radial force must vanish:

$$F_{\text{eff}}(r) = \frac{\ell^2}{\mu r^3} + F(r) = \frac{\ell^2}{\mu r^3} - \frac{k}{r^{3-\beta^2}} = 0 . \quad (4.147)$$

Solving for $r = r_0$, we have $r_0 = (\ell^2/\mu k)^{1/\beta^2}$. The second derivative of $U_{\text{eff}}(r)$ at this point is

$$U''_{\text{eff}}(r_0) = -F'_{\text{eff}}(r_0) = \frac{3\ell^2}{\mu r_0^4} + (\beta^2 - 3) \frac{k}{r_0^{4-\beta^2}} = \frac{\beta^2 \ell^2}{\mu r_0^4} , \quad (4.148)$$

which is manifestly positive. Thus, the circular orbit at $r = r_0$ is stable.

(b) Show that the geometric equation for the shape of the orbit may be written

$$\frac{d^2 s}{d\phi^2} + s = K(s) \quad (4.149)$$

where $s = 1/r$, and

$$K(s) = s_0 \left(\frac{s}{s_0} \right)^{1-\beta^2}, \quad (4.150)$$

with $s_0 = 1/r_0$.

Solution : We have previously derived (e.g. in the notes) the equation

$$\frac{d^2s}{d\phi^2} + s = -\frac{\mu}{\ell^2 s^2} F(s^{-1}) \quad . \quad (4.151)$$

From the given $F(r)$, we then have

$$\frac{d^2s}{d\phi^2} + s = \frac{\mu k}{\ell^2} s^{1-\beta^2} \equiv K(s) \quad , \quad (4.152)$$

where $s_0 \equiv (\mu k / \ell^2)^{1/\beta^2} = 1/r_0$, and where

$$K(s) = s_0 \left(\frac{s}{s_0} \right)^{1-\beta^2} \quad . \quad (4.153)$$

(c) Writing $s \equiv (1+u) s_0$, show that u satisfies

$$\frac{1}{\beta^2} \frac{d^2u}{d\phi^2} + u = a_1 u^2 + a_2 u^3 + \dots \quad . \quad (4.154)$$

Find a_1 and a_2 .

Solution : Writing $s \equiv s_0 (1+u)$, we have

$$\begin{aligned} \frac{d^2u}{d\phi^2} + 1 + u &= (1+u)^{1-\beta^2} \\ &= 1 + (1-\beta^2)u + \frac{1}{2}(-\beta^2)(1-\beta^2)u^2 \\ &\quad + \frac{1}{6}(-1-\beta^2)(-\beta^2)(1-\beta^2)u^3 + \dots \quad . \end{aligned} \quad (4.155)$$

Thus,

$$\frac{1}{\beta^2} \frac{d^2u}{d\phi^2} + u = a_1 u^2 + a_2 u^3 + \dots \quad , \quad (4.156)$$

where

$$a_1 = -\frac{1}{2}(1-\beta^2) \quad , \quad a_2 = \frac{1}{6}(1-\beta^4) \quad . \quad (4.157)$$

(d) Now let us associate a power of ε with each power of the deviation u and write

$$\frac{1}{\beta^2} \frac{d^2u}{d\phi^2} + u = \varepsilon a_1 u^2 + \varepsilon^2 a_2 u^3 + \dots \quad , \quad (4.158)$$

Solve this equation using the method of multiple scale analysis (MSA). You will have to go to second order in the multiple scale expansion, writing

$$X \equiv \beta\phi \quad , \quad Y \equiv \varepsilon\beta\phi \quad , \quad Z \equiv \varepsilon^2\beta\phi \quad (4.159)$$

and hence

$$\frac{1}{\beta} \frac{d}{d\phi} = \frac{\partial}{\partial X} + \varepsilon \frac{\partial}{\partial Y} + \varepsilon^2 \frac{\partial}{\partial Z} + \dots \quad . \quad (4.160)$$

Further writing

$$u = u_0 + \varepsilon u_1 + \varepsilon^2 u_2 + \dots \quad , \quad (4.161)$$

derive the equations for the multiple scale analysis, up to second order in ε .

Solution : We now associate one power of ε with each additional power of u beyond order u^1 . In this way, a uniform expansion in terms of ε will turn out to be an expansion in powers of the amplitude of the oscillations. We'll see how this works below. We then have

$$\frac{1}{\beta^2} \frac{d^2 u}{d\phi^2} + u = a_1 \varepsilon u^2 + a_2 \varepsilon^2 u^3 + \dots \quad , \quad (4.162)$$

with $\varepsilon = 1$. We now perform a multiple scale analysis, writing

$$X \equiv \beta\phi \quad , \quad Y \equiv \varepsilon\beta\phi \quad , \quad Z \equiv \varepsilon^2\beta\phi \quad . \quad (4.163)$$

This entails

$$\frac{1}{\beta} \frac{d}{d\phi} = \frac{\partial}{\partial X} + \varepsilon \frac{\partial}{\partial Y} + \varepsilon^2 \frac{\partial}{\partial Z} + \dots \quad . \quad (4.164)$$

We also expand u in powers of ε , as

$$u = u_0 + \varepsilon u_1 + \varepsilon^2 u_2 + \dots \quad . \quad (4.165)$$

Thus, we obtain

$$\begin{aligned} & (\partial_X + \varepsilon \partial_Y + \varepsilon^2 \partial_Z + \dots)^2 (u_0 + \varepsilon u_1 + \varepsilon^2 u_2 + \dots) + (u_0 + \varepsilon u_1 + \varepsilon^2 u_2 + \dots) \\ &= \varepsilon a_1 (u_0 + \varepsilon u_1 + \varepsilon^2 u_2 + \dots)^2 + \varepsilon^2 a_2 (u_0 + \varepsilon u_1 + \varepsilon^2 u_2 + \dots)^3 + \dots \quad . \end{aligned} \quad (4.166)$$

We now extract a hierarchy of equations, order by order in powers of ε .

We find, out to order ε^2 ,

$$\begin{aligned} \mathcal{O}(\varepsilon^0): \quad & \frac{\partial^2 u_0}{\partial X^2} + u_0 = 0 \\ \mathcal{O}(\varepsilon^1): \quad & \frac{\partial^2 u_1}{\partial X^2} + u_1 = -2 \frac{\partial^2 u_0}{\partial Y \partial X} + a_1 u_0^2 \\ \mathcal{O}(\varepsilon^2): \quad & \frac{\partial^2 u_2}{\partial X^2} + u_2 = -2 \frac{\partial^2 u_0}{\partial Z \partial X} - \frac{\partial^2 u_0}{\partial Y^2} - 2 \frac{\partial^2 u_1}{\partial Z \partial X} + 2a_1 u_0 u_1 + a_2 u_0^3 \quad . \end{aligned} \quad (4.167)$$

(e) Show that there is no shift of the angular period $\Delta\phi = 2\pi/\beta$ if one works only to leading order in ε .

Solution : The $\mathcal{O}(\varepsilon^0)$ equation in the hierarchy is solved by writing

$$u_0 = A \cos(X + \psi) , \quad (4.168)$$

where

$$A = A(Y, Z) , \quad \psi = \psi(Y, Z) . \quad (4.169)$$

We define $\theta \equiv X + \psi(Y, Z)$, so we may write $u_0 = A \cos \theta$. At the next order, we obtain

$$\begin{aligned} \frac{\partial^2 u_1}{\partial \theta^2} + u_1 &= 2 \frac{\partial A}{\partial Y} \sin \theta + 2A \frac{\partial \psi}{\partial Y} \cos \theta + a_1 A^2 \cos \theta \\ &= 2 \frac{\partial A}{\partial Y} \sin \theta + 2A \frac{\partial \psi}{\partial Y} \cos \theta + \frac{1}{2} a_1 A^2 + \frac{1}{2} a_1 A^2 \cos 2\theta . \end{aligned} \quad (4.170)$$

In order that there be no resonantly forcing terms on the RHS of eqn. 4.170, we demand

$$\frac{\partial A}{\partial Y} = 0 , \quad \frac{\partial \psi}{\partial Y} = 0 \Rightarrow A = A(Z) , \quad \psi = \psi(Z) . \quad (4.171)$$

The solution for u_1 is then

$$u_1(\theta) = \frac{1}{2} a_1 A^2 - \frac{1}{6} a_1 A^2 \cos 2\theta . \quad (4.172)$$

Were we to stop at this order, we could ignore $Z = \varepsilon^2 \beta \phi$ entirely, since it is of order ε^2 , and the solution would be

$$u(\phi) = A_0 \cos(\beta\phi + \psi_0) + \frac{1}{2} \varepsilon a_1 A_0^2 - \frac{1}{6} \varepsilon a_1 A_0^2 \cos(2\beta\phi + 2\psi_0) . \quad (4.173)$$

The angular period is still $\Delta\phi = 2\pi/\beta$, and, starting from a small amplitude solution at order ε^0 we find that to order ε we must add a constant shift proportional to A_0^2 , as well as a second harmonic term, also proportional to A_0^2 .

(f) Carrying out the MSA to second order in ε , show that the shift of the angular period vanishes only if $\beta^2 = 1$ or $\beta^2 = 4$.

Solution : Carrying out the MSA to the next order, $\mathcal{O}(\varepsilon^2)$, we obtain

$$\begin{aligned} \frac{\partial^2 u_2}{\partial \theta^2} + u_2 &= 2 \frac{\partial A}{\partial Z} \sin \theta + 2A \frac{\partial \psi}{\partial Z} \cos \theta + 2a_1 A \cos \theta \left(\frac{1}{2} a_1 A^2 - \frac{1}{6} a_1 A^2 \cos 2\theta \right) + a_2 A^3 \cos^3 \theta \\ &= 2 \frac{\partial A}{\partial Z} \sin \theta + 2A \frac{\partial \psi}{\partial Z} \cos \theta + \left(\frac{5}{6} a_1^2 + \frac{3}{4} a_2 \right) A^3 \cos \theta + \left(-\frac{1}{6} a_1^2 + \frac{1}{4} a_2 \right) A^3 \cos 3\theta . \end{aligned} \quad (4.174)$$

Now in order to make the resonant forcing terms on the RHS vanish, we must choose

$$\frac{\partial A}{\partial Z} = 0 \quad (4.175)$$

as well as

$$\begin{aligned} \frac{\partial \psi}{\partial Z} &= - \left(\frac{5}{12} a_1^2 + \frac{3}{8} a_2 \right) A^2 \\ &= -\frac{1}{24} (\beta^2 - 4)(\beta^2 - 1) . \end{aligned} \quad (4.176)$$

The solutions to these equations are trivial:

$$A(Z) = A_0 \quad , \quad \psi(Z) = \psi_0 - \frac{1}{24}(\beta^2 - 1)(\beta^2 - 4)A_0^2 Z \quad . \quad (4.177)$$

With the resonant forcing terms eliminated, we may write

$$\frac{\partial^2 u_2}{\partial \theta^2} + u_2 = \left(-\frac{1}{6}a_1^2 + \frac{1}{4}a_2 \right) A^3 \cos 3\theta \quad , \quad (4.178)$$

with solution

$$\begin{aligned} u_2 &= \frac{1}{96}(2a_1^2 - 3a_2) A^3 \cos 3\theta \\ &= \frac{1}{96} \beta^2 (\beta^2 - 1) A_0^2 \cos (3X + 3\psi(Z)) \quad . \end{aligned} \quad (4.179)$$

The full solution to second order in this analysis is then

$$\begin{aligned} u(\phi) &= A_0 \cos(\beta'\phi + \psi_0) + \frac{1}{2}\varepsilon a_1 A_0^2 - \frac{1}{6}\varepsilon a_1 A_0^2 \cos(2\beta'\phi + 2\psi_0) \\ &\quad + \frac{1}{96}\varepsilon^2 (2a_1^2 - 3a_2) A_0^3 \cos(3\beta'\phi + 3\psi_0) \quad . \end{aligned} \quad (4.180)$$

with

$$\beta' = \beta \cdot \left\{ 1 - \frac{1}{24}\varepsilon^2 (\beta^2 - 1)(\beta^2 - 4)A_0^2 \right\} \quad . \quad (4.181)$$

The angular period shifts:

$$\Delta\phi = \frac{2\pi}{\beta'} = \frac{2\pi}{\beta} \cdot \left\{ 1 + \frac{1}{24}\varepsilon^2 (\beta^2 - 1)(\beta^2 - 4)A_0^2 \right\} + \mathcal{O}(\varepsilon^3) \quad . \quad (4.182)$$

Note that there is no shift in the period, for any amplitude, if $\beta^2 = 1$ (*i.e.* Kepler potential) or $\beta^2 = 4$ (*i.e.* harmonic oscillator).

4.7.2 Solution using Poincaré-Lindstedt method

Recall that geometric equation for the shape of the (relative coordinate) orbit for the two body central force problem is

$$\begin{aligned} \frac{d^2 s}{d\phi^2} + s &= K(s) \\ K(s) &= s_0 \left(\frac{s}{s_0} \right)^{1-\beta^2} \end{aligned} \quad (4.183)$$

where $s = 1/r$, $s_0 = (l^2/\mu k)^{1/\beta^2}$ is the inverse radius of the stable circular orbit, and $f(r) = -kr^{\beta^2-3}$ is the central force. Expanding about the stable circular orbit, one has

$$\frac{d^2 y}{d\phi^2} + \beta^2 y = \frac{1}{2}K''(s_0) y^2 + \frac{1}{6}K'''(s_0) y^3 + \dots \quad , \quad (4.184)$$

where $s = s_0(1 + y)$, with

$$\begin{aligned} K'(s) &= (1 - \beta^2) \left(\frac{s_0}{s} \right)^{\beta^2} \\ K''(s) &= -\beta^2 (1 - \beta^2) \left(\frac{s_0}{s} \right)^{1+\beta^2} \\ K'''(s) &= \beta^2 (1 - \beta^2) (1 + \beta^2) \left(\frac{s_0}{s} \right)^{2+\beta^2} . \end{aligned} \quad (4.185)$$

Thus,

$$\frac{d^2y}{d\phi^2} + \beta^2 y = \epsilon a_1 y^2 + \epsilon^2 a_2 y^3 , \quad (4.186)$$

with $\epsilon = 1$ and

$$\begin{aligned} a_1 &= -\frac{1}{2} \beta^2 (1 - \beta^2) \\ a_2 &= +\frac{1}{6} \beta^2 (1 - \beta^2) (1 + \beta^2) . \end{aligned} \quad (4.187)$$

Note that we assign one factor of ϵ for each order of nonlinearity beyond order y^1 . Note also that while y here corresponds to u in eqn. 4.156, the constants $a_{1,2}$ here are a factor of β^2 larger than those defined in eqn. 4.157.

We now apply the Poincaré-Lindstedt method, by defining $\theta = \Omega \phi$, with

$$\Omega^2 = \Omega_0^2 + \epsilon \Omega_1^2 + \epsilon^2 \Omega_2^2 + \dots \quad (4.188)$$

and

$$y(\theta) = y_0(\theta) + \epsilon y_1(\theta) + \epsilon^2 y_2(\theta) + \dots . \quad (4.189)$$

We therefore have

$$\frac{d}{d\phi} = \Omega \frac{d}{d\theta} \quad (4.190)$$

and

$$\begin{aligned} (\Omega_0^2 + \epsilon \Omega_1^2 + \epsilon^2 \Omega_2^2 + \dots) (y_0'' + \epsilon y_1'' + \epsilon^2 y_2'' + \dots) + \beta^2 (y_0 + \epsilon y_1 + \epsilon^2 y_2 + \dots) \\ = \epsilon a_1 (y_0 + \epsilon y_1 + \epsilon^2 y_2 + \dots)^2 + \epsilon^2 a_2 (y_0 + \epsilon y_1 + \epsilon^2 y_2 + \dots)^3 . \end{aligned} \quad (4.191)$$

We now extract equations at successive orders of ϵ . The first three in the hierarchy are

$$\Omega_0^2 y_0'' + \beta^2 y_0 = 0$$

$$\Omega_1^2 y_0'' + \Omega_0^2 y_1'' + \beta^2 y_1 = a_1 y_0^2 \quad (4.192)$$

$$\Omega_2^2 y_0'' + \Omega_1^2 y_1'' + \Omega_0^2 y_2'' + \beta^2 y_2 = 2 a_1 y_0 y_1 + a_2 y_0^3 ,$$

where prime denotes differentiation with respect to θ .

To order ϵ^0 , the solution is $\Omega_0^2 = \beta^2$ and

$$y_0(\theta) = A \cos(\theta + \delta) , \quad (4.193)$$

where A and δ are constants.

At order ϵ^1 , we have

$$\begin{aligned} \beta^2(y_1'' + y_1) &= -\Omega_1^2 y_0'' + a_1 y_0^2 \\ &= \Omega_1^2 A \cos(\theta + \delta) + a_1 A^2 \cos^2(\theta + \delta) \\ &= \Omega_1^2 A \cos(\theta + \delta) + \frac{1}{2} a_1 A^2 + \frac{1}{2} a_1 A^2 \cos(2\theta + 2\delta) . \end{aligned} \quad (4.194)$$

The secular forcing terms on the RHS are eliminated by the choice $\Omega_1^2 = 0$. The solution is then

$$y_1(\theta) = \frac{a_1 A^2}{2\beta^2} \left\{ 1 - \frac{1}{3} \cos(2\theta + 2\delta) \right\} . \quad (4.195)$$

At order ϵ^2 , then, we have

$$\begin{aligned} \beta^2(y_2'' + y_2) &= -\Omega_2^2 y_0'' - \Omega_1^2 y_1'' + 2a_1 y_1 y_1 + a_2 y_0^3 \\ &= \Omega_2^2 A \cos(\theta + \delta) + \frac{a_1^2 A^3}{\beta^2} \left\{ 1 - \frac{1}{3} \cos(2\theta + 2\delta) \right\} \cos(\theta + \delta) + a_2 A^3 \cos^2(\theta + \delta) \\ &= \left\{ \Omega_2^2 + \frac{5a_1^2 A^3}{6\beta^2} + \frac{3}{4} a_2 A^3 \right\} A \cos(\theta + \delta) + \left\{ -\frac{a_1^2 A^3}{6\beta^2} + \frac{1}{4} a_2 A^3 \right\} \cos(3\theta + 3\delta) . \end{aligned} \quad (4.196)$$

The resonant forcing terms on the RHS are eliminated by the choice

$$\begin{aligned} \Omega_2^2 &= -\left(\frac{5}{6}\beta^{-2}a_1^2 + \frac{3}{4}a_2\right)A^3 \\ &= -\frac{1}{24}\beta^2(1-\beta^2)\left[5(1-\beta^2) + 3(1+\beta^2)\right] \\ &= -\frac{1}{12}\beta^2(1-\beta^2)(4-\beta^2) . \end{aligned} \quad (4.197)$$

Thus, the frequency shift to this order vanishes whenever $\beta^2 = 0$, $\beta^2 = 1$, or $\beta^2 = 4$. Recall the force law is $F(r) = -C r^{\beta^2-3}$, so we see that there is no shift – hence no precession – for inverse cube, inverse square, or linear forces.

4.8 Appendix III : Modified van der Pol Oscillator

Consider the nonlinear oscillator

$$\ddot{x} + \epsilon(x^4 - 1)\dot{x} + x = 0 . \quad (4.198)$$

Analyze this using the same approach we apply to the van der Pol oscillator.

- (a) Sketch the vector field $\dot{\varphi}$ for this problem. It may prove convenient to first identify the *nullclines*, which are the curves along which $\dot{x} = 0$ or $\dot{v} = 0$ (with $v = \dot{x}$). Argue that a limit cycle exists.

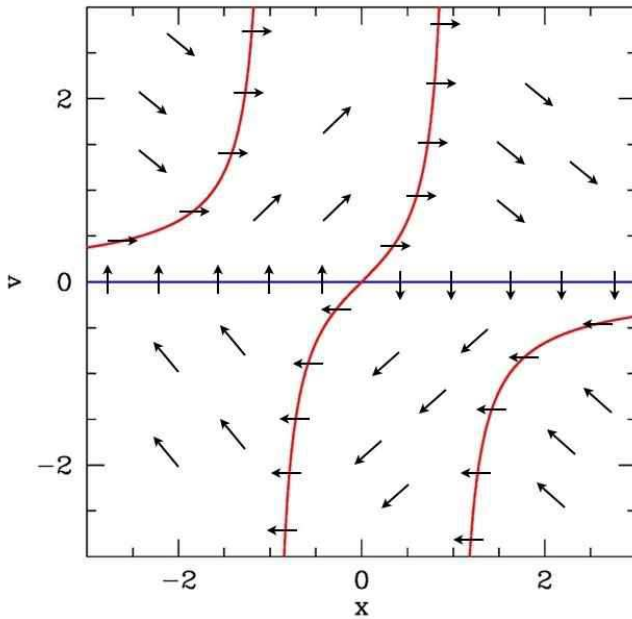


Figure 4.16: Phase flow and nullclines for the oscillator $\ddot{x} + \epsilon(x^4 - 1)\dot{x} + x = 0$. Red nullclines: $\dot{v} = 0$; blue nullcline: $\dot{x} = 0$.

Solution : There is a single fixed point, at the origin $(0, 0)$, for which the linearized dynamics obeys

$$\frac{d}{dt} \begin{pmatrix} x \\ v \end{pmatrix} = \begin{pmatrix} 0 & 1 \\ -1 & \epsilon \end{pmatrix} \begin{pmatrix} x \\ v \end{pmatrix} + \mathcal{O}(x^4 v) . \quad (4.199)$$

One finds $T = \epsilon$ and $D = 1$ for the trace and determinant, respectively. The origin is an unstable spiral for $0 < \epsilon < 2$ and an unstable node for $\epsilon > 2$.

The nullclines are sketched in Fig. 4.16. One has

$$\dot{x} = 0 \leftrightarrow v = 0 , \quad \dot{v} = 0 \leftrightarrow v = \frac{1}{\epsilon} \frac{x}{1 - x^4} . \quad (4.200)$$

The flow at large distances from the origin winds once around the origin and spirals in. The flow close to the origin spirals out ($\epsilon < 2$) or flows radially out ($\epsilon > 2$). Ultimately the flow must collapse to a limit cycle, as can be seen in the accompanying figures.

(b) In the limit $0 < \epsilon \ll 1$, use multiple time scale analysis to obtain a solution which reveals the approach to the limit cycle.

Solution : We seek to solve the equation

$$\ddot{x} + x = \epsilon h(x, \dot{x}) , \quad (4.201)$$

with

$$h(x, \dot{x}) = (1 - x^4) \dot{x} . \quad (4.202)$$

Employing the multiple time scale analysis to lowest nontrivial order, we write $T_0 \equiv t, T_1 \equiv \epsilon t$,

$$x = x_0 + \epsilon x_1 + \dots \quad (4.203)$$

and identify terms order by order in ϵ . At $\mathcal{O}(\epsilon^0)$, this yields

$$\frac{\partial^2 x_0}{\partial T_0^2} + x_0 = 0 \quad \Rightarrow \quad x_0 = A \cos(T_0 + \phi) \quad , \quad (4.204)$$

where $A = A(T_1)$ and $\phi = \phi(T_1)$. At $\mathcal{O}(\epsilon^1)$, we have

$$\begin{aligned} \frac{\partial^2 x_1}{\partial T_0^2} + x_1 &= -2 \frac{\partial^2 x_0}{\partial T_0 \partial T_1} + h\left(x_0, \frac{\partial x_0}{\partial T_0}\right) \\ &= 2 \frac{\partial A}{\partial T_1} \sin \theta + 2A \frac{\partial \phi}{\partial T_1} \cos \theta + h(A \cos \theta, -A \sin \theta) \end{aligned} \quad (4.205)$$

with $\theta = T_0 + \phi(T_1)$ as usual. We also have

$$\begin{aligned} h(A \cos \theta, -A \sin \theta) &= A^5 \sin \theta \cos \theta - A \sin \theta \\ &= \left(\frac{1}{8}A^5 - A\right) \sin \theta + \frac{3}{16}A^5 \sin 3\theta + \frac{1}{16}A^5 \sin 5\theta \end{aligned} \quad . \quad (4.206)$$

To eliminate the resonant terms in eqn. 4.205, we must choose

$$\frac{\partial A}{\partial T_1} = \frac{1}{2}A - \frac{1}{16}A^5 \quad , \quad \frac{\partial \phi}{\partial T_1} = 0 \quad . \quad (4.207)$$

The A equation is similar to the logistic equation. Clearly $A = 0$ is an unstable fixed point, and $A = 8^{1/4} \approx 1.681793$ is a stable fixed point. Thus, the amplitude of the oscillations will asymptotically approach $A^* = 8^{1/4}$. (Recall the asymptotic amplitude in the van der Pol case was $A^* = 2$.)

To integrate the A equation, substitute $y = \frac{1}{\sqrt{8}}A^2$, and obtain

$$dT_1 = \frac{dy}{y(1-y^2)} = \frac{1}{2}d\ln \frac{y^2}{1-y^2} \quad \Rightarrow \quad y^2(T_1) = \frac{1}{1+(y_0^{-2}-1)\exp(-2T_1)} \quad . \quad (4.208)$$

We then have

$$A(T_1) = 8^{1/4} \sqrt{y(T_1)} = \left(\frac{8}{1+(8A_0^{-4}-1)\exp(-2T_1)} \right)^{1/4} \quad . \quad (4.209)$$

(c) In the limit $\epsilon \gg 1$, find the period of relaxation oscillations, using Liénard plane analysis. Sketch the orbit of the relaxation oscillation in the Liénard plane.

Solution : Our nonlinear oscillator may be written in the form

$$\ddot{x} + \epsilon \frac{dF(x)}{dt} + x = 0 \quad , \quad (4.210)$$

with

$$F(x) = \frac{1}{5}x^5 - x \quad . \quad (4.211)$$

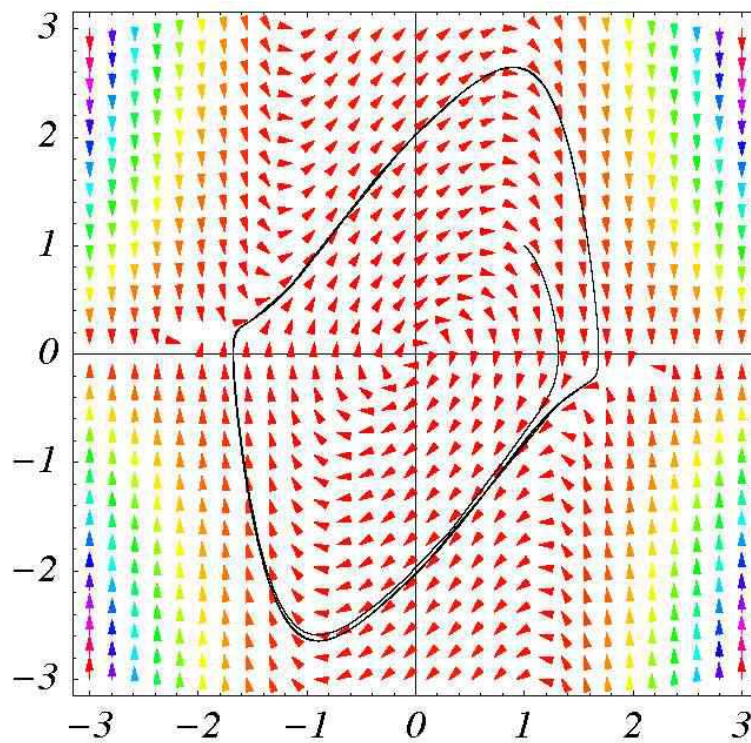


Figure 4.17: Vector field and phase curves for the oscillator $\ddot{x} + \epsilon(x^4 - 1)\dot{x} + x = 0$, with $\epsilon = 1$ and starting from $(x_0, v_0) = (1, 1)$.

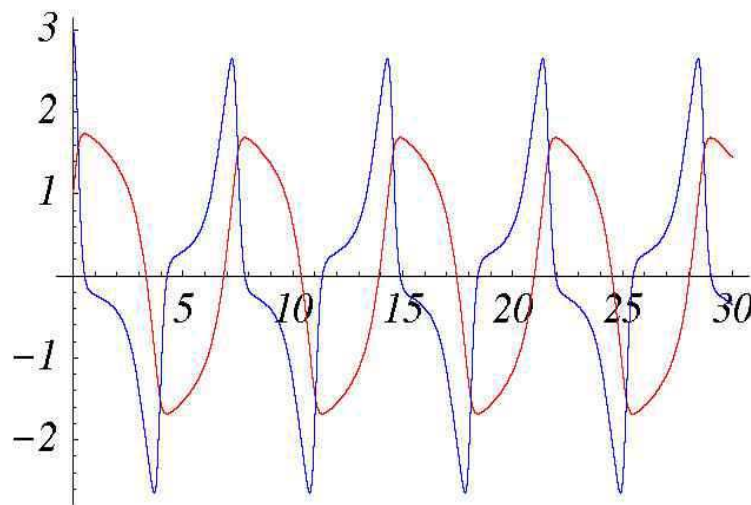


Figure 4.18: Solution to the oscillator equation $\ddot{x} + \epsilon(x^4 - 1)\dot{x} + x = 0$ with $\epsilon = 1$ and initial conditions $(x_0, v_0) = (1, 3)$. $x(t)$ is shown in red and $v(t)$ in blue. Note that $x(t)$ resembles a relaxation oscillation for this moderate value of ϵ .

Note $\dot{F} = (x^4 - 1) \dot{x}$. Now we define the Liénard variable

$$y \equiv \frac{\dot{x}}{\epsilon} + F(x) \quad , \quad (4.212)$$

and in terms of (x, y) we have

$$\dot{x} = \epsilon [y - F(x)] \quad , \quad \dot{y} = -\frac{x}{\epsilon} \quad . \quad (4.213)$$

As we have seen in the notes, for large ϵ the motion in the (x, y) plane is easily analyzed. $x(t)$ must move quickly over to the curve $y = F(x)$, at which point the motion slows down and slowly creeps along this curve until it can no longer do so, at which point another big fast jump occurs. The jumps take place between the local extrema of $F(x)$, which occur for $F'(a) = a^4 - 1 = 0$, i.e. at $a = \pm 1$, and points on the curve with the same values of $F(a)$. Thus, we solve $F(-1) = \frac{4}{5} = \frac{1}{5}b^5 - b$ and find the desired root at $b^* \approx 1.650629$. The period of the relaxation oscillations, for large ϵ , is

$$T \approx 2\epsilon \int_a^b dx \frac{F'(x)}{x} = \epsilon \cdot \left[\frac{1}{2}x^4 - 2 \ln x \right]_a^b \approx 2.20935 \epsilon \quad . \quad (4.214)$$

(d) Numerically integrate the equation (4.198) starting from several different initial conditions.

Solution : The accompanying Mathematica plots show $x(t)$ and $v(t)$ for this system for two representative values of ϵ .

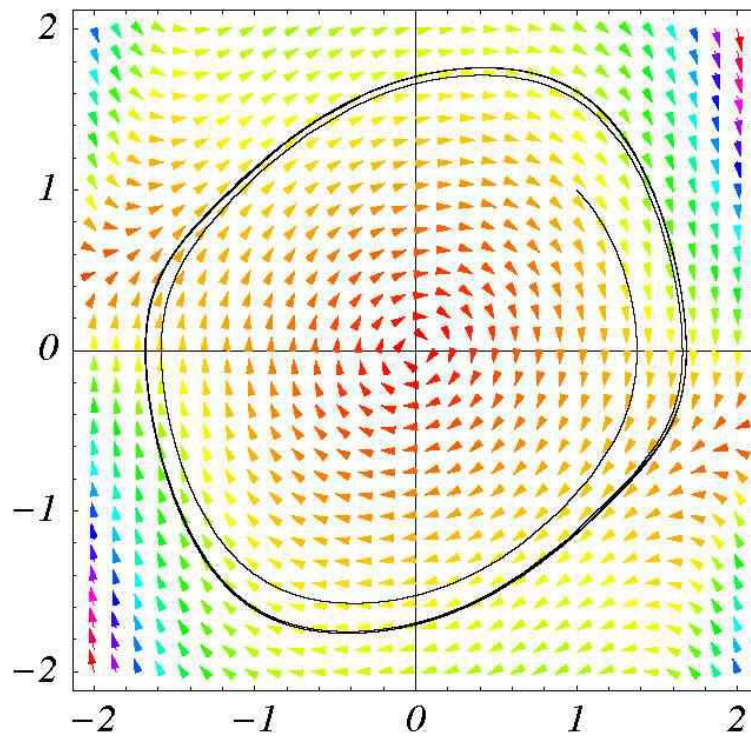


Figure 4.19: Vector field and phase curves for the oscillator $\ddot{x} + \epsilon(x^4 - 1)\dot{x} + x = 0$, with $\epsilon = 0.25$ and starting from $(x_0, v_0) = (1, 1)$. As $\epsilon \rightarrow 0$, the limit cycle is a circle of radius $A^* = 8^{1/4} \approx 1.682$.

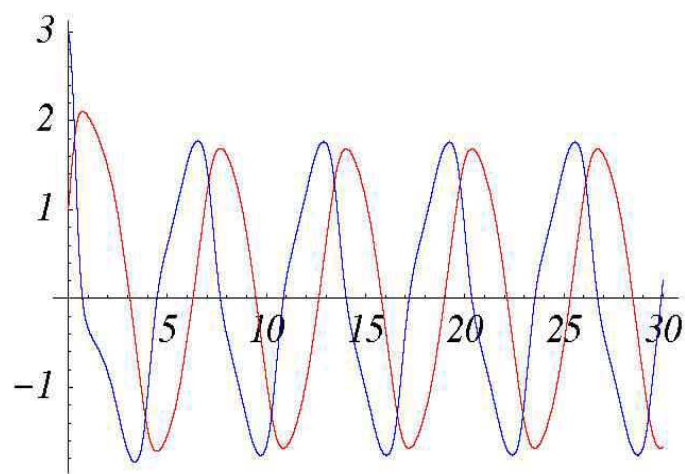


Figure 4.20: Solution to the oscillator equation $\ddot{x} + \epsilon(x^4 - 1)\dot{x} + x = 0$ with $\epsilon = 0.25$ and initial conditions $(x_0, v_0) = (1, 3)$. $x(t)$ is shown in red and $v(t)$ in blue. As $\epsilon \rightarrow 0$, the amplitude of the oscillations tends to $A^* = 8^{1/4} \approx 1.682$.

Chapter 5

Maps, Strange Attractors, and Chaos

5.1 Motion on Resonant Tori

Consider an integrable Hamiltonian with two degrees of freedom. The energy $E(J_1, J_2)$ is then a function of the two action coordinates, so at fixed energy we may regard $J_2(J_1; E)$ as being determined by J_1 . The motion is then given by $\phi_j(t) = \omega_j(J_1; E)t + \beta_j$, and, at fixed E , is confined to a two-torus \mathbb{T}^2 specified by the action J_1 , as depicted in Fig. 5.1. For a system with N freedoms (*i.e.* a phase space of dimension $2n$), integrable motion is confined to an n -torus $\mathbb{T}^N = \mathbb{S}^1 \times \cdots \times \mathbb{S}^1$. The frequencies $\omega_j = \partial E / \partial J_j = \omega_j(J_1, \dots, J_{N-1}; E)$ are specified, at fixed E , by $N - 1$ action variables. If, on a given torus, the frequency ratios $\omega_j / \omega_{j'}$ are rational numbers for all j and j' , then the motion is periodic, and all frequencies are said to be in resonance. In this case we may write $\omega_j = k_j \omega_0$ for some set $\{k_1, \dots, k_N\} \in \mathbb{Z}^N$, and some quantity ω_0 which has dimensions of frequency. One can Fourier decompose the original coordinates $q_\sigma(\phi, \mathbf{J})$ as

$$q_\sigma(\phi, \mathbf{J}) = \sum_m \hat{q}_{\sigma, m}(\mathbf{J}) e^{im \cdot \phi} , \quad (5.1)$$

and similarly for $p_\sigma(\phi, \mathbf{J})$, where $\mathbf{m} \in \mathbb{Z}^N$. Invoking the solution $\phi_\sigma(t) = k_\sigma \omega_0 t + \beta_\sigma$, one sees that the motion is periodic in time with period $T = 2\pi/\omega_0$. That all the frequencies are in resonance further means that for some of the \mathbf{m} vectors, one has $\mathbf{m} \cdot \mathbf{k} = 0$.

5.1.1 The twist map

Consider the motion $\phi(t) = \omega(\mathbf{J})t + \beta$ along a resonant torus, and let us plot consecutive intersections of the trajectory with the (J_1, ϕ_1) plane, *i.e.* the subset of phase space where both E (or J_2) and ϕ_2 are fixed. Such a plot is called a *surface of section*. Successive intersections of this surface occur at time interval $\Delta t = 2\pi/\omega_2$, during which the angle ϕ_1 changes by $\Delta\phi_1 = \omega_1 \Delta t = 2\pi\alpha$, where $\alpha = \omega_1/\omega_2$. Focusing only on the surface of section, we write $\phi \equiv \phi_1$ and $J \equiv J_1$. The relation between (ϕ, J) values

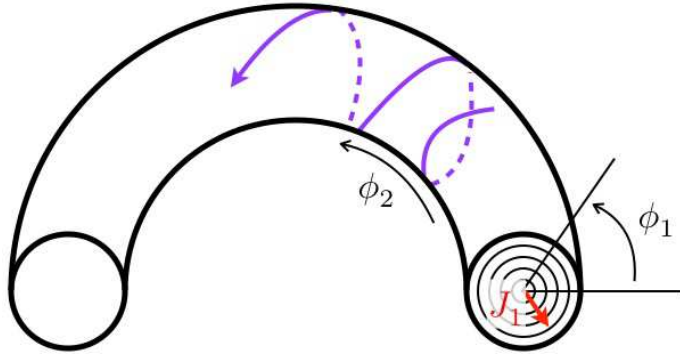


Figure 5.1: Motion of an $n = 2$ system on an invariant torus specified by action J_1 , with $E(J_1, J_2)$ fixed.

at successive crossings of this surface is

$$\begin{aligned}\phi_{n+1} &= \phi_n + 2\pi\alpha(J_{n+1}) \\ J_{n+1} &= J_n\end{aligned}\quad (5.2)$$

Formally, we may write the map as $\varphi_{n+1} = \hat{T}\varphi_n$, where $\varphi_n = (\phi_n, J_n)$ and \hat{T} is the map. Note that the action variable is unchanged during the motion¹, and hence is fixed under the map. We are left with a mapping of the circle onto itself, called the *twist map*. Since the map faithfully represents Hamiltonian evolution, it must be canonical, meaning

$$\{\phi_{n+1}, J_{n+1}\}_{(\phi_n, J_n)} = \det \frac{\partial(\phi_{n+1}, J_{n+1})}{\partial(\phi_n, J_n)} = \frac{\partial\phi_{n+1}}{\partial\phi_n} \frac{\partial J_{n+1}}{\partial J_n} - \frac{\partial\phi_{n+1}}{\partial J_n} \frac{\partial J_{n+1}}{\partial\phi_n} = 1 \quad , \quad (5.3)$$

which is indeed satisfied. If $\alpha(J) \in \mathbb{Q}$ is rational, certain iterations of the map leave the circle fixed. Specifically, let $\alpha = r/s$. Then \hat{T}^s acts as the identity, leaving the entire circle (and indeed the entire (ϕ, J) plane) fixed.

For systems with N degrees of freedom, with (ϕ_N, J_N) as the surface of section, one defines $\phi = (\phi_1, \dots, \phi_{N-1})$ and $\mathbf{J} = (J_1, \dots, J_{N-1})$ and $\boldsymbol{\alpha} = (\omega_1/\omega_N, \dots, \omega_{N-1}/\omega_N)$, one has

$$\begin{aligned}\phi_{n+1} &= \phi_n + 2\pi\boldsymbol{\alpha}(\mathbf{J}_{n+1}) \\ \mathbf{J}_{n+1} &= \mathbf{J}_n\end{aligned}\quad (5.4)$$

One can check that this map is also area-preserving (canonical).

5.1.2 The perturbed twist map

Now consider a perturbed Hamiltonian $H(\mathbf{J}, \phi) = H_0(\mathbf{J}) + \epsilon H_1(\mathbf{J}, \phi)$, again for $N = 2$. Once more we consider the surface of section defined by the (ϕ_1, J_1) plane. We expect a perturbed twist map \hat{T}_ϵ of the form

$$\begin{aligned}\phi_{n+1} &= \phi_n + 2\pi\alpha(J_{n+1}) + \epsilon f(\phi_n, J_{n+1}) \\ J_{n+1} &= J_n + \epsilon g(\phi_n, J_{n+1})\end{aligned}\quad , \quad (5.5)$$

¹It is for this reason that we may write $\alpha(J_{n+1})$ in the first equation, rather than $\alpha(J_n)$. The reason will soon be apparent.

for some functions f and g . Is the perturbed twist map canonical? We could investigate this by computing the Poisson bracket $\{\phi_{n+1}, J_{n+1}\}$, but here we take another approach, which is to exhibit explicitly a type-II generator $F_2(\phi_n, J_{n+1})$ which effects the canonical transformation $(\phi_n, J_n) \rightarrow (\phi_{n+1}, J_{n+1})$. Consider the generator

$$F_2(\phi_n, J_{n+1}) = \phi_n J_{n+1} + 2\pi A(J_{n+1}) + \epsilon B(\phi_n, J_{n+1}) . \quad (5.6)$$

The CT generated is

$$\begin{aligned} \phi_{n+1} &= \frac{\partial F_2}{\partial J_{n+1}} = \phi_n + 2\pi \frac{\partial A}{\partial J_{n+1}} + \epsilon \frac{\partial B}{\partial J_{n+1}} \\ J_n &= \frac{\partial F_2}{\partial \phi_n} = J_{n+1} + \epsilon \frac{\partial B}{\partial \phi_n} . \end{aligned} \quad (5.7)$$

We therefore identify $\alpha(J_{n+1}) = A'(J_{n+1})$ as well as

$$f(J_{n+1}, \phi_n) = \frac{\partial B}{\partial J_{n+1}} , \quad g(J_{n+1}, \phi_n) = -\frac{\partial B}{\partial \phi_n} . \quad (5.8)$$

This, in turn, requires

$$\frac{\partial f}{\partial \phi_n} + \frac{\partial g}{\partial J_{n+1}} = 0 , \quad (5.9)$$

which is a necessary and sufficient condition in order that the map \hat{T}_ϵ be canonical.

In the case $g = g(\phi_n)$, the above condition requires $f = f(J_{n+1})$, and we may absorb $f(J)$ into the definition of $\alpha(J)$. We then have the map

$$\begin{aligned} \phi_{n+1} &= \phi_n + 2\pi\alpha(J_{n+1}) \\ J_{n+1} &= J_n + \epsilon g(\phi_n) . \end{aligned} \quad (5.10)$$

For $\alpha(J) = J$ and $g(\phi) = -\sin \phi$, we obtain the *standard map*, about which we shall have more to say below.

5.2 Maps from Time-Dependent Hamiltonian Systems

5.2.1 Parametric Oscillator

Consider the equation

$$\ddot{x} + \omega_0^2(t)x = 0 , \quad (5.11)$$

where the oscillation frequency is a function of time. Equivalently,

$$\frac{d}{dt} \begin{pmatrix} x \\ \dot{x} \end{pmatrix} = \underbrace{\begin{pmatrix} M(t) & \\ 0 & 1 \end{pmatrix}}_{\varphi(t)} \underbrace{\begin{pmatrix} x \\ \dot{x} \end{pmatrix}}_{\varphi(t)} . \quad (5.12)$$

The formal solution is the path-ordered exponential,

$$\varphi(t) = \mathcal{P} \exp \left\{ \int_0^t dt' M(t') \right\} \varphi(0). \quad (5.13)$$

Let's consider an example in which

$$\omega(t) = \begin{cases} (1 + \epsilon) \omega_0 & \text{if } 2n\tau \leq t \leq (2n+1)\tau \\ (1 - \epsilon) \omega_0 & \text{if } (2n+1)\tau \leq t \leq (2n+2)\tau. \end{cases} \quad (5.14)$$

Define $\varphi_n \equiv \varphi(2n\tau)$. Then

$$\varphi_{n+1} = \exp(M_- \tau) \exp(M_+ \tau) \varphi_n \equiv \mathcal{U} \varphi_n, \quad (5.15)$$

where

$$M_\pm = \begin{pmatrix} 0 & 1 \\ -\omega_\pm^2 & 0 \end{pmatrix}, \quad (5.16)$$

with $\omega_\pm \equiv (1 \pm \epsilon) \omega_0$. Note that $M_\pm^2 = -\omega_\pm^2 \mathbb{I}$ is a multiple of the identity. Evaluating the Taylor series for the exponential, one finds

$$\mathcal{U}_\pm \equiv \exp(M_\pm t) = \begin{pmatrix} \cos \omega_\pm \tau & \omega_\pm^{-1} \sin \omega_\pm \tau \\ -\omega_\pm \sin \omega_\pm \tau & \cos \omega_\pm \tau \end{pmatrix}, \quad (5.17)$$

from which we derive the evolution matrix

$$\mathcal{U} \equiv \mathcal{U}_- \mathcal{U}_+ = \begin{pmatrix} \cos \omega_- \tau & \omega_-^{-1} \sin \omega_- \tau \\ -\omega_- \sin \omega_- \tau & \cos \omega_- \tau \end{pmatrix} \begin{pmatrix} \cos \omega_+ \tau & \omega_+^{-1} \sin \omega_+ \tau \\ -\omega_+ \sin \omega_+ \tau & \cos \omega_+ \tau \end{pmatrix} \equiv \begin{pmatrix} a & b \\ c & d \end{pmatrix}$$

with

$$\begin{aligned} a &= \cos \omega_- \tau \cos \omega_+ \tau - \frac{\omega_+}{\omega_-} \sin \omega_- \tau \sin \omega_+ \tau \\ b &= \frac{1}{\omega_+} \cos \omega_- \tau \sin \omega_+ \tau + \frac{1}{\omega_-} \sin \omega_- \tau \cos \omega_+ \tau \\ c &= -\omega_+ \cos \omega_- \tau \sin \omega_+ \tau - \omega_- \sin \omega_- \tau \cos \omega_+ \tau \\ d &= \cos \omega_- \tau \cos \omega_+ \tau - \frac{\omega_-}{\omega_+} \sin \omega_- \tau \sin \omega_+ \tau. \end{aligned} \quad (5.18)$$

Note that \mathcal{U}_\pm are each symplectic, hence $\det \exp(M_\pm \tau) = 1$, and therefore \mathcal{U} is also symplectic with $\det \mathcal{U} = 1$. Also note that

$$P(\lambda) = \det(\mathcal{U} - \lambda \cdot \mathbb{I}) = \lambda^2 - T\lambda + \Delta, \quad (5.19)$$

where $T = a + d = \text{Tr } \mathcal{U}$ and $\Delta = ad - bc = \det \mathcal{U}$. The eigenvalues of \mathcal{U} are

$$\lambda_\pm = \frac{1}{2}T \pm \frac{1}{2}\sqrt{T^2 - 4\Delta}. \quad (5.20)$$

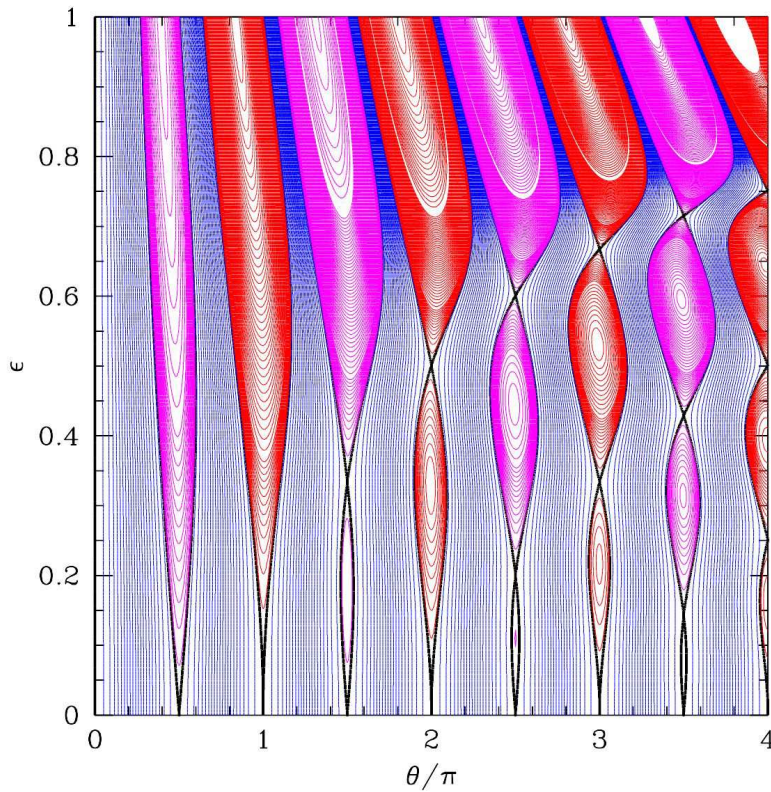


Figure 5.2: Phase diagram for the parametric oscillator in the (θ, ϵ) plane. Thick black lines correspond to $T = \pm 2$. Blue regions: $|T| < 2$. Red regions: $T > 2$. Magenta regions: $T < -2$.

In our case, $\Delta = 1$. There are two cases to consider:

$$\begin{aligned} |T| < 2 : \lambda_+ &= \lambda_-^* = e^{i\delta} \quad , \quad \delta = \cos^{-1} \frac{1}{2}T \\ |T| > 2 : \lambda_+ &= \lambda_-^{-1} = \pm e^\mu \quad , \quad \mu = \cosh^{-1} \frac{1}{2}|T| . \end{aligned} \quad (5.21)$$

When $|T| < 2$, φ remains bounded; when $|T| > 2$, $|\varphi|$ increases exponentially with time. Note that phase space volumes are preserved by the dynamics.

To investigate more fully, let $\theta \equiv \omega_0\tau$. The period of the frequency oscillations is $\Delta t = 2\tau$, i.e. $\omega_{\text{pump}} = \pi/\tau$ is the frequency at which the system is ‘pumped’, so

$$\frac{\theta}{\pi} = \frac{\omega_0}{\omega_{\text{pump}}} = \frac{T_{\text{pump}}}{T_0} \quad , \quad (5.22)$$

where $T_0 = 2\pi/\omega_0$ is the unperturbed natural frequency and $T_{\text{pump}} = \Delta t = 2\tau$. One finds $T = \text{Tr}\mathcal{U}$ is given by

$$T = \frac{2 \cos(2\theta) - 2\epsilon^2 \cos(2\epsilon\theta)}{1 - \epsilon^2} . \quad (5.23)$$

We are interested in the boundaries in the (θ, ϵ) plane where $|T| = 2$. Setting $T = +2$, we write $\theta = n\pi + \delta$, which means $T_{\text{pump}} \approx nT_0$. Expanding for small δ and ϵ , we obtain the relation

$$\delta^2 = \epsilon^4 \theta^2 \quad \Rightarrow \quad \epsilon = \pm \left| \frac{\delta}{n\pi} \right|^{1/2}. \quad (5.24)$$

Setting $T = -2$, we write $\theta = (n + \frac{1}{2})\pi + \delta$, i.e. $T_{\text{pump}} \approx (n + \frac{1}{2})T_0$. This gives

$$\delta^2 = \epsilon^2 \quad \Rightarrow \quad \epsilon = \pm \delta. \quad (5.25)$$

The full phase diagram in the (θ, ϵ) plane is shown in Fig. 5.2. A physical example is pumping a swing. By extending your legs periodically, you effectively change the length $\ell(t)$ of the pendulum, resulting in a time-dependent $\omega_0(t) = \sqrt{g/\ell(t)}$.

5.2.2 Kicked dynamics

A related model is described by the *kicked dynamics* of the Hamiltonian

$$H(t) = T(p) + V(q) K(t), \quad (5.26)$$

where

$$K(t) = \tau \sum_{n=-\infty}^{\infty} \delta(t - n\tau) \quad (5.27)$$

is the kicking function. The potential thus winks on and off with period τ . Note that

$$\lim_{\tau \rightarrow 0} K(t) = 1. \quad (5.28)$$

In the $\tau \rightarrow 0$ limit, the system is continuously kicked, and is equivalent to motion in a time-independent external potential $V(q)$.

The equations of motion are

$$\dot{q} = T'(p) \quad , \quad \dot{p} = -V'(q) K(t). \quad (5.29)$$

Integrating these equations, we obtain the map

$$\begin{aligned} q_{n+1} &= q_n + \tau T'(p_n) \\ p_{n+1} &= p_n - \tau V'(q_{n+1}). \end{aligned} \quad (5.30)$$

Note that the determinant of Jacobean of the map is unity:

$$\det \frac{\partial(q_{n+1}, p_{n+1})}{\partial(q_n, p_n)} = \det \begin{pmatrix} 1 & \tau T''(p_n) \\ -\tau V''(q_{n+1}) & 1 - \tau^2 T''(p_n) V''(q_{n+1}) \end{pmatrix} = 1. \quad (5.31)$$

This means that the map preserves phase space volumes.

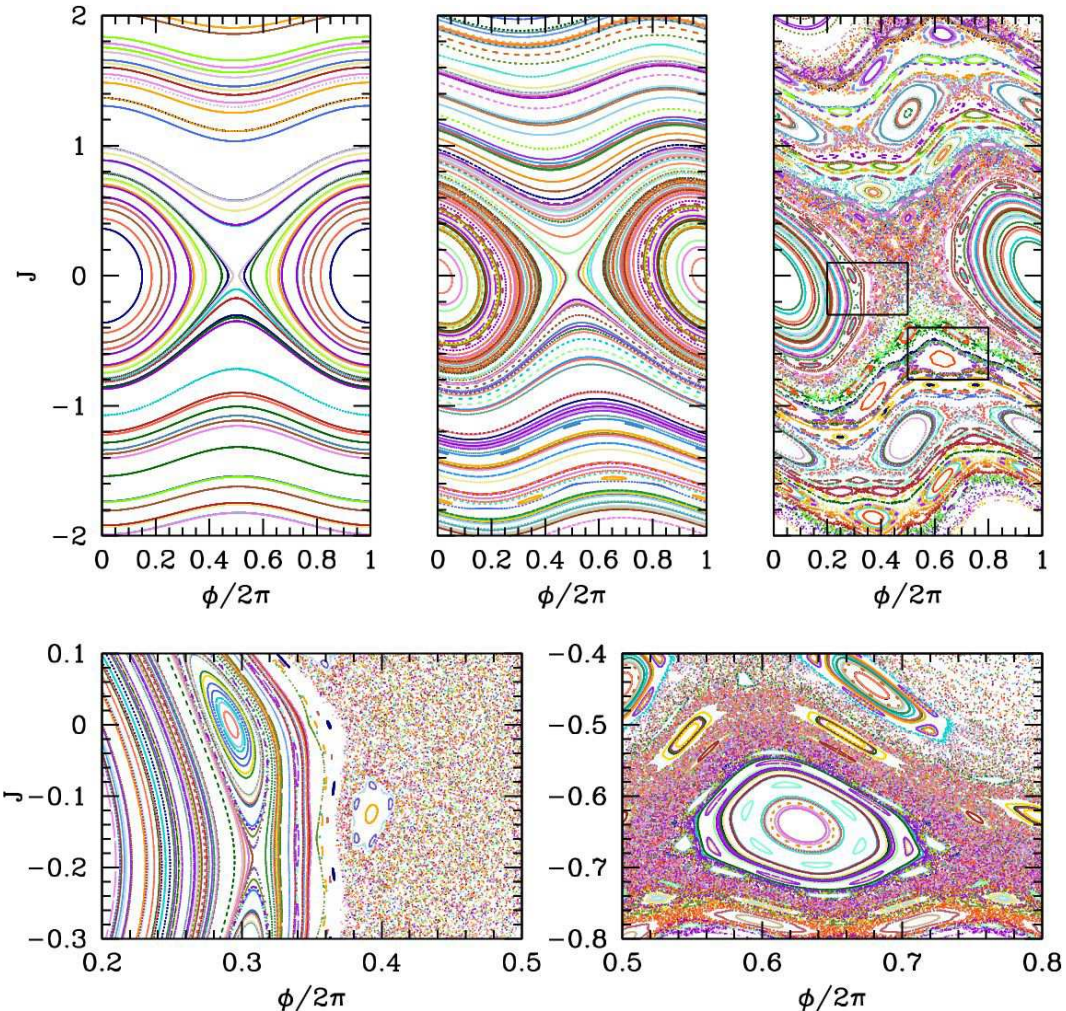


Figure 5.3: Top: the standard map, as defined in the text. Four values of the ϵ parameter are shown: $\epsilon = 0.01$ (left), $\epsilon = 0.2$ (center), and $\epsilon = 0.4$ (right). Bottom: details of the $\epsilon = 0.4$ map.

Consider, for example, the Hamiltonian $H(t) = \frac{L^2}{2I} - V\cos(\phi) K(t)$, where L is the angular momentum conjugate to ϕ . This results in the map

$$\begin{aligned}\phi_{n+1} &= \phi_n + 2\pi\epsilon J_n \\ J_{n+1} &= J_n - \epsilon \sin \phi_{n+1},\end{aligned}\tag{5.32}$$

where $J_n = L_n/\sqrt{2\pi IV}$ and $\epsilon = \tau\sqrt{V/2\pi I}$. This is the standard map², which we encountered earlier, albeit in a slightly different form. In the limit $\epsilon \rightarrow 0$, we may define $\dot{\phi} = (\phi_{n+1} - \phi_n)/\epsilon$ and $\dot{J} = (J_{n+1} - J_n)/\epsilon$, and we recover the continuous time dynamics $\dot{\phi} = 2\pi J$ and $\dot{J} = -\sin \phi$. These dynamics preserve the energy function $E = \pi J^2 - \cos \phi$. There is a separatrix at $E = 1$, given by $J(\phi) = \pm \frac{2}{\pi} |\cos(\phi/2)|$. We see from fig. 5.3 that this separatrix is the first structure to be replaced by a chaotic fuzz as ϵ increases

²The standard map us usually written in the form $x_{n+1} = x_n + \mathcal{J}_n$ and $\mathcal{J}_{n+1} = \mathcal{J}_n - k \sin(2\pi x_{n+1})$. We can recover our version by rescaling $\phi_n = 2\pi x_n$, $\mathcal{J}_n \equiv \sqrt{k} J_n$ and defining $\epsilon \equiv \sqrt{k}$.

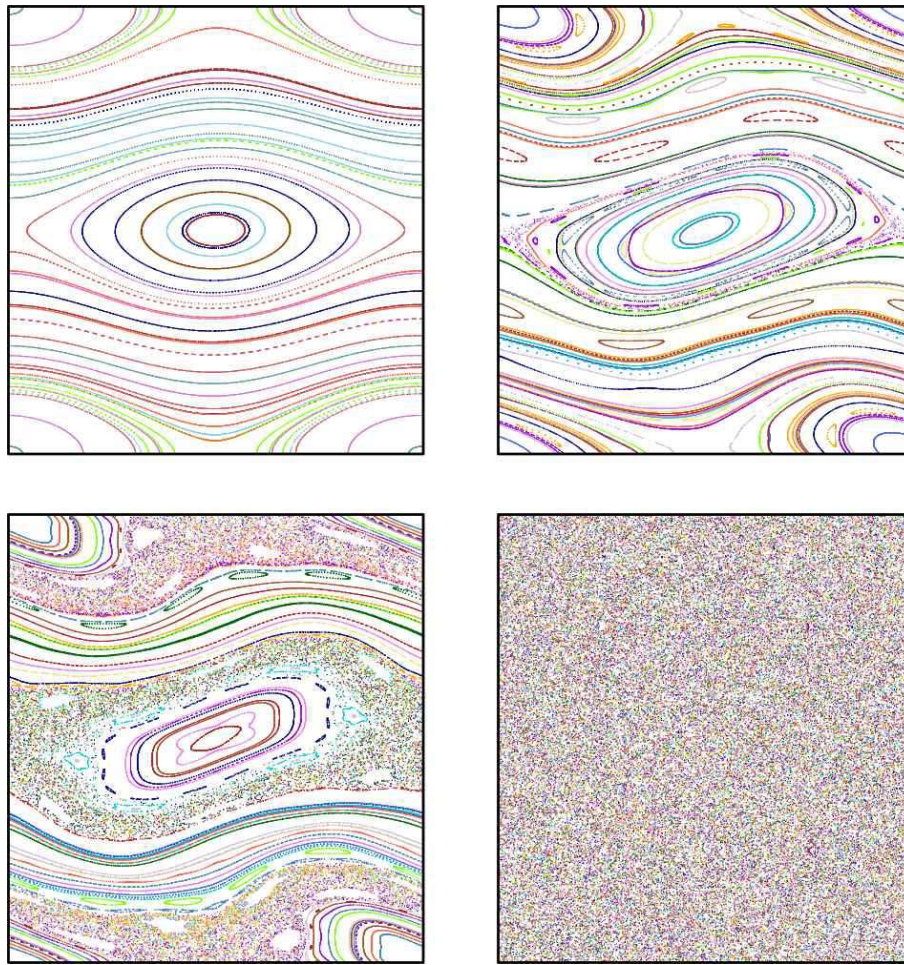


Figure 5.4: The kicked Harper map, with $\alpha = 2$, and with $\epsilon = 0.01, 0.125, 0.2$, and 5.0 (clockwise from upper left). The phase space here is the unit torus, $\mathbb{T}^2 = [0, 1] \times [0, 1]$.

from zero to a small finite value.

Another well-studied system is the *kicked Harper model*, for which

$$H(t) = -V_1 \cos\left(\frac{2\pi p}{P}\right) - V_2 \cos\left(\frac{2\pi q}{Q}\right) K(t) . \quad (5.33)$$

With $x = q/Q$ and $y = p/P$, Hamilton's equations generate the map

$$\begin{aligned} x_{n+1} &= x_n + \epsilon \alpha \sin(2\pi y_n) \\ y_{n+1} &= y_n - \frac{\epsilon}{\alpha} \sin(2\pi x_{n+1}) , \end{aligned} \quad (5.34)$$

where $\epsilon = 2\pi\tau\sqrt{V_1 V_2}/PQ$ and $\alpha = \sqrt{V_1/V_2}$ are dimensionless parameters. In this case, the conserved energy is

$$E = -\alpha^{-1} \cos(2\pi x) - \alpha \cos(2\pi y) . \quad (5.35)$$

There are then two separatrices, at $E = \pm(\alpha - \alpha^{-1})$, with equations $\alpha \cos(\pi y) = \pm \sin(\pi x)$ and $\alpha \sin(\pi y) = \pm \cos(\pi x)$. Again, as is apparent from fig. 5.4, the separatrix is the first structure to be destroyed at finite ϵ . This also occurs for the standard map – there is a transition to *global stochasticity* at a critical value of ϵ .

Note that the kicking function may be written as

$$K(t) = \tau \sum_{n=-\infty}^{\infty} \delta(t - n\tau) = \sum_{m=-\infty}^{\infty} \cos\left(\frac{2\pi mt}{\tau}\right) , \quad (5.36)$$

a particularly handy result known as the *Poisson summation formula*. This, a kicked Hamiltonian may be written as

$$H(J, \phi, t) = H_0(J) + V(\phi) \sum_{m=-\infty}^{\infty} \cos\left(\frac{2\pi mt}{\tau}\right) . \quad (5.37)$$

The $m = 0$ term generates the continuous time dynamics $\dot{\phi} = \omega_0(J)$, $\dot{J} = -V'(\phi)$. For the standard map, these are the dynamics of a simple pendulum. The $m \neq 0$ terms are responsible for resonances and the formation of so-called ‘stochastic layers’.

5.3 Local Stability and Lyapunov Exponents

5.3.1 The fate of nearly separated initial conditions under iteration

Consider a map \hat{T} acting on a phase space of dimension $2N$ (*i.e.* N position degrees of freedom). We ask what is the fate of two nearby initial conditions, ξ_0 and $\xi_0 + d\xi$, under the iterated map. Under the first iteration, we have $\xi_0 \rightarrow \xi_1 = \hat{T}\xi_0$ and

$$\xi_0 + d\xi \longrightarrow \xi_1 + M(\xi_0) d\xi , \quad (5.38)$$

where $M(\xi)$ is a matrix given by the *linearization of \hat{T} at ξ* , *viz.*

$$M_{ij}(\xi) = \frac{\partial(\hat{T}\xi)_i}{\partial\xi_j} . \quad (5.39)$$

Let’s iterate again. Clearly $\xi_1 \rightarrow \xi_2 = \hat{T}^2\xi_0$ and

$$\xi_1 + M(\xi_0) d\xi \longrightarrow \xi_2 + M(\xi_1)M(\xi_0) d\xi . \quad (5.40)$$

After n iterations, we clearly have $\hat{T}^n\xi_0 = \xi_n$ and

$$\hat{T}^n(\xi_0 + d\xi) = \xi_n + M(\xi_{n-1}) \cdots M(\xi_0) d\xi , \quad (5.41)$$

and we define $R^{(n)}(\xi) = M(\hat{T}^n\xi) \cdots M(\hat{T}\xi)M(\xi)$, whose matrix elements may be written as $R_{ij}^{(n)}(\xi) = \partial(\hat{T}^n\xi)_i / \partial\xi_j$.

Since the map \hat{T} is presumed to be canonical, at each stage $M(\xi_j) \in \text{Sp}(2N)$, and since the product of symplectic matrices is a symplectic matrix, $R^{(n)}(\xi) \in \text{Sp}(2N)$. It is easy to see that for any real symplectic

matrix R , the eigenvalues come in unimodular conjugate pairs $\{e^{i\delta}, e^{-i\delta}\}$, in real pairs $\{\lambda, \lambda^{-1}\}$ with $\lambda \in \mathbb{R}$, or in quartets $\{\lambda, \lambda^{-1}, \lambda^*, \lambda^{*-1}\}$ with $\lambda \in \mathbb{C}$, where λ^* is the complex conjugate of λ . This follows from analysis of the characteristic polynomial $P(\lambda) = \det(\lambda - R)$ given the symplectic condition³ $R^t \mathbb{J} R = \mathbb{J}$. Let $\{\lambda_j^{(n)}(\xi)\}$ be the eigenvalues of $R^{(n)}(\xi)$, with $j \in \{1, \dots, 2N\}$. One defines the *Lyapunov exponents*,

$$\nu_j(\xi) = \lim_{n \rightarrow \infty} \frac{1}{n} \ln |\lambda_j^{(n)}(\xi)| . \quad (5.42)$$

These may be ordered such that $\nu_1 \leq \nu_2 \leq \dots \leq \nu_{2N}$. Positive Lyapunov exponents correspond to an exponential stretching (as a function of the iteration number n), while negative ones correspond to an exponential squeezing.

As an example, consider the Arnol'd cat map, which is an automorphism of the torus $\mathbb{T}^2 = \mathbb{S}^1 \times \mathbb{S}^1$, given by⁴

$$\begin{aligned} q_{n+1} &= (K + 1) q_n + p_n \\ p_{n+1} &= K q_n + p_n , \end{aligned} \quad (5.43)$$

where $K \in \mathbb{Z}$, and where both q_n and p_n are defined modulo unity, so $(q_n, p_n) \in [0, 1] \times [0, 1]$. Note that K must be an integer in order for the map to be smooth on the torus, *i.e.* it is left unchanged by displacing either coordinate by an integer distance. The map is already linear, hence we can read off

$$M = \frac{\partial(q_{n+1}, p_{n+1})}{\partial(q_n, p_n)} = \begin{pmatrix} K + 1 & 1 \\ K & 1 \end{pmatrix} , \quad (5.44)$$

which is independent of (q_n, p_n) . The inverse map also has integer coefficients:

$$M^{-1} = \begin{pmatrix} 1 & -1 \\ -K & K + 1 \end{pmatrix} . \quad (5.45)$$

Since $\det M = 1$, the cat map is canonical, *i.e.* it preserves phase space volumes. The eigenvalues of M are the roots of the characteristic polynomial $P(\lambda) = \lambda^2 - (K + 2)\lambda - K$, and are given by

$$\lambda_{\pm} = 1 + \frac{1}{2}K \pm \sqrt{K + \frac{1}{4}K^2} . \quad (5.46)$$

Thus, for $K \in \{-4, -3, -2, -1, 0\}$, the eigenvalues come in pairs $e^{\pm i\delta_K}$, with $\delta_{-4} = \pi$, $\delta_{-3} = \frac{2}{3}\pi$, $\delta_{-2} = \frac{1}{2}\pi$, $\delta_{-1} = \frac{1}{3}\pi$, and $\delta_0 = 0$. For $K < -4$ or $K > 0$, the eigenvalues are (λ, λ^{-1}) with $\lambda > 1$ and $0 < \lambda^{-1} < 1$, corresponding, respectively, to stretching and squeezing. The Lyapunov exponents are $\nu_{\pm} = \ln |\lambda_{\pm}|$.

5.3.2 Kolmogorov-Sinai entropy

Let $\Gamma < \infty$ be our phase space (at constant energy, for a Hamiltonian system), and $\{\Delta_j\}$ a partition of disjoint sets whose union is Γ . The simplest arrangement to think of is for each Δ_j to correspond to a

³One has $P(\lambda) = \det(\lambda - R) = \det(\lambda - R^t) = \det(\lambda + \mathbb{J}R^{-1}\mathbb{J}) = \det(\lambda^{-1} - R) \cdot \lambda^{2N}/\det R$ and therefore if λ is a root of the characteristic polynomial, then so is λ^{-1} . Since $R = R^*$, one also has $P(\lambda^*) = [P(\lambda)]^*$, hence if λ is a root, then so is λ^* . From $\text{Pf}(R^t \mathbb{J} R) = \det(R) \text{Pf}(\mathbb{J})$, where Pf is the Pfaffian, one has $\det R = 1$.

⁴The map in Eqn. 5.43 is a generalized version of Arnol'd's original cat map, which had $K = 1$.

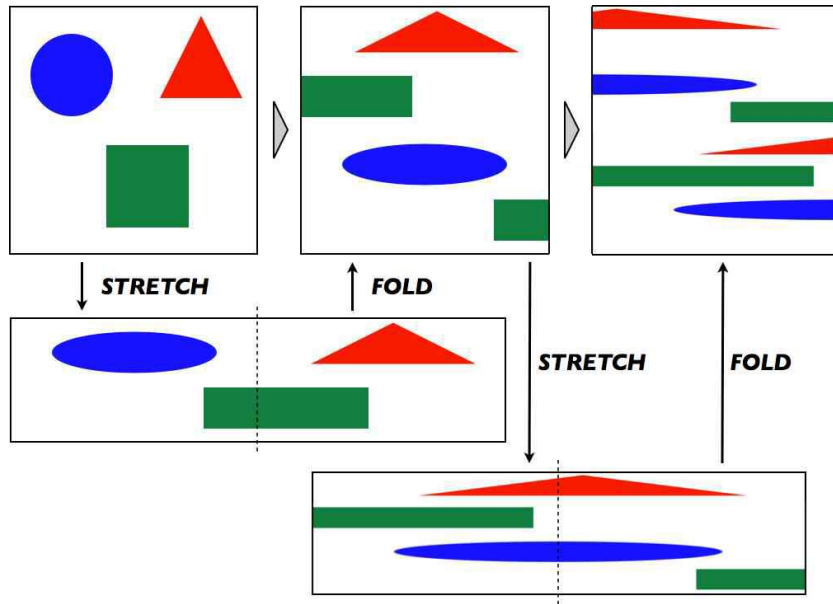


Figure 5.5: The baker's transformation involves stretching/squeezing and 'folding' (cutting and restacking).

little hypercube; stacking up all the hypercube builds the entire phase space. Now apply the inverse map \hat{T}^{-1} to each Δ_j , and form the intersections $\Delta_{jk} \equiv \Delta_j \cap \hat{T}^{-1}\Delta_k$. If $\sum_j \mu(\Delta_j) = \mu(\Gamma) \equiv 1$, then $\sum_{j,k} \mu(\Delta_{jk}) = 1$. Iterating further, we obtain $\Delta_{jkl} = \Delta_{jk} \equiv \Delta_j \cap \hat{T}^{-1}\Delta_k \cap \hat{T}^{-2}\Delta_l$, etc.

The entropy of a distribution $\{p_a\}$ is defined to be $S = -\sum_a p_a \ln p_a$. Accordingly we define

$$S_L(\Delta) = - \sum_{j_1} \cdots \sum_{j_L} \mu(\Delta_{j_1 \cdots j_L}) \ln \mu(\Delta_{j_1 \cdots j_L}) . \quad (5.47)$$

This is a function of both the iteration number L as well as the initial set $\Delta = \{\Delta_1, \dots, \Delta_r\}$, where r is the number of subregions in our original partition. We then define the Kolmogorov-Sinai entropy to be

$$h_{\text{KS}} \equiv \sup_{\Delta} \lim_{L \rightarrow \infty} \frac{1}{L} S_L(\Delta) . \quad (5.48)$$

Here \sup stands for *supremum*, meaning we maximize over all partitions Δ .

Consider, for example, the *baker's transformation* (see Fig. 5.5), which stretches, cuts, stacks, and compresses the torus according to

$$(q', p') = \hat{T}(q, p) = \begin{cases} (2q, \frac{1}{2}p) & \text{if } 0 \leq p < \frac{1}{2} \\ (2q-1, \frac{1}{2}p + \frac{1}{2}) & \text{if } \frac{1}{2} \leq p < 1 \end{cases} \quad (5.49)$$

It is not difficult to convince oneself that the KS entropy for the baker's transformation is $h_{\text{KS}} = \ln 2$. On the other hand, for a simple translation map which takes $(q, p) \rightarrow (q', p') = (q + \alpha, p + \beta)$, it is easy to see that $h_{\text{KS}} = 0$. The KS entropy is related to the Lyapunov exponents through the formula

$$h_{\text{KS}} = \sum_j \nu_j \Theta(\nu_j) . \quad (5.50)$$

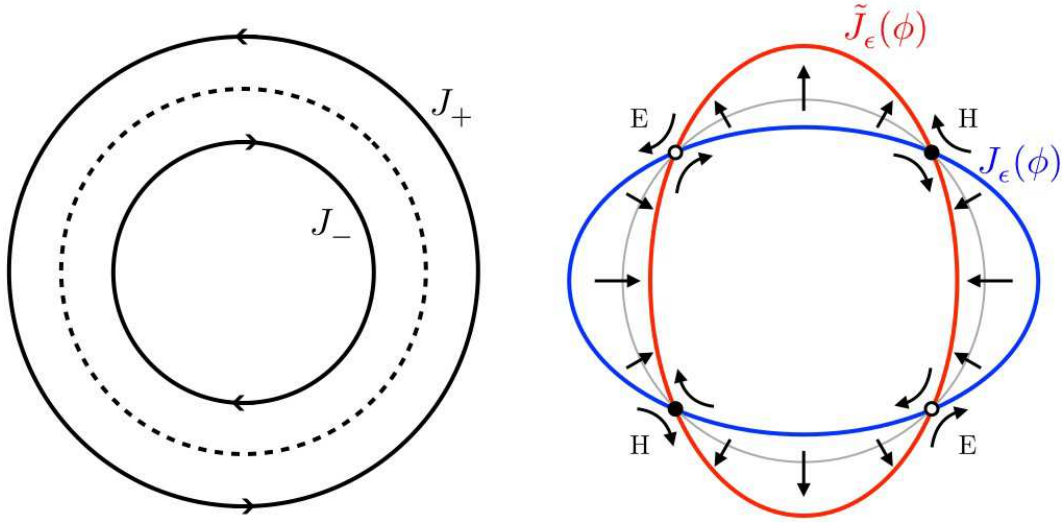


Figure 5.6: Left: The action of the iterated map \hat{T}_0^s leaves the circle with $\alpha(J) = r/s$ invariant (dotted curve), but rotates slightly counterclockwise and clockwise on the circles $J = J_+$ and $J = J_-$, respectively. Right: The blue curve $J_\epsilon(\phi)$ is the locus of points where \hat{T}_ϵ^s acts purely radially and preserves ϕ , resulting in the red curve $\tilde{J}_\epsilon(\phi)$. Since \hat{T}_ϵ^s is volume-preserving, these curves must intersect in an alternating sequence of elliptic and hyperbolic fixed points.

The RHS is the sum over all the positive Lyapunov exponents $\gamma_j > 0$. Actually, this formula presumes that the γ_j do not vary in phase space, but in general this is not the case. The more general result is known as *Pesin's entropy formula*,

$$h_{\text{KS}} = \int d\mu(\xi) \sum_j \nu_j(\xi) \Theta(\nu_j(\xi)) . \quad (5.51)$$

5.4 The Poincaré-Birkhoff Theorem

Let's return to our discussion of the perturbed twist map,

$$\begin{pmatrix} \phi_{n+1} \\ J_{n+1} \end{pmatrix} = \hat{T}_\epsilon \begin{pmatrix} \phi_n \\ J_n \end{pmatrix} = \begin{pmatrix} \phi_n + 2\pi\alpha(J_{n+1}) + \epsilon f(\phi_n, J_{n+1}) \\ J_n + \epsilon g(\phi_n, J_{n+1}) \end{pmatrix} , \quad (5.52)$$

with $\frac{\partial f}{\partial \phi_n} + \frac{\partial g}{\partial J_{n+1}} = 0$ in order that the map be canonical. For $\epsilon = 0$, the map \hat{T}_0 leaves J invariant, and takes circles to circles. If $\alpha(J) \neq \mathbb{Q}$, the images of the iterated map become dense on the circle.

Consider now a circle with fixed J for which $\alpha(J) = r/s$ is rational⁵, and without loss of generality let us presume $\alpha'(J) > 0$ so that on circles $J_\pm = J \pm \Delta J$ we have $\alpha(J_+) > r/s$ and $\alpha(J_-) < r/s$. Under \hat{T}_0^s , all the points on the circle $\mathcal{C} = \mathcal{C}(J)$ are fixed, whereas those on \mathcal{C}_+ rotate slightly counterclockwise, and those on \mathcal{C}_- slightly clockwise (see left panel of Fig. 5.6), where $\mathcal{C}_\pm = \mathcal{C}(J_\pm)$. Now consider the

⁵We may assume r and s are relatively prime.

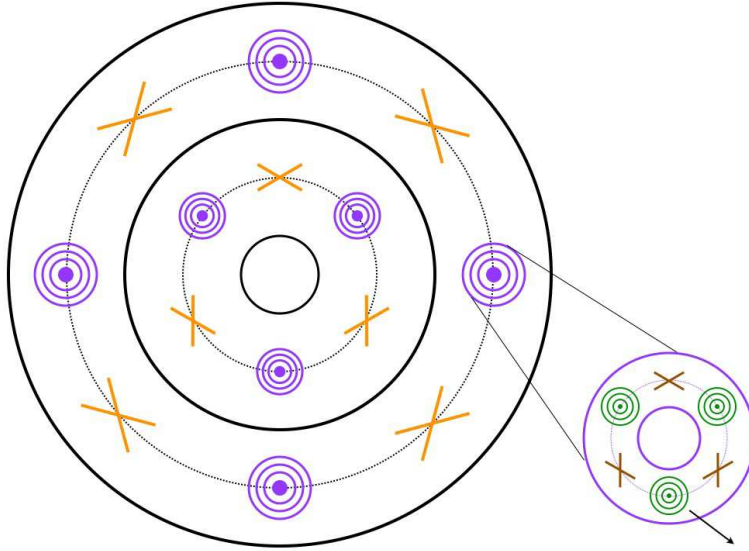


Figure 5.7: Self-similar structures in the iterated twist map.

action of the iterated perturbed map \hat{T}_ϵ^s . Acting on \mathcal{C}_+ , the action is still a net counterclockwise shift (assuming $\epsilon \ll \frac{\Delta J}{J}$, with some small $\mathcal{O}(\epsilon)$ radial component. Similarly, acting on \mathcal{C}_- , the action is a net clockwise shift plus $\mathcal{O}(\epsilon)$ radial component. By the intermediate value theorem, for a given fixed ϕ , as one proceeds radially outward from \mathcal{C}_- to \mathcal{C}_+ , there must be a point $J = J_\epsilon(\phi)$ where the angular shift vanishes. This defines an entire curve $J_\epsilon(\phi)$ along which the action of \hat{T}_ϵ^s is purely radial. Now consider the curve $\tilde{J}_\epsilon(\phi) = \hat{T}_\epsilon^s J_\epsilon(\phi)$, i.e. the action of \hat{T}_ϵ^s on the curve $J_\epsilon(\phi)$. We know that each point along $J_\epsilon(\phi)$ is displaced radially, but we also know that \hat{T}_ϵ^s is volume-preserving. Therefore, the curves $J_\epsilon(\phi)$ and $\tilde{J}_\epsilon(\phi)$ must intersect at an even number of points⁶. These intersections are fixed points of the map \hat{T}_ϵ^s . The situation is depicted in the right panel of Fig. 5.6. From the figure, it is clear that the set $J_\epsilon(\phi) \cap \tilde{J}_\epsilon(\phi)$ consists of alternating elliptic and hyperbolic fixed points.

What we have just described is the content of the *Poincaré-Birkhoff theorem*: A small perturbation of a resonant torus with $\alpha(J) = r/s$ results in an equal number elliptic and hyperbolic fixed points for the iterated map \hat{T}_ϵ^s . Since T_ϵ has period s acting on these fixed points, the number of EFPs and HFPs must be equal and also a multiple of s . In the vicinity of the EFPs, this structure repeats, as depicted in Fig. 5.7.

Stable/unstable manifolds and homoclinic/heteroclinic intersections

Now consider the HFPs. Emanating from a given HFP ξ^* are *stable and unstable manifolds*, $\Sigma^{S/U}(\xi^*)$, defined by:

$$\begin{aligned}\xi \in \Sigma^S(\xi^*) &\Rightarrow \lim_{n \rightarrow \infty} \hat{T}_\epsilon^{+ns} \xi = \xi^* \quad (\text{to } \xi^*) \\ \xi \in \Sigma^U(\xi^*) &\Rightarrow \lim_{n \rightarrow \infty} \hat{T}_\epsilon^{-ns} \xi = \xi^* \quad (\text{from } \xi^*)\end{aligned}. \tag{5.53}$$

⁶Tangency is nongeneric and broken by a small change in ϵ .

Note that $\Sigma^U(\xi_i^*)$ can never intersect $\Sigma^U(\xi_j^*)$ for any i and j , nor can $\Sigma^S(\xi_i^*)$ ever intersect $\Sigma^S(\xi_j^*)$. However, $\Sigma^U(\xi_i^*)$ can intersect $\Sigma^S(\xi_j^*)$. If $i = j$, such an intersection is called a *homoclinic point*, while for $i \neq j$ the intersection is called a *heteroclinic point*. Because \hat{T}_ϵ^s is continuous and invertible, its action at a homoclinic/heteroclinic point will produce a *new* homoclinic/heteroclinic point, *ad infinitum*! For homoclinic intersections, the resulting structure is known as a *homoclinic tangle*, an example of which is shown in Fig. 5.8.

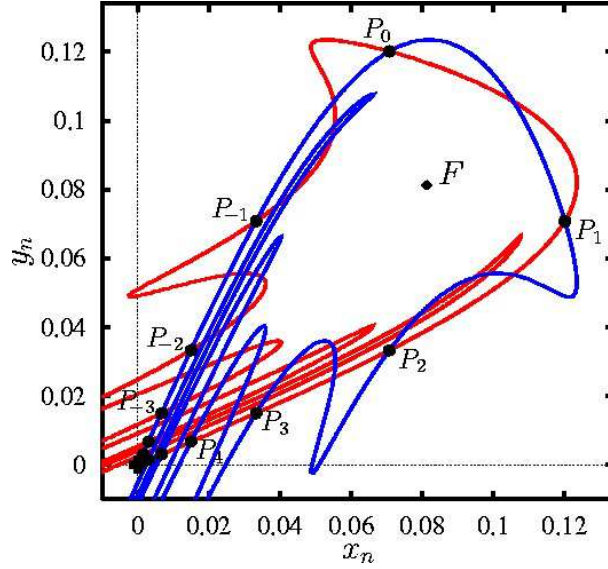


Figure 5.8: Homoclinic tangle for the map $x_{n+1} = y_n$ and $y_{n+1} = (a + b y_n^2) y_n - x_n$ for parameters $a = 2.693$, $b = -104.888$. Stable (blue) and unstable (red) manifolds emanating from the HFP at $(0, 0)$ are shown.

5.5 One-dimensional Maps

Consider now an even simpler case of a purely one-dimensional map,

$$x_{n+1} = f(x_n). \quad (5.54)$$

A fixed point of the map satisfies $x = f(x)$. Writing the solution as x^* and expanding about the fixed point, we write $x = x^* + u$ and obtain

$$u_{n+1} = f'(x^*) u_n + \mathcal{O}(u^2). \quad (5.55)$$

Thus, the fixed point is stable if $|f'(x^*)| < 1$, since successive iterates of u then get smaller and smaller. The fixed point is unstable if $|f'(x^*)| > 1$.

Perhaps the most important and most studied of the one-dimensional maps is the logistic map, where $f(x) = rx(1-x)$, defined on the interval $x \in [0, 1]$. This has a fixed point at $x^* = 1 - r^{-1}$ if $r > 1$. We then have $f'(x^*) = 2 - r$, so the fixed point is stable if $r \in (1, 3)$. What happens for $r > 3$? We can

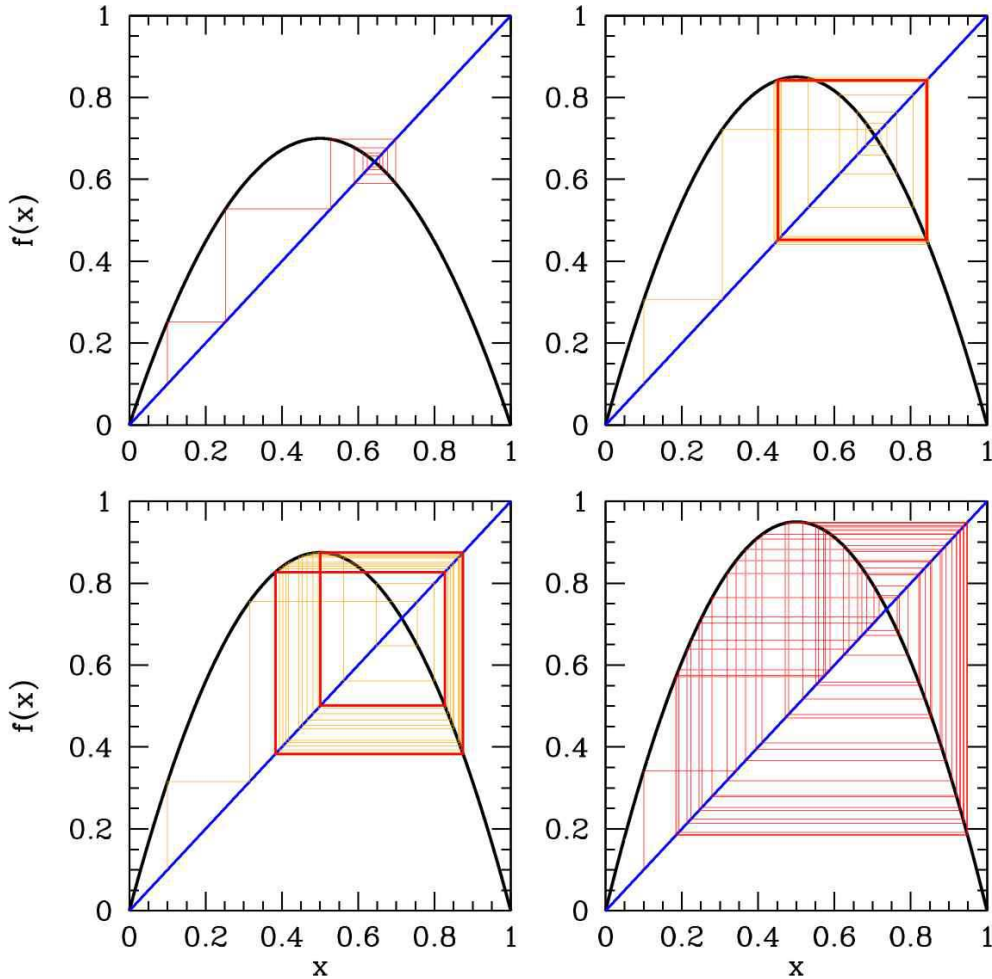


Figure 5.9: Cobweb diagram showing iterations of the logistic map $f(x) = rx(1 - x)$ for $r = 2.8$ (upper left), $r = 3.4$ (upper right), $r = 3.5$ (lower left), and $r = 3.8$ (lower right). Note the single stable fixed point for $r = 2.8$, the stable two-cycle for $r = 3.4$, the stable four-cycle for $r = 3.5$, and the chaotic behavior for $r = 3.8$.

explore the behavior of the iterated map by drawing a *cobweb diagram*, shown in fig. 5.9. We sketch, on the same graph, the curves $y = x$ (in blue) and $y = f(x)$ (in black). Starting with a point x on the line $y = x$, we move vertically until we reach the curve $y = f(x)$. To iterate, we then move horizontally to the line $y = x$ and repeat the process. We see that for $r = 3.4$ the fixed point x^* is unstable, but there is a stable two-cycle, defined by the equations

$$\begin{aligned} x_2 &= rx_1(1 - x_1) \\ x_1 &= rx_2(1 - x_2). \end{aligned} \tag{5.56}$$

The second iterate of $f(x)$ is then

$$f^{(2)}(x) = f(f(x)) = r^2x(1 - x)(1 - rx + rx^2). \tag{5.57}$$

Setting $x = f^{(2)}(x)$, we obtain a cubic equation. Since $x - x^*$ must be a factor, we can divide out by this monomial and obtain a quadratic equation for x_1 and x_2 . We find

$$x_{1,2} = \frac{1 + r \pm \sqrt{(r+1)(r-3)}}{2r}. \quad (5.58)$$

How stable is this 2-cycle? We find

$$\frac{d}{dx}f^{(2)}(x) = r^2(1-2x_1)(1-2x_2) = -r^2 + 2r + 4. \quad (5.59)$$

The condition that the 2-cycle be stable is then

$$-1 < r^2 - 2r - 4 < 1 \implies r \in [3, 1 + \sqrt{6}]. \quad (5.60)$$

At $r = 1 + \sqrt{6} = 3.4494897\dots$ there is a bifurcation to a 4-cycle, as can be seen in fig. 5.10.

5.5.1 Lyapunov Exponents

The *Lyapunov exponent* $\lambda(x)$ of the iterated map $f(x)$ at point x is defined to be

$$\lambda(x) = \lim_{n \rightarrow \infty} \frac{1}{n} \ln \left| \frac{df^{(n)}(x)}{dx} \right| = \lim_{n \rightarrow \infty} \frac{1}{n} \sum_{j=1}^n \ln |f'(x_j)|, \quad (5.61)$$

where $x_{j+1} \equiv f(x_j)$. The significance of the Lyapunov exponent is the following. If $\text{Re}(\lambda(x)) > 0$ then two initial conditions near x will exponentially separate under the iterated map. For the *tent map*,

$$f(x) = \begin{cases} 2rx & \text{if } x < \frac{1}{2} \\ 2r(1-x) & \text{if } x \geq \frac{1}{2}, \end{cases} \quad (5.62)$$

one easily finds $\lambda(x) = \ln(2r)$ independent of x . Thus, if $r > \frac{1}{2}$ the Lyapunov exponent is positive, meaning that every neighboring pair of initial conditions will eventually separate exponentially under repeated application of the map. The Lyapunov exponent for the logistic map is depicted in fig. 5.11.

5.5.2 Chaos in the logistic map

What happens in the logistic map for $r > 1 + \sqrt{6}$? At this point, the 2-cycle becomes unstable and a stable 4-cycle develops. However, this soon goes unstable and is replaced by a stable 8-cycle, as the right hand panel of fig. 5.10 shows. The first eight values of r where bifurcations occur are given by

$$\begin{aligned} r_1 &= 3, & r_2 &= 1 + \sqrt{6} = 3.4494897, & r_3 &= 3.544096, & r_4 &= 3.564407, \\ r_5 &= 3.568759, & r_6 &= 3.569692, & r_7 &= 3.569891, & r_8 &= 3.569934, \dots \end{aligned} \quad (5.63)$$

Feigenbaum noticed that these numbers seemed to be converging exponentially. With the *Ansatz*

$$r_\infty - r_k = \frac{c}{\delta^k}, \quad (5.64)$$

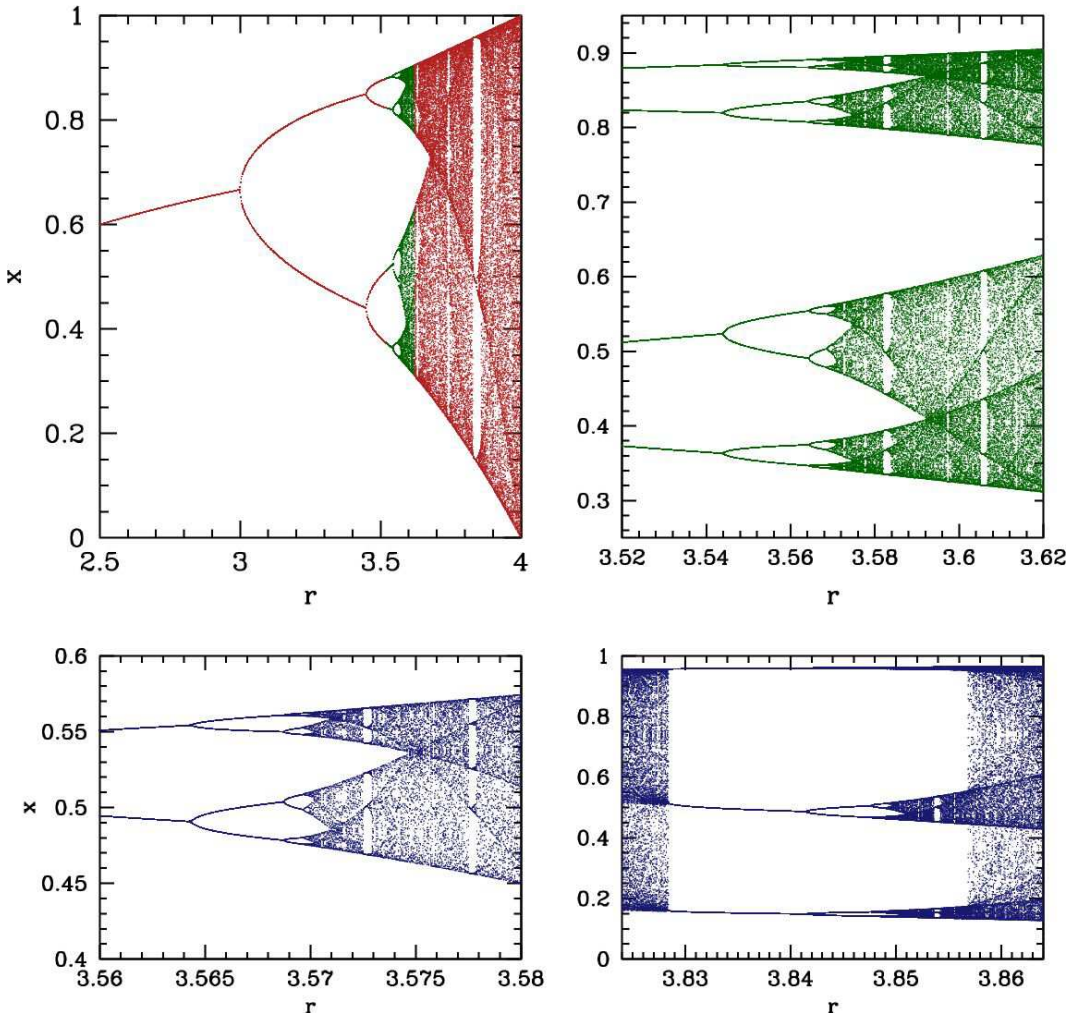


Figure 5.10: Iterates of the logistic map $f(x) = rx(1 - x)$.

one finds

$$\delta = \frac{r_k - r_{k-1}}{r_{k+1} - r_k}, \quad (5.65)$$

and taking the limit $k \rightarrow \infty$ from the above data one finds

$$\delta = 4.669202 , \quad c = 2.637 , \quad r_\infty = 3.5699456 . \quad (5.66)$$

There's a very nifty way of thinking about the chaos in the logistic map at the special value $r = 4$. If we define $x_n \equiv \sin^2 \theta_n$, then we find

$$\theta_{n+1} = 2\theta_n . \quad (5.67)$$

Now let us write

$$\theta_0 = \pi \sum_{k=1}^{\infty} \frac{b_k}{2^k} , \quad (5.68)$$

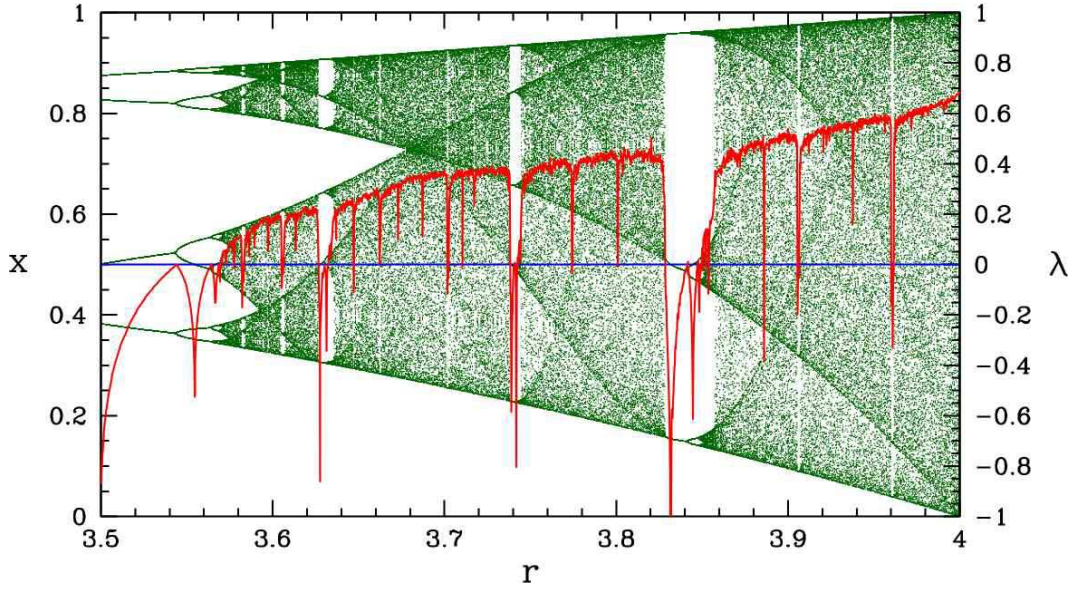


Figure 5.11: Lyapunov exponent (in red) for the logistic map.

where each b_k is either 0 or 1. In other words, the $\{b_k\}$ are the digits in the binary decimal expansion of θ_0/π . Now $\theta_n = 2^n \theta_0$, hence

$$\theta_n = \pi \sum_{k=1}^{\infty} \frac{b_{n+k}}{2^k}. \quad (5.69)$$

We now see that the logistic map has the effect of *shifting* to the left the binary digits of θ_n/π to yield θ_{n+1}/π . With each such shift, leftmost digit falls off the edge of the world, as it were, since it results in an overall contribution to θ_{n+1} which is zero modulo π . This very emphatically demonstrates the sensitive dependence on initial conditions which is the hallmark of chaotic behavior, for eventually two very close initial conditions, differing by $\Delta\theta \sim 2^{-m}$, will, after m iterations of the logistic map, come to differ by $\mathcal{O}(1)$.

5.5.3 Intermittency

Successive period doubling is one route to chaos, as we've just seen. Another route is *intermittency*. Intermittency works like this. At a particular value of our control parameter r , the map exhibits a stable periodic cycle, such as the stable 3-cycle at $r = 3.829$, as shown in the bottom panel of fig. 5.13. If we then vary the control parameter slightly in a certain direction, the periodic behavior persists for a finite number of iterations, followed by a *burst*, which is an interruption of the regular periodicity, followed again by periodic behavior, *ad infinitum*. There are three types of intermittent behavior, depending on whether the Lyapunov exponent λ goes through $\text{Re}(\lambda) = 0$ while $\text{Im}(\lambda) = 0$ (type-I intermittency), or with $\text{Im}(\lambda) = \pi$ (type-III intermittency), or, as is possible for two-dimensional maps, with $\text{Im}(\lambda) = \eta$, a general real number.

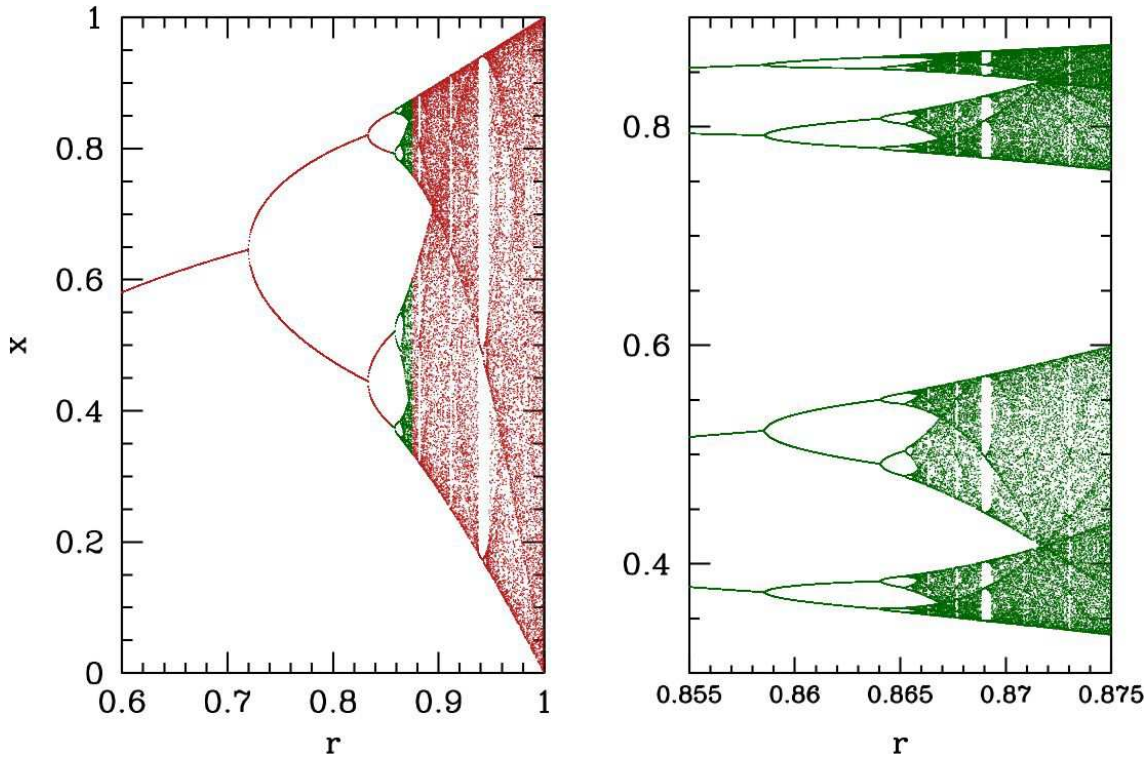


Figure 5.12: Iterates of the sine map $f(x) = r \sin(\pi x)$.

5.6 Attractors

An *attractor* of a dynamical system $\dot{\varphi} = V(\varphi)$ is the set of φ values that the system evolves to after a sufficiently long time. For $N = 1$ the only possible attractors are stable fixed points. For $N = 2$, we have stable nodes and spirals, but also stable limit cycles. For $N > 2$ the situation is qualitatively different, and a fundamentally new type of set, the *strange attractor*, emerges.

A strange attractor is basically a bounded set on which nearby orbits diverge exponentially (*i.e.* there exists at least one positive Lyapunov exponent). To envision such a set, consider a flat rectangle, like a piece of chewing gum. Now fold the rectangle over, stretch it, and squash it so that it maintains its original volume. Keep doing this. Two points which started out nearby to each other will eventually, after a sufficiently large number of folds and stretches, grow far apart. Formally, a strange attractor is a *fractal*, and may have *noninteger Hausdorff dimension*. (We won't discuss fractals and Hausdorff dimension here.)

5.7 The Lorenz Model

The canonical example of an $N = 3$ strange attractor is found in the Lorenz model. E. N. Lorenz, in a seminal paper from the early 1960's, reduced the essential physics of the coupled *partial* differential

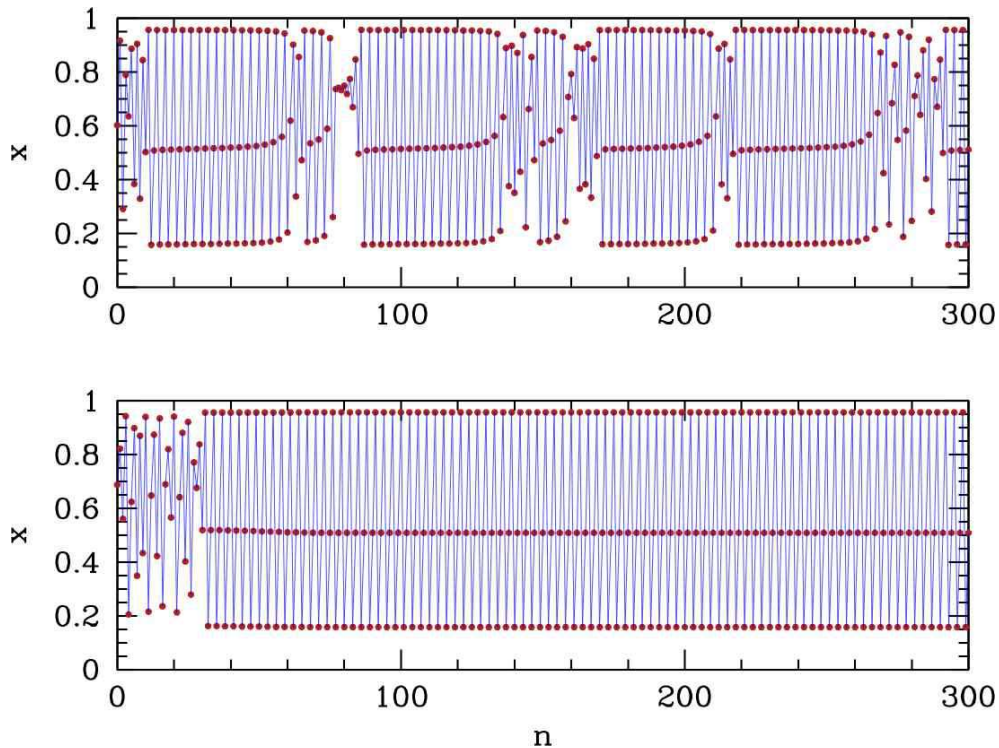


Figure 5.13: Intermittency in the logistic map in the vicinity of the 3-cycle. Top panel: $r = 3.828$, showing intermittent behavior. Bottom panel: $r = 3.829$, showing a stable 3-cycle.

equations describing Rayleigh-Benard convection (a fluid slab of finite thickness, heated from below – in Lorenz’s case a model of the atmosphere warmed by the ocean) to a set of twelve coupled nonlinear *ordinary* differential equations. Lorenz’s intuition was that his weather model should exhibit recognizable patterns over time. What he found instead was that in some cases, changing his initial conditions by a part in a thousand rapidly led to totally different behavior. This *sensitive dependence on initial conditions* is a hallmark of chaotic systems.

The essential physics (or mathematics?) of Lorenz’s $N = 12$ system is elicited by the reduced $N = 3$ system,

$$\begin{aligned}\dot{X} &= -\sigma X + \sigma Y \\ \dot{Y} &= rX - Y - XZ \\ \dot{Z} &= XY - bZ,\end{aligned}\tag{5.70}$$

where σ , r , and b are all real and positive. Here t is the familiar time variable (appropriately scaled), and (X, Y, Z) represent linear combinations of physical fields, such as global wind current and poleward temperature gradient. These equations possess a symmetry under $(X, Y, Z) \rightarrow (-X, -Y, Z)$, but what is most important is the presence of nonlinearities in the second and third equations.

The Lorenz system is *dissipative* because phase space volumes contract:

$$\nabla \cdot \mathbf{V} = \frac{\partial \dot{X}}{\partial X} + \frac{\partial \dot{Y}}{\partial Y} + \frac{\partial \dot{Z}}{\partial Z} = -(\sigma + b + 1).\tag{5.71}$$

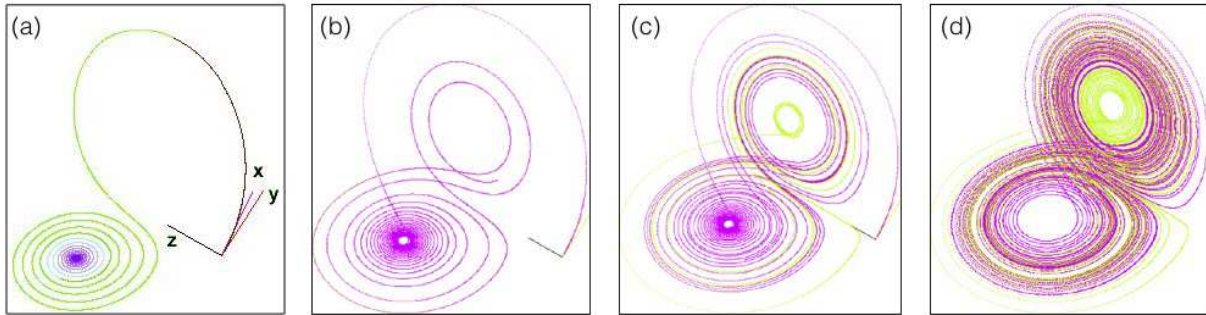


Figure 5.14: (a) Evolution of the Lorenz equations for $\sigma = 10$, $b = \frac{8}{3}$, and $r = 15$, with initial conditions $(X, Y, Z) = (0, 1, 0)$, projected onto the (X, Z) plane. The attractor is a stable spiral. (b) - (d) Chaotic regime ($r = 28$) evolution showing sensitive dependence on initial conditions. The magenta and green curves differ in their initial X coordinate by 10^{-5} . (Source: Wikipedia)

Thus, volumes contract under the flow. Another property is the following. Let

$$F(X, Y, Z) = \frac{1}{2}X^2 + \frac{1}{2}Y^2 + \frac{1}{2}(Z - r - \sigma)^2 . \quad (5.72)$$

Then

$$\begin{aligned} \dot{F} &= X\dot{X} + Y\dot{Y} + (Z - r - \sigma)\dot{Z} \\ &= -\sigma X^2 - Y^2 - b(Z - \frac{1}{2}r - \frac{1}{2}\sigma)^2 + \frac{1}{4}b(r + \sigma)^2 . \end{aligned} \quad (5.73)$$

Thus, $\dot{F} < 0$ outside an ellipsoid, which means that all solutions must remain bounded in phase space for all times.

5.7.1 Fixed point analysis

Setting $\dot{X} = \dot{Y} = \dot{Z} = 0$, we find three solutions. One solution which is always present is $X^* = Y^* = Z^* = 0$. If we linearize about this solution, we obtain

$$\frac{d}{dt} \begin{pmatrix} \delta X \\ \delta Y \\ \delta Z \end{pmatrix} = \begin{pmatrix} -\sigma & \sigma & 0 \\ r & -1 & 0 \\ 0 & 0 & -b \end{pmatrix} \begin{pmatrix} \delta X \\ \delta Y \\ \delta Z \end{pmatrix} . \quad (5.74)$$

The eigenvalues of the linearized dynamics are found to be

$$\begin{aligned} \lambda_{1,2} &= -\frac{1}{2}(1 + \sigma) \pm \frac{1}{2}\sqrt{(1 + \sigma)^2 + 4\sigma(r - 1)} \\ \lambda_3 &= -b , \end{aligned} \quad (5.75)$$

and thus if $0 < r < 1$ all three eigenvalues are negative, and the fixed point is a stable node. If, however, $r > 1$, then $\lambda_2 > 0$ and the fixed point is attractive in two directions but repulsive in a third, corresponding to a three-dimensional version of a saddle point.

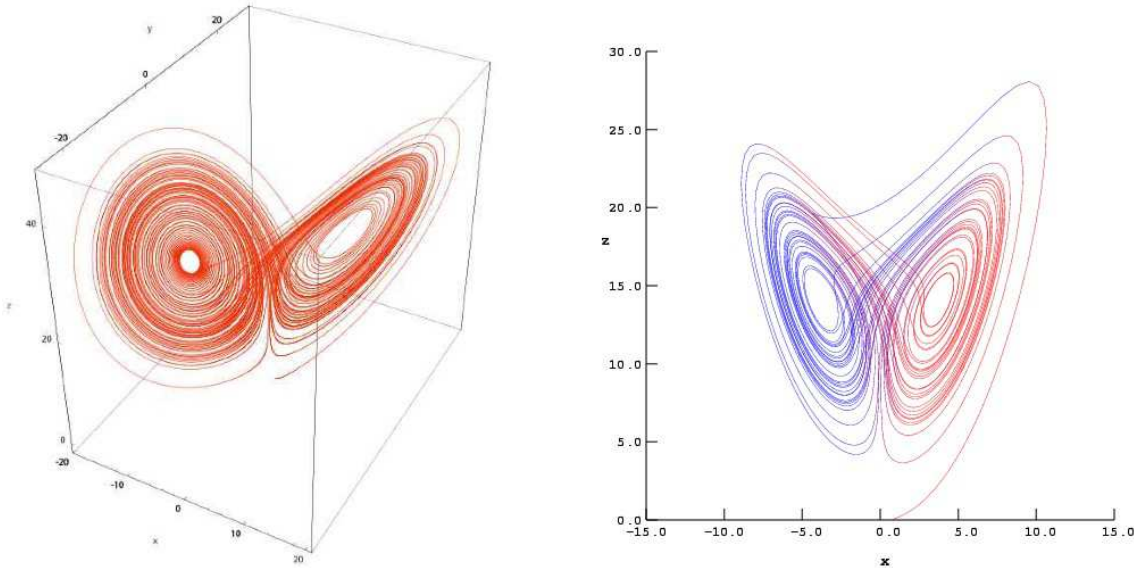


Figure 5.15: Left: Evolution of the Lorenz equations for $\sigma = 10$, $b = \frac{8}{3}$, and $r = 28$, with initial conditions $(X_0, Y_0, Z_0) = (0, 1, 0)$, showing the ‘strange attractor’. Right: The Lorenz attractor, projected onto the (X, Z) plane. (Source: Wikipedia)

For $r > 1$, a new pair of solutions emerges, with

$$X^* = Y^* = \pm \sqrt{b(r-1)} \quad , \quad Z^* = r - 1 . \quad (5.76)$$

Linearizing about either one of these fixed points, we find

$$\frac{d}{dt} \begin{pmatrix} \delta X \\ \delta Y \\ \delta Z \end{pmatrix} = \begin{pmatrix} -\sigma & \sigma & 0 \\ 1 & -1 & -X^* \\ X^* & X^* & -b \end{pmatrix} \begin{pmatrix} \delta X \\ \delta Y \\ \delta Z \end{pmatrix} . \quad (5.77)$$

The characteristic polynomial of the linearized map is

$$P(\lambda) = \lambda^3 + (b + \sigma + 1)\lambda^2 + b(\sigma + r)\lambda + 2b(r - 1) . \quad (5.78)$$

Since b , σ , and r are all positive, $P'(\lambda) > 0$ for all $\lambda \geq 0$. Since $P(0) = 2b(r-1) > 0$, we may conclude that there is always at least one eigenvalue λ_1 which is real and negative. The remaining two eigenvalues are either both real and negative, or else they occur as a complex conjugate pair: $\lambda_{2,3} = \alpha \pm i\beta$. The fixed point is stable provided $\alpha < 0$. The stability boundary lies at $\alpha = 0$. Thus, we set

$$P(i\beta) = [2b(r-1) - (b + \sigma + 1)\beta^2] + i[b(\sigma + r) - \beta^2]\beta = 0 , \quad (5.79)$$

which results in two equations. Solving these two equations for $r(\sigma, b)$, we find

$$r_c = \frac{\sigma(\sigma + b + 3)}{\sigma - b - 1} . \quad (5.80)$$

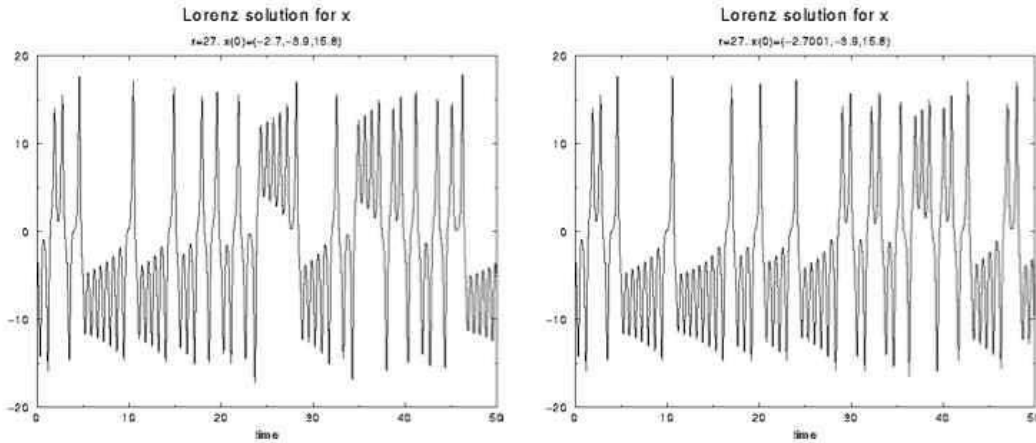


Figure 5.16: $X(t)$ for the Lorenz equations with $\sigma = 10$, $b = \frac{8}{3}$, $r = 28$, and initial conditions $(X_0, Y_0, Z_0) = (-2.7, -3.9, 15.8)$, and initial conditions $(X_0, Y_0, Z_0) = (-2.7001, -3.9, 15.8)$.

The fixed point is stable for $r \in [1, r_c]$. These fixed points correspond to steady convection. The approach to this fixed point is shown in Fig. 5.14.

The Lorenz system has commonly been studied with $\sigma = 10$ and $b = \frac{8}{3}$. This means that the volume collapse is very rapid, since $\nabla \cdot \mathbf{V} = -\frac{41}{3} \approx -13.67$, leading to a volume contraction of $e^{-41/3} \simeq 1.16 \times 10^{-6}$ per unit time. For these parameters, one also has $r_c = \frac{470}{19} \approx 24.74$. The capture by the strange attractor is shown in Fig. 5.15.

In addition to the new pair of fixed points, a strange attractor appears for $r > r_s \simeq 24.06$. In the narrow interval $r \in [24.06, 24.74]$ there are then *three* stable attractors, two of which correspond to steady convection and the third to chaos. Over this interval, there is also hysteresis. *I.e.* starting with a convective state for $r < 24.06$, the system remains in the convective state until $r = 24.74$, when the convective fixed point becomes unstable. The system is then driven to the strange attractor, corresponding to chaotic dynamics. Reversing the direction of r , the system remains chaotic until $r = 24.06$, when the strange attractor loses its own stability.

5.7.2 Poincaré section

One method used by Lorenz in analyzing his system was to plot its *Poincaré section*. This entails placing one constraint on the coordinates (X, Y, Z) to define a two-dimensional surface Σ , and then considering the intersection of this surface Σ with a given phase curve for the Lorenz system. Lorenz chose to set $\dot{Z} = 0$, which yields the surface $Z = b^{-1}XY$. Note that since $\dot{Z} = 0$, $Z(t)$ takes its maximum and minimum values on this surface; see the left panel of Fig. 5.17. By plotting the values of the maxima Z_N as the integral curve successively passed through this surface, Lorenz obtained results such as those shown in the right panel of Fig. 5.17, which has the form of a one-dimensional map and may be analyzed as such. Thus, chaos in the Lorenz attractor can be related to chaos in a particular one-dimensional map, known as the *return map* for the Lorenz system.

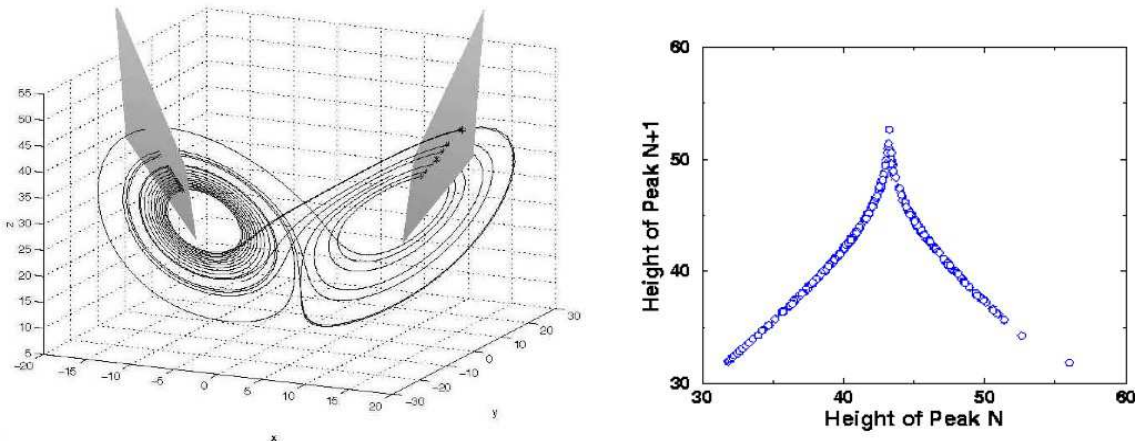


Figure 5.17: Left: Lorenz attractor for $b = \frac{8}{3}$, $\sigma = 10$, and $r = 28$. Maxima of Z are depicted by stars. Right: Relation between successive maxima Z_N along the strange attractor.

5.7.3 Rössler System

The strange attractor is one of the hallmarks of the Lorenz system. Another simple dynamical system which possesses a strange attractor is the Rössler system. This is also described by $N = 3$ coupled ordinary differential equations, *viz.*

$$\begin{aligned}\dot{X} &= -Y - Z \\ \dot{Y} &= Z + aY \\ \dot{Z} &= b + Z(X - c),\end{aligned}\tag{5.81}$$

typically studied as a function of c for $a = b = \frac{1}{5}$. In Fig. 5.19, we present results from work by Crutchfield *et al.* (1980). The transition from simple limit cycle to strange attractor proceeds via a sequence of period-doubling bifurcations, as shown in the figure. A convenient diagnostic for examining this period-doubling route to chaos is the *power spectral density*, or PSD, defined for a function $F(t)$ as

$$\Phi_F(\omega) = \left| \int_{-\infty}^{\infty} \frac{d\omega}{2\pi} F(t) e^{-i\omega t} \right|^2 = |\hat{F}(\omega)|^2.\tag{5.82}$$

As one sees in Fig. 5.19, as c is increased past each critical value, the PSD exhibits a series of frequency halvings (*i.e.* period doublings). All harmonics of the lowest frequency peak are present. In the chaotic region, where $c > c_\infty \approx 4.20$, the PSD also includes a noisy broadband background.

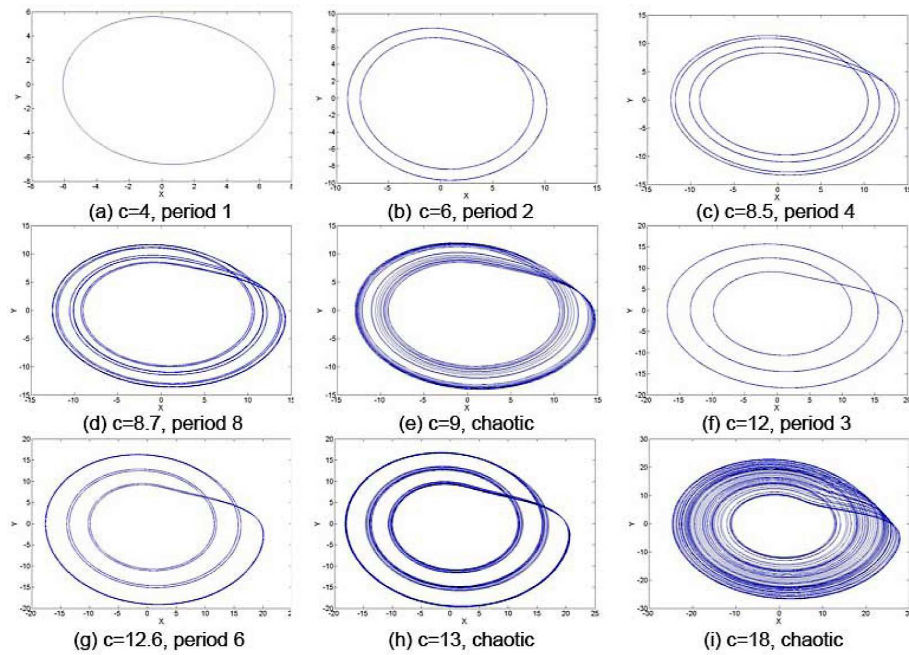


Figure 5.18: Period doubling bifurcations of the Rössler attractor, projected onto the (x, y) plane, for nine values of c , with $a = b = \frac{1}{10}$.

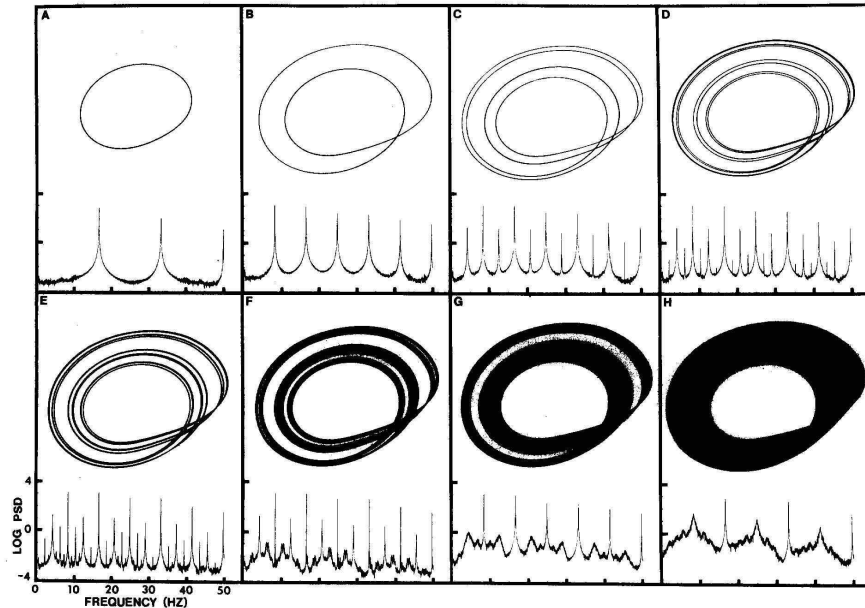


Figure 5.19: Period doubling bifurcations of the Rössler attractor with $a = b = \frac{1}{5}$, projected onto the (X, Y) plane, for eight values of c , and corresponding power spectral density for $Z(t)$. (a) $c = 2.6$; (b) $c = 3.5$; (c) $c = 4.1$; (d) $c = 4.18$; (e) $c = 4.21$; (f) $c = 4.23$; (g) $c = 4.30$; (h) $c = 4.60$.

Chapter 6

Front Propagation

6.1 Reaction-Diffusion Systems

We've studied simple $N = 1$ dynamical systems of the form

$$\frac{du}{dt} = R(u) \quad . \quad (6.1)$$

Recall that the dynamics evolves $u(t)$ monotonically toward the first stable fixed point encountered. Now let's extend the function $u(t)$ to the spatial domain as well, i.e. $u(\mathbf{x}, t)$, and add a diffusion term:

$$\frac{\partial u}{\partial t} = D \nabla^2 u + R(u) \quad , \quad (6.2)$$

where D is the diffusion constant. This is an example of a *reaction-diffusion system*. If we extend $u(\mathbf{x}, t)$ to a multicomponent field $\mathbf{u}(\mathbf{x}, t)$, we obtain the general reaction-diffusion equation (RDE)

$$\frac{\partial u_i}{\partial t} = D_{ij} \nabla^2 u_i + R_i(u_1, \dots, u_N) \quad . \quad (6.3)$$

Here, \mathbf{u} is interpreted as a *vector of reactants*, $\mathbf{R}(\mathbf{u})$ describes the *nonlinear local reaction kinetics*, and D_{ij} is the *diffusivity matrix*. If diffusion is negligible, this PDE reduces to decoupled local ODEs of the form $\dot{\mathbf{u}} = \mathbf{R}(\mathbf{u})$, which is to say a dynamical system at each point in space. Thus, any fixed point \mathbf{u}^* of the local reaction dynamics also describes a spatially homogeneous, time-independent solution to the RDE. These solutions may be characterized as dynamically stable or unstable, depending on the eigenspectrum of the Jacobian matrix $M_{ij} = \partial_i R_j(\mathbf{u}^*)$. At a stable fixed point, $\text{Re}(\lambda_i) < 0$ for all eigenvalues.

6.1.1 Single component systems

We first consider the single component system,

$$\frac{\partial u}{\partial t} = D \nabla^2 u + R(u) \quad . \quad (6.4)$$

Note that the right hand side can be expressed as the functional derivative of a *Lyapunov functional*,

$$L[u] = \int d^d x \left[\frac{1}{2} D(\nabla u)^2 - U(u) \right] , \quad (6.5)$$

where

$$U(u) = \int_0^u du' R(u') . \quad (6.6)$$

(The lower limit in the above equation is arbitrary.) Thus, eqn. 6.4 is equivalent to

$$\frac{\partial u}{\partial t} = - \frac{\delta L}{\delta u(\mathbf{x}, t)} . \quad (6.7)$$

Thus, the Lyapunov functional runs strictly downhill, *i.e.* $\dot{L} < 0$, except where $u(\mathbf{x}, t)$ solves the RDE, at which point $\dot{L} = 0$.

6.1.2 Propagating front solutions

Suppose the dynamical system $\dot{u} = R(u)$ has two or more fixed points. Each such fixed point represents a static, homogeneous solution to the RDE. We now seek a dynamical, inhomogeneous solution to the RDE in the form of a *propagating front*, described by

$$u(x, t) = u(x - Vt) , \quad (6.8)$$

where V is the (as yet unknown) front propagation speed. With this *Ansatz*, the PDE of eqn. 6.4 is converted to an ODE,

$$D \frac{d^2 u}{d\xi^2} + V \frac{du}{d\xi} + R(u) = 0 , \quad (6.9)$$

where $\xi = x - Vt$. With $R(u) \equiv U'(u)$ as in eqn. 6.6, we have the following convenient interpretation. If we substitute $u \rightarrow q$, $\xi \rightarrow s$, $D \rightarrow m$, and $v \rightarrow \gamma$, this equation describes the damped motion of a massive particle under friction: $m\ddot{q} + \gamma\dot{q} = -U'(q)$, where $\dot{q} = dq/ds$. The fixed points q^* satisfy $U'(q^*) = 0$ and are hence local extrema of $U(q)$. The propagating front solution we seek therefore resembles the motion of a massive particle rolling between extrema of the potential $U(q)$. Note that the stable fixed points of the local reaction kinetics have $R'(q) = U''(q) < 0$, corresponding to *unstable* mechanical equilibria. Conversely, unstable fixed points of the local reaction kinetics have $R'(q) = U''(q) > 0$, corresponding to *stable* mechanical equilibria. Note that

$$\mathcal{E} \equiv \frac{1}{2} D u_\xi^2 + U(u) \quad \Rightarrow \quad \frac{d\mathcal{E}}{d\xi} = -V u_\xi^2 \quad (6.10)$$

and thus $\mathcal{E}_\xi \leq 0$ if $V > 0$ while $\mathcal{E}_\xi > 0$ if $V < 0$.

Eqn. 6.9 is an $N = 2$ dynamical system of the form

$$\frac{d}{d\xi} \begin{pmatrix} u \\ v \end{pmatrix} = \begin{pmatrix} v \\ -D^{-1}R(u) - D^{-1}Vv \end{pmatrix} , \quad (6.11)$$

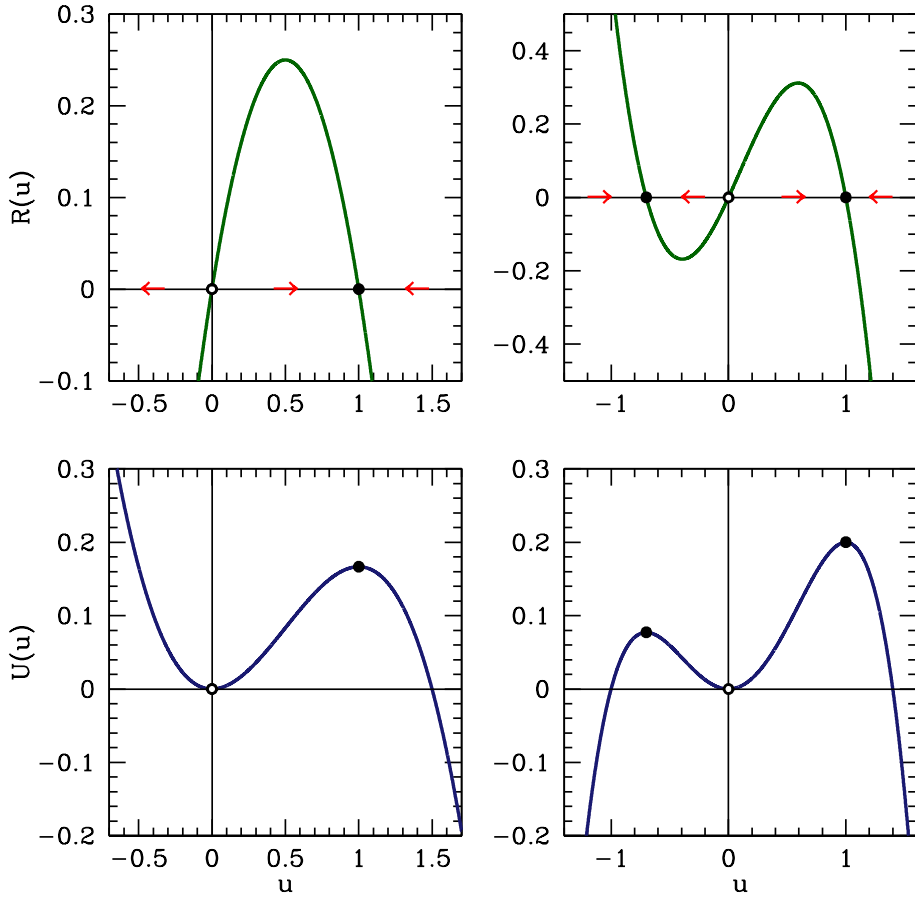


Figure 6.1: Reaction functions $R(u) = ru(a - u)$ with $r = a = 1$ (top left) and $R(u) = -ru(u - a)(u - b)$ with $r = 1, a = 1, b = -0.7$ (top right), along with corresponding potentials $U(u)$ (bottom panels). Stable fixed points for the local reaction kinetics are shown with a solid black dot, and unstable fixed points as a hollow black dot. Note that $R(u) = U'(u)$, so stable fixed points for the local reaction kinetics have $R'(u) = U''(u) < 0$, and thus correspond to *unstable* mechanical equilibria in the potential $U(u)$. Similarly, unstable fixed points for the local reaction kinetics correspond to stable mechanical equilibria.

with $v \equiv u'(\xi)$. At a fixed point (u^*, v^*) we must have $R(u^*) = 0$ and $v^* = 0$. The linearized dynamics at a fixed point are given by

$$\frac{d}{d\xi} \begin{pmatrix} \delta u \\ \delta v \end{pmatrix} = \underbrace{\begin{pmatrix} M(u^*) & \\ & \end{pmatrix}}_{\begin{pmatrix} 0 & 1 \\ -D^{-1}R'(u^*) & -D^{-1}V \end{pmatrix}} \begin{pmatrix} \delta u \\ \delta v \end{pmatrix} \quad (6.12)$$

We thus have

$$\tau(u^*) \equiv \text{Tr } M(u^*) = -D^{-1}V \quad , \quad \Delta(u^*) \equiv \det M(u^*) = D^{-1}R'(u^*) \quad . \quad (6.13)$$

Thus, if $R'(u^*) < 0$ the fixed point is a saddle, whereas if $R'(u^*) > 0$ the fixed point is stable if $V > 0$ and unstable if $V < 0$, and is a node if $R'(u^*) < V^2/4D$ and a spiral if $R'(u^*) > V^2/4D$.

A front solution corresponds to a mechanical motion interpolating between two equilibria at $u(\xi = \pm\infty)$. If the front propagates to the right then $V > 0$, corresponding to a positive (*i.e.* usual) friction coefficient γ . Any solution, therefore must start from an unstable equilibrium point u_I^* and end at another equilibrium u_{II}^* . The final state, however, may be either a stable or an unstable equilibrium for the potential $U(q)$. Consider the functions $R(u)$ and $U(u)$ in the left panels of fig. 6.1. Starting at ‘time’ $\xi = -\infty$ with $u = u_I^* = 1$, a particle with positive friction rolls down hill and eventually settles at position $u_{II}^* = 0$. If the motion is underdamped, it will oscillate as it approaches its final value, but there will be a solution connecting the two fixed points for an entire range of V values. Consider a model where

$$\begin{aligned} R(u) &= ru(u - a)(b - u) \\ U(u) &= -\frac{r}{4}u^4 + \frac{r}{3}(a + b)u^3 - \frac{r}{2}abu^2 \quad , \end{aligned} \tag{6.14}$$

with $a > 0 > b$, which is depicted in the right panels of fig. 6.1. Assuming $r > 0$, there are two stable fixed points for the local reaction kinetics: $u^* = a$ and $u^* = b$. Since $U(a) - U(b) = \frac{1}{12}r(a - b)^2(a^2 - b^2)$, the fixed point which is farther from $u = 0$ has the higher value. Without loss of generality, let us assume $|a| > |b|$, as is the case in the figure. One can then roll off the peak at $u^* = a$ and eventually settle in at the local minimum $u^* = 0$ for a range of V values, provided V is sufficiently large that the motion does not take u beyond the other fixed point at $u^* = b$. If we start at $u^* = b$, then a solution interpolating between this value and $u^* = 0$ exists for any positive value of V . As we shall see, this makes the issue of velocity selection a subtle one, as at this stage it appears a continuous family of propagating front solutions are possible. At any rate, for this type of front we have $u(\xi = -\infty) = u_I^*$ and $u(\xi = +\infty) = u_{II}^*$, where $u_{I,II}^*$ correspond to stable and unstable fixed points of the local dynamics. If we fix x and examine what happens as a function of t , we have $\xi \rightarrow \mp\infty$ as $t \rightarrow \pm\infty$, since $V > 0$, meaning that we start out in the unstable fixed point and eventually as the front passes over our position we transition to the stable fixed point. Accordingly, this type of front describes a *propagation into an unstable phase*. Note that for $V < 0$, corresponding to left-moving fronts, we have negative friction, meaning we move uphill in the potential $U(u)$. Thus, we start at $\xi = -\infty$ with $u(-\infty) = 0$ and end up at $u(+\infty) = u_{I,II}^*$. But now we have $\xi \rightarrow \pm\infty$ as $t \rightarrow \pm\infty$, hence once again *the stable phase invades the unstable phase*.

Another possibility is that one stable phase invades another. For the potential in the lower right panel of fig. 6.1, this means starting at the leftmost fixed point where $u(-\infty) = a$ and, with $V > 0$ and positive friction, rolling down hill past $u = 0$, then back up the other side, asymptotically coming to a perfect stop at $u(+\infty) = b$. Clearly this requires that V be finely tuned to a specific value so that the system dissipates an energy exactly equal to $U(a) - U(b)$ to friction during its motion. If $V < 0$ we have the time reverse of this motion. The fact that V is finely tuned to a specific value in order to have a solution means that we have a *velocity selection* taking place. Thus, if $R(a) = R(b) = 0$, then defining

$$\Delta U = \int_a^b du R(u) = U(b) - U(a) \quad , \tag{6.15}$$

we have that $u^* = a$ invades $u^* = b$ if $\Delta U > 0$, and $u^* = b$ invades $u^* = a$ if $\Delta U < 0$. The front velocity in either case is fixed by the selection criterion that we asymptotically approach both local maxima of $U(u)$ as $t \rightarrow \pm\infty$.

For the equation

$$Du'' + Vu' = ru(u - a)(u - b) \quad , \tag{6.16}$$

we can find an exact solution of the form

$$u(\xi) = \left(\frac{a+b}{2} \right) + \left(\frac{b-a}{2} \right) \tanh(A\xi) . \quad (6.17)$$

Direct substitution shows this is a solution when

$$\begin{aligned} A &= |a-b| \left(\frac{r}{8D} \right)^{1/2} \\ V &= \sqrt{\frac{Dr}{2}} (a+b). \end{aligned} \quad (6.18)$$

6.1.3 Stability and zero mode

We assume a propagating front solution $u(x - Vt)$ connecting $u(-\infty) = u_L$ and $u(+\infty) = u_R$. For $|\xi|$ very large, we can linearize about the fixed points $u_{L,R}$. For $\xi \rightarrow -\infty$ we write $R(u_L + \delta u) \approx R'(u_L) \delta u$ and the linearized front equation is

$$D \delta u'' + V \delta u' + R'(u_L) \delta u = 0 . \quad (6.19)$$

This equation possesses solutions of the form $\delta u = A e^{\kappa_L \xi}$, where

$$D \kappa_L^2 + V \kappa_L + R'(u_L) = 0 . \quad (6.20)$$

The solutions are

$$\kappa_L = -\frac{V}{2D} \pm \sqrt{\left(\frac{V}{2D} \right)^2 - \frac{R'(u_L)}{D}} . \quad (6.21)$$

We assume that u_L is a stable fixed point of the local dynamics, which means $R'(u_L) < 0$. Thus, $\kappa_{L,-} < 0 < \kappa_{L,+}$, and the allowed solution, which does not blow up as $\xi \rightarrow -\infty$ is to take $\kappa_L = \kappa_{L,+}$. If we choose $\xi_L < 0$ such that $\kappa_+ \xi_L \ll -1$, then we can take as initial conditions $u(\xi_L) = u_L + A_L e^{\kappa_L \xi_L}$ and $u'(x_L) = \kappa_L A_L e^{\kappa_L \xi_L}$. We can then integrate forward to $\xi = +\infty$ where $u'(+\infty) = 0$ using the ‘shooting method’ to fix the propagation speed V .

For $\xi \rightarrow +\infty$, we again linearize, writing $u = u_R + \delta u$ and obtaining

$$D \delta u'' + V \delta u' + R'(u_R) \delta u = 0 . \quad (6.22)$$

We find

$$\kappa_R = -\frac{V}{2D} \pm \sqrt{\left(\frac{V}{2D} \right)^2 - \frac{R'(u_R)}{D}} . \quad (6.23)$$

If we are invading another stable (or metastable) phase, then $R'(u_R) < 0$ and we must choose $\kappa_R = \kappa_{R,-}$ in order for the solution not to blow up as $\xi \rightarrow +\infty$. If we are invading an unstable phase, however, then $R'(u_R) > 0$ and there are two possible solutions, with $\kappa_{R,-} < \kappa_{R,+} < 0$. In the $\xi \rightarrow \infty$ limit, the $\kappa_{R,+}$ mode dominates, hence asymptotically we have $\kappa_R = \kappa_{R,+}$, however in general both solutions are present asymptotically, which means the corresponding boundary value problem is underdetermined.

Next we investigate stability of the front solution. To do this, we must return to our original reaction-diffusion PDE and linearize, writing

$$u(x, t) = u(x - Vt) + \delta u(x, t) , \quad (6.24)$$

where $f(\xi)$ is a solution to $Du'' + Vu' + R(u) = 0$. Linearizing in δu , we obtain the PDE

$$\frac{\partial \delta u}{\partial t} = D \frac{\partial^2 \delta u}{\partial x^2} + R'(u(x - Vt)) \delta u . \quad (6.25)$$

While this equation is linear, it is not autonomous, due to the presence of $u(x - Vt)$ on the in the argument of R' on the right hand side.

Let's shift to a moving frame defined by $\xi = x - Vt$ and $s = t$. Then

$$\begin{aligned} \frac{\partial}{\partial x} &= \frac{\partial \xi}{\partial x} \frac{\partial}{\partial \xi} + \frac{\partial s}{\partial x} \frac{\partial}{\partial s} = \frac{\partial}{\partial \xi} \\ \frac{\partial}{\partial t} &= \frac{\partial \xi}{\partial t} \frac{\partial}{\partial \xi} + \frac{\partial s}{\partial t} \frac{\partial}{\partial s} = -V \frac{\partial}{\partial \xi} + \frac{\partial}{\partial s} . \end{aligned} \quad (6.26)$$

So now we have the linear PDE

$$\delta u_s = D \delta u_{\xi\xi} + V \delta u_\xi + R'(u(\xi)) \delta u . \quad (6.27)$$

This equation, unlike eqn. 6.25, is linear and autonomous. We can spot one solution immediately. Let $\delta u(\xi, s) = Cu'(\xi)$, where C is a constant. Then the RHS of the above equation is

$$\begin{aligned} \text{RHS} &= D u_{\xi\xi\xi} + V u_{\xi\xi} + R'(u) u_\xi \\ &= \frac{d}{d\xi} \left[D u_{\xi\xi} + V u_\xi + R(u) \right] = 0 , \end{aligned} \quad (6.28)$$

by virtue of the front equation for $u(\xi)$ itself. This solution is called the *zero mode*. It is easy to understand why such a solution must exist. Due to translation invariance in space and time, if $u(x, t) = u(x - Vt)$ is a solution, then so must $u(x - a, t) = u(x - a - Vt)$ be a solution, and for all values of a . Now differentiate with respect to a and set $a = 0$. The result is the zero mode, $u'(x - Vt)$.

If we define (writing $t = s$)

$$\delta u(\xi, t) = e^{-V\xi/2D} \psi(\xi, t) , \quad (6.29)$$

then we obtain a Schrödinger-like equation for $\psi(\xi, t)$, i.e.

$$-\psi_t = \hat{K}\psi , \quad \hat{K} = -D \frac{\partial^2}{\partial \xi^2} + W(\xi) , \quad (6.30)$$

with

$$W(\xi) = \frac{V^2}{4D} - R'(u(\xi)) . \quad (6.31)$$

The Schrödinger equation is separable, so we can write $\psi(\xi, t) = e^{-Et} \phi(\xi)$, obtaining

$$E \phi = -D \phi_{\xi\xi} + W(\xi) \phi . \quad (6.32)$$

Since the zero mode solution $\delta u = u'(\xi)$ is an $E = 0$ solution, and since $u'(\xi)$ must be nodeless, the zero mode energy must be the ground state for this system, and all other eigenvalues must lie at positive energy. This proves that the front solution $u(x - Vt)$ is *stable*, provided the zero mode lies within the eigenspectrum of eqn. 6.32.

For $\xi \rightarrow -\infty$ we have $u \rightarrow u_L$ with $R'(u_L) < 0$ by assumption. Thus, $W(-\infty) > 0$ and all $E > 0$ solutions are exponentially decaying. As $\xi \rightarrow +\infty$, the solutions decay exponentially if $R'(u_R) < 0$, i.e. if u_R is a stable fixed point of the local dynamics. If on the other hand u_R is an *unstable* fixed point, then $R'(u_R) > 0$. We see immediately that propagation velocities with $V < V_c = 2\sqrt{DR'(u_R)}$ are unstable, since $W(+\infty) < 0$ in such cases. On the other hand, for $V > V_c$, we have that

$$\psi(\xi) = e^{V\xi/2D} \delta u(\xi) \sim A_R \exp\left(\sqrt{V^2 - V_c^2} \xi/2D\right) , \quad (6.33)$$

which is unnormalizable! Hence, the zero mode is no longer part of the eigenspectrum – translational invariance has been lost! One possible resolution is that $V = V_c$, where the threshold of normalizability lies. This is known as the *Fisher velocity*.

6.1.4 Fisher's equation

If we take $R(u) = ru(1 - u)$, the local reaction kinetics are those of the logistic equation $\dot{u} = ru(1 - u)$. With $r > 0$, this system has an unstable fixed point at $u = 0$ and a stable fixed point at $u = 1$. Rescaling time to eliminate the rate constant r , and space to eliminate the diffusion constant D , the corresponding one-dimensional RDE is

$$\frac{\partial u}{\partial t} = \frac{\partial^2 u}{\partial x^2} + u(1 - u) , \quad (6.34)$$

which is known as Fisher's equation (1937), originally proposed to describe the spreading of biological populations. Note that the physical length scale is $\ell = (D/r)^{1/2}$ and the physical time scale is $\tau = r^{-1}$. Other related RDEs are the Newell-Whitehead Segel equation, for which $R(u) = u(1 - u^2)$, and the Zeldovich equation, for which $R(u) = u(1 - u)(a - u)$ with $0 < a < 1$.

To study front propagation, we assume $u(x, t) = u(x - Vt)$, resulting in

$$\frac{d^2 u}{d\xi^2} + V \frac{du}{d\xi} = -U'(u) , \quad (6.35)$$

where

$$U(u) = -\frac{1}{3}u^3 + \frac{1}{2}u^2 . \quad (6.36)$$

Let $v = du/d\xi$. Then we have the $N = 2$ dynamical system

$$\frac{du}{d\xi} = v , \quad \frac{dv}{d\xi} = -u(1 - u) - Vv , \quad (6.37)$$

with fixed points at $(u^*, v^*) = (0, 0)$ and $(u^*, v^*) = (1, 0)$. The Jacobian matrix is

$$M = \begin{pmatrix} 0 & 1 \\ 2u^* - 1 & -V \end{pmatrix} \quad (6.38)$$

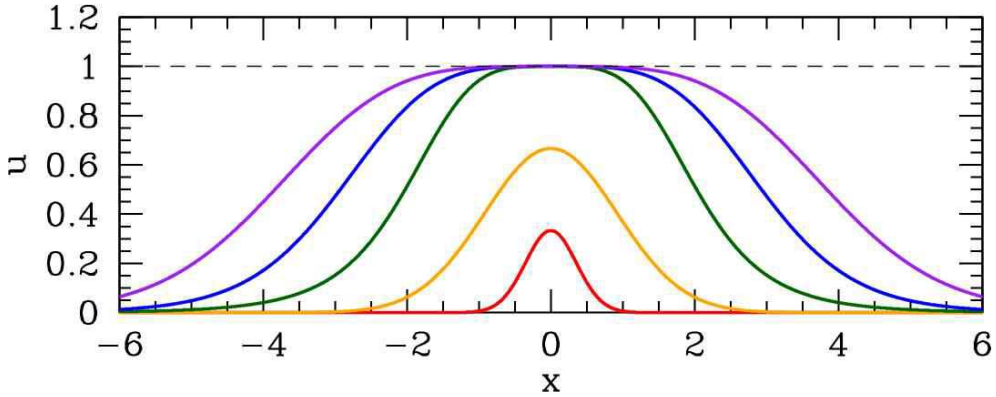


Figure 6.2: Evolution of a blip in the Fisher equation. The initial configuration is shown in red. Progressive configurations are shown in orange, green, blue, and purple. Asymptotically the two fronts move with speed $V = 2$.

At $(u^*, v^*) = (1, 0)$, we have $\det(M) = -1$ and $\text{Tr}(M) = -V$, corresponding to a saddle. At $(u^*, v^*) = (0, 0)$, we have $\det(M) = 1$ and $\text{Tr}(M) = -V$, corresponding to a stable node if $V > 2$ and a stable spiral if $0 < V < 2$. If $u(x, t)$ describes a density, then we must have $u(x, t) \geq 0$ for all x and t , and this rules out $0 < V < 2$ since the approach to the $u^* = 0$ fixed point is oscillating (and damped).

6.1.5 Velocity selection and stability

Is there a preferred velocity V ? According to our analysis thus far, any $V \geq V_c = 2$ will yield an acceptable front solution with $u(x, t) > 0$. However, Kolmogorov and collaborators proved that starting with the initial conditions $u(x, t = 0) = \Theta(-x)$, the function $u(x, t)$ evolves to a traveling wave solution with $V = 2$, which is the minimum allowed propagation speed. That is, the system exhibits *velocity selection*.

We can begin to see why if we assume an asymptotic solution $u(\xi) = A e^{-\kappa\xi}$ as $\xi \rightarrow \infty$. Then since $u^2 \ll u$ we have the linear equation

$$u'' + Vu' + u = 0 \quad \Rightarrow \quad V = \kappa + \kappa^{-1} . \quad (6.39)$$

Thus, any $\kappa > 0$ yields a solution, with $V = V(\kappa)$. Note that the minimum allowed value is $V_{\min} = 2$, achieved at $\kappa = 1$. If $\kappa < 1$, the solution falls off more slowly than for $\kappa = 1$, and we apparently have a propagating front with $V > 2$. However, if $\kappa > 1$, the solution decays more rapidly than for $\kappa = 1$, and the $\kappa = 1$ solution will dominate.

We can make further progress by deriving a formal asymptotic expansion. We start with the front equation

$$u'' + Vu' + u(1 - u) = 0 , \quad (6.40)$$

and we define $z = \xi/V$, yielding

$$\epsilon \frac{d^2u}{dz^2} + \frac{du}{dz} + u(1 - u) = 0 , \quad (6.41)$$

with $\epsilon = V^{-2} \leq \frac{1}{4}$. We now develop a perturbation expansion:

$$u(z; \epsilon) = u_0(z) + \epsilon u_1(z) + \dots , \quad (6.42)$$

and isolating terms of equal order in ϵ , we obtain a hierarchy. At order $\mathcal{O}(\epsilon^0)$, we have

$$u'_0 + u_0(1 - u_0) = 0 , \quad (6.43)$$

which is to say

$$\frac{du_0}{u_0(u_0 - 1)} = d\ln(u_0^{-1} - 1) = dz . \quad (6.44)$$

Thus,

$$u_0(z) = \frac{1}{\exp(z - a) + 1} , \quad (6.45)$$

where a is a constant of integration. At level k of the hierarchy, with $k > 1$ we have

$$u''_{k-1} + u'_k + u_k - \sum_{l=0}^k u_l u_{k-l} = 0 , \quad (6.46)$$

which is a first order ODE relating u_k at level k to the set $\{u_j\}$ at levels $j < k$. Separating out the terms, we can rewrite this as

$$u'_k + (1 - 2u_0) u_k = -u''_{k-1} - \sum_{l=1}^{k-1} u_l u_{k-l} . \quad (6.47)$$

At level $k = 1$, we have

$$u'_1 + (1 - 2u_0) u_1 = -u''_0 . \quad (6.48)$$

Plugging in our solution for $u_0(z)$, this inhomogeneous first order ODE may be solved via elementary means. The solution is

$$u_1(z) = -\frac{\ln \cosh(\frac{z-a}{2})}{2 \cosh^2(\frac{z-a}{2})} . \quad (6.49)$$

Here we have adjusted the constant of integration so that $u_1(a) \equiv 0$. Without loss of generality we may set $a = 0$, and we obtain

$$u(\xi) = \frac{1}{\exp(\xi/V) + 1} - \frac{1}{2V^2} \frac{\ln \cosh(\xi/2V)}{\cosh^2(\xi/2V)} + \mathcal{O}(V^{-4}) . \quad (6.50)$$

At $\xi = 0$, where the front is steepest, we have

$$-u'(0) = \frac{1}{4V} + \mathcal{O}(V^{-3}) . \quad (6.51)$$

Thus, the *slower* the front moves, the *steeper* it gets. Recall that we are assuming $V \geq 2$ here.

6.2 Multi-Species Reaction-Diffusion Systems

We've already introduced the general multi-species RDE,

$$\frac{\partial u_i}{\partial t} = D_{ij} \nabla^2 u_i + R_i(u_1, \dots, u_N) . \quad (6.52)$$

We will be interested in stable traveling wave solutions to these coupled nonlinear PDEs. We'll start with a predator-prey model,

$$\begin{aligned} \frac{\partial N_1}{\partial t} &= rN_1 \left(1 - \frac{N_1}{K}\right) - \alpha N_1 N_2 + D_1 \frac{\partial^2 N_1}{\partial x^2} \\ \frac{\partial N_2}{\partial t} &= \beta N_1 N_2 - \gamma N_2 + D_2 \frac{\partial^2 N_2}{\partial x^2} . \end{aligned} \quad (6.53)$$

Rescaling x, t, N_1 , and N_2 , this seven parameter system can be reduced to one with only three parameters, all of which are assumed to be positive:

$$\begin{aligned} \frac{\partial u}{\partial t} &= u(1 - u - v) + \mathcal{D} \frac{\partial^2 u}{\partial x^2} \\ \frac{\partial v}{\partial t} &= av(u - b) + \frac{\partial^2 v}{\partial x^2} . \end{aligned} \quad (6.54)$$

The interpretation is as follows. According to the local dynamics, species v is parasitic in that it decays as $\dot{v} = -abv$ in the absence of u . The presence of u increases the growth rate for v . Species u on the other hand will grow in the absence of v , and the presence of v decreases its growth rate and can lead to its extinction. Thus, v is the predator and u is the prey.

Before analyzing this reaction-diffusion system, we take the opportunity to introduce some notation on partial derivatives. We will use subscripts to denote partial differentiation, e.g.

$$\phi_t = \frac{\partial \phi}{\partial t} , \quad \phi_{xx} = \frac{\partial^2 \phi}{\partial x^2} , \quad \phi_{xxt} = \frac{\partial^3 \phi}{\partial x^2 \partial t} , \quad \text{etc.} \quad (6.55)$$

Thus, our two-species RDE may be written

$$\begin{aligned} u_t &= u(1 - u - v) + \mathcal{D} u_{xx} \\ v_t &= av(u - b) + v_{xx} . \end{aligned} \quad (6.56)$$

We assume $0 < b < 1$, in which case there are three fixed points:

$$\text{empty state: } (u^*, v^*) = (0, 0)$$

$$\text{prey at capacity: } (u^*, v^*) = (1, 0)$$

$$\text{coexistence: } (u^*, v^*) = (b, 1 - b) .$$

We now compute the Jacobian for the local dynamics:

$$M = \begin{pmatrix} \dot{u}_u & \dot{u}_v \\ \dot{v}_u & \dot{v}_v \end{pmatrix} = \begin{pmatrix} 1 - 2u - v & -u \\ av & a(u - b) \end{pmatrix} \quad . \quad (6.57)$$

We now examine the three fixed points.

- At $(u^*, v^*) = (0, 0)$ we have

$$M_{(0,0)} = \begin{pmatrix} 1 & 0 \\ 0 & -b \end{pmatrix} \quad \Rightarrow \quad T = 1 - b \quad , \quad D = -b \quad , \quad (6.58)$$

corresponding to a saddle.

- At $(u^*, v^*) = (1, 0)$,

$$M_{(1,0)} = \begin{pmatrix} -1 & -1 \\ 0 & a(1 - b) \end{pmatrix} \quad \Rightarrow \quad T = a(1 - b) - 1 \quad , \quad D = -a(1 - b) \quad , \quad (6.59)$$

which is also a saddle, since $0 < b < 1$.

- Finally, at $(u^*, v^*) = (b, 1 - b)$,

$$M_{(b,1-b)} = \begin{pmatrix} -b & -b \\ a(1 - b) & 0 \end{pmatrix} \quad \Rightarrow \quad T = -b \quad , \quad D = ab(1 - b) \quad . \quad (6.60)$$

Since $T < 0$ and $D > 0$ this fixed point is stable. For $D > \frac{1}{4}T^2$ it corresponds to a spiral, and otherwise a node. In terms of a and b , this transition occurs at $a = b/4(1 - b)$. That is,

$$\text{stable node: } a < \frac{b}{4(1 - b)} \quad , \quad \text{stable spiral: } a > \frac{b}{4(1 - b)}. \quad (6.61)$$

The local dynamics has an associated Lyapunov function,

$$L(u, v) = ab \left[\frac{u}{b} - 1 - \ln \left(\frac{u}{v} \right) \right] + (1 - b) \left[\frac{v}{1 - b} - 1 - \ln \left(\frac{v}{1 - b} \right) \right] \quad . \quad (6.62)$$

The constants in the above Lyapunov function are selected to take advantage of the relation $x - 1 - \ln x \geq 0$; thus, $L(u, v) \geq 0$, and $L(u, v)$ achieves its minimum $L = 0$ at the stable fixed point $(b, 1 - b)$. Ignoring diffusion, under the local dynamics we have

$$\frac{dL}{dt} = -a(u - b)^2 \leq 0 \quad . \quad (6.63)$$

6.2.1 Propagating front solutions

We now look for a propagating front solution of the form

$$u(x, t) = u(x - Vt) \quad , \quad v(x, t) = v(x - Vt) \quad . \quad (6.64)$$

This results in the coupled ODE system,

$$\begin{aligned} \mathcal{D} u'' + Vu' + u(1 - u - v) &= 0 \\ v'' + Vv' + av(u - b) &= 0 \end{aligned} \quad , \quad (6.65)$$

where once again the independent variable is $\xi = x - Vt$. These two coupled second order ODEs may be written as an $N = 4$ system.

We will make a simplifying assumption and take $\mathcal{D} = D_1/D_2 = 0$. This is appropriate if one species diffuses very slowly. An example might be plankton ($D_1 \approx 0$) and an herbivorous species ($D_2 > 0$). We then have $\mathcal{D} = 0$, which results in the $N = 3$ dynamical system,

$$\begin{aligned} \frac{du}{d\xi} &= -V^{-1} u (1 - u - v) \\ \frac{dv}{d\xi} &= w \\ \frac{dw}{d\xi} &= -av (u - b) - Vw \end{aligned} \quad , \quad (6.66)$$

where $w = v'$. In terms of the $N = 3$ phase space $\varphi = (u, v, w)$, the three fixed points are

$$\begin{aligned} (u^*, v^*, w^*) &= (0, 0, 0) \\ (u^*, v^*, w^*) &= (1, 0, 0) \\ (u^*, v^*, w^*) &= (b, 1 - b, 0) \end{aligned} \quad . \quad (6.67)$$

The first two are unstable and the third is stable. We will look for solutions where the stable solution invades one of the two unstable solutions. Since the front is assumed to propagate to the right, we must have the stable solution at $\xi = -\infty$, i.e. $\varphi(-\infty) = (b, 1 - b, 0)$. There are then two possibilities: either (i) $\varphi(+\infty) = (0, 0, 0)$, or (ii) $\varphi(+\infty) = (1, 0, 0)$. We will call the former a type-I front and the latter a type-II front.

For our analysis, we will need to evaluate the Jacobian of the system at the fixed point. In general, we have

$$M = \begin{pmatrix} -V^{-1}(1 - 2u^* - v^*) & V^{-1}u^* & 0 \\ 0 & 0 & 1 \\ -av^* & -a(u^* - b) & -V \end{pmatrix} \quad . \quad (6.68)$$

We now evaluate the behavior at the fixed points.

- Let's first look in the vicinity of $\varphi = (0, 0, 0)$. The linearized dynamics then give

$$\frac{d\eta}{d\xi} = M\eta \quad , \quad M = \begin{pmatrix} -V^{-1} & 0 & 0 \\ 0 & 0 & 1 \\ 0 & ab & -V \end{pmatrix} \quad , \quad (6.69)$$

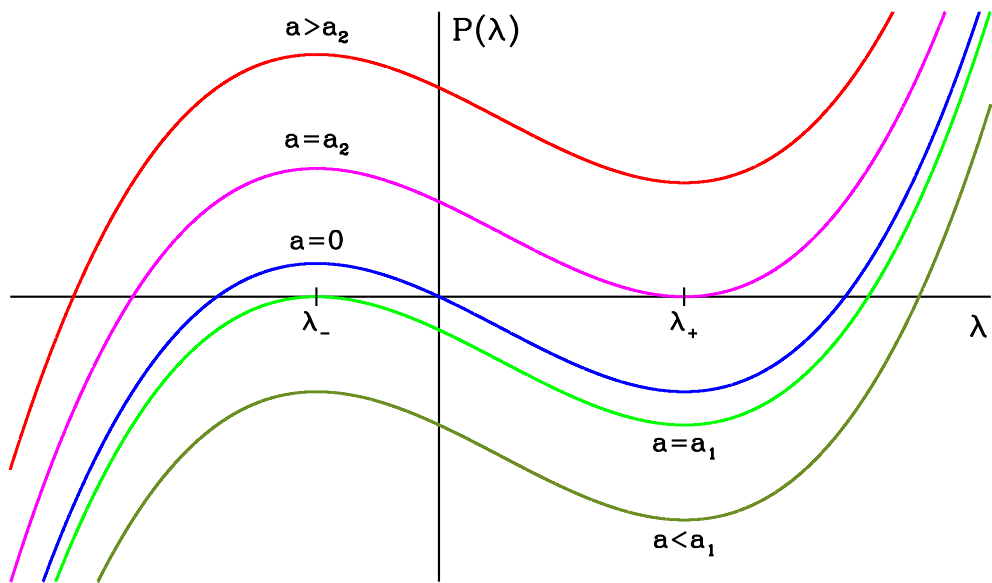


Figure 6.3: Analysis of the characteristic polynomial for the Jacobian of the linearized map at the fixed point $(u^*, v^*, w^*) = (b, 1 - b, 0)$.

where $\varphi = \varphi^* + \eta$. The eigenvalues are

$$\lambda_1 = -V^{-1} \quad , \quad \lambda_{2,3} = -\frac{1}{2}V \pm \frac{1}{2}\sqrt{V^2 + 4ab} \quad . \quad (6.70)$$

We see that $\lambda_{1,2} < 0$ while $\lambda_3 > 0$.

- In the vicinity of $\varphi = (1, 0, 0)$, we have

$$\frac{d\eta}{d\xi} = M\eta \quad , \quad M = \begin{pmatrix} V^{-1} & V^{-1} & 0 \\ 0 & 0 & 1 \\ 0 & a(b-1) & -V \end{pmatrix} \quad , \quad (6.71)$$

The eigenvalues are

$$\lambda_1 = V^{-1} \quad , \quad \lambda_{2,3} = -\frac{1}{2}V \pm \frac{1}{2}\sqrt{V^2 - 4a(1-b)} \quad . \quad (6.72)$$

We now have $\lambda_1 > 0$ and $\text{Re}(\lambda_{2,3}) < 0$. If we exclude oscillatory solutions, then we must have

$$V > V_{\min} = 2\sqrt{a(1-b)} \quad . \quad (6.73)$$

- Finally, let's examine the structure of the fixed point at $\varphi = (b, 1 - b, 0)$, where

$$\frac{d\eta}{d\xi} = M\eta \quad , \quad M = \begin{pmatrix} bV^{-1} & bV^{-1} & 0 \\ 0 & 0 & 1 \\ -a(1-b) & 0 & -V \end{pmatrix} \quad , \quad (6.74)$$

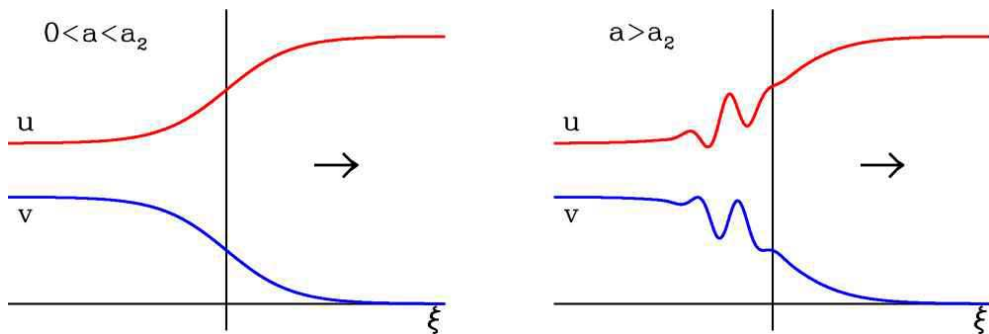


Figure 6.4: Sketch of the type-II front. Left panel: $0 < a < a_2$, for which the trailing edge of the front is monotonic. Right panel: $a > a_2$, for which the trailing edge of the front is oscillatory. In both cases, $\frac{1}{2} < b < 1$, and the front propagates to the right.

The characteristic polynomial is

$$\begin{aligned} P(\lambda) &= \det(\lambda \cdot \mathbb{I} - M) \\ &= \lambda^3 + (V - b V^{-1}) \lambda^2 - b \lambda + ab(1 - b)V^{-1} . \end{aligned} \quad (6.75)$$

Although physically we want to restrict $a > 0$, we will analyze this cubic for general a , but still $0 < b_1$. First, note that $P(\lambda)$ has extrema when $P'(\lambda) = 0$, which is to say

$$\lambda = \lambda_{\pm} = -\frac{1}{3}(V - b V^{-1}) \pm \frac{1}{3}\sqrt{(V - b V^{-1})^2 + 3b} . \quad (6.76)$$

Note that $\lambda_- < 0 < \lambda_+$. Since the sign of the cubic term in $P(\lambda)$ is positive, we must have that λ_- is a local maximum and λ_+ a local minimum. Note furthermore that both λ_+ and λ_- are independent of the constant a , and depend only on b and c . Thus, the situation is as depicted in fig. 6.3. The constant a merely shifts the cubic $P(\lambda)$ uniformly up or down. When $a = 0$, $P(0) = 0$ and the curve runs through the origin. There exists an $a_1 < 0$ such that for $a = a_1$ we have $P(\lambda_-) = 0$. Similarly, there exists an $a_2 > 0$ such that for $a = a_2$ we have $P(\lambda_+) = 0$. Thus,

$$\begin{aligned} a < a_1 < 0 &: \quad \operatorname{Re}(\lambda_{1,2}) < 0 < \lambda_3 \\ a_1 < a < 0 &: \quad \lambda_1 < \lambda_2 < 0 < \lambda_3 \\ a = 0 &: \quad \lambda_1 < \lambda_2 = 0 < \lambda_3 \\ 0 < a < a_2 &: \quad \lambda_1 < 0 < \lambda_2 < \lambda_3 \\ 0 < a_2 < a &: \quad \lambda_1 < 0 < \operatorname{Re}(\lambda_{2,3}) . \end{aligned} \quad (6.77)$$

Since this is the fixed point approached as $\xi \rightarrow -\infty$, we must approach it along one of its *unstable* manifolds, *i.e.* along a direction corresponding to a positive eigenvalue. Thus, we conclude that if $a > a_2$ that the approach is oscillatory, while for $0 < a < a_2$ the approach is monotonic.

In fig. 6.4 we sketch the solution for a type-II front, where the stable coexistence phase invades the unstable ‘prey at capacity’ phase.

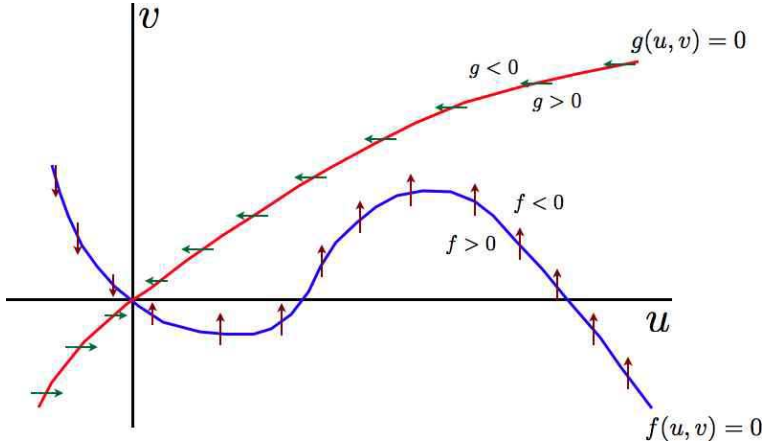


Figure 6.5: Sketch of the nullclines for the dynamical system described in the text.

6.3 Excitable Media

Consider the following $N = 2$ system:

$$\begin{aligned}\dot{u} &= f(u, v) \\ \dot{v} &= \epsilon g(u, v)\end{aligned}, \quad (6.78)$$

where $0 < \epsilon \ll 1$. The first equation is ‘fast’ and the second equation ‘slow’. We assume the nullclines for $f = 0$ and $g = 0$ are as depicted in fig. 6.5. As should be clear from the figure, the origin is a stable fixed point. In the vicinity of the origin, we can write

$$\begin{aligned}f(u, v) &= -au - bv + \dots \\ g(u, v) &= +cu - dv + \dots\end{aligned}, \quad (6.79)$$

where a, b, c , and d are all positive real numbers. The equation for the nullclines in the vicinity of the origin is then $au + bv = 0$ for the $f = 0$ nullcline, and $cu - dv = 0$ for the $g = 0$ nullcline. Note that

$$M \equiv \left. \frac{\partial(\dot{u}, \dot{v})}{\partial(u, v)} \right|_{(0,0)} = \begin{pmatrix} -a & -b \\ \epsilon c & -\epsilon d \end{pmatrix}. \quad (6.80)$$

We then have $\text{Tr } M = -(a + \epsilon d) < 0$ and $\det M = \epsilon(ad + bc) > 0$. Since the trace is negative and the determinant positive, the fixed point is stable. The boundary between spiral and node solutions is $\det M = \frac{1}{4}(\text{Tr } M)^2$, which means

$$\begin{aligned}|a - \epsilon d| &> 2\sqrt{\epsilon bc} : \text{stable node} \\ |a - \epsilon d| &< 2\sqrt{\epsilon bc} : \text{stable spiral}\end{aligned}. \quad (6.81)$$

Although the trivial fixed point $(u^*, v^*) = (0, 0)$ is stable, it is still *excitable* in the sense that a large enough perturbation will result in a big excursion. Consider the sketch in fig. 6.6. Starting from A, v initially increases as u decreases, but eventually both u and v get sucked into the stable fixed point at

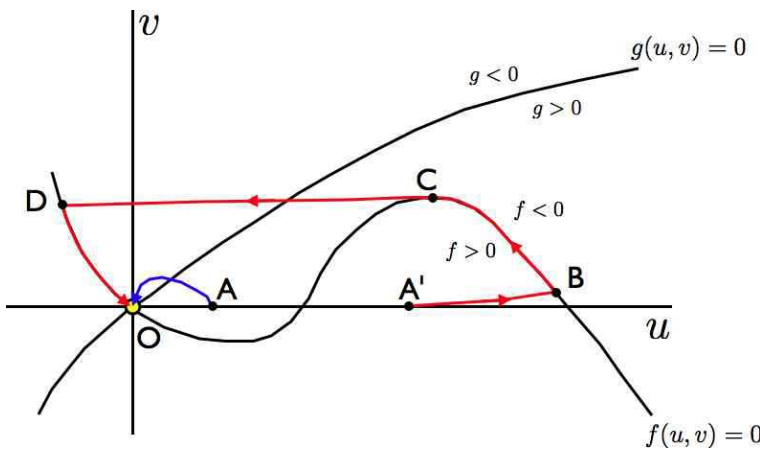


Figure 6.6: Sketch of the *fizzle*, which starts from A , and the *burst*, which starts from A' .

O. We call this path the *fizzle*. Starting from A' , however, u begins to increase rapidly and v increases slowly until the $f = 0$ nullcline is reached. At this point the fast dynamics has played itself out. The phase curve follows the nullcline, since any increase in v is followed by an immediate readjustment of u back to the nullcline. This state of affairs continues until C is reached, at which point the phase curve makes a large rapid excursion to D , following which it once again follows the $f = 0$ nullcline to the origin O. We call this path a *burst*. The behavior of $u(t)$ and $v(t)$ during these paths is depicted in fig. 6.7.

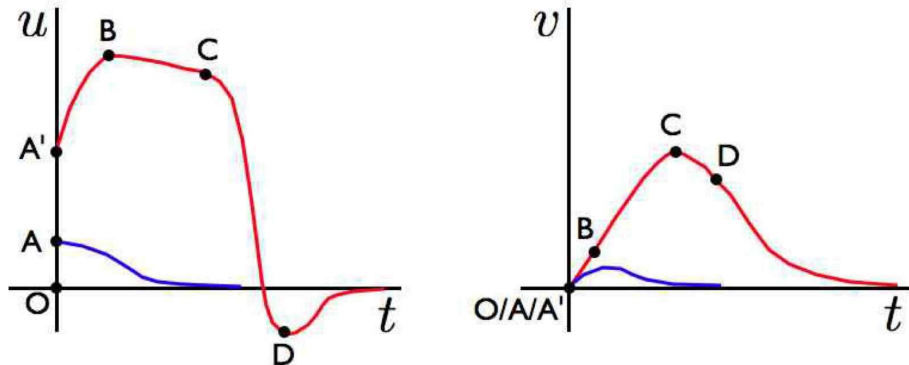


Figure 6.7: Sketch of $u(t)$ and $v(t)$ for the fizzle and burst.

It is also possible for there to be multiple bursts. Consider for example the situation depicted in fig. 6.8, in which the $f = 0$ and $g = 0$ nullclines cross three times. Two of these crossings correspond to stable (attractive) fixed points, while the third is unstable. There are now two different large scale excursion paths, depending on which stable fixed point one ends up at¹.

¹For a more egregious example of a sentence ending in several prepositions: “What did you bring that book I didn’t want to be read to out of up around for?”

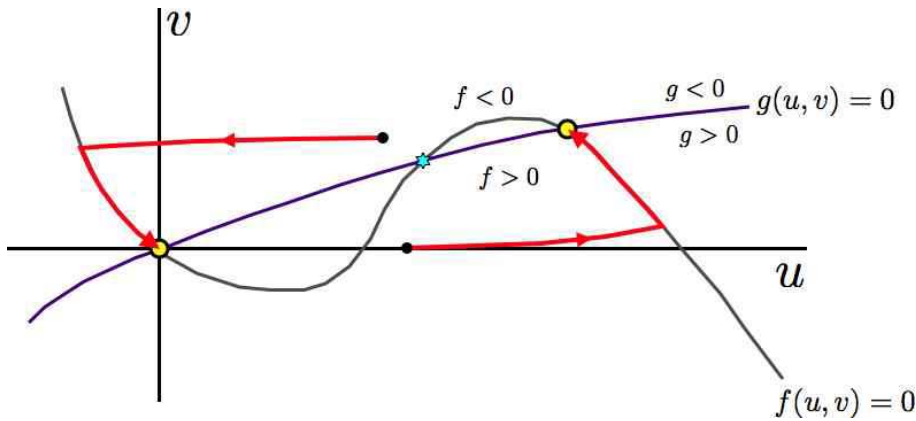


Figure 6.8: With three nullcline crossings, there are two stable fixed points, and hence two types of burst. The yellow-centered circles denote stable fixed points, and the blue-centered star denotes an unstable fixed point.

6.3.1 Front propagation in excitable media

Now let's add in diffusion:

$$\begin{aligned} u_t &= D_1 u_{xx} + f(u, v) \\ v_t &= D_2 v_{xx} + \epsilon g(u, v) \end{aligned} \quad . \quad (6.82)$$

We will consider a specific model,

$$\begin{aligned} u_t &= u(a - u)(u - 1) - v + D u_{xx} \\ v_t &= b u - \gamma v \end{aligned} \quad . \quad (6.83)$$

This is known as the *FitzHugh-Nagumo model* of nerve conduction (1961-2). It represents a tractable simplification and reduction of the famous Hodgkin-Huxley model (1952) of electrophysiology. Very briefly, u represents the membrane potential, and v the contributions to the membrane current from Na^+ and K^+ ions. We have $0 < a < 1$, $b > 0$, and $\gamma > 0$. The nullclines for the local dynamics resemble those in fig. 6.5, with the nullcline for the slow reaction perfectly straight.

We are interested in wave (front) solutions, which might describe wave propagation in muscle (*e.g.* heart) tissue. Let us once again define $\xi = x - Vt$ and assume a propagating front solution. We then arrive at the coupled ODEs,

$$\begin{aligned} D u'' + V u' + h(u) - v &= 0 \\ V v' + b u - \gamma v &= 0 \end{aligned} \quad , \quad (6.84)$$

where

$$h(u) = u(a - u)(u - 1) \quad . \quad (6.85)$$

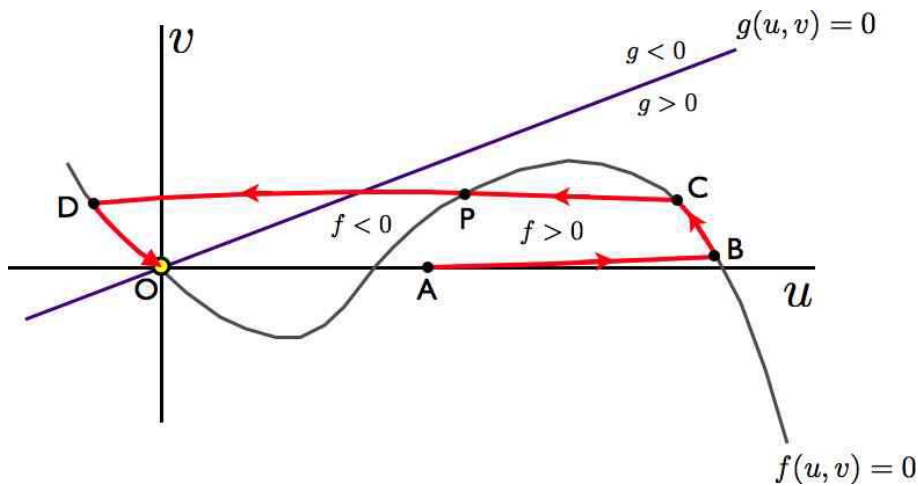


Figure 6.9: Excitation cycle for the FitzHugh-Nagumo model.

Once again, we have an $N = 3$ dynamical system:

$$\begin{aligned} \frac{du}{d\xi} &= w \\ \frac{dv}{d\xi} &= -b V^{-1} u + \gamma V^{-1} v \\ \frac{dw}{d\xi} &= -D^{-1} h(u) + D^{-1} v - V D^{-1} w \quad , \end{aligned} \tag{6.86}$$

where $w = u'$.

We assume that b and γ are both small, so that the v dynamics are slow. Furthermore, v remains small throughout the motion of the system. Then, assuming an initial value $(u_0, 0, 0)$, we may approximate

$$u_t \approx D u_{xx} + h(u) \quad . \tag{6.87}$$

With $D = 0$, the points $u = 1$ and $u = 1$ are both linearly stable and $u = a$ is linearly unstable. For finite D there is a wave connecting the two stable fixed points with a unique speed of propagation.

The equation $Du'' + Vu' = -h(u)$ may again be interpreted mechanically, with $h(u) = U'(u)$. Then since the cubic term in $h(u)$ has a negative sign, the potential $U(u)$ resembles an inverted asymmetric double well, with local maxima at $u = 0$ and $u = 1$, and a local minimum somewhere in between at $u = a$. Since

$$U(0) - U(1) = \int_0^1 du h(u) = \frac{1}{12}(1 - 2a) \quad , \tag{6.88}$$

hence if $V > 0$ we must have $a < \frac{1}{2}$ in order for the left maximum to be higher than the right maximum. The constant V is adjusted so as to yield a solution. This entails

$$V \int_{-\infty}^{\infty} d\xi u_\xi^2 = V \int_0^1 du u_\xi = U(0) - U(1) \quad . \tag{6.89}$$

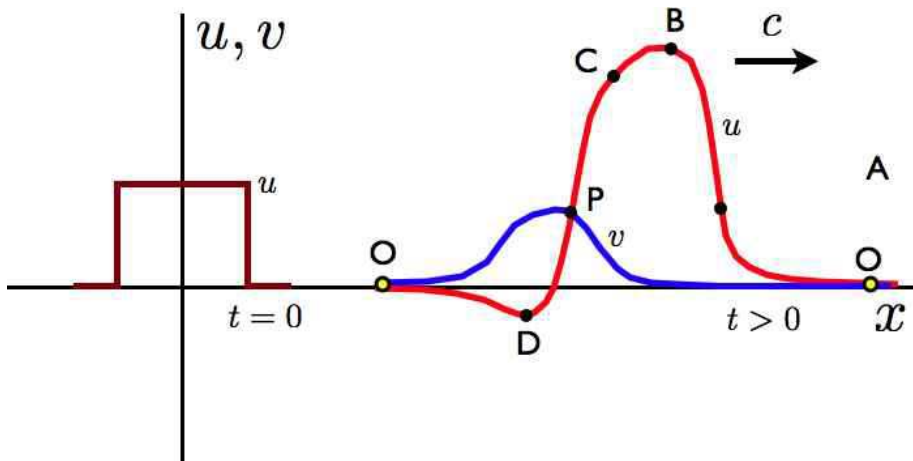


Figure 6.10: Sketch of the excitation pulse of the FitzHugh-Nagumo model.

The solution makes use of some very special properties of the cubic $h(u)$ and is astonishingly simple:

$$V = (D/2)^{1/2} (1 - 2a) \quad . \quad (6.90)$$

We next must find the speed of propagation on the CD leg of the excursion. There we have

$$u_t \approx D u_{xx} + h(u) - v_C \quad , \quad (6.91)$$

with $u(-\infty) = u_D$ and $u(+\infty) = u_C$. The speed of propagation is

$$\tilde{V} = (D/2)^{1/2} (u_C - 2u_P + u_D) \quad . \quad (6.92)$$

We then set $V = \tilde{V}$ to determine the location of C. The excitation pulse is sketched in fig. 6.10

Calculation of the wave speed

Consider the second order ODE,

$$\mathcal{L}(u) \equiv D u'' + V u' + A(u - u_1)(u_2 - u)(u - u_3) = 0 \quad . \quad (6.93)$$

We assume $u_{1,2,3}$ are all distinct. Remarkably, a solution may be found. We claim that if

$$u' = \lambda(u - u_1)(u - u_2) \quad , \quad (6.94)$$

then, by suitably adjusting λ , the solution to eqn. 6.94 also solves eqn. 6.93. To show this, note that under the assumption of eqn. 6.94 we have

$$\begin{aligned} u'' &= \frac{du'}{du} \cdot \frac{du}{d\xi} \\ &= \lambda(2u - u_1 - u_2) u' \\ &= \lambda^2(u - u_1)(u - u_2)(2u - u_1 - u_2) \quad . \end{aligned} \quad (6.95)$$

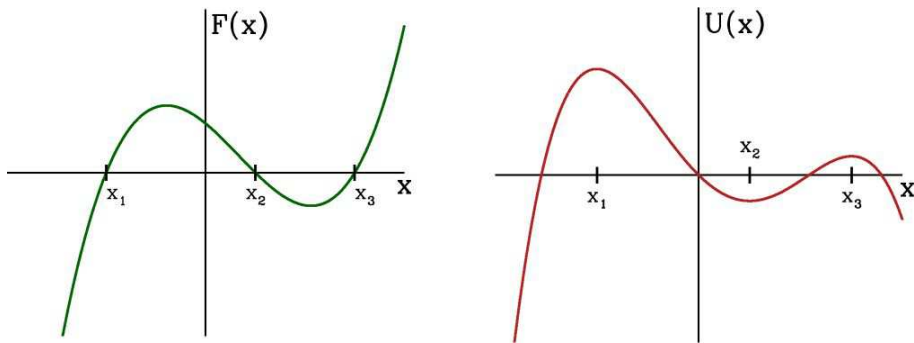


Figure 6.11: Mechanical analog for the front solution, showing force $F(x)$ and corresponding potential $U(x)$.

Thus,

$$\begin{aligned}\mathcal{L}(u) &= (u - u_1)(u - u_2) \left[\lambda^2 D(2u - u_1 - u_2) + \lambda V + A(u_3 - u) \right] \\ &= (u - u_1)(u - u_2) \left[(2\lambda^2 D - A)u + (\lambda V + Au_3 - \lambda^2 D(u_1 + u_2)) \right] .\end{aligned}\quad (6.96)$$

Therefore, if we choose

$$\lambda = \sigma \sqrt{\frac{A}{2D}} \quad , \quad V = \sigma \sqrt{\frac{AD}{2}} (u_1 + u_2 - 2u_3) \quad , \quad (6.97)$$

with $\sigma = \pm 1$, we obtain a solution to $\mathcal{L}(u) = 0$. Note that the velocity V has been *selected*.

The integration of eqn. 6.94 is elementary, yielding the kink solution

$$\begin{aligned}u(\xi) &= \frac{u_2 + u_1 \exp [\lambda(u_2 - u_1)(\xi - \xi_0)]}{1 + \exp [\lambda(u_2 - u_1)(\xi - \xi_0)]} \\ &= \frac{1}{2}(u_1 + u_2) + \frac{1}{2}(u_1 - u_2) \tanh \left[\frac{1}{2}\lambda(u_2 - u_1)(\xi - \xi_0) \right] ,\end{aligned}\quad (6.98)$$

where ξ_0 is a constant which is the location of the center of the kink. This front solution connects $u = u_1$ and $u = u_2$. There is also a front solution connecting u_1 and u_3 :

$$u(\xi) = \frac{1}{2}(u_1 + u_3) + \frac{1}{2}(u_1 - u_3) \tanh \left[\frac{1}{2}\lambda(u_3 - u_1)(\xi - \xi_0) \right] , \quad (6.99)$$

with the same value of $\lambda = \sigma \sqrt{A/2D}$, but with a different velocity of front propagation, given by $V = \sigma(AD/2)^{1/2}(u_1 + u_3 - 2u_2)$, again with $\sigma = \pm 1$.

It is instructive to consider the analogue mechanical setting of eqn. 6.93. We write $D \rightarrow M$ and $V \rightarrow \gamma$, and $u \rightarrow x$, giving

$$M\ddot{x} + \gamma \dot{x} = A(x - x_1)(x - x_2)(x - x_3) \equiv F(x) , \quad (6.100)$$

where we take $x_1 < x_2 < x_3$. Mechanically, the points $x = x_{1,3}$ are unstable equilibria. A front solution interpolates between these two stationary states. If $\gamma = V > 0$, the friction is of the usual sign, and the

path starts from the equilibrium at which the potential $U(x)$ is greatest. Note that

$$U(x_1) - U(x_3) = \int_{x_1}^{x_3} dx F(x) = \frac{1}{12}(x_3 - x_1)^2 \left[(x_2 - x_1)^2 - (x_3 - x_2)^2 \right] . \quad (6.101)$$

so if, for example, the integral of $F(x)$ between x_1 and x_3 is positive, then $U(x_1) > U(x_3)$. For our cubic force $F(x)$, this occurs if $x_2 > \frac{1}{2}(x_1 + x_3)$.

Chapter 7

Pattern Formation

Patterning is a common occurrence found in a wide variety of physical systems, including chemically active media, fluids far from equilibrium, liquid crystals, *etc.* In this chapter we will touch very briefly on the basic physics of patterning instabilities.

7.1 Reaction-Diffusion Dynamics Revisited

Let $\{\phi_i(\mathbf{r}, t)\}$ denote a set of scalar fields satisfying

$$\partial_t \phi_i + \nabla \cdot \mathbf{J}_i = R_i \quad , \quad (7.1)$$

where

$$J_i^\alpha = -D_{ij}^{\alpha\beta} \partial_\beta \phi_j \quad (7.2)$$

is the α component of the current density of species i . We assume that the local reaction kinetics is given by

$$R_i = R_i(\{\phi_j\}, \lambda) \quad , \quad (7.3)$$

where λ is a control parameter, or possibly a set of control parameters. Thus,

$$\partial_t \phi_i = \partial_\alpha D_{ij}^{\alpha\beta} \partial_\beta \phi_j + R_i(\{\phi_j\}, \lambda) \quad . \quad (7.4)$$

Let us expand about a homogeneous solution to the local dynamics, $R(\{\phi_i^*\}, \lambda) = 0$, writing

$$\phi_i(\mathbf{r}, t) = \phi_i^* + \eta_i(\mathbf{r}, t) \quad . \quad (7.5)$$

We then have

$$\partial_t \eta_i = \frac{\partial R_i}{\partial \phi_j} \Big|_{\phi^*} \eta_j + \partial_\alpha D_{ij}^{\alpha\beta} \partial_\beta \eta_j \quad . \quad (7.6)$$

Assuming $D_{ij}^{\alpha\beta}$ is constant in space, we obtain the linear equation

$$\partial_t \hat{\eta}(\mathbf{q}, t) = L_{ij}(\mathbf{q}; \lambda) \hat{\eta}_j(\mathbf{q}, t) \quad , \quad (7.7)$$

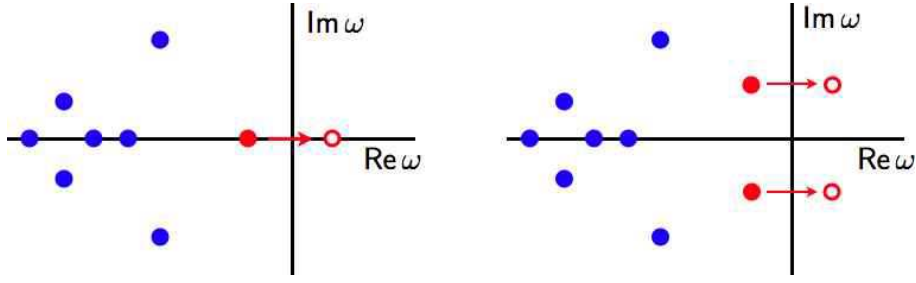


Figure 7.1: Instabilities in linear systems $\dot{\eta} = L\eta$ occur when the eigenvalue with the largest real part crosses the line $\text{Re}(\omega) = 0$. If L is a real operator, its eigenvalues are either real or come in complex conjugate pairs.

where

$$L_{ij}(\mathbf{q}; \lambda) = \frac{\partial R_i}{\partial \phi_j} \Big|_{\phi^*} - D_{ij}^{\alpha\beta} q_\alpha q_\beta . \quad (7.8)$$

Let

$$P(\omega) = \det(\omega \mathbb{I} - L) \quad (7.9)$$

be the characteristic polynomial for $L(\mathbf{q}; \lambda)$. The eigenvalues $\omega_a(\mathbf{q}; \lambda)$ satisfy $P(\omega_a) = 0$. If we assume that $L_{ij}(\mathbf{q}; \lambda) \in \mathbb{R}$ is real, then $P(\omega^*) = [P(\omega)]^*$, which means that the eigenvalues ω_a are either purely real or else come in complex conjugate pairs $\omega_{a,1} \pm i\omega_{a,2}$. The eigenvectors $\psi_i^a(\mathbf{q}; \lambda)$ need not be real, since L is not necessarily Hermitian. The general solution is then

$$\eta_i(\mathbf{q} t) = \sum_a C_a \psi_i^a(\mathbf{q}; \lambda) e^{\omega_a(\mathbf{q}; \lambda) t} . \quad (7.10)$$

Modes with $\text{Re } \omega_a > 0$ are stabilized by nonlinear terms, *e.g.* $\dot{A} = rA - A^3$.

Let's assume the eigenvalues are ordered so that $\text{Re } (\omega_a) \geq \text{Re } (\omega_{a+1})$, and that $\text{Re } (\omega_1) \leq 0$ for $\lambda \leq \lambda_c$.

- If $\omega_1(\mathbf{q} = 0; \lambda_c) = 0$, we expect a transition between homogeneous ($\mathbf{q} = 0$) states at $\lambda = \lambda_c$.
- If $\omega_1(\mathbf{q} = \mathbf{Q}; \lambda_c) = 0$, we expect a transition to a spatially modulated structure with wavevector \mathbf{Q} .
- If $\text{Re } \omega_1(\mathbf{q} = 0; \lambda_c) = 0$ but $\text{Im } \omega_1(\mathbf{q} = 0; \lambda_c) \neq 0$ we expect a Hopf bifurcation and limit cycle behavior.
- If $\text{Re } \omega_1(\mathbf{q} = \mathbf{Q}; \lambda_c) = 0$ but $\text{Im } \omega_1(\mathbf{q} = \mathbf{Q}; \lambda_c) \neq 0$ we expect a Hopf bifurcation to a spatiotemporal pattern structure.

In the vicinity of a bifurcation, space and time scales associated with the unstable mode(s) tend to infinity. This indicates a *critical slowing down*. If the unstable modes evolve very slowly, the faster, non-critical modes may be averaged over (*i.e.* 'adiabatically eliminated').

For the most unstable mode $\omega \equiv \omega_1$, we envisage the following possibilities:

$\omega = \epsilon - A q^2$	homogeneous states ; $q = 0$ least stable
$\omega = \epsilon - A(q^2 - Q^2)^2$	modulated: $q = Q$ is least stable
$\omega = \epsilon - A(q^2 - Q^2)^2 - B q^2 \sin^2 \theta_q$	θ_q between q and symmetry axis
$\omega = \epsilon - A q^2 \pm i\Omega_0$	Hopf, to homogeneous state
$\omega = \epsilon - A(q^2 - Q^2)^2 \pm i\Omega_0$	Hopf, to modulated state

where

$$\epsilon \propto \frac{\lambda - \lambda_c}{\lambda_c} . \quad (7.11)$$

7.2 Turing and Hopf Instabilities

As an explicit example in $d = 1$ dimension, consider the coupled RDEs,

$$\begin{aligned} u_t &= D_u u_{xx} + f(u, v) \\ v_t &= D_v v_{xx} + g(u, v) \end{aligned} . \quad (7.12)$$

We linearize about the fixed point $u = v = 0$, obtaining

$$\begin{pmatrix} \delta \hat{u}_t \\ \delta \hat{v}_t \end{pmatrix} = \overbrace{\begin{pmatrix} f_u - D_u q^2 & f_v \\ g_u & g_v - D_v q^2 \end{pmatrix}}^{L(q)} \begin{pmatrix} \delta \hat{u} \\ \delta \hat{v} \end{pmatrix} + \dots \quad (7.13)$$

for the Fourier transforms

$$\begin{pmatrix} \delta \hat{u}(q, t) \\ \delta \hat{v}(q, t) \end{pmatrix} = \int_{-\infty}^{\infty} dx \begin{pmatrix} \delta u(x, t) \\ \delta v(x, t) \end{pmatrix} e^{-iqx} . \quad (7.14)$$

Please note that $f_u \equiv \partial f / \partial u$ whereas D_u is the self-diffusion coefficient for the u field (and does not signify a partial derivative with respect to u). We now examine the eigenvalues of L . Clearly we have

$$\begin{aligned} \mathcal{T} &\equiv \text{Tr}(L) = f_u + g_v - (D_u + D_v) q^2 \\ \mathcal{D} &\equiv \det(L) = D_u D_v q^4 - (D_u g_v + D_v f_u) q^2 + \Delta \end{aligned} , \quad (7.15)$$

where

$$\Delta = f_u g_v - f_v g_u \quad (7.16)$$

is the determinant at $q = 0$. The eigenvalues are

$$\omega_{\pm} = \frac{1}{2} \mathcal{T} \pm \sqrt{\frac{1}{4} \mathcal{T}^2 - \mathcal{D}} . \quad (7.17)$$

Recall that in the $(\mathcal{T}, \mathcal{D})$ plane, it is the upper left quadrant, with $\mathcal{T} < 0$ and $\mathcal{D} > 0$, where the fixed point is stable. There are then two instability boundary, both of which are straight lines. The first

boundary is the positive \mathcal{D} axis, *i.e.* ($\mathcal{T} = 0, \mathcal{D} > 0$), which separates the stable spiral from the unstable spiral, corresponding to the onset of an *oscillatory (Hopf) instability*. Since the q^2 term in \mathcal{T} has a negative coefficient¹, this instability first occurs at $q = 0$, *i.e.* in the spatially homogeneous mode. The condition for the Hopf instability is then

$$f_u + g_v = 0 \quad , \quad (7.18)$$

and $\Delta > 0$. The latter condition guarantees that we cross the \mathcal{D} axis in the upper half $(\mathcal{T}, \mathcal{D})$ plane.

The second instability boundary is the half-line ($\mathcal{T} < 0, \mathcal{D} = 0$), which forms the border with the saddle point region. If the coefficient of the q^2 term in \mathcal{D} is negative, *i.e.* if $(D_u g_v + D_v f_u) > 0$, then the minimum of $\mathcal{D}(q)$ occurs at a finite value, $q = \pm Q$, where

$$Q^2 = \frac{D_u g_v + D_v f_u}{2D_u D_v} \quad . \quad (7.19)$$

In this case, the instability is to a spatially inhomogeneous state. This is the *Turing instability*. This requires that at least one of f_u and g_v is positive, or *autocatalytic*. However, if both are positive, then the condition for the Hopf instability will already have been satisfied. So for the Turing instability we must require $f_u + g_v < 0$, which says that only one of the species is autocatalytic. Setting $\mathcal{D}(Q) = 0$, we eliminate Q and obtain the condition

$$D_u g_v + D_v f_u = 2\sqrt{\Delta D_u D_v} \quad , \quad (7.20)$$

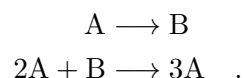
hence, at the threshold of instability, the ordering wavevector is

$$Q^2 = \sqrt{\frac{\Delta}{D_u D_v}} \quad . \quad (7.21)$$

For the Turing instability, we may assume, without loss of generality, that $g_v < 0 < f_u$. Since $\Delta > 0$, we must have $f_v g_u < f_u g_v < 0$. The Turing instability *preempts* the Hopf instability when eqn. 7.20 is satisfied before eqn. 7.18. It is therefore a necessary (but not sufficient) condition that $D_v > D_u$. *The Turing instability preempts the Hopf instability when only one species is autocatalytic, and the autocatalytic species is less diffusive.* This requires a slowly diffusing *activator* and a more rapidly diffusing *inhibitor*.

7.3 The Brusselator

Consider the so-called Brusselator model of Prigogine and Lefever (1968). The Brusselator is a model for two fictitious chemical reactions,



¹We assume both diffusion constants are positive: $D_{u,v} > 0$.

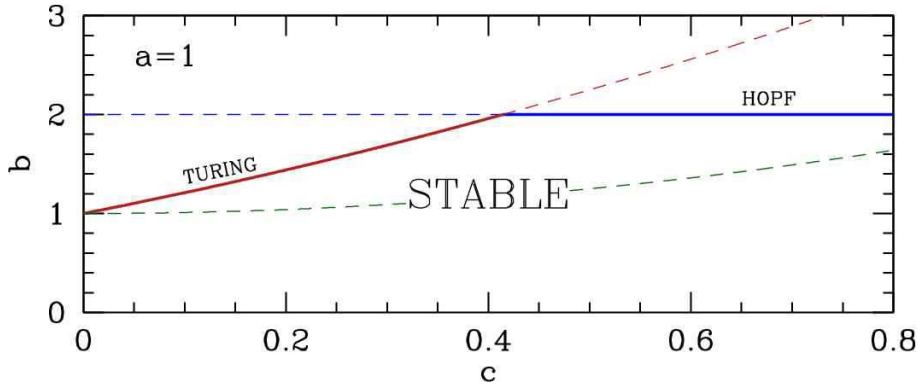


Figure 7.2: Instability lines for the Brusselator. The thick blue line denotes a Hopf instability and the thick red line a Turing instability. The dashed light green line is the locus of points below which the minimum of \mathcal{D} lies at $Q = 0$.

The species A is assumed to be supplied and removed from the system, in which case, after adding diffusion, we have two coupled RDEs with

$$\begin{aligned} f(u, v) &= a - (1 + b)u + u^2v \\ g(u, v) &= bu - u^2v \end{aligned} \quad . \quad (7.22)$$

The fixed point $f = g = 0$ occurs at $(u^*, v^*) = (a, b/a)$. Linearizing the local dynamics about the fixed point, we obtain

$$\begin{pmatrix} f_u & f_v \\ g_u & g_v \end{pmatrix} = \begin{pmatrix} b-1 & a^2 \\ -b & -a^2 \end{pmatrix} \quad . \quad (7.23)$$

Thus, $\Delta = a^2 > 0$. The Hopf instability sets in when $f_u + g_v = 0$, i.e. when $b = b_H$, where

$$b_H = 1 + a^2 \quad . \quad (7.24)$$

For the Turing instability, eqn. 7.20 gives $b = b_T$, where

$$b_T = (1 + c)^2 \quad , \quad (7.25)$$

where we have defined

$$c \equiv a \sqrt{\frac{D_u}{D_v}} \quad . \quad (7.26)$$

Note that $c < a$ for the Turing instability. These two curves intersect at

$$c^* = -1 + \sqrt{1 + a^2} \quad . \quad (7.27)$$

Note that

$$Q^2 = \frac{a}{\sqrt{D_u D_v}} \quad \Rightarrow \quad D_u Q^2 = c \quad , \quad D_v Q^2 = \frac{a^2}{c} \quad . \quad (7.28)$$

Suppose we are close to the Turing instability, and we write $b = b_T + \epsilon$ with $|\epsilon| \ll 1$. We first expand the coupled RDEs about the fixed point, writing

$$u = u^* + \delta u \quad , \quad v = v^* + \delta v \quad , \quad (7.29)$$

with $u^* = a$ and $v^* = \frac{b}{a}$. Written in terms of δu and δv , the coupled RDEs take the form

$$\delta u_t = D_u \delta u_{xx} - \delta u + \left(b \delta u + a^2 \delta v \right) + \left(\frac{b}{a} (\delta u)^2 + 2a \delta u \delta v + (\delta u)^2 \delta v \right) \quad (7.30)$$

$$\delta v_t = D_v \delta v_{xx} - \left(b \delta u + a^2 \delta v \right) - \left(\frac{b}{a} (\delta u)^2 + 2a \delta u \delta v + (\delta u)^2 \delta v \right) . \quad (7.31)$$

If we ignore the nonlinear terms, we obtain a linear equation which has a solution

$$\begin{aligned} \delta u(x, t) &= U_{11} A(t) \cos(Qx) \\ \delta v(x, t) &= V_{11} A(t) \cos(Qx) \end{aligned} , \quad (7.32)$$

where $A(t) = A_0 \exp(\omega t)$ is an amplitude, and where the eigenvector $(U_{11} \ V_{11})^t$ satisfies

$$\begin{pmatrix} b - c - 1 & a^2 \\ -b & -a^2 - \frac{a^2}{c} \end{pmatrix} \begin{pmatrix} U_{11} \\ V_{11} \end{pmatrix} = \omega \begin{pmatrix} U_{11} \\ V_{11} \end{pmatrix} . \quad (7.33)$$

If we set $b = b_T$, and, without loss of generality, take $U_{11} \equiv 1$, we have

$$U_{11} = 1 \quad , \quad V_{11} = -\frac{c(1+c)}{a^2} . \quad (7.34)$$

If $b > b_T$, then there exists an eigenvalue ω which is real and positive, in which case the amplitude $A(t)$ grows exponentially.

7.3.1 The amplitude equation

The exponential growth of the amplitude $A(t)$ is valid only insofar as the nonlinear terms in the dynamics are small. Our goal here will be to develop a nonlinear ODE governing the growth of $A(t)$, assuming $|b - b_T| \ll 1$. We follow the treatment of Kessler and Levine (2009, unpublished).

We assume one Fourier mode will be excited, with $q = \pm Q$, along with its harmonics. We therefore write

$$\delta u = \sum_{m=1}^{\infty} \sum_{n=0}^{\infty} U_{mn} A^m \cos(nQx) \quad (7.35)$$

$$\delta v = \sum_{m=1}^{\infty} \sum_{n=0}^{\infty} V_{mn} A^m \cos(nQx) . \quad (7.36)$$

We shall only need the first few terms:

$$\begin{aligned} \delta u &= (U_{11}A + U_{31}A^3) \cos(Qx) + U_{20}A^2 + U_{22}A^2 \cos(2Qx) + \dots \\ \delta v &= (V_{11}A + V_{31}A^3) \cos(Qx) + V_{20}A^2 + V_{22}A^2 \cos(2Qx) + \dots . \end{aligned} \quad (7.37)$$

Note that we assume $U_{10} = V_{10} = 0$ because the leading behavior is in the U_{11} and V_{11} terms. It is through the quadratic nonlinearities that terms with $n = 0$ are generated.

Note that we also set $U_{21} = V_{21} = 0$, because starting with a solution proportional to $A \cos(Qx)$, the quadratic nonlinearities produce terms with spatial wavevectors $q = 0$ and $q = 2Q$, with amplitude proportional to A^2 , corresponding to $(m, n) = (2, 0)$ and $(m, n) = (2, 2)$, respectively. The cubic nonlinearities generate wavevectors $q = Q$ and $q = 3Q$, with amplitude A^3 , corresponding to $(m, n) = (3, 1)$ and $(3, 3)$, of which we require only the former. Starting from $A \cos(Qx)$, we *never* generate terms with $(m, n) = (2, 1)$. We could include such terms, assigning to them an amplitude B , and derive an amplitude equation for B , but it would give a subleading contribution to the spatial patterning.

We now undertake the tedious process of working out the RHS of eqns. 7.30 and 7.31 to order A^3 . Throughout our derivation, we shall include only the $n = 0$, $n = 1$ and $n = 2$ harmonics and drop all other terms. We will also assume $b = b_T$ whenever it multiplies A^m with $m > 1$, since $\epsilon = b - b_T$ is presumed small, and, as we shall see, the amplitude itself will be proportional to $\sqrt{\epsilon}$. Let's roll up our sleeves and get to work!

The first terms we need are all the ones linear in δu and δv . Thus, we need

$$\begin{aligned} D_u \delta u_{xx} - \delta u &= -(1 + c) \left(U_{11} A + U_{31} A^3 \right) \cos(Qx) - U_{20} A^2 - (1 + 4c) U_{22} A^2 \cos(2Qx) \\ D_v \delta v_{xx} &= -\frac{a^2}{c} \left(V_{11} A + V_{31} A^3 \right) \cos(Qx) - \frac{4a^2}{c} V_{22} A^2 \cos(2Qx) \end{aligned} \quad (7.38)$$

as well as

$$\begin{aligned} b \delta u + a^2 \delta v &= \left\{ b \left(U_{11} A + U_{31} A^3 \right) + a^2 \left(V_{11} A + V_{31} A^3 \right) \right\} \cos(Qx) \\ &\quad + \left(b U_{20} + a^2 V_{20} \right) A^2 + \left(b U_{22} + a^2 V_{22} \right) A^2 \cos(2Qx) . \end{aligned} \quad (7.39)$$

Next, we need the nonlinear terms, starting with

$$(\delta u)^2 = \frac{1}{2} U_{11}^2 A^2 + \frac{1}{2} U_{11}^2 A^2 \cos(2Qx) + U_{11} (2 U_{20} + U_{22}) A^3 \cos(Qx) + \dots , \quad (7.40)$$

where the remaining terms are of $\mathcal{O}(A^4)$ or are proportional to $\cos(3Qx)$. We also require

$$\begin{aligned} 2 \delta u \delta v &= U_{11} V_{11} A^2 + U_{11} V_{11} A^2 \cos(2Qx) \\ &\quad + \left(2 U_{11} V_{20} + 2 V_{11} U_{20} + U_{11} V_{22} + V_{11} U_{22} \right) A^3 \cos(Qx) + \dots . \end{aligned} \quad (7.41)$$

Finally, we need

$$(\delta u)^2 \delta v = \frac{3}{4} U_{11}^2 V_{11} A^3 \cos(Qx) + \dots . \quad (7.42)$$

On the left hand side of eqns. 7.30 and 7.31, we have the time derivative terms. Again, as we shall see, the amplitude A will be proportional to $\sqrt{\epsilon}$, where $\epsilon = b - b_T$ is presumed small. Its time derivative A_t will be proportional to $\epsilon^{3/2}$. Therefore, terms such as $(A^2)_t = 2AA_t$ will be negligible and we shall drop them from the outset. Thus,

$$\begin{aligned} \delta u_t &= U_{11} A_t \cos(Qx) + \dots \\ \delta v_t &= V_{11} A_t \cos(Qx) + \dots . \end{aligned} \quad (7.43)$$

We now set to zero the coefficients of $\cos(nQx)$ for $n = 0, 1$, and 2 in each of eqns. 7.30 and 7.31. Setting the $n = 0$ terms on the RHS of these equations to zero, we obtain

$$\begin{aligned} U_{20} &= 0 \\ \frac{b}{2a} U_{11}^2 + a U_{11} V_{11} + a^2 V_{20} &= 0 \end{aligned} \quad . \quad (7.44)$$

Doing the same for the $n = 2$ terms, we get

$$\begin{aligned} \frac{b}{2a} U_{11}^2 + a U_{11} V_{11} + b U_{22} + a^2 (1 + 4c^{-1}) V_{22} &= 0 \\ (1 + 4c) U_{22} + \frac{4a^2}{c} V_{22} &= 0 \end{aligned} \quad . \quad (7.45)$$

Solving, we obtain

$$U_{20} = 0 \quad , \quad U_{22} = \frac{2(1 - c^2)}{9ac} \quad , \quad V_{20} = -\frac{1 - c^2}{2a^3} \quad , \quad V_{22} = -\frac{(1 - c^2)(1 + 4c)}{18a^3} \quad . \quad (7.46)$$

Finally, we need the $n = 1$ terms. There are three contributions. One comes from the linear terms, restoring the small differences proportional to $\epsilon = b - b_T$. These terms contribute a coefficient for $\cos(Qx)$ of ϵA in the RHS of eqn. 7.30 and $-\epsilon A$ on the RHS of eqn. 7.31. A second contribution comes from the nonlinear terms. We invoke eqns. 7.40 and 7.41, multiplying the former by $\frac{b}{a}$ and the latter by a . The term we seek is proportional to $A^3 \cos(Qx)$, with a coefficient

$$\frac{b}{a} U_{22} + a(2V_{20} + V_{22} + V_{11}U_{22}) + \frac{3}{4}V_{11} = \frac{(1+c)(2+c)(8c^2 - 21c + 4)}{36a^2c} \quad . \quad (7.47)$$

We define

$$\lambda = -\frac{(1+c)(2+c)(8c^2 - 21c + 4)}{36a^2c} \quad . \quad (7.48)$$

Note that $\lambda > 0$ for $c \in [c_-, c_+]$, where $c_{\pm} = \frac{1}{16}(21 \pm \sqrt{313})$. Numerically, $c_- \approx 0.20676$ and $c_+ \approx 2.4182$. Finally, we have the U_{31} and V_{31} terms themselves. Thus, dividing out the common $\cos(Qx)$ factor on both sides of both equations, we have

$$\begin{aligned} A_t &= \epsilon A + \left[c(1+c)U_{31} + a^2 V_{31} - \lambda \right] A^3 \\ -\frac{c(1+c)}{a^2} A_t &= -\epsilon A - \left[(1+c)^2 U_{31} + \frac{a^2}{c} (1+c) V_{31} + \lambda \right] A^3 \end{aligned} \quad . \quad (7.49)$$

We can rewrite these equations as a linear system for the coefficients U_{31} and V_{31} , viz.

$$A^3 \underbrace{\begin{pmatrix} c(1+c) & a^2 \\ -(1+c)^2 & -a^2 - \frac{a^2}{c} \end{pmatrix}}_M \begin{pmatrix} U_{31} \\ V_{31} \end{pmatrix} = \begin{pmatrix} A_t - \epsilon A + \lambda A^3 \\ -a^{-2} c(1+c) A_t + \epsilon A - \lambda A^3 \end{pmatrix} \quad . \quad (7.50)$$

In order to be able to satisfy the above equation, the RHS must be orthogonal to the left eigenvector of the matrix M corresponding to the zero eigenvalue. This is called the *solvability condition*. It is easy to see that this zero left eigenvector is proportional to

$$\phi = (1 + c \quad c) \quad . \quad (7.51)$$

Thus, we demand

$$(1+c)\left(A_t - \epsilon A + \lambda A^3\right) - c\left(a^{-2}c(1+c)A_t - \epsilon A + \lambda A^3\right) = 0 \quad . \quad (7.52)$$

This, at long last, yields our amplitude equation:

$$A_t = \eta A - gA^3 \quad , \quad (7.53)$$

where

$$\eta = \frac{a^2(b - b_T)}{(1+c)(a^2 - c^2)} \quad , \quad g = -\frac{a^2(2+c)(8c^2 - 21c + 4)}{36a^2c(a^2 - c^2)} \quad . \quad (7.54)$$

The amplitude equation has a fixed point when $A_t = 0$, which says $\eta = gA^2$. Since $c < a$, we have that η is positive for $b > b_T$ and negative for $b < b_T$. Furthermore g is positive for $c \in [c_-, c_+]$ and negative outside this region. Thus, A has a fixed point $A^* = \sqrt{\eta/g}$ (in addition to the one at $A = 0$) if both η and g are positive, or if both η and g are negative. In the former case, $A = 0$ is unstable and $A = A^*$ is stable. In the latter case, $A = 0$ is stable and $A = A^*$ is unstable.

7.4 Rayleigh-Bénard Instability

Consider a layer of fluid between two horizontal plates, as depicted in fig. 7.3. The top plate is held at temperature T_1 and the bottom plate at temperature T_2 , with $\Delta T = T_2 - T_1 > 0$. As the fluid near the bottom plate is heated, it expands, and an upward buoyancy force per unit volume $f_{\text{buoy}} = \rho g \alpha \Delta T$ results, where $\alpha = \frac{1}{V} \frac{\partial V}{\partial T}$ is the thermal expansion coefficient and ρ is the fluid density. This buoyancy force is a destabilizing effect, and is opposed by a stabilizing dissipative force per unit volume $f_{\text{diss}} = \nu \kappa \rho / d^3$, where ν is the kinematic viscosity, κ the thermal diffusivity, and d the distance between the plates. The dimensionless ratio of these two force densities is known as the *Rayleigh number*,

$$\mathcal{R} = \frac{f_{\text{buoy}}}{f_{\text{diss}}} = \frac{g d^3 \alpha \Delta T}{\nu \kappa} \quad . \quad (7.55)$$

When $\mathcal{R} > \mathcal{R}_c \approx 1708$, the destabilizing effects are sufficient to destroy the homogeneous state. Due to mass conservation, the entire fluid cannot rise uniformly, hence the instability occurs at a finite wavelength λ , owing to the formation of *convective rolls* known as *Bénard cells* (see fig. 7.3).

Swift and Hohenberg (1977) showed that the dynamics for this problem reduces to the following equation for the real field $\sigma(\mathbf{r}, t)$ ²:

$$\frac{\partial \sigma}{\partial t} = \left[\varepsilon - (Q^2 + \nabla^2)^2 \right] \sigma - \sigma^3 \quad . \quad (7.56)$$

Here, $\varepsilon \propto \mathcal{R} - \mathcal{R}_c$ measures the distance from the instability, and $\nabla = \hat{x} \partial_x + \hat{y} \partial_y$ is the in-plane gradient. Distances are measured in units of d , and the maximally unstable wavevector is $Q \approx 3.12$.

We assume a plane wave disturbance, and we first separate out the oscillating features of $\sigma(\mathbf{r}, t)$ so that we may talk of a slowly varying amplitude function $A(\mathbf{r}, t)$:

$$\sigma(\mathbf{r}, t) = A(\mathbf{r}, t) e^{i Q x} + A^*(\mathbf{r}, t) e^{-i Q x} \quad , \quad (7.57)$$

²The field σ is actually a combination of temperature and vertical velocity fields.

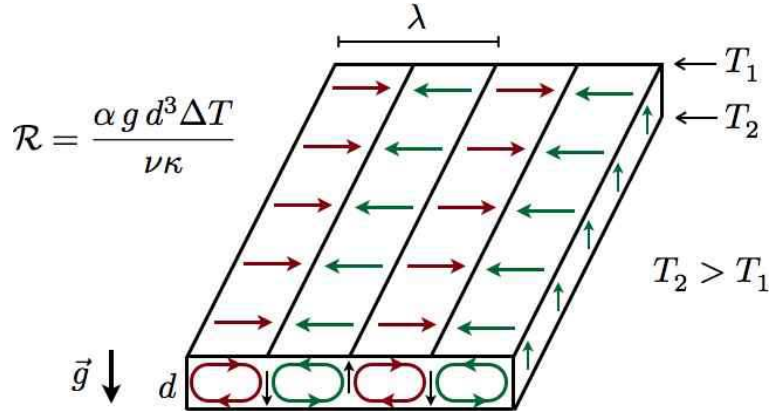


Figure 7.3: Bénard convection cells in a fluid heated from below.

where \hat{n} is a unit vector which we henceforth assume to be $\hat{n} = \hat{x}$. We then have

$$\begin{aligned} \sigma^3 &= A^3 e^{3iQx} + 3|A|^2 A e^{iQx} + 3|A|^2 A^* e^{-iQx} + A^{*3} e^{-3iQx} \\ (Q^2 + \nabla^2) A e^{iQx} &= e^{iQx} \cdot (2iQ \partial_x + \partial_x^2 + \partial_y^2) A . \end{aligned} \quad (7.58)$$

Matching coefficients of e^{iQx} , we find

$$\partial_t A = \left\{ \varepsilon - (2iQ \partial_x + \partial_x^2 + \partial_y^2)^2 \right\} A - 3|A|^2 A . \quad (7.59)$$

If we assume that the solution for A is such that $\partial_x \propto \epsilon^{1/2}$ and $\partial_y \propto \epsilon^{1/4}$ when acting on A , then the ∂_x^2 term is subleading relative to $Q \partial_x$ and ∂_y^2 , and we may drop it for $|\epsilon| \ll 1$ and write

$$\partial_t A = \left\{ \varepsilon - (2iQ \partial_x + \partial_y^2)^2 \right\} A - 3|A|^2 A . \quad (7.60)$$

For $\varepsilon > 0$ there is a family of stationary solutions of the form

$$A(x, y) = A_q e^{iq \cdot r} e^{i\delta} , \quad (7.61)$$

where

$$A_q = \frac{1}{\sqrt{3}} \left(\varepsilon - (2Qq_x + q_y^2)^2 \right)^{1/2} . \quad (7.62)$$

The instability first occurs at $q = 0$, at $\varepsilon = 0$. As we shall see, the nonlinearity severely limits what multimode structures may form.

The derivation of the Swift-Hohenberg equation utilizes something called the *Boussinesq approximation*, in which the density variation of the fluid enters only in the buoyancy equation. For *non-Boussinesq* fluids, the symmetry $\sigma \rightarrow -\sigma$ is broken, and one has

$$\partial_t \sigma = \left[\varepsilon - (Q^2 + \nabla^2)^2 \right] \sigma + v \sigma^2 - \sigma^3 , \quad (7.63)$$

for which the bifurcation is subcritical. This is called the *Haken model*.

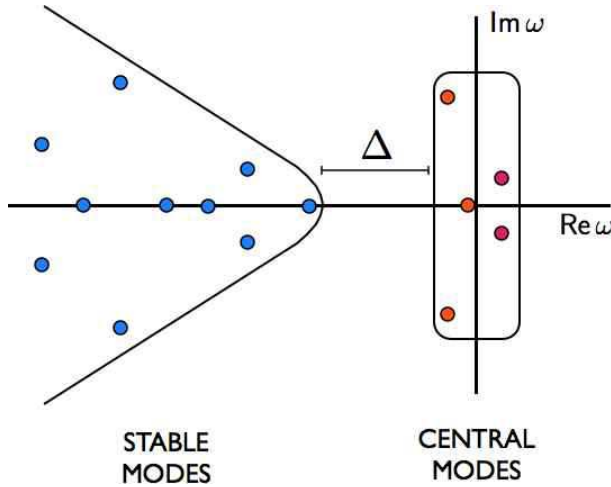


Figure 7.4: Sketch showing separation of frequency scales owing to gap Δ . The fast, stable modes are to the left, and the slow central modes all have $\text{Re } \omega_a \approx 0$.

7.5 Center Manifold Reduction

Consider a dynamical system in the vicinity of a fixed point: $\dot{\phi}_i = L_{ij} \phi_j + \mathcal{O}(\phi^2)$. If we expand the variables ϕ_i in terms of the eigenvectors ψ_i^a of L , writing $\phi_i = \sum_a A_a \psi_i^a$, then we can treat the A_a as new variables. Furthermore, we assume that the eigenspectrum $\{\omega_a\}$ exhibits a gap Δ , as shown in fig. 7.4, which allows us to classify these normal modes as either stable or central. The stable normal modes have large ($\text{Re } \omega_a < -\Delta$) negative real parts to their frequencies, and hence relax rapidly. On this time scales $\tau \lesssim \Delta^{-1}$, the central modes are roughly constant. We label these modes as A_a^c and A_a^s , respectively. The dynamics of these modes may be written as

$$\begin{aligned} \frac{dA_a^c}{dt} &= J_{ab} A_b^c + M_a(\mathbf{A}^c, \mathbf{A}^s) \\ \frac{dA_a^s}{dt} &= K_{ab} A_b^s + N_a(\mathbf{A}^c, \mathbf{A}^s) \quad , \end{aligned} \tag{7.64}$$

where M_a and N_a are nonlinear. If we assume that the fast, stable modes come to equilibrium, we set $\dot{A}_a^s = 0$ and solve the nonlinear equations $K_{ab} A_b^s + N_a(\mathbf{A}^c, \mathbf{A}^s) = 0$ to obtain $A_a^s = A_a^s(\mathbf{A}^c)$. Inserting this into the first of the previous sets of equations, we arrive at a new set of equations for the central modes alone. These new equations, obtained by substituting the solution for the stable modes, which are slaved to the slower central modes, into the function $M_a(\mathbf{A}^c, \mathbf{A}^s)$, are of the form

$$\frac{dA_a^c}{dt} = L_{ab} A_b^c + P_a(\mathbf{A}^c) \quad . \tag{7.65}$$

where P_a is nonlinear.

It is convenient to consider a nonlinear change of variables $(\mathbf{A}^c, \mathbf{A}^s) \rightarrow (\mathbf{B}^c, \mathbf{B}^s)$ so that the center manifold is described by $\mathbf{B}^s = 0$. To this end, we write $\mathbf{B} = \mathbf{A} + \mathbf{F}(\mathbf{A})$, or equivalently, $\mathbf{A} = \mathbf{B} + \mathbf{G}(\mathbf{B})$.

Note that to linear order the transformation is the identity $\mathbf{A} = \mathbf{B}$ because we wish to preserve the identification of the stable and central modes.

As a simple example, consider the system

$$\frac{dA_1}{dt} = 2A_1 A_2 , \quad \frac{dA_2}{dt} = -5A_2 - A_1^2 . \quad (7.66)$$

We identify A_1 as the central mode and A_2 as the stable fast mode. We now try a nonlinear transformation of the form

$$\begin{aligned} A_1 &= B_1 + \alpha B_1^2 + \beta B_1 B_2 + \gamma B_2^2 \\ A_2 &= B_2 + \alpha' B_1^2 + \beta' B_1 B_2 + \gamma' B_2^2 . \end{aligned} \quad (7.67)$$

We then have

$$\frac{dA_2}{dt} = \frac{dB_2}{dt} + 2\alpha' B_1 \frac{dB_1}{dt} + \beta' B_1 \frac{dB_2}{dt} + \beta' B_2 \frac{dB_1}{dt} + 2\gamma' B_2 \frac{dB_2}{dt} . \quad (7.68)$$

Setting $\beta' = 0$ we obtain the equation

$$(1 + 2\gamma' B_2) \frac{dB_2}{dt} = -5B_2 - (1 + 5\alpha') B_1^2 - 5\gamma' B_2^2 + \mathcal{O}(B^3) \quad (7.69)$$

We see that B_2 becomes isolated from B_1 if we choose $\alpha' = -\frac{1}{5}$. We are free to choose any value of γ' we please; for simplicity we choose $\gamma' = 0$. The B_2 equation is then

$$\frac{dB_2}{dt} = -5B_2 . \quad (7.70)$$

The fixed point is $B_2 = 0$. Note that

$$A_2 = B_2 - \frac{1}{5}B_1^2 \quad (7.71)$$

and so at the fixed point we conclude

$$A_2 = -\frac{1}{5}A_1^2 + \mathcal{O}(A_1^3) , \quad (7.72)$$

which is obvious from inspection of the second of eqn. 7.66 as well.

7.6 Selection and Stability of Spatial Patterns

Consider the spatiotemporal dynamics for a real field $\sigma(\mathbf{r}, t)$ close to an instability which lies at $|\mathbf{q}| = Q$. We assume a form

$$\sigma(\mathbf{r}, t) = \sum_{\ell=1}^M \left(A_\ell(t) e^{i\mathbf{q}_\ell \cdot \mathbf{r}} + A_\ell^*(t) e^{-i\mathbf{q}_\ell \cdot \mathbf{r}} \right) , \quad (7.73)$$

where $\mathbf{q}_\ell = Q \hat{\mathbf{n}}_\ell$ and $\hat{\mathbf{n}}_\ell^2 = 1$. By assuming $A_\ell = A_\ell(t)$, i.e. with no spatial (\mathbf{r}) dependence, we are considering a system whose spatial structure is ‘perfect’ and whose growth rate is maximum. We now consider the amplitude equations for the $A_\ell(t)$. Note that the set of allowed wavevectors in the Fourier decomposition of $\sigma(\mathbf{r}, t)$ consists of $2M$ elements, which we can order $\{\mathbf{q}_1, \dots, \mathbf{q}_M, -\mathbf{q}_1, \dots, -\mathbf{q}_M\}$. With this ordering, we have $\mathbf{q}_{\ell+M} = -\mathbf{q}_\ell$ and $A_{\ell+M} = A_\ell^*$, where $1 \leq \ell \leq M$. We will use indices $i, j, etc.$ to refer to the entire set: $1 \leq j \leq 2M$.

7.6.1 $d = 1$

For systems in one spatial dimension, the amplitude equation is quite limited, since $\hat{\mathbf{n}} = \hat{x}$ is the only possibility, and consequently $M = 1$. The simplest case is the logistic type equation,

$$\frac{dA}{dt} = \varepsilon A - g |A|^2 A \quad . \quad (7.74)$$

Here, $\varepsilon \propto \lambda - \lambda_c$ is a measure of the system's proximity to an instability, where λ is a control parameter. There are fixed points at $A = 0$ and, for $g > 0$, at $|A| = \sqrt{\varepsilon/g}$. Fixed points at finite A are in fact fixed *rings* in the Cartesian space ($\text{Re } A$, $\text{Im } A$), since the phase of A is undetermined and amplitude remains fixed if the phase is varied globally.

With $g > 0$, eqn. 7.74 describes a *supercritical pitchfork bifurcation*. The flow is sketched in the left panel of fig. 7.5. If $g < 0$, the bifurcation is *subcritical*, and the finite A fixed point occurs for $\varepsilon < 0$ and is unstable. In such a case, we must proceed to the next order in the amplitude equation,

$$\frac{dA}{dt} = \varepsilon A - g_1 |A|^2 A - g_2 |A|^4 A \quad , \quad (7.75)$$

with $g_1 < 0$ and $g_2 > 0$. The bifurcation diagram for this equation is sketched in the right panel of fig. 7.5.

7.6.2 Remarks on the amplitude equations for $d > 1$

In dimensions $d > 1$ we have the possibility for nonlinear mixing of K different modes, provided

$$\sum_{j=1}^K \mathbf{q}_j = Q \sum_{j=1}^K \hat{\mathbf{n}}_j = 0 \quad . \quad (7.76)$$

Recall also that A_j is associated with $e^{i\mathbf{q}_j \cdot \mathbf{r}}$ and A_j^* with $e^{-i\mathbf{q}_j \cdot \mathbf{r}}$. Under these conditions, the amplitude equations take the following general form:

$$\begin{aligned} \frac{dA_i}{dt} = & \varepsilon A_i + v \sum_{j,k} A_j^* A_k^* \delta_{\hat{\mathbf{n}}_i + \hat{\mathbf{n}}_j + \hat{\mathbf{n}}_k, 0} - g |A_i|^2 A_i - g \sum_j' \gamma_{ij} |A_j|^2 A_i \\ & - \sum_{j,k,l} \lambda_{ijkl} A_j^* A_k^* A_l^* \delta_{\hat{\mathbf{n}}_i + \hat{\mathbf{n}}_j + \hat{\mathbf{n}}_k + \hat{\mathbf{n}}_l, 0} + \mathcal{O}(A^4) \quad . \end{aligned} \quad (7.77)$$

The prime on the sum indicates that the term with $j = i$ is excluded. Taking the complex conjugate, we obtain the equation with index i replaced by $i + M$. The couplings γ_{ij} and λ_{ijkl} are functions of the relative angles:

$$\begin{aligned} \gamma_{ij} &= \gamma(\hat{\mathbf{n}}_i \cdot \hat{\mathbf{n}}_j) \\ \lambda_{ijkl} &= \lambda(\hat{\mathbf{n}}_i \cdot \hat{\mathbf{n}}_j, \hat{\mathbf{n}}_i \cdot \hat{\mathbf{n}}_k, \dots) \quad . \end{aligned} \quad (7.78)$$

Note that if we associate A_j with $e^{i\mathbf{q}_j \cdot \mathbf{r}}$ we can define $A_{-j} \equiv A_j^*$, associated with $e^{-i\mathbf{q}_j \cdot \mathbf{r}}$. Also note that v is a constant independent of j and k because the dot products in that case necessarily are all identical: $\hat{\mathbf{n}}_i \cdot \hat{\mathbf{n}}_j = \hat{\mathbf{n}}_j \cdot \hat{\mathbf{n}}_k = \hat{\mathbf{n}}_k \cdot \hat{\mathbf{n}}_i$.

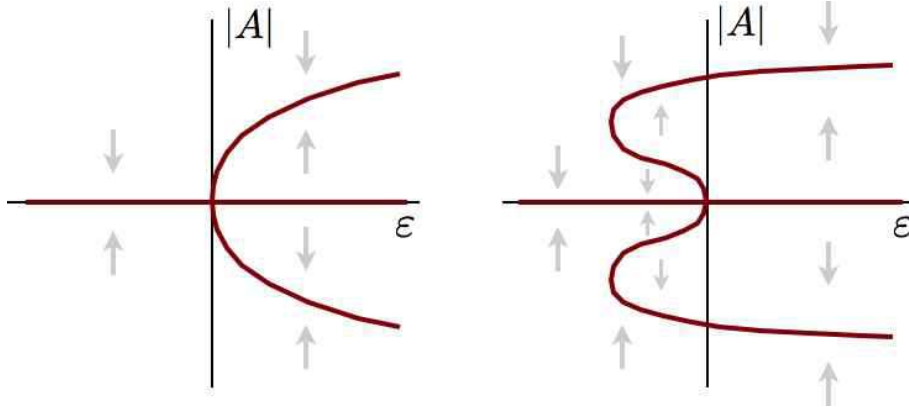


Figure 7.5: Flow diagrams for one-dimensional bifurcations $\dot{A} = \varepsilon A - g |A|^2 A$ with $g > 0$ (left) and $\dot{A} = \varepsilon A - g_1 |A|^2 A - g_2 |A|^4 A$ with $g_1 < 0$ and $g_2 > 0$ (right).

7.6.3 $d = 2$

For $d = 2$ systems all the allowed wavevectors lie on the circle $|\mathbf{q}_j| = Q$. Let's consider the cases $M = 1$, $M = 2$, and $M = 3$.

For $M = 1$ we recapitulate the $d = 1$ case. We have $\mathbf{q}_1 = Q\hat{x}$ and $\mathbf{q}_2 = -Q\hat{x}$ (up to continuous rotations). The amplitude equation is of the form $\dot{A} = \varepsilon A - g |A|^2 A$, and the patterned state is one with bands (stripes). This is not the last word, however, since we must check its stability with respect to $M = 2$ and $M = 3$ patterns.

$M = 2$ case

For $M = 2$, we write

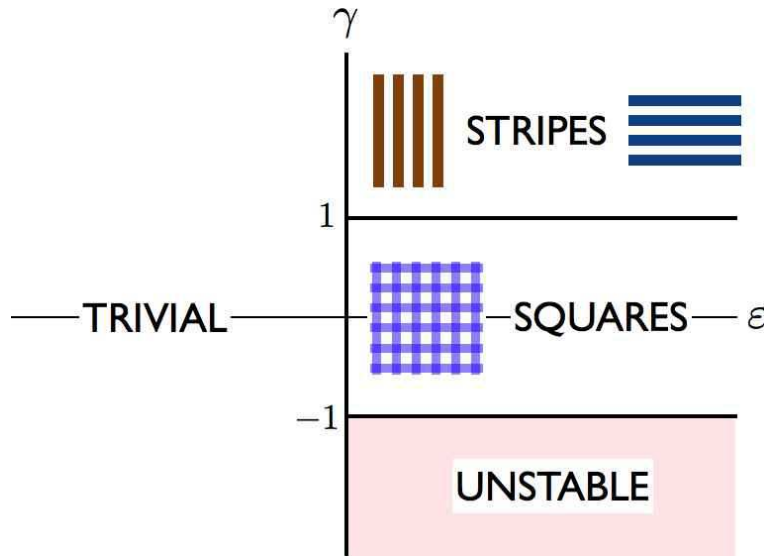
$$\sigma(x, y, t) = A_1(t) e^{iQx} + A_1^*(t) e^{-iQx} + A_2(t) e^{iQy} + A_2^*(t) e^{-iQy} . \quad (7.79)$$

The amplitude equations are

$$\begin{aligned} \dot{A}_1 &= \varepsilon A_1 - g |A_1|^2 A_1 - \gamma g |A_2|^2 A_1 \\ \dot{A}_2 &= \varepsilon A_2 - g |A_2|^2 A_2 - \gamma g |A_1|^2 A_2 . \end{aligned} \quad (7.80)$$

We assume $g > 0$. There are four possible fixed points $(\mathcal{A}_1, \mathcal{A}_2)$:

- | | |
|--|----------------------------|
| $(\mathcal{A}_1, \mathcal{A}_2) = (0, 0)$ | (I: trivial state) |
| $(\mathcal{A}_1, \mathcal{A}_2) = \sqrt{\varepsilon/g} \cdot (e^{i\alpha_1}, 0)$ | (II: y -directed bands) |
| $(\mathcal{A}_1, \mathcal{A}_2) = \sqrt{\varepsilon/g} \cdot (0, e^{i\alpha_2})$ | (III: x -directed bands) |
| $(\mathcal{A}_1, \mathcal{A}_2) = \sqrt{\varepsilon/g(1 + \gamma)} \cdot (e^{i\alpha_1}, e^{i\alpha_2})$ | (IV: squares) |

Figure 7.6: Phase diagram for the $M = 2$ system.

Note that $\mathcal{A}_1 \rightarrow \mathcal{A}_1 e^{-i\beta}$ is equivalent to a translation of the pattern in the \hat{x} -direction by $\Delta x = \beta/Q$.

To assess the stability of these fixed points, we write

$$A_j = \mathcal{A}_j (1 + \eta_j) \quad , \quad (7.81)$$

and we find

$$\begin{pmatrix} \dot{\eta}_1 \\ \dot{\eta}_2 \end{pmatrix} = \overbrace{\begin{pmatrix} \varepsilon - 3g|\mathcal{A}_1|^2 - \gamma g|\mathcal{A}_2|^2 & -2\gamma g|\mathcal{A}_2|^2 \\ -2\gamma g|\mathcal{A}_1|^2 & \varepsilon - \gamma g|\mathcal{A}_1|^2 - 3g|\mathcal{A}_2|^2 \end{pmatrix}}^L \begin{pmatrix} \eta_1 \\ \eta_2 \end{pmatrix} + \mathcal{O}(\eta^2) \quad . \quad (7.82)$$

Evaluating L at the four fixed points, we find

$$L_{\text{I}} = \begin{pmatrix} \varepsilon & 0 \\ 0 & \varepsilon \end{pmatrix} \quad , \quad L_{\text{II}} = \begin{pmatrix} -2\varepsilon & 0 \\ -2\gamma\varepsilon & (1-\gamma)\varepsilon \end{pmatrix} \quad (7.83)$$

and

$$L_{\text{III}} = \begin{pmatrix} (1-\gamma)\varepsilon & -2\gamma\varepsilon \\ 0 & -2\varepsilon \end{pmatrix} \quad , \quad L_{\text{IV}} = -\frac{2\varepsilon}{1+\gamma} \begin{pmatrix} 1 & \gamma \\ \gamma & 1 \end{pmatrix} \quad . \quad (7.84)$$

Computing $\mathcal{T} = \text{Tr}(L)$ and $\mathcal{D} = \det(L)$, we find:

- (I) In the trivial phase, we have $\mathcal{T} = 2\varepsilon$ and $\mathcal{D} = \varepsilon^2$. This fixed point is stable star if $\varepsilon < 0$ and an unstable star if $\varepsilon > 0$.³

³The star is a nongeneric fixed point, arising here because the eigenspace is degenerate. Note that $\mathcal{D} = \frac{1}{4}\mathcal{T}^2$ for the type I case.

- (II) In the striped phase, we have $\mathcal{T} = -(1 + \gamma)\varepsilon$ and $\mathcal{D} = 2(\gamma - 1)\varepsilon^2$. Thus, if $\gamma < 1$ the stripes are unstable as the fixed point is a saddle. Now suppose $\gamma > 1$, meaning $\mathcal{D} > 0$. The fixed point is therefore stable since $\varepsilon > 0$. If $\varepsilon < 0$, there is no solution for the fixed point at all. We next compute $\mathcal{D} - \frac{1}{4}\mathcal{T}^2 = -\frac{1}{4}(\gamma - 3)^2\varepsilon^2$ which is always negative, indicating that the fixed point is always a stable node.
- (III) Same as case II.
- (IV) We find $\mathcal{T} = -4\varepsilon/(\gamma + 1)$ and $\mathcal{D} = 4\varepsilon^2(1 - \gamma)/(1 + \gamma)$. The condition $\mathcal{D} > 0$ is equivalent to $|\gamma| < 1$. For $|\gamma| > 1$, this fixed point is a saddle, and is unstable. Note that $|\mathcal{A}_{1,2}|^2 = -\mathcal{T}/4g$ at the fixed point, so if a solution exists we must have $\mathcal{T} < 0$. If $|\gamma| < 1$ then, the fixed point is stable, and we find $\mathcal{D} - \frac{1}{4}\mathcal{T}^2 = -4\varepsilon^2\gamma^2/(1 + \gamma)^2 < 0$, indicating a stable node. Note that a fixed point solution exists for $\varepsilon < 0$ if $1 + \gamma < 0$, which means $\gamma < -1$, which is a saddle and unstable.

The phase diagram is shown in fig. 7.6.

$M = 3$ case

For $M = 3$ we write

$$\hat{\mathbf{n}}_1 = \hat{\mathbf{x}} \quad , \quad \hat{\mathbf{n}}_2 = -\frac{1}{2}\hat{\mathbf{x}} + \frac{\sqrt{3}}{2}\hat{\mathbf{y}} \quad , \quad \hat{\mathbf{n}}_3 = -\frac{1}{2}\hat{\mathbf{x}} - \frac{\sqrt{3}}{2}\hat{\mathbf{y}} \quad , \quad (7.85)$$

with $\mathbf{q}_j = Q\hat{\mathbf{n}}_j$, with $\hat{\mathbf{n}}_{r+3} = -\hat{\mathbf{n}}_r$. The σ field is then given by the sum

$$\sigma(\mathbf{r}, t) = A_1 e^{i\mathbf{q}_1 \cdot \mathbf{r}} + A_2 e^{i\mathbf{q}_2 \cdot \mathbf{r}} + A_3 e^{i\mathbf{q}_3 \cdot \mathbf{r}} + A_1^* e^{-i\mathbf{q}_1 \cdot \mathbf{r}} + A_2^* e^{-i\mathbf{q}_2 \cdot \mathbf{r}} + A_3^* e^{-i\mathbf{q}_3 \cdot \mathbf{r}} \quad . \quad (7.86)$$

Let's suppose the $\sigma \rightarrow -\sigma$ symmetry is broken, leaving us with the Haken model,

$$\frac{\partial \sigma}{\partial t} = \left[\varepsilon - \left(Q^2 + \nabla^2 \right)^2 \right] \sigma + v\sigma^2 - \sigma^3 \quad . \quad (7.87)$$

The resulting amplitude equations are then

$$\frac{dA_\ell}{dt} = \varepsilon A_\ell + v A_{\ell-1}^* A_{\ell+1}^* - g |A_\ell|^2 A_\ell - \gamma g \left(|A_{\ell-1}|^2 + |A_{\ell+1}|^2 \right) A_\ell \quad , \quad (7.88)$$

Our notation is cyclic in $\ell \bmod 3$, so $A_{\ell+1} = A_1$ when $\ell = 3$, and $A_{\ell-1} = A_3$ when $\ell = 1$.

We now convert to amplitude and phase variables, writing

$$A_\ell = R_\ell e^{i\phi_\ell} \quad . \quad (7.89)$$

Plugging this into the amplitude equations and taking the real part, we obtain

$$\frac{dR_\ell}{dt} = \varepsilon R_\ell + v R_{\ell-1} R_{\ell+1} \cos \phi - g R_\ell^3 - \gamma g (R_{\ell-1}^2 + R_{\ell+1}^2) R_\ell \quad (7.90)$$

where

$$\phi = \phi_1 + \phi_2 + \phi_3 \quad . \quad (7.91)$$

The imaginary part yields the equations

$$\frac{d\phi_\ell}{dt} = -\frac{R_{\ell-1}R_{\ell+1}}{R_\ell} \cdot v \sin \phi \quad . \quad (7.92)$$

Adding these last three equations, we obtain a single equation for the total phase angle ϕ :

$$\frac{d\phi}{dt} = -\frac{R_1^2 R_2^2 + R_2^2 R_3^2 + R_3^2 R_1^2}{R_1 R_2 R_3} \cdot v \sin \phi \quad . \quad (7.93)$$

Thus, $\sin \phi = 0$ is a fixed point for these dynamics, and in steady state, we have

$$\begin{aligned} v < 0 &\Rightarrow \phi = \pi \\ v > 0 &\Rightarrow \phi = 0 \end{aligned} \quad .$$

Thus, $v \cos \phi > 0$ in steady state, i.e. $v \cos \phi = |v|$. Assuming the phase angle has reached its steady state value, the amplitude equations are given by

$$\begin{aligned} \frac{dR_1}{dt} &= \varepsilon R_1 + |v|R_2R_3 - gR_1^3 - \gamma g(R_2^2 + R_3^2)R_1 \\ \frac{dR_2}{dt} &= \varepsilon R_2 + |v|R_3R_1 - gR_2^3 - \gamma g(R_3^2 + R_1^2)R_2 \\ \frac{dR_3}{dt} &= \varepsilon R_3 + |v|R_1R_2 - gR_3^3 - \gamma g(R_1^2 + R_2^2)R_3 \end{aligned} \quad . \quad (7.94)$$

Subtracting the first equation from the second gives

$$\frac{d}{dt}(R_1 - R_2) = \left[\varepsilon - |v|R_3 - g(R_1^2 + R_1R_2 + R_2^2) - \gamma gR_3^2 + \gamma gR_1R_2 \right] (R_1 - R_2) \quad . \quad (7.95)$$

For sufficiently small ε , we suspect that the term in brackets is negative, indicating that the difference $R_1 - R_2$ tends to zero. As we could have chosen any two distinct indices for R , we are motivated to consider the symmetric case $R_1 = R_2 = R_3 = R$. This results in the equation

$$\frac{dR}{dt} = \varepsilon R + |v|R^2 - g(1 + 2\gamma)R^3 \quad . \quad (7.96)$$

The fixed points $\dot{R} = 0$ occur at $R = 0$ and at $R = R_\pm$, where

$$R_\pm = \frac{|v| \pm \sqrt{v^2 + 4\varepsilon g(1 + 2\gamma)}}{2g(1 + 2\gamma)} \quad . \quad (7.97)$$

This solution describes a hexagonal structure.

To assess the stability of these solutions, it is *incorrect* to analyze the stability of eqn. 7.96. Rather, we must go back to the full $N = 4$ system (R_1, R_2, R_3, ϕ) . Since the partial derivatives $\partial \dot{R}_\ell / \partial \phi =$

$-vR_{\ell-1}R_{\ell+1}\sin\phi$ all vanish at the fixed point, we only need consider the $N = 3$ system (R_1, R_2, R_3) in eqns. 7.94. We must examine the Jacobian

$$J_{\ell\ell'} = \frac{\partial \dot{R}_\ell}{\partial R_{\ell'}} = \begin{pmatrix} a & b & b \\ b & a & b \\ b & b & a \end{pmatrix} = (a - b)\mathbb{I} + 3b|\psi\rangle\langle\psi| \quad , \quad (7.98)$$

where $\psi^t = \frac{1}{\sqrt{3}}(1, 1, 1)$. Thus, $|\psi\rangle$ is an eigenvector with eigenvalue $\lambda_+ = a + 2b$, while the two-dimensional subspace orthogonal to $|\psi\rangle$ has the (doubly degenerate) eigenvalue $\lambda_- = a - b$. Thus,

$$\begin{aligned} \lambda_+ &= \varepsilon + 2|v|R - 3(1 + 2\gamma)gR^2 \\ &= -2\varepsilon - |v|R \end{aligned} \quad (7.99)$$

and

$$\begin{aligned} \lambda_- &= \varepsilon - |v|R - 3gR^2 \\ &= \frac{2}{1 + 2\gamma} \left((\gamma - 1)\varepsilon - (2 + \gamma)|v|R \right) \quad . \end{aligned} \quad (7.100)$$

We have used the fixed point equation

$$g(1 + 2\gamma)R^2 - |v|R - \varepsilon = 0 \quad (7.101)$$

to eliminate the quadratic terms in R in these expressions for λ_\pm .

Consider the $R = R_+$ fixed point. Plugging the expression for R_+ into the expressions for λ_\pm , the stability criteria $\lambda_\pm < 0$ can be investigated. We find that the $R = R_+$ solution is stable for

$$-\frac{v^2}{4g(1 + 2\gamma)} < \varepsilon < \frac{(2 + \gamma)v^2}{g(\gamma - 1)^2} \quad . \quad (7.102)$$

The lower limit for ε is set by the condition $\lambda_+ = 0$, and the upper limit by $\lambda_- = 0$. The $R = R_-$ solution and all other fixed points (such as when $v \cos\phi < 0$) are unstable. For example, there are so-called mixed modes, where

$$R_1 = \frac{|v|}{g(\gamma - 1)} \quad , \quad R_2 = R_3 = \sqrt{\frac{\varepsilon - gR_1^2}{g(\gamma + 1)}} \quad . \quad (7.103)$$

These are also unstable.

The hexagonal pattern is described by

$$\sigma(\mathbf{r}, t) = 2R(t) \left[\cos(Q\hat{\mathbf{n}}_1 \cdot \mathbf{r} + \phi_1) + \cos(Q\hat{\mathbf{n}}_2 \cdot \mathbf{r} + \phi_2) \pm \cos(Q\hat{\mathbf{n}}_3 \cdot \mathbf{r} - \phi_1 - \phi_2) \right] \quad . \quad (7.104)$$

where the upper sign is taken when $v > 0$ ($\phi = 0$), and the lower sign when $v < 0$ ($\phi = \pi$). Let us define the primitive *reciprocal lattice vectors*

$$\mathbf{b}_1 = Q\hat{\mathbf{x}} \quad , \quad \mathbf{b}_2 = Q\left(\frac{1}{2}\hat{\mathbf{x}} + \frac{\sqrt{3}}{2}\hat{\mathbf{y}}\right) \quad . \quad (7.105)$$

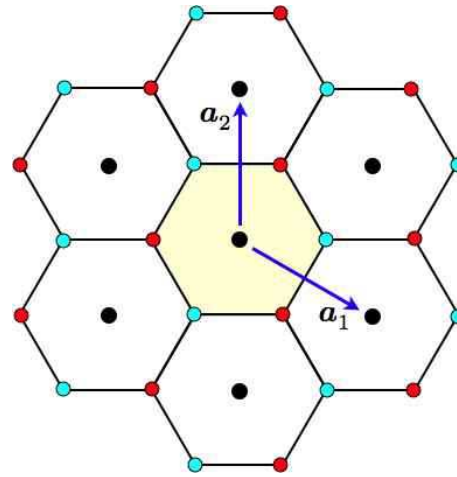


Figure 7.7: Points of high symmetry in the honeycomb lattice. The black dots label the Γ sublattice, the blue dots the K sublattice, and the red dots the K' sublattice.

With this definition, we have

$$\begin{aligned} \mathbf{q}_1 &= \mathbf{b}_1 & \mathbf{q}_2 &= \mathbf{b}_2 - \mathbf{b}_1 & \mathbf{q}_3 &= -\mathbf{b}_2 \\ \mathbf{q}_4 &= -\mathbf{b}_1 & \mathbf{q}_5 &= \mathbf{b}_1 - \mathbf{b}_2 & \mathbf{q}_6 &= \mathbf{b}_2 \end{aligned} .$$

We also define the primitive *direct lattice vectors*

$$\mathbf{a}_1 = \frac{4\pi}{\sqrt{3}Q} \left(\frac{\sqrt{3}}{2}\hat{x} - \frac{1}{2}\hat{y} \right) , \quad \mathbf{a}_2 = \frac{4\pi}{\sqrt{3}Q} \hat{y} . \quad (7.106)$$

Note that

$$\mathbf{a}_\mu \cdot \mathbf{b}_\nu = 2\pi \delta_{\mu\nu} . \quad (7.107)$$

We can expand \mathbf{r} in the basis of primitive direct lattice vectors as

$$\mathbf{r} \equiv \frac{\zeta_1}{2\pi} \mathbf{a}_1 + \frac{\zeta_2}{2\pi} \mathbf{a}_2 . \quad (7.108)$$

Then

$$\begin{aligned} \sigma(\mathbf{r}, t) &= 2R(t) \left[\cos(\mathbf{b}_1 \cdot \mathbf{r} + \phi_1) + \cos((\mathbf{b}_2 - \mathbf{b}_1) \cdot \mathbf{r} + \phi_2) \pm \cos(\mathbf{b}_2 \cdot \mathbf{r} + \phi_1 + \phi_2) \right] \\ &= 2R(t) \left[\cos(\zeta_1 + \phi_1) + \cos(\zeta_2 - \zeta_1 + \phi_2) \pm \cos(\zeta_2 + \phi_1 + \phi_2) \right] . \end{aligned} \quad (7.109)$$

If we now shift the origin of coordinates, defining

$$\tilde{\zeta}_1 = \begin{cases} \zeta_1 + \phi_1 & \text{if } v > 0 \\ \zeta_1 + \phi_1 + \pi & \text{if } v < 0 \end{cases} , \quad \tilde{\zeta}_2 = \zeta_2 + \phi_2 , \quad (7.110)$$

then we have

$$\sigma(\mathbf{r}, t) = \pm 2R(t) \left[\cos \tilde{\zeta}_1 + \cos(\tilde{\zeta}_2 - \tilde{\zeta}_1) + \cos \tilde{\zeta}_2 \right] , \quad (7.111)$$

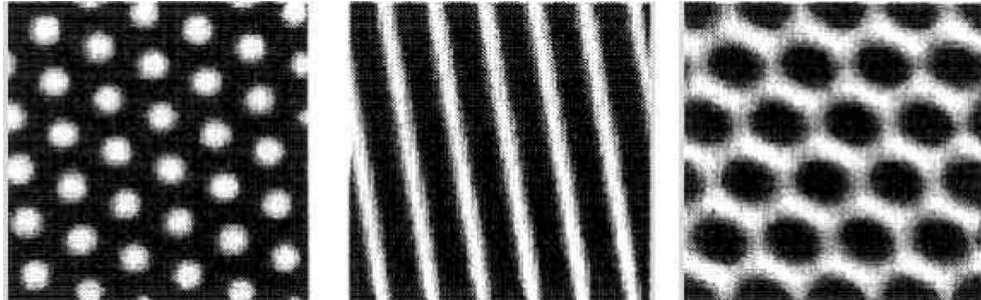


Figure 7.8: Two-dimensional stationary Turing patterns, showing H0 (left), striped (center), and H π (right) structures. White areas correspond to local maxima of the concentration field. From A. De Wit, *Adv. Chem. Phys.* **109**, 435 (1999).

where again the upper sign is for $v > 0$ and the lower sign for $v < 0$. Consider the case $v > 0$. At a fixed time t , the function $\sigma(\mathbf{r}, t)$ achieves its maxima $\sigma_{\max} = 6R$ when $\tilde{\zeta}_1 = 0$ modulo 2π and $\tilde{\zeta}_2 = 0$ modulo 2π , which is to say when \mathbf{r} lies on a triangular lattice of points, which we call the Γ sublattice. This pattern is known as the H0 hexagonal pattern. The minima lie on a honeycomb lattice, which can be described as two interpenetrating triangular lattices. The K sublattice is defined by the set of points equivalent to $\tilde{\zeta}_1 = \frac{4\pi}{3}$ and $\tilde{\zeta}_2 = \frac{2\pi}{3}$, while the K' sublattice consists of the points equivalent to $\tilde{\zeta}_1 = \frac{2\pi}{3}$ and $\tilde{\zeta}_2 = \frac{4\pi}{3}$, again modulo 2π in either component. The sum of the three cosines is then $-\frac{3}{2}$, hence $\sigma_{\min} = -3R$. For $v < 0$ the roles of minima and maxima are reversed, and the maxima lie on the vertices of a honeycomb lattice; this is the H π structure. See figs. 7.7 and 7.8.

Hexagons are not the only stable pattern, however. We can find stripe solutions where $R_1 = R$ and $R_2 = R_3 = 0$. Nontrivial solutions occur for $\varepsilon > 0$, where $R = \sqrt{\varepsilon/g}$, as in the one-dimensional case. The Jacobian at this fixed point is given by

$$J_{\ell\ell'} = \begin{pmatrix} -2\varepsilon & 0 & 0 \\ 0 & (1-\gamma)\varepsilon & |v|\sqrt{\frac{\varepsilon}{g}} \\ 0 & |v|\sqrt{\frac{\varepsilon}{g}} & (1-\gamma)\varepsilon \end{pmatrix} . \quad (7.112)$$

The eigenvalues are $\lambda_1 = -2\varepsilon$ and $\lambda_{2,3} = (1-\gamma)\varepsilon \pm |v|\sqrt{\frac{\varepsilon}{g}}$. Since $\varepsilon > 0$ in order to have a nontrivial solution, $\lambda_1 < 0$ and we can focus on $\lambda_{2,3}$. If $\gamma < 1$ then $\lambda_2 > 0$, so stripes are unstable for $\gamma < 1$. If $\gamma > 1$, we have that $\lambda_3 < 0$, and the condition $\lambda_2 < 0$ requires

$$\varepsilon > \frac{v^2}{g(1-\gamma)^2} \quad (7.113)$$

for the stripes to be stable, along with $\gamma > 1$.

It is convenient to rescale, defining

$$|v| \equiv u \cdot \sqrt{4g(1+2\gamma)} \quad , \quad R \equiv S \cdot \frac{u}{\sqrt{g}} \quad , \quad \varepsilon \equiv \eta \cdot u^2 \quad . \quad (7.114)$$

Then we find

$$S_{\text{HEX}}(\eta) = \frac{1 \pm \sqrt{1+\eta}}{\sqrt{1+2\gamma}} \quad , \quad S_{\text{STRIPE}}(\eta) = \sqrt{\eta} \quad . \quad (7.115)$$

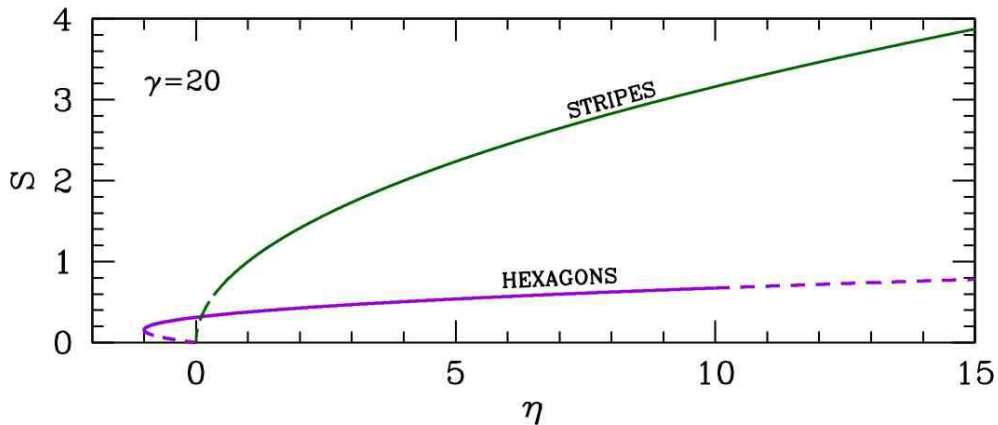


Figure 7.9: Dimensionless amplitude S versus dimensionless coupling η for the $M = 3$ system discussed in the text, showing stable (solid) and unstable (dashed) solutions.

The upper solution for the hexagons is stable for $\eta_- < \eta < \eta_+$, whereas the stripe solution is stable for $\eta > \eta_s$, where

$$\eta_- = -1 \quad , \quad \eta_s = \frac{4(1+2\gamma)}{(\gamma-1)^2} \quad , \quad \eta_+ = \frac{4(1+2\gamma)(2+\gamma)}{(\gamma-1)^2} \quad . \quad (7.116)$$

These results are plotted in fig. 7.9.

7.6.4 $d = 3$

We can extend the previous $d = 2$ results to $d = 3$ dimensions simply by assuming there is no variation in the along z , the coordinate in the third direction. Thus, stripes in $d = 2$ become lamellae in $d = 3$. New structures emerge as well:

$$\begin{aligned} M = 3 : 2M = 6 &\Rightarrow \text{simple cubic in reciprocal and real space} \\ M = 4 : 2M = 8 &\Rightarrow \text{BCC reciprocal lattice, FCC direct lattice} \\ M = 6 : 2M = 12 &\Rightarrow \text{FCC reciprocal lattice, BCC direct lattice} \end{aligned} .$$

For a description of the many patterned structures which can form under these periodicities, see T. K. Callahan and E. Knobloch, *Nonlinearity* **10**, 1179 (1997) and *idem, Physica D* **132**, 339 (1999).

7.7 Anisotropy

Many physical systems exhibit intrinsic spatial anisotropies. To see how these might affect patterning, consider a modification of the Brusselator with anisotropic diffusion:

$$\begin{aligned} u_t &= D_{u,\parallel} u_{xx} + D_{u,\perp} u_{yy} + a - (b+1)u + u^2v \\ v_t &= D_{v,\parallel} v_{xx} + D_{v,\perp} v_{yy} + b u - u^2v \end{aligned} . \quad (7.117)$$

The linearized dynamics, from eqn. 7.13, are given by the matrix

$$L(q) = \begin{pmatrix} b - 1 - \tilde{D}_u(\phi) q^2 & a^2 \\ -b & -a^2 - \tilde{D}_v(\phi) q^2 \end{pmatrix} . \quad (7.118)$$

where

$$q_x = q \cos \phi \quad , \quad q_y = q \sin \phi \quad (7.119)$$

and

$$\begin{aligned} \tilde{D}_u(\phi) &= D_{u,\parallel} \cos^2 \phi - D_{u,\perp} \sin^2 \phi \\ \tilde{D}_v(\phi) &= D_{v,\parallel} \cos^2 \phi - D_{v,\perp} \sin^2 \phi \end{aligned} . \quad (7.120)$$

We identify the maximally unstable wavevector for the Turing instability $\det(L) = 0$ as before, *i.e.* by minimizing $\det(L)$ with respect to q^2 . We then invoke $\det(L) = 0$, which gives us a second equation. From these two equations we obtain the critical value of b at the transition and the critical wavevector at the transition:

$$\begin{aligned} b_T(\phi) &= \left(1 + a \sqrt{\frac{\tilde{D}_u(\phi)}{\tilde{D}_v(\phi)}} \right)^2 \\ Q^2(\phi) &= \frac{a}{\sqrt{\tilde{D}_u(\phi) \tilde{D}_v(\phi)}} \end{aligned} . \quad (7.121)$$

We have thus described a one-parameter family of Turing instabilities, as a function of the angle ϕ . The earliest (smallest $b_T(\phi)$ value) of these will preempt the others. Examining $b_T(\phi)$, we find

$$\begin{aligned} \frac{D_{u,\perp}}{D_{u,\parallel}} > \frac{D_{v,\parallel}}{D_{v,\perp}} &\Rightarrow \phi = 0 \\ \frac{D_{u,\perp}}{D_{u,\parallel}} < \frac{D_{v,\parallel}}{D_{v,\perp}} &\Rightarrow \phi = \frac{\pi}{2} . \end{aligned} \quad (7.122)$$

7.8 Phase Diffusion : Eckhaus and Zigzag Instabilities

Starting from the Swift-Hohenberg equation, the dynamics of a striped configuration, with $\sigma(x, y, t) = 2 \operatorname{Re} [A(x, y, t) e^{iQx}]$ are governed by the Newell-Whitehead-Segel equation,

$$\frac{\partial A}{\partial T} = \mu A + \left(\frac{\partial}{\partial X} + \frac{i}{2} \frac{\partial^2}{\partial Y^2} \right)^2 A - |A|^2 A , \quad (7.123)$$

where X , Y , and T are scaled ‘slow variables’, $X = \varepsilon_0 Q x$, $Y = |\varepsilon_0|^{1/2} Q y$, $T = 4Q^2 |\varepsilon_0| t$, and $\varepsilon = 4Q^2 |\varepsilon_0| \mu$, where $|\varepsilon_0| \ll 1$. The amplitude has also been scaled by a factor of $\frac{2}{\sqrt{3}} Q^2 |\varepsilon_0|^{1/2}$.

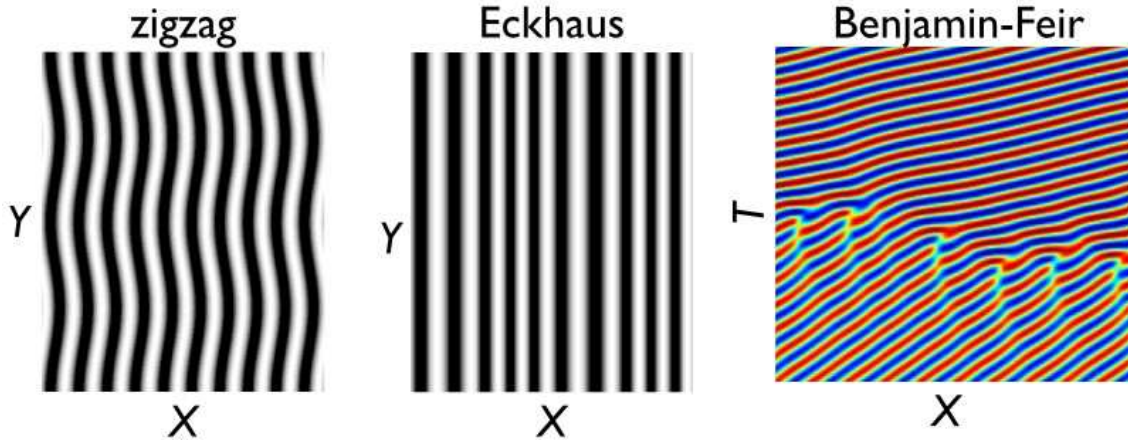


Figure 7.10: Zigzag, Eckhaus, and Benjamin-Feir instabilities.

The optimal pattern is given by the constant solution $A = \sqrt{\mu}$, for $\mu > 0$, corresponding to $\sigma(x) = 2\sqrt{\mu} \cos(Qx)$. However, for $\varepsilon > 0$ an entire band of wavevectors is linearly unstable, since $\varepsilon - (Q^2 + \nabla^2)^2$ acting on any plane wave $e^{iq \cdot r}$ will yield a positive growth rate so long as $|q^2 - Q^2| < \sqrt{\varepsilon}$. Thus the Newell-Whitehead-Segel (NWS) equation admits a band of static solutions,

$$A(X, Y) = \sqrt{\mu - k^2} e^{ikX} , \quad (7.124)$$

for $|k| < \sqrt{\mu}$. We now investigate the stability of these solutions, writing

$$A(X, Y, T) = \left(\sqrt{\mu - k^2} + \rho(X, Y, T) \right) e^{ikX} e^{i\phi(X, Y, T)} , \quad (7.125)$$

and linearizing in the amplitude and phase variations ρ and ϕ .

We start by defining $\Lambda = kX + \phi$. Then

$$\begin{aligned} e^{-i\Lambda} \frac{\partial}{\partial X} e^{i\Lambda} &= \frac{\partial}{\partial X} + ik + i \frac{\partial \phi}{\partial X} \\ e^{-i\Lambda} \frac{\partial}{\partial Y} e^{i\Lambda} &= \frac{\partial}{\partial Y} + i \frac{\partial \phi}{\partial Y} . \end{aligned} \quad (7.126)$$

Thus,

$$e^{-i\Lambda} \left(\partial_X - \frac{i}{2} \partial_Y^2 \right) e^{i\Lambda} = ik + \partial_X - \frac{i}{2} \partial_Y^2 + i\phi_X + \frac{1}{2}\phi_{YY} + \phi_Y \partial_Y + \frac{i}{2}\phi_Y^2 \quad (7.127)$$

We need to square the RHS and then apply it to $(\sqrt{\mu - k^2} + \rho)$, and then keep only terms up to linear order in ρ , ϕ , and their derivatives. Clearly we can drop the last two terms on the RHS above since $\phi_Y \partial_Y$ will be nonzero only when acting on ρ or ϕ , resulting in a nonlinear contribution; the last term ϕ_Y^2 is already nonlinear. Even with the reduction from seven to five terms, squaring is a slightly tedious process, and we skip the intermediate steps. Multiplying the NWS equation on the left by $e^{-i\Lambda}$ and then

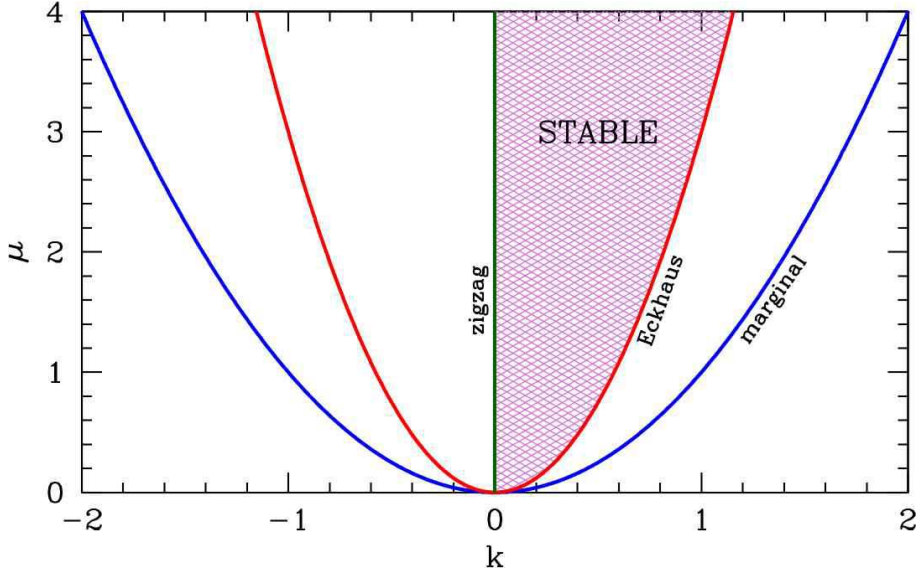


Figure 7.11: Boundary curves for Eckhaus and zigzag instabilities. Structures within the shaded region are stable.

collecting real and imaginary terms, we obtain the coupled equations

$$\begin{aligned} \rho_T &= -2(\mu - k^2) \rho - 2k\sqrt{\mu - k^2} \phi_X + \rho_{XX} + k\rho_{YY} + \sqrt{\mu - k^2} \phi_{XYY} - \frac{1}{4} \rho_{YYYY} \\ \phi_T &= \frac{2k}{\sqrt{\mu - k^2}} \rho_X + \phi_{XX} + k\phi_{YY} - \frac{1}{2\sqrt{\mu - k^2}} \rho_{XYY} - \frac{1}{4} \phi_{YYYY} . \end{aligned} \quad (7.128)$$

The terms on the RHS of these equations are ordered by increasing powers of derivatives. We assume a long wavelength disturbance, meaning we can neglect all but the lowest nontrivial terms. From the RHS of the first equation, we take the first two terms, which yield

$$\rho = -\frac{k}{\sqrt{\mu - k^2}} \phi_X . \quad (7.129)$$

Note that $\rho \propto \phi_X$, which means that the LHS of the first equation is $\rho_T \propto \phi_{XT}$, which has one more derivative. Substituting this result into the second equation, we obtain

$$\phi_T = \left(\frac{\mu - 3k^2}{\mu - k^2} \right) \phi_{XX} + k\phi_{YY} . \quad (7.130)$$

This is an anisotropic diffusion equation. We identify

$$D_{\phi,X} = \frac{\mu - 3k^2}{\mu - k^2} , \quad D_{\phi,Y} = k . \quad (7.131)$$

An instability occurs when either diffusion constant is negative. Note that $\mu = k^2$ is the so-called *marginal stability boundary* and that no patterned solution exists for $k^2 > \mu$. The condition $D_{\phi,X} < 0$

corresponds to the *Eckhaus instability* and $D_{\phi,Y} < 0$ to the *zigzag instability*. A sketch of the stability boundaries is provided in fig. 7.11.

These are many other patterning instabilities. For example, the *Benjamin-Feir instability* is an analog of the Eckhaus instability which occurs in travelling plane waves. This and other such examples are discussed in detail in the books by R. Hoyle and by M. Cross and H. Greenside, both listed in chapter 0 of these notes.

Chapter 8

Solitons

Starting in the 19th century, researchers found that certain nonlinear PDEs admit exact solutions in the form of solitary waves, known today as *solitons*. There's a famous story of the Scottish engineer, John Scott Russell, who in 1834 observed a hump-shaped disturbance propagating undiminished down a canal. In 1844, he published this observation¹, writing,

"I was observing the motion of a boat which was rapidly drawn along a narrow channel by a pair of horses, when the boat suddenly stopped - not so the mass of water in the channel which it had put in motion; it accumulated round the prow of the vessel in a state of violent agitation, then suddenly leaving it behind, rolled forward with great velocity, assuming the form of a large solitary elevation, a rounded, smooth and well-defined heap of water, which continued its course along the channel apparently without change of form or diminution of speed. I followed it on horseback, and overtook it still rolling on at a rate of some eight or nine miles an hour, preserving its original figure some thirty feet long and a foot to a foot and a half in height. Its height gradually diminished, and after a chase of one or two miles I lost it in the windings of the channel. Such, in the month of August 1834, was my first chance interview with that singular and beautiful phenomenon which I have called the Wave of Translation".

Russell was so taken with this phenomenon that subsequent to his discovery he built a thirty foot wave tank in his garden to reproduce the effect, which was precipitated by an initial sudden displacement of water. Russell found empirically that the velocity obeyed $v \simeq \sqrt{g(h + u_m)}$, where h is the average depth of the water and u_m is the maximum vertical displacement of the wave. He also found that a sufficiently large initial displacement would generate two solitons, and, remarkably, that solitons can pass through one another undisturbed. It was not until 1890 that Korteweg and deVries published a theory of shallow water waves and obtained a mathematical description of Russell's soliton.

Nonlinear PDEs which admit soliton solutions typically contain two important classes of terms which feed off each other to produce the effect:

$$\text{DISPERSION} \iff \text{NONLINEARITY}$$

¹J. S. Russell, *Report on Waves*, 14th Meeting of the British Association for the Advancement of Science, pp. 311-390.

The effect of dispersion is to spread out pulses, while the effect of nonlinearities is, often, to draw in the disturbances. We saw this in the case of front propagation, where dispersion led to spreading and nonlinearity to steepening.

In the 1970's it was realized that several of these nonlinear PDEs yield entire families of exact solutions, and not just isolated solitons. These families contain solutions with arbitrary numbers of solitons of varying speeds and amplitudes, and undergoing mutual collisions. The three most studied systems have been

- The *Korteweg-deVries equation*,

$$u_t + 6uu_x + u_{xxx} = 0 \quad . \quad (8.1)$$

This is a generic equation for 'long waves' in a dispersive, energy-conserving medium, to lowest order in the nonlinearity.

- The *Sine-Gordon equation*,

$$\phi_{tt} - \phi_{xx} + \sin \phi = 0 \quad . \quad (8.2)$$

The name is a play on the Klein-Gordon equation, $\phi_{tt} - \phi_{xx} + \phi = 0$. Note that the Sine-Gordon equation is periodic under $\phi \rightarrow \phi + 2\pi$.

- The *nonlinear Schrödinger equation*,

$$i\psi_t \pm \psi_{xx} + 2|\psi|^2\psi = 0 \quad . \quad (8.3)$$

Here, ψ is a complex scalar field. Depending on the sign of the second term, we denote this equation as either NLS(+) or NLS(-), corresponding to the so-called *focusing* (+) and *defocusing* (-) cases.

Each of these three systems supports soliton solutions, including exact N -soliton solutions, and nonlinear periodic waves.

8.1 The Korteweg-deVries Equation

Let h_0 denote the resting depth of water in a one-dimensional channel, and $y(x, t)$ the vertical displacement of the water's surface. Let L be a typical horizontal scale of the wave. When $|y| \ll h_0 \ll L$, and $v \approx 0$ (speed of propagation small compared with c_0), the evolution of an x -directed wave is described by the KdV equation,

$$y_t + c_0 y_x + \frac{3c_0}{2h_0} yy_x + \frac{1}{6}c_0 h_0^2 y_{xxx} = 0 \quad , \quad (8.4)$$

where $c_0 = \sqrt{gh_0}$. For small amplitude disturbances, only the first two terms are consequential, and we have

$$y_t + c_0 y_x \approx 0 \quad , \quad (8.5)$$

the solution to which is

$$y(x, t) = f(x - c_0 t) \quad , \quad (8.6)$$

where $f(\xi)$ is an *arbitrary* shape; the disturbance propagates with velocity c_0 . When the dispersion and nonlinearity are included, only a *particular* pulse shape can propagate in an undistorted manner; this is the soliton.

It is convenient to shift to a moving frame of reference:

$$x' = x - c_0 t \quad , \quad t' = t \quad , \quad (8.7)$$

hence

$$\frac{\partial}{\partial x} = \frac{\partial}{\partial x'} \quad , \quad \frac{\partial}{\partial t} = \frac{\partial}{\partial t'} - c_0 \frac{\partial}{\partial x'} \quad . \quad (8.8)$$

Thus,

$$y_{t'} + \frac{3c_0}{2h_0} y y_{x'} + \frac{1}{6} c_0 h_0^2 y_{x'x'x'} = 0 \quad . \quad (8.9)$$

Finally, rescaling position, time, and displacement, and dropping the primes, we arrive at the KdV equation,

$$u_t + 6uu_x + u_{xxx} = 0 \quad , \quad (8.10)$$

which is a convenient form.

8.1.1 KdV solitons

We seek a solution to the KdV equation of the form $u(x, t) = u(x - Vt)$. Then with $\xi \equiv x - Vt$, we have $\partial_x = \partial_\xi$ and $\partial_t = -V\partial_\xi$ when acting on $u(x, t) = u(\xi)$. Thus, we have

$$-Vu' + 6uu' + u''' = 0 \quad . \quad (8.11)$$

Integrating once, we have

$$-Vu + 3u^2 + u'' = A \quad , \quad (8.12)$$

where A is a constant. We can integrate once more, obtaining

$$-\frac{1}{2}Vu^2 + u^3 + \frac{1}{2}(u')^2 = Au + B \quad , \quad (8.13)$$

where now both A and B are constants. We assume that u and all its derivatives vanish in the limit $\xi \rightarrow \pm\infty$, which entails $A = B = 0$. Thus,

$$\frac{du}{d\xi} = \pm u \sqrt{V - 2u} \quad . \quad (8.14)$$

With the substitution

$$u = \frac{1}{2}V \operatorname{sech}^2 \theta \quad , \quad (8.15)$$

we find $d\theta = \mp \frac{1}{2}\sqrt{V} d\xi$, hence we have the solution

$$u(x, t) = \frac{1}{2}V \operatorname{sech}^2 \left(\frac{\sqrt{V}}{2} (x - Vt - \xi_0) \right) \quad . \quad (8.16)$$

Note that the maximum amplitude of the soliton is $u_{\max} = \frac{1}{2}V$, which is proportional to its velocity V . The KdV equation imposes no limitations on V other than $V \geq 0$.

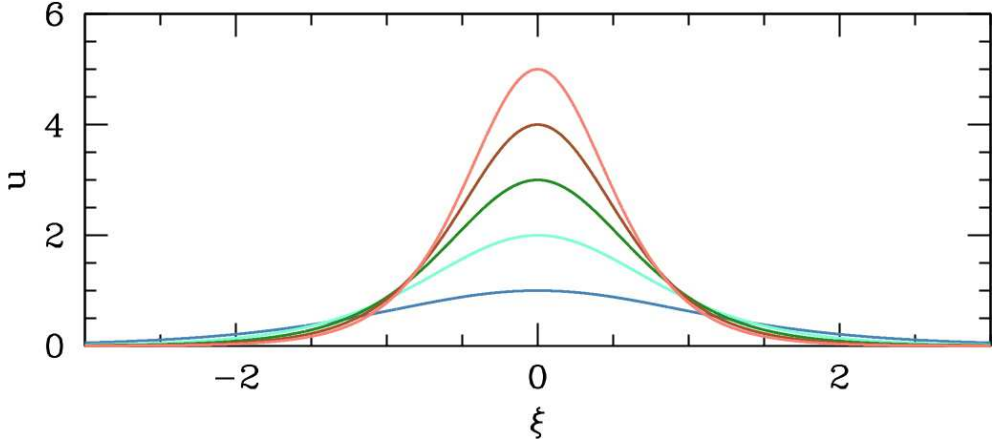


Figure 8.1: Soliton solutions to the KdV equation, with five evenly spaced V values ranging from $V = 2$ (blue) to $V = 10$ (orange). The greater the speed, the narrower the shape.

8.1.2 Periodic solutions : soliton trains

If we relax the condition $A = B = 0$, new solutions to the KdV equation arise. Define the cubic

$$\begin{aligned} P(u) &= 2u^3 - Vu^2 - 2Au - 2B \\ &\equiv 2(u - u_1)(u - u_2)(u - u_3) \quad , \end{aligned} \tag{8.17}$$

where $u_i = u_i(A, B, V)$. We presume that A , B , and V are such that all three roots $u_{1,2,3}$ are real and nondegenerate. Without further loss of generality, we may then assume $u_1 < u_2 < u_3$. Then

$$\frac{du}{d\xi} = \pm \sqrt{-P(u)} \quad . \tag{8.18}$$

Since $P(u) < 0$ for $u_2 < u < u_3$, we conclude $u(\xi)$ must lie within this range. Therefore, we have

$$\xi - \xi_0 = \pm \int_{u_2}^u \frac{ds}{\sqrt{-P(s)}} = \pm \left(\frac{2}{u_3 - u_1} \right)^{1/2} \int_0^\phi \frac{d\theta}{\sqrt{1 - k^2 \sin^2 \theta}} \quad , \tag{8.19}$$

where

$$u \equiv u_3 - (u_3 - u_2) \sin^2 \phi \quad , \quad k^2 \equiv \frac{u_3 - u_2}{u_3 - u_1} \quad . \tag{8.20}$$

The solution for $u(\xi)$ is then

$$u(\xi) = u_3 - (u_3 - u_2) \operatorname{sn}^2(\zeta, k) \quad , \tag{8.21}$$

where

$$\zeta = \sqrt{\frac{u_3 - u_1}{2}} (\xi - \xi_0) \tag{8.22}$$

and $\operatorname{sn}(\zeta, k)$ is the Jacobi elliptic function.

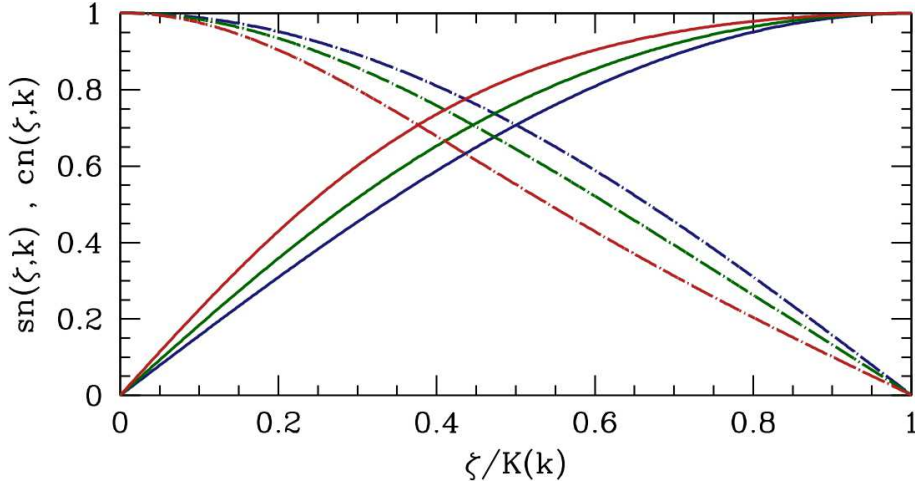


Figure 8.2: The Jacobi elliptic functions $\text{sn}(\zeta, k)$ (solid) and $\text{cn}(\zeta, k)$ (dot-dash) *versus* $\zeta/K(k)$, for $k = 0$ (blue), $k = \frac{1}{\sqrt{2}}$ (green), and $k = 0.9$ (red).

8.1.3 Interlude: primer on elliptic functions

We assume $0 \leq k^2 \leq 1$ and we define

$$\zeta(\phi, k) = \int_0^\phi \frac{d\theta}{\sqrt{1 - k^2 \sin^2 \theta}} \quad . \quad (8.23)$$

The sn and cn functions are defined by the relations

$$\begin{aligned} \text{sn}(\zeta, k) &= \sin \phi \\ \text{cn}(\zeta, k) &= \cos \phi \end{aligned} \quad . \quad (8.24)$$

Note that $\text{sn}^2(\zeta, k) + \text{cn}^2(\zeta, k) = 1$. One also defines the function dn(ζ, k) from the relation

$$\text{dn}^2(\zeta, k) + k^2 \text{sn}^2(\zeta, k) = 1 \quad . \quad (8.25)$$

When ϕ advances by one period, we have $\Delta\phi = 2\pi$, and therefore $\Delta\zeta = Z$, where

$$Z = \int_0^{2\pi} \frac{d\theta}{\sqrt{1 - k^2 \sin^2 \theta}} = 4 \mathbb{K}(k) \quad , \quad (8.26)$$

where $\mathbb{K}(k)$ is the complete elliptic integral of the first kind. Thus, $\text{sn}(\zeta + Z, k) = \text{sn}(\zeta, k)$, and similarly for the cn function. In fig. 8.2, we sketch the behavior of the elliptic functions over one quarter of a period. Note that for $k = 0$ we have $\text{sn}(\zeta, 0) = \sin \zeta$ and $\text{cn}(\zeta, 0) = \cos \zeta$.

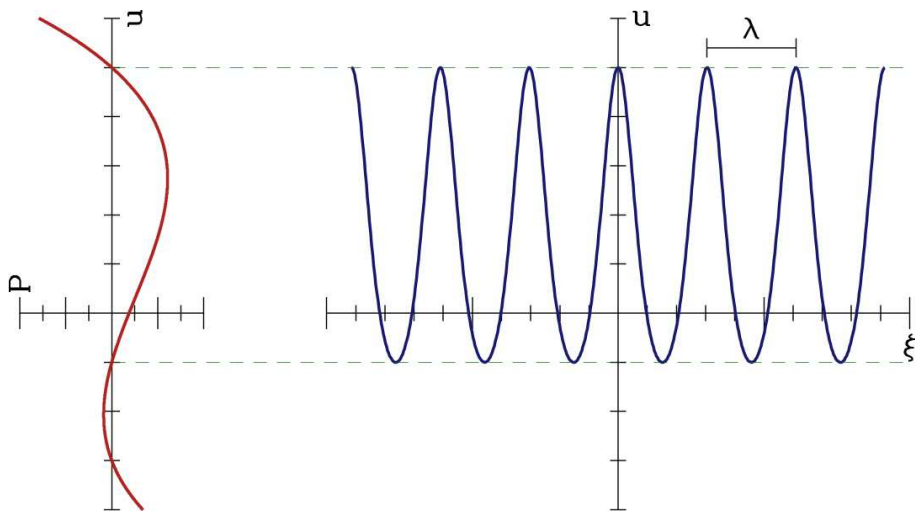


Figure 8.3: The cubic function $P(u)$ (left), and the soliton lattice (right) for the case $u_1 = -1.5$, $u_2 = -0.5$, and $u_3 = 2.5$.

8.1.4 The soliton lattice

Getting back to our solution in eqn. 8.21, we see that the solution describes a *soliton lattice* with a wavelength

$$\lambda = \frac{\sqrt{8} K(k)}{\sqrt{u_3 - u_1}} . \quad (8.27)$$

Note that our definition of $P(u)$ entails

$$V = 2(u_1 + u_2 + u_3) . \quad (8.28)$$

There is a simple mechanical analogy which merits illumination. Suppose we define

$$W(u) \equiv u^3 - \frac{1}{2}Vu^2 - Au , \quad (8.29)$$

and furthermore $E \equiv B$. Then

$$\frac{1}{2} \left(\frac{du}{d\xi} \right)^2 + W(u) = E , \quad (8.30)$$

which takes the form of a one-dimensional Newtonian mechanical system, if we replace $\xi \rightarrow t$ and interpret u_ξ as a velocity. The potential is $W(u)$ and the total energy is E . In terms of the polynomial $P(u)$, we have $P = 2(W - E)$. Accordingly, the ‘motion’ $u(\xi)$ is flattest for the lowest values of u , near $u = u_2$, which is closest to the local maximum of the function $W(u)$.

Note that specifying $u_{\min} = u_2$, $u_{\max} = u_3$, and the velocity V specifies all the parameters. Thus, we have a three parameter family of soliton lattice solutions.

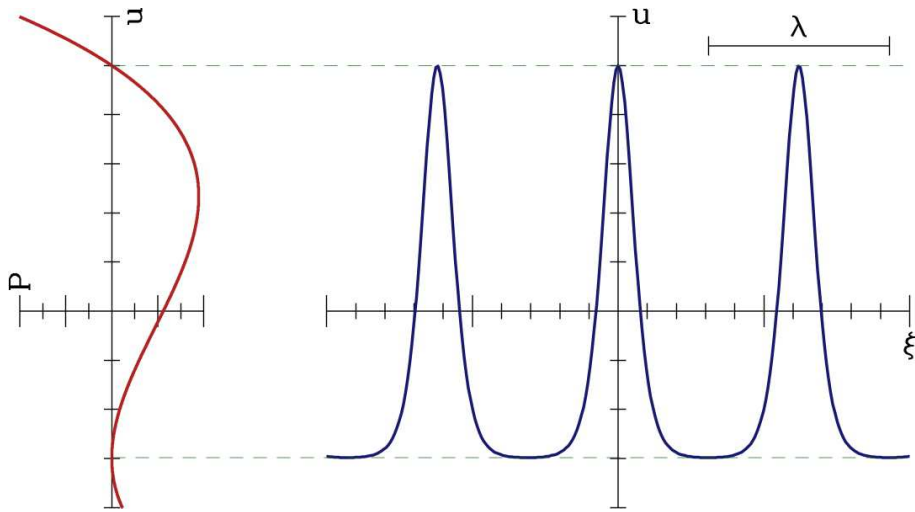


Figure 8.4: The cubic function $P(u)$ (left), and the soliton lattice (right) for the case $u_1 = -1.5$, $u_2 = -1.49$, and $u_3 = 2.50$.

8.1.5 N -soliton solutions to KdV

In 1971, Ryogo Hirota² showed that exact N -soliton solutions to the KdV equation exist. Here we discuss the Hirota solution, following the discussion in the book by Whitham.

The KdV equation may be written as

$$u_t + \{3u^2 + u_{xx}\}_x = 0 \quad , \quad (8.31)$$

which is in the form of the one-dimensional continuity equation $u_t + j_x = 0$, where the current is $j = 3u^2 + u_{xx}$. Let us define $u = p_x$. Then our continuity equation reads $p_{tx} + j_x = 0$, which can be integrated to yield $p_t + j = C$, where C is a constant. Demanding that u and its derivatives vanish at spatial infinity requires $C = 0$. Hence, we have

$$p_t + 3p_x^2 + p_{xxx} = 0 \quad . \quad (8.32)$$

Now consider the nonlinear transformation

$$p = 2(\ln F)_x = \frac{2F_x}{F} \quad . \quad (8.33)$$

We then have

$$p_t = \frac{2F_{xt}}{F} - \frac{2F_x F_t}{F^2} \quad , \quad p_x = \frac{2F_{xx}}{F} - \frac{2F_x^2}{F^2} \quad (8.34)$$

and

$$\begin{aligned} p_{xx} &= \frac{2F_{xxx}}{F} - \frac{6F_x F_{xx}}{F^2} + \frac{4F_x^3}{F^3} \\ p_{xxx} &= \frac{2F_{xxxx}}{F} - \frac{8F_x F_{xxx}}{F^2} - \frac{6F_x x^2}{F^2} + \frac{24F_x^2 F_{xx}}{F^3} - \frac{12F_x^4}{F^4} \end{aligned} \quad . \quad (8.35)$$

²R. Hirota, *Phys. Rev. Lett.* **27**, 1192 (1971).

When we add up the combination $p_t + 3p_x^2 + p_{xxx} = 0$, we find, remarkably, that the terms with F^3 and F^4 in the denominator cancel. We are then left with

$$F(F_t + F_{xxx})_x - F_x(F_t + F_{xxx}) + 3(F_{xx}^2 - F_x F_{xxx}) = 0 \quad . \quad (8.36)$$

This equation has the two-parameter family of solutions

$$F(x, t) = 1 + e^{\phi(x, t)} \quad . \quad (8.37)$$

where

$$\phi(x, t) = \alpha(x - b - \alpha^2 t) \quad , \quad (8.38)$$

with α and b constants. Note that these solutions are all annihilated by the operator $\partial_t + \partial_x^3$, and also by the last term in eqn. 8.36 because of the homogeneity of the derivatives. Converting back to our original field variable $u(x, t)$, we have that these solutions are single solitons:

$$u = p_x = \frac{2(F F_{xx} - F_x^2)}{F^2} = \frac{\alpha^2 f}{(1+f)^2} = \frac{1}{2}\alpha^2 \operatorname{sech}^2(\frac{1}{2}\phi) \quad . \quad (8.39)$$

The velocity for these solutions is $V = \alpha^2$.

If eqn. 8.36 were linear, our job would be done, and we could superpose solutions. We will meet up with such a felicitous situation when we discuss the Cole-Hopf transformation for the one-dimensional Burgers' equation. But for KdV the situation is significantly more difficult. We will write

$$F = 1 + F^{(1)} + F^{(2)} + \dots + F^{(N)} \quad , \quad (8.40)$$

with

$$F^{(1)} = f_1 + f_2 + \dots + f_N \quad , \quad (8.41)$$

where

$$\begin{aligned} f_j(x, t) &= e^{\phi_j(x, t)} \\ \phi_j(x, t) &= \alpha_j(x - \alpha_j^2 t - b_j) \quad . \end{aligned} \quad (8.42)$$

We may then derive a hierarchy of equations, the first two levels of which are

$$\begin{aligned} (F_t^{(1)} + F_{xxx}^{(1)})_x &= 0 \\ (F_t^{(2)} + F_{xxx}^{(2)})_x &= -3(F_{xx}^{(1)} F_{xx}^{(1)} - F_x^{(1)} F_{xxx}^{(1)}) \quad . \end{aligned} \quad (8.43)$$

Let's explore the case $N = 2$. The equation for $F^{(2)}$ becomes

$$(F_t^{(2)} + F_{xxx}^{(2)})_x = 3\alpha_1\alpha_2(\alpha_2 - \alpha_1)^2 f_1 f_2 \quad , \quad (8.44)$$

with solution

$$F^{(2)} = \left(\frac{\alpha_1 - \alpha_2}{\alpha_1 + \alpha_2}\right)^2 f_1 f_2 \quad . \quad (8.45)$$

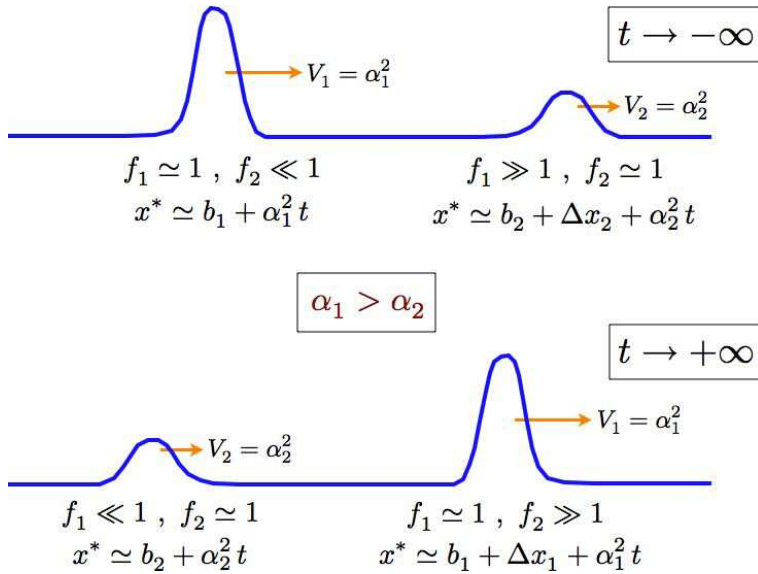


Figure 8.5: Early and late time configuration of the two soliton solution to the KdV equation.

Remarkably, this completes the hierarchy for $N = 2$. Thus,

$$\begin{aligned} F &= 1 + f_1 + f_2 + \left(\frac{\alpha_1 - \alpha_2}{\alpha_1 + \alpha_2} \right)^2 f_1 f_2 \\ &= \det \begin{pmatrix} 1 + f_1 & \frac{2\sqrt{\alpha_1 \alpha_2}}{\alpha_1 + \alpha_2} f_1 \\ \frac{2\sqrt{\alpha_1 \alpha_2}}{\alpha_1 + \alpha_2} f_2 & 1 + f_2 \end{pmatrix} . \end{aligned} \quad (8.46)$$

What Hirota showed, quite amazingly, is that this result generalizes to the N -soliton case,

$$F = \det Q , \quad (8.47)$$

where Q is matrix

$$Q_{mn} = \delta_{mn} + \frac{2\sqrt{\alpha_m \alpha_n}}{\alpha_m + \alpha_n} f_m . \quad (8.48)$$

Note that for $N = 2$ this agrees with Eqn. 8.46. Thus, N -soliton solutions to the KdV equation may be written in the form

$$u(x, t) = 2 \frac{\partial^2}{\partial x^2} \ln \det Q(x, t) . \quad (8.49)$$

Here we are free to make a similarity transformation $Q \rightarrow S^{-1} Q S$ for any nonsingular matrix S . If we take $S_{mn} = e^{\phi_n/2} \delta_{mn}$, then $Q \rightarrow \tilde{Q}$, where

$$\tilde{Q} = e^{-\phi_m/2} Q_{mn} e^{+\phi_n/2} = \delta_{mn} + \frac{2\sqrt{\alpha_m \alpha_n}}{\alpha_m + \alpha_n} \sqrt{f_m f_n} \quad (8.50)$$

is symmetric.

Consider the case $N = 2$. Direct, if tedious, calculations lead to the expression

$$u = 2 \frac{\alpha_1^2 f_1 + \alpha_2^2 f_2 + 2(\alpha_1 - \alpha_2)^2 f_1 f_2 + \left(\frac{\alpha_1 - \alpha_2}{\alpha_1 + \alpha_2}\right)^2 (\alpha_1^2 f_1 f_2^2 + \alpha_2^2 f_1^2 f_2)}{\left[1 + f_1 + f_2 + \left(\frac{\alpha_1 - \alpha_2}{\alpha_1 + \alpha_2}\right)^2 f_1 f_2\right]^2} . \quad (8.51)$$

Recall that

$$f_j(x, t) = \exp[\alpha_j(x_j - \alpha_j^2 t - b_j)] . \quad (8.52)$$

Let's consider (x, t) values for which $f_1 \simeq 1$ is neither large nor small, and investigate what happens in the limits $f_2 \ll 1$ and $f_2 \gg 1$. In the former case, we find

$$u \simeq \frac{2\alpha_1^2 f_1}{(1 + f_1)^2} \quad (f_2 \ll 1) , \quad (8.53)$$

which is identical to the single soliton case of eqn. 8.39. In the opposite limit, we have

$$u \simeq \frac{2\alpha_1^2 g_1}{(1 + g_1)^2} \quad (f_2 \gg 1) , \quad (8.54)$$

where

$$g_1 = \left(\frac{\alpha_1 - \alpha_2}{\alpha_1 + \alpha_2}\right)^2 f_1 \quad (8.55)$$

But multiplication of f_j by a constant C is equivalent to a translation:

$$C f_j(x, t) = f_j(x + \alpha_j^{-1} \ln C, t) \equiv f_j(x - \Delta x_j, t) . \quad (8.56)$$

Thus, depending on whether f_2 is large or small, the solution either acquires or does not acquire a spatial shift Δx_1 , where

$$\Delta x_j = \frac{2}{\alpha_j} \ln \left| \frac{\alpha_1 + \alpha_2}{\alpha_1 - \alpha_2} \right| . \quad (8.57)$$

The function $f(x, t) = \exp[\alpha(x - \alpha^2 t - b)]$ is monotonically increasing in x (assuming $\alpha > 0$). Thus, if at fixed t the spatial coordinate x is such that $f \ll 1$, this means that the soliton lies to the right. Conversely, if $f \gg 1$ the soliton lies to the left. Suppose $\alpha_1 > \alpha_2$, in which case soliton #1 is stronger (*i.e.* greater amplitude) and faster than soliton #2. The situation is as depicted in figs. 8.5 and 8.6. Starting at early times, the strong soliton lies to the left of the weak soliton. It moves faster, hence it eventually overtakes the weak soliton. As the strong soliton passes through the weak one, it is shifted *forward*, and the weak soliton is shifted *backward*. It hardly seems fair that the strong fast soliton gets pushed even further ahead at the expense of the weak slow one, but sometimes life is just like that³.

³See T. Piketty, *Capital in the Twenty-First Century* (Belknap Press, 2014).

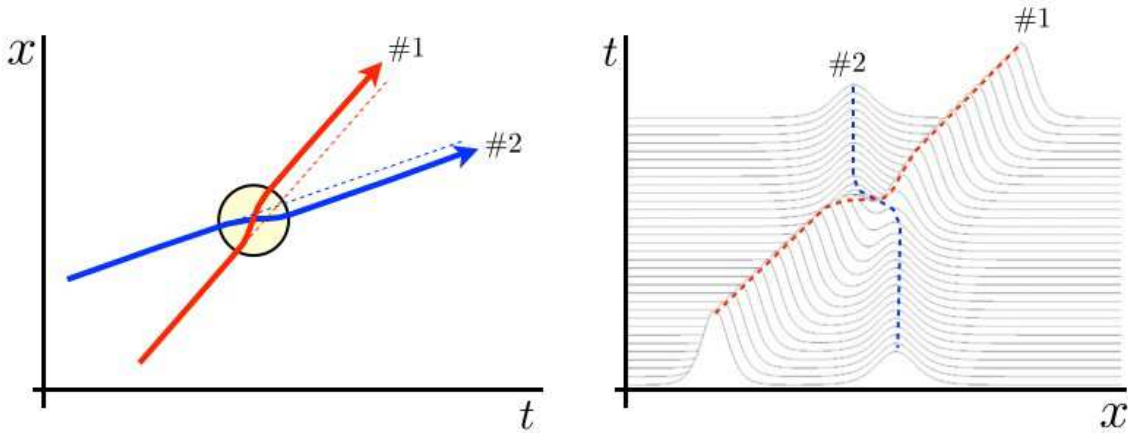


Figure 8.6: Left: Spacetime diagram (x versus t) for the collision of two KdV solitons. The strong, fast soliton (#1) is shifted forward and the weak slow one (#2) is shifted backward. The red and blue lines indicate the centers of the two solitons. The yellow shaded circle is the ‘interaction region’ where the solution is not simply a sum of the two single soliton waveforms. Right: t versus x showing the soliton waveforms through the collision. Here, the velocity of the slow soliton is close to zero. Note that the slow soliton is again shifted backward. From P. J. Caudrey, *Phil. Trans. Roy. Soc. A* **28**, 1215 (2011).

8.1.6 Bäcklund transformations

For certain nonlinear PDEs, a given solution may be used as a ‘seed’ to generate an entire hierarchy of solutions. This is familiar from the case of Riccati equations, which are nonlinear and nonautonomous ODEs, but for PDEs it is even more special. The general form of the Bäcklund transformation (BT) is

$$u_{1,t} = P(u_1, u_0, u_{0,t}, u_{0,x}) \quad (8.58)$$

$$u_{1,x} = Q(u_1, u_0, u_{0,t}, u_{0,x}) \quad , \quad (8.59)$$

where $u_0(x, t)$ is the known solution.

A Bäcklund transformation for the KdV equation was first obtained in 1973⁴. This provided a better understanding of the Hirota hierarchy. To proceed, following the discussion in the book by Scott, we consider the earlier (1968) result of Miura⁵, who showed that if $v(x, t)$ satisfies the modified KdV (MKdV) equation⁶,

$$v_t - 6v^2 v_x + v_{xxx} = 0 \quad , \quad (8.60)$$

then

$$u = -(v^2 + v_x) \quad (8.61)$$

solves KdV:

$$\begin{aligned} u_t + 6uu_x + u_{xxx} &= -(v^2 + v_x)_t + 6(v^2 + v_x)(v^2 + v_x)_x - (v^2 + v_x)_{xxx} \\ &= -(2v + \partial_x)(v_t - 6v^2 v_x + v_{xxx}) = 0 \quad . \end{aligned} \quad (8.62)$$

⁴H. D. Wahlquist and F. B. Eastabrook, *Phys. Rev. Lett.* **31**, 1386 (1973).

⁵R. M. Miura, *J. Math. Phys.* **9**, 1202 (1968).

⁶Note that the second term in the MKdV equation is proportional to $v^2 v_x$, as opposed to uu_x which appears in KdV.



Figure 8.7: “Wrestling’s living legend” Bob Backlund, in a 1983 match, is subjected to a devastating *camel clutch* by the Iron Sheikh. The American Bob Backlund has nothing to do with the Bäcklund transformations discussed in the text, which are named for the 19th century Swedish mathematician Albert Bäcklund. Note that Bob Backlund’s manager has thrown in the towel (lower right).

From this result, we have that if

$$v_t - 6(v^2 + \lambda) v_x + v_{xxx} = 0 \quad , \quad (8.63)$$

then

$$u = -(v^2 + v_x + \lambda) \quad (8.64)$$

solves KdV. The MKdV equation, however, is symmetric under $v \rightarrow -v$, hence

$$\begin{aligned} u_0 &= -v_x - v^2 - \lambda \\ u_1 &= +v_x - v^2 - \lambda \end{aligned} \quad (8.65)$$

both solve KdV. Now define $u_0 \equiv -w_{0,x}$ and $u_1 \equiv -w_{1,x}$. Subtracting the above two equations, we find

$$u_0 - u_1 = -2v_x \quad \Rightarrow \quad w_0 - w_1 = 2v \quad . \quad (8.66)$$

Adding the equations instead gives

$$\begin{aligned} w_{0,x} + w_{1,x} &= 2(v^2 + \lambda) \\ &= \frac{1}{2}(w_0 - w_1)^2 + 2\lambda \quad . \end{aligned} \quad (8.67)$$

Substituting for $v = \frac{1}{2}(w_0 - w_1)$ and $v^2 + \lambda = \frac{1}{2}(w_{0,x} + w_{1,x})$ into the MKdV equation, we have

$$(w_0 - w_1)_t - 3(w_{0,x}^2 - w_{1,x}^2) + (w_0 - w_1)_{xxx} = 0 \quad . \quad (8.68)$$

This last equation is a Bäcklund transformation (BT), although in a somewhat nonstandard form, since the RHS of eqn. 8.58, for example, involves only the ‘new’ solution u_1 and the ‘old’ solution u_0 and its first derivatives. Our equation here involves third derivatives. However, we can use eqn. 8.67 to express $w_{1,x}$ in terms of w_0 , $w_{0,x}$, and w_1 .

Starting from the trivial solution $w_0 = 0$, eqn. 8.67 gives

$$w_{1,x} = \frac{1}{2}w_1^2 + 2\lambda \quad . \quad (8.69)$$

With the choice $\lambda = -\frac{1}{4}\alpha^2 < 0$, we integrate and obtain

$$w_1(x, t) = -\alpha \tanh\left(\frac{1}{2}\alpha x + \varphi(t)\right) , \quad (8.70)$$

where $\varphi(t)$ is at this point arbitrary. We fix $\varphi(t)$ by invoking eqn. 8.68, which says

$$w_{1,t} = 3w_{1,x}^2 - w_{1,xxx} = 0 . \quad (8.71)$$

Invoking $w_{1,x} = \frac{1}{2}w_1^2 + \lambda$ and differentiating twice to obtain $w_{1,xxx}$, we obtain an expression for the RHS of the above equation. The result is $w_{1,t} + \alpha^2 w_{1,x} = 0$, hence

$$\begin{aligned} w_1(x, t) &= -\alpha \tanh\left[\frac{1}{2}\alpha(x - \alpha^2 t - b)\right] \\ u_1(x, t) &= \frac{1}{2}\alpha^2 \operatorname{sech}^2\left[\frac{1}{2}\alpha(x - \alpha^2 t - b)\right] , \end{aligned} \quad (8.72)$$

which recapitulates our earlier result. Of course we would like to do better, so let's try to insert this solution into the BT and the turn the crank and see what comes out. This is unfortunately a rather difficult procedure. It becomes tractable if we assume that successive Bäcklund transformations commute, which is the case, but which we certainly have not yet proven. That is, we assume that $w_{12} = w_{21}$, where

$$\begin{array}{ccccc} w_0 & \xrightarrow{\lambda_1} & w_1 & \xrightarrow{\lambda_2} & w_{12} \\ w_0 & \xrightarrow{\lambda_2} & w_2 & \xrightarrow{\lambda_1} & w_{21} \end{array} . \quad (8.73)$$

Invoking this result, we find that the Bäcklund transformation gives

$$w_{12} = w_{21} = w_0 - \frac{4(\lambda_1 - \lambda_2)}{w_1 - w_2} . \quad (8.74)$$

Successive applications of the BT yield Hirota's multiple soliton solutions:

$$w_0 \xrightarrow{\lambda_1} w_1 \xrightarrow{\lambda_2} w_{12} \xrightarrow{\lambda_3} w_{123} \xrightarrow{\lambda_4} \dots . \quad (8.75)$$

8.2 Sine-Gordon Model

Consider transverse electromagnetic waves propagating down a superconducting transmission line, shown in fig. 8.8. The transmission line is modeled by a set of inductors, capacitors, and Josephson junctions such that for a length dx of the transmission line, the capacitance is $dC = \mathcal{C} dx$, the inductance is $dL = \mathcal{L} dx$, and the critical current is $dI_0 = \mathcal{I}_0 dx$. Dividing the differential voltage drop dV and shunt current dI by dx , we obtain

$$\begin{aligned} \frac{\partial V}{\partial x} &= -\mathcal{L} \frac{\partial I}{\partial t} \\ \frac{\partial I}{\partial x} &= -\mathcal{C} \frac{\partial V}{\partial t} - \mathcal{I}_0 \sin \phi , \end{aligned} \quad (8.76)$$

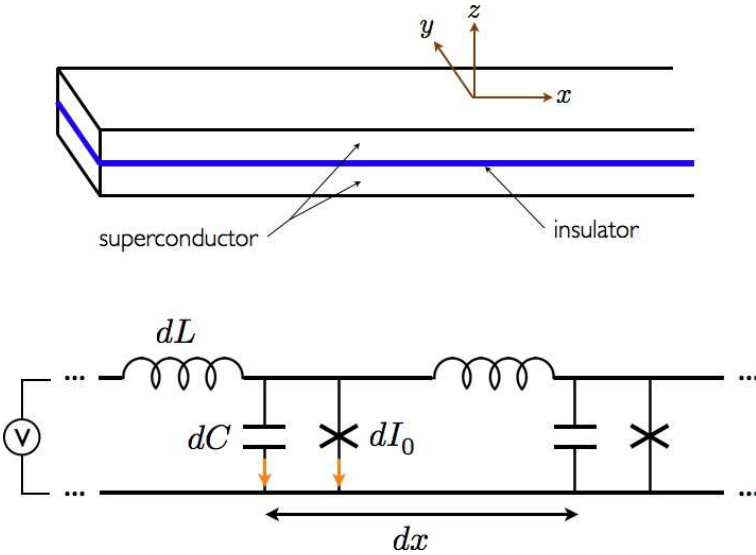


Figure 8.8: A superconducting transmission line is described by a capacitance per unit length \mathcal{C} , an inductance per unit length \mathcal{L} , and a critical current per unit length \mathcal{I}_0 . Based on fig. 3.4 of A. Scott, *Nonlinear Science*.

where ϕ is the difference $\phi = \phi_{\text{upper}} - \phi_{\text{lower}}$ in the superconducting phases. The voltage is related to the rate of change of ϕ through the Josephson equation,

$$\frac{\partial \phi}{\partial t} = \frac{2eV}{\hbar} , \quad (8.77)$$

and therefore

$$\frac{\partial \phi}{\partial x} = -\frac{2e\mathcal{L}}{\hbar} I . \quad (8.78)$$

Thus, we arrive at the equation

$$\frac{1}{c^2} \frac{\partial^2 \phi}{\partial t^2} - \frac{\partial^2 \phi}{\partial x^2} + \frac{1}{\lambda_J^2} \sin \phi = 0 , \quad (8.79)$$

where $c = (\mathcal{L}\mathcal{C})^{-1/2}$ is the *Swihart velocity* and $\lambda_J = (\hbar/2e\mathcal{L}\mathcal{I}_0)^{1/2}$ is the *Josephson length*. We may now rescale lengths by λ_J and times by λ_J/c to arrive at the *sine-Gordon equation*,

$$\phi_{tt} - \phi_{xx} + \sin \phi = 0 . \quad (8.80)$$

This equation of motion may be derived from the Lagrangian density

$$\mathcal{L} = \frac{1}{2} \phi_t^2 - \frac{1}{2} \phi_x^2 - U(\phi) . \quad (8.81)$$

We then obtain

$$\phi_{tt} - \phi_{xx} = -\frac{\partial U}{\partial \phi} , \quad (8.82)$$

and the sine-Gordon equation follows for $U(\phi) = 1 - \cos \phi$.

Assuming $\phi(x, t) = \phi(x - Vt)$ we arrive at $(1 - V^2) \phi_{\xi\xi} = U'(\xi)$, and integrating once we obtain

$$\frac{1}{2}(1 - V^2) \phi_{\xi\xi}^2 - U(\phi) = E \quad . \quad (8.83)$$

This describes a particle of mass $M = 1 - V^2$ moving in the *inverted potential* $-U(\phi)$. Assuming $V^2 < 1$, we may solve for ϕ_{ξ} :

$$\phi_{\xi\xi}^2 = \frac{2(E + U(\phi))}{1 - V^2} \quad , \quad (8.84)$$

which requires $E \geq -U_{\max}$ in order for a solution to exist. For $-U_{\max} < E < -U_{\min}$, the motion is bounded by turning points. The situation for the sine-Gordon (SG) model is sketched in fig. 8.9. For the SG model, the turning points are at $\phi_{\pm}^* = \pm \cos^{-1}(E + 1)$, with $-2 < E < 0$. We can write

$$\phi_{\pm}^* = \pi \pm \delta \quad , \quad \delta = 2 \cos^{-1} \sqrt{-\frac{E}{2}} \quad . \quad (8.85)$$

This class of solutions describes periodic waves. From

$$\frac{\sqrt{2} d\xi}{\sqrt{1 - V^2}} = \frac{d\phi}{\sqrt{E + U(\phi)}} \quad , \quad (8.86)$$

we have that the spatial period λ is given by

$$\lambda = \sqrt{2(1 - V^2)} \int_{\phi^*}^{2\pi - \phi^*} \frac{d\phi}{\sqrt{E + U(\phi)}} \quad , \quad (8.87)$$

where $\phi^* \in [0, \pi]$. If $E > -U_{\min}$, then ϕ_{ξ} is always of the same sign, and $\phi(\xi)$ is a monotonic function of ξ . If $U(\phi) = U(\phi + 2\pi)$ is periodic, then the solution is a ‘soliton lattice’ where the spatial period of $\phi \bmod 2\pi$ is

$$\tilde{\lambda} = \sqrt{\frac{1 - V^2}{2}} \int_0^{2\pi} \frac{d\phi}{\sqrt{E + U(\phi)}} \quad . \quad (8.88)$$

For the sine-Gordon model, with $U(\phi) = 1 - \cos \phi$, one finds

$$\lambda = \sqrt{8(1 - V^2)} \mathbb{K} \left(\sqrt{\frac{E + 2}{2}} \right) \quad , \quad (8.89)$$

where $\mathbb{K}(k)$ is the complete elliptic integral of the first kind⁷ and

$$\tilde{\lambda} = \sqrt{\frac{8(1 - V^2)}{E + 2}} \mathbb{K} \left(\sqrt{\frac{2}{E + 2}} \right) \quad . \quad (8.90)$$

⁷See the *NIST Handbook of Mathematical Functions*, ch. 19

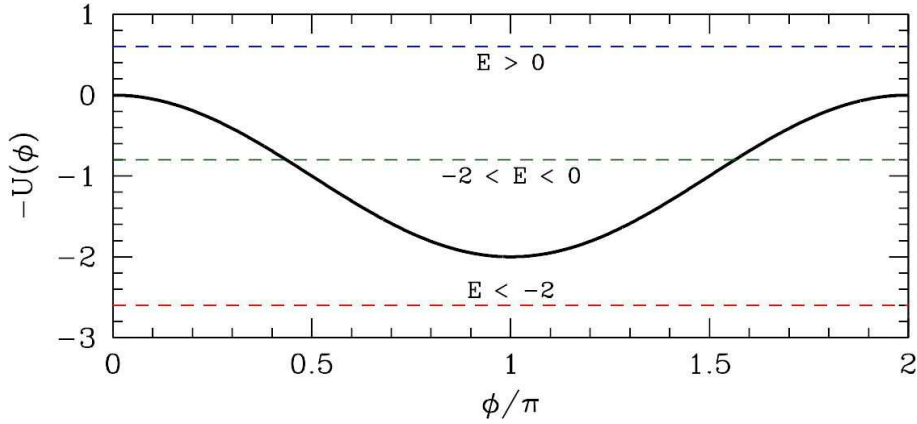


Figure 8.9: The inverted potential $-U(\phi) = \cos \phi - 1$ for the sine-Gordon problem.

8.2.1 Tachyon solutions

When $V^2 > 1$, we have

$$\frac{1}{2}(V^2 - 1)\phi_\xi^2 + U(\phi) = -E \quad . \quad (8.91)$$

Such solutions are called *tachyonic*. There are again three possibilities:

- $E > U_{\min}$: no solution.
- $-U_{\max} < E < -U_{\min}$: periodic $\phi(\xi)$ with oscillations about $\phi = 0$.
- $E < -U_{\max}$: tachyon lattice with monotonic $\phi(\xi)$.

It turns out that the tachyon solution is unstable.

8.2.2 Hamiltonian formulation

The Hamiltonian density is

$$\mathcal{H} = \pi \phi_t - \mathcal{L} \quad , \quad (8.92)$$

where

$$\pi = \frac{\partial \mathcal{L}}{\partial \phi_t} = \phi_t \quad (8.93)$$

is the momentum density conjugate to the field ϕ . Then

$$\mathcal{H}(\pi, \phi) = \frac{1}{2}\pi^2 + \frac{1}{2}\phi_x^2 + U(\phi) \quad . \quad (8.94)$$

Note that the total momentum in the field is

$$\begin{aligned} P &= \int_{-\infty}^{\infty} dx \pi = \int_{-\infty}^{\infty} dx \phi_t = -V \int_{-\infty}^{\infty} dx \phi_x \\ &= -V [\phi(\infty) - \phi(-\infty)] = -2\pi n V \quad , \end{aligned} \quad (8.95)$$

where $n = [\phi(\infty) - \phi(-\infty)]/2\pi$ is the *winding number*.

8.2.3 Phonons

The Hamiltonian density for the SG system is minimized when $U(\phi) = 0$ everywhere. The ground states are then classified by an integer $n \in \mathbb{Z}$, where $\phi(x, t) = 2\pi n$ for ground state n . Suppose we linearize the SG equation about one of these ground states, writing

$$\phi(x, t) = 2\pi n + \eta(x, t) , \quad (8.96)$$

and retaining only the first order term in η from the nonlinearity. The result is the Klein-Gordon (KG) equation,

$$\eta_{tt} - \eta_{xx} + \eta = 0 . \quad (8.97)$$

This is a linear equation, whose solutions may then be superposed. Fourier transforming from (x, t) to (k, ω) , we obtain the equation

$$(-\omega^2 + k^2 + 1) \hat{\eta}(k, \omega) = 0 , \quad (8.98)$$

which entails the dispersion relation $\omega = \pm\omega(k)$, where

$$\omega(k) = \sqrt{1 + k^2} . \quad (8.99)$$

Thus, the most general solution to the $(1+1)$ -dimensional KG equation is

$$\eta(x, t) = \int_{-\infty}^{\infty} \frac{dk}{2\pi} \left\{ A(k) e^{ikx} e^{-i\sqrt{1+k^2}t} + B(k) e^{ikx} e^{i\sqrt{1+k^2}t} \right\} . \quad (8.100)$$

For the Helmholtz equation $\eta_{tt} - \eta_{xx} = 0$, the dispersion is $\omega(k) = |k|$, and the solution may be written as $\eta(x, t) = f(x-t) + g(x+t)$, which is the sum of arbitrary right-moving and left-moving components. The fact that the Helmholtz equation preserves the shape of the wave is a consequence of the absence of dispersion, *i.e.* the phase velocity $v_p(k) = \frac{\omega}{k}$ is the same as the group velocity $v_g(k) = \frac{\partial\omega}{\partial k}$. This is not the case for the KG equation, obviously, since

$$v_p(k) = \frac{\omega}{k} = \frac{\sqrt{1+k^2}}{k} , \quad v_g(k) = \frac{\partial\omega}{\partial k} = \frac{k}{\sqrt{1+k^2}} , \quad (8.101)$$

hence $v_p v_g = 1$ for KG.

8.2.4 Mechanical realization

The sine-Gordon model can be realized mechanically by a set of pendula elastically coupled. The kinetic energy T and potential energy U are given by

$$\begin{aligned} T &= \sum_n \frac{1}{2} m \ell^2 \dot{\phi}_n^2 \\ U &= \sum_n \left[\frac{1}{2} \kappa (\phi_{n+1} - \phi_n)^2 + mg\ell(1 - \cos \phi_n) \right] . \end{aligned} \quad (8.102)$$

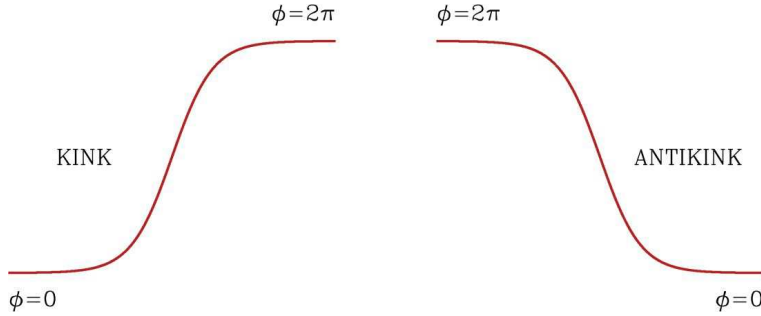


Figure 8.10: Kink and antikink solutions to the sine-Gordon equation.

Here ℓ is the distance from the hinge to the center-of-mass of the pendulum, and κ is the torsional coupling. From the Euler-Lagrange equations we obtain

$$m\ell^2 \ddot{\phi}_n = -\kappa(\phi_{n+1} + \phi_{n-1} - 2\phi_n) - mg\ell \sin \phi_n . \quad (8.103)$$

Let a be the horizontal spacing between the pendula. Then we can write the above equation as

$$\ddot{\phi}_n \overset{\equiv c^2}{=} \frac{\kappa a^2}{m\ell^2} \cdot \overbrace{\frac{1}{a} \left[\left(\frac{\phi_{n+1} - \phi_n}{a} \right) - \left(\frac{\phi_n - \phi_{n-1}}{a} \right) \right]}^{\approx \phi''_n} - \frac{g}{\ell} \sin \phi_n . \quad (8.104)$$

The continuum limit of these coupled ODEs yields the PDE

$$\frac{1}{c^2} \phi_{tt} - \phi_{xx} + \frac{1}{\lambda^2} \sin \phi = 0 , \quad (8.105)$$

which is the sine-Gordon equation, with $\lambda = (\kappa a^2 / mg\ell)^{1/2}$.

8.2.5 Kinks and antikinks

Let us return to eqn. 8.83 and this time set $E = -U_{\min}$. With $U(\phi) = 1 - \cos \phi$, we have $U_{\min} = 0$, and thus

$$\frac{d\phi}{d\xi} = \pm \frac{2}{\sqrt{1 - V^2}} \sin \left(\frac{1}{2}\phi \right) . \quad (8.106)$$

This equation may be integrated:

$$\pm \frac{d\xi}{\sqrt{1 - V^2}} = \frac{d\phi}{2 \sin \frac{1}{2}\phi} = d \ln \tan \frac{1}{4}\phi . \quad (8.107)$$

Thus, the solution is

$$\phi(x, t) = 4 \tan^{-1} \exp \left(\pm \frac{x - Vt - x_0}{\sqrt{1 - V^2}} \right) . \quad (8.108)$$

where ξ_0 is a constant of integration. This describes either a kink (with $d\phi/dx > 0$) or an antikink (with $d\phi/dx < 0$) propagating with velocity V , instantaneously centered at $x = x_0 + Vt$. Unlike the

KdV soliton, the amplitude of the SG soliton is independent of its velocity. The SG soliton is *topological*, interpolating between two symmetry-related vacuum states, namely $\phi = 0$ and $\phi = 2\pi$.

Note that the width of the kink and antikink solutions decreases as V increases. This is a Lorentz contraction, and should have been expected since the SG equation possesses a Lorentz invariance under transformations

$$x = \frac{x' + vt'}{\sqrt{1 - v^2}} \quad , \quad t = \frac{t' + vx'}{\sqrt{1 - v^2}} \quad . \quad (8.109)$$

One then readily finds

$$\partial_t^2 - \partial_x^2 = \partial_{t'}^2 - \partial_{x'}^2 \quad . \quad (8.110)$$

The moving soliton solutions may then be obtained by a Lorentz transformation of the stationary solution,

$$\phi(x, t) = 4 \tan^{-1} e^{\pm(x-x_0)} \quad . \quad (8.111)$$

The field ϕ itself is a Lorentz scalar, and hence does not change in magnitude under a Lorentz transformation.

8.2.6 Bäcklund transformation for the sine-Gordon system

Recall D'Alembert's method of solving the Helmholtz equation, by switching to variables

$$\zeta = \frac{1}{2}(x-t) \quad , \quad \tau = \frac{1}{2}(x+t) \quad , \quad \partial_x = \frac{1}{2}\partial_\zeta + \frac{1}{2}\partial_\tau \quad , \quad \partial_t = -\frac{1}{2}\partial_\zeta + \frac{1}{2}\partial_\tau \quad . \quad (8.112)$$

The D'Alembertian operator then becomes

$$\partial_t^2 - \partial_x^2 = -\partial_\zeta \partial_\tau \quad . \quad (8.113)$$

This transforms the Helmholtz equation $\phi_{tt} - \phi_{xx} = 0$ to $\phi_{\zeta\tau} = 0$, with solutions $\phi(\zeta, \tau) = f(\zeta) + g(\tau)$, with f and g arbitrary functions of their arguments. As applied to the SG equation, we have

$$\phi_{\zeta\tau} = \sin \phi \quad . \quad (8.114)$$

Suppose we have a solution ϕ_0 to this equation. Suppose further that ϕ_1 satisfies the pair of equations,

$$\phi_{1,\zeta} = 2\lambda \sin\left(\frac{\phi_1 + \phi_0}{2}\right) + \phi_{0,\zeta} \quad (8.115)$$

$$\phi_{1,\tau} = \frac{2}{\lambda} \sin\left(\frac{\phi_1 - \phi_0}{2}\right) - \phi_{0,\tau} \quad . \quad (8.116)$$

Thus,

$$\begin{aligned} \phi_{1,\zeta\tau} - \phi_{0,\zeta\tau} &= \lambda \cos\left(\frac{\phi_1 + \phi_0}{2}\right) (\phi_{1,\tau} + \phi_{0,\tau}) \\ &= 2 \cos\left(\frac{\phi_1 + \phi_0}{2}\right) \sin\left(\frac{\phi_1 - \phi_0}{2}\right) \\ &= \sin \phi_1 - \sin \phi_0 \quad . \end{aligned} \quad (8.117)$$

Thus, if $\phi_{0,\zeta\tau} = \sin \phi_0$, then $\phi_{1,\zeta\tau} = \sin \phi_1$ as well, and ϕ_1 satisfies the SG equation. Eqns. 8.115 and 8.116 constitute a Bäcklund transformation for the SG system.

Let's give the 'Bäcklund crank' one turn, starting with the trivial solution $\phi_0 = 0$. We then have

$$\phi_{1,\zeta} = 2\lambda \sin \frac{1}{2}\phi_1 \quad (8.118)$$

$$\phi_{1,\tau} = 2\lambda^{-1} \sin \frac{1}{2}\phi_1 \quad . \quad (8.119)$$

The solution to these equations is easily found by direct integration:

$$\phi(\zeta, \tau) = 4 \tan^{-1} e^{\lambda\zeta} e^{\tau/\lambda} \quad . \quad (8.120)$$

In terms of our original independent variables (x, t) , we have

$$\lambda\zeta + \lambda^{-1}\tau = \frac{1}{2}(\lambda + \lambda^{-1})x - \frac{1}{2}(\lambda - \lambda^{-1})t = \pm \frac{x - vt}{\sqrt{1 - v^2}} \quad , \quad (8.121)$$

where

$$v \equiv \frac{\lambda^2 - 1}{\lambda^2 + 1} \iff \lambda = \pm \left(\frac{1+v}{1-v} \right)^{1/2} \quad . \quad (8.122)$$

Thus, we generate the kink/antikink solution

$$\phi_1(x, t) = 4 \tan^{-1} \exp \left(\pm \frac{x - vt}{\sqrt{1 - v^2}} \right) \quad . \quad (8.123)$$

As was the case with the KdV system, successive Bäcklund transformations commute. Thus,

$$\begin{array}{c} \phi_0 \xrightarrow{\lambda_1} \phi_1 \xrightarrow{\lambda_2} \phi_{12} \\ \phi_0 \xrightarrow{\lambda_2} \phi_2 \xrightarrow{\lambda_1} \phi_{21} \end{array} \quad , \quad (8.124)$$

with $\phi_{12} = \phi_{21}$. This allows one to eliminate the derivatives and write

$$\tan \left(\frac{\phi_{12} - \phi_0}{4} \right) = \left(\frac{\lambda_1 + \lambda_2}{\lambda_1 - \lambda_2} \right) \tan \left(\frac{\phi_2 - \phi_1}{4} \right) \quad . \quad (8.125)$$

We can now create new solutions from individual kink pairs (KK), or kink-antikink pairs (KK). For KK, taking $v_1 = v_2 = v$ yields

$$\phi_{\text{KK}}(x, t) = 4 \tan^{-1} \left(\frac{v \sinh(\gamma x)}{\cosh(\gamma vt)} \right) \quad , \quad (8.126)$$

where γ is the Lorentz factor,

$$\gamma = \frac{1}{\sqrt{1 - v^2}} \quad . \quad (8.127)$$

Note that $\phi_{\text{KK}}(\pm\infty, t) = \pm 2\pi$ and $\phi_{\text{KK}}(0, t) = 0$, so there is a phase increase of 2π on each of the negative and positive half-lines for x , and an overall phase change of $+4\pi$. For the KK system, if we take $v_1 = -v_2 = v$, we obtain the solution

$$\phi_{\text{KK}}(x, t) = 4 \tan^{-1} \left(\frac{\sinh(\gamma vt)}{v \cosh(\gamma x)} \right) \quad . \quad (8.128)$$

In this case, analytically continuing to imaginary v with

$$v = \frac{i\omega}{\sqrt{1 - \omega^2}} \implies \gamma = \sqrt{1 - \omega^2} \quad (8.129)$$

yields the *stationary breather* solution,

$$\phi_B(x, t) = 4 \tan^{-1} \left(\frac{\sqrt{1 - \omega^2} \sin(\omega t)}{\omega \cosh(\sqrt{1 - \omega^2} x)} \right) . \quad (8.130)$$

The breather is a localized solution to the SG system which oscillates in time. By applying a Lorentz transformation of the spacetime coordinates, one can generate a moving breather solution as well.

Please note, in contrast to the individual kink/antikink solutions, the solutions ϕ_{KK} , $\phi_{K\bar{K}}$, and ϕ_B are not functions of a single variable $\xi = x - Vt$. Indeed, a given multisoliton solution may involve components moving at several different velocities. Therefore the total momentum P in the field is no longer given by the simple expression $P = V(\phi(-\infty) - \phi(+\infty))$. However, in cases where the multikink solutions evolve into well-separated solutions, as happens when the individual kink velocities are distinct, the situation simplifies, as we may consider each isolated soliton as linearly independent. We then have

$$P = -2\pi \sum_i n_i V_i , \quad (8.131)$$

where $n_i = +1$ for kinks and $n_i = -1$ for antikinks.

8.3 Nonlinear Schrödinger Equation

The Nonlinear Schrödinger (NLS) equation arises in several physical contexts. One is the Gross-Pitaevskii action for an interacting bosonic field,

$$S[\psi, \psi^*] = \int dt \int d^d x \left\{ i\psi^* \frac{\partial \psi}{\partial t} - \frac{\hbar^2}{2m} \nabla \psi^* \cdot \nabla \psi - U(|\psi|^2) + \mu \psi^* \psi \right\} , \quad (8.132)$$

where $\psi(x, t)$ is a complex scalar field. The local interaction $U(|\psi|^2)$ is taken to be quartic,

$$U(|\psi|^2) = \frac{1}{2}g |\psi|^4 . \quad (8.133)$$

Note that

$$U(|\psi|^2) - \mu |\psi|^2 = \frac{1}{2}g \left(|\psi|^2 - \frac{\mu}{g} \right)^2 - \frac{\mu^2}{2g} . \quad (8.134)$$

Extremizing the action with respect to ψ^* yields the equation

$$\frac{\delta S}{\delta \psi^*} = 0 = i \frac{\partial \psi}{\partial t} + \frac{\hbar^2}{2m} \nabla^2 \psi - U'(\psi^* \psi) \psi + \mu \psi . \quad (8.135)$$

Extremization with respect to ψ yields the complex conjugate equation. In $d = 1$, we have

$$i\psi_t = -\frac{\hbar^2}{2m} \psi_{xx} + U'(\psi^*\psi) \psi - \mu \psi . \quad (8.136)$$

We can absorb the chemical potential by making a time-dependent gauge transformation

$$\psi(x, t) \longrightarrow e^{i\mu t} \psi(x, t) . \quad (8.137)$$

Further rescalings of the field and independent variables yield the generic form

$$i\psi_t \pm \psi_{xx} + 2|\psi|^2 \psi = 0 , \quad (8.138)$$

where the $+$ sign pertains for the case $g < 0$ (attractive interaction), and the $-$ sign for the case $g > 0$ (repulsive interaction). These cases are known as *focusing*, or NLS(+), and *defocusing*, or NLS($-$), respectively.

8.3.1 Amplitude-phase representation

We can decompose the complex scalar ψ into its amplitude and phase:

$$\psi = A e^{i\phi} . \quad (8.139)$$

We then find

$$\begin{aligned} \psi_t &= (A_t + iA\phi_t) e^{i\phi} \\ \psi_x &= (A_x + iA\phi_x) e^{i\phi} \\ \psi_{xx} &= (A_{xx} - A\phi_x^2 + 2iA_x\phi_x + iA\phi_{xx}) e^{i\phi} . \end{aligned} \quad (8.140)$$

Multiplying the NLS(\pm) equations by $e^{-i\phi}$ and taking real and imaginary parts, we obtain the coupled nonlinear PDEs,

$$\begin{aligned} -A\phi_t \pm (A_{xx} - A\phi_x^2) + 2A^3 &= 0 \\ A_t \pm (2A_x\phi_x + A\phi_{xx}) &= 0 . \end{aligned} \quad (8.141)$$

Note that the second of these equations may be written in the form of a continuity equation,

$$\rho_t + j_x = 0 , \quad (8.142)$$

where

$$\begin{aligned} \rho &= A^2 \\ j &= \pm 2A^2\phi_x . \end{aligned} \quad (8.143)$$

8.3.2 Phonons

One class of solutions to NLS(\pm) is the spatially uniform case

$$\psi_0(x, t) = A_0 e^{2iA_0^2 t} , \quad (8.144)$$

with $A = A_0$ and $\phi = 2A_0^2 t$. Let's linearize about these solutions, writing

$$\begin{aligned} A(x, t) &= A_0 + \delta A(x, t) \\ \phi(x, t) &= 2A_0^2 t + \delta\phi(x, t) . \end{aligned} \quad (8.145)$$

Our coupled PDEs then yield

$$\begin{aligned} 4A_0^2 \delta A \pm \delta A_{xx} - A_0 \delta\phi_t &= 0 \\ \delta A_t \pm A_0 \delta\phi_{xx} &= 0 . \end{aligned} \quad (8.146)$$

Fourier transforming, we obtain

$$\begin{pmatrix} 4A_0^2 \mp k^2 & iA_0 \omega \\ -i\omega & \mp A_0 k^2 \end{pmatrix} \begin{pmatrix} \delta\hat{A}(k, \omega) \\ \delta\hat{\phi}(k, \omega) \end{pmatrix} = 0 . \quad (8.147)$$

Setting the determinant to zero, we obtain

$$\omega^2 = \mp 4A_0^2 k^2 + k^4 . \quad (8.148)$$

For NLS($-$), we see that $\omega^2 \geq 0$ for all k , meaning that the initial solution $\psi_0(x, t)$ is stable. For NLS($+$), however, we see that wavevectors $k \in [-2A_0, 2A_0]$ are *unstable*. This is known as the *Benjamin-Feir instability*.

8.3.3 Soliton solutions for NLS(+)

Let's consider moving soliton solutions for NLS(+). We try a two-parameter solution of the form

$$\begin{aligned} A(x, t) &= A(x - ut) \\ \phi(x, t) &= \phi(x - vt) . \end{aligned} \quad (8.149)$$

This results in the coupled ODEs

$$\begin{aligned} A_{xx} - A \phi_x^2 + vA \phi_x + 2A^3 &= 0 \\ A \phi_{xx} + 2A_x \phi_x - uA_x &= 0 . \end{aligned} \quad (8.150)$$

Multiplying the second equation by $2A$ yields

$$\left((2\phi_x - u) A^2 \right)_x = 0 \implies \phi_x = \frac{1}{2}u + \frac{P}{2A^2} , \quad (8.151)$$

where P is a constant of integration. Inserting this in the first equation results in

$$A_{xx} + 2A^3 + \frac{1}{4}(2uv - u^2)A + \frac{1}{2}(v - u)PA^{-1} - \frac{1}{4}PA^{-3} = 0 \quad . \quad (8.152)$$

We may write this as

$$A_{xx} + W'(A) = 0 \quad , \quad (8.153)$$

where

$$W(A) = \frac{1}{2}A^4 + \frac{1}{8}(2uv - u^2)A^2 + \frac{1}{2}(v - u)P \ln A + \frac{1}{8}PA^{-2} \quad (8.154)$$

plays the role of a potential. We can integrate eqn. 8.153 to yield

$$\frac{1}{2}A_x^2 + W(A) = E \quad , \quad (8.155)$$

where E is second constant of integration. This may be analyzed as a one-dimensional mechanics problem.

The simplest case to consider is $P = 0$, in which case

$$W(A) = \frac{1}{2}(A^2 + \frac{1}{2}uv - \frac{1}{4}u^2)A^2 \quad . \quad (8.156)$$

If $u^2 < 2uv$, then $W(A)$ is everywhere nonnegative and convex, with a single global minimum at $A = 0$, where $W(0) = 0$. The analog mechanics problem tells us that A will oscillate between $A = 0$ and $A = A^*$, where $W(A^*) = E > 0$. There are no solutions with $E < 0$. If $u^2 > 2uv$, then $W(A)$ has a double well shape⁸. If $E > 0$ then the oscillations are still between $A = 0$ and $A = A^*$, but if $E < 0$ then there are two positive solutions to $W(A) = E$. In this latter case, we may write

$$F(A) \equiv 2[E - W(A)] = (A^2 - A_0^2)(A_1^2 - A^2) \quad , \quad (8.157)$$

where $A_0 < A_1$ and

$$\begin{aligned} E &= -\frac{1}{2}A_0^2 A_1^2 \\ \frac{1}{4}u^2 - \frac{1}{2}uv &= A_0^2 + A_1^2 \quad . \end{aligned} \quad (8.158)$$

The amplitude oscillations are now between $A = A_0^*$ and $A = A_1^*$. The solution is given in terms of Jacobi elliptic functions:

$$\psi(x, t) = A_1 \exp \left[\frac{i}{2}u(x - vt) \right] \operatorname{dn}(A_1(x - ut - \xi_0), k) \quad , \quad (8.159)$$

where

$$k^2 = 1 - \frac{A_0^2}{A_1^2} \quad . \quad (8.160)$$

The simplest case is $E = 0$, for which $A_0 = 0$. We then obtain

$$\psi(x, t) = A^* \exp \left[\frac{i}{2}u(x - vt) \right] \operatorname{sech}(A^*(x - ut - \xi_0)) \quad , \quad (8.161)$$

where $4A^{*2} = u^2 - 2uv$. When $u = 0$ we obtain the stationary breather solution, for which the entire function $\psi(x, t)$ oscillates uniformly.

⁸Although we have considered $A > 0$ to be an amplitude, there is nothing wrong with allowing $A < 0$. When $A(t)$ crosses $A = 0$, the phase $\phi(t)$ jumps by $\pm \pi$.

8.3.4 Dark solitons for NLS(–)

The small oscillations of NLS(–) are stable, as we found in our phonon calculation. It is therefore perhaps surprising to note that this system also supports solitons. We write

$$\psi(x, t) = \sqrt{\rho_0} e^{2i\rho_0 t} e^{i\alpha} Z(x, t) , \quad (8.162)$$

with α an arbitrary constant. This yields

$$iZ_t = Z_{xx} + 2\rho_0(1 - |Z|^2)Z . \quad (8.163)$$

We then write $Z = X + iY$, yielding

$$\begin{aligned} X_t &= Y_{xx} + 2\rho_0(1 - X^2 - Y^2)Y \\ -Y_t &= X_{xx} + 2\rho_0(1 - X^2 - Y^2)X . \end{aligned} \quad (8.164)$$

We try $Y = Y_0$, a constant, and set $X(x, t) = X(x - Vt)$. Then

$$\begin{aligned} -VX_\xi &= 2\rho_0 Y_0(1 - Y_0^2 - X^2) \\ 0 &= X_{\xi\xi} + 2\rho_0(1 - Y_0^2 - X^2)X \end{aligned} \quad (8.165)$$

Thus,

$$X_\xi = -\frac{2\rho_0 Y_0}{V}(1 - Y_0^2 - X^2) , \quad (8.166)$$

from which it follows that

$$\begin{aligned} X_{\xi\xi} &= \frac{4\rho_0 Y_0}{V} XX_\xi \\ &= -\frac{8\rho_0^2 Y_0^2}{V}(1 - Y_0^2 - X^2)X = \frac{4\rho_0 Y_0^2}{V^2} X_{\xi\xi} . \end{aligned} \quad (8.167)$$

Thus, in order to have a solution, we must have

$$V = \pm 2\sqrt{\rho_0} Y_0 . \quad (8.168)$$

We now write $\xi = x - Vt$, in which case, from Eqn. 8.166,

$$\sqrt{\rho_0} d\xi = \mp \frac{dX}{1 - Y_0^2 - X^2} . \quad (8.169)$$

From this point, the derivation is elementary. One writes $X = \sqrt{1 - Y_0^2} \tilde{X}$, and integrates to obtain

$$\tilde{X}(\xi) = \mp \tanh\left(\sqrt{\rho_0(1 - Y_0^2)} (\xi - \xi_0)\right) . \quad (8.170)$$

We simplify the notation by writing $Y_0 = \sin \beta$. Then

$$\psi(x, t) = \sqrt{\rho_0} e^{i\alpha} e^{2i\rho_0 t} \left[\mp \tanh\left(\sqrt{\rho_0} \cos \beta (x - Vt - \xi_0)\right) \cos \beta + i \sin \beta \right] , \quad (8.171)$$

where α is a constant and $V = \pm 2\sqrt{\rho_0} \sin \beta$. The density $\rho = |\psi|^2$ is then given by

$$\rho(x, t) = \rho_0 \left[1 - \operatorname{sech}^2 \left(\sqrt{\rho_0} \cos \beta (x - Vt - \xi_0) \right) \right] . \quad (8.172)$$

This is called a *dark soliton* because the density $\rho(x, t)$ is minimized at the center of the soliton, where $\rho = \rho_0 \sin^2 \beta$, which is smaller than the asymptotic $|x| \rightarrow \infty$ value of $\rho(\pm\infty, t) = \rho_0$.

Chapter 9

Shock Waves

Here we shall follow closely the pellucid discussion in chapter 2 of the book by G. Whitham, beginning with the simplest possible PDE, describing *chiral* (unidirectional motion) waves,

$$\rho_t + c_0 \rho_x = 0 \quad . \quad (9.1)$$

The solution to this equation is an arbitrary right-moving wave (assuming $c_0 > 0$), with profile

$$\rho(x, t) = f(x - c_0 t) \quad , \quad (9.2)$$

where the initial conditions on Eqn. 9.1 are $\rho(x, t = 0) = f(x)$. This is even simpler than the Helmholtz equation, $\rho_{tt} = c_0^2 \rho_{xx}$, which is nonchiral, *i.e.* waves move in either direction. Anyway, nothing to see here, so move along.

9.1 Nonlinear Chiral Wave Equation

The simplest nonlinear PDE is a generalization of Eqn. 9.1,

$$\rho_t + c(\rho) \rho_x = 0 \quad . \quad (9.3)$$

This equation arises in a number of contexts. One example comes from the theory of vehicular traffic flow along a single lane roadway. Starting from the continuity equation,

$$\rho_t + j_x = 0 \quad , \quad (9.4)$$

one posits a constitutive relation $j = J(\rho)$, in which case $c(\rho) = J'(\rho)$. If the individual vehicles move with a velocity $v = v(\rho)$, then

$$J(\rho) = \rho v(\rho) \quad \Rightarrow \quad c(\rho) = v(\rho) + \rho v'(\rho) \quad . \quad (9.5)$$

It is natural to assume a form $v(\rho) = c_0(1 - a\rho)$, so that at low densities one has $v \approx c_0$, with $v(\rho)$ decreasing monotonically to $v = 0$ at a critical density $\rho = a^{-1}$, presumably corresponding to bumper-to-bumper traffic. The current $J(\rho)$ then takes the form of an inverted parabola. Note the difference

between the individual vehicle velocity $v(\rho)$ and what turns out to be the group velocity of a traffic wave, $c(\rho)$. For $v(\rho) = c_0(1 - a\rho)$, one has $c(\rho) = c_0(1 - 2a\rho)$, which is negative for $\rho \in [\frac{1}{2}a^{-1}, a^{-1}]$. For vehicular traffic, we have $c'(\rho) = J''(\rho) < 0$ but in general $J(\rho)$ and thus $c(\rho)$ can be taken to be arbitrary.

Another example comes from the study of chromatography, which refers to the spatial separation of components in a mixture which is forced to flow through an immobile absorbing ‘bed’. Let $\rho(x, t)$ denote the density of the desired component in the fluid phase and $n(x, t)$ be its density in the solid phase. Then continuity requires

$$n_t + \rho_t + V\rho_x = 0 \quad , \quad (9.6)$$

where V is the velocity of the flow, which is assumed constant. The net rate at which the component is deposited from the fluid onto the solid is given by an equation of the form

$$n_t = F(n, \rho) \quad . \quad (9.7)$$

In equilibrium, we then have $F(n, \rho) = 0$, which may in principle be inverted to yield $n = n_{\text{eq}}(\rho)$. If we assume that the local deposition processes run to equilibrium on fast time scales, then we may substitute $n(x, t) \approx n_{\text{eq}}(\rho(x, t))$ into Eqn. 9.6 and obtain

$$\rho_t + c(\rho)\rho_x = 0 \quad , \quad c(\rho) = \frac{V}{1 + n'_{\text{eq}}(\rho)} \quad . \quad (9.8)$$

9.1.1 The method of characteristics

We solve Eqn. 9.3 using the *method of characteristics*. Suppose we have the solution $\rho = \rho(x, t)$. Consider then the family of curves obeying the ODE

$$\frac{dx}{dt} = c(\rho(x, t)) \quad . \quad (9.9)$$

This is a family of curves, rather than a single curve, because it is parameterized by the initial condition $x(0) \equiv \zeta$. Now along any one of these curves we must have

$$\frac{d\rho}{dt} = \frac{\partial\rho}{\partial t} + \frac{\partial\rho}{\partial x} \frac{dx}{dt} = \frac{\partial\rho}{\partial t} + c(\rho) \frac{\partial\rho}{\partial x} = 0 \quad . \quad (9.10)$$

Thus, $\rho(x, t)$ is a constant along each of these curves, which are called *characteristics*. For Eqn. 9.3, the family of characteristics is a set of straight lines¹,

$$x_\zeta(t) = \zeta + c(\rho) t \quad . \quad (9.11)$$

The initial conditions for the function $\rho(x, t)$ are

$$\rho(x = \zeta, t = 0) = f(\zeta) \quad , \quad (9.12)$$

¹The existence of straight line characteristics is a special feature of the equation $\rho_t + c(\rho)\rho_x = 0$. For more general hyperbolic first order PDEs to which the method of characteristics may be applied, the characteristics are curves. See the discussion in the Appendix.

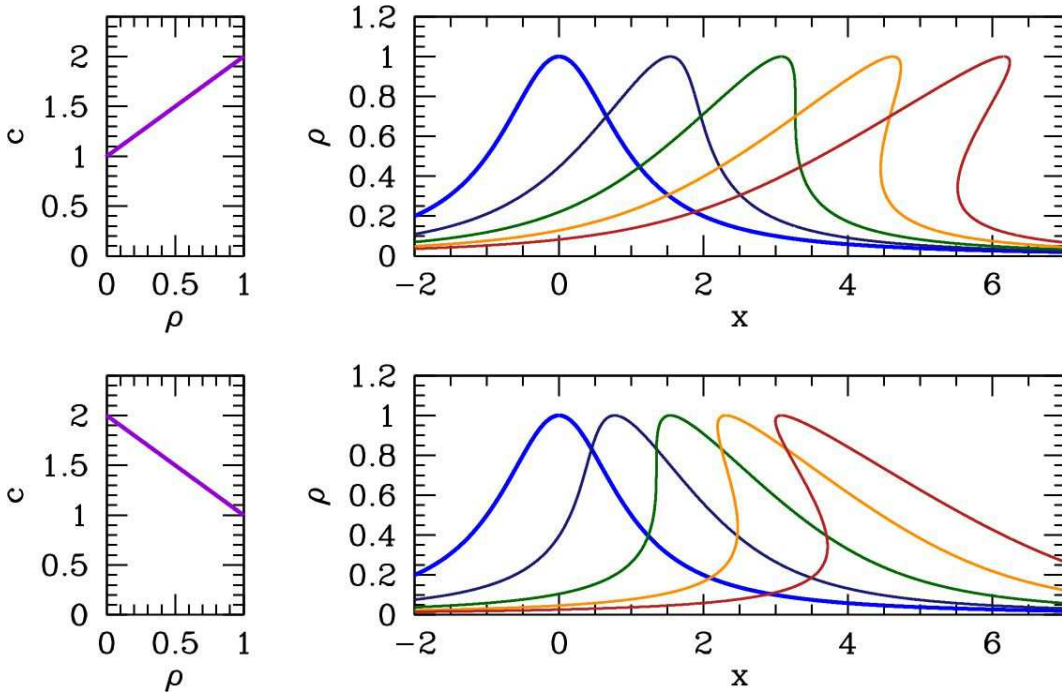


Figure 9.1: Forward and backward breaking waves for the nonlinear chiral wave equation $\rho_t + c(\rho) \rho_x = 0$, with $c(\rho) = 1 + \rho$ (top panels) and $c(\rho) = 2 - \rho$ (bottom panels). The initial conditions are $\rho(x, t = 0) = 1/(1 + x^2)$, corresponding to a break time of $t_B = \frac{16}{3\sqrt{3}}$. Successive $\rho(x, t)$ curves are plotted for $t = 0$ (thick blue), $t = \frac{1}{2}t_B$ (dark blue), $t = t_B$ (dark green), $t = \frac{3}{2}t_B$ (orange), and $t = 2t_B$ (dark red).

where $f(\zeta)$ is arbitrary. Thus, in the (x, t) plane, if the characteristic curve $x(t)$ intersects the line $t = 0$ at $x = \zeta$, then its slope is constant and equal to $c(f(\zeta))$. We then define

$$g(\zeta) \equiv c(f(\zeta)) . \quad (9.13)$$

This is a known function, computed from $c(\rho)$ and $f(\zeta) = \rho(x = \zeta, t = 0)$. The equation of the characteristic $x_\zeta(t)$ is then

$$x_\zeta(t) = \zeta + g(\zeta) t . \quad (9.14)$$

Do not confuse the subscript in $x_\zeta(t)$ for a derivative!

To find $\rho(x, t)$, we follow this prescription:

- (i) Given any point in the (x, t) plane, we find the characteristic $x_\zeta(t)$ on which it lies. This means we invert the equation $x = \zeta + g(\zeta) t$ to find $\zeta(x, t)$.
- (ii) The value of $\rho(x, t)$ is then $\rho = f(\zeta(x, t))$.
- (iii) Equivalently, at fixed t , for $\zeta \in (-\infty, +\infty)$ plot $\rho = f(\zeta)$ vs. $x = \zeta + g(\zeta)t$. This obviates the inversion in (i).

- (iv) This procedure yields a unique value for $\rho(x, t)$ provided the characteristics do not cross, *i.e.* provided that there is a unique ζ such that $x = \zeta + g(\zeta)t$. If the characteristics do cross, then $\rho(x, t)$ is either *multi-valued*, or else the method has otherwise broken down. As we shall see, the crossing of characteristics, under the conditions of single-valuedness for $\rho(x, t)$, means that a *shock* has developed, and that $\rho(x, t)$ is *discontinuous*.

We can verify that this procedure yields a solution to the original PDE of Eqn. 9.3 in the following manner. Suppose we invert

$$x = \zeta + g(\zeta)t \quad \Rightarrow \quad \zeta = \zeta(x, t) . \quad (9.15)$$

We then have

$$\rho(x, t) = f(\zeta(x, t)) \quad \Rightarrow \quad \begin{cases} \rho_t = f'(\zeta)\zeta_t \\ \rho_x = f'(\zeta)\zeta_x \end{cases} \quad (9.16)$$

To find ζ_t and ζ_x , we invoke $x = \zeta + g(\zeta)t$, hence

$$\begin{aligned} 0 &= \frac{\partial}{\partial t} [\zeta + g(\zeta)t - x] = \zeta_t + \zeta_t g'(\zeta)t + g(\zeta) \\ 0 &= \frac{\partial}{\partial x} [\zeta + g(\zeta)t - x] = \zeta_x + \zeta_x g'(\zeta)t - 1 , \end{aligned} \quad (9.17)$$

from which we conclude

$$\rho_t = -\frac{f'(\zeta)g(\zeta)}{1+g'(\zeta)t} , \quad \rho_x = \frac{f'(\zeta)}{1+g'(\zeta)t} . \quad (9.18)$$

Thus, $\rho_t + c(\rho)\rho_x = 0$, since $c(\rho) = g(\zeta)$.

As any wave disturbance propagates, different values of ρ propagate with their own velocities. Thus, the solution $\rho(x, t)$ can be constructed by splitting the curve $\rho(x, t=0)$ into level sets of constant ρ , and then shifting each such set by a distance $c(\rho)t$. For $c(\rho) = c_0$, the entire curve is shifted uniformly. When $c(\rho)$ varies, different level sets are shifted by different amounts.

9.1.2 Breaking waves: when characteristics intersect

We see that ρ_x diverges when $1 + g'(\zeta)t = 0$. At this time, the wave is said to *break*. The break time t_B is defined to be the smallest value of t for which $\rho_x = \infty$ anywhere. Thus,

$$t_B = \min_{\substack{\zeta \\ g'(\zeta) < 0}} \left(-\frac{1}{g'(\zeta)} \right) \equiv -\frac{1}{g'(\zeta_B)} . \quad (9.19)$$

Breaking can only occur when $g'(\zeta) < 0$, and differentiating $g(\zeta) = c(f(\zeta))$, we have that $g'(\zeta) = c'(f)f'(\zeta)$. We then conclude

$$\begin{aligned} c' < 0 &\implies \text{need } f' > 0 \text{ to break} \\ c' > 0 &\implies \text{need } f' < 0 \text{ to break} \end{aligned} . \quad (9.20)$$

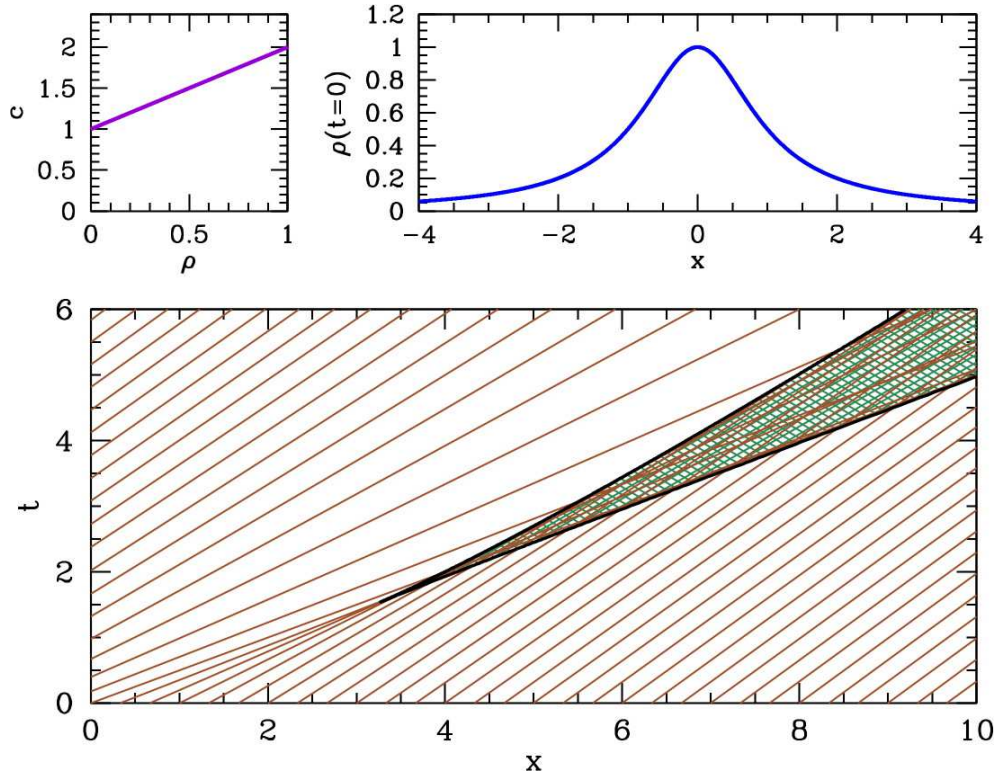


Figure 9.2: Crossing of characteristics of the nonlinear chiral wave equation $\rho_t + c(\rho) \rho_x = 0$, with $c(\rho) = 1 + \rho$ and $\rho(x, t = 0) = 1/(1 + x^2)$. Within the green hatched region of the (x, t) plane, the characteristics cross, and the function $\rho(x, t)$ is apparently multivalued.

Thus, if $\rho(x = \zeta, t = 0) = f(\zeta)$ has a hump profile, then the wave breaks forward (*i.e.* in the direction of its motion) if $c' > 0$ and backward (*i.e.* opposite to the direction of its motion) if $c' < 0$. In Fig. 9.1 we sketch the breaking of a wave with $\rho(x, t = 0) = 1/(1 + x^2)$ for the cases $c = 1 + \rho$ and $c = 2 - \rho$. Note that it is possible for different regions of a wave to break at different times, if, say, it has multiple humps.

Wave breaking occurs when neighboring characteristic cross. We can see this by comparing two neighboring characteristics,

$$x_\zeta(t) = \zeta + g(\zeta) t \quad (9.21)$$

and

$$\begin{aligned} x_{\zeta+\delta\zeta}(t) &= \zeta + \delta\zeta + g(\zeta + \delta\zeta) t \\ &= \zeta + g(\zeta) t + (1 + g'(\zeta) t) \delta\zeta + \dots \end{aligned} \quad (9.22)$$

For these characteristics to cross, we demand

$$x_\zeta(t) = x_{\zeta+\delta\zeta}(t) \implies t = -\frac{1}{g'(\zeta)} . \quad (9.23)$$

Usually, in most physical settings, the function $\rho(x, t)$ is single-valued. In such cases, when the wave

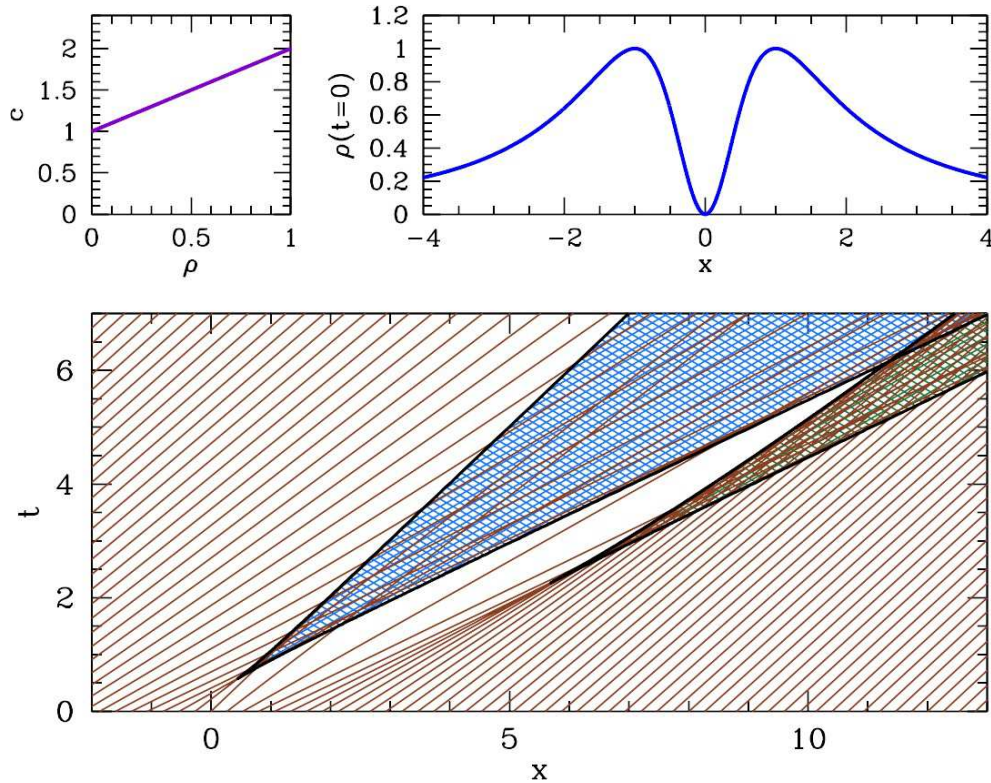


Figure 9.3: Crossing of characteristics of the nonlinear chiral wave equation $\rho_t + c(\rho) \rho_x = 0$, with $c(\rho) = 1 + \rho$ and $\rho(x, t = 0) = [x/(1 + x^2)]^2$. The wave now breaks in two places and is multivalued in both hatched regions. The left hump is the first to break.

breaks, the multivalued solution ceases to be applicable². Generally speaking, this means that some important physics has been left out. For example, if we neglect viscosity η and thermal conductivity κ , then the equations of gas dynamics have breaking wave solutions similar to those just discussed. When the gradients are steep – just before breaking – the effects of η and κ are no longer negligible, even if these parameters are small. This is because these parameters enter into the coefficients of higher derivative terms in the governing PDEs, and even if they are small their effect is magnified in the presence of steep gradients. In mathematical parlance, they constitute *singular perturbations*. The shock wave is then a thin region in which η and κ are crucially important, and the flow changes rapidly throughout this region. If one is not interested in this small scale physics, the shock region can be approximated as being infinitely thin, *i.e.* as a discontinuity in the inviscid limit of the theory. What remains is a set of *shock conditions* which govern the discontinuities of various quantities across the shocks.

²This is even true for water waves, where one might think that a multivalued height function $h(x, t)$ is physically possible.

9.2 Shocks

We now show that a solution to Eqn. 9.3 exists which is single valued for almost all (x, t) , i.e. everywhere with the exception of a set of zero measure, but which has a discontinuity along a curve $x = x_s(t)$. This discontinuity is the shock wave.

The velocity of the shock is determined by mass conservation, and is most easily obtained in the frame of the shock. The situation is as depicted in Fig. 9.4. If the density and current are (ρ_-, j_-) to the left of the shock and (ρ_+, j_+) to the right of the shock, and if the shock moves with velocity v_s , then making a Galilean transformation to the frame of the shock, the densities do not change but the currents transform as $j \rightarrow j' = j - \rho v$. Thus, in the frame where the shock is stationary, the current on the left and right are $j_{\pm} = j_{\pm} - \rho_{\pm} v_s$. Current conservation then requires

$$v_s = \frac{j_+ - j_-}{\rho_+ - \rho_-} = \frac{\Delta j}{\Delta \rho} . \quad (9.24)$$

The special case of quadratic $J(\rho)$ bears mention. Suppose

$$J(\rho) = \alpha\rho^2 + \beta\rho + \gamma . \quad (9.25)$$

Then $c = 2\alpha\rho + \beta$ and

$$\begin{aligned} v_s &= \alpha(\rho_+ + \rho_-) + \beta \\ &= \frac{1}{2}(c_+ + c_-) . \end{aligned} \quad (9.26)$$

So for quadratic $J(\rho)$, the shock velocity is simply the average of the flow velocity on either side of the shock.

Consider, for example, a model with $J(\rho) = 2\rho(1 - \rho)$, for which $c(\rho) = 2 - 4\rho$. Consider an initial condition $\rho(x = \zeta, t = 0) = f(\zeta) = \frac{3}{16} + \frac{1}{8}\Theta(\zeta)$, so initially $\rho = \rho_1 = \frac{3}{16}$ for $x < 0$ and $\rho = \rho_2 = \frac{5}{16}$ for $x > 0$. The lower density part moves faster, so in order to avoid multiple-valuedness, a shock must propagate. We find $c_- = \frac{5}{4}$ and $c_+ = \frac{3}{4}$. The shock velocity is then $v_s = 1$. This situation is depicted in Fig. 9.5.

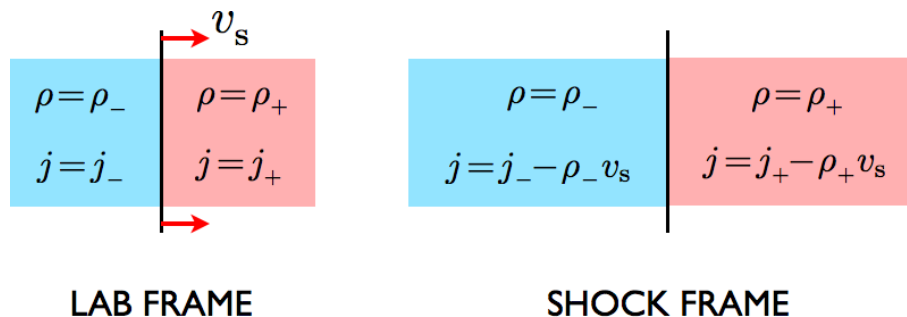


Figure 9.4: Current conservation in the shock frame yields the shock velocity, $v_s = \Delta j / \Delta \rho$.

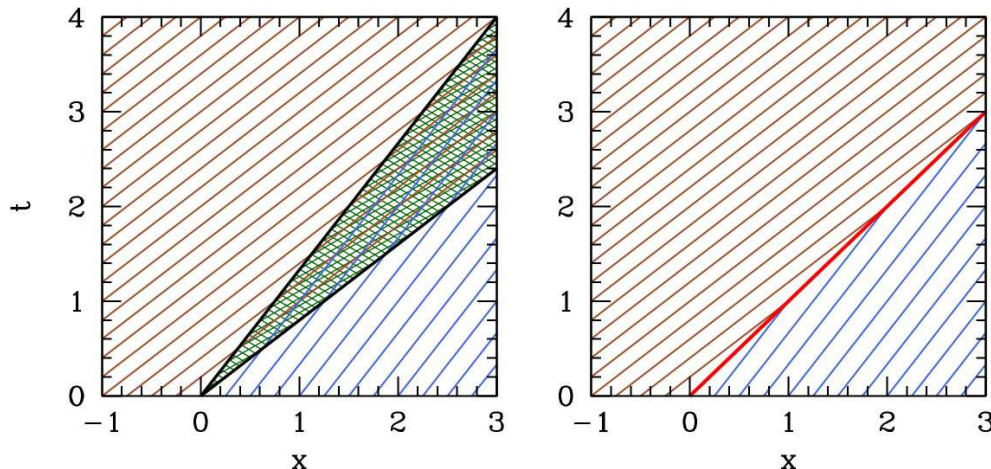


Figure 9.5: A resulting shock wave arising from $c_- = \frac{5}{4}$ and $c_+ = \frac{3}{4}$. With no shock fitting, there is a region of (x, t) where the characteristics cross, shown as the hatched region on the left. With the shock, the solution remains single valued. A quadratic behavior of $J(\rho)$ is assumed, leading to $v_s = \frac{1}{2}(c_+ + c_-) = 1$.

9.3 Internal Shock Structure

At this point, our model of a shock is a discontinuity which propagates with a finite velocity. This may be less problematic than a multivalued solution, but it is nevertheless unphysical. We should at least understand how the discontinuity is resolved in a more complete model. To this end, consider a model where

$$j = J(\rho, \rho_x) = J(\rho) - \nu \rho_x . \quad (9.27)$$

The $J(\rho)$ term contains a nonlinearity which leads to steepening and broadening of regions where $\frac{dc}{dx} > 0$ and $\frac{dc}{dx} < 0$, respectively. The second term, $-\nu \rho_x$, is due to diffusion, and recapitulates *Fick's law*, which says that a diffusion current flows in such a way as to reduce gradients. The continuity equation then reads

$$\rho_t + c(\rho) \rho_x = \nu \rho_{xx} , \quad (9.28)$$

with $c(\rho) = J'(\rho)$. Even if ν is small, its importance is enhanced in regions where $|\rho_x|$ is large, and indeed $-\nu \rho_x$ dominates over $J(\rho)$ in such regions. Elsewhere, if ν is small, it may be neglected, or treated perturbatively.

General solutions to Eqn. 9.28 are of the form $\rho = \rho(x, t)$. In §9.9 below, we will show how to obtain such general solutions for the case where $c(\rho)$ is a linear function of the density, *i.e.* $c''(\rho) = 0$, using a nifty nonlinear transformation. Here, we will content ourselves with obtaining a special class of solution to Eqn. 9.28 by assuming a form corresponding to *front propagation*,

$$\rho(x, t) = \rho(x - v_s t) \equiv \rho(\xi) \quad ; \quad \xi = x - v_s t , \quad (9.29)$$

where the propagation speed v_s is a constant to be determined. The above form of solution corresponds to a fixed shape $\rho(\xi)$ which moves with constant propagation speed. Thus, $\rho_t = -v_s \rho_x$ and $\rho_x = \rho_\xi$,

leading to

$$-v_s \rho_\xi + c(\rho) \rho_\xi = \nu \rho_{\xi\xi} . \quad (9.30)$$

By assuming the propagating front form, we have achieved a remarkable simplification, transforming a first order PDE in two variables to a second order ODE. Moreover, the ODE is simple to integrate. Integrating once, we have

$$J(\rho) - v_s \rho + A = \nu \rho_\xi , \quad (9.31)$$

where A is a constant. Integrating a second time, we have

$$\xi - \xi_0 = \nu \int_{\rho_0}^{\rho} \frac{d\rho'}{J(\rho') - v_s \rho' + A} . \quad (9.32)$$

Suppose ρ interpolates between the values ρ_1 and ρ_2 over the interval $\xi \in (-\infty, +\infty)$. Then we must have

$$\begin{aligned} J(\rho_1) - v_s \rho_1 + A &= 0 \\ J(\rho_2) - v_s \rho_2 + A &= 0 , \end{aligned} \quad (9.33)$$

which in turn requires

$$v_s = \frac{J_2 - J_1}{\rho_2 - \rho_1} , \quad (9.34)$$

where $J_{1,2} = J(\rho_{1,2})$, exactly as before! We also conclude that the constant A must be

$$A = \frac{\rho_1 J_2 - \rho_2 J_1}{\rho_2 - \rho_1} . \quad (9.35)$$

9.3.1 Quadratic $J(\rho)$

For the special case where $J(\rho)$ is quadratic, with $J(\rho) = \alpha\rho^2 + \beta\rho + \gamma$, we may write

$$J(\rho) - v_s \rho + A = \alpha(\rho - \rho_2)(\rho - \rho_1) . \quad (9.36)$$

We then have $v_s = \alpha(\rho_1 + \rho_2) + \beta$, as well as $A = \alpha\rho_1\rho_2 - \gamma$. The moving front solution then obeys

$$d\xi = \frac{\nu d\rho}{\alpha(\rho - \rho_2)(\rho - \rho_1)} = \frac{\nu}{\alpha(\rho_2 - \rho_1)} d \ln \left(\frac{\rho_2 - \rho}{\rho - \rho_1} \right) , \quad (9.37)$$

which is integrated to yield

$$\rho(x, t) = \frac{\rho_2 + \rho_1 \exp \left[\alpha(\rho_2 - \rho_1)(x - v_s t)/\nu \right]}{1 + \exp \left[\alpha(\rho_2 - \rho_1)(x - v_s t)/\nu \right]} . \quad (9.38)$$

We consider the case $\alpha > 0$ and $\rho_1 < \rho_2$. Then $\rho(\pm\infty, t) = \rho_{1,2}$. Note that

$$\rho(x, t) = \begin{cases} \rho_1 & \text{if } x - v_s t \gg \delta \\ \rho_2 & \text{if } x - v_s t \ll -\delta \end{cases} , \quad (9.39)$$

where

$$\delta = \frac{\nu}{\alpha(\rho_2 - \rho_1)} \quad (9.40)$$

is the thickness of the shock region. In the limit $\nu \rightarrow 0$, the shock is discontinuous. All that remains is the *shock condition*,

$$v_s = \alpha(\rho_1 + \rho_2) + \beta = \frac{1}{2}(c_1 + c_2) \quad . \quad (9.41)$$

We stress that we have limited our attention here to the case where $J(\rho)$ is quadratic. It is worth remarking that for *weak shocks* where $\Delta\rho = \rho_+ - \rho_-$ is small, we can expand $J(\rho)$ about the average $\frac{1}{2}(\rho_+ + \rho_-)$, in which case we find $v_s = \frac{1}{2}(c_+ + c_-) + \mathcal{O}((\Delta\rho)^2)$.

9.4 Shock Fitting

When we neglect diffusion currents, we have $j = J$. We now consider how to fit discontinuous shocks satisfying

$$v_s = \frac{J_+ - J_-}{\rho_+ - \rho_-} \quad (9.42)$$

into the continuous solution of Eqn. 9.3, which are described by

$$x = \zeta + g(\zeta)t \quad , \quad \rho = f(\zeta) \quad , \quad (9.43)$$

with $g(\zeta) = c(f(\zeta))$, such that the multivalued parts of the continuous solution are eliminated and replaced with the shock discontinuity. The guiding principle here is number conservation:

$$\frac{d}{dt} \int_{-\infty}^{\infty} dx \rho(x, t) = 0 \quad . \quad (9.44)$$

We'll first learn how do fit shocks when $J(\rho)$ is quadratic, with $J(\rho) = \alpha\rho^2 + \beta\rho + \gamma$. We'll assume $\alpha > 0$ for the sake of definiteness.

9.4.1 An important caveat

Let's multiply the continuity equation $\rho_t + c(\rho)\rho_x = 0$ by $c'(\rho)$. Thus results in

$$c_t + c c_x = 0 \quad . \quad (9.45)$$

If we define $q = \frac{1}{2}c^2$, then this takes the form of a continuity equation:

$$c_t + q_x = 0 \quad . \quad (9.46)$$

Now consider a shock wave. Invoking Eqn. 9.24, we would find, *mutatis mutandis*, a shock velocity

$$u_s = \frac{q_+ - q_-}{c_+ - c_-} = \frac{1}{2}(c_+ + c_-) \quad . \quad (9.47)$$

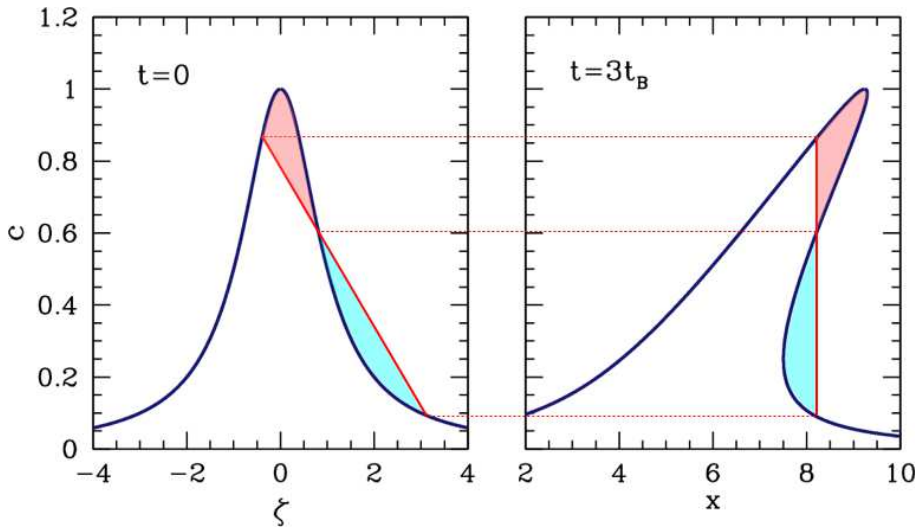


Figure 9.6: Shock fitting for quadratic $J(\rho)$.

This agrees with the velocity $v_s = \Delta j / \Delta \rho$ only when $J(\rho)$ is quadratic. Something is wrong – there cannot be two velocities for the same shock.

The problem is that Eqn. 9.45 is not valid across the shock and cannot be used to determine the shock velocity. There is no conservation law for c as there is for ρ . One way we can appreciate the difference is to add diffusion into the mix. Multiplying Eqn. 9.28 by $c'(\rho)$, and invoking $c_{xx} = c'(\rho) \rho_{xx} + c''(\rho) \rho_x^2$, we obtain

$$c_t + c c_x = \nu c_{xx} - \nu c''(\rho) \rho_x^2 . \quad (9.48)$$

We now see explicitly how nonzero $c''(\rho)$ leads to a different term on the RHS. When $c''(\rho) = 0$, the above equation is universal, independent of the coefficients in the quadratic $J(\rho)$, and is known as *Burgers' equation*,

$$c_t + c c_x = \nu c_{xx} . \quad (9.49)$$

Later on we shall see how this nonlinear PDE may be linearized, and how we can explicitly solve for shock behavior, including the merging of shocks.

9.4.2 Recipe for shock fitting when $J'''(\rho) = 0$

Number conservation means that when we replace the multivalued solution by the discontinuous one, the area under the curve must remain the same. If $J(\rho)$ is quadratic, then we can base our analysis on the equation $c_t + c c_x = 0$, since it gives the correct shock velocity $v_s = \frac{1}{2}(c_+ + c_-)$. We then may then follow the following rules:

- (i) Sketch $c(\zeta) = c(x = \zeta, t = 0)$.
- (ii) Draw a straight line connecting two points on this curve at ζ_- and ζ_+ which obeys the equal area

law, i.e.

$$\frac{1}{2}(\zeta_+ - \zeta_-)(c(\zeta_+) + c(\zeta_-)) = \int_{\zeta_-}^{\zeta_+} d\zeta c(\zeta) . \quad (9.50)$$

(iii) This line evolves into the shock front after a time t such that

$$x_s(t) = \zeta_- + c(\zeta_-)t = \zeta_+ + c(\zeta_+)t . \quad (9.51)$$

Thus,

$$t = \frac{\zeta_+ - \zeta_-}{c(\zeta_-) - c(\zeta_+)} . \quad (9.52)$$

Alternatively, we can fix t and solve for ζ_\pm . See Fig. 9.6 for a graphical description.

- (iv) The position of the shock at this time is $x = x_s(t)$. The strength of the shock is $\Delta c = c(\zeta_-) - c(\zeta_+)$. Since $J(\rho) = \alpha\rho^2 + \beta\rho + \gamma$, we have $c(\rho) = 2\alpha\rho + \beta$ and hence the density discontinuity at the shock is $\Delta\rho = \Delta c/2\alpha$.
- (v) The break time, when the shock first forms, is given by finding the steepest chord satisfying the equal area law. Such a chord is tangent to $c(\zeta)$ and hence corresponds to zero net area. The break time is

$$t_B = \min_{\zeta} \left(-\frac{1}{c'(\zeta)} \right) \equiv -\frac{1}{c'(\zeta_B)} . \quad (9.53)$$

- (vi) If $c(\infty) = c(-\infty)$, the shock strength vanishes as $t \rightarrow \infty$. If $c(-\infty) > c(+\infty)$ then asymptotically the shock strength approaches $\Delta c = c(-\infty) - c(+\infty)$.
- (vii) To plot $c(x, t)$ versus x at fixed t : If $t \leq t_B$, plot $c(\zeta)$ versus $x = \zeta + c(\zeta)t$ for $\zeta \in (-\infty, +\infty)$. If $t > t_B$, plot $c(\zeta)$ versus $x = \zeta + c(\zeta)t$ separately for $\zeta \in (-\infty, \zeta_-]$ and $\zeta \in [\zeta_+, +\infty)$.

9.4.3 Example : shock fitting an inverted parabola

Consider the shock fitting problem for the initial condition

$$c(x, t=0) = c_0 \left(1 - \frac{x^2}{a^2} \right) \Theta(a^2 - x^2) , \quad (9.54)$$

which is to say a truncated inverted parabola. We assume $J'''(\rho) = 0$. Clearly $-c_x(x, 0)$ is maximized at $x = a$, where $-c_x(a, 0) = 2c_0/a$, hence breaking first occurs at

$$(x_B, t_B) = \left(a, \frac{a}{2c_0} \right) . \quad (9.55)$$

Clearly $\zeta_+ > a$, hence $c_+ = 0$. Shock fitting then requires

$$\frac{1}{2}(\zeta_+ - \zeta_-)(c_+ + c_-) = \int_{\zeta_-}^{\zeta_+} d\zeta c(\zeta) = \frac{c_0}{3a^2} (2a + \zeta_-)(a - \zeta_+)^2 . \quad (9.56)$$

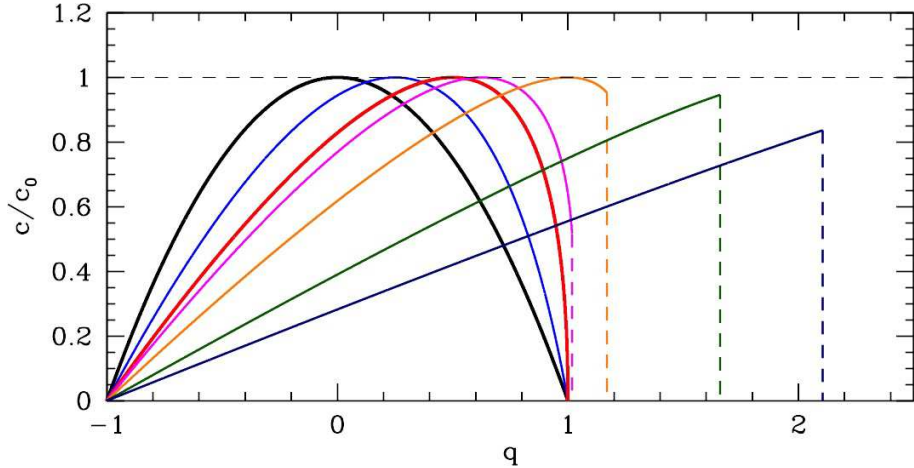


Figure 9.7: Evolution of the inverted parabola profile for $\tau = 0$ (black), $\tau = 0.5$ (blue), $\tau = 1$ (red), $\tau = 1.25$ (magenta), $\tau = 2.0$ (green), and $\tau = 6.0$ (navy blue). The wave first breaks at time $\tau = \tau_B = 1$.

Since $c_+ + c_- = \frac{c_0}{a^2} (a^2 - \zeta_-^2)$, we have

$$\zeta_+ - \zeta_- = \frac{2}{3} (2a + \zeta_-) \left(\frac{a - \zeta_-}{a + \zeta_-} \right) . \quad (9.57)$$

The second shock-fitting equation is $\zeta_+ - \zeta_- = (c_- - c_+) t$. Eliminating ζ_+ from the two shock-fitting equations, and invoking $c_+ = 0$, we have

$$t = \frac{2a^2}{3c_0} \cdot \frac{2a + \zeta_-}{(a + \zeta_-)^2} . \quad (9.58)$$

Inverting to find $\zeta_-(t)$, we obtain

$$\frac{\zeta_-(t)}{a} = \frac{a}{3c_0 t} - 1 + \frac{a}{3c_0 t} \sqrt{1 + \frac{6c_0 t}{a}} . \quad (9.59)$$

The shock position is then $x_s(t) = \zeta_-(t) + c_- (\zeta_-(t)) t = \zeta_+(t)$.

It is convenient to rescale lengths by a and times by $t_B = a/2c_0$, defining q and τ from $x \equiv aq$ and $t \equiv a\tau/2c_0$. Then we have, for $q_{\pm}(\tau) = \zeta_{\pm}(t)/a$,

$$\begin{aligned} q_-(\tau) &= \frac{2}{3\tau} - 1 + \frac{2}{3\tau} \sqrt{1 + 3\tau} \\ q_s(\tau) &= q_+(\tau) = \frac{2}{9\tau} - 1 + \frac{2}{9\tau} (1 + 3\tau)^{3/2} . \end{aligned} \quad (9.60)$$

The dimensionless break time is $\tau_B = 1$. Note that $q_-(1) = q_+(1) = 1$, i.e. the wave starts breaking at $q_B = 1$. The dimensionless shock discontinuity is given by

$$\frac{\Delta c(\tau)}{c_0} = 1 - q_-^2 = -\frac{8}{9\tau^2} [1 + \sqrt{1 + 3\tau}] + \frac{4}{3\tau} \sqrt{1 + 3\tau} . \quad (9.61)$$

Note also that $\Delta c(\tau_B) = 0$. The dimensionless shock velocity is

$$\begin{aligned}\dot{q}_s &= -\frac{2}{9\tau^2} \left[1 + (1+3\tau)^{3/2} \right] + \frac{1}{\tau} (1+3\tau)^{1/2} \\ &= \frac{3}{4}(\tau-1) + \frac{81}{64}(\tau-1)^2 + \dots \quad ,\end{aligned}\tag{9.62}$$

with $v_s = 2c_0 \dot{q}_s = \frac{1}{2}c_-$, if we restore units. Note that $\dot{q}_s(\tau=1)=0$, so the shock curve initially rises vertically in the (x,t) plane. In Fig. 9.7 we plot the evolution of $c(x,t)$. Another example of shock fitting is worked out in the appendix §9.11 below. Interestingly, $v_s \propto (\tau-1)$ here, while for the example in §9.11, where $c(x,0)$ has a similar profile, we find $v_s \propto (\tau-1)^{1/2}$ (see Eqn. 9.170).

9.5 Long-time Behavior of Shocks

Starting with an initial profile $\rho(x,t)$, almost all the original details are lost in the $t \rightarrow \infty$ limit. What remains is a set of propagating triangular waves, where only certain gross features of the original shape, such as its area, are preserved.

9.5.1 Fate of a hump

Once again, we consider the case $c''(\rho) = 0$ and analyze the equation $c_t + c c_x = 0$. The late time profile of $c(x,t)$ in Fig. 9.14 is that of a triangular wave. This is a general result. Following Whitham, we consider the late time evolution of a hump profile $c(\zeta) = c(x=\zeta, t=0)$. We assume $c(\zeta) = c_0$ for $|\zeta| > L$. Shock fitting requires

$$\frac{1}{2} \left[c(\zeta_+) + c(\zeta_-) - 2c_0 \right] (\zeta_+ - \zeta_-) = \int_{\zeta_-}^{\zeta_+} d\zeta (c(\zeta) - c_0) \quad .\tag{9.63}$$

Eventually the point ζ_+ must pass $x = L$, in which case $c(\zeta_+) = c_0$. Then

$$\frac{1}{2} \left[c(\zeta_+) - c_0 \right] (\zeta_+ - \zeta_-) = \int_{\zeta_-}^L d\zeta (c(\zeta) - c_0) \quad .\tag{9.64}$$

and therefore

$$t = \frac{\zeta_+ - \zeta_-}{c(\zeta_-) - c_0} \quad .\tag{9.65}$$

Using this equation to eliminate ζ_+ , we have

$$\frac{1}{2} (c(\zeta_-) - c_0)^2 t = \int_{\zeta_-}^L d\zeta (c(\zeta) - c_0) \quad .\tag{9.66}$$

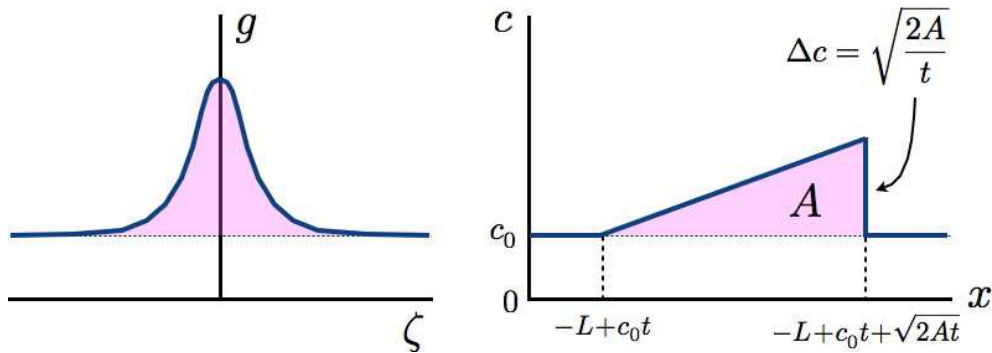


Figure 9.8: Initial and late time configurations for a hump profile. For late times, the profile is triangular, and all the details of the initial shape are lost, save for the area A .

As $t \rightarrow \infty$ we must have $\zeta_- \rightarrow -L$, hence

$$\frac{1}{2}(c(\zeta_-) - c_0)^2 t \approx \int_{-L}^L d\zeta (c(\zeta) - c_0) \equiv A \quad , \quad (9.67)$$

where A is the area under the hump to the line $c = c_0$. Thus,

$$c(\zeta_-) - c_0 \approx \sqrt{\frac{2A}{t}} \quad , \quad (9.68)$$

and the late time motion of the shock is given by

$$\begin{aligned} x_s(t) &= -L + c_0 t + \sqrt{2At} \\ v_s(t) &= c_0 + \sqrt{\frac{A}{2t}} \quad . \end{aligned} \quad (9.69)$$

The shock strength is $\Delta c = c(\zeta_-) - c_0 = \sqrt{2A/t}$. Behind the shock, we have $c = c(\zeta)$ and $x = \zeta + c(\zeta)t$, hence

$$c = \frac{x + L}{t} \quad \text{for} \quad -L + c_0 t < x < -L + c_0 t + \sqrt{2At} \quad . \quad (9.70)$$

As $t \rightarrow \infty$, the details of the original profile $c(x, 0)$ are lost, and all that remains conserved is the area A . Both shock velocity and the shock strength decrease as $t^{-1/2}$ at long times, with $v_s(t) \rightarrow c_0$ and $\Delta c(t) \rightarrow 0$.

9.5.2 N-wave and P-wave

Consider the initial profile in the top left panel of Fig. 9.9. Now there are two propagating shocks, since there are two compression regions where $g'(\zeta) < 0$. As $t \rightarrow \infty$, we have $(\zeta_-, \zeta_+)_A \rightarrow (0, \infty)$ for the A shock, and $(\zeta_-, \zeta_+)_B \rightarrow (-\infty, 0)$ for the B shock. Asymptotically, the shock strength

$$\Delta c(t) \equiv c(x_s^-(t), t) - c(x_s^+(t), t) \quad (9.71)$$

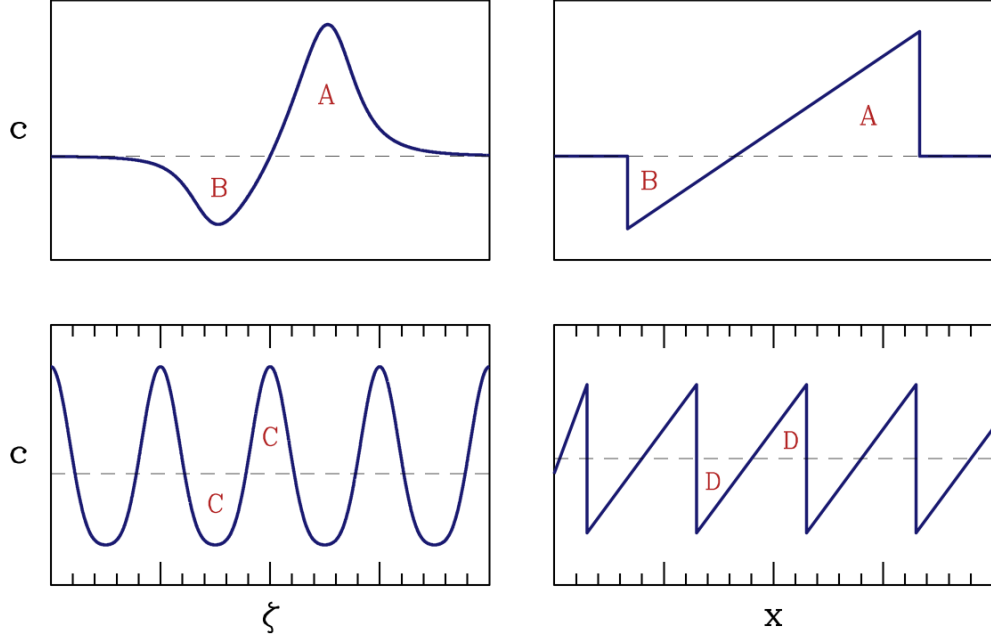


Figure 9.9: Top panels : An N-wave, showing initial (left) and late time (right) profiles. As the N-wave propagates, the areas A and B are preserved. Bottom panels : A P-wave. The area D eventually decreases to zero as the shock amplitude dissipates.

for the two shocks is given by

$$\begin{aligned} x_s^A(t) &\approx c_0 t + \sqrt{2At} \quad , \quad \Delta c_A \approx +\sqrt{\frac{2A}{t}} \\ x_s^B(t) &\approx c_0 t - \sqrt{2Bt} \quad , \quad \Delta c_B \approx -\sqrt{\frac{2B}{t}} \end{aligned} \quad (9.72)$$

where A and B are the areas associated with the two features. This feature is called an N-wave, for its N (or inverted N) shape.

The initial and late stages of a periodic (P) wave, where $g(\zeta + \lambda) = g(\zeta)$, are shown in the bottom panels of Fig. 9.9. In the $t \rightarrow \infty$ limit, we evidently have $\zeta_+ - \zeta_- = \lambda$, the wavelength. Asymptotically the shock strength is given by

$$\Delta c(t) \equiv g(\zeta_-) - g(\zeta_+) = \frac{\zeta_+ - \zeta_-}{t} = \frac{\lambda}{t} \quad , \quad (9.73)$$

where we have invoked Eqn. 9.52. In this limit, the shock train travels with constant velocity c_0 , which is the spatial average of $c(x, 0)$ over one wavelength:

$$c_0 = \frac{1}{\lambda} \int_0^\lambda d\zeta g(\zeta) \quad . \quad (9.74)$$

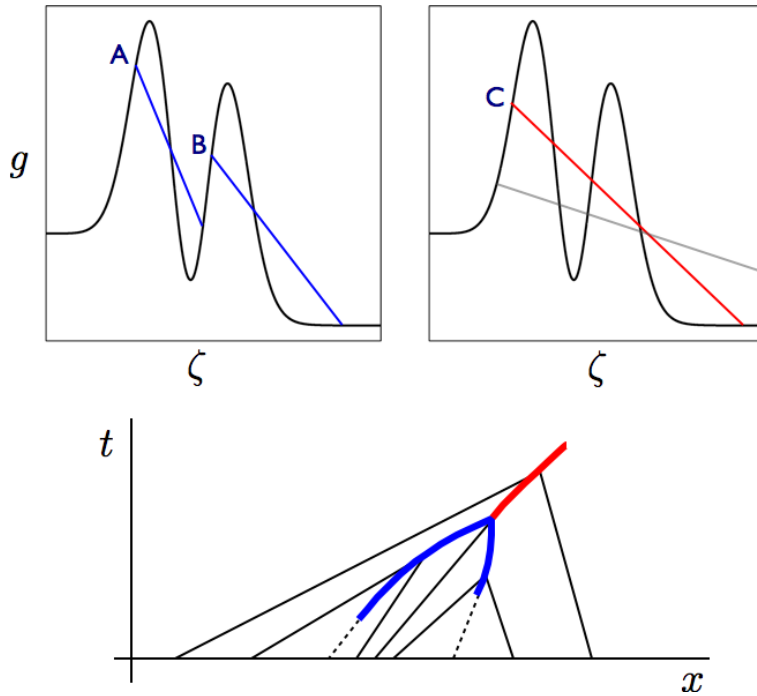


Figure 9.10: Merging of two shocks. The shocks initially propagate independently (upper left), and then merge and propagate as a single shock (upper right). Bottom : characteristics for the merging shocks.

9.6 Shock Merging

It is possible for several shock waves to develop, and in general these shocks form at different times, have different strengths, and propagate with different velocities. Under such circumstances, it is quite possible that one shock overtakes another. These two shocks then merge and propagate on as a single shock. The situation is depicted in Fig. 9.10. We label the shocks by A and B when they are distinct, and the late time single shock by C. We must have

$$\begin{aligned} v_s^A &= \frac{1}{2} g(\zeta_+^A) + \frac{1}{2} g(\zeta_-^A) \\ v_s^B &= \frac{1}{2} g(\zeta_+^B) + \frac{1}{2} g(\zeta_-^B) \end{aligned} \quad . \quad (9.75)$$

The merging condition requires

$$\zeta_+^A = \zeta_-^B \equiv \xi \quad (9.76)$$

as well as

$$\zeta_+^C = \zeta_-^B \quad , \quad \zeta_-^C = \zeta_-^A \quad . \quad (9.77)$$

The merge occurs at time \$t\$, where

$$t = \frac{\zeta_+ - \xi}{g(\xi) - g(\zeta_+)} = \frac{\xi - \zeta_-}{g(\zeta_-) - g(\xi)} \quad . \quad (9.78)$$

Thus, the slopes of the A and B shock construction lines are equal when they merge.

9.7 Shock Fitting for General $J(\rho)$

When $J(\rho)$ is quadratic, we may analyze the equation $c_t + c c_x$, as it is valid across any shocks in that it yields the correct shock velocity. If $J'''(\rho) \neq 0$, this is no longer the case, and we must base our analysis on the original equation $\rho_t + c(\rho) \rho_x = 0$.

The coordinate transformation

$$(x, c) \rightarrow (x + ct, c) \quad (9.79)$$

preserves areas in the (x, c) plane and also maps lines to lines. However, while

$$(x, \rho) \rightarrow (x + c(\rho)t, \rho) \quad (9.80)$$

does preserve areas in the (x, ρ) plane, it does not map lines to lines. Thus, the ‘pre-image’ of the shock front in the (x, ρ) plane is not a simple straight line, and our equal area construction fails. Still, we can make progress. We once again follow Whitham, §2.9.

Let $x(\rho, t)$ be the inverse of $\rho(x, t)$, with $\zeta(\rho) \equiv x(\rho, t = 0)$. Then

$$x(\rho, t) = \zeta(\rho) + c(\rho)t \quad . \quad (9.81)$$

Note that $\rho(x, t)$ is in general multi-valued. We still have that the shock solution covers the same area as the multivalued solution $\rho(x, t)$. Let ρ_{\pm} denote the value of ρ just to the right (+) or left (-) of the shock. For purposes of illustration, we assume $c'(\rho) > 0$, which means that $\rho_x < 0$ is required for breaking, although the method works equally well for $c'(\rho) < 0$. Assuming a hump-like profile, we then have $\rho_- > \rho_+$, with the shock breaking to the right. Area conservation requires

$$\int_{\rho_+}^{\rho_-} d\rho x(\rho, t) = \int_{\rho_+}^{\rho_-} d\rho [\zeta(\rho) + c(\rho)t] = (\rho_- - \rho_+) x_s(t) \quad . \quad (9.82)$$

Since $c(\rho) = J'(\rho)$, the above equation may be written as

$$(J_+ - J_-)t - (\rho_+ - \rho_-)x_s(t) = \int_{\rho_+}^{\rho_-} d\rho \zeta(\rho) = \rho_- \zeta_- - \rho_+ \zeta_+ - \int_{\zeta_+}^{\zeta_-} d\zeta \rho(\zeta) \quad , \quad (9.83)$$

where we have integrated by parts in obtaining the RHS, writing $\zeta d\rho = d(\rho \zeta) - \rho d\zeta$. Next, the shock position $x_s(t)$ is given by

$$x_s(t) = \zeta_- + c_- t = \zeta_+ + c_+ t \quad , \quad (9.84)$$

which yields

$$t = \frac{\zeta_- - \zeta_+}{c_+ - c_-} \quad , \quad (9.85)$$

and therefore

$$[(J_+ - \rho_+ c_+) - (J_- - \rho_- c_-)] = -\frac{c_+ - c_-}{\zeta_+ - \zeta_-} \int_{\zeta_-}^{\zeta_+} d\zeta \rho(\zeta) \quad . \quad (9.86)$$

This is a useful result because J_{\pm} , ρ_{\pm} , and c_{\pm} are all functions of ζ_{\pm} , hence what we have here is a relation between ζ_+ and ζ_- . When $J(\rho)$ is quadratic, this reduces to our earlier result in Eqn. 9.50. For a hump, we still have $x_s \approx c_0 t + \sqrt{2A}t$ and $c - c_0 \approx \sqrt{2A/t}$ as before, with

$$A = c'(\rho_0) \int_{-\infty}^{\infty} d\zeta [\rho(\zeta) - \rho_0] . \quad (9.87)$$

9.8 Sources

Consider the continuity equation in the presence of a source term,

$$\rho_t + c \rho_x = \sigma , \quad (9.88)$$

where $c = c(x, t, \rho)$ and $\sigma = \sigma(x, t, \rho)$. Note that we are allowing for more than just $c = c(\rho)$ here. According to the discussion in the Appendix, the characteristic obey the coupled ODEs³,

$$\frac{dx}{dt} = c(x, t, \rho) , \quad \frac{d\rho}{dt} = \sigma(x, t, \rho) . \quad (9.89)$$

In general, the characteristics no longer are straight lines.

9.8.1 Examples

Whitham analyzes the equation

$$c_t + c c_x = -\alpha c , \quad (9.90)$$

so that the characteristics obey

$$\frac{dc}{dt} = -\alpha c , \quad \frac{dx}{dt} = c . \quad (9.91)$$

The solution is

$$\begin{aligned} c_{\zeta}(t) &= e^{-\alpha t} g(\zeta) \\ x_{\zeta}(t) &= \zeta + \frac{1}{\alpha} (1 - e^{-\alpha t}) g(\zeta) , \end{aligned} \quad (9.92)$$

where $\zeta = x_{\zeta}(0)$ labels the characteristics. Clearly $x_{\zeta}(t)$ is not a straight line. Neighboring characteristics will cross at time t if

$$\frac{\partial x_{\zeta}(t)}{\partial \zeta} = 1 + \frac{1}{\alpha} (1 - e^{-\alpha t}) g'(\zeta) = 0 . \quad (9.93)$$

Thus, the break time is

$$t_B = \min_{\substack{\zeta \\ t_B > 0}} \left[-\frac{1}{\alpha} \ln \left(1 + \frac{\alpha}{g'(\zeta)} \right) \right] . \quad (9.94)$$

³We skip the step where we write $dt/ds = 1$ since this is immediately integrated to yield $s = t$.

This requires $g'(\zeta) < -\alpha$ in order for wave breaking to occur.

For another example, consider

$$c_t + c c_x = -\alpha c^2 \quad , \quad (9.95)$$

so that the characteristics obey

$$\frac{dc}{dt} = -\alpha c^2 \quad , \quad \frac{dx}{dt} = c \quad . \quad (9.96)$$

The solution is now

$$\begin{aligned} c_\zeta(t) &= \frac{g(\zeta)}{1 + \alpha g(\zeta)t} \\ x_\zeta(t) &= \zeta + \frac{1}{\alpha} \ln(1 + \alpha g(\zeta)t) \quad . \end{aligned} \quad (9.97)$$

9.8.2 Moving sources

Consider a source moving with velocity u . We then have

$$c_t + c c_x = \sigma(x - ut) \quad , \quad (9.98)$$

where u is a constant. We seek a moving wave solution $c = c(\xi) = c(x - ut)$. This leads immediately to the ODE

$$(c - u) c_\xi = \sigma(\xi) \quad . \quad (9.99)$$

This may be integrated to yield

$$\frac{1}{2}(u - c_\infty)^2 - \frac{1}{2}(u - c)^2 = \int_{\xi}^{\infty} d\xi' \sigma(\xi') \quad . \quad (9.100)$$

Consider the supersonic case where $u > c$. Then we have a smooth solution,

$$c(\xi) = u - \left[(u - c_\infty)^2 - 2 \int_{\xi}^{\infty} d\xi' \sigma(\xi') \right]^{1/2} \quad , \quad (9.101)$$

provided that the term inside the large rectangular brackets is positive. This is always the case for $\sigma < 0$. For $\sigma > 0$ we must require

$$u - c_\infty > \sqrt{2 \int_{\xi}^{\infty} d\xi' \sigma(\xi')} \quad (9.102)$$

for all ξ . If $\sigma(\xi)$ is monotonic, the lower limit on the above integral may be extended to $-\infty$. Thus, if the source strength is sufficiently small, no shocks are generated. When the above equation is satisfied as an equality, a shock develops, and transients from the initial conditions overtake the wave. A complete solution of the problem then requires a detailed analysis of the transients. What is surprising here is that a supersonic source need not produce a shock wave, if the source itself is sufficiently weak.

9.9 Burgers' Equation

The simplest equation describing both nonlinear wave propagation and diffusion equation is the one-dimensional *Burgers' equation*,

$$c_t + c c_x = \nu c_{xx} . \quad (9.103)$$

As we've seen, this follows from the continuity equation $\rho_t + j_x$ when $j = J(\rho) - \nu \rho_x$, with $c = J'(\rho)$ and $c''(\rho) = 0$.

We have already obtained, in §9.3.1, a solution to Burgers' equation in the form of a propagating front. However, we can do much better than this; we can find *all* the solutions to the one-dimensional Burgers' equation. The trick is to employ a nonlinear transformation of the field $c(x, t)$, known as the *Cole-Hopf transformation*, which linearizes the PDE. Once again, we follow the exceptionally clear discussion in the book by Whitham (ch. 4).

The Cole-Hopf transformation is defined as follows:

$$c \equiv -2\nu \frac{\varphi_x}{\varphi} = \frac{\partial}{\partial x} (-2\nu \ln \varphi) . \quad (9.104)$$

Plugging into Burgers' equation, one finds that $\varphi(x, t)$ satisfies the *linear* diffusion equation,

$$\varphi_t = \nu \varphi_{xx} . \quad (9.105)$$

Isn't that just about the coolest thing you've ever heard?

Suppose the initial conditions on $\varphi(x, t)$ are

$$\varphi(x, 0) = \Phi(x) . \quad (9.106)$$

We can then solve the diffusion equation 9.105 by Laplace transform. The result is

$$\varphi(x, t) = \frac{1}{\sqrt{4\pi\nu t}} \int_{-\infty}^{\infty} dx' e^{-(x-x')^2/4\nu t} \Phi(x') . \quad (9.107)$$

Thus, if $c(x, t=0) = g(x)$, then the solution for subsequent times is

$$c(x, t) = \frac{\int_{-\infty}^{\infty} dx' (x - x') e^{-H(x, x', t)/2\nu}}{t \int_{-\infty}^{\infty} dx' e^{-H(x, x', t)/2\nu}} , \quad (9.108)$$

where

$$H(x, x', t) = \int_0^{x'} dx'' g(x'') + \frac{(x - x')^2}{2t} . \quad (9.109)$$

9.9.1 The limit $\nu \rightarrow 0$

In the limit $\nu \rightarrow 0$, the integrals in the numerator and denominator of Eqn. 9.108 may be computed via the method of steepest descents. This means that extremize $H(x, x', t)$ with respect to x' , which entails solving

$$\frac{\partial H}{\partial x'} = g(x') - \frac{x - x'}{t} \quad . \quad (9.110)$$

Let $\zeta = \zeta(x, t)$ be a solution to this equation for x' , so that

$$x = \zeta + g(\zeta) t \quad . \quad (9.111)$$

We now expand about $x' = \zeta$, writing $x' = \zeta + s$, in which case

$$H(x') = H(\zeta) + \frac{1}{2} H''(\zeta) s^2 + \mathcal{O}(s^3) \quad , \quad (9.112)$$

where the x and t dependence is here implicit. If $F(x')$ is an arbitrary function which is slowly varying on distance scales on the order of $\nu^{1/2}$, then we have

$$\int_{-\infty}^{\infty} dx' F(x') e^{-H(x')/2\nu} \approx \sqrt{\frac{4\pi\nu}{H''(\zeta)}} e^{-H(\zeta)/2\nu} F(\zeta) \quad . \quad (9.113)$$

Applying this result to Eqn. 9.108, we find

$$c \approx \frac{x - \zeta}{t} \quad , \quad (9.114)$$

which is to say

$$\begin{aligned} c &= g(\zeta) \\ x &= \zeta + g(\zeta) t \quad . \end{aligned} \quad (9.115)$$

This is precisely what we found for the characteristics of $c_t + c c_x = 0$.

What about multivaluedness? This is obviated by the presence of an additional saddle point solution. *I.e.* beyond some critical time, we have a discontinuous change of saddles as a function of x :

$$x = \zeta_{\pm} + g(\zeta_{\pm}) t \quad \longrightarrow \quad \zeta_{\pm} = \zeta_{\pm}(x, t) \quad . \quad (9.116)$$

Then

$$c \sim \frac{1}{t} \cdot \frac{\frac{x - \zeta_-}{\sqrt{H''(\zeta_-)}} e^{-H(\zeta_-)/2\nu} + \frac{x - \zeta_+}{\sqrt{H''(\zeta_+)}} e^{-H(\zeta_+)/2\nu}}{\frac{1}{\sqrt{H''(\zeta_-)}} e^{-H(\zeta_-)/2\nu} + \frac{1}{\sqrt{H''(\zeta_+)}} e^{-H(\zeta_+)/2\nu}} \quad . \quad (9.117)$$

Thus,

$$\begin{aligned} H(\zeta_+) > H(\zeta_-) &\Rightarrow c \approx \frac{x - \zeta_-}{t} \\ H(\zeta_+) < H(\zeta_-) &\Rightarrow c \approx \frac{x - \zeta_+}{t} \quad . \end{aligned} \quad (9.118)$$

At the shock, these solutions are degenerate:

$$H(\zeta_+) = H(\zeta_-) \quad \Rightarrow \quad \frac{1}{2}(\zeta_+ - \zeta_-)(g(\zeta_+) + g(\zeta_-)) = \int_{\zeta_-}^{\zeta_+} d\zeta g(\zeta) \quad , \quad (9.119)$$

which is again exactly as before. We stress that for ν small but finite the shock fronts are smoothed out on a distance scale proportional to ν .

What does it mean for ν to be small? The dimensions of ν are $[\nu] = L^2/T$, so we must find some other quantity in the problem with these dimensions. The desired quantity is the area,

$$A = \int_{-\infty}^{\infty} dx [g(x) - c_0] \quad , \quad (9.120)$$

where $c_0 = c(x = \pm\infty)$. We can now define the dimensionless ratio,

$$R \equiv \frac{A}{2\nu} \quad , \quad (9.121)$$

which is analogous to the Reynolds number in viscous fluid flow. R is proportional to the ratio of the nonlinear term $(c - c_0)c_x$ to the diffusion term νc_{xx} .

9.9.2 Examples

Whitham discusses three examples: diffusion of an initial step, a hump, and an N-wave. Here we simply reproduce the functional forms of these solutions. For details, see chapter 4 of Whitham's book.

For an initial step configuration,

$$c(x, t=0) = \begin{cases} c_1 & \text{if } x < 0 \\ c_2 & \text{if } x > 0 \end{cases} . \quad (9.122)$$

We are interested in the case $c_1 > c_2$. Using the Cole-Hopf transformation and applying the appropriate initial conditions to the resulting linear diffusion equation, one obtains the complete solution,

$$c(x, t) = c_2 + \frac{c_1 - c_2}{1 + h(x, t) \exp [(c_1 - c_2)(x - v_s t)/2\nu]} \quad , \quad (9.123)$$

where

$$v_s = \frac{1}{2}(c_1 + c_2) \quad (9.124)$$

and

$$h(x, t) = \frac{\operatorname{erfc}\left(-\frac{x-c_2 t}{\sqrt{4 \nu t}}\right)}{\operatorname{erfc}\left(+\frac{x-c_1 t}{\sqrt{4 \nu t}}\right)} . \quad (9.125)$$

Recall that $\text{erfc}(z)$ is the complimentary error function:

$$\begin{aligned}\text{erf}(z) &= \frac{2}{\sqrt{\pi}} \int_0^z du e^{-u^2} \\ \text{erfc}(z) &= \frac{2}{\sqrt{\pi}} \int_z^\infty du e^{-u^2} = 1 - \text{erf}(z) .\end{aligned}\quad (9.126)$$

Note the limiting values $\text{erfc}(-\infty) = 2$, $\text{erfc}(0) = 1$ and $\text{erfc}(\infty) = 0$. If $c_2 < x/t < c_1$, then $h(x, t) \rightarrow 1$ as $t \rightarrow \infty$, in which case the solution resembles a propagating front. It is convenient to adimensionalize $(x, t) \rightarrow (y, \tau)$ by writing

$$x = \frac{\nu y}{\sqrt{c_1 c_2}} , \quad t = \frac{\nu \tau}{c_1 c_2} , \quad r \equiv \sqrt{\frac{c_1}{c_2}} . \quad (9.127)$$

We then have

$$\frac{c(z, \tau)}{\sqrt{c_1 c_2}} = r^{-1} + \frac{2\alpha}{1 + h(z, \tau) \exp(\alpha z)} , \quad (9.128)$$

where

$$h(z, \tau) = \text{erfc}\left(-\frac{z + \alpha\tau}{2\sqrt{\tau}}\right) / \text{erfc}\left(+\frac{z - \alpha\tau}{2\sqrt{\tau}}\right) \quad (9.129)$$

and

$$\alpha \equiv \frac{1}{2}(r - r^{-1}) , \quad z \equiv y - \frac{1}{2}(r + r^{-1})\tau . \quad (9.130)$$

The second example involves the evolution of an infinitely thin hump, where

$$c(x, t = 0) = c_0 + A \delta(x) . \quad (9.131)$$

The solution for subsequent times is

$$c(x, t) = c_0 + \sqrt{\frac{\nu}{\pi t}} \cdot \frac{(e^R - 1) \exp\left(-\frac{x - c_0 t}{4\nu t}\right)}{1 + \frac{1}{2}(e^R - 1) \text{erfc}\left(\frac{x - c_0 t}{\sqrt{4\nu t}}\right)} , \quad (9.132)$$

where $R = A/2\nu$. Defining

$$z \equiv \frac{x - c_0 t}{\sqrt{2At}} , \quad (9.133)$$

we have the solution

$$c = c_0 + \left(\frac{2A}{t}\right)^{1/2} \frac{1}{\sqrt{4\pi R}} \cdot \frac{(e^R - 1) e^{-Rz^2}}{1 + \frac{1}{2}(e^R - 1) \text{erfc}(\sqrt{R}z)} . \quad (9.134)$$

Asymptotically, for $t \rightarrow \infty$ with x/t fixed, we have

$$c(x, t) = \begin{cases} x/t & \text{if } 0 < x < \sqrt{2At} \\ 0 & \text{otherwise} \end{cases} . \quad (9.135)$$

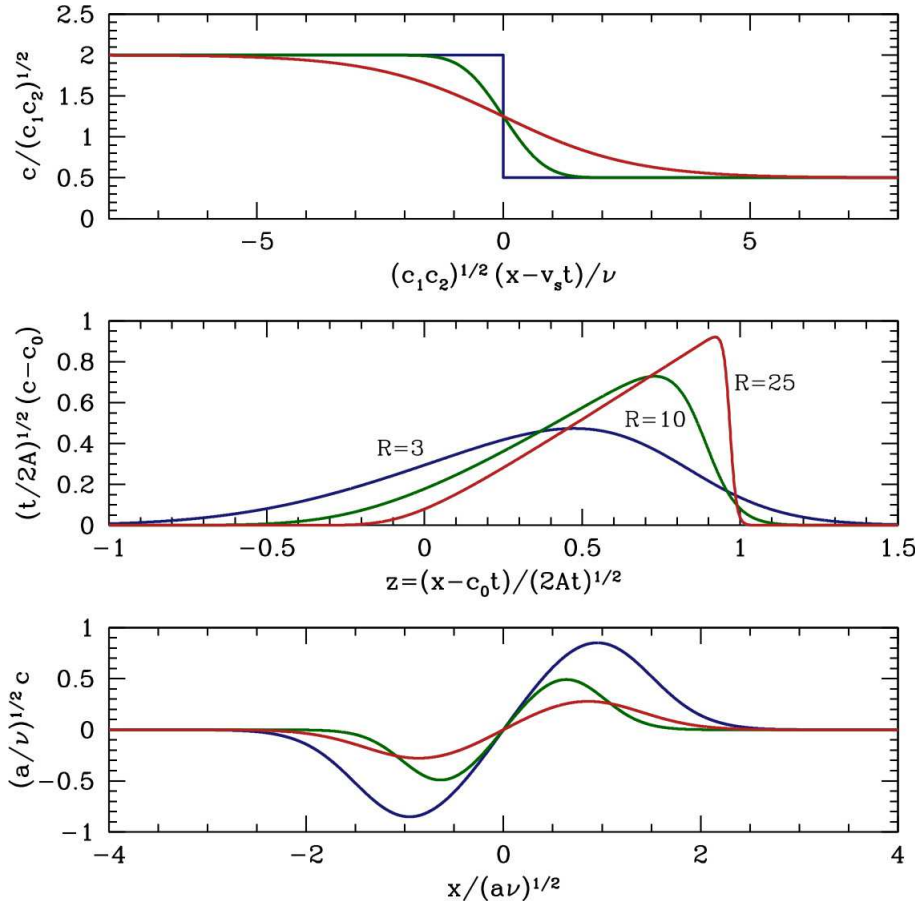


Figure 9.11: Evolution of profiles for Burgers' equation. Top : a step discontinuity evolving into a front at times $\tau = 0$ (blue), $\tau = \frac{1}{5}$ (green), and $\tau = 5$ (red).. Middle : a narrow hump $c_0 + A\delta(x)$ evolves into a triangular wave. Bottom : dissipation of an N-wave at times $\tau = \frac{1}{4}$ (blue), $\tau = \frac{1}{2}$ (green), and $\tau = 1$ (red).

This recapitulates the triangular wave solution with the two counterpropagating shock fronts and dissipating shock strengths.

Finally, there is the N-wave. If we take the following solution to the linear diffusion equation,

$$\varphi(x, t) = 1 + \sqrt{\frac{a}{t}} e^{-x^2/4\nu t} , \quad (9.136)$$

then we obtain

$$c(x, t) = \frac{x}{t} \cdot \frac{e^{-x^2/4\nu t}}{\sqrt{\frac{t}{a} + e^{-x^2/4\nu t}}} . \quad (9.137)$$

In terms of dimensionless variables (y, τ) , where

$$x = \sqrt{a\nu} y \quad , \quad t = a\tau \quad , \quad (9.138)$$

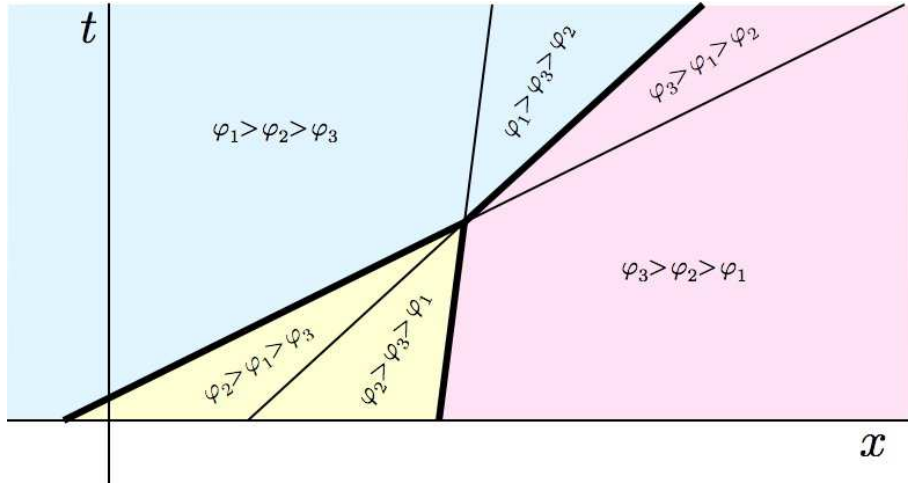


Figure 9.12: Merging of two shocks for piecewise constant initial data. The (x, t) plane is broken up into regions labeled by the local value of $c(x, t)$. For the shocks to form, we require $c_1 > c_2 > c_3$. When the function $\varphi_j(x, t)$ dominates over the others, then $c(x, t) \approx c_j$.

we have

$$c = \sqrt{\frac{\nu}{a}} \frac{y}{\tau} \cdot \frac{e^{-y^2/4\tau}}{\sqrt{\tau + e^{-y^2/4\tau}}} . \quad (9.139)$$

The evolving profiles for these three cases are plotted in Fig. 9.11.

9.9.3 Confluence of shocks

The fact that the diffusion equation 9.105 is linear means that we can superpose solutions:

$$\varphi(x, t) = \varphi_1(x, t) + \varphi_2(x, t) + \dots + \varphi_N(x, t) , \quad (9.140)$$

where

$$\varphi_j(x, t) = e^{-c_j(x-b_j)/2\nu} e^{+c_j^2 t/4\nu} . \quad (9.141)$$

We then have

$$c(x, t) = -\frac{2\nu\varphi_x}{\varphi} = \frac{\sum_i c_i \varphi_i(x, t)}{\sum_i \varphi_i(x, t)} . \quad (9.142)$$

Consider the case $N = 2$, which describes a single shock. If $c_1 > c_2$, then at a fixed time t we have that φ_1 dominates as $x \rightarrow -\infty$ and φ_2 as $x \rightarrow +\infty$. Therefore $c(-\infty, t) = c_1$ and $c(+\infty) = c_2$. The shock center is defined by $\varphi_1 = \varphi_2$, where $x = \frac{1}{2}(c_1 + c_2)t$.

Next consider $N = 3$, where there are two shocks. We assume $c_1 > c_2 > c_3$. We identify regions in the

(x, t) plane where φ_1 , φ_2 , and φ_3 are dominant. One finds

$$\begin{aligned}\varphi_1 > \varphi_2 &: x < \frac{1}{2}(c_1 + c_2)t + \frac{b_1 c_1 - b_2 c_2}{c_1 - c_2} \\ \varphi_1 > \varphi_3 &: x < \frac{1}{2}(c_1 + c_3)t + \frac{b_1 c_1 - b_3 c_3}{c_1 - c_3} \\ \varphi_2 > \varphi_3 &: x < \frac{1}{2}(c_2 + c_3)t + \frac{b_2 c_2 - b_3 c_3}{c_2 - c_3} .\end{aligned}\quad (9.143)$$

These curves all meet in a single point at (x_m, t_m) , as shown in Fig. 9.12. The shocks are the locus of points along which two of the φ_j are equally dominant. We assume that the intercepts of these lines with the x -axis are ordered as in the figure, with $x_{12}^* < x_{13}^* < x_{23}^*$, where

$$x_{ij}^* \equiv \frac{b_i c_i - b_j c_j}{c_i - c_j} . \quad (9.144)$$

When a given $\varphi_i(x, t)$ dominates over the others, we have from Eqn. 9.142 that $c \approx c_i$. We see that for $t < t^*$ one has that φ_1 is dominant for $x < x_{12}^*$, and φ_3 is dominant for $x > x_{23}^*$, while φ_2 dominates in the intermediate regime $x_{12}^* < x < x_{23}^*$. The boundaries between these different regions are the two propagating shocks. After the merge, for $t > t_m$, however, φ_2 never dominates, and hence there is only one shock.

9.10 Appendix I : The Method of Characteristics

Consider the quasilinear PDE

$$a_1(\mathbf{x}, \phi) \frac{\partial \phi}{\partial x_1} + a_2(\mathbf{x}, \phi) \frac{\partial \phi}{\partial x_2} + \dots + a_N(\mathbf{x}, \phi) \frac{\partial \phi}{\partial x_N} = b(\mathbf{x}, \phi) . \quad (9.145)$$

This PDE is called ‘quasilinear’ because it is linear in the derivatives $\partial \phi / \partial x_j$. The N independent variables are the elements of the vector $\mathbf{x} = (x_1, \dots, x_N)$. A solution is a function $\phi(\mathbf{x})$ which satisfies the PDE.

Now consider a curve $\mathbf{x}(s)$ parameterized by a single real variable s satisfying

$$\frac{dx_j}{ds} = a_j(\mathbf{x}, \phi(\mathbf{x})) , \quad (9.146)$$

where $\phi(\mathbf{x})$ is a solution of Eqn. 9.145. Along such a curve, which is called a *characteristic*, the variation of ϕ is

$$\frac{d\phi}{ds} = \sum_{j=1}^N \frac{\partial \phi}{\partial x_j} \frac{dx_j}{ds} = b(\mathbf{x}(s), \phi) . \quad (9.147)$$

Thus, we have converted our PDE into a set of $(N + 1)$ ODEs. To integrate, we must supply some initial conditions of the form

$$g(\mathbf{x}, \phi) \Big|_{s=0} = 0 . \quad (9.148)$$

This defines an $(N - 1)$ -dimensional hypersurface, parameterized by $\{\zeta_1, \dots, \zeta_{N-1}\}$:

$$\begin{aligned} x_j(s=0) &= h_j(\zeta_1, \dots, \zeta_{N-1}) \quad , \quad j = 1, \dots, N \\ \phi(s=0) &= f(\zeta_1, \dots, \zeta_{N-1}) \quad . \end{aligned} \quad (9.149)$$

If we can solve for all the characteristic curves, then the solution of the PDE follows. For every x , we identify the characteristic curve upon which x lies. The characteristics are identified by their parameters $(\zeta_1, \dots, \zeta_{N-1})$. The value of $\phi(x)$ is then $\phi(x) = f(\zeta_1, \dots, \zeta_{N-1})$. If two or more characteristics cross, the solution is multi-valued, or a shock has occurred.

9.10.1 Example

Consider the PDE

$$\phi_t + t^2 \phi_x = -x \phi \quad . \quad (9.150)$$

We identify $a_1(t, x, \phi) = 1$ and $a_2(t, x, \phi) = t^2$, as well as $b(t, x, \phi) = -x \phi$. The characteristics are curves $(t(s), x(s))$ satisfying

$$\frac{dt}{ds} = 1 \quad , \quad \frac{dx}{ds} = t^2 \quad . \quad (9.151)$$

The variation of ϕ along each of the characteristics is given by

$$\frac{d\phi}{ds} = -x \phi \quad . \quad (9.152)$$

The initial data are expressed parametrically as

$$t(s=0) = 0 \quad , \quad x(s=0) = \zeta \quad , \quad \phi(s=0) = f(\zeta) \quad . \quad (9.153)$$

We now solve for the characteristics. We have

$$\frac{dt}{ds} = 1 \quad \Rightarrow \quad t(s, \zeta) = s \quad . \quad (9.154)$$

It then follows that

$$\frac{dx}{ds} = t^2 = s^2 \quad \Rightarrow \quad x(s, \zeta) = \zeta + \frac{1}{3}s^3 \quad . \quad (9.155)$$

Finally, we have

$$\frac{d\phi}{ds} = -x \phi = -\left(\zeta + \frac{1}{3}s^3\right) \phi \quad \Rightarrow \quad \phi(s, \zeta) = f(\zeta) \exp\left(-\frac{1}{12}s^4 - s\zeta\right) \quad . \quad (9.156)$$

We may now eliminate (ζ, s) in favor of (x, t) , writing $s = t$ and $\zeta = x - \frac{1}{3}t^3$, yielding the solution

$$\phi(x, t) = f\left(x - \frac{1}{3}t^3\right) \exp\left(\frac{1}{4}t^4 - xt\right) \quad . \quad (9.157)$$

9.11 Appendix II : Worked Problem in Shock Fitting

Consider the equation $c_t + c c_x = 0$. Suppose the $c(\rho)$ and $\rho(x, t = 0)$ are such that $c(x, t = 0)$ is given by

$$c(x, 0) = c_0 \cos\left(\frac{\pi x}{2\ell}\right) \Theta(\ell - |x|) , \quad (9.158)$$

where $\Theta(s)$ is the step function, which vanishes identically for negative values of its argument. Thus, $c(x, 0) = 0$ for $|x| \geq \ell$.

(a) Find the time t_B at which the wave breaks and a shock front develops. Find the position of the shock $x_s(t_B)$ at the moment it forms.

Solution : Breaking first occurs at time

$$t_B = \min_x \left(-\frac{1}{c'(x, 0)} \right) . \quad (9.159)$$

Thus, we look for the maximum negative slope in $g(x) \equiv c(x, 0)$, which occurs at $x = \ell$, where $c'(\ell, 0) = -\pi c_0 / 2\ell$. Therefore,

$$t_B = \frac{2\ell}{\pi c_0} , \quad x_B = \ell . \quad (9.160)$$

(b) Use the shock-fitting equations to derive $\zeta_{\pm}(t)$.

Solution : The shock fitting equations are

$$\frac{1}{2} (\zeta_+ - \zeta_-) (g(\zeta_+) + g(\zeta_-)) = \int_{\zeta_-}^{\zeta_+} d\zeta g(\zeta) \quad (9.161)$$

and

$$t = \frac{\zeta_+ - \zeta_-}{g(\zeta_-) - g(\zeta_+)} . \quad (9.162)$$

Clearly $\zeta_+ > \ell$, hence $g(\zeta_+) = 0$ and

$$\int_{\zeta_-}^{\zeta_+} d\zeta g(\zeta) = c_0 \cdot \frac{2\ell}{\pi} \int_{\pi\zeta_-/2\ell}^{\pi/2} dz \cos z = \frac{2\ell c_0}{\pi} \left\{ 1 - \sin\left(\frac{\pi\zeta_-}{2\ell}\right) \right\} . \quad (9.163)$$

Thus, the first shock fitting equation yields

$$\frac{1}{2} (\zeta_+ - \zeta_-) c_0 \cos\left(\frac{\pi\zeta_-}{2\ell}\right) = \frac{2\ell c_0}{\pi} \left\{ 1 - \sin\left(\frac{\pi\zeta_-}{2\ell}\right) \right\} . \quad (9.164)$$

The second shock fitting equation gives

$$t = \frac{\zeta_+ - \zeta_-}{c_0 \cos\left(\frac{\pi\zeta_-}{2\ell}\right)} . \quad (9.165)$$

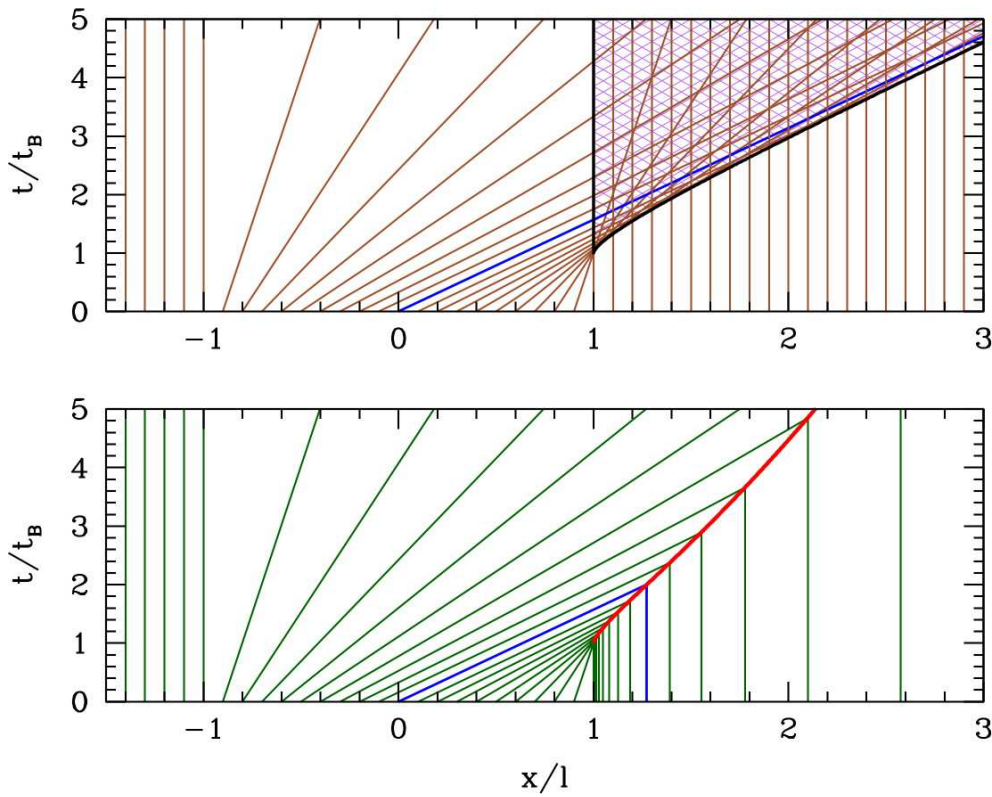


Figure 9.13: Top : crossing characteristics (purple hatched region) in the absence of shock fitting. Bottom : characteristics in the presence of the shock.

Eliminating $\zeta_+ - \zeta_-$, we obtain the relation

$$\sin\left(\frac{\pi\zeta_-}{2\ell}\right) = \frac{4\ell}{\pi c_0 t} - 1 \quad . \quad (9.166)$$

Thus,

$$\zeta_-(t) = \frac{2\ell}{\pi} \sin^{-1}\left(\frac{4\ell}{\pi c_0 t} - 1\right) \quad (9.167)$$

and

$$\begin{aligned} \zeta_+(t) &= \zeta_- + \frac{4\ell}{\pi} \cdot \frac{1 - \sin(\pi\zeta_-/2\ell)}{\cos(\pi\zeta_-/2\ell)} \\ &= \frac{2\ell}{\pi} \left\{ \sin^{-1}\left(\frac{4\ell}{\pi c_0 t} - 1\right) + 2 \sqrt{\frac{\pi c_0 t}{2\ell} - 1} \right\} \quad , \end{aligned} \quad (9.168)$$

where $t \geq t_B = 2\ell/\pi c_0$.

(c) Find the shock motion $x_s(t)$.

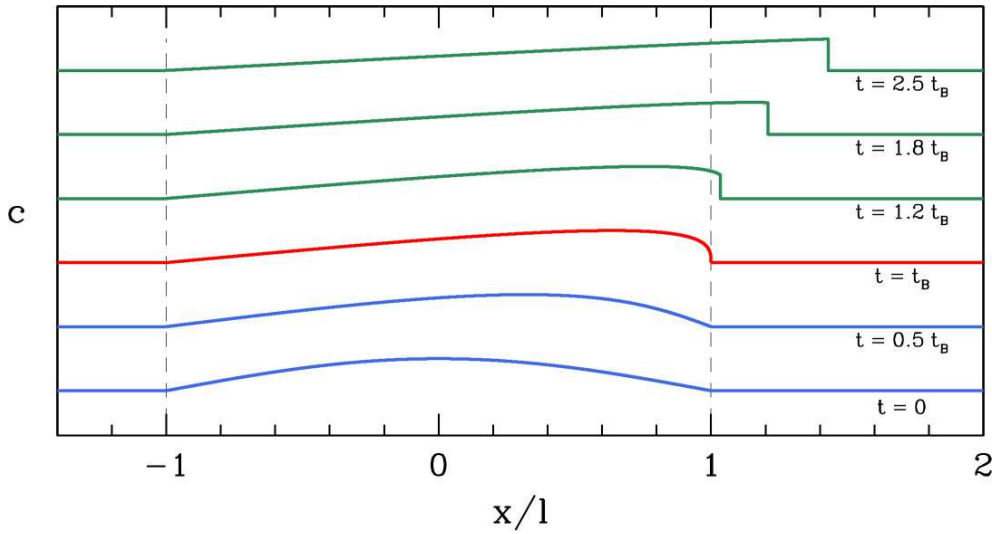


Figure 9.14: Evolution of $c(x, t)$ for a series of time values.

Solution : The shock position is

$$\begin{aligned} x_s(t) &= \zeta_- + g(\zeta_-) t \\ &= \frac{2\ell}{\pi} \sin^{-1}\left(\frac{2}{\tau} - 1\right) + \frac{4\ell}{\pi} \sqrt{\tau - 1} \quad , \end{aligned} \quad (9.169)$$

where $\tau = t/t_B = \pi c_0 t / 2\ell$, and $\tau \geq 1$.

(d) Sketch the characteristics for the multivalued solution with no shock fitting, identifying the region in (x, t) where characteristics cross. Then sketch the characteristics for the discontinuous shock solution.

Solution : See Fig. 9.13.

(e) Find the shock discontinuity $\Delta c(t)$.

Solution : The shock discontinuity is

$$\begin{aligned} \Delta c(t) &= g(\zeta_-) - g(\zeta_+) = c_0 \cos\left(\frac{\pi \zeta_-}{2\ell}\right) \\ &= \sqrt{\frac{8\ell c_0}{\pi t} \left(1 - \frac{2\ell}{\pi c_0 t}\right)} = 2c_0 \frac{\sqrt{\tau - 1}}{\tau} \quad . \end{aligned} \quad (9.170)$$

(f) Find the shock velocity $v_s(t)$.

Solution : The shock wave velocity is

$$\begin{aligned} c_s(t) &= \frac{1}{2} [g(\zeta_-) + g(\zeta_+)] = \frac{1}{2} \Delta c(t) \\ &= \sqrt{\frac{2\ell c_0}{\pi t} \left(1 - \frac{2\ell}{\pi c_0 t}\right)} . \end{aligned} \quad (9.171)$$

(g) Sketch the evolution of the wave, showing the breaking of the wave at $t = t_B$ and the subsequent evolution of the shock front.

Solution : A sketch is provided in Fig. 9.14.

9.12 Appendix III : The Traffic Light

Problem : Consider vehicular traffic flow where the flow velocity is given by

$$u(\rho) = u_0 \left(1 - \frac{\rho^2}{\rho_{BB}^2}\right) . \quad (9.172)$$

Solve for the density $\rho(x, t)$ with the initial conditions appropriate to a green light starting at $t = 0$, i.e. $\rho(x, 0) = \rho_{BB} \Theta(-x)$. Solve for the motion of a vehicle in the flow, assuming initial position $x(0) = x_0 < 0$. How long does it take the car to pass the light?

Solution : Consider the one-parameter family of velocity functions,

$$u(\rho) = u_0 \left(1 - \frac{\rho^\alpha}{\rho_{BB}^\alpha}\right) , \quad (9.173)$$

where $\alpha > 0$. The speed of wave propagation is

$$\begin{aligned} c(\rho) &= u(\rho) + \rho u'(\rho) \\ &= u_0 \left(1 - (1 + \alpha) \frac{\rho^\alpha}{\rho_{BB}^\alpha}\right) . \end{aligned} \quad (9.174)$$

The characteristics are shown in figure 9.15. At $t = 0$, the characteristics emanating from the x -axis have slope $-1/(\alpha u_0)$ for $x < 0$ and slope $+1/u_0$ for $x > 0$. This is because the slope is $1/c$ (we're plotting t on the y -axis), and $c(0) = u_0$ while $c(\rho_{BB}) = -\alpha u_0$. Interpolating between these two sets is the fan region, shown in blue in the figure. All characteristics in the fan emanate from $x = 0$, where the density is discontinuous at $t = 0$. Hence, the entire interval $[0, \rho_{BB}]$ is represented at $t = 0$.

For the fan region, the characteristics satisfy

$$c(\rho) = \frac{x}{t} \Rightarrow \frac{\rho^\alpha}{\rho_{BB}^\alpha} = \frac{1}{1 + \alpha} \left(1 - \frac{x}{u_0 t}\right) . \quad (9.175)$$

This is valid throughout the region $-\alpha u_0 < x/t < u_0$. The motion of a vehicle in this flow is determined by the equation

$$\frac{dx}{dt} = u(\rho) = \frac{\alpha u_0}{1 + \alpha} + \frac{1}{1 + \alpha} \frac{x}{t} , \quad (9.176)$$

which is obtained by eliminating ρ in terms of the ratio x/t . Thus, we obtain the linear, non-autonomous, inhomogeneous equation

$$t \frac{dx}{dt} - \frac{x}{1 + \alpha} = \frac{\alpha u_0 t}{1 + \alpha} , \quad (9.177)$$

whose solution is

$$x(t) = \mathcal{C} t^{1/(1+\alpha)} + u_0 t , \quad (9.178)$$

where \mathcal{C} is a constant, fixed by the initial conditions.

What are the initial conditions? Consider a vehicle starting at $x(t = 0) = -|x_0|$. It remains stationary until a time $t^* = |x_0|/\alpha u_0$, at which point $x/t^* = -\alpha u_0$, and it enters the fan region. At this point (see figure 9.16), the trailing edge of the smoothing front region, which was absolutely sharp and discontinuous at $t = 0$, passes by the vehicle, the local density decreases below ρ_{BB} , and it starts to move. We solve for \mathcal{C} by setting

$$x(t^*) = -|x_0| \Rightarrow \mathcal{C} = -(1 + \alpha) \alpha^{-\alpha/(1+\alpha)} |x_0|^{\alpha/(1+\alpha)} u_0^{1/(1+\alpha)} . \quad (9.179)$$

Thus,

$$\begin{aligned} x(t) &= -|x_0| \quad (t < t^* = |x_0|/\alpha u_0) \\ &= u_0 t - (1 + \alpha) \alpha^{-\alpha/(1+\alpha)} |x_0|^{\alpha/(1+\alpha)} (u_0 t)^{1/(1+\alpha)} \quad (t > t^*) . \end{aligned} \quad (9.180)$$

Finally, we set $x(t_c) = 0$ to obtain

$$x(t_c) = 0 \Rightarrow t_c = \frac{1}{\alpha} (1 + \alpha)^{1+\alpha^{-1}} \cdot \frac{|x_0|}{u_0} . \quad (9.181)$$

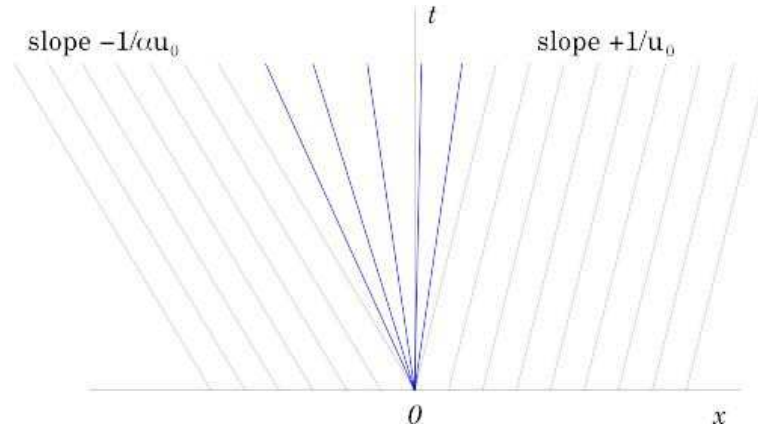


Figure 9.15: Characteristics for the green light problem. For $x < 0$, the density at $t = 0$ is $\rho = \rho_{BB}$, and $c(x < 0, t = 0) = -\alpha u_0$. For $x > 0$, the density at $t = 0$ is $\rho = 0$ and $c(x > 0, t = 0) = u_0$.

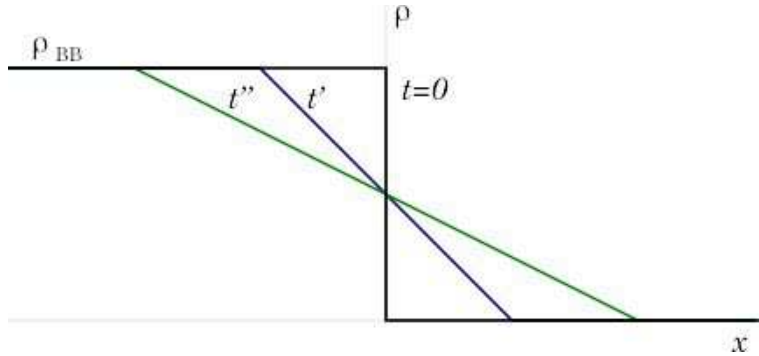


Figure 9.16: Density *versus* position for the green light problem at three successive times. The initial discontinuity at $x = 0$ is smoothed into a straight line interpolating between $\rho = \rho_{\text{BB}}$ and $\rho = 0$. Because $dc/dx > 0$ for this problem, the initial profile smooths out. When $dc/dx < 0$, the wave steepens.

For $\alpha = 2$, find $t_c = \frac{3\sqrt{3}}{2} |x_0|/u_0$.

9.13 Appendix IV : Characteristics for a Periodic Signal

Problem : Consider traffic flow in the presence of a signal on a single-lane roadway. Assume initial conditions $\rho(x, 0) = \rho_1$. At time $t = 0$, the signal turns red for an interval $T_{\text{red}} = rT$, after which the signal is green for $T_{\text{green}} = gT$, with $r + g = 1$. The cycle length is T . (Traffic engineers call g the ‘green-to-cycle ratio’.) It is useful to work with dimensionless quantities,

$$\bar{\rho} \equiv \rho/\rho_{\text{BB}} \quad \bar{c} \equiv c/u_0 \quad \bar{x} \equiv x/u_0 T \quad (9.182)$$

$$\bar{j} \equiv j/u_0 \rho_{\text{BB}} \quad \bar{u} \equiv u/u_0 \quad \tau \equiv t/T \quad .$$

The continuity equation is then

$$\frac{\partial \bar{\rho}}{\partial \tau} + \bar{c}(\bar{\rho}) \frac{\partial \bar{\rho}}{\partial \bar{x}} = 0 \quad . \quad (9.183)$$

Note : Assume $\bar{j}(\bar{\rho}) = \bar{\rho}(1 - \bar{\rho})$, so

$$\bar{u}(\bar{\rho}) = 1 - \bar{\rho} \quad , \quad \bar{c}(\bar{\rho}) = 1 - 2\bar{\rho} \quad . \quad (9.184)$$

(a) During the red phase, two shocks propagate – one behind the light (*i.e.* $\bar{x}_s^- < 0$) and one ahead of the light (*i.e.* $\bar{x}_s^+ > 0$). Find the velocities and discontinuities at these shocks.

Solution : During the red phase, $0 \leq \tau \leq r$, a shock is formed behind the light at the boundary of the $\bar{\rho} = \bar{\rho}_1$ and $\bar{\rho} = 1$ regions. The velocity of this shock is

$$v_s = \frac{\bar{j}(1) - \bar{j}(\bar{\rho}_1)}{1 - \bar{\rho}_1} = -\bar{\rho}_1 \quad . \quad (9.185)$$

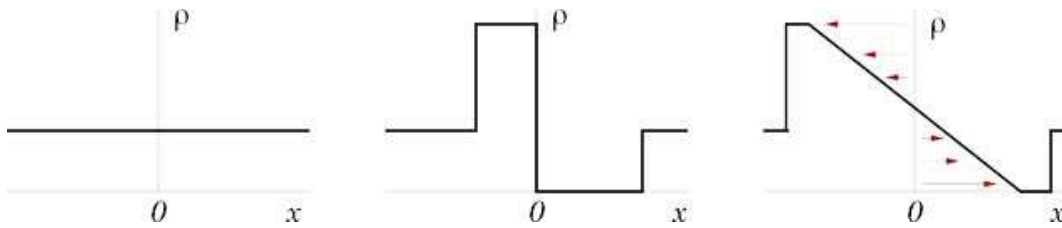


Figure 9.17: Evolution of traffic density before, during, and after a red light.

This shock forms immediately upon the appearance of the red light, hence $\bar{x}_s^-(\tau) = -\bar{\rho}_1 \tau$. Another shock forms ahead of the light, at the boundary between $\bar{\rho} = 0$ and $\bar{\rho} = \bar{\rho}_1$ regions. There,

$$v_s = \frac{\bar{j}(\bar{\rho}_1) - \bar{j}(0)}{\bar{\rho}_1 - 0} = 1 - \bar{\rho}_1 \quad . \quad (9.186)$$

Thus, $\bar{x}_s^+(\tau) = (1 - \bar{\rho}_1) \tau$.

(b) When the light changes to green, the characteristics develop a fan, and the discontinuity at $x = 0$ starts to spread. Let $\bar{x}_>(\tau)$ denote the minimum value of \bar{x} for which $\bar{\rho}(\tau) = 0$, and $\bar{x}_<(\tau)$ the maximum value of \bar{x} for which $\bar{\rho}(\tau) = 1$. Show that $\bar{x}_>$ overtakes \bar{x}_s^+ after a time τ_+ and that $\bar{x}_<$ overtakes \bar{x}_s^- after a time τ_- . Compute τ_{\pm} .

Solution : The situation is depicted in figure 9.17. At $\tau = r$, the light turns green, and the queue behind the light is released. The discontinuity at $\bar{x} = 0$ spreads as shown in the figure. (Recall that regions with $dc/dx > 0$ spread while those with $dc/dx < 0$ steepen.) The boundaries of the spreading region are $\bar{x}_>(\tau) = \tau - r$ and $\bar{x}_<(\tau) = r - \tau$, and travel at speeds $\bar{c}_> = +1$ and $\bar{c}_< = -1$. Setting $\bar{x}_s^+(\tau_+) = \bar{x}_>(\tau_+)$ gives $\tau_+ = r/\bar{\rho}_1$. Similarly, setting $\bar{x}_s^-(\tau_-) = \bar{x}_<(\tau_-)$ gives $\tau_- = r/(1 - \bar{\rho}_1)$. For light traffic ($\bar{\rho}_1 < \frac{1}{2}$), we have $\tau_- < \tau_+$, while for heavy traffic ($\bar{\rho}_1 > \frac{1}{2}$), $\tau_- > \tau_+$.

(c) Impose the proper shock conditions at \bar{x}_s^{\pm} for $\tau > \tau_{\pm}$, respectively. Show that each shock obeys the equation

$$\frac{d\bar{x}_s}{d\tau} = \frac{1}{2} - \bar{\rho}_1 + \frac{\bar{x}_s}{2(\tau - r)} \quad .$$

Apply the proper boundary conditions for the ahead and behind shocks and obtain explicit expressions for $\bar{x}_s^{\pm}(\tau)$ for all $\tau \geq 0$. (You will have to break up your solution into different cases, depending on τ .)

Solution : For a shock discontinuity between $\bar{\rho} = \bar{\rho}_-$ and $\bar{\rho} = \bar{\rho}_+$, we have in general

$$v_s = \frac{\bar{j}_+ - \bar{j}_-}{\bar{\rho}_+ - \bar{\rho}_-} = 1 - \bar{\rho}_+ - \bar{\rho}_- \quad . \quad (9.187)$$

Let's first apply this at the shock \bar{x}_s^+ for $\tau > \tau_+$. For $x < \bar{x}_s^+$, we are in a fan region of the characteristics, with

$$\bar{x}(\tau) = \bar{c}(\bar{\rho})(\tau - r) = (1 - 2\bar{\rho})(\tau - r) \quad . \quad (9.188)$$

Thus,

$$\bar{\rho} = \frac{1}{2} \left(1 - \frac{\bar{x}}{\tau - r} \right) \quad . \quad (9.189)$$

Now invoke the shock condition at $\bar{x} = \bar{x}_s^+$:

$$\begin{aligned}\frac{d\bar{x}_s^+}{d\tau} &= 1 - \bar{\rho}_1 - \frac{1}{2} \left(1 - \frac{\bar{x}_s^+}{\tau - r} \right) \\ &= \frac{1}{2} - \bar{\rho}_1 - \frac{\bar{x}_s^+}{2(\tau - r)} ,\end{aligned}\quad (9.190)$$

the solution of which is

$$\bar{x}_s^+(\tau) = A_+ (\tau - r)^{1/2} + (1 - 2\bar{\rho}_1)(\tau - r) . \quad (9.191)$$

The constant A_+ is determined by setting

$$\bar{x}_s^+(\tau_+) = \bar{x}_>(\tau_+) = \frac{\bar{\rho}_1 r}{1 - \bar{\rho}_1} \Rightarrow A_+ = 2\sqrt{r\bar{\rho}_1(1 - \bar{\rho}_1)} . \quad (9.192)$$

Putting this all together, we have

$$\bar{x}_s^+(\tau) = \begin{cases} (1 - \bar{\rho}_1)\tau & \text{for } \tau < \frac{r}{\bar{\rho}_1} \\ \sqrt{4r\bar{\rho}_1(1 - \bar{\rho}_1)}(\tau - r)^{1/2} + (1 - 2\bar{\rho}_1)(\tau - r) & \text{for } \tau > \frac{r}{\bar{\rho}_1} \end{cases} . \quad (9.193)$$

The identical analysis can be applied to the shock at \bar{x}_s^- for $\tau > \tau_-$. The solution is once again of the form

$$\bar{x}_s^-(\tau) = A_- (\tau - r)^{1/2} + (1 - 2\bar{\rho}_1)(\tau - r) , \quad (9.194)$$

now with A_- chosen to satisfy

$$\bar{x}_s^-(\tau_-) = \bar{x}_<(\tau_-) = -\frac{\bar{\rho}_1 r}{1 - \bar{\rho}_1} \Rightarrow A_- = -2\sqrt{r\bar{\rho}_1(1 - \bar{\rho}_1)} = -A_+ . \quad (9.195)$$

Thus,

$$\bar{x}_s^-(\tau) = \begin{cases} -\bar{\rho}_1\tau & \text{for } \tau < \frac{r}{1 - \bar{\rho}_1} \\ -\sqrt{4r\bar{\rho}_1(1 - \bar{\rho}_1)}(\tau - r)^{1/2} + (1 - 2\bar{\rho}_1)(\tau - r) & \text{for } \tau > \frac{r}{1 - \bar{\rho}_1} \end{cases} . \quad (9.196)$$

(d) Compute the discontinuity $\Delta\bar{\rho}^\pm(\tau)$ at the shocks.

Solution : For the shock at \bar{x}_s^+ , we have

$$\begin{aligned}\Delta\bar{\rho}^+(\tau) &= \bar{\rho}_1 - \frac{1}{2} \left(1 - \frac{\bar{x}_s^+}{\tau - r} \right) \\ &= \sqrt{r\bar{\rho}_1(1 - \bar{\rho}_1)}(\tau - r)^{-1/2} ,\end{aligned}\quad (9.197)$$

which is valid for $\tau > \tau_+ = r/\bar{\rho}_1$. For the shock at \bar{x}_s^- ,

$$\begin{aligned}\Delta\bar{\rho}^-(\tau) &= \frac{1}{2} \left(1 - \frac{\bar{x}_s^-}{\tau - r} \right) - \bar{\rho}_1 \\ &= \sqrt{r\bar{\rho}_1(1 - \bar{\rho}_1)}(\tau - r)^{-1/2} ,\end{aligned}\quad (9.198)$$

which is valid for $\tau > \tau_- = r/(1 - \bar{\rho}_1)$. Note $\Delta\bar{\rho}^+(\tau) = \Delta\bar{\rho}^-(\tau)$ for $\tau > \max(\tau_+, \tau_-)$.

(e) If $\bar{\rho}_1 < \frac{1}{2}$, show that the shock which starts out behind the light passes the light after a finite time τ^* . What is the condition that the shock passes the light before the start of the next red phase? Show that this condition is equivalent to demanding that the number of cars passing the light during the green phase must be greater than the incoming flux at $\bar{x} = -\infty$, integrated over the cycle length, under the assumption that the shock just barely manages to pass through before the next red.

Solution : For light traffic with $\bar{\rho}_1 < \frac{1}{2}$, the shock behind the light passes the signal at time τ^* , where $\bar{x}_s^-(\tau^*) = 0$, i.e.

$$\bar{x}_s^-(\tau^*) = (1 - 2\bar{\rho}_1)(\tau^* - r) - \sqrt{4r\bar{\rho}_1(1 - \bar{\rho}_1)}(\tau^* - r)^{1/2} = 0 \quad . \quad (9.199)$$

Solving for τ^* , we have

$$\tau^* = r + \frac{4r\bar{\rho}_1(1 - \bar{\rho}_1)}{(1 - 2\bar{\rho}_1)^2} = \frac{r}{(1 - 2\bar{\rho}_1)^2} \quad . \quad (9.200)$$

Similarly, if $\bar{\rho}_1 > \frac{1}{2}$, the shock ahead of the light reverses direction and passes behind the signal at time $\tau^* = r/(2\bar{\rho}_1 - 1)^2$.

For the case of light traffic, we see that if $r > (1 - 2\bar{\rho}_1)^2$, the trailing shock remains behind the signal when the next green phase starts – the shock never clears the signal. In traffic engineering parlance, the capacity of the intersection is insufficient, and the traffic will back up. We can derive the result in a very simple way. Until the trailing shock at \bar{x}_s^- passes the signal, the density of vehicles at the signal is fixed at $\bar{\rho} = \frac{1}{2}$. Hence the flux of vehicles at the signal is maximum, and equal to $\bar{j}(\bar{\rho} = \frac{1}{2}) = \frac{1}{4}$. The maximum number of vehicles that the signal can clear is therefore $\frac{1}{4}g = \frac{1}{4}(1 - r)$, which pertains when the trailing shock just barely passes the signal before the start of the next red phase. We now require that the incident flux of cars from $\bar{x} = -\infty$, integrated over the *entire* cycle, is less than this number:

$$\bar{j}(\bar{\rho}_1) \times 1 = \bar{\rho}_1(1 - \bar{\rho}_1) < \frac{1}{4}(1 - r) \Rightarrow r < (1 - 2\bar{\rho}_1)^2 \quad . \quad (9.201)$$

Merging shocks : So far, so good. We now ask: does the shock at $\bar{x}_s^-(\tau)$ ever catch up with the shock at $\bar{x}_s^+(\tau - 1)$ from the next cycle? Let's assume that the equation $\bar{x}_s^-(\tau) = \bar{x}_s^+(\tau - 1)$ has a solution, which means we set

$$-a\sqrt{\tau - r} + b(\tau - r) = \begin{cases} a\sqrt{\tau - 1 - r} + b(\tau - 1 - r) & \text{if } \tau > 1 + \frac{r}{\bar{\rho}_1} \\ (1 - \bar{\rho}_1)(\tau - 1) & \text{if } 1 < \tau < 1 + \frac{r}{\bar{\rho}_1} \end{cases} \quad (9.202)$$

with

$$a \equiv \sqrt{4r\bar{\rho}_1(1 - \bar{\rho}_1)} \quad , \quad b \equiv 1 - 2\bar{\rho}_1 \quad . \quad (9.203)$$

We first look for a solution satisfying $\tau > 1 + \tau_+ = 1 + \frac{r}{\bar{\rho}_1}$. Let us call this a ‘case I merge’. It is convenient to define $s = \tau - \frac{1}{2} - r$, in which case

$$a\sqrt{s - \frac{1}{2}} + a\sqrt{s + \frac{1}{2}} = b \quad , \quad (9.204)$$

which is solved by

$$s = \frac{1}{4}\left(\frac{a^2}{b^2} + \frac{b^2}{a^2}\right) \quad . \quad (9.205)$$

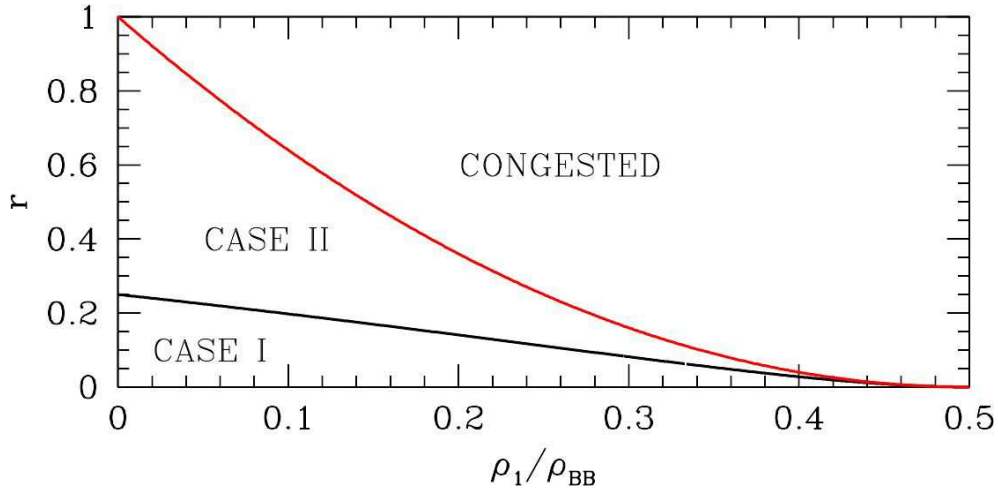


Figure 9.18: Phase diagram for the shock merge analysis. For $r > (1 - 2\bar{\rho}_1)^2$ (red line), the signal is congested, and the trailing shock does not clear the signal before the start of the following red phase. In case II, the shocks merge when the leading shock is still in its constant velocity phase. In case I, the shocks merge after the leading shock has already begun to decelerate.

Note $s > \frac{1}{2}$, so $\tau > 1 + r$. Solving for τ , we obtain

$$\tau = \tau_I \equiv 1 + r + \frac{1}{4} \left(\frac{a}{b} - \frac{b}{a} \right)^2 . \quad (9.206)$$

We must now check that $\tau > 1 + \frac{r}{\bar{\rho}_1}$. We have

$$\begin{aligned} 0 &> f(r) \equiv 1 + \frac{r}{\bar{\rho}_1} - \tau_I \\ &= \frac{(1 - \bar{\rho}_1)^2(1 - 3\bar{\rho}_1)}{(1 - 2\bar{\rho}_1)^2\bar{\rho}_1} r + \frac{1}{2} - \frac{(1 - 2\bar{\rho}_1)^2}{16r\bar{\rho}_1(1 - \bar{\rho}_1)} \\ &\equiv \frac{(1 - \bar{\rho}_1)^2(1 - 3\bar{\rho}_1)}{(1 - 2\bar{\rho}_1)^2\bar{\rho}_1 r} (r - r_1)(r - r_2) \end{aligned} \quad (9.207)$$

with

$$r_1 = \left(\frac{1 - 2\bar{\rho}_1}{2 - 2\bar{\rho}_1} \right)^2 , \quad r_2 = -\frac{(1 - 2\bar{\rho}_1)^2}{4(1 - \bar{\rho}_1)(1 - 3\bar{\rho}_1)} . \quad (9.208)$$

When $\bar{\rho}_1 < \frac{1}{3}$, we have $r_2 > 0 > r_1$, and we require $0 < r < r_2$. When $\bar{\rho}_1 > \frac{1}{3}$, $r_1 > r_2$ so again we require $0 < r < r_2$.

Now let's solve for the merging shocks. We write the condition that two characteristics meet. Thus,

$$\alpha(\tau - r) = \beta(\tau - 1 - r) \quad (9.209)$$

with $\bar{x} = \alpha(\tau - r)$. Let $\sigma = \tau - r$. Then $\bar{x} = \alpha\sigma = \beta(\sigma - 1)$, which yields

$$\alpha = \frac{\bar{x}}{\sigma} , \quad \beta = \frac{\bar{x}}{\sigma - 1} . \quad (9.210)$$

The combined shock moves at velocity v_s , where

$$v_s = \dot{x} = \frac{1}{2}(\alpha + \beta) = \frac{\bar{x}}{2\sigma} + \frac{\bar{x}}{2(\sigma - 1)} . \quad (9.211)$$

This equation is easily integrated to yield

$$\bar{x}^I(\sigma) = \mathcal{C} \sqrt{\sigma(\sigma - 1)} . \quad (9.212)$$

The constant \mathcal{C} is fixed by the initial conditions at time τ_I , when the shocks merge. We have

$$\begin{aligned} \tau_I - r &= \frac{1}{4} \left(\frac{a}{b} + \frac{b}{a} \right)^2 \\ \bar{x}(\tau_I) &= -a \sqrt{\tau_I - r} + b(\tau_I - r) \\ &= \frac{1}{4} \left(\frac{b^2}{a^2} - \frac{a^2}{b^2} \right) b . \end{aligned} \quad (9.213)$$

We then have

$$\sigma(\sigma - 1) = \frac{1}{16} \left(\frac{a^2}{b^2} - \frac{b^2}{a^2} \right)^2 ,$$

and we set

$$\frac{1}{4} \left(\frac{a^2}{b^2} - \frac{b^2}{a^2} \right) \mathcal{C} = \frac{1}{4} \left(\frac{b^2}{a^2} - \frac{a^2}{b^2} \right) b ,$$

which simply yields $\mathcal{C} = b = 1 - 2\bar{\rho}_1$.

Finally, consider the ‘case II merge’ where $\bar{x}_s^-(\tau) = \bar{x}_s^+(\tau - 1)$ requires $\tau < 1 + \frac{r}{\bar{\rho}_1}$. We now must solve

$$-a \sqrt{\tau - r} + b(\tau - r) = (1 - \bar{\rho}_1)(\tau - 1) , \quad (9.214)$$

the solution of which is

$$\tau_{II} = r + (1 - \sqrt{r})^2 \frac{1 - \bar{\rho}_1}{\bar{\rho}_1} . \quad (9.215)$$

One can check that $\tau_{II} < 1 + \frac{r}{\bar{\rho}_1}$ is equivalent to $r > r_2$. In this case, the characteristics to the right of the shock all have slope 1, corresponding to $\bar{\rho} = 0$, and are not part of the fan. Thus, the shock condition becomes

$$\dot{x} = \frac{1}{2} \left(1 + \frac{\bar{x}}{\sigma} \right) \quad (9.216)$$

with $\sigma = \tau - r$ as before. The solution here is

$$\bar{x}^{II} = \mathcal{C}' \sqrt{\sigma} + \sigma . \quad (9.217)$$

Again, \mathcal{C}' is determined by the merging shock condition, $\bar{x}_s^-(\tau) = \bar{x}_s^+(\tau - 1)$. We therefore set

$$\mathcal{C}' (1 - \sqrt{r}) \sqrt{\frac{1 - \bar{\rho}_1}{\bar{\rho}_1}} + (1 - \sqrt{r})^2 \frac{1 - \bar{\rho}_1}{\bar{\rho}_1} = (1 - \bar{\rho}_1) \left\{ r + (1 - \sqrt{r})^2 \frac{1 - \bar{\rho}_1}{\bar{\rho}_1} - 1 \right\} , \quad (9.218)$$

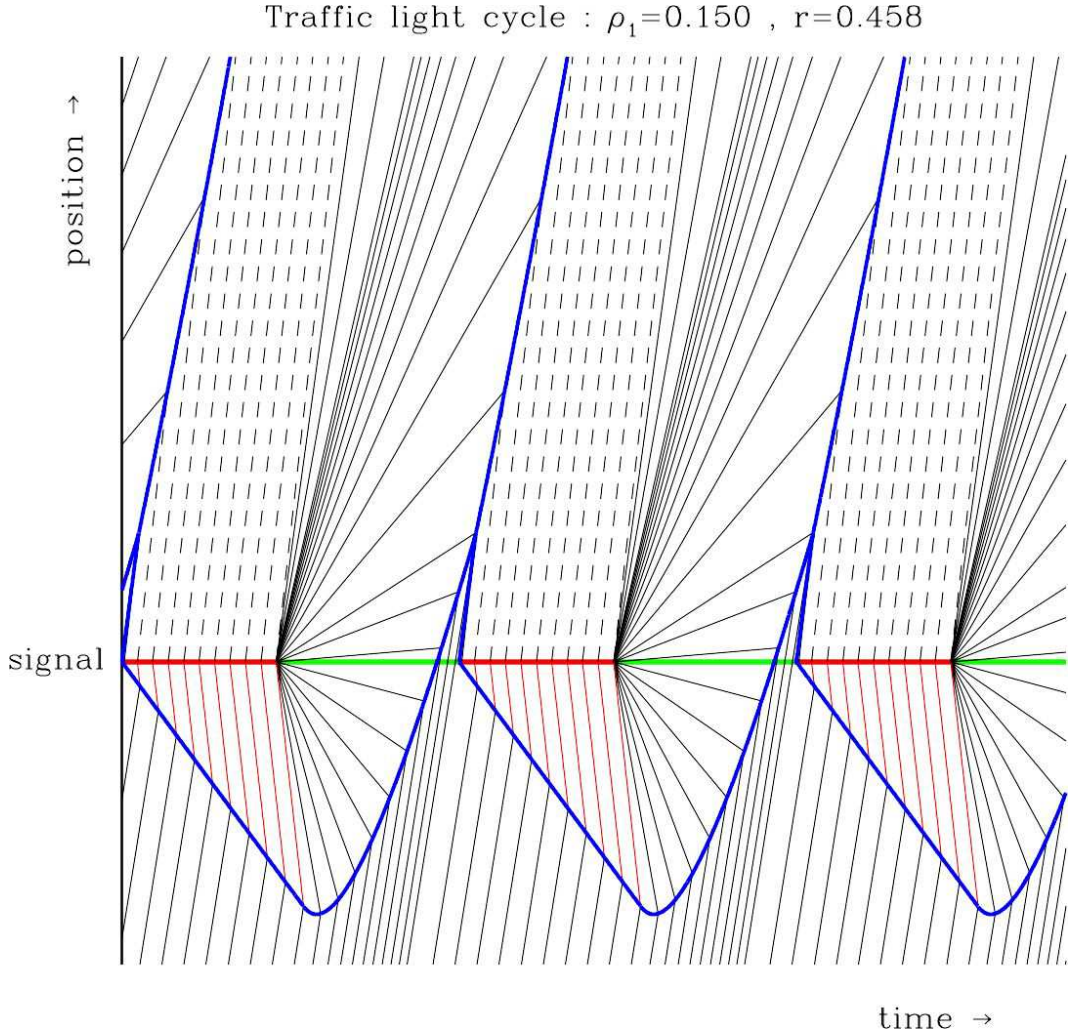


Figure 9.19: Characteristics for the light cycle problem. Red interval signifies red light; green interval signifies green light. Red characteristics correspond to bumper-to-bumper traffic, i.e. $\bar{\rho} = 1$. Dotted line characteristics correspond to $\bar{\rho} = 0$. Note the merging of shocks. Congested regions are those with negatively-sloped characteristics, since $\bar{c} < 0$ for $\bar{\rho} > \frac{1}{2}$.

yielding

$$\mathcal{C}' = -\sqrt{4\bar{\rho}_1(1-\bar{\rho}_1)} = -\frac{a}{\sqrt{r}} \quad . \quad (9.219)$$

This solution is valid until the characteristics on the right side of the shock extrapolate back to the \bar{x} axis at time $\tau = 1 + r$, when the fan begins. Thus,

$$\bar{x} = \tau - 1 - r = \sigma - 1 = \mathcal{C}' \sqrt{\sigma} + \sigma \quad , \quad (9.220)$$

which yields $\sigma = \sigma_m \equiv \frac{1}{4\bar{\rho}_1(1-\bar{\rho}_1)}$.

For $\sigma > \sigma_m$, we match with the profile $C'' \sqrt{\sigma(\sigma - 1)}$, which we obtained earlier. Thus,

$$C'' \sqrt{\sigma_m(\sigma_m - 1)} = \sigma_m - \sqrt{4\bar{\rho}_1(1 - \bar{\rho}_1)} \sqrt{\sigma_m} , \quad (9.221)$$

which yields $C'' = b = 1 - 2\bar{\rho}_1$, as before.

Putting this all together, we plot the results in figure 9.19. The regions with negatively-sloped characteristics are regions of local congestion, since $\bar{c} < 0$ implies $\bar{\rho} > \frac{1}{2}$. Note that the diagram is periodic in time, and it is presumed that several cycles have passed in order for the cycle to equilibrate. *I.e.* the conditions at $t = 0$ in the diagram do not satisfy $\bar{\rho}(x) = \bar{\rho}_1$ for $x > 0$.

9.14 Appendix V : Car-Following Models

So-called ‘car-following’ models are defined by equations of motion for individual vehicles. Let $x_n(t)$ be the motion of the n^{th} vehicle in a group, with $x_{n+1} < x_n$, so that the lead vehicle ($n = 0$) is the rightmost vehicle. Three classes of models have traditionally been considered in the literature:

- *Traditional car-following model (CFM)* – Cars accelerate (or decelerate) in an attempt to match velocity with the car ahead, subject to a delay time τ :

$$\ddot{x}_n(t + \tau) = \alpha \left\{ \dot{x}_{n-1}(t) - \dot{x}_n(t) \right\} .$$

- *Optimal velocity model (OVM)* – Drivers instantaneously accelerate in order to maintain a velocity which is optimally matched to the distance to the next car. (The distance to the next vehicle is known as the *headway* in traffic engineering parlance.) Thus,

$$\ddot{x}_n = \alpha \left\{ V(x_{n-1} - x_n) - \dot{x}_n \right\} , \quad (9.222)$$

where $V(\Delta x)$ is the optimum velocity function.

- *Optimal headway model (OHM)* – Drivers instantaneously accelerate in order to maintain an optimal headway, given their current velocity:

$$\ddot{x}_n = \alpha \left\{ H(\dot{x}_n) - (x_{n-1} - x_n) \right\} . \quad (9.223)$$

The optimal headway function is just the inverse of the optimal velocity function of the OVM: $H = V^{-1}$.

- (a) The CFM equation above is a linear equation. Solve it by Fourier transforming the function $v_n(t) = \dot{x}_n(t)$. Show that

$$\hat{v}_n(\omega) = r(\omega) e^{i\theta(\omega)} \hat{v}_{n-1}(\omega) . \quad (9.224)$$

Thus, given the velocity $v_0(t)$ of the lead vehicle, the velocity of every other vehicle is determined, since $\hat{v}_n(\omega) = r^n(\omega) e^{in\theta(\omega)} \hat{v}_0(\omega)$. Derive the stability criterion $|r| < 1$ in terms of ω , τ , and α . Show that, if

the motion is stable, no matter how erratic the lead vehicle moves, for $n \rightarrow \infty$ the variations in $v_n(t)$ are damped out and the velocity approaches a constant.

Solution : We have the linear equation

$$\dot{v}_n(t + \tau) = \alpha \left\{ v_{n-1}(t) - v_n(t) \right\} . \quad (9.225)$$

Solve by Fourier transform:

$$v_n(t) = \int_{-\infty}^{\infty} \frac{d\omega}{2\pi} \hat{v}_n(\omega) e^{-i\omega t} . \quad (9.226)$$

This yields

$$\hat{v}_n(\omega) = z(\omega) \hat{v}_{n-1}(\omega) \quad (9.227)$$

with

$$z(\omega) = \frac{\alpha}{\alpha - i\omega \exp(-i\omega\tau)} . \quad (9.228)$$

Thus, writing $z = r e^{i\theta}$, we have

$$\theta(\omega) = \tan^{-1} \left(\frac{\omega \cos \omega\tau}{\alpha - \omega \sin \omega\tau} \right) \quad (9.229)$$

and

$$r(\omega) = \frac{\alpha}{\sqrt{\alpha^2 + \omega^2 - 2\alpha\omega \sin(\omega\tau)}} . \quad (9.230)$$

The velocity of the n^{th} vehicle is now given in terms of that of the lead vehicle, according to the relation

$$\hat{v}_n(\omega) = r^n(\omega) e^{in\theta(\omega)} \hat{v}_0(\omega) . \quad (9.231)$$

For $\omega = 0$ we have $z(\omega) = 1$, which says that the time-averaged velocity of each vehicle is the same. For $\hat{v}_{n \rightarrow \infty}(\omega)$ to be bounded requires $r(\omega) \leq 1$, which gives

$$r(\omega) \leq 1 \iff 2\alpha\tau \cdot \frac{\sin \omega\tau}{\omega\tau} \leq 1 . \quad (9.232)$$

The maximum of the function $x^{-1} \sin x$ is unity, for $x = 0$. This means that the instability first sets in for infinitesimal ω . We can ensure that every frequency component is stable by requiring

$$\alpha\tau < \frac{1}{2} . \quad (9.233)$$

The interpretation of this result is straightforward. The motion is stable if the product of the response time τ and the sensitivity α is sufficiently small. Slow response times and hypersensitive drivers result in an unstable flow. This is somewhat counterintuitive, as we expect that increased driver awareness should improve traffic flow.

(b) Linearize the OVM about the steady state solution,

$$x_n^0(t) = -na + V(a)t , \quad (9.234)$$

where a is the distance between cars. Write $x_n(t) = x_n^0(t) + \delta x_n(t)$ and find the linearized equation for $\delta x_n(t)$. Then try a solution of the form

$$\delta x_n(t) = A e^{ikna} e^{-\beta t} , \quad (9.235)$$

and show this solves the linearized dynamics provided $\beta = \beta(k)$. What is the stability condition in terms of α , k , and a ? Show that all small perturbations about the steady state solution are stable provided $V'(a) < \frac{1}{2}\alpha$. Interpret this result physically. If you get stuck, see M. Bando *et al.*, *Phys. Rev. E* **51**, 1035 (1995).

Solution : Writing $x_n = -na + V(a)t + \delta x_n$, we linearize the OVM and obtain

$$\delta \ddot{x}_n = \alpha \left\{ V'(a)(\delta x_{n-1} - \delta x_n) - \delta \dot{x}_n \right\} + \dots . \quad (9.236)$$

We now write

$$\delta x_n(t) = A e^{inka} e^{-\beta t} , \quad (9.237)$$

and obtain the equation

$$\beta^2 - \alpha\beta + \alpha V'(a)(1 - e^{-ika}) = 0 . \quad (9.238)$$

This determines the growth rate $\beta(k)$ for each wavelength k . Solving the quadratic equation,

$$\beta(k) = \frac{1}{2}\alpha \pm \frac{1}{2}\sqrt{\alpha^2 - 4\alpha V'(a)(1 - e^{-ika})} . \quad (9.239)$$

Let us separate β into its real and imaginary parts: $\beta \equiv \mu + i\nu$. Then

$$\mu - \frac{1}{2}\alpha + i\nu = \pm \frac{1}{2}\sqrt{\alpha^2 - 4\alpha V'(a)(1 - e^{-ika})} \quad (9.240)$$

which, when squared, gives two equations for the real and imaginary parts:

$$\begin{aligned} \nu^2 + \mu\alpha - \mu^2 &= \alpha V'(a)(1 - \cos ka) \\ \alpha\nu - 2\mu\nu &= \alpha V'(a) \sin ka . \end{aligned} \quad (9.241)$$

We set $\mu = \text{Re } \beta = 0$ to obtain the stability boundary. We therefore obtain

$$V'(a) < \frac{\alpha}{2 \cos^2 \frac{1}{2}ka} \Leftrightarrow \text{Re } \beta(k) > 0 . \quad (9.242)$$

The uniform $k = 0$ mode is the first to go unstable. We therefore have that all k modes are linearly stable provided

$$V'(a) < \frac{1}{2}\alpha . \quad (9.243)$$

This says that the stability places a *lower* limit on the sensitivity α – exactly the opposite of what we found for the CFM. The OVM result is more intuitive. Physically, we expect that the OVM is more realistic as well, since drivers generally find it easier to gauge the distance to the next car than to gauge the difference in velocity.